frontiers | Research Topics

NLRP3 activation and regulation in innate immune responses

Edited by
Alessandra Mortellaro and Chaofeng Han

Published in
Frontiers in Immunology

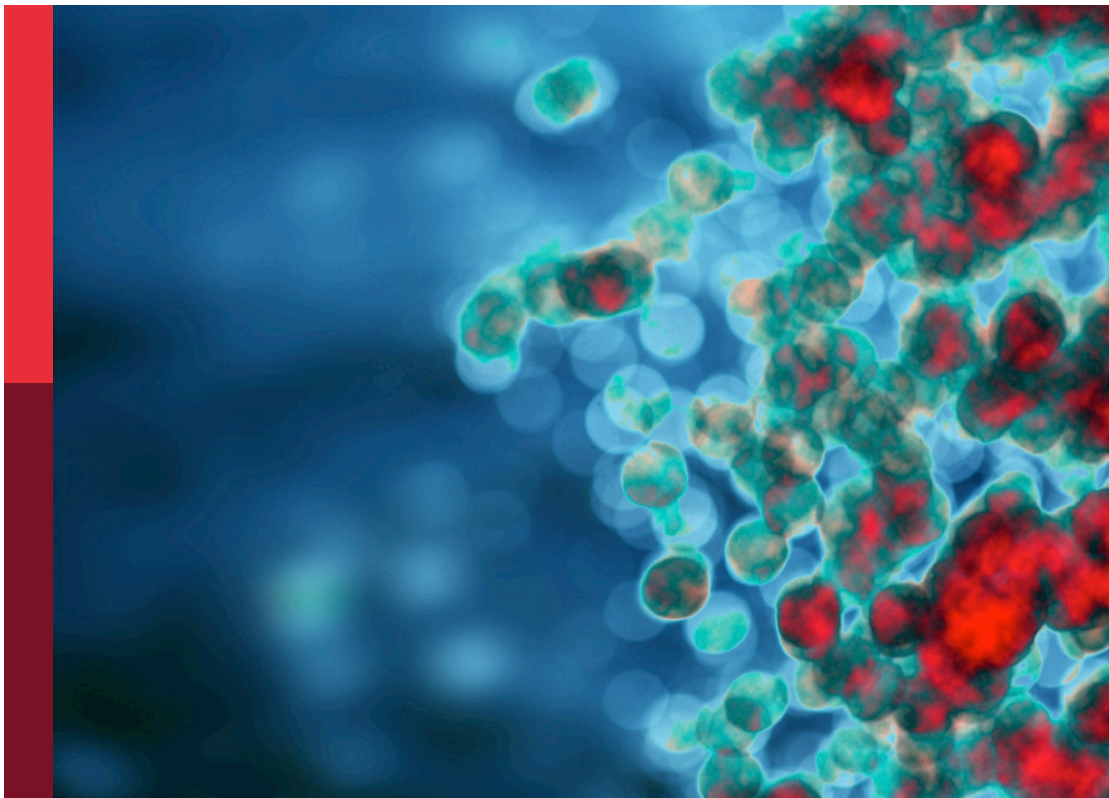

ISSN 1664-8714
ISBN 978-2-83251-987-5
DOI 10.3389/978-2-83251-987-5

About Frontiers

Frontiers is more than just an open access publisher of scholarly articles: it is a pioneering approach to the world of academia, radically improving the way scholarly research is managed. The grand vision of Frontiers is a world where all people have an equal opportunity to seek, share and generate knowledge. Frontiers provides immediate and permanent online open access to all its publications, but this alone is not enough to realize our grand goals.

Frontiers journal series

The Frontiers journal series is a multi-tier and interdisciplinary set of open-access, online journals, promising a paradigm shift from the current review, selection and dissemination processes in academic publishing. All Frontiers journals are driven by researchers for researchers; therefore, they constitute a service to the scholarly community. At the same time, the *Frontiers journal series* operates on a revolutionary invention, the tiered publishing system, initially addressing specific communities of scholars, and gradually climbing up to broader public understanding, thus serving the interests of the lay society, too.

Dedication to quality

Each Frontiers article is a landmark of the highest quality, thanks to genuinely collaborative interactions between authors and review editors, who include some of the world's best academicians. Research must be certified by peers before entering a stream of knowledge that may eventually reach the public - and shape society; therefore, Frontiers only applies the most rigorous and unbiased reviews. Frontiers revolutionizes research publishing by freely delivering the most outstanding research, evaluated with no bias from both the academic and social point of view. By applying the most advanced information technologies, Frontiers is catapulting scholarly publishing into a new generation.

What are Frontiers Research Topics?

Frontiers Research Topics are very popular trademarks of the *Frontiers journals series*: they are collections of at least ten articles, all centered on a particular subject. With their unique mix of varied contributions from Original Research to Review Articles, Frontiers Research Topics unify the most influential researchers, the latest key findings and historical advances in a hot research area.

Find out more on how to host your own Frontiers Research Topic or contribute to one as an author by contacting the Frontiers editorial office: frontiersin.org/about/contact

NLRP3 activation and regulation in innate immune responses

Topic editors

Alessandra Mortellaro — San Raffaele Telethon Institute for Gene Therapy (SR-Tiget), Italy

Chaofeng Han — Second Military Medical University, China

Citation

Mortellaro, A., Han, C., eds. (2023). *NLRP3 activation and regulation in innate immune responses*. Lausanne: Frontiers Media SA. doi: 10.3389/978-2-83251-987-5

Table of contents

frontiers | Frontiers in Immunology

TYPE Editorial
PUBLISHED 08 March 2023
DOI 10.3389/fimmu.2023.1171138

OPEN ACCESS

EDITED AND REVIEWED BY
Francesca Granucci,
University of Milano-Bicocca, Italy

*CORRESPONDENCE
Alessandra Mortellaro
mortellaro.alessandra@hsr.it

SPECIALTY SECTION
This article was submitted to Molecular Innate Immunity, a section of the journal Frontiers in Immunology

RECEIVED 21 February 2023
ACCEPTED 27 February 2023
PUBLISHED 08 March 2023

CITATION
Mortellaro A (2023) Editorial: NLRP3 activation and regulation in innate immune responses.
Front. Immunol. 14:1171138.
doi: 10.3389/fimmu.2023.1171138

Editorial: NLRP3 activation and regulation in innate immune responses

Alessandra Mortellaro*

San Raffaele Telethon Institute for Gene Therapy (SR-Tiget), IRCCS San Raffaele Scientific Institute, Milan, Italy

KEYWORDS

NLRP3, inflammasome, pyroptosis, chronic inflammation, IL-1 (interleukin-1)

Editorial on the Research Topic
NLRP3 activation and regulation in innate immune responses

The NLRP3 inflammasome is a multiprotein complex involved in the regulation of the immune system and inflammation (1). It comprises three main proteins: NLRP3 (Nod-like receptor protein 3), ASC (apoptosis-associated speck-like protein containing a caspase recruitment domain), and caspase-1. When activated, NLRP3 recruits the adaptor protein ASC and caspase-1 to form the inflammasome. Caspase-1 cleaves pro-inflammatory cytokines, such as interleukin-1β (IL-1β) and interleukin-18 (IL-18), into their active forms, which help recruit and activate immune cells to remove the stressor. Gasdermin D (GSDMD) is another inflammasome effector protein cleaved by caspase-1 downstream of inflammasome activation (Magnani et al.) The cleavage of GSDMD releases its N-terminal domain, which can form pores in the cell membrane, leading to a type of programmed cell death called pyroptosis.

Excessive or chronic activation of the N LRP3 inflammasome can contribute to various inflammatory diseases, including autoinflammatory diseases, such as cryopyrin-associated periodic syndrome (CAPS), autoimmune diseases, cancer, cardiovascular diseases, and neurological disorders (Alehashemi and Goldbach-Mansky) (2, 3). Understanding how NLRP3 inflammasome works and how its activation is regulated is important for developing new ways to prevent or treat inflammatory diseases.

This Research Topic brings together original articles related to the identification of new danger signals and pathways that activate the NLRP3 inflammasome. Moreover, some contributions highlight new mechanisms of inflammasome activation in human primary cells, like macrophages and neutrophils. Furthermore, some studies implicate chronic NLRP3 inflammasome activation in the pathogenesis of diseases, like chronic and acute pulmonary inflammation, spinal cord injury and liver fibrosis.

The NLRP3 inflammasome is known to sense a wide range of stimuli, including pathogen-associated molecular patterns (PAMPs) and danger-associated molecular patterns (DAMPs). PAMPs are molecular patterns associated with pathogens, such as bacteria, viruses, and fungi; on the other hand, DAMPs are molecules released from damaged or dying cells and tissues. These can include ATP, uric acid, or cholesterol crystals. Original articles in this Research Topic identify new endogenous activators and repressors of the NLRP3 inflammasome. The finding that the internalization of membrane

attack complex (MAC), a component of the complement system, drives NLRP3 inflammasome activation and IL-1β secretion is highlighted by Diaz-del-Olmo et al. Upon endocytosis, the colocalization of MAC with NLRP3-ASC proteins leads to the assembly of the NLRP3 inflammasome. Wisitpongpun et al. describe that oleamide, a natural oleic acid derivative, can induce NLRP3 inflammasome-mediated release of IL-1β, potentiating the polarization of primary human macrophages toward a pro-inflammatory M1 phenotype. Kienes et al. report a new mechanism of how NLRP11, a member of the Nod-like receptor family, inhibits the activation of the NLRP3 inflammasome. They identified the ATP-dependent RNA helicase DDX3X as a protein binding to NLRP11. Therefore, by sequestering DDX3X, NLRP11 negatively regulates NLRP3-mediated caspase-1 activation, thereby, limiting inflammasome activation.

The tight regulation of the NLRP3 inflammasome pathway is crucial for maintaining proper immune function and preventing excessive inflammation. The mechanisms of NLRP3 inflammasome activation may depend on the specific context and cell type. While priming is a well-established step for NLRP3 inflammasome activation in many cell types, including murine macrophages, Gritsenko et al. report that priming might be dispensable for NLRP3 inflammasome activation in human monocytes *in vitro*. When human monocytes are treated with nigericin, it induces K+ and Cl- efflux, which triggers the assembly of the NLRP3 inflammasome complex, leading to IL-1β and IL-18 release. Inflammasome activation is also peculiar in neutrophils in several ways. Inflammasome activation in neutrophils is often associated with NETosis, a specialized form of programmed cell death in which neutrophils release net-like structures called neutrophil extracellular traps (NETs). Münzer et al. show that, under sterile conditions, neutrophils can assemble and activate the NLRP3 inflammasome with the support of the enzyme PAD4 (peptidyl arginine deiminase 4), which is involved in chromatin decondensation and NET formation. In addition, Keitelman et al. reveal that serine proteases support caspase-1 in the processing and secretion of IL-1β in human neutrophils *via* the autophagic pathway. Son et al. present another key feature of inflammasome activation in neutrophils. When exposed to a milieu enriched in DAMPs, neutrophils are resistant to pyroptosis and mitochondrial depolarization in response to a NLRP3 inflammasome activator. In contrast, macrophages are desensitized *via* a mechanism leading to mitochondrial depolarization and pyroptosis. Based on these results, they propose that neutrophils are the primary source of IL-1β released in DAMP-rich inflammatory districts.

On this Research Topic, some articles emphasize the contribution of excessive and chronic inflammasome activation in the pathogenesis of various inflammatory diseases. Huot-Marchand et al. demonstrate that the NLRP3 inflammasome and GSDMD are key players in pulmonary inflammation and remodeling upon acute or sub-chronic mouse exposure to cigarette smoke. Li et al. report that a 4-benzene-indol derivative ameliorates LPS-induced sepsis-related acute lung injury by disrupting NLRP3-NEK7 interaction and the subsequent inflammasome assembly and activation. Wang et al. focus on the role of the inflammasome-induced IL-1 release in the development and progression of spinal cord injury. Inhibition of caspase-4 (involved in NLRP3 inflammasome activation) and IL-1-mediated pathway attenuate inflammation and promote repair of the injured spinal cord by inhibiting NF-kB signaling, NLRP3 inflammasome, and GSDMD-mediated pyroptosis. The potential role of inflammasomes and pyroptosis in relation to liver fibrosis is reviewed in Gan et al. They particularly focus on the effect of inflammasome activation in various liver cells (i.e., hepatocytes, cholangiocytes, hepatic stellate cells, hepatic macrophages, and liver sinusoidal endothelial cells) and how the pharmacological treatment of inflammasomes can be exploited as a potential strategy for attenuating liver fibrosis.

To summarize, this Research Topic, with a variety of articles, has provided important new insights into the activation mechanisms of the NLRP3 inflammasome and its link with a number of diseases and conditions.

Author contributions

The author confirms being the sole contributor of this work and has approved it for publication.

Funding

This work was supported by the Else Kröner Fresenius Prize for Medical Research 2020 and a grant from Fondazione Telethon (SR-Tiget Core Grant, Tele21-A5).

Conflict of interest

The author declares that the research was conducted in the absence of any commercial or financial relationships that could be construed as a potential conflict of interest.

Publisher's note

References

1. Blevins HM, Xu Y, Biby S, Zhang S. The NLRP3 inflammasome pathway: A review of mechanisms and inhibitors for the treatment of inflammatory diseases. *Front Aging Neurosci* (2022) 14:879021. doi: 10.3389/fnagi.2022.879021

2. Zheng Y, Xu L, Dong N, Li F. NLRP3 inflammasome: The rising star in cardiovascular diseases. *Front Cardiovasc Med* (2022) 9:927061. doi: 10.3389/fcvm.2022.927061

3. Song L, Pei L, Yao S, Wu Y, Shang Y. NLRP3 inflammasome in neurological diseases, from functions to therapies. *Front Cell Neurosci* (2017) 11:63. doi: 10.3389/fncel.2017.00063

frontiers in Immunology

ORIGINAL RESEARCH
published: 30 September 2020
doi: 10.3389/fimmu.2020.565924

Priming Is Dispensable for NLRP3 Inflammasome Activation in Human Monocytes *In Vitro*

*Anna Gritsenko[1], Shi Yu[2], Fatima Martin-Sanchez[1], Ines Diaz-del-Olmo[1], Eva-Maria Nichols[3], Daniel M. Davis[1], David Brough[2] and Gloria Lopez-Castejon[1]**

[1] Division of Infection, Immunity and Respiratory Medicine, Faculty of Biology, Medicine and Health, Lydia Becker Institute of Immunology and Inflammation, University of Manchester, Manchester Academic Health Science Centre, Manchester, United Kingdom, [2] Division of Neuroscience and Experimental Psychology, Faculty of Biology, Medicine and Health, Lydia Becker Institute of Immunology and Inflammation, University of Manchester, Manchester Academic Health Science Centre, Manchester, United Kingdom, [3] Adaptive Immunity Research Unit, GSK, Stevenage, United Kingdom

OPEN ACCESS

Edited by:
Alessandra Mortellaro, San Raffaele Telethon Institute for Gene Therapy (SR-Tiget), Italy

Reviewed by:
Deepika Sharma, University of Chicago, United States
Etienne Meunier, UMR5089 Institut de Pharmacologie et de Biologie Structurale (IPBS), France

***Correspondence:**
Gloria Lopez-Castejon
Gloria.lopez-castejon@manchester.ac.uk

Specialty section:
This article was submitted to Molecular Innate Immunity, a section of the journal Frontiers in Immunology

Received: *26 May 2020*
Accepted: *14 September 2020*
Published: *30 September 2020*

Citation:
Gritsenko A, Yu S, Martin-Sanchez F, Diaz-del-Olmo I, Nichols E-M, Davis DM, Brough D and Lopez-Castejon G (2020) Priming Is Dispensable for NLRP3 Inflammasome Activation in Human Monocytes In Vitro. Front. Immunol. 11:565924. doi: 10.3389/fimmu.2020.565924

Interleukin (IL)-18 and IL-1β are potent pro-inflammatory cytokines that contribute to inflammatory conditions such as rheumatoid arthritis and Alzheimer's disease. They are produced as inactive precursors that are activated by large macromolecular complexes called inflammasomes upon sensing damage or pathogenic signals. NLRP3 inflammasome activation is regarded to require a priming step that causes NLRP3 and IL-1β gene upregulation, and also NLRP3 post-translational licencing. A subsequent activation step leads to the assembly of the complex and the cleavage of pro-IL-18 and pro-IL-1β by caspase-1 into their mature forms, allowing their release. Here we show that human monocytes, but not monocyte derived macrophages, are able to form canonical NLRP3 inflammasomes in the absence of priming. NLRP3 activator nigericin caused the processing and release of constitutively expressed IL-18 in an unprimed setting. This was mediated by the canonical NLRP3 inflammasome that was dependent on K^+ and Cl^- efflux and led to ASC oligomerization, caspase-1 and Gasdermin-D (GSDMD) cleavage. IL-18 release was impaired by the NLRP3 inhibitor MCC950 and by the absence of NLRP3, but also by deficiency of GSDMD, suggesting that pyroptosis is the mechanism of release. This work highlights the readiness of the NLRP3 inflammasome to assemble in the absence of priming in human monocytes and hence contribute to the very early stages of the inflammatory response when IL-1β has not yet been produced. It is important to consider the unprimed setting when researching the mechanisms of NLRP3 activation, as to not overshadow the pathways that occur in the absence of priming stimuli, which might only enhance this response.

Keywords: macrophage, inflammasome, NLRP3, priming, monocytes, IL-18, GSDMD

INTRODUCTION

Inflammasomes are molecular complexes formed by immune cells such as macrophages and monocytes in response to tissue injury or infection (1). Inflammasomes are required to process proinflammatory cytokine precursors of the Interleukin (IL-1) family, such as pro-IL-1β and pro-IL-18, into their mature and secreted active forms (mIL-1β and mIL-18), thus initiating inflammation (2). NOD-like receptor pyrin domain-containing protein 3 (NLRP3) is the best studied inflammasome sensor, the activation of which can occur in sterile inflammation. Its dysregulation is suggested to play a role in the progression of non-communicable diseases such as rheumatoid arthritis, Alzheimer's disease, and cancer (3).

Classical or canonical NLRP3 inflammasome activation is considered to be a two-step process. The first or priming step is achieved through the activation of the nuclear factor kappa B (NF-κB) pathway, leading to the upregulation of NLRP3 and pro-IL-1β proteins (4) and to changes in NLRP3 post-translational modifications (PTMs) such as ubiquitination (5) and phosphorylation (6) that licence NLRP3 and promote inflammasome assembly. This step can be initiated by pathogen-associated molecular patterns (PAMPs) or damage-associated molecular patterns (DAMPs) binding toll like receptors (TLRs), or IL-1β and TNF-α binding to their respective receptors (7). The second or activating step leads to changes in NLRP3 conformation (8) and PTMs (9, 10) that allow NLRP3 oligomerization and consequently inflammasome activation. This step can be induced by a broad range of factors including PAMPs and DAMPs, e.g. nigericin toxin, extracellular ATP, as well as lysosomal destabilization agents such as silica and cholesterol crystals (1). Upon activation, oligomerized NLRP3 polymerizes the adaptor protein ASC, recruiting pro-caspase-1, which undergoes proximity-dependent auto-activation and as a result cleaves pro-IL-18 and pro-IL-1β into their mature forms. Simultaneously, mature caspase-1 induces the cleavage of gasdermin-D (GSDMD) (11) into N-terminal fragments that form lytic pores, facilitating the release of mature IL-1β and IL-18 as well as promoting pyroptotic cell death (12). GSDMD dependent lytic cell death also leads to the release of damage associated molecules such as high-mobility group box 1 (HMGB1), ATP, DNA and even inflammasome components themselves, e.g. ASC, which are able to propagate inflammation (13).

Although the current dogma is that the formation of an active NLRP3 inflammasome is a two-step process (14), this is not always the case. Human monocytes, in response to just the priming signal LPS, can induce the release of IL-1β in a NLRP3 dependent manner in a process that has been described as the alternative NLRP3 inflammasome (15). While pro-IL-1β is not expressed basally, pro-IL-18 is constitutively expressed in different cell types including macrophages, monocytes, dendritic cells, astrocytes and microglia (16). There are several reports that have described caspase-1 activation and IL-18 release in the absence of a priming step and just in response to the second or activating signal, especially in human cells (17–21). Despite this evidence, whether this process is dependent on the NLRP3 inflammasome has not been explored. Here, we report that primary human monocytes are equipped with a ready to assemble NLRP3 inflammasome that leads to the processing and release of constitutively expressed caspase-1 substrates such as IL-18 and GSDMD in response to just an activating signal in a sterile setting. This pathway is dependent on NLRP3, ion efflux and PTMs, which are hallmarks of the classical primed inflammasome activation. These results highlight the fact that priming might not be as necessary as initially thought for the assembly of an active inflammasome although it is required to potentiate the inflammasome response and generate IL-1β dependent inflammatory pathways.

EXPERIMENTAL PROCEDURES

LPS (*Escherichia coli* 026:B6); nigericin sodium salt (N7143); protease inhibitor cocktail (P8340); penicillin-streptomycin (Pen/Strep, P4333); MCC950 (PZ0280); Punicalagin (P0023), 5Z-7-Oxozeaenol (O9890), Ca-074-Me (C5857), SB220025 (S9070), and Z-VAD-FMK (V116-2MG) were obtained from Sigma. JSH-23 (CAY15036) was sourced from Cambridge Bioscience. Fetal bovine serum (FBS) was purchased from Gibco. 5-Nitro-2-(3-phenylpropylamino)benzoic acid (NPPB, 0593) was sourced from Calbiochem.

Primary antibodies for Western blot assays and their final concentrations were as follows: anti-human IL-18 (0.5 μg/ml, rabbit polyclonal, LifeSpan BioSciences, LS-C313397), anti-human IL-1β (0.1 μg/ml, goat polyclonal, R&D Systems, AF-201-NA), anti-human caspase-1 p20 (1:1000, mouse monoclonal, Cell Signalling Technology, 3866), anti-NLRP3 (1 μg/ml, mouse monoclonal, Adipogen, AG-20B-0014), anti-NLRP3 (1:1000, Sigma, HPA012878), anti-β-actin-HRP (0.2 μg/ml, mouse monoclonal, Sigma, A3854), anti-human UBE2L3 (0.2 μg/ml, mouse monoclonal, Santa Cruz, sc-390032), anti-human GSDMD (0.07 μg/ml, Novus Biologicals, NBP2-33422), anti-human IκBα (1:1000, Cell Signalling Technology, 4812). HRP conjugated secondary antibodies used for Western blotting were anti-rabbit-HRP (0.25 μg/ml, goat polyclonal, Dako, P0448), anti-mouse-HRP (1.3 μg/ml, rabbit polyclonal, Dako, P0260), and anti-goat-HRP (0.13 μg/ml, rabbit polyclonal, Sigma, A5420). We used the Adipogen (AG-20B-001) anti-NLRP3 antibody to detect NLRP3 in THP-1 cells and the anti-NLRP3 from Sigma (HPA012878) to detect NLRP3 from human blood monocytes by western blot.

Cell Culture and Treatments

THP-1 cells were cultured in complete media (RPMI-1640 supplemented with 2 mM L-glutamine, 10% FBS and Pen/Strep (100 U/ml)) and plated at a density of 1×10^6 cells/ml. Leukocyte cones were obtained from the National Blood Transfusion Service (Manchester, UK) with full ethical approval from the Research Governance, Ethics, and Integrity Committee at the University of Manchester (ref. 2018-2696-5711). Fresh blood was isolated from healthy volunteers following approval from Ethics Committee 05/Q0401/108 and 2017-2551-3945 (University of Manchester). In both cases, PBMCs were isolated from blood by density centrifugation

using a 30% Ficoll gradient. The PBMC layer was separated and washed with MACS buffer (PBS, 0.5% BSA, 2 mM EDTA) to remove platelets. Monocytes were positively selected from PBMCs from leukocyte cones with magnetic $CD14^+$ MicroBeads (Miltenyi, 130-050-201) for 15 min at 4°C and eluted using a LS column (Miltenyi, 130-042-401). To differentiate monocyte-derived macrophages (MDMs), monocytes were plated for 7 days (at a concentration of 5×10^5 cells/ml) in RPMI-1640 supplemented with 2 mM L-glutamine, 10% FBS, Pen/Strep (100 U/ml) and 0.5 ng/ml M-CSF (Peprotech, 300-25). On day 3, half of the media was removed and replaced with fresh media.

GSDMD knockout THP-1 cells were lentivirally generated using guide RNA oligonucleotide sequences 5'-CACCGACCAGCC TGCAGAGCTCCAC-3' and 5'-AAACGTGGAGCTCTGC AGGCTGGTC-3' (22) by utilizing the lentiCRISPR v2 plasmid system. lentiCRISPR v2 was a gift from Feng Zhang (Addgene plasmid #52961; http://n2t.net/addgene:52961; RRID: Addgene_52961). NLRP3 deficient THP-1 cells were a gift from Prof Veit Hornung (Ludwig Maximilian University of Munich).

When comparing primed and unprimed inflammasome responses, cells were seeded in the presence/absence of LPS (1 μg/ml) for 4 h in complete media. The priming stimulus was then removed and replaced with ET buffer (147 mM NaCl, 10 mM HEPES, 13 mM D-glucose, 2 mM KCl, 2 mM $CaCl_2$, and 1 mM $MgCl_2$). When priming experiments were not performed in parallel, cells were plated directly into ET buffer. Cells were then treated with nigericin toxin (10 μM, 45 min or 2 h as indicated) to activate the NLRP3 inflammasome.

Cell Death Assay

Cell death was measured using quantitative assay for the release of lactate dehydrogenase (LDH) into cell supernatants. The supernatant was gently centrifuged for 5 min at 500*g* at 4°C to remove any remaining cells. LDH release in cell supernatants were measured using CytoTox 96® Non-Radioactive Cytotoxicity Assay (G1780, Promega), according to the manufacturer's instructions. Absorbance values were recorded at 490 nm and the results were expressed as a percentage of LDH release normalized to total lysis.

Enzyme-Linked Immunosorbent Assay (ELISA)

Levels of human IL-1β (DY201) and IL-18 (DY318) were measured in the cell supernatants using ELISA kits from R&D Systems. Human IL-6 (# 88-7066-86) and TNF-α (# 88-7346-86) were detected using Invitrogen ELISA kits. ELISAs were performed following the manufacturer's instructions.

Western Blot

Cells were lysed on ice using a RIPA lysis buffer (50 mM Tris–HCl, pH 8, 150 mM NaCl, 1% NP-40, 0.5% sodium deoxycholate, and 0.1% sodium dodecyl sulphate [SDS]), supplemented with a protease inhibitors cocktail (Sigma-Aldrich, P8340, 1:100). Lysates were then clarified at 21,000*g* for 10 min in order to remove the insoluble fraction. Protein concentrations of each sample were measured using BCA assays (Thermo Scientific Pierce, 23225), following the manufacturer's guidelines, so an equal amount of protein was loaded for each sample. Cell supernatants were centrifuged at 500*g* for 5 min to remove dead cells and concentrated using 10 kDa MW cut-off filters (Amicon, Merck Millipore), as described by the manufacturer. Supernatants and whole-cell lysates were diluted in 1× reducing Laemmli buffer containing 1% β-mercaptoethanol. Samples were boiled at 95°C for 5 min and separated by Tris-glycine SDS-PAGE. Proteins were transferred onto nitrocellulose membranes (0.2 μm) and blocked in PBS-Tween (PBS-T, 0.1%) containing 5% skimmed milk for 1 h at room temperature. Membranes were then incubated overnight with the specific primary antibody in blocking buffer at 4°C. following day, membranes were labeled with a horseradish peroxidase-conjugated secondary antibody for 1 h at room temperature. Membranes were then washed, developed and captured digitally using Clarity™ Western ECL Blotting Substrate (Bio-Rad, 1705061) in a ChemiDoc™ MP Imager (Bio-Rad).

ASC Oligomerization Assay

After inflammasome stimulation, undifferentiated WT and NLRP3 KO THP-1 cells and monocytes were placed on ice. 1% (v/v) NP-40 and protease inhibitor cocktail were added directly to wells. Cell total lysates were separated into NP-40 soluble and insoluble fractions using differential centrifugation at 6,800*g* for 20 min at 4°C. The soluble fraction containing cell supernatant and lysates was utilized for western blotting analysis, whereas the NP-40 insoluble pellets were chemically crosslinked with 2 mM disuccinimidyl suberate (DSS) (Thermo Fisher) for 30 min at RT. Crosslinked pellets were further centrifuged at 6,800*g* for 20 min and resuspended in boiled 1× Laemmli buffer for standard SDS-PAGE.

Caspase-Glo® 1 Inflammasome Assay

Caspase-1 activity was measured in the supernatants using Caspase-Glo® 1 Inflammasome Assay (Promega). Briefly, cell supernatants were combined with Z-WEHD aminoluciferin substrate and illuminescence measured following 1 h incubation.

Cell Vitality Assay

Cells were stimulated as required, washed in 1× PBS, and resuspended at 1×10^6 cells/ml in PBS. Cells were then stained with LIVE/DEAD Cell Vitality Assay Kit (L34951) with C12-Resazurin and SYTOX ® Green Stain (Thermo Scientific) as per manufacturer's instructions. 100,000 cells per sample were acquired using a 3-laser Fortessa with BD FACSDiva software and analyzed with FlowJo software (version 10, TreeStar).

Statistical Analysis

GraphPad Prism 8 software was used to carry out all statistical analysis. Differences between 2 groups were analyzed using t-test. Differences between 3+ groups were analyzed using one-way ANOVA with the *post hoc* Dunnett's test or two-way ANOVA with the *post hoc* Tukey's test for multiple comparisons. Data was shown as mean +/- standard deviation (S.D.). Accepted levels of significance were $^*P < 0.05$, $^{**}P < 0.01$, $^{***}P < 0.001$, $^{****}P < 0.0001$.

RESULTS

Priming Is Not Required for NLRP3 Inflammasome Activation in Human Monocytes *In Vitro*

To determine if NLRP3 inflammasome activation occurs in human monocytes in the absence of priming, we first compared the release of mIL-18 and mIL-1β, as pro-IL-18 gene expression is constitutive, while pro-IL-1β requires upregulation by priming (23). Undifferentiated THP-1 cells were primed with LPS (1 μg/ml) for 4 h, or left unprimed, followed by treatment with the NLRP3 activator nigericin (10 μM, 45 min). Nigericin induced mIL-18 release and cell death in both primed and unprimed cells to the same extent, while it only induced mIL-1β release in LPS primed THP-1 cells (**Figures 1A, B**). In line with this, caspase-1 cleavage into its active form (p20) was also detected in both primed and unprimed cells, as well as IL-18 processing and release (**Figure 1B**). Nigericin treatment, with or without priming, led to GSDMD cleavage, detected by the appearance of a GSDMD fragment of 31 kDa, corresponding to the pore-forming N-terminus (GSDMD NT) (**Figure 1B**). GSDMD cleavage is a consequence of caspase-1 activation and is required for pyroptosis (11). However, we could not detect statistically significant elevated levels of cell death following nigericin treatment by measuring LDH release (**Figure 1A**) or by uptake of the SYTOX Green nuclear dye (**Figure S1**). Caspase-1 activation leads to the direct or

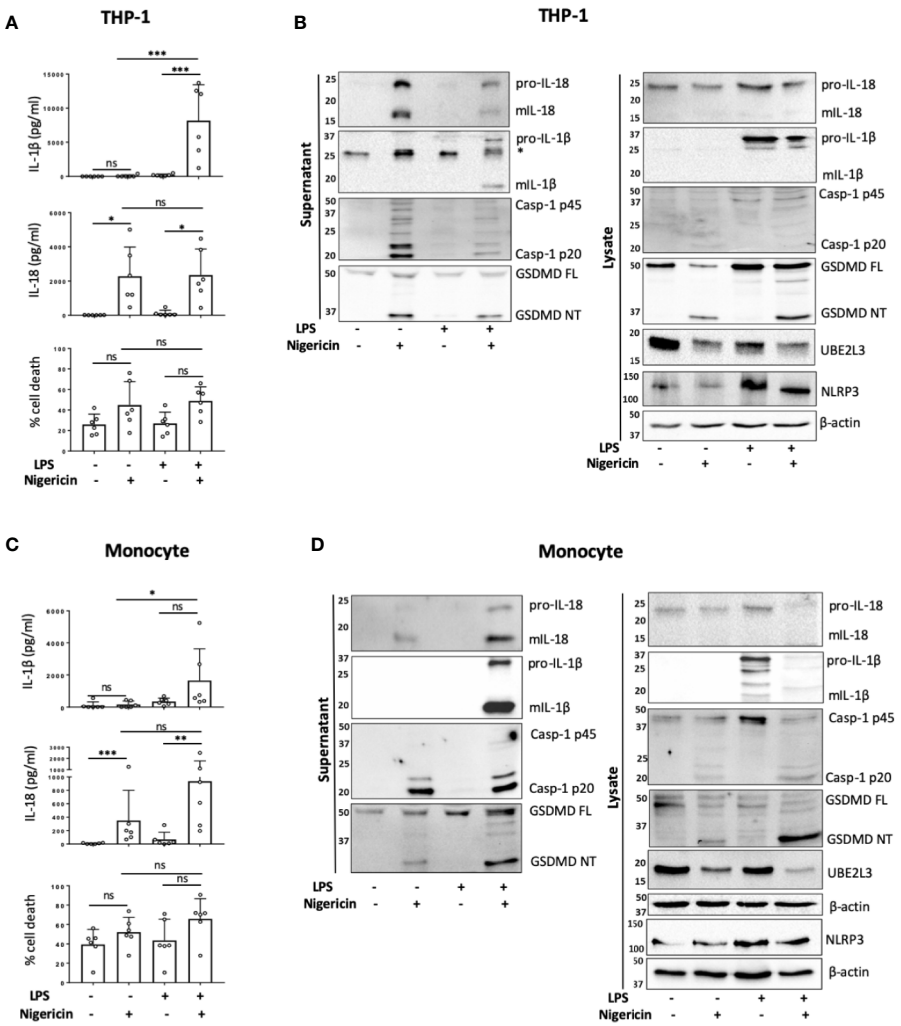

FIGURE 1 | Priming is not required for NLRP3 inflammasome activation in human monocytes *in vitro*. **(A, B)** Undifferentiated THP-1 cells (n=6 independent biological replicates) and **(C, D)** primary CD14$^+$ monocytes (n=6 independent biological replicates (each point represents a different blood donor)) were left untreated or primed with LPS (1 μg/ml, 4 h) prior to treatment with nigericin (10 μM, 45 min) to activate the NLRP3 inflammasome. **(A, C)** IL-1β and IL-18 were measured by ELISA and cell death was measured by LDH assay and shown as percentage relative to total cell death, mean ± S.D., *P < 0.05; **P < 0.01; ***P < 0.001; ns (non significant) using one-way ANOVA comparing all groups. **(B, D)** Western blot analysis for mIL-18 (18 kDa), pro-IL-18 (24 kDa), mIL-1β (17 kDa), pro-IL-1β (34 kDa), mCaspase-1 (20 kDa), pro-Caspase-1 (45 kDa), GSDMD full length (FL, 53 kDa), GSDMD N-terminus (NT, 31 kDa), UBE2L3 (17.9 kDa), NLRP3 (113 kDa), as well as loading control β-actin (42 kDa). Blots are representative of at least 3 independent biological experiments and in case of monocytes 3 different blood donors.

indirect processing of substrates other than IL-1β, IL-18, and GSDMD (24–26). For example, caspase-1 can mediate the degradation of the E2 ubiquitin-conjugating enzyme UBE2L3 involved in NF-κB activation and pro-IL-1β turnover (27). To assess if active caspase-1 in unprimed cells can be involved in other cellular processes, we investigated whether the second signal alone was sufficient to induce degradation of UBE2L3. Nigericin treatment alone was enough to reduce UBE2L3 levels, suggesting that caspase-1 is active and able to cleave substrates other than IL-1β and IL-18 (**Figure 1B**). The NLRP3 protein was detected in THP-1 cells without any treatment, and was upregulated following exposure to LPS (**Figure 1B**). Despite this, caspase-1 and GSDMD cleavage, UBE2L3 degradation and mIL-18 release were not potentiated by LPS stimulation in THP-1 cells suggesting that changes in NLRP3 expression are not solely responsible for intensity of inflammasome activation. Overall, this highlights that inflammasome activation without prior priming can lead to the cleavage of a number of constitutively expressed caspase-1 substrates.

Next we tested whether unprimed inflammasome activation occurred in freshly isolated primary human $CD14^+$ monocytes from healthy donors. We observed that the treatment of $CD14^+$ human monocytes with nigericin alone was sufficient to trigger significant mIL-18 secretion (**Figures 1C, D**). Western blot analysis revealed that, like THP-1 cells, unprimed monocytes responded to nigericin treatment with caspase-1 activation, GSDMD cleavage, UBE2L3 degradation and the release of IL-18, but not IL-1β (**Figures 1C, D**). We observed that priming human monocytes with LPS, unlike THP-1 cells, potentiated nigericin-induced secretion of mIL-18 and cell death, although this was not significantly different to the unprimed response (**Figure 1C**). We also observed a slight increase in NLRP3 levels after LPS priming, as was also the case in THP-1 cells (**Figure 1D**).

To exclude the possibility of a priming effect by engagement of CD14 receptor during monocyte purification, we also analyzed IL-18 release and cell death in response to nigericin in the CD14 negative peripheral blood mononuclear cell (PBMC) fraction in the absence of LPS priming. Similarly to $CD14^+$ monocytes, we also found mIL-18 release in response to nigericin, although at much lower levels likely due to the lower number of inflammasome forming cells in this fraction (**Figure S2A**). As most experiments were carried out on cells isolated from leukocyte cones, we wanted to ensure that packaging and storing blood in these cones did not prime the cells. We therefore tested freshly isolated PBMCs from healthy volunteers. When stimulated with nigericin, these PBMCs showed unprimed IL-18 release (**Figure S2B**). This suggests that inflammasome activation occurs in recently isolated, not previously packaged cells that also have not undergone $CD14^+$ magnetic separation. Small levels of IL-1β release were detected in unprimed PBMCs, which could be explained by higher pro-IL-1β expression in human PBMCs compared to monocytes and macrophages (28).

To determine whether unprimed NLRP3 inflammasome assembly is unique to monocytes, we also carried out parallel experiments in human monocyte derived macrophages (MDMs). We observed non-significant mIL-18 release from MDMs in the absence of priming (**Figure S3A**). The levels of secreted mIL-18 released by LPS primed cells activated with nigericin were significantly higher than in unprimed MDMs. Unlike in primary monocytes, the cleavage of caspase-1 by inflammasome activation without LPS stimulation was also much lower than in LPS primed cells (**Figures S3B, C**). The cleavage of GSDMD and maturation of IL-18 occurred without priming at lower levels than in LPS primed cells (**Figure S3B**). UBE2L3 did not appear to be degraded without LPS priming. Therefore, although there is a small response to inflammasome activation in human macrophages, unlike monocytes, priming is required for a full response.

TAK1 and NF-κB Differentially Contribute to Unprimed Inflammasome Activation

TAK1 (transforming growth factor beta-activated kinase 1) is an upstream regulator of the crucial intracellular kinases: I-kappa B kinase complex (IKK), p38, and JNK that mediate activation of the transcription factors NF-κB and AP-1, thus contributing to the priming step of NLRP3 inflammasome formation (4, 29). TAK1 is also activated in response to inflammasome activating signals such as the lysosomotropic agent Leu-Leu-O-methyl ester (LLMe) (30) or hypotonic stress-induced cell volume change (31) and mediates TLR induced non-transcriptional activation of the NLRP3 inflammasome (32). However, whether TAK1 controls NLRP3 inflammasome activation in the absence of TLR4 sensitization has not been explored. To test whether TAK1 was involved in unprimed NLRP3 activation, we pre-treated human monocytes with an inhibitor of TAK1 catalytic activity: 5z-7-oxozeaenol (5z-7) (0.5 μM) for 15 min prior to nigericin stimulation. We found that TAK1 inhibition significantly impaired mIL-18 release in primary human monocytes (**Figures 2A, B**) as well as reduced the cleavage of caspase-1 into its mature form (p20) (**Figure 2B**). However, TAK1 inhibition did not alter unprimed inflammasome activation in THP-1 cells (**Figure S4A**).

To assess if TAK1 contributed to unprimed inflammasome activation through NF-κB or p38 pathways, we treated human monocytes with either the NF-κB nuclear translocation inhibitor JSH-23 (33) (40 μM, 13 h) or p38 inhibitor SB220025 (34) (20 μM, 30 min) followed by nigericin or vehicle treatment (10 μM, 45 min). We found that in human monocytes, JSH-23 treatment did not significantly affect IL-18 release, cell death or caspase-1 activity (**Figure 2C**) in response to nigericin. However, JSH-23 treatment in THP-1 cells led to a reduction in IL-18 release, cell death and caspase-1 activation (**Figure S4B**). As expected, LPS treatment (1 μg/ml, 4 h) induced the release of IL-6 and TNF-α in primary monocytes and TNF-α in THP-1 cells. Minimal levels of IL-6 and TNF-α were found in the supernatants of untreated cells, suggesting that the isolated monocytes and THP-1 cells are unprimed without LPS treatment (**Figure 2D**, **Figure S4C**). Pre-treatment with JSH-23 reduced LPS induced IL-6 and TNF-α release in both cell types although this was not statistically significant in human monocytes given the high variability among monocytes from different donors (**Figure 2D**, **Figure**

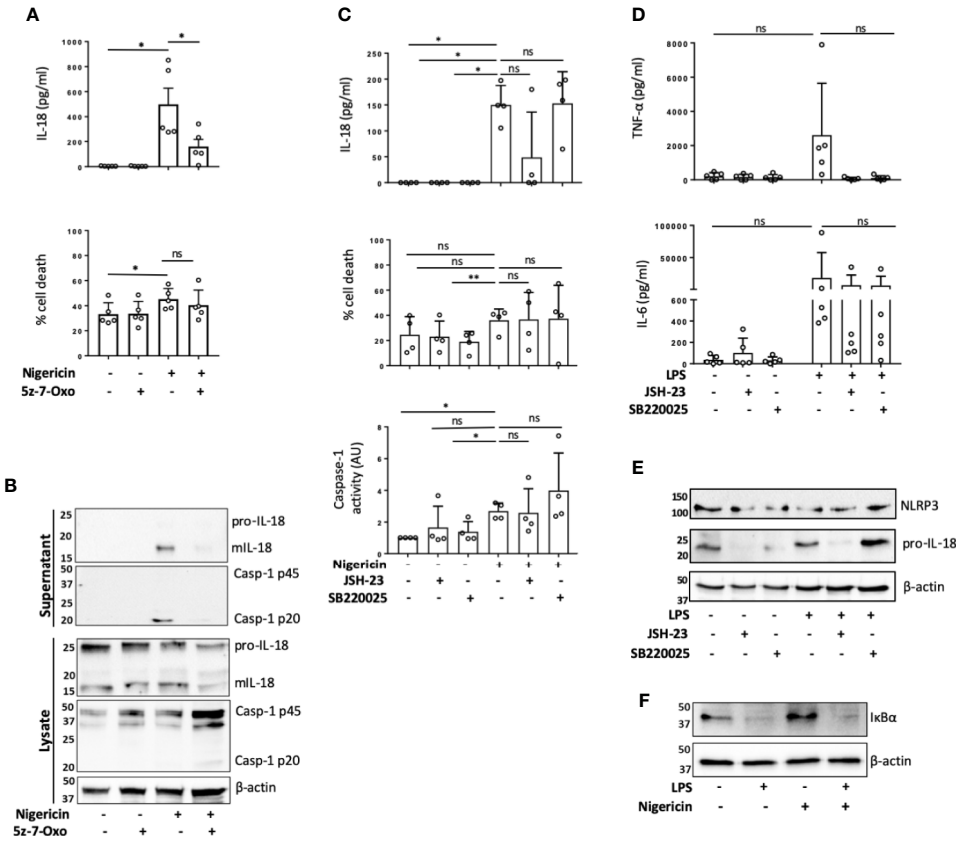

FIGURE 2 | TAK1 and NF-κB differentially contribute to unprimed inflammasome activation in human monocytes. **(A, B)** Primary human monocytes were pre-incubated with 5z-7-Oxozeaenol (0.5 μM) for 15 min prior to treatment with nigericin (10 μM, 45 min). **(A)** Secreted IL-18 was measured by ELISA and cell death was measured by LDH assay and shown as percentage relative to total cell death. n=5 independent biological replicates (each point represents a different blood donor). Error bars represent mean ± S.D., *P < 0.05 using one-way ANOVA comparing each sample to the nigericin only treated sample. **(B)** Supernatants and lysates were analyzed for mIL-18 (18 kDa), pro-IL-18 (24 kDa), mCaspase-1 (20 kDa), pro-Caspase-1 (45 kDa), as well as loading control β-actin (42 kDa). Blots are representative of at least 3 independent experiments. **(C)** Primary human monocytes were left untreated or pre-treated with JSH-23 (40 μM, 13 h) or SB220025 (20 μM, 30 min) followed by treatment with nigericin (10 μM, 45 min). Cell supernatants were assayed for the release of IL-18, cell death by LDH release and caspase-1 activity by caspase-1-Glo assay. n=4 independent biological replicates (each point represents a different blood donor). Error bars represent mean ± S.D., * = P < 0.05; ** = P < 0.01; ns (not significant) using one-way ANOVA comparing each sample to the nigericin only treated sample. **(D, E)** Primary human monocytes were left untreated or pre-treated with JSH-23 (40 μM, 13 h) or SB220025 (20 μM, 30 min) following treatment with LPS (1 μg/ml, 4 h) or left untreated. **(D)** Cell supernatants were assayed for TNF-α and IL-6 release. n=5 independent biological replicates (each point represents a different blood donor). Error bars represent mean ± S.D., *P < 0.05 using one-way ANOVA comparing each sample to the LPS only treated sample. **(E)** Lysates were analyzed for proIL-18 (24 kDa) and NLRP3 (113 kDa) as well as loading control β-actin (42 kDa). **(F)** Western blot analysis of human monocyte lysates for IκBα (39 kDa) and loading control β-actin (42 kDa) from cells left untreated or treated with nigericin (10 μM, 45 min). All blots are representative of 2 independent biological experiments (each from a different blood donor).

S4C). When we normalized the data to the maximum IL-6 or TNF-α release induced by LPS alone in each donor, we observed that the levels of IL-6 were reduced to 67.4% ±; 21.4% (mean ±; S.D.; p=0.02) and the levels of TNF-α release reduced to 4.7% ±; 4.3% (mean ±; S.D.; p=0.054) (Friedman test, *post hoc* Dunn's test), indicating a clear effect of JSH-23 in these cells. JSH-23 did not affect NLRP3 levels in either human monocytes nor THP-1 cells. However, while JSH-23 reduced pro-IL-18 levels in human monocytes (**Figure 2E**), it did not alter proIL-18 levels in THP-1 cells (**Figure S2D**). This could explain why we observed reduced levels of nigericin-induced IL-18 release in several donors compared to untreated cells. To exclude the possibility that nigericin itself was activating NF-κB, we assessed the degradation of IκBα in the presence or absence of nigericin or LPS. While LPS treatment reduced IκBα levels, nigericin stimulation resulted in no changes in IκBα levels in either human monocytes or THP-1 cells (**Figure 2F**, **Figure S4E**). Inhibition of p38 with SB220025 did not affect IL-18 release in response to nigericin in human monocytes or THP-1 cells despite impairing IL-6 and TNF-α release induced by LPS (1 μg/ml, 4 h) treatment (**Figures 2C, D**; **Figures S4B, C**). In this case, when we normalized the data to the maximum IL-6 or TNF-α release level induced by LPS alone in each donor, we observed that SB220025 reduced IL-6 levels to 65.2% ±; 21.4%

(mean ±; S.D.; p=0.054) and TNF-α release to 3% ±; 2.5% (mean ±; S.D.; p=0.02) (Friedman test, *post hoc* Dunn's test), validating that the inhibitor works on human monocytes. These results suggests that TAK1 and NF-κB might be active at basal levels in human monocytes and THP-1s and differentially contribute to the unprimed inflammasome response, while MAPK p38 activity may not be necessary.

mIL-18 Release in the Absence of Priming Is NLRP3-Dependent

Unprimed release of mIL-18 in response to nigericin has initially been described, prior to discovery of the NLRP3 inflammasome, as a necrosis dependent pathway mediated by cathepsin B and lysosomal disruption but independent of caspase-1 activity (17). As cathepsin B and lysosomal destabilization have been closely linked to inflammasome activation, we first tested the effect of cathepsin B inhibitor Ca-074-Me on unprimed IL-18 release in THP-1 cells. However, we did not observe any inhibition of nigericin induced mIL-18 release in the presence of cathepsin B inhibitor (**Figure S5**). Upon treating THP-1 cells (**Figures 3A, B**) or primary monocytes (**Figures 3C, D**) with NLRP3 inhibitor MCC950 (1 μM, 15 min) prior to the addition of nigericin (10 μM, 45 min), we found that MCC950 inhibited nigericin-induced mIL-18 release, caspase-1 cleavage into its active form, and cell death in both cell types. Similar effects were observed when either human monocytes or THP-1 cells were pre-treated with an irreversible pan-caspase inhibitor Z-VAD-FMK (ZVAD, 50 μM, 15 min) (**Figures 3A–D**). To further confirm the involvement of NLRP3 in this process, we utilized NLRP3 knock out (KO) THP-1 cells and revealed that IL-18 processing and release, caspase-1 activation and cell death following unprimed inflammasome activation did not occur in NLRP3 deficient cells compared to WT (**Figures 3E, F**).

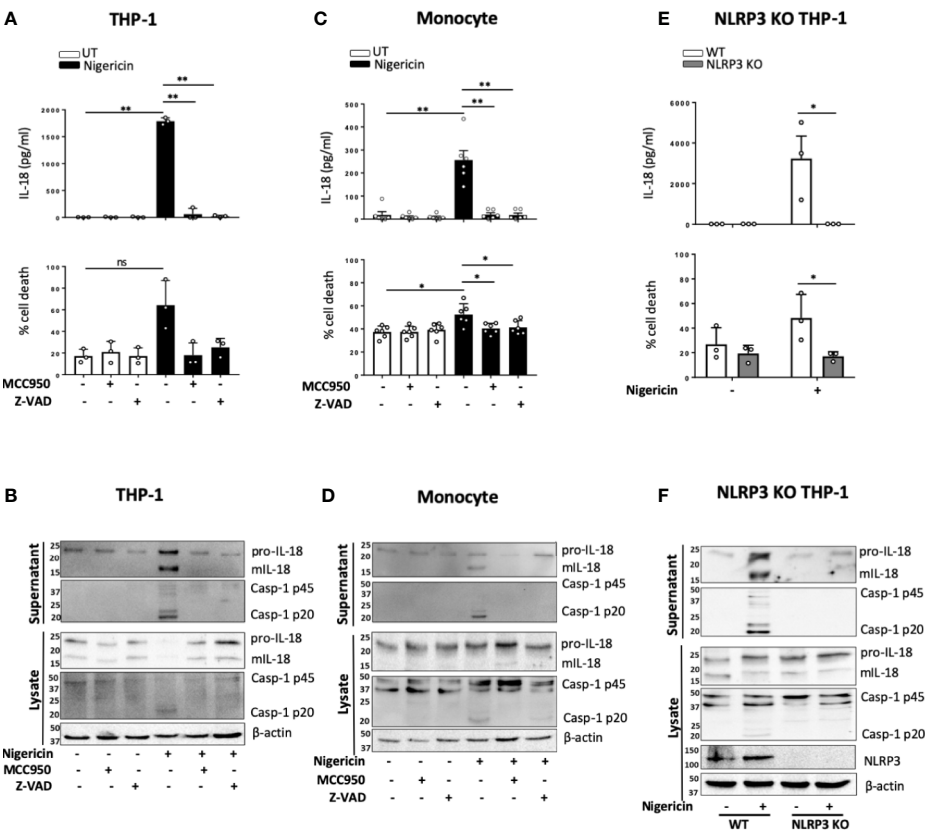

FIGURE 3 | mIL-18 release in the absence of priming is NLRP3 dependent. THP-1 cells **(A, B)** and monocytes **(C, D)** were pre-incubated with MCC950 (1 μM) or Z-VAD (50 μM) for 15 min prior to treatment with nigericin (10 μM, 45 min). **(A, C)** Secreted IL-18 was measured by ELISA and cell death was measured by LDH assay and shown as percentage relative to total cell death, n=3 independent biological replicates for THP-1 and n=6 independent blood donors for human monocytes, mean ± S.D., *P < 0.05; **P < 0.01; ns (not significant) using one-way ANOVA comparing each sample to the nigericin only treated sample. **(E, F)** Unprimed WT or NLRP3 KO THP-1 were treated with nigericin (10 μM, 45 min). **(E)** Secreted IL-18 was measured by ELISA and cell death was measured by LDH assay and shown as percentage relative to total cell death, n=3 independent biological replicates, mean ± S.D., * = P < 0.05; ns (not significant) using two-way ANOVA comparing nigericin treated WT and NLRP3 KO THP-1s. **(B, D, F)** Western blot analysis for mIL-18 (18 kDa), pro-IL-18 (24 kDa), mCaspase-1 (20 kDa), pro-Caspase-1 (45 kDa), and in some cases NLRP3 (113 kDa), as well as loading control β-actin (42 kDa). Blots are representative of at least 3 independent biological experiments and blood donors.

Unprimed NLRP3 Inflammasome Activation Has the Same Requirements as the Canonical Inflammasome

NLRP3 inflammasome activation in monocytes can occur through different pathways (35). In primed monocytes, nigericin is a trigger of canonical NLRP3 inflammasome activation, which is characterized by the oligomerization of ASC (36). We therefore tested whether ASC oligomerization also occurred in unprimed monocytes. We found that nigericin treatment (10 μM, 2 h) of unprimed THP-1 cells resulted in ASC oligomerization that was detected in the crosslinked NP-40 insoluble fraction of the total lysate, and that this was absent in NLRP3 KO cells (**Figure 4A**). Similarly, unprimed primary human monocytes formed ASC oligomers following stimulation with nigericin and this did not occur in monocytes pre-treated with the NLRP3 inhibitor MCC950 (10 μM, 15 min) (**Figure 4B**).

As well as ASC oligomerization, the classical primed canonical NLRP3 inflammasome activation in response to nigericin is dependent on potassium (K^+) (37) and chloride (Cl^-) (38) efflux. This is unlike the alternative NLRP3 inflammasome that occurs in human monocytes and assembles following prolonged priming signals in a K^+ (15) and Cl^- independent manner (38). We tested the requirement of K^+ and Cl^- efflux during unprimed inflammasome activation in response to nigericin. We incubated unprimed THP-1 cells either in high K^+ containing media or pre-treated these cells with

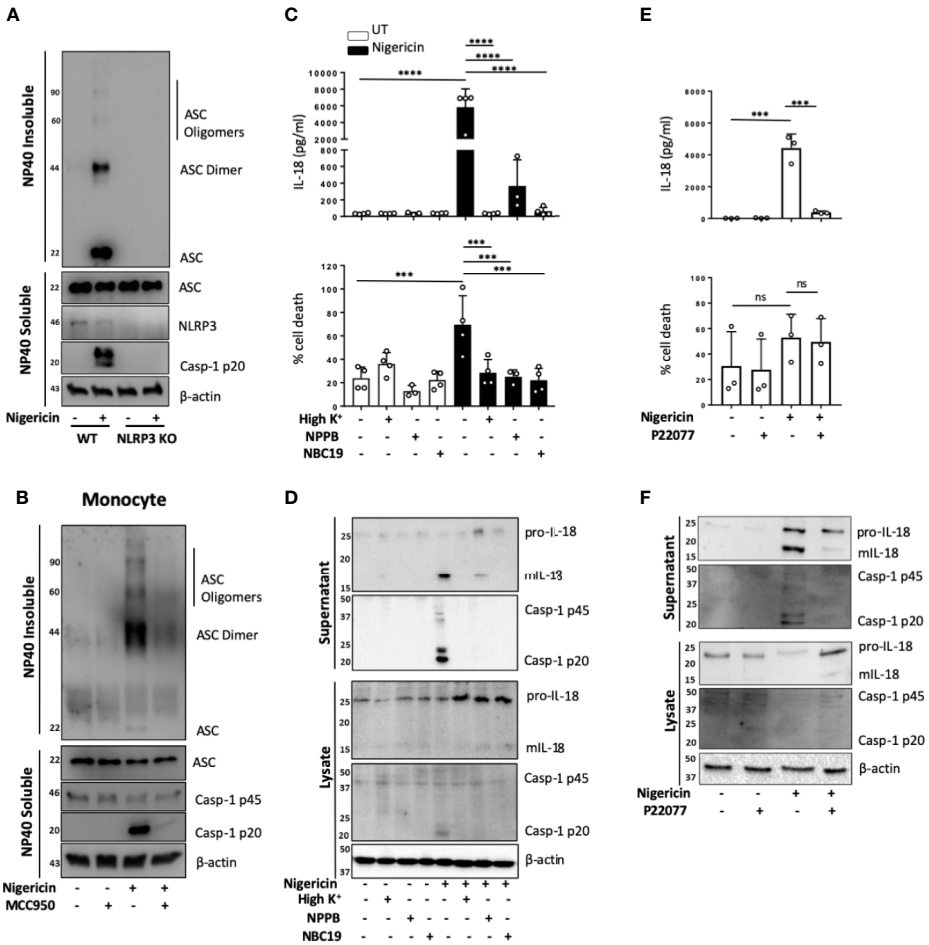

FIGURE 4 | Unprimed NLRP3 inflammasome activation has the same requirements as the canonical inflammasome. **(A)** WT and NLRP3 KO THP-1 cells were left unprimed prior to treatment with nigericin (10 μM, 2 h) to activate NLRP3 inflammasome. **(B)** Primary human monocytes were pre-incubated with MCC950 (1 μM) for 15 min prior to treatment with nigericin (10 μM, 45 min). The NP-40 soluble fraction and DSS crosslinked insoluble fraction were immunoblotted for ASC monomers, dimers and oligomers. Blots are representative of 3 independent biological experiments and blood donors. **(C, D)** THP-1 cells were left unprimed and pre-incubated with high K^+ buffer, NPPB (50 μM) or NBC19 (25 μM) for 15 min prior to treatment with nigericin (10 μM, 45 min). **(E, F)** THP-1 cells were left unprimed pre-incubated with P22077 (2.5 μM, 15 min) prior to treatment with nigericin (10 μM, 45 min). n=3 independent biological replicates, mean ±; S.D., ***$P < 0.001$; ****$P < 0.0001$; ns (not significant) using one-way ANOVA comparing each sample to nigericin only treated sample. **(D, F)** Supernatants and lysates were analyzed for mIL-18 (18 kDa), pro-IL-18 (24 kDa), mCaspase-1 (20 kDa), pro-Caspase-1 (45 kDa), as well as loading control β-actin (42 kDa). Blots are representative of at least 3 independent experiments and in the case of primary monocytes, blood donors.

broad-spectrum chloride channel inhibitor NPPB (50 μM), or NBC19: a recently described NLRP3 inhibitor (25 μM) (39), as a positive control, for 15 min prior to nigericin treatment (**Figures 4C, D**). This revealed that unprimed mIL-18 release, caspase-1 cleavage and cell death following nigericin stimulation were dependent on K^+ efflux and were also sensitive to Cl^- channel inhibitor NPPB (**Figures 4C, D**), as they were reduced to the same extent as in the presence of inflammasome inhibitor NBC19.

Deubiquitination of NLRP3 by the priming and activating step has been described as necessary for the formation of an active NLRP3 inflammasome (5). We have recently shown that deubiquitinases USP7 and USP47 mediate canonical NLRP3 inflammasome activation in human macrophages independently of transcriptional priming (9). Hence we hypothesized that DUBs might also mediate inflammasome activation in an unprimed context. To test this, we investigated the effect of the dual USP7/USP47 inhibitor P22077 (9) on inflammasome activation without priming. We found that pre-incubation of THP-1 cells with P22077 (2.5 μM, 15 min) prior to nigericin treatment significantly reduced IL-18 release (**Figure 4E**). This was accompanied by a reduction in caspase-1 maturation (**Figure 4F**), although no significant reduction in cell death was observed. Similar results were found in primary human monocytes (**Figure S6**). These data show that USP7 and USP47 can control inflammasome activation independently of the priming step.

mIL-18 Release From Unprimed Monocytes Is Dependent on GSDMD

NLRP3 inflammasome mediated IL-1 release, membrane permeabilization and pyroptotic cell death are closely associated, and these events are tightly linked to GSDMD cleavage and pore formation. However, certain NLRP3 activators such as changes in cell volume can induce mIL-1β and mIL-18 release in the absence of pyroptosis. As we observed that levels of cell death triggered by nigericin in unprimed cells were lower and more variable than those expected from murine cells, we set out to determine whether inflammasome-induced membrane permeabilization in unprimed monocytes was involved in the release of mIL-18. We first tested the effect of the polyphenolic compound punicalagin, known to inhibit plasma membrane permeability, as well as mIL-1β and mIL-18 release induced by inflammasome activation, while allowing caspase-1 activity (40, 41). In unprimed THP-1 cells, 15 min pre-treatment with 50 μM punicalagin prior to nigericin significantly blocked IL-18 release (**Figure 5A**). Western blot analysis revealed that punicalagin treated cells still displayed caspase-1 activation, indicating inflammasome activation, but the release of mature caspase-1 (p20) was blocked (**Figure 5B**). Similarly, pro-IL-18 was cleaved into its mature form but its release was inhibited by punicalagin.

The effect of punicalagin on inflammasome activation resembles that of GSDMD KO (40–42). Similar to pro-IL-18, GSDMD is constitutively expressed in unprimed THP-1 and human monocytes. As the GSDMD pore has been proposed as a mediator of mIL-1β release (42) and we observed GSDMD cleavage in unprimed monocytes, we investigated if GSDMD was required for mIL-18 release. IL-18 release caused by nigericin was significantly lower in cells lacking GSDMD compared to WT control (**Figure 5C**). Like with punicalagin treatment, GSDMD deficient cells where still able to activate caspase-1 and process pro-IL-18 into its mature form (**Figure 5D**) but its released was impaired. Overall, these data suggest that caspase-1 cleavage of GSDMD and subsequent pyroptosis may be a key mechanism for the release of inflammasome regulated cytokines following inflammasome assembly in the absence of priming.

DISCUSSION

Our work shows that human monocytes are able to assemble a functional NLRP3 inflammasome in response to an activating signal even in the absence of a priming step. The priming step has long been regarded as an essential stage for the assembly of an active NLRP3 inflammasome. Initially, it was believed that priming was only required to upregulate NLRP3 and pro-IL-1β proteins in response to the activation of NF-κB signaling (4). In recent years, however, a role for priming independent of transcriptional regulation has been uncovered and is believed to be mediated by PTMs such as changes in the ubiquitination or phosphorylation of NLRP3 (5, 43). Our data shows that an initial priming step is not required for the formation of an active NLRP3 canonical inflammasome but might be required to enhance inflammasome activation and the inflammatory response, depending on the cell type.

Evidence linking the ability of human monocytes to activate caspase-1 and induce the release of mIL-18 in the absence of priming was first described by Perregaux et al. (18) and Mehta et al. (20). The first group reported that ATP treatment of human blood in the absence of LPS priming leads to IL-18 release, while Mehta et al. showed that ATP treated human PBMCs activate caspase-1 in the absence of LPS priming but do not release IL-18 (20). It was later shown, in THP-1 cells and human monocytes, that lysosomal rupture induced by nigericin contributes to caspase-1 activation and IL-18 release in what was thought to be necrosis (17). In this report, IL-18 release was impaired with a cathepsin B inhibitor but not by caspase-1 inhibition. Here, we have further characterized the release of IL-18 in unprimed human monocytes and THP-1 cells and showed that it is dependent on the activation of the canonical NLRP3 inflammasome as it is a process blocked by preventing K^+ efflux and by Cl^- channel inhibition. This results in the formation of ASC oligomers, caspase-1 activation and GDSMD cleavage and pyroptosis. Although we cannot completely rule out an unknown priming effect of monocytes *in vivo*, our data on THP-1 cells, human PBMCs, $CD14^+$ monocytes and human $CD14^-$ PBMC fraction, as well as previous reports using human blood, purified PBMCs (17, 18) and human derived DCs (19), all show the dispensability of priming for inflammasome activation *in vitro*. Moreover, primary human monocytes that were seeded

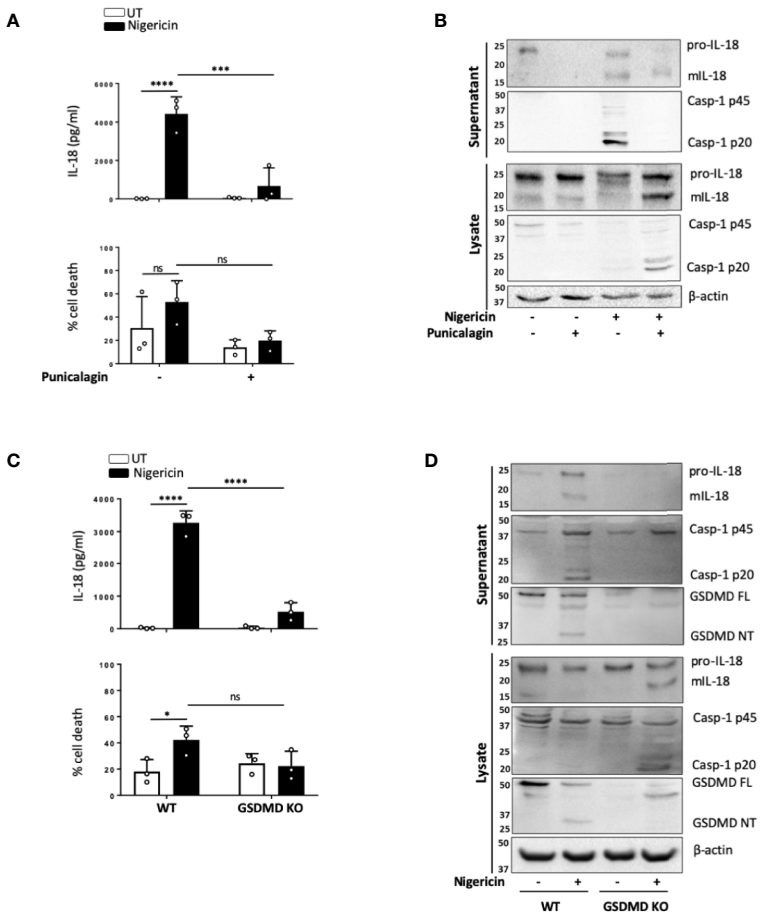

FIGURE 5 | mIL-18 release from unprimed monocytes is dependent on GSDMD. **(A, B)** Unprimed THP-1 cells pre-incubated with punicalagin (50 μM, 15 min) prior to treatment with nigericin (10 μM, 45 min). **(C, D)** Unprimed WT and GSDMD KO THP-1s were treated with nigericin (10 μM, 45 min). **(A, C)** Secreted IL-18 was measured by ELISA and cell death was measured by LDH assay and shown as percentage relative to total cell death, n=3 independent biological replicates, mean ± S.D., *P < 0.05; ***P <0.001; ****P <0.0001; ns (not significant) using one-way ANOVA comparing each sample to nigericin only treated sample **(A)** or two-way ANOVA comparing UT to nigericin treated WT THP-1s as well as nigericin treated WT THP-1s to nigericin treated GSDMD KO THP-1s. **(C)**. **(B, D)** Western blot analysis of THP-1 cells for mIL-18 (18 kDa), pro-IL-18 (24 kDa), mCaspase-1 (20 kDa), pro-Caspase-1 (45 kDa), GSDMD full length (FL, 53 kDa), GSDMD N-terminus (NT, 31 kDa), as well as loading control β-actin (42 kDa). Blots are representative of at least 3 independent experiments.

and stimulated directly in serum free buffer behaved the same as those cultured in complete media, ruling out any priming effect of serum (**Figures 1C, D** vs **Figures 3C, D**). Together, this evidence suggests that unprimed inflammasome assembly is not an effect of sample preparation or cell culture conditions.

It has been previously evidenced that certain mouse cells are activated by signal 2 alone. For example, unprimed primary murine peritoneal macrophages from both LPS-sensitive FVBN mice and from LPS-unresponsive C3H/HeJ mice secrete significant levels of IL-18 in response to nigericin treatment, also suggesting inflammasome activation (17). Unprimed monocytes from C57BL/6 mice have been shown to respond to nigericin with elevated LDH release, suggesting possible inflammasome activation and pyroptosis but whether this leads to inflammasome activation has not been directly tested (15). On the contrary, mouse BMDMs appear to require a priming signal for NLRP3 inflammasome assembly, as demonstrated in a number of studies (6, 44). Taken together, this evidence suggests that both human and murine monocytes are capable of TLR independent NLRP3 activation, whereas human MDMs and murine BMDMs, but not murine peritoneal macrophages, do not have this ability. Whether this is a product of culturing cells *ex vivo* for prolonged periods of time or due to differences between cell types remains to be explored.

A feature of the canonical NLRP3 inflammasome is its regulation by kinases such as TAK1, JNK (c-Jun N-terminal kinase) and protein kinase D (PKD) (6, 45, 46) and phosphatases such as protein phosphatase 2A (PP2A), protein tyrosine phosphatase non-receptor type 22 (PTPN22) (47) and PTEN (48). Whether these enzymes contribute to the NLRP3 priming, licencing, or activating step is not clear. TAK1 kinase is described to regulate the canonical NLRP3 inflammasome at the priming

level by either mediating transcriptional priming through its role in NF-κB signaling downstream of TLR4 (29) or *via* non transcriptional priming (32). TAK1 activation is also induced by NLRP3 activating signals such as hypotonicity, ATP or lysosomotropic agents (30, 31, 49) in macrophages that have been previously engaged with TLR activators. Lysomal destabilization has been previously linked to an unprimed inflammasome response and is an established activator of TAK1, downstream of which JNK regulates the NLRP3 inflammasome through the oligomerization of ASC (49). Whether TAK1 plays a role in inflammasome activation in a setting where TLR4 is not engaged has not been explored. We found that TAK1 inhibition significantly reduced inflammasome activation in unprimed human monocytes but not in THP-1 cells. TAK1 activation can be induced by only osmotic stress in mouse embryonic fibroblasts (MEFs) (50) and is closely linked to lysosomal destabilization. It is hence plausible that in human monocytes, nigericin and potentially other activating signals induce TAK1 activation independently of priming but dependent on lysosomal rupture and hence contribute to NLRP3 inflammasome assembly. It has recently been suggested that in human myeloid cells, NLRP3 inflammasome can form in the absence of NEK7, which was once considered an essential component of this inflammasome (51). This work proposes that NEK7 contributes to inflammasome activation as a priming factor, required at the initial stages of the response. This requirement is bypassed after prolonged priming by active TAK1 (51). However the roles of NEK7 and TAK1 in NLRP3 activation were not explored in an unprimed setting.

Constitutive NF-κB activation by tonic signals, independent of IL-1R, TNFR, or TLR priming, occurs in the bone marrow (52) and has also been found in human monocytes as well as mouse peritoneal and bone marrow derived macrophages. However, the mechanisms that control this basal activation are not clear (53). High constitutive NF-κB levels are also a feature of acute myeloid leukemia (AML) (54) and hence this might be reflected in THP-1 cells. We found that preventing NF-κB nuclear translocation with the inhibitor JSH-23 did not alter NLRP3 levels, but differentially affected IL-18 in human monocytes and THP-1 cells. In human monocytes, inhibition of NF-κB nuclear translocation led to a reduction in basal pro-IL-18 levels but had no effect on inflammasome activation (cell death and caspase-1 activity) while in THP-1 cells it blocked inflammasome activation without affecting IL-18 protein levels. It is possible that high basal activation of NF-κB contributes to higher levels of IL-18 and inflammasome activation observed in THP-1 cells. Our results however differ from previous work (32) that found that TAK1 inhibition impaired inflammasome activation but JSH-23 did not. These differences can be explained by the fact that our THP-1 cells have not been differentiated with PMA and primed with LPS as done by Gong et al. (32) and that we did a long pre-treatment with JSH-23 (13 h) while Gong *et al.* added the inhibitor at the same time as the NLRP3 activating stimuli nigericin or ATP (30 min). Our data also showed no degradation of IκBα in response to nigericin, indicating that contribution of NF-κB to unprimed inflammasome is not mediated by the activating signal as previously shown for LLME (55). Despite the regulation of p38 activity downstream of TAK1 and the contribution of p38 activity to NLRP3 inflammasome activation (56, 57), we observed no effect of p38 inhibition on unprimed NLRP3 inflammasome activation. Our data highlight an important role for TAK1 and basal NF-κB activity in unprimed inflammasome activation. However the mechanisms by which they do so remain unknown.

It is now evident that changes in PTMs such as ubiquitination or phosphorylation induced by priming or activating signals are essential for the assembly of an active NLRP3 inflammasome (5, 43). Both human and mouse NLRP3 have been described to require TLR4 priming for rapid deubiquitination to be able to respond to the subsequent activating signal (5). Juliana et al. also reported that cell lines overexpressing NLRP3 do not require TLR signaling to respond to an inflammasome activator. However, our results showed that human monocytes and THP-1 cells have basal NLRP3 protein levels, suggesting that this is not the reason why TLR4 engagement is needed for inflammasome assembly. Moreover, our THP-1 data reveals that increased NLRP3 protein expression is not associated with enhanced inflammasome activation. The same study also reported that in the absence of LPS, ATP (signal 2) can cause the deubiquitination of NLRP3 (5). Several deubiquitinases such as USP7, USP47, and BRCC3 have been reported to licence NLRP3 (9, 10). USP7 and USP47 upregulate their activity in response to inflammasome activating signals, even in the absence of priming, and their activity is required to form a canonical NLRP3 inflammasome independently of transcriptional priming (9). Our new data takes this a step further by showing that inhibition of USP7 and USP47 activity prevents the canonical NLRP3 inflammasome activation in unprimed human monocytes. This highlights the role of USP7 and USP47 in sensing danger independently of the priming state of the cell and their ability to mediate inflammasome formation, hence facilitating a fast inflammatory response. Further characterization of basal NLRP3 modifications, especially ubiquitination, as well the activity of various deubiquitinases across species and cell types would greatly expand our understanding of the mechanisms of inflammasome activation.

Pyroptotic cell death is a very well established feature of NLRP3 inflammasome activation. It is mediated by caspase-1 and GSDMD cleavage. Our results, however showed that cell death levels induced by nigericin in both primed and unprimed human cells (monocytes and macrophages) were lower than those traditionally observed in murine cells. This was not just due to a sensitivity issue of the LDH detection assay as cell death measured by nuclear dye uptake showed very similar results. This could be explained by some mouse to human differences, however this has not been addressed in this study and will require further investigation.

Caspase-1 has a broad range of substrate specificity and its activation by the inflammasome regulate cellular responses beyond those attributed to IL-1β and IL-18 activation (58). These include the release of alarmins such as HMGB1 and

ASC *via* pyroptosis (13), FADD (Fas-Associated Death Domain) release *via* microvesicle shedding (59) or the degradation of UBE2L3 (E2 ubiquitin-conjugating enzyme L3) involved in NF-κB activation and pro-IL-1β turnover (27). We have shown that UBE2L3 degradation occurs in the absence of TLR-priming, as does FADD release (59), indicating the ability of active caspase-1 to cleave the same substrates independently of its priming state. This suggests that inflammasome activation can contribute to the amplification of the inflammatory response by mechanisms other than IL-18 signaling in an unprimed setting. This is not yet fully explored and needs to be further researched.

IL-18, unlike IL-1β, is constitutively expressed and is an important initiator of the inflammatory response through driving neutrophil recruitment, and further cytokine and chemokine release (60). IL-18 is involved in the progression of sterile inflammatory diseases including atherosclerosis, metabolic and neuro-inflammatory disorders (61). In these conditions, IL-18 mediates the activation of the NF-κB pathway and upregulation and secretion of TNF-α, adhesion molecules and chemokines (62). IL-18 is a key player in autoinflammatory syndromes, such as familial Mediterranean fever (FMF) caused by pyrin mutations (63) and the Macrophage Activation Syndrome (MAS) caused by NLRC4 gain of function mutations (64) that are characterized by systemically elevated IL-18 levels. IL-18 also plays a key role in the autoinflammatory Cryopyrin-associated periodic syndromes (CAPS) caused by mutations of NLRP3 (65), as IL-18R deletion lessens the disease phenotype to a greater extent than IL-1R deletion in a CAPS mouse model (66). Moreover, the release of damage associated signals such as ATP in transplantation can lead to P2X7R-mediated activation of the inflammasome, inducing the release of IL-18, but not IL-1β, which in turn plays an important role in allograft rejection through IFN-γ production and $CD8^+$ T cell proliferation (67). This highlights the importance of IL-18 release by the rapid assembly of NLRP3 inflammasome in the initiation and progression of the inflammatory response.

Based on our results, we propose that the NLRP3 inflammasome in human monocytes is a "ready to assemble" complex, capable of propagating inflammatory responses at the early stages of inflammation when IL-1β has not yet been produced. The definition of priming in inflammasome research refers to transcriptional or post-translational changes required for NLRP3 to form an active inflammasome in response to a second signal. Based on our results it is possible that the second signal alone provides the licensing step required to allow NLRP3 oligomerization and consequent activation if NLRP3 is already present in the cell. However, we still know very little about what triggers this licensed state and the level of priming that cells present *in vivo*. Specifically what contributes to basal TAK1 and NF-κB activities is poorly characterized. Therefore, it is important to investigate the molecular mechanisms of NLRP3 activation in the absence of priming signals as this might reveal core regulatory mechanisms otherwise overshadowed by the different cellular processes and inflammatory status provided by diverse priming stimuli. We have shown the extent of NLRP3 activation varies between cell types; whether this is different between species, especially human and mouse has not been explored. One possible explanation to our results could be that humans are exposed to pathogenic and non-pathogenic danger signals throughout life and hence monocytes could exist in a basal primed state, allowing the inflammasome to assemble rapidly in response to danger. However, this remains poorly understood and requires further research in the future.

DATA AVAILABILITY STATEMENT

All datasets presented in this study are included in the article/ **Supplementary Material**.

AUTHOR CONTRIBUTIONS

AG, SY, DB, and GL-C designed research. AG, SY, FM and ID-O, performed research. DD and EM-N contributed new reagents/analytic tools. AG, SY, FM-S, DB, and GL-C analyzed and discussed data. AG and GL-C wrote the paper. All authors contributed to the article and approved the submitted version.

FUNDING

This work is supported by: a Medical Research Council PhD DTP studentship to AG (MR/N013751/1); a GSK funded PhD studentship to ID-O; a joint University of Manchester and China Council Scholarship (201608060031) and President's Doctoral Scholar award to SY; a Medical Research Council grant (MR/N029992/1) to DB; a Wellcome Trust Investigator Award (110091) to DD and a Wellcome Trust and Royal Society Henry Dale Fellowship to GL-C (104192/Z/14/Z).

ACKNOWLEDGMENTS

We thank Dr. Veit Hornung (Ludwig Maximilian University, Munich) for providing the NLRP3 KO THP-1 cells, Dr. Kevin Stacey (Lydia Becker Institute of Immunology and Inflammation, Manchester) for his support in providing PBMCs and Dr Gareth J. Howell and the University of Manchester Flow Cytometry Facility. This work has been previously published as a preprint on BioRxiv (68).

SUPPLEMENTARY MATERIAL

The Supplementary Material for this article can be found online at: https://www.frontiersin.org/articles/10.3389/fimmu.2020.565924/full#supplementary-material

REFERENCES

1. Broz P, Dixit VM. Inflammasomes: mechanism of assembly, regulation and signalling. *Nat Rev Immunol* (2016) 16(7):407–20. doi: 10.1038/nri.2016.58
2. Barker BR, Taxman DJ, Ting JP. Cross-regulation between the IL-1β/IL-18 processing inflammasome and other inflammatory cytokines. *Curr Opin Immunol* (2011) 23(5):591–7. doi: 10.1016/j.coi.2011.07.005
3. Ren K, Torres R. Role of interleukin-1beta during pain and inflammation. *Brain Res Rev* (2009) 60(1):57–64. doi: 10.1016/j.brainresrev.2008.12.020
4. Bauernfeind FG, Horvath G, Stutz A, Alnemri ES, MacDonald K, Speert D, et al. Cutting edge: NF-kappaB activating pattern recognition and cytokine receptors license NLRP3 inflammasome activation by regulating NLRP3 expression. *J Immunol* (2009) 183(2):787–91. doi: 10.4049/jimmunol.0901363
5. Juliana C, Fernandes-Alnemri T, Kang S, Farias A, Qin F, Alnemri ES. Non-transcriptional priming and deubiquitination regulate NLRP3 inflammasome activation. *J Biol Chem* (2012) 287(43):36617–22. doi: 10.1074/jbc.M112.407130
6. Song N, Liu ZS, Xue W, Bai ZF, Wang QY, Dai J, et al. NLRP3 Phosphorylation Is an Essential Priming Event for Inflammasome Activation. *Mol Cell* (2017) 68(1):185–97.e6. doi: 10.1016/j.molcel.2017.08.017
7. Kuno K, Matsushima K. The IL-1 receptor signaling pathway. *J Leukoc Biol* (1994) 56(5):542–7. doi: 10.1002/jlb.56.5.542
8. Tapia-Abellán A, Angosto-Bazarra D, Martínez-Banaclocha H, de Torre-Minguela C, Cerón-Carrasco JP, Pérez-Sánchez H, et al. MCC950 closes the active conformation of NLRP3 to an inactive state. *Nat Chem Biol* (2019) 15(6):560–4. doi: 10.1038/s41589-019-0278-6
9. Palazón-Riquelme P, Worboys JD, Green J, Valera A, Martín-Sánchez F, Pellegrini C, et al. USP7 and USP47 deubiquitinases regulate NLRP3 inflammasome activation. *EMBO Rep* (2018) 19. doi: 10.15252/embr.201744766
10. Py BF, Kim MS, Vakifahmetoglu-Norberg H, Yuan J. Deubiquitination of NLRP3 by BRCC3 critically regulates inflammasome activity. *Mol Cell* (2013) 49(2):331–8. doi: 10.1016/j.molcel.2012.11.009
11. Shi J, Zhao Y, Wang K, Shi X, Wang Y, Huang H, et al. Cleavage of GSDMD by inflammatory caspases determines pyroptotic cell death. *Nature* (2015) 526(7575):660–5. doi: 10.1038/nature15514
12. Ding J, Wang K, Liu W, She Y, Sun Q, Shi J, et al. Pore-forming activity and structural autoinhibition of the gasdermin family. *Nature* (2016) 535(7610):111–6. doi: 10.1038/nature18590
13. Baroja-Mazo A, Martín-Sánchez F, Gomez AI, Martínez CM, Amores-Iniesta J, Compan V, et al. The NLRP3 inflammasome is released as a particulate danger signal that amplifies the inflammatory response. *Nat Immunol* (2014) 15(8):738–48. doi: 10.1038/ni.2919
14. Latz E, Xiao TS, Stutz A. Activation and regulation of the inflammasomes. *Nat Rev Immunol* (2013) 13(6):397–411. doi: 10.1038/nri3452
15. Gaidt MM, Ebert TS, Chauhan D, Schmidt T, Schmid-Burgk JL, Rapino F, et al. Human Monocytes Engage an Alternative Inflammasome Pathway. *Immunity* (2016) 44(4):833–46. doi: 10.1016/j.immuni.2016.01.012
16. Liu T, Zhang L, Joo D, Sun SC. NF-κB signaling in inflammation. *Signal Transduct Target Ther* (2017) 2. doi: 10.1038/sigtrans.2017.23
17. Hentze H, Lin XY, Choi MS, Porter AG. Critical role for cathepsin B in mediating caspase-1-dependent interleukin-18 maturation and caspase-1-independent necrosis triggered by the microbial toxin nigericin. *Cell Death Differ* (2003) 10(9):956–68. doi: 10.1038/sj.cdd.4401264
18. Perregaux DG, McNiff P, Laliberte R, Conklyn M, Gabel CA. ATP acts as an agonist to promote stimulus-induced secretion of IL-1 beta and IL-18 in human blood. *J Immunol* (2000) 165(8):4615–23. doi: 10.4049/jimmunol.165.8.4615
19. Fernandez MV, Miller E, Krammer F, Gopal R, Greenbaum BD, Bhardwaj N. Ion efflux and influenza infection trigger NLRP3 inflammasome signaling in human dendritic cells. *J Leukoc Biol* (2016) 99(5):723–34. doi: 10.1189/jlb.3A0614-313RRR
20. Mehta V, Hart J, Wewers MD. ATP-stimulated Release of Interleukin (IL)-1β and IL-18 Requires Priming by Lipopolysaccharide and Is Independent of Caspase-1 Cleavage. *J Biol Chem* (2000) 3820–6. doi: 10.1074/jbc.M006814200
21. O'Brien M, Moehring D, Muñoz-Planillo R, Núñez G, Callaway J, Ting J, et al. A bioluminescent caspase-1 activity assay rapidly monitors inflammasome activation in cells. *J Immunol Methods* (2017) 447:1–13. doi: 10.1016/j.jim.2017.03.004
22. Platnich JM, Chung H, Lau A, Sandall CF, Bondzi-Simpson A, Chen HM, et al. Shiga Toxin/Lipopolysaccharide Activates Caspase-4 and Gasdermin D to Trigger Mitochondrial Reactive Oxygen Species Upstream of the NLRP3 Inflammasome. *Cell Rep* (2018) 25(6):1525–36.e7. doi: 10.1016/j.celrep.2018.09.071
23. Gabellec MM, Griffais R, Fillion G, Haour F. Expression of interleukin 1 alpha, interleukin 1 beta and interleukin 1 receptor antagonist mRNA in mouse brain: regulation by bacterial lipopolysaccharide (LPS) treatment. *Brain Res Mol Brain Res* (1995) 31(1-2):122–30. doi: 10.1016/0169-328X(95)00042-Q
24. Shao W, Yeretssian G, Doiron K, Hussain SN, Saleh M. The caspase-1 digestome identifies the glycolysis pathway as a target during infection and septic shock. *J Biol Chem* (2007) 282(50):36321–9. doi: 10.1074/jbc.M708182200
25. Jamilloux Y, Lagrange B, Di Micco A, Bourdonnay E, Provost A, Tallant R, et al. A proximity-dependent biotinylation (BioID) approach flags the p62/sequestosome-1 protein as a caspase-1 substrate. *J Biol Chem* (2018) 293(32):12563–75. doi: 10.1074/jbc.RA117.000435
26. Agard NJ, Maltby D, Wells JA. Inflammatory stimuli regulate caspase substrate profiles. *Mol Cell Proteomics* (2010) 9(5):880–93. doi: 10.1074/mcp.M900528-MCP200
27. Eldridge MJG, Sanchez-Garrido J, Hoben GF, Goddard PJ, Shenoy AR. The Atypical Ubiquitin E2 Conjugase UBE2L3 Is an Indirect Caspase-1 Target and Controls IL-1β Secretion by Inflammasomes. *Cell Rep* (2017) 18(5):1285–97. doi: 10.1016/j.celrep.2017.01.015
28. Awad F, Assrawi E, Jumeau C, Georgin-Lavialle S, Cobret L, Duquesnoy P, et al. Impact of human monocyte and macrophage polarization on NLR expression and NLRP3 inflammasome activation. *PloS One* (2017) 12(4):e0175336. doi: 10.1371/journal.pone.0175336
29. Landstrom M. The TAK1-TRAF6 signalling pathway. *Int J Biochem Cell Biol* (2010) 42(5):585–9. doi: 10.1016/j.biocel.2009.12.023
30. Katsnelson MA, Lozada-Soto KM, Russo HM, Miller BA, Dubyak GR. NLRP3 inflammasome signaling is activated by low-level lysosome disruption but inhibited by extensive lysosome disruption: roles for K+ efflux and Ca2+ influx. *Am J Physiol Cell Physiol* (2016) 311(1):C83–C100. doi: 10.1152/ajpcell.00298.2015
31. Compan V, Baroja-Mazo A, López-Castejón G, Gomez AI, Martínez CM, Angosto D, et al. Cell volume regulation modulates NLRP3 inflammasome activation. *Immunity* (2012) 37(3):487–500. doi: 10.1016/j.immuni.2012.06.013
32. Gong YN, Wang XM, Wang JY, Yang ZX, Li S, Yang JL, et al. Chemical probing reveals insights into the signaling mechanism of inflammasome activation. *Cell Res* (2010) 20(12):1289–305. doi: 10.1038/cr.2010.135
33. Shin HM, Kim MH, Kim BH, Jung SH, Kim YS, Park HJ, et al. Inhibitory action of novel aromatic diamine compound on lipopolysaccharide-induced nuclear translocation of NF-kappaB without affecting IkappaB degradation. *FEBS Lett* (2004) 571(1-3):50–4. doi: 10.1016/j.febslet.2004.06.056
34. Jackson JR, Bolognese B, Hillegass L, Kassis S, Adams J, Griswold DE, et al. Pharmacological effects of SB 220025, a selective inhibitor of P38 mitogen-activated protein kinase, in angiogenesis and chronic inflammatory disease models. *J Pharmacol Exp Ther* (1998) 284(2):687–92.
35. He Y, Hara H, Núñez G. Mechanism and Regulation of NLRP3 Inflammasome Activation. *Trends Biochem Sci* (2016) 41(12):1012–21. doi: 10.1016/j.tibs.2016.09.002
36. Stutz A, Horvath GL, Monks BG, Latz E. ASC speck formation as a readout for inflammasome activation. *Methods Mol Biol* (2013) 1040:91–101. doi: 10.1007/978-1-62703-523-1_8
37. Muñoz-Planillo R, Kuffa P, Martínez-Colón G, Smith BL, Rajendiran TM, Núñez G. K^+ efflux is the common trigger of NLRP3 inflammasome activation by bacterial toxins and particulate matter. *Immunity* (2013) 38(6):1142–53. doi: 10.1016/j.immuni.2013.05.016
38. Green JP, Yu S, Martín-Sánchez F, Pelegrin P, Lopez-Castejon G, Lawrence CB, et al. Chloride regulates dynamic NLRP3-dependent ASC oligomerization and inflammasome priming. *Proc Natl Acad Sci U S A* (2018) 115:9371–80. doi: 10.1073/pnas.1812744115
39. Baldwin AG, Rivers-Auty J, Daniels MJD, White CS, Schwalbe CH, Schilling T, et al. Boron-Based Inhibitors of the NLRP3 Inflammasome. *Cell Chem Biol* (2017) 24(11):1321–35.e5. doi: 10.1016/j.chembiol.2017.08.011
40. Martín-Sánchez F, Diamond C, Zeitler M, Gomez AI, Baroja-Mazo A, Bagnall J, et al. Inflammasome-dependent IL-1β release depends upon membrane

permeabilisation. *Cell Death Differ* (2016) 23(7):1219–31. doi: 10.1038/cdd.2015.176
41. Tapia VS, Daniels MJD, Palazón-Riquelme P, Dewhurst M, Luheshi NM, Rivers-Auty J, et al. The three cytokines IL-1β, IL-18, and IL-1α share related but distinct secretory routes. *J Biol Chem* (2019) 294(21):8325–35. doi: 10.1074/jbc.RA119.008009
42. He WT, Wan H, Hu L, Chen P, Wang X, Huang Z, et al. Gasdermin D is an executor of pyroptosis and required for interleukin-1β secretion. *Cell Res* (2015) 25(12):1285–98. doi: 10.1038/cr.2015.139
43. Stutz A, Kolbe CC, Stahl R, Horvath GL, Franklin BS, van Ray O, et al. NLRP3 inflammasome assembly is regulated by phosphorylation of the pyrin domain. *J Exp Med* (2017) 214(6):1725–36. doi: 10.1084/jem.20160933
44. Lin KM, Hu W, Troutman TD, Jennings M, Brewer T, Li X, et al. IRAK-1 bypasses priming and directly links TLRs to rapid NLRP3 inflammasome activation. *Proc Natl Acad Sci U S A* (2014) 111(2):775–80. doi: 10.1073/pnas.1320294111
45. Mortimer L, Moreau F, MacDonald JA, Chadee K. NLRP3 inflammasome inhibition is disrupted in a group of auto-inflammatory disease CAPS mutations. *Nat Immunol* (2016) 17(10):1176–+. doi: 10.1038/ni.3538
46. Zhang Z, Meszaros G, He WT, Xu Y, de Fatima Magliarelli H, Mailly L, et al. Protein kinase D at the Golgi controls NLRP3 inflammasome activation. *J Exp Med* (2017) 214(9):2671–93. doi: 10.1084/jem.20162040
47. Spalinger MR, Kasper S, Gottier C, Lang S, Atrott K, Vavricka SR, et al. NLRP3 tyrosine phosphorylation is controlled by protein tyrosine phosphatase PTPN22. *J Clin Invest* (2016) 126(11):4388. doi: 10.1172/JCI90897
48. Huang Y, Wang H, Hao Y, Lin H, Dong M, Ye J, et al. Myeloid PTEN promotes chemotherapy-induced NLRP3-inflammasome activation and antitumour immunity. *Nat Cell Biol* (2020) 22:716–27. doi: 10.1038/s41556-020-0510-3
49. Okada M, Matsuzawa A, Yoshimura A, Ichijo H. The lysosome rupture-activated TAK1-JNK pathway regulates NLRP3 inflammasome activation. *J Biol Chem* (2014) 289(47):32926–36. doi: 10.1074/jbc.M114.579961
50. Inagaki M, Omori E, Kim JY, Komatsu Y, Scott G, Ray MK, et al. TAK1-binding protein 1, TAB1, mediates osmotic stress-induced TAK1 activation but is dispensable for TAK1-mediated cytokine signaling. *J Biol Chem* (2008) 283(48):33080–6. doi: 10.1074/jbc.M807574200
51. Schmacke NA, Gaidt MM, Szymanska I, O'Duill F, Stafford CA, Chauhan D, et al. Priming enables a NEK7-independent route of NLRP3 activation. *bioRxiv* (2019). doi: 10.1101/799320
52. Fang J, Muto T, Kleppe M, Bolanos LC, Hueneman KM, Walker CS, et al. TRAF6 Mediates Basal Activation of NF-κB Necessary for Hematopoietic Stem Cell Homeostasis. *Cell Rep* (2018) 22(5):1250–62. doi: 10.1016/j.celrep.2018.01.013
53. Bagaev AV, Garaeva AY, Lebedeva ES, Pichugin AV, Ataullakhanov RI, Ataullakhanov FI. Elevated pre-activation basal level of nuclear NF-κB in native macrophages accelerates LPS-induced translocation of cytosolic NF-κB into the cell nucleus. *Sci Rep* (2019) 9(1):4563. doi: 10.1038/s41598-018-36052-5
54. Zhou J, Ching YQ, Chng WJ. Aberrant nuclear factor-kappa B activity in acute myeloid leukemia: from molecular pathogenesis to therapeutic target. *Oncotarget* (2015) 6(8):5490–500. doi: 10.18632/oncotarget.3545
55. Ono H, Ohta R, Kawasaki Y, Niwa A, Takada H, Nakahata T, et al. Lysosomal membrane permeabilization causes secretion of IL-1β in human vascular smooth muscle cells. *Inflammation Res* (2018) 67(10):879–89. doi: 10.1007/s00011-018-1178-z
56. Fenini G, Grossi S, Gehrke S, Beer HD, Satoh TK, Contassot E, et al. The p38 Mitogen-Activated Protein Kinase Critically Regulates Human Keratinocyte Inflammasome Activation. *J Invest Dermatol* (2018) 138(6):1380–90. doi: 10.1016/j.jid.2017.10.037
57. Wang C, Hockerman S, Jacobsen EJ, Alippe Y, Selness SR, Hope HR, et al. Selective inhibition of the p38α MAPK-MK2 axis inhibits inflammatory cues including inflammasome priming signals. *J Exp Med* (2018) 215(5):1315–25. doi: 10.1084/jem.20172063
58. Denes A, Lopez-Castejon G, Brough D. Caspase-1: is IL-1 just the tip of the ICEberg? *Cell Death Dis* (2012) 3:e338. doi: 10.1038/cddis.2012.86
59. Mouasni S, Gonzalez V, Schmitt A, Bennana E, Guillonneau F, Mistou S, et al. The classical NLRP3 inflammasome controls FADD unconventional secretion through microvesicle shedding. *Cell Death Dis* (2019) 10(3):190. doi: 10.1038/s41419-019-1412-9
60. Leung BP, Culshaw S, Gracie JA, Hunter D, Canetti CA, Campbell C, et al. A role for IL-18 in neutrophil activation. *J Immunol* (2001) 167(5):2879–86. doi: 10.4049/jimmunol.167.5.2879
61. Patel MN, Carroll RG, Galván-Peña S, Mills EL, Olden R, Triantafilou M, et al. Inflammasome Priming in Sterile Inflammatory Disease. *Trends Mol Med* (2017) 23(2):165–80. doi: 10.1016/j.molmed.2016.12.007
62. Felderhoff-Mueser U, Schmidt OI, Oberholzer A, Bührer C, Stahel PF. IL-18: a key player in neuroinflammation and neurodegeneration? *Trends Neurosci* (2005) 28(9):487–93. doi: 10.1016/j.tins.2005.06.008
63. Wada T, Toma T, Miyazawa H, Koizumi E, Shirahashi T, Matsuda Y, et al. Longitudinal analysis of serum interleukin-18 in patients with familial Mediterranean fever carrying MEFV mutations in exon 10. *Cytokine* (2018) 104:143–6. doi: 10.1016/j.cyto.2017.10.007
64. Canna SW, Girard C, Malle L, de Jesus A, Romberg N, Kelsen J, et al. Life-threatening NLRC4-associated hyperinflammation successfully treated with IL-18 inhibition. *J Allergy Clin Immunol* (2017) 139(5):1698–701. doi: 10.1016/j.jaci.2016.10.022
65. Feldmann J, Prieur AM, Quartier P, Berquin P, Certain S, Cortis E, et al. Chronic infantile neurological cutaneous and articular syndrome is caused by mutations in CIAS1, a gene highly expressed in polymorphonuclear cells and chondrocytes. *Am J Hum Genet* (2002) 71(1):198–203. doi: 10.1086/341357
66. Brydges SD, Broderick L, McGeough MD, Pena CA, Mueller JL, Hoffman HM. Divergence of IL-1, IL-18, and cell death in NLRP3 inflammasomopathies. *J Clin Invest* (2013) 123(11):4695–705. doi: 10.1172/JCI71543
67. Amores-Iniesta J, Barbera-Cremades M, Martinez CM, Pons JA, Revilla-Nuin B, Martinez-Alarcon L, et al. Extracellular ATP Activates the NLRP3 Inflammasome and Is an Early Danger Signal of Skin Allograft Rejection. *Cell Rep* (2017) 21(12):3414–26. doi: 10.1016/j.celrep.2017.11.079
68. Gritsenko A, Yu S, Martin-Sanchez F, Diaz- del-Olmo I, Nichols E-M, View ORCID Profile Davis DM, et al. Priming is dispensable for NLRP3 inflammasome activation in human monocytes. *BioRxiv* (2020). doi: 10.1101/2020.01.30.925248

Conflict of Interest: EN is an employee of the GSK group of companies.

The remaining authors declare that the research was conducted in the absence of any commercial or financial relationships that could be construed as a potential conflict of interest.

frontiers in Immunology

ORIGINAL RESEARCH
published: 13 May 2021
doi: 10.3389/fimmu.2021.653883

DDX3X Links NLRP11 to the Regulation of Type I Interferon Responses and NLRP3 Inflammasome Activation

Ioannis Kienes[1], Sarah Bauer[1], Clarissa Gottschild[1], Nora Mirza[1], Jens Pfannstiel[2], Martina Schröder[3†] and Thomas A. Kufer[1†]*

[1] Department of Immunology, Institute of Nutritional Medicine, University of Hohenheim, Stuttgart, Germany, [2] Core Facility University of Hohenheim, Mass Spectrometry Module, University of Hohenheim, Stuttgart, Germany, [3] Kathleen Lonsdale Institute for Human Health Research, Department of Biology, Maynooth University, Maynooth, Ireland

OPEN ACCESS

Edited by:
Bernd Lepenies,
University of Veterinary Medicine Hannover, Germany

Reviewed by:
Pin Ling,
National Cheng Kung University, Taiwan
Santosh Chauhan,
Institute of Life Sciences (ILS), India

****Correspondence:***
Thomas A. Kufer
thomas.kufer@uni-hohenheim.de

†These authors share last authorship

Specialty section:
This article was submitted to Molecular Innate Immunity, a section of the journal Frontiers in Immunology

Received: *15 January 2021*
Accepted: *19 April 2021*
Published: *13 May 2021*

Citation:
Kienes I, Bauer S, Gottschild C, Mirza N, Pfannstiel J, Schröder M and Kufer TA (2021) DDX3X Links NLRP11 to the Regulation of Type I Interferon Responses and NLRP3 Inflammasome Activation. Front. Immunol. 12:653883. doi: 10.3389/fimmu.2021.653883

Tight regulation of inflammatory cytokine and interferon (IFN) production in innate immunity is pivotal for optimal control of pathogens and avoidance of immunopathology. The human Nod-like receptor (NLR) NLRP11 has been shown to regulate type I IFN and pro-inflammatory cytokine responses. Here, we identified the ATP-dependent RNA helicase DDX3X as a novel binding partner of NLRP11, using co-immunoprecipitation and LC-MS/MS. DDX3X is known to enhance type I IFN responses and NLRP3 inflammasome activation. We demonstrate that NLRP11 can abolish IKKε-mediated phosphorylation of DDX3X, resulting in lower type I IFN induction upon viral infection. These effects were dependent on the LRR domain of NLRP11 that we mapped as the interaction domain for DDX3X. In addition, NLRP11 also suppressed NLRP3-mediated caspase-1 activation in an LRR domain-dependent manner, suggesting that NLRP11 might sequester DDX3X and prevent it from promoting NLRP3-induced inflammasome activation. Taken together, our data revealed DDX3X as a central target of NLRP11, which can mediate the effects of NLRP11 on type I IFN induction as well as NLRP3 inflammasome activation. This expands our knowledge of the molecular mechanisms underlying NLRP11 function in innate immunity and suggests that both NLRP11 and DDX3X might be promising targets for modulation of innate immune responses.

Keywords: innate immunity, nod-like receptors, anti-viral, DEAD-box helicase, inflammasome, IL-1, type I interferon

INTRODUCTION

In mammals, viral infections are detected by anti-viral pattern-recognition receptors (PRRs), including RIG-I-like receptors (RLRs), cytosolic DNA receptors, and endosomal Toll-like receptors (TLRs). Their activation induces antiviral cytokine responses dominated by release of type I interferons (IFNs), which are crucial for limiting replication of most viruses (1–4). Hence, failure to initiate an effective IFN response correlates with higher pathogenicity in many viral infections (5–7). Thus, robust early IFN induction is crucial for controlling viral replication,

but failure to resolve this response can result in severe immunopathology in the host (8–10). In particular an altered balance between type I IFN responses and pro-inflammatory cytokine release can lead to pathology in the host, as seen for example in COVID-19 disease (11, 12). It is therefore critical to understand how type I IFN and pro-inflammatory cytokine responses are balanced during viral infections.

RLRs, most prominently RIG-I, are essential sensors for cytosolic viral RNA (13). Following the binding of viral RNAs, RIG-I oligomerizes and binds to the mitochondrial antiviral signaling protein (MAVS) *via* CARD-CARD interactions (14). MAVS then recruits downstream signaling proteins, such as TNF-associated factor 2 (TRAF2) (15), TRAF6 (16), and TRAF3 (17), which ultimately lead to induction of pro-inflammatory cytokines and type I IFNs. IFN induction is dependent on phosphorylation of the transcription factors interferon regulatory factor 3 (IRF3) and IRF7 (18–21) mediated by two related kinases, inhibitor of NF-κB kinase subunit epsilon (IKKε) and TANK binding kinase 1 (TBK1) (22, 23). TBK1 is necessary for IFN-β induction and ubiquitously expressed in different cell types, while IKKε may not be essential for IFN-β induction and has been suggested to directly regulate a subset of interferon-stimulated genes (ISGs) (24).

NOD-like receptors (NLRs) are another important group of PRRs and a total of 22 human NLR proteins have been discovered (25), many of which remain to be functionally characterized. NLRs consist of an N-terminal effector domain, a central NACHT domain, and a C-terminal leucine-rich repeat region (LRRs), and can be subcategorized by their effector domains into pyrin-domain (PYD) containing NLRP proteins, CARD-domain containing NLRC proteins, baculovirus inhibitor of apoptosis (BIR)-domain containing NLRB proteins, and CARD-transcriptional activation-domain (CARD-AD) containing NLRA proteins (26).

Signaling pathways induced by NLRs are heterogeneous. While NOD1 and NOD2 induce NF-κB activation upon recognition of bacterial ligands (27–29), NLRP1, NLRP3 and NLRC4 activation leads to formation of a large multiprotein signaling platform called the inflammasome (30–32). Inflammasome formation starts with recruitment of the adaptor protein apoptosis-associated speck-like protein (ASC), which then recruits and activates pro-caspase-1, enabling maturation and release of IL-1β and IL-18. Other NLRP proteins including NLRP6, NLRP7, NLRP12, and possibly NLRC5 might also form inflammasomes (33–36). However, not all mammalian NLR proteins act as PRRs. For example, NLRC5 and CIITA are transcriptional enhancers for MHC class I and class II genes, respectively (37, 38), and some NLRs have been identified as negative regulators of innate immune responses. An example is NLRC3 that negatively regulates DNA sensing-PRRs by interfering with the adaptor molecule stimulator of interferon genes (STING) (39). Furthermore, NLRP4 (40–42), NLRP12 (43, 44) and NLRP14 (45), were reported to modulate IFN responses (for an overview see (46)).

We and others have previously shown that NLRP11 can negatively regulate both NF-κB activation (47) and type I IFN induction (48, 49). It was shown that NLRP11 interferes with the MAVS signaling complex (47, 49), but it can also block type I IFN induction downstream of TBK1 (48), suggesting that NLRP11 might intervene at multiple levels in the RLR pathway.

A well-established positive regulator of the RLR-pathway is the human DEAD-box protein 3 (DDX3X). DDX3X physically interacts with MAVS (50), IKKε (51), TBK1 (52), TRAF3 (53) and IRF3 (54), resulting in enhanced type I IFN production (50, 51, 53, 54). DDX3X might also be directly involved in recognition of viral RNA (50). Activation of the RIG-I pathway triggers binding of DDX3X to IKKε, which leads to enhanced IKKε activation (51, 54) and IKKε-mediated phosphorylation of DDX3X in its N-terminal region, which enables recruitment of IRF3 into the complex, resulting in enhanced activation of IRF3 by IKKε phosphorylation (54). TBK1 can also phosphorylate DDX3X and enhance IFNβ production (52). The physiological importance of DDX3X's role in anti-viral immune signaling is underlined by the fact that several viruses, including Vaccinia virus, Hepatitis B virus and Influenza A virus, evolved immune evasion mechanisms targeting DDX3X (51, 55–59). Thus DDX3X is a central regulator of the RIG-I anti-viral signaling pathway, where it interacts with signaling intermediates in a complex manner that is still not completely understood.

Recently, a further role for DDX3X as a positive regulator of NLRP3 inflammasome activation was reported. Sequestration of DDX3X into cytosolic stress granules during cellular stress results in reduced NLRP3/caspase-1 activation and suppression of IL-1β and IL-18 release (60).

A better understanding of the complex molecular circuits that control innate immune responses will advance our understanding of host-pathogen interactions and help to identify novel targets for therapeutic intervention. Here we provide evidence that NLRP11, *via* its leucine-rich repeats (LRRs), interacts with DDX3X. This interaction inhibited IKKε-induced phosphorylation of DDX3X and type I IFN induction. Using caspase-1 activation assays and ASC speck formation assays, we revealed that NLRP11 can also counteract the positive effect of DDX3X on NLRP3 inflammasome activation. Taken together, our work identified DDX3X as a novel target of NLRP11 that contributes to the inhibitory effects on both type I IFN induction and IL-1β release.

MATERIALS AND METHODS

Plasmids and Reagents

Myc-NLRP11 and myc-NLRP11 domain constructs were previously described (48). The plasmids pcDNA5/FRT/TO-NLRP11-eGFP and pEGFP-DDX3X were generated by molecular cloning from myc-NLRP11 or myc-DDX3X respectively. The Myc-DDX3X construct is described in (51). piGLuc caspase-1 reporter plasmid, pCI-caspase-1 and pCI-ASC-HA were kindly provided by Veit Hornung and are described in (61, 62). FLAG-IKKε was kindly provided by Eliane Meurs (63). Myc-DDX3X mutants were previously

described in (54). All plasmids (inserts, tags and flanking regions) were verified by Sanger sequencing.

Cell Culture

HEK293T cells (ATCC, CRL-3216) were grown in DMEM supplemented with 10% heat-inactivated FBS. HEK Blue IFN-α/β (hkb-ifnab, InvivoGen) were maintained in DMEM, supplemented with 10% heat-inactivated FBS, 30 µg/ml blasticidin and 100 µg/ml zeocin. THP1 cells with a doxycycline inducible shRNA targeting DDX3X and non-silencing controls (NSC) are described in (64). Cells were grown in RPMI 1640 supplemented with 10% heat-inactivated FBS, gentamycin and puromycin. Knock-down of DDX3X was induced by 1 µg/ml doxycycline for 48 h.

Stable, inducible cell lines expressing NLRP11-eGFP were generated by co-transfection of pOG44 and pcDNA5/FRT/TO-NLRP11-eGFP at 9:1 ratio into Flp-In T-REx HEK293 (Invitrogen/ThermoFischer, R78007) and HeLa FlpIn T-REx cells (kindly provided by the Hentze Lab, EMBL Heidelberg) using Lipofectamin 2000 (Thermo Fisher Scientific) and selected with 10 µg/ml blasticidin and either 100 µg/ml (HEK) or 600 µg/ml (HeLa) hygromycin. Single clones were selected, and expression was induced by 1 µg/ml doxycycline for at least 16 h prior to further experiments. All cell culture media were supplemented with penicillin and streptomycin. Cells were routinely monitored for absence of mycoplasma infection by PCR.

For viral infection, cells were incubated with 160 hemagglutination units (HAU)/ml Sendai virus (Cantell Strain in allantoic fluid, Charles River).

siRNA- and shRNA Mediated Silencing

THP1 and THP1shDDX3X cells were differentiated with 100 nM PMA for 16 h. Medium was changed and cells were incubated for 24 h prior to siRNA-mediated knock-down with 100 nM siRNA, transfected using HiPerFect transfection reagent (Qiagen) according to (65). AllStars negative control siRNA and siNLRP11_6 CACGACCTTGCAGCTGTCGAA (48) (Qiagen) were used. Knock-down of NLRP11 was performed for 72 h. For double knock-down of NLRP11 and DDX3X, 24 h after transfection of the siRNA, THP1 shDDX3X cells were induced with 1 µg/ml doxycycline for 48 h.

Knock-down efficiency of NLRP11 was monitored with endpoint PCR as described in (48). Knock-down of DDX3X was monitored by end-point PCR using the following primer pair: fwd: TGCTGGCCTAGACCTGAACT rev: TTGATCCACTTCCACGATCA.

Co-Immunoprecipitation and Protein Binding Assays

Co-immunoprecipitation of NLRP11-eGFP, from HEK293 and HeLa FlpIn eGFP and NLRP11-eGFP cell lines, or of eGFP-DDX3X from HEK293T cells, transiently transfected with Lipofectamine 2000 (Thermo Fisher Scientific), was performed with GFP-Trap Agarose resin (Chromotek). Cells were lysed in Triton buffer [50 mM Tris/HCl pH 7.4, 150 mM NaCl, 1% Triton-X100, 1% Na-Deoxycholate, 100 nM β-glycerophosphate, 100 nM sodium orthovanadate, 1 mM NaF and cOmplete Mini Protease inhibitor Cocktail (Roche)]. Lysates were cleared by centrifugation (15 min, 4°C, 21000 x *g*) before the supernatants were loaded onto the matrix. Precipitation was performed at 4°C for 3 h, before the matrix was washed with washing buffer (50 mM Tris/HCl pH 7.4, 150 mM NaCl, 1% Na-Deoxycholate).

NanoLC-MS/MS Analysis

Proteins were digested on beads using trypsin (Roche, Germany) in 6 M urea, 50 mM Tris-HCl pH 8.5. Cysteines were reduced using 1,4-dithiothreitol (DTT) and then alkylated by chloroacetamide. Samples were then diluted to a final concentration of 2 M urea. 750 ng trypsin were added, and samples were digested overnight at 25°C. The digests were stopped by adding trifluoroacetic acid (TFA). Next, peptide mixtures were concentrated and desalted on C18 stage tips and dried under vacuum. Samples were dissolved in 0.1% TFA and were subjected to nanoLC-MS/MS analysis on an EASY-nLC 1000 system (Thermo Fisher Scientific, Germany) coupled to a Q-Exactive Plus mass spectrometer (Thermo Fisher Scientific, Germany) using an EASY-Spray nanoelectrospray ion source (Thermo Fisher Scientific, Germany). The system was controlled by Xcalibur 3.0.63 software. Tryptic peptides were directly injected to a 25 cm x 75 µm EASY-Spray analytical column (2 µm, 100 Å, PepMap C18) operated at 35°C. Peptides were separated at a flow rate of 250 nL/min using a 120 min gradient with the following profile: 3% - 10% solvent B in 50 min, 10% - 22% solvent B in 40 min, 22% - 45% solvent B in 30 min, 45% - 90% solvent B in 10 min, 15 min isocratic at 90% solvent B, followed by 90% - 3% solvent B in 10 min and re-equilibration at 3% solvent B for 15 min. (solvent A: 0.5% acetic acid; solvent B: acetonitrile/H_2O (80/20, v/v), 0.5% acetic acid).

MS spectra (m/z = 300-1600) were detected at a resolution of 70000 (m/z = 200) using a maximum injection time (MIT) of 100 ms and an automatic gain control (AGC) value of 1×10^6. MS/MS spectra were generated for the 10 most abundant peptide precursors using high energy collision dissociation (HCD) fragmentation at a resolution of 17500, normalized collision energy of 27 and an intensity threshold of 1.3×10^5. Only ions with charge states from +2 to +5 were selected for fragmentation using an isolation width of 1.6 Da. For each MS/MS scan, the AGC was set at 5×10^5 and the MIT was 100 ms. Mascot 2.6 (Matrix Science, UK) was used as search engine for protein identification. Spectra were searched against the human UniProt database (66). Scaffold 4.8.6. (Proteome Software, USA) was used to evaluate peptide identifications. These were accepted with a peptide probability greater than 80% as specified by the Peptide Prophet algorithm (67). Proteins had to be identified by at least one unique peptide and a protein probability of at least 99% to be accepted.

Reporter Assays

For iGLuc caspase-1 reporter assays, HEK293T cells were seeded in a 96-well plate (Greiner) at a density of 35,000 cells per well and transiently transfected using Xtreme Gene 9 transfection reagent (Sigma Aldrich) with 8.6 ng β-galactosidase plasmid, 42 ng of the iGLuc reporter plasmid (61), and expression plasmids of NLRP3, NLRP11, ASC, caspase-1 and DDX3X,

DDX3X S102A, or DDX3X 4A as indicated. 20 h after transfection, cells were stimulated with 15 µM nigericin (InvivoGen) for 3 h. Cells were then lysed in 100 µl passive lysis buffer (Promega) per well. 50 µl of the cell lysate were transferred into a non-transparent 96-well plate. Luciferase activity was measured in a multiplate reader (Enspire, PerkinElmer LifeSciences) after addition of 100 µl of 3.33 µM Coelenterazine (Carl Roth) per well. 100 µl of 1 mg/ml O-nitrohpenyl-β-D-galactoryranoside in 60 mM Na_2HPO_4, 40 mM NaH_2PO_4, 10 mM KCl and 1 mM $MgSO_4$ were added to the remaining 50 µl lysate, incubated at 37°C and absorption was measured at 405 nm (620 nm reference) as β-galactosidase activity. Luciferase activity was normalized to β-galactosidase activity.

Ifnβ luciferase reporter assays were performed as described in (48), with 5 ng FLAG-IKKε plasmid for activation.

Assays were performed in technical triplicates and repeated independently three times unless indicated otherwise.

Indirect Immunofluorescence

HeLa FlpIn cells were seeded into 24-well plates at a density of 75,000 cells per well on glass coverslips, HEK FlpIn cells at 100,000 cells per well on poly-L-lysin pretreated glass coverslips and expression of eGFP or eGFP-NLRP11 was induced with 1 µg/ml doxycycline. After overnight expression, cells were either infected with 160 hemagglutination units (HAU)/ml Sendai virus (SeV) for different durations, or directly fixed with 4% PFA in PBS, permeabilized with 0.5% Triton X-100 and blocked with 5% FBS in PBS. Cells were then incubated with primary and secondary antibody sequentially. Antibodies used: Primary: DDX3X (A300-474A Bethyl Laboratories), AIF (Cell Signalling # 4642). Secondary: Alexa-546 goat anti-rabbit IgG, Alexa-405 goat anti-mouse (Molecular Probes). DNA was stained with Hoechst 33258 (Sigma). Images were captured with a Leica DMi8 microscope using a HCX PL FL L 40X/0.60 or a HC PL APO 63X/1.40-0.60 OIL objective and processed using the Leica LasX software and ImageJ. For 3D deconvolution, Z-stacks of 4.05 µm depth were captured, with individual planes every 0.2 µm. Blind 3D-deconvolution was performed using the Leica LasX software, performing 10 iterations at a refractive index of 1.52. For quantitative analysis, sample pictures were blinded and counted by eye.

Immunoblotting

Immunoblotting was performed as described in (65). Antibodies used: β-actin (C-4; Santa Cruz sc-47778), GFP (Roche 11 814 460 001), myc (9E10; Sigma Aldrich M4439), DDX3X (Bethyl Laboratories A300-474A), FLAG (Sigma Aldrich F7425), GAPDH (Santa Cruz sc-25778), pIRF3 (Cell Signalling #29047T).

Measurement of Cytokines

IL-1β and IFNβ release was measured in cell supernatants by ELISA (DY201, DY814, R&D Systems) according to the manufacturer's instructions. A bioassay for type I interferons was performed using HEK Blue IFN-α/β cells (Invivogen). HEK Blue IFN-α/β cells were stimulated for 20 h with supernatant from SeV infected THP1 cells and SEAP activity in the supernatant was measured by Quantiblue solution (rep-qbs, InvivoGen) according to the manufacturer's conditions.

Statistical Analysis

Data were analyzed by unequal variances t-test (Welch test) and plotted using GraphPad Prism version 7.05. $p < 0.05$ was regarded as significant.

RESULTS

NLRP11 Interacts With the ATP-Dependent RNA Helicase DDX3X

We recently demonstrated that NLRP11 is a negative regulator of inflammatory cytokine induction (48). In order to study the underlying molecular mechanism, we generated an eGFP-tagged NLRP11 (NLRP11-eGFP) expression construct and confirmed that NLRP11-eGFP retained its negative regulatory effect on IKKε induced *ifnβ*-reporter gene expression in comparison to our previously used myc-NLRP11 construct (**Figure 1A**). Stable cell lines allowing for inducible expression of NLRP11-eGFP were generated using the doxycycline inducible single site recombination system Flp-In T-REx. We obtained stable HeLa and HEK293 lines that showed inducible expression of NLRP11-eGFP after doxycycline treatment, as well as control cell lines expressing eGFP only. We selected for cell lines with tight regulation, uniform expression in all cells, and well detectable expression upon induction (**Figure 1B**). We noticed that NLRP11-eGFP tended to form high molecular weight SDS-stable aggregates in both HEK293 and HeLa cells (**Figure 1B**, upper band), which we also observed for myc-NLRP11 (data not shown). However, we always also detected monomeric NLRP11 in SDS-PAGE, and fluorescent microscopy also confirmed that NLRP11-eGFP was distributed in the cytoplasm without formation of larger aggregates, consistent with earlier reports (48, 49). Nonetheless, we noticed that NLRP11 was not completely evenly distributed in the cytosol, suggesting it might associate with cellular organelles (**Figure 1C**).

Next, we used these stable cell lines to identify interaction partners of NLRP11. NLRP11-eGFP protein complexes were immunoprecipitated from the HeLa-NLRP11-eGFP cells using anti-GFP antibody. Co-immunoprecipitated proteins were identified by mass spectrometry. We obtained several putative NLRP11 interactors that were not detected in two independent control immunoprecipitation experiments conducted with the corresponding eGFP-expressing HeLa cell line (**Supplementary Table 1**). Due to its well-described functions in anti-viral innate immune signaling (51, 52, 68), we selected the DEAD-box protein DDX3X as the most interesting candidate for further analysis. To validate the interaction, we used a specific antibody directed against DDX3X. In independent experiments we could confirm the presence of endogenous DDX3X in co-immunoprecipitations from HEK293-NLRP11-eGFP cells, while it was absent in co-immunoprecipitations conducted with HEK293-eGFP control cells (**Figure 1D**). Unfortunately, due to lack of a specific antibody against human NLRP11, we could not assess the interaction with endogenous NLRP11.

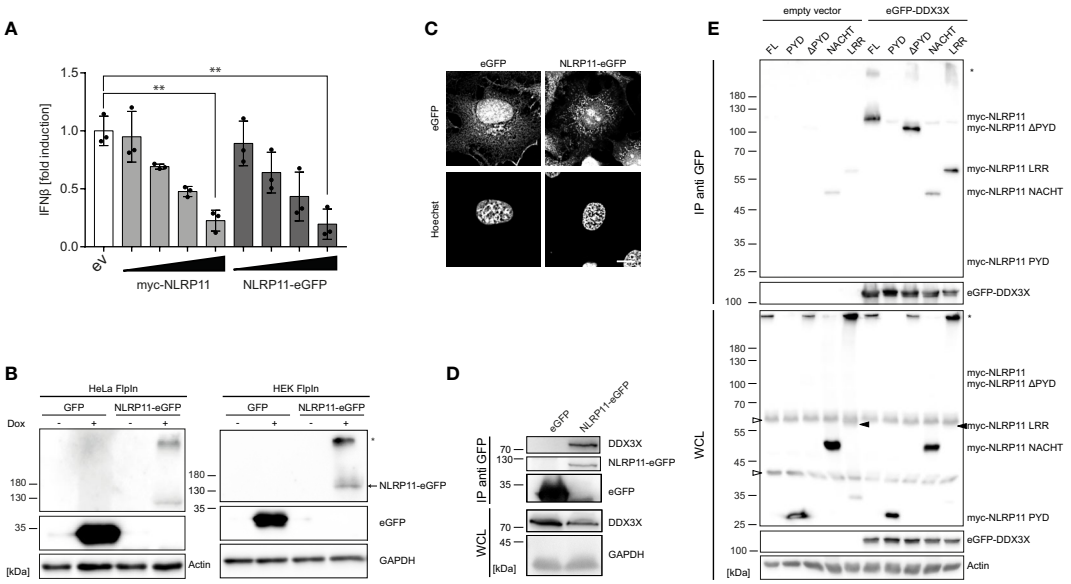

FIGURE 1 | NLRP11 interacts with DDX3X. **(A)** *ifnb* luciferase reporter assay in HEK293T cells overexpressing FLAG-IKKε (5 ng) and either empty vector (ev), myc-NLRP11, or NLRP11-eGFP. Means of three independent experiments conducted in triplicates, relative to the mean of 0 ng NLRP11, ± SEM are shown. **p < 0.01; Welch's two-sided t-test. **(B)** Immunoblot of protein lysates of HEK293- and HeLa-eGFP and -NLRP11-eGFP cells, induced overnight with doxycycline. Probing for GFP and actin, or GAPDH as loading control is shown. Monomeric NLRP11-eGFP is marked by an arrow and aggregated NLRP11 by an asterisk. **(C)** Immunofluorescence micrographs of HeLa-NLRP11-eGFP cells. Cells were induced with doxycycline overnight, fixed and nuclei were stained. 3D-deconvolution of z-stacks of the signal of DNA (lower images) and eGFP (upper images) are shown. Stack size = 0.2 µm. Scale bar = 10 µm. **(D)** Immunoblots from anti-GFP immunoprecipitations (IP) from HEK293T-eGFP and HEK293-NLRP11-eGFP cells induced over night with doxycycline. IPs were probed for DDX3X and GFP, whole cell lysates (WCL) were probed for DDX3X and GAPDH as loading control. Representative blots for two independent experiments are shown. **(E)** Immunoblots from anti-GFP IPs from HEK293T cells expressing empty vector, or eGFP-DDX3X and the indicated myc-NLRP11 construct. IP lysates were probed for myc and GFP, whole cell lysates were probed for myc, GFP and actin as a loading control. Representative blots of two independent experiments are shown. *, NLRP11 aggregate; Δ, unspecific bands.

To map the interaction domain for DDX3X in NLRP11, we expressed myc-tagged NLRP11 truncation mutants in HEK293T cells together with eGFP-DDX3X or empty vector and performed immunoprecipitations using anti-GFP antibody. We also confirmed binding of myc-NLRP11 to DDX3X in these experiments (**Figure 1E**). Deletion of the NLRP11 PYD did not influence binding, nor was the PYD sufficient to facilitate binding to DDX3X. While the LRR domain alone showed a strong interaction with DDX3X, we only observed limited binding of the NACHT domain to DDX3X (**Figure 1E**). This finding is in line with results obtained in our previous work, where we showed that the LRR domain of NLRP11 is sufficient for inhibition of TBK1-induced type I IFN (48).

We next set out to analyze the functional relevance of the DDX3X-NLRP11 interaction. First, we tested whether the NLRP11-DDX3X complex formation changed during Sendai virus (SeV) infection. Starting at 4 h post infection, we observed increased expression levels and co-immunoprecipitation of endogenous DDX3X with NLRP11-eGFP in HEK293 cells that was strongest at 6 h and 16 h post infection (**Figure 2A**). We next analyzed the subcellular localization dynamics of NLRP11 and DDX3X during infection with SeV by indirect immunofluorescence microscopy. In HEK293-NLRP11-eGFP cells we confirmed co-localization of NLRP11 and DDX3X in the cytosol. This co-localization was maintained and appeared slightly enhanced during SeV infection with more pronounced co-localization at 16 h post infection compared to steady state levels (**Figure 2B**). Co-localization of DDX3X and NLRP11-eGFP was also observed in HeLa-NLRP11-eGFP cells, where NLRP11-eGFP continued to stably co-localize with DDX3X over the course of 16 h of infection in the majority of cells (**Figure 2C**). However, NLRP11 was not recruited to distinct DDX3X clusters that appeared at 16 h post infection in a minority of cells (**Figure 2D**). The formation of these structures was also not influenced by the presence, or absence of NLRP11-eGFP (**Figure 2D**). These structures likely represent stress granules that DDX3X is known to be recruited into (60, 69, 70) and were only present in a minority of the cells. In line with data previously published by Qin et al. (49), HEK293-NLRP11-eGFP cells showed no co-localization of NLRP11-eGFP with the mitochondrial marker apoptosis-inducing factor (AIF) at steady state conditions, but we observed recruitment of NLRP11 to mitochondria at 16 h post infection (**Figure 2E**). In HeLa NLRP11-eGFP cells, NLRP11 was localized in proximity to mitochondria in untreated cells and this localization pattern persisted during 16 h of SeV infection, with partial co-localization observed at 16 h post infection (**Figure 2F**).

Taken together, we identified DDX3X as a novel binding partner of NLRP11. Mapping of the interaction domain in NLRP11 identified that the LRR region was sufficient for DDX3X binding. We further demonstrated that the interaction

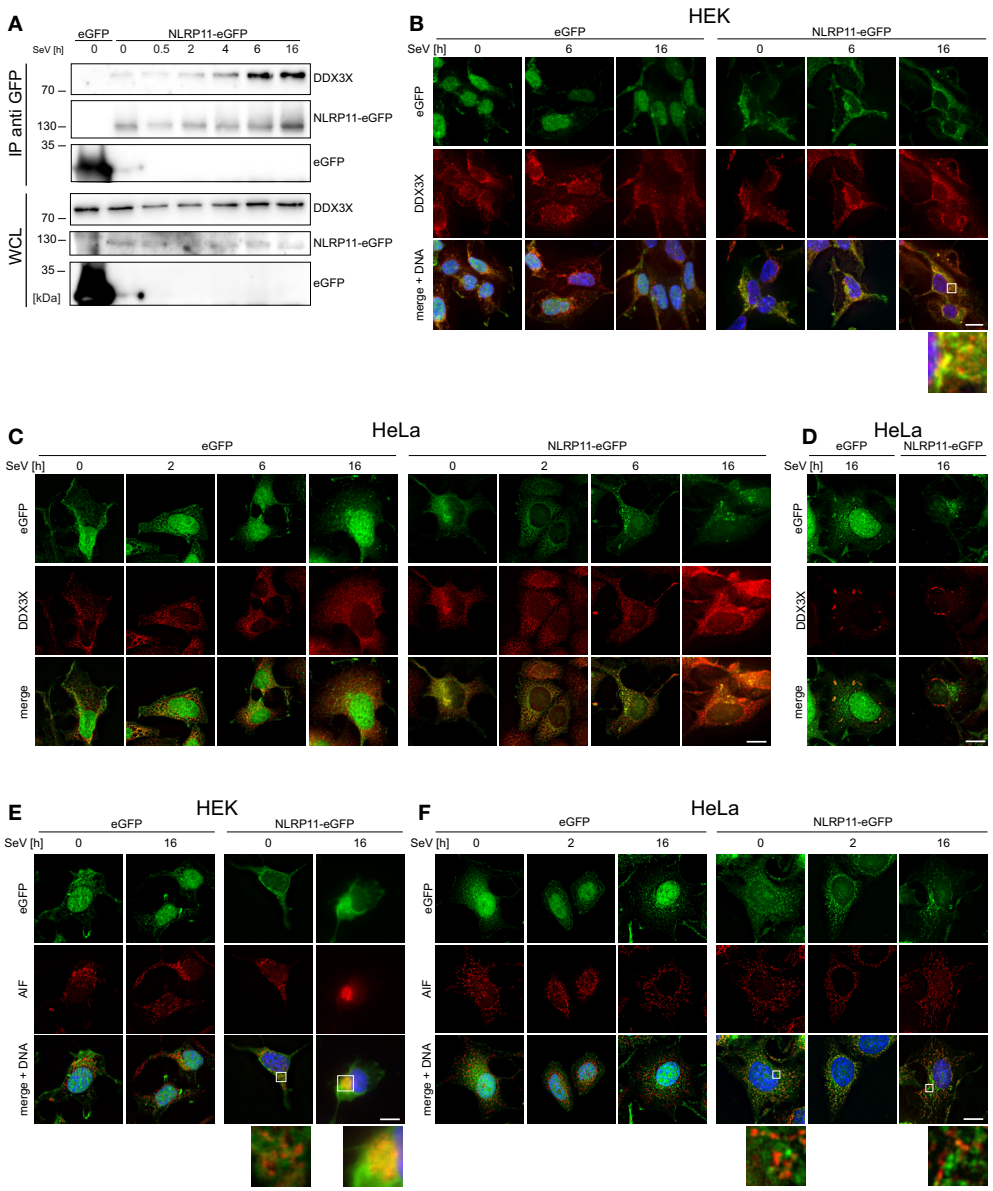

FIGURE 2 | Interaction and co-localization of NLRP11 and DDX3X upon infection. **(A)** Co-immunoprecipitation of NLRP11-eGFP from HEK293-eGFP and HEK293-NLRP11-eGFP cells after induction with doxycycline overnight and infection with SeV for the indicated time. Immunoblots of the IPs and whole cell lysates (WCL) were probed for DDX3X and GFP. The blots are representative of two independent experiments. **(B–F)** Indirect immunofluorescence micrographs of HEK293 **(B, E)**, or HeLa- **(C, D, F)**, eGFP or NLRP11-eGFP cells induced with doxycycline overnight and infected with SeV for the indicated time. 3D deconvolution of DDX3X **(B–D)**, or AIF **(E, F)** staining (red), together with the eGFP signal (green) are shown. Nuclei are stained with Hoechst (blue). Scale bars = 10 µm.

between NLRP11 and DDX3X occurred in the cytosol in proximity to mitochondria.

NLRP11 Prevents the Post-Translational Modification of DDX3X by IKKε

Gu et al. reported that IKKε can phosphorylate DDX3X and that this is a prerequisite for the interaction of DDX3X with IRF3 and subsequent activation of the *Ifnb* promotor (54). We therefore investigated whether NLRP11 influences this posttranslational modification of DDX3X. As shown before, co-expression of IKKε and DDX3X in HEK293T cells induced a change in the electrophoretic mobility of DDX3X, which is indicative of phosphorylation (54). This up-shift of DDX3X was clearly suppressed by co-expression of NLRP11 (**Figure 3A**).

We have previously shown that the ability of NLRP11 to inhibit TBK1-induced IFNβ production is dependent on its LRRs (48). Given that the LRR region also interacted with DDX3 (**Figure 1E**), we tested whether this domain is required and

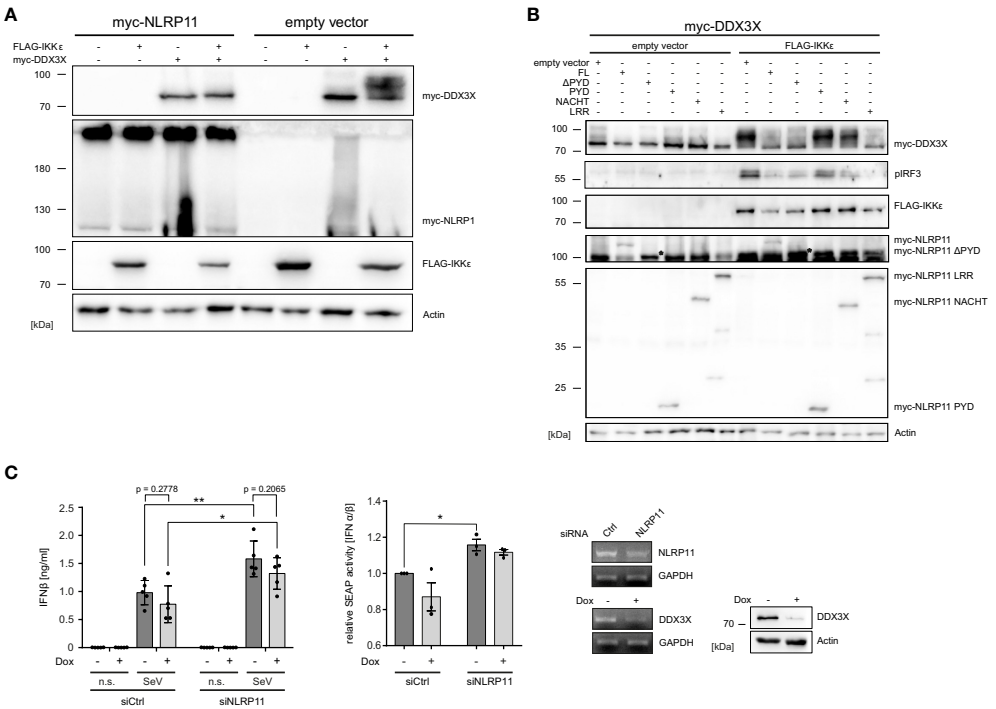

FIGURE 3 | NLRP11 inhibits the phosphorylation of DDX3X by IKKε. **(A, B)** Immunoblot of whole cell lysates from HEK293T cells expressing FLAG-IKKε, myc-DDX3X and either myc-NLRP11 **(A)**, or myc-NLRP11 deletion constructs **(B)** as indicated. Blots were probed for myc, FLAG, pIRF3 and actin as loading control. Representative blots of at least two independent experiments are shown. *, myc-NLRP11 ΔPYD **(C)** IFNβ release from macrophage-like differentiated shDDX3 THP1 cells. DDX3X targeting shRNA was expressed by induction with doxycycline (Dox) for 48 h and NLRP11 was targeted by siRNA transfection for 72 h, as indicated. Cells were infected with SeV for 16 h. IFNβ quantification by ELISA (left graph) and bioassay (right graph) are shown as means ± SEM (IFNβ: n = 5, SEAP: n = 3, ± SEM). *p < 0.05; **p < 0.01 Welch's, two-sided t-test. Knock-down efficiency of NLRP11 and DDX3X was validated by endpoint PCR, and protein levels of DDX3X by immunoblot (upper panels). Immunoblots were probed for DDX3X and actin as loading control. n.s., not stimulated.

sufficient to inhibit IKKε-mediated DDX3X phosphorylation and, consequently, downstream activation of IRF3 (54). Expression of full-length NLRP11, NLRP11-ΔPYD and NLRP11-LRR reduced the IKKε-induced upshift of DDX3X, while this was not observed for the PYD or NACHT domain of NLRP11. Consistent with this data, activation of IRF3, assessed by serine 396 phosphorylation, was also strongly reduced when NLRP11 full length, ΔPYD or the LRRs were expressed (**Figure 3B**).

Next, in order to interrogate the consequences of the DDX3X-NLRP11 interaction on IFNβ induction, we performed siRNA-mediated knock-down of NLRP11 in macrophage-like differentiated human THP1 cells in which DDX3X expression can be suppressed by Tet-inducible expression of a specific short hairpin RNA (shRNA) (THP1 shDDX3X) (64). THP1 cells were used for these experiments because they express higher levels of endogenous NLRP11 and IKKε compared to HeLa and HEK293T cells (48). In accordance with recent data (48, 49), knock-down of NLRP11 led to significantly increased IFNβ production in response to SeV infection (**Figure 3C**). As reported previously (51), shRNA-mediated knock-down of DDX3X had the opposite effect and reduced SeV-induced IFNβ expression (**Figure 3C**). However, DDX3X depletion resulted in a similar ratio of IFNβ reduction compared to control (-Dox) in both siCtrl cells and siNLRP11 treated cells (**Figure 3C**). Qualitatively similar results were obtained when measuring IFNβ activity in a bioassay (**Figure 3C**).

Overall, our data suggest that NLRP11 represses type I interferon responses by affecting IKKε-mediated posttranslational modification of DDX3X.

NLRP11 Counteracts the Effect of DDX3X on NLRP3 Inflammasome Activation

Considering the recent identification of DDX3X as a positive regulator of NLRP3 inflammasome formation (60), we next investigated whether NLRP11 affects DDX3X's function in this context. We previously showed that NLRP11 cannot induce caspase-1 activation itself, nor does NLRP11 recruit the inflammasome adaptor ASC (48), suggesting that NLRP11 does not form a classical inflammasome when ectopically expressed in cells. Instead, we observed a trend towards reduced caspase-1 activation when NLRP11 was overexpressed (48). We therefore now investigated whether NLRP11 interferes with NLRP3 inflammasome activation, conceivably *via* sequestration of DDX3X. In line with the report from the Kanneganti lab (60), DDX3X enhanced nigericin-induced

pro-caspase-1 cleavage, as measured by the iGLuc reporter assay, where a luciferase protein gets activated by caspase-1 cleavage in HEK293T cells (61) (**Figure 4A**). Expression of increasing amounts of myc-NLRP11 did not significantly affect NLRP3 inflammasome activation in the absence of exogenous DDX3X expression but led to a dose-dependent reduction of caspase-1 activation back to baseline levels in DDX3X overexpressing cells (**Figure 4A**).

To determine whether the LRRs of NLRP11 were involved in the negative regulation of the NLRP3 inflammasome, we performed caspase-1 activation assays with our different NLRP11 truncation mutants. Expression of full-length NLRP11

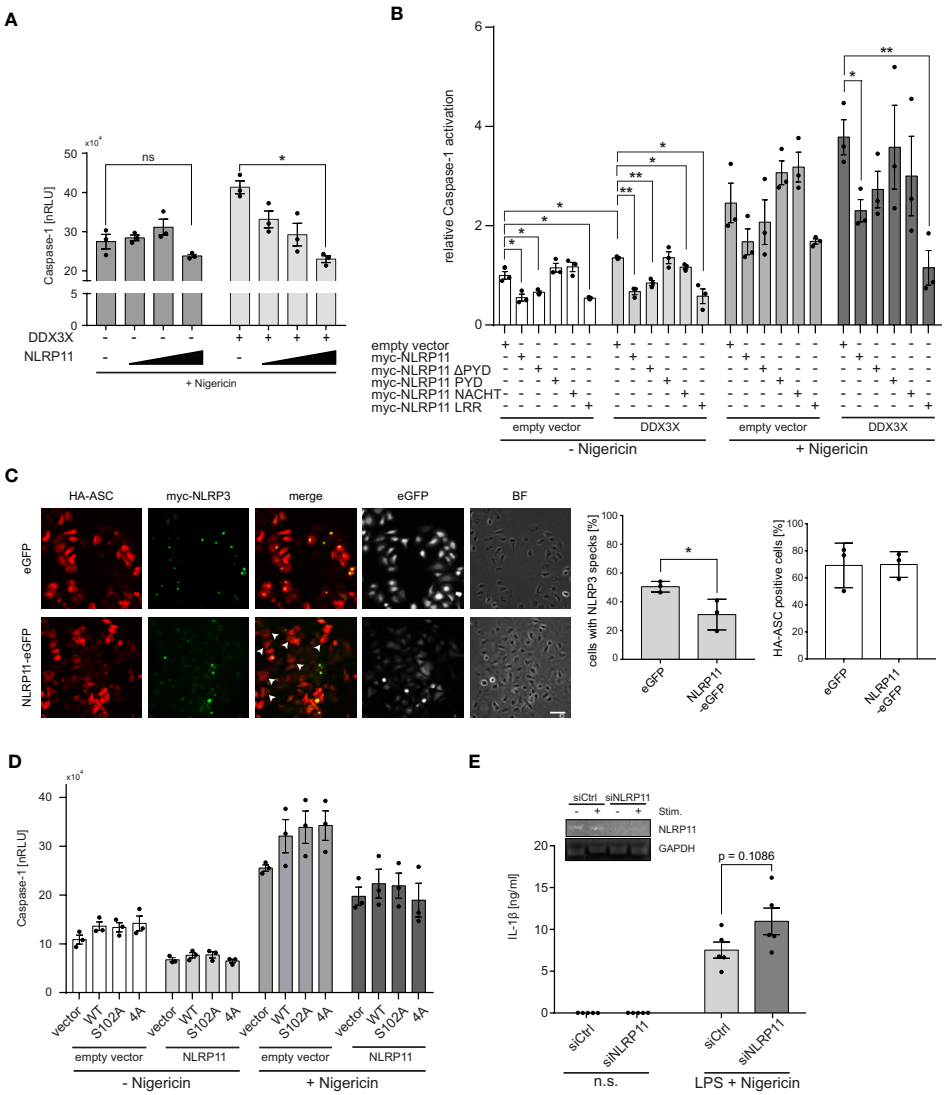

FIGURE 4 | NLRP11 suppresses NLRP3 inflammasome activation by DDX3X. **(A, B)** iGLuc caspase-1 reporter assay in HEK293T cells expressing myc-NLRP3 (15 ng), HA-ASC, and caspase-1 (10 ng each) together with the indicated proteins. Cells were treated with 15 μM nigericin for 3 h. Means of three independent experiments (each conducted in triplicates) ± SEM are shown. *p < 0.05; **p < 0.01 Welch's, two-sided t-test. **(B)**, values relative to the mean of three independent experiments conducted in triplicates of cells, transfected with the reporter plasmid, NLRP3, ASC and caspase-1, not treated with nigericin, are shown. **(C)** Indirect immunofluorescent micrographs of HeLa-eGFP or HeLa-NLRP11-eGFP cells, induced with doxycycline overnight and transfected with HA-ASC and myc-NLRP3. Staining for HA and myc, as well as eGFP-signal is shown. Images representative of three independent experiments are shown. Scale bar = 50 μm. HA-ASC expressing cells without speck-formation are indicated with white arrow heads. Right panels: Quantification of cells with myc-NLRP3 specks and quantification of cells with HA-ASC staining (blinded counting of 150 cells per condition from n = 3). **(D)** iGLuc caspase-1 reporter assay in HEK293T cells expressing myc-NLRP3 (15 ng), HA-ASC, and caspase-1 (10 ng each) together with the indicated proteins. Cells were treated with 15 μM nigericin for 3 h. Means of three independent experiments (each conducted in triplicates) ± SEM are shown. **(E)** IL-1β release from macrophage-like differentiated THP1 cells after 72 h of siRNA-mediated knock-down. Cells were primed for 4 h with 100 ng/ml LPS followed by stimulation with 10 μM nigericin for 2 h. Means of five independent experiments ± SEM are shown. *Inlay:* endpoint PCR for NLRP11 and GAPDH of a representative experiment for validation of knock-down efficiency. n.s., not stimulated.

or the LRRs led to a significant reduction of nigericin-induced caspase-1 activation. The same trend was observed in cells expressing only endogenous DDX3X (**Figures 4A, B**). NLRP11, NLRP11-ΔPYD and NLRP11-LRRs also caused a significant decrease in baseline caspase-1 activity (in the absence of nigericin) both in the presence and absence of exogenous DDX3X (**Figure 4B**). Taken together, this data shows that the LRRs of NLRP11 are both necessary and sufficient to dampen NLRP3 inflammasome activation, which might be a result of DDX3X recruitment and sequestration *via* the LRR domain of NLRP11. To provide further evidence we performed ASC speck-formation assays. When we co-expressed HA-ASC together with myc-NLRP3 in our HeLa cell lines, we found fewer ASC specks in NLRP11-eGFP-expressing cells compared to eGFP-expressing cells that served as control. Quantitative analysis revealed a reduction from about 51% speck-containing cells for HeLa-eGFP cells to about 31% for HeLa-NLRP11-eGFP cells (**Figure 4C**). Equal transfection efficiency of both cell lines was confirmed by blinded counting of HA-ASC positive cells (**Figure 4C**). This data strongly suggests that NLRP11 can inhibit assembly of NLRP3 inflammasomes.

In **Figures 3A, B**, we showed that NLRP11 suppresses IKKε-mediated phosphorylation of DDX3X. We next asked whether this phosphorylation plays a role in the regulation of NLRP3 inflammasome activation by DDX3X. To this end, we performed iGLuc reporter assays with the S102A mutant of DDX3X lacking the IKKε-phosphorylation site shown to be critical for IRF3 recruitment to DDX3X and IFNβ induction. We also tested another DDX3X mutant in which three further IKKε-phosphorylation sites in the N-terminus of DDX3X (S71A, S82A, S83A) are mutated in addition to S102 (54). We did not observe any differences in the capacity of these DDX3X mutants to enhance caspase-1 activation both in presence and absence of NLRP11 expression (**Figure 4D**), suggesting that these DDX3 phosphorylation events do not regulate its effect on inflammasome formation.

Finally, to corroborate a negative regulatory role for NLRP11 in inflammasome induced caspase-1 activation, we knocked down endogenous NLRP11 expression in macrophage-like differentiated THP1 cells using a specific siRNA (48). We first primed the differentiated THP1 cells with LPS and then induced NLRP3 inflammasome activation with nigericin. IL-1β secretion, a well-established read-out for NLRP3 inflammasome activation, was measured. Knock-down of NLRP11 resulted in increased IL-1β secretion (**Figure 4E**), albeit this effect was not significant (p=0.1086).

Taken together, these data provide evidence that NLRP11 can negatively regulate NLRP3 inflammasome activation and suggest that this is mediated via its interaction with DDX3X.

DISCUSSION

Tight control and coordinated resolution of pro-inflammatory signaling pathways is an essential part of the immune response. While insufficient activation of innate immunity might provide pathogens the opportunity to thrive, an overshooting immune response can result in immunopathology. Many control mechanisms have therefore evolved that meticulously regulate the activation level of innate immune responses. We and others previously showed that NLRP11 can act as a negative regulator of antiviral type I IFN expression (48, 49) and NF-κB-dependent pro-inflammatory cytokine responses (47). Here we expand the mechanistical understanding of NLRP11's regulation of antiviral responses by showing that it interacts with and inhibits the DEAD-box protein DDX3X (**Figure 5**). DDX3X has previously been shown to enhance the RIG-I-mediated antiviral response at multiple levels (50–54). Interestingly, other DEAD-box helicases have also been shown to form complexes with NLR family members: In mice, Nlrp9b uses the DEAD-box protein Dhx9 as a sensor for double-stranded RNA to induce inflammasome activation and pyroptosis following infection with dsRNA viruses (71). Dhx15 has also been shown to sense viral RNA and to bind to Nlrp6, mediating its interaction with MAVS (72). Sensing of viral and bacterial RNA by DHX33 has been shown to induce an interaction with NLRP3, enhancing inflammasome formation and caspase-1 activation (73). The latter interaction was shown to be dependent on the NACHT domain of NLRP3. Similarly, the DDX3X interaction with NLRP3 was also mediated by the NACHT domain, resulting in enhanced activation of caspase-1 (60). In contrast, we demonstrated that the interaction between NLRP11 and DDX3X is mediated by the LRRs of NLRP11. This difference in binding domains might explain why some interactions between DExD/H-box proteins and NLR proteins result in increased activation of immune signaling pathways, whereas the interaction we describe here has a negative regulatory effect. The LRR domain of NLRP11 has already been shown to inhibit type I IFN induction upon viral challenge (48, 49). Here we show that the LRR domain is also sufficient to inhibit hyperphosphorylation of DDX3X induced by IKKε (51, 54). This supports our hypothesis that NLRP11's repression of IFN induction is at least partially mediated by targeting DDX3X.

DDX3X is known to positively regulate the RIG-I pathway by interacting with multiple downstream signaling molecules. RIG-I signals *via* its mitochondrial adaptor protein MAVS to induce type I IFN transcription (50). Previously, NLRP11 was shown to be recruited to MAVS *via* its LRRs to modulate TRAF6 function and stability (49). However, no direct physical interaction between NLRP11 and MAVS was shown in this study. This raises the possibility that DDX3X could be involved in mediating this NLRP11-MAVS interaction. In our HEK293-NLRP11-eGFP cell line, we confirmed recruitment of NLRP11 to mitochondria 16 h post infection, as visualized by co-staining with AIF, however, the cellular morphology was heavily disturbed after 16 h of virus infection. The physiological relevance of the change in subcellular localization of NLRP11 in this cell type thus remains elusive.

Surprisingly, NLRP11 knock-down still increased IFNβ induction in DDX3X knock-down cells (**Figures 3C, D**). However, our DDX3X knock-down was only partial as

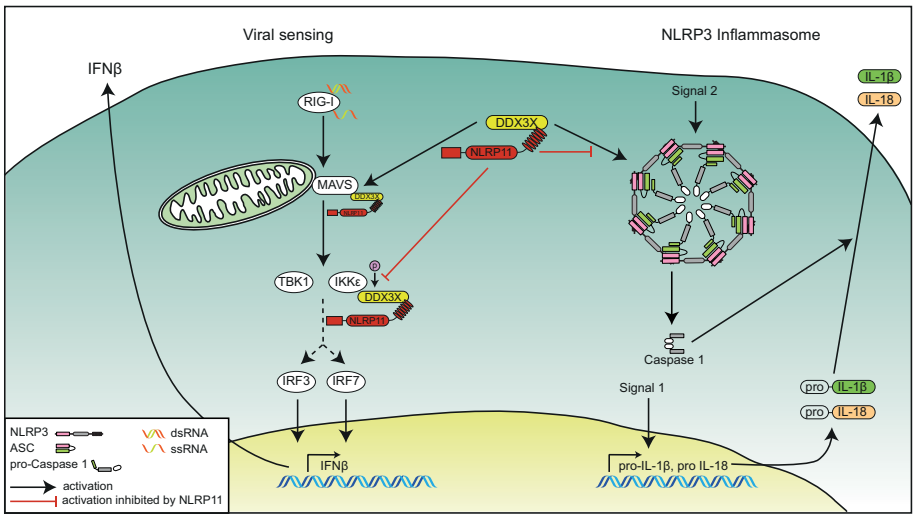

FIGURE 5 | Schematic overview of the functional interplay of DDX3X and NLRP11 in innate immunity. The role of NLRP11 in attenuating RIG-I-induced type I interferon responses (left side) and in the activation of the NLRP3 inflammasome (right side) is depicted. NLRP11 interacts with DDX3X *via* its LRR domain. NLRP11 reduces type I interferon responses downstream of RIG-I activation by negative regulation of the activity of DDX3X in type I interferon induction. NLRP11 can also interfere with DDX3X-mediated NLRP3 inflammasome activation, leading to reduced IL-1β processing.

DDX3X is required for cell viability, and therefore residual DDX3X protein levels might have affected the outcome of this experiment. It is also possible, that the NLRP11-DDX3X interaction more strongly perturbs the function of IKKε in ISG induction (74, 75) than IFNβ induction which is more TBK1-mediated (23, 76). This would explain why NLRP11 interferes with antiviral signaling at multiple steps downstream of RIG-I, enabling it to negatively regulate expression of both IFN (47–49) and ISGs that are directly regulated by IKKε.

In addition to this role in regulating antiviral gene expression, we provide evidence that NLRP11 can act as a negative regulator of the NLRP3 inflammasome. We confirmed that DDX3X is a positive regulator of the NLRP3 inflammasome, as reported recently (60) and show that expression of NLRP11 counteracts this effect of DDX3X. We also observed a trend towards higher IL-1β secretion upon NLRP11 knock-down in macrophage-like differentiated THP1 cells, but the rather low NLRP11 expression levels in THP1 cells (48) might limit the effect of siRNA-mediated knock-down.

The PYD domain of NLRP11 was not required for blocking the DDX3X effect on the NLRP3 inflammasome, instead expression of the NLRP11 LRRs was sufficient. Samir et al. proposed that recruitment of DDX3X by NLRP3 is critical for functional inflammasome formation (60). This is in line with our data, which suggests that NLRP11 binding to DDX3X *via* its LRRs reduces caspase-1 activation. It would be interesting whether this effect results from DDX3X sequestration by NLRP11 or competition between NLRP3 and NLRP11 for binding sites on DDX3X. When overexpressing NLRP11-eGFP in HeLa cells, we did not observe an obvious change in the subcellular localization of endogenous DDX3X, arguing against the sequestration mechanism. Another possibility is that NLRP11 inhibits posttranslational modifications of DDX3X that are important for its involvement in the NLRP3 inflammasome. This hypothesis is based on our finding that the NLRP11 LRRs inhibited the NLRP3 inflammasome and prevented IKKε-mediated hyperphosphorylation of DDX3X. Although we were unable to implicate the phosphorylation sites of DDX3X that are involved in IRF3 activation (54) in its regulatory effect on the NLRP3 inflammasome, it is likely that other DDX3X post-translational modifications could also be affected by NLRP11.

In summary, we show that NLRP11 is an NLR family member that negatively regulates NLRP3 inflammasome activity and interferes with the induction of antiviral type I IFN. For both regulatory effects, we identified a novel role for DDX3X, which we discovered as a novel binding partner of NLRP11, putting a further spotlight on this interesting DEAD-box protein.

DATA AVAILABILITY STATEMENT

The original contributions presented in the study are included in the article/**Supplementary Material**. Further inquiries can be directed to the corresponding author.

AUTHOR CONTRIBUTIONS

IK, SB, and CG performed the experiments and analyzed data. JP performed MS analysis and data interpretation. MS provided reagents. NM provided essential conceptional input and edited

the manuscript. IK, MS, and TK wrote and edited the manuscript and figures. MS and TK conceptualized the study, analyzed data, and assured funding. All authors contributed to the article and approved the submitted version.

FUNDING

IK acknowledges support by the Landesgraduiertenförderung of Baden-Württemberg. Research in the MS laboratory was funded by Science Foundation Ireland and the Irish Health Research Board.

ACKNOWLEDGMENTS

We thank Yvonne Postma for technical assistance with experiments and Camille Vaslin for help with cloning and the characterization of the NLRP11 constructs.

SUPPLEMENTARY MATERIAL

The Supplementary Material for this article can be found online at: https://www.frontiersin.org/articles/10.3389/fimmu.2021.653883/full#supplementary-material

REFERENCES

1. Daffis S, Samuel MA, Keller BC, Gale MJr., Diamond MS. Cell-Specific IRF-3 Responses Protect Against West Nile Virus Infection by Interferon-Dependent and -Independent Mechanisms. *PLoS Pathog* (2007) 3(7):e106. doi: 10.1371/journal.ppat.0030106
2. Chopy D, Detje CN, Lafage M, Kalinke U, Lafon M. The Type I Interferon Response Bridles Rabies Virus Infection and Reduces Pathogenicity. *J Neurovirol* (2011) 17(4):353–67. doi: 10.1007/s13365-011-0041-6
3. Detje CN, Meyer T, Schmidt H, Kreuz D, Rose JK, Bechmann I, et al. Local Type I IFN Receptor Signaling Protects Against Virus Spread Within the Central Nervous System. *J Immunol* (2009) 182(4):2297–304. doi: 10.4049/jimmunol.0800596
4. Schilte C, Couderc T, Chretien F, Sourisseau M, Gangneux N, Guivel-Benhassine F, et al. Type I IFN Controls Chikungunya Virus Via its Action on Nonhematopoietic Cells. *J Exp Med* (2010) 207(2):429–42. doi: 10.1084/jem.20090851
5. Channappanavar R, Fehr AR, Vijay R, Mack M, Zhao J, Meyerholz DK, et al. Dysregulated Type I Interferon and Inflammatory Monocyte-Macrophage Responses Cause Lethal Pneumonia in SARS-CoV-Infected Mice. *Cell Host Microbe* (2016) 19(2):181–93. doi: 10.1016/j.chom.2016.01.007
6. Shepardson KM, Larson K, Johns LL, Stanek K, Cho H, Wellham J, et al. Ifnar2 Is Required for Anti-influenza Immunity and Alters Susceptibility to Post-influenza Bacterial Superinfections. *Front Immunol* (2018) 9:2589. doi: 10.3389/fimmu.2018.02589
7. Sandler NG, Bosinger SE, Estes JD, Zhu RT, Tharp GK, Boritz E, et al. Type I Interferon Responses in Rhesus Macaques Prevent SIV Infection and Slow Disease Progression. *Nature* (2014) 511(7511):601–5. doi: 10.1038/nature13554
8. Channappanavar R, Fehr AR, Zheng J, Wohlford-Lenane C, Abrahante JE, Mack M, et al. IFN-I Response Timing Relative to Virus Replication Determines MERS Coronavirus Infection Outcomes. *J Clin Invest* (2019) 129(9):3625–39. doi: 10.1172/jci126363
9. Rotger M, Dalmau J, Rauch A, McLaren P, Bosinger SE, Martinez R, et al. Comparative Transcriptomics of Extreme Phenotypes of Human HIV-1 Infection and SIV Infection in Sooty Mangabey and Rhesus Macaque. *J Clin Invest* (2011) 121(6):2391–400. doi: 10.1172/jci45235
10. Chi B, Dickensheets HL, Spann KM, Alston MA, Luongo C, Dumoutier L, et al. Alpha and Lambda Interferon Together Mediate Suppression of CD4 T Cells Induced by Respiratory Syncytial Virus. *J Virol* (2006) 80(10):5032–40. doi: 10.1128/jvi.80.10.5032-5040.2006
11. Acharya D, Liu G, Gack MU. Dysregulation of Type I Interferon Responses in COVID-19. *Nat Rev Immunol* (2020) 20(7):397–8. doi: 10.1038/s41577-020-0346-x
12. Jamilloux Y, Henry T, Belot A, Viel S, Fauter M, El Jammal T, et al. Should We Stimulate or Suppress Immune Responses in COVID-19? Cytokine and Anti-Cytokine Interventions. *Autoimmun Rev* (2020) 19(7):102567. doi: 10.1016/j.autrev.2020.102567
13. Rehwinkel J, Gack MU. Rig-I-like Receptors: Their Regulation and Roles in RNA Sensing. *Nat Rev Immunol* (2020) 20(9):537–51. doi: 10.1038/s41577-020-0288-3
14. Hou F, Sun L, Zheng H, Skaug B, Jiang QX, Chen ZJ. MAVS Forms Functional Prion-Like Aggregates to Activate and Propagate Antiviral Innate Immune Response. *Cell* (2011) 146(3):448–61. doi: 10.1016/j.cell.2011.06.041
15. Lad SP, Yang G, Scott DA, Chao TH, Correia Jda S, de la Torre JC, et al. Identification of MAVS Splicing Variants That Interfere With RIGI/MAVS Pathway Signaling. *Mol Immunol* (2008) 45(8):2277–87. doi: 10.1016/j.molimm.2007.11.018
16. Xu LG, Wang YY, Han KJ, Li LY, Zhai Z, Shu HB. VISA is an Adapter Protein Required for Virus-Triggered IFN-beta Signaling. *Mol Cell* (2005) 19(6):727–40. doi: 10.1016/j.molcel.2005.08.014
17. Saha SK, Pietras EM, He JQ, Kang JR, Liu SY, Oganesyan G, et al. Regulation of Antiviral Responses by a Direct and Specific Interaction Between TRAF3 and Cardif. *EMBO J* (2006) 25(14):3257–63. doi: 10.1038/sj.emboj.7601220
18. Au WC, Moore PA, Lowther W, Juang YT, Pitha PM. Identification of a Member of the Interferon Regulatory Factor Family That Binds to the Interferon-Stimulated Response Element and Activates Expression of Interferon-Induced Genes. *Proc Natl Acad Sci USA* (1995) 92(25):11657–61. doi: 10.1073/pnas.92.25.11657
19. Juang YT, Lowther W, Kellum M, Au WC, Lin R, Hiscott J, et al. Primary Activation of Interferon A and Interferon B Gene Transcription by Interferon Regulatory Factor 3. *Proc Natl Acad Sci USA* (1998) 95(17):9837–42. doi: 10.1073/pnas.95.17.9837
20. Lin R, Heylbroeck C, Pitha PM, Hiscott J. Virus-Dependent Phosphorylation of the IRF-3 Transcription Factor Regulates Nuclear Translocation, Transactivation Potential, and Proteasome-Mediated Degradation. *Mol Cell Biol* (1998) 18(5):2986–96. doi: 10.1128/mcb.18.5.2986
21. Au WC, Moore PA, LaFleur DW, Tombal B, Pitha PM. Characterization of the Interferon Regulatory Factor-7 and its Potential Role in the Transcription Activation of Interferon A Genes. *J Biol Chem* (1998) 273(44):29210–7. doi: 10.1074/jbc.273.44.29210
22. Fitzgerald KA, McWhirter SM, Faia KL, Rowe DC, Latz E, Golenbock DT, et al. Ikkepsilon and TBK1 are Essential Components of the IRF3 Signaling Pathway. *Nat Immunol* (2003) 4(5):491–6. doi: 10.1038/ni921
23. Hemmi H, Takeuchi O, Sato S, Yamamoto M, Kaisho T, Sanjo H, et al. The Roles of Two IkappaB Kinase-Related Kinases in Lipopolysaccharide and Double Stranded RNA Signaling and Viral Infection. *J Exp Med* (2004) 199(12):1641–50. doi: 10.1084/jem.20040520
24. Hiscott J. Convergence of the NF-kappaB and IRF Pathways in the Regulation of the Innate Antiviral Response. *Cytokine Growth factor Rev* (2007) 18(5-6):483–90. doi: 10.1016/j.cytogfr.2007.06.002
25. Liwinski T, Zheng D, Elinav E. The Microbiome and Cytosolic Innate Immune Receptors. *Immunol Rev* (2020) 297(1):207–24. doi: 10.1111/imr.12901
26. Ting JP, Davis BK. CATERPILLER: A Novel Gene Family Important in Immunity, Cell Death, and Diseases. *Annu Rev Immunol* (2005) 23:387–414. doi: 10.1146/annurev.immunol.23.021704.115616
27. Girardin SE, Boneca IG, Carneiro LA, Antignac A, Jehanno M, Viala J, et al. Nod1 Detects a Unique Muropeptide From Gram-Negative Bacterial Peptidoglycan. *Science* (2003) 300(5625):1584–7. doi: 10.1126/science.1084677
28. Girardin SE, Boneca IG, Viala J, Chamaillard M, Labigne A, Thomas G, et al. Nod2 is a General Sensor of Peptidoglycan Through Muramyl Dipeptide

(MDP) Detection. *J Biol Chem* (2003) 278(11):8869–72. doi: 10.1074/jbc.C200651200
29. Inohara N, Koseki T, del Peso L, Hu Y, Yee C, Chen S, et al. Nod1, an Apaf-1-like Activator of Caspase-9 and Nuclear Factor-Kappab. *J Biol Chem* (1999) 274(21):14560–7. doi: 10.1074/jbc.274.21.14560
30. Srinivasula SM, Poyet JL, Razmara M, Datta P, Zhang Z, Alnemri ES. The PYRIN-CARD Protein ASC is an Activating Adaptor for Caspase-1. *J Biol Chem* (2002) 277(24):21119–22. doi: 10.1074/jbc.C200179200
31. Martinon F, Burns K, Tschopp J. The Inflammasome: A Molecular Platform Triggering Activation of Inflammatory Caspases and Processing of Proil-Beta. *Mol Cell* (2002) 10(2):417–26. doi: 10.1016/s1097-2765(02)00599-3
32. Sutterwala FS, Mijares LA, Li L, Ogura Y, Kazmierczak BI, Flavell RA. Immune Recognition of Pseudomonas Aeruginosa Mediated by the IPAF/NLRC4 Inflammasome. *J Exp Med* (2007) 204(13):3235–45. doi: 10.1084/jem.20071239
33. Grenier JM, Wang L, Manji GA, Huang WJ, Al-Garawi A, Kelly R, et al. Functional Screening of Five PYPAF Family Members Identifies PYPAF5 as a Novel Regulator of NF-kappaB and Caspase-1. *FEBS Lett* (2002) 530(1-3):73–8. doi: 10.1016/s0014-5793(02)03416-6
34. Wang L, Manji GA, Grenier JM, Al-Garawi A, Merriam S, Lora JM, et al. PYPAF7, a Novel PYRIN-containing Apaf1-like Protein That Regulates Activation of NF-Kappa B and caspase-1-dependent Cytokine Processing. *J Biol Chem* (2002) 277(33):29874–80. doi: 10.1074/jbc.M203915200
35. Khare S, Dorfleutner A, Bryan NB, Yun C, Radian AD, de Almeida L, et al. An NLRP7-containing Inflammasome Mediates Recognition of Microbial Lipopeptides in Human Macrophages. *Immunity* (2012) 36(3):464–76. doi: 10.1016/j.immuni.2012.02.001
36. Davis BK, Roberts RA, Huang MT, Willingham SB, Conti BJ, Brickey WJ, et al. Cutting Edge: NLRC5-dependent Activation of the Inflammasome. *J Immunol* (2011) 186(3):1333–7. doi: 10.4049/jimmunol.1003111
37. Steimle V, Otten LA, Zufferey M, Mach B. Complementation Cloning of an MHC Class II Transactivator Mutated in Hereditary MHC Class II Deficiency (or Bare Lymphocyte Syndrome). *Cell* (1993) 75(1):135–46. doi: 10.1016/S0092-8674(05)80090-X
38. Meissner TB, Li A, Biswas A, Lee KH, Liu YJ, Bayir E, et al. NLR Family Member NLRC5 is a Transcriptional Regulator of MHC Class I Genes. *Proc Natl Acad Sci U S A* (2010) 107(31):13794–9. doi: 10.1073/pnas.1008684107
39. Zhang L, Mo J, Swanson KV, Wen H, Petrucelli A, Gregory SM, et al. NLRC3, a Member of the NLR Family of Proteins, is a Negative Regulator of Innate Immune Signaling Induced by the DNA Sensor STING. *Immunity* (2014) 40(3):329–41. doi: 10.1016/j.immuni.2014.01.010
40. Charoenthongtrakul S, Gao L, Harhaj EW. The NLRP4-DTX4 Axis: A Key Suppressor of TBK1 and Innate Antiviral Signaling. *Cell Mol Immunol* (2012) 9(6):431–3. doi: 10.1038/cmi.2012.49
41. Cui J, Li Y, Zhu L, Liu D, Songyang Z, Wang HY, et al. NLRP4 Negatively Regulates Type I Interferon Signaling by Targeting the Kinase TBK1 for Degradation Via the Ubiquitin Ligase DTX4. *Nat Immunol* (2012) 13(4):387–95. doi: 10.1038/ni.2239
42. Lin M, Zhao Z, Yang Z, Meng Q, Tan P, Xie W, et al. Usp38 Inhibits Type I Interferon Signaling by Editing Tbk1 Ubiquitination Through NLRP4 Signalosome. *Mol Cell* (2016) 64(2):267–81. doi: 10.1016/j.molcel.2016.08.029
43. Chen ST, Chen L, Lin DS, Chen SY, Tsao YP, Guo H, et al. Nlrp12 Regulates Anti-Viral RIG-I Activation Via Interaction With TRIM25. *Cell Host Microbe* (2019) 25(4):602–16.e7. doi: 10.1016/j.chom.2019.02.013
44. Normand S, Waldschmitt N, Neerincx A, Martinez-Torres RJ, Chauvin C, Couturier-Maillard A, et al. Proteasomal Degradation of NOD2 by NLRP12 in Monocytes Promotes Bacterial Tolerance and Colonization by Enteropathogens. *Nat Commun* (2018) 9(1):5338. doi: 10.1038/s41467-018-07750-5
45. Abe T, Lee A, Sitharam R, Kesner J, Rabadan R, Shapira SD. Germ-Cell-Specific Inflammasome Component NLRP14 Negatively Regulates Cytosolic Nucleic Acid Sensing to Promote Fertilization. *Immunity* (2017) 46(4):621–34. doi: 10.1016/j.immuni.2017.03.020
46. Kienes I, Weidl T, Mirza N, Chamaillard M, Kufer TA. Role of NLRs in the Regulation of Type I Interferon Signaling, Host Defense and Tolerance to Inflammation. *Int J Mol Sci* (2021) 22(3):1301. doi: 10.3390/ijms22031301
47. Wu C, Su Z, Lin M, Ou J, Zhao W, Cui J, et al. NLRP11 Attenuates Toll-like Receptor Signalling by Targeting TRAF6 for Degradation Via the Ubiquitin Ligase RNF19A. *Nat Commun* (2017) 8(1):1977. doi: 10.1038/s41467-017-02073-3
48. Ellwanger K, Becker E, Kienes I, Sowa A, Postma Y, Cardona Gloria Y, et al. The NLR Family Pyrin Domain-Containing 11 Protein Contributes to the Regulation of Inflammatory Signaling. *J Biol Chem* (2018) 293(8):2701–10. doi: 10.1074/jbc.RA117.000152
49. Qin Y, Su Z, Wu Y, Wu C, Jin S, Xie W, et al. NLRP11 Disrupts MAVS Signalosome to Inhibit Type I Interferon Signaling and Virus-Induced Apoptosis. *EMBO Rep* (2017) 18(12):2160–71. doi: 10.15252/embr.201744480
50. Oshiumi H, Sakai K, Matsumoto M, Seya T. Dead/H BOX 3 (DDX3) Helicase Binds the RIG-I Adaptor IPS-1 to Up-Regulate IFN-beta-inducing Potential. *Eur J Immunol* (2010) 40(4):940–8. doi: 10.1002/eji.200940203
51. Schroder M, Baran M, Bowie AG. Viral Targeting of DEAD Box Protein 3 Reveals its Role in TBK1/IKKepsilon-mediated IRF Activation. *EMBO J* (2008) 27(15):2147–57. doi: 10.1038/emboj.2008.143
52. Soulat D, Burckstummer T, Westermayer S, Goncalves A, Bauch A, Stefanovic A, et al. The DEAD-box Helicase DDX3X is a Critical Component of the TANK-binding Kinase 1-Dependent Innate Immune Response. *EMBO J* (2008) 27(15):2135–46. doi: 10.1038/emboj.2008.126
53. Gu L, Fullam A, McCormack N, Höhn Y, Schröder M. DDX3 Directly Regulates TRAF3 Ubiquitination and Acts as a Scaffold to Co-Ordinate Assembly of Signalling Complexes Downstream From MAVS. *Biochem J* (2017) 474(4):571–87. doi: 10.1042/bcj20160956
54. Gu L, Fullam A, Brennan R, Schröder M. Human DEAD Box Helicase 3 Couples Iκb Kinase ϵ to Interferon Regulatory Factor 3 Activation. *Mol Cell Biol* (2013) 33(10):2004–15. doi: 10.1128/mcb.01603-12
55. Kalverda AP, Thompson GS, Vogel A, Schröder M, Bowie AG, Khan AR, et al. Poxvirus K7 Protein Adopts a Bcl-2 Fold: Biochemical Mapping of its Interactions With Human DEAD Box RNA Helicase DDX3. *J Mol Biol* (2009) 385(3):843–53. doi: 10.1016/j.jmb.2008.09.048
56. Oda S, Schröder M, Khan AR. Structural Basis for Targeting of Human RNA Helicase DDX3 by Poxvirus Protein K7. *Structure* (2009) 17(11):1528–37. doi: 10.1016/j.str.2009.09.005
57. Wang H, Ryu WS. Hepatitis B Virus Polymerase Blocks Pattern Recognition Receptor Signaling Via Interaction With DDX3: Implications for Immune Evasion. *PLoS Pathog* (2010) 6(7):e1000986. doi: 10.1371/journal.ppat.1000986
58. Yu S, Chen J, Wu M, Chen H, Kato N, Yuan Z. Hepatitis B Virus Polymerase Inhibits RIG-I- and Toll-like Receptor 3-Mediated Beta Interferon Induction in Human Hepatocytes Through Interference With Interferon Regulatory Factor 3 Activation and Dampening of the Interaction Between TBK1/IKKepsilon and DDX3. *J Gen Virol* (2010) 91(Pt 8):2080–90. doi: 10.1099/vir.0.020552-0
59. Park ES, Byun YH, Park S, Jang YH, Han WR, Won J, et al. Co-Degradation of Interferon Signaling Factor DDX3 by PB1-F2 as a Basis for High Virulence of 1918 Pandemic Influenza. *EMBO J* (2019) 38(10):e99475. doi: 10.15252/embj.201899475
60. Samir P, Kesavardhana S, Patmore DM, Gingras S, Malireddi RKS, Karki R, et al. DDX3X Acts as a Live-or-Die Checkpoint in Stressed Cells by Regulating NLRP3 Inflammasome. *Nature* (2019) 573(7775):590–4. doi: 10.1038/s41586-019-1551-2
61. Bartok E, Bauernfeind F, Khaminets MG, Jakobs C, Monks B, Fitzgerald KA, et al. iGLuc: A Luciferase-Based Inflammasome and Protease Activity Reporter. *Nat Methods* (2013) 10(2):147–54. doi: 10.1038/nmeth.2327
62. Hornung V, Ablasser A, Charrel-Dennis M, Bauernfeind F, Horvath G, Caffrey DR, et al. AIM2 Recognizes Cytosolic dsDNA and Forms a caspase-1-activating Inflammasome With ASC. *Nature* (2009) 458(7237):514–8. doi: 10.1038/nature07725
63. Sharma S, tenOever BR, Grandvaux N, Zhou GP, Lin R, Hiscott J. Triggering the Interferon Antiviral Response Through an IKK-related Pathway. *Science* (2003) 300(5622):1148–51. doi: 10.1126/science.1081315
64. Fullam A, Gu L, Höhn Y, Schröder M. DDX3 Directly Facilitates Ikkα Activation and Regulates Downstream Signalling Pathways. *Biochem J* (2018) 475(22):3595–607. doi: 10.1042/bcj20180163
65. Neerincx A, Lautz K, Menning M, Kremmer E, Zigrino P, Hösel M, et al. A Role for the Human Nucleotide-Binding Domain, Leucine-Rich Repeat-Containing Family Member NLRC5 in Antiviral Responses. *J Biol Chem* (2010) 285(34):26223–32. doi: 10.1074/jbc.M110.109736
66. UniProt Consortium T. UniProt: The Universal Protein Knowledgebase. *Nucleic Acids Res* (2018) 46(5):2699. doi: 10.1093/nar/gky092

67. Keller A, Nesvizhskii AI, Kolker E, Aebersold R. Empirical Statistical Model to Estimate the Accuracy of Peptide Identifications Made by MS/MS and Database Search. *Anal Chem* (2002) 74(20):5383–92. doi: 10.1021/ac025747h
68. Szappanos D, Tschismarov R, Perlot T, Westermayer S, Fischer K, Platanitis E, et al. The RNA Helicase DDX3X is an Essential Mediator of Innate Antimicrobial Immunity. *PLoS Pathog* (2018) 14(11):e1007397. doi: 10.1371/journal.ppat.1007397
69. Pene V, Li Q, Sodroski C, Hsu CS, Liang TJ. Dynamic Interaction of Stress Granules, DDX3X, and IKK-alpha Mediates Multiple Functions in Hepatitis C Virus Infection. *J Virol* (2015) 89(10):5462–77. doi: 10.1128/JVI.03197-14
70. Shih JW, Wang WT, Tsai TY, Kuo CY, Li HK, Wu Lee YH. Critical Roles of RNA Helicase DDX3 and its Interactions With eIF4E/PABP1 in Stress Granule Assembly and Stress Response. *Biochem J* (2012) 441(1):119–29. doi: 10.1042/BJ20110739
71. Zhu S, Ding S, Wang P, Wei Z, Pan W, Palm NW, et al. Nlrp9b Inflammasome Restricts Rotavirus Infection in Intestinal Epithelial Cells. *Nature* (2017) 546(7660):667–70. doi: 10.1038/nature22967
72. Wang P, Zhu S, Yang L, Cui S, Pan W, Jackson R, et al. Nlrp6 Regulates Intestinal Antiviral Innate Immunity. *Science* (2015) 350(6262):826–30. doi: 10.1126/science.aab3145
73. Mitoma H, Hanabuchi S, Kim T, Bao M, Zhang Z, Sugimoto N, et al. The DHX33 RNA Helicase Senses Cytosolic RNA and Activates the NLRP3 Inflammasome. *Immunity* (2013) 39(1):123–35. doi: 10.1016/j.immuni.2013.07.001
74. Matsui K, Kumagai Y, Kato H, Sato S, Kawagoe T, Uematsu S, et al. Cutting Edge: Role of TANK-binding Kinase 1 and Inducible IkappaB Kinase in IFN Responses Against Viruses in Innate Immune Cells. *J Immunol* (2006) 177 (9):5785–9. doi: 10.4049/jimmunol.177.9.5785
75. Tenoever BR, Ng SL, Chua MA, McWhirter SM, García-Sastre A, Maniatis T. Multiple Functions of the IKK-related Kinase IKKepsilon in Interferon-Mediated Antiviral Immunity. *Science* (2007) 315(5816):1274–8. doi: 10.1126/science.1136567
76. Perry AK, Chow EK, Goodnough JB, Yeh WC, Cheng G. Differential Requirement for TANK-binding Kinase-1 in Type I Interferon Responses to Toll-Like Receptor Activation and Viral Infection. *J Exp Med* (2004) 199 (12):1651–8. doi: 10.1084/jem.20040528

Conflict of Interest: The authors declare that the research was conducted in the absence of any commercial or financial relationships that could be construed as a potential conflict of interest.

frontiers in Immunology

ORIGINAL RESEARCH
published: 28 May 2021
doi: 10.3389/fimmu.2021.683803

NLRP3 Inflammasome Assembly in Neutrophils Is Supported by PAD4 and Promotes NETosis Under Sterile Conditions

*Patrick Münzer[1,2,3,4], Roberto Negro[1,5], Shoichi Fukui[1,2], Lucas di Meglio[1,4,6], Karen Aymonnier[1,2,4], Long Chu[1,2], Deya Cherpokova[1,2], Sarah Gutch[1,2], Nicoletta Sorvillo[1,2], Lai Shi[1,2], Venkat Giri Magupalli[1,5], Alexander N. R. Weber[7], Rüdiger E. Scharf[1,2,8], Clare M. Waterman[4,9], Hao Wu[1,5] and Denisa D. Wagner[1,2,4,10]**

[1] Program in Cellular and Molecular Medicine, Boston Children's Hospital, Boston, MA, United States, [2] Department of Pediatrics, Harvard Medical School, Boston, MA, United States, [3] Department of Cardiology and Angiology, University of Tübingen, Tübingen, Germany, [4] Whitman Center, Marine Biological Laboratory, Woods Hole, MA, United States, [5] Department of Biological Chemistry and Molecular Pharmacology, Harvard Medical School, Boston, MA, United States, [6] Laboratory of Vascular Translational Science, U1148 INSERM University of Paris, Paris, France, [7] Department of Immunology, Interfaculty Institute of Cell Biology, University of Tübingen, Tübingen, Germany, [8] Division of Experimental and Clinical Hemostasis, Hemotherapy, and Transfusion Medicine, and Hemophilia Comprehensive Care Center, Institute of Transplantation Diagnostics and Cell Therapy, Heinrich Heine University Medical Center, Düsseldorf, Germany, [9] Cell Biology and Physiology Center, National Heart, Lung, and Blood Institute of the National Institutes of Health, Bethesda, MD, United States, [10] Division of Hematology/Oncology, Boston Children's Hospital, Boston, MA, United States

Neutrophil extracellular trap formation (NETosis) and the NLR family pyrin domain containing 3 (NLRP3) inflammasome assembly are associated with a similar spectrum of human disorders. While NETosis is known to be regulated by peptidylarginine deiminase 4 (PAD4), the role of the NLRP3 inflammasome in NETosis was not addressed. Here, we establish that under sterile conditions the cannonical NLRP3 inflammasome participates in NETosis. We show apoptosis-associated speck-like protein containing a CARD (ASC) speck assembly and caspase-1 cleavage in stimulated mouse neutrophils without LPS priming. PAD4 was needed for optimal NLRP3 inflammasome assembly by regulating NLRP3 and ASC protein levels post-transcriptionally. Genetic ablation of NLRP3 signaling resulted in impaired NET formation, because NLRP3 supported both nuclear envelope and plasma membrane rupture. Pharmacological inhibition of NLRP3 in either mouse or human neutrophils also diminished NETosis. Finally, NLRP3 deficiency resulted in a lower density of NETs in thrombi produced by a stenosis-induced mouse model of deep vein thrombosis. Altogether, our results indicate a PAD4-dependent formation of the NLRP3 inflammasome in neutrophils and implicate NLRP3 in NETosis under noninfectious conditions *in vitro* and *in vivo*.

Keywords: Neutrophils, NETs, NLRP3 inflammasome, MCC950, deep vein thrombosis, PAD4

OPEN ACCESS

Edited by:
Chaofeng Han, Second Military Medical University, China

Reviewed by:
Kaiwen Chen, National University of Singapore, Singapore
Jia-feng Wang, Second Military Medical University, China

***Correspondence:**
Denisa D. Wagner
denisa.wagner@childrens.harvard.edu

Specialty section:
This article was submitted to Molecular Innate Immunity, a section of the journal Frontiers in Immunology

Received: *22 March 2021*
Accepted: *10 May 2021*
Published: *28 May 2021*

Citation:
Münzer P, Negro R, Fukui S, di Meglio L, Aymonnier K, Chu L, Cherpokova D, Gutch S, Sorvillo N, Shi L, Magupalli VG, Weber ANR, Scharf RE, Waterman CM, Wu H and Wagner DD (2021) NLRP3 Inflammasome Assembly in Neutrophils Is Supported by PAD4 and Promotes NETosis Under Sterile Conditions. Front. Immunol. 12:683803. doi: 10.3389/fimmu.2021.683803

INTRODUCTION

Initially described as part of the innate immune response to microbes (1), there is now increasing evidence that neutrophil extracellular traps (NETs) are produced under sterile conditions. They are implicated in a wide variety of inflammatory, (auto) immune, and thrombo-occlusive disorders. In particular, NETs are known to foster thrombosis (2, 3), contribute to ischemia/reperfusion injury (4), and age-related tissue fibrosis (5). NETs also likely contribute to the severe side effects of a COVID-19 infection (6). Moreover, NET formation is stimulated by diseases, such as diabetes (7) and cancer (8), and contributes to cancer progression (9, 10).

NETs are decondensed chromatin meshworks ejected by neutrophils upon inflammatory stimulation or hypoxia. A key characteristic of the extracellular neutrophil chromatin is the inclusion of pro-thrombotic, pro-inflammatory, and cytotoxic components, in particular histones and microbicidal proteases (3, 11). While the clinical relevance of NETs is recognized, the underlying cellular mechanisms of their induction are poorly defined. Recently, NET formation (NETosis) was determined to be a well-orchestrated sequence of cellular events, including disassembly of the cellular cytoskeletons, endomembrane fragmentation, nuclear rounding, plasma membrane permeabilization, and finally nuclear and plasma membrane rupture (12).

A major prerequisite for NETosis is the peptidylarginine deiminase 4 (PAD4)-dependent post-translational modification of histones (13, 14). In general, PAD enzymes are calcium-dependent enzymes which deiminate the positively charged arginine residue of proteins, thus transforming arginine to a neutral citrulline. PAD4 is mainly expressed in granulocytes and transferred into an enzymatic active conformation upon calcium binding. Moreover, since PAD4 is the only PAD isoform that contains a nuclear localization sequence, it is required for nuclear histone citrullination (12, 15). During the course of NETosis, it is thought that citrullination of histones reduces their DNA/histone binding ability which causes chromatin decondensation and subsequently culminates in chromatin expulsion.

Effective inducers of NETosis *in vitro* are the calcium ionophore ionomycin, the protein kinase C activator phorbol 12-myristate 13-acetate (PMA), and the potassium ionophore nigericin (16, 17). Interestingly, nigericin is widely used in macrophages to induce assembly of the NLR family pyrin domain containing 3 (NLRP3) inflammasome, which is also expressed in neutrophils (18, 19). In neutrophils the NLRP3 inflammasome was found to be activated after bacterial infection (20, 21) or after lipopolysaccharide (LPS) pretreatment with subsequent ATP stimulation (22). In addition, an activating mutation (A352V) in NLRP3 leading to Muckle Wells syndrome is associated with excessive neutrophil granule exocytosis (23) and a gain-of-function mutation in NLRP3, which results in Familial Mediterranean Fever (FMF) is subsequently linked to augmented NETosis (24, 25).

Inflammasomes are multiprotein signaling platforms, described mainly in macrophages, that mediate pivotal responses of innate immunity after activation by pathogen- and danger-associated molecular patterns (PAMPs and DAMPs). The most prominent and best studied inflammasome is NLRP3 (26, 27). Assembly of the NLRP3 inflammasome in macrophages *in vitro* requires a two-step mechanism. First, protein expression levels of NLRP3 have to be increased transcriptionally by priming macrophages with lipopolysaccharide (LPS) and, second, subsequent stimulation for example with pore-forming toxins (nigericin), results in a prominent NIMA (never in mitosis gene a)-related kinase 7 (NEK7)-dependent oligomerization of NLRP3 (28, 29). Successively, apoptosis-associated speck-like protein containing a CARD (ASC) is recruited, polymerized, and crosslinked with pro-caspase-1 leading to the formation of a macromolecular multiprotein structure designated ASC speck (30). ASC speck formation results in activation of caspase-1 (31), which in turn allows processing of the pro-inflammatory cytokines IL-1ß and IL-18, as well as the pore-forming protein gasdermin D (GSDMD) (32). Specific inhibition by the small molecule MCC950, an established NLRP3 inhibitor that binds to NLRP3 (33), results in impaired ATP hydrolysis with a subsequent blockade of NLRP3 inflammasome formation (34, 35).

Interestingly, neutrophils also have been described as a source of NLRP3/ASC-dependent IL-1ß production after *Staphylococcus aureus* infection (36). NLRP3-linked disorders, like hypoxia-induced venous thromboembolism (37), atherosclerosis (27), and tissue damage after ischemia/reperfusion (38) have an inflammatory thrombo-occlusive pathology in common that is associated with PAD4 and NETosis. So far, NLRP3 assembly and ASC speck formation have been described in neutrophils only after pathogen-induced infections (19, 20) or in the presence of LPS (22). Nothing is known about NLRP3 inflammasome assembly in neutrophils in sterile inflammation or their potential role in NETosis.

Here, we demonstrate that the formation of the NLRP3 inflammasome supports NETosis in the absence of LPS both *in vitro* and *in vivo*, and that PAD4, in addition to its known role in chromatin decondensation, also regulates NLRP3 inflammasome assembly in neutrophils. Our studies provide an important link between NETosis and the NLRP3 inflammasome, explaining, at least in part, the overlapping features of disorders in which both components are involved.

MATERIALS AND METHODS

Materials

A detailed list of used material and corresponding ordering informations can be found in the **Supplementary Informations**.

Animals

Nlrp3$^{-/-}$ (stock no. #021302) and corresponding wild-type (C57BL/6J; stock no. #000664) mice were obtained from Jackson Laboratory (Bar Harbor, ME, USA). *Padi4*$^{-/-}$ mice were originally generated by Y. Wang (13) and back-crossed with C57BL/6J in the Wagner laboratory. All mouse lines were housed in the animal facility of Boston Children's Hospital.

Padi4$^{fl/fl}$ mice (stock no. #026708), previously described by Hemmers and colleagues (39), and *Vav1-iCre* mice (stock no #008610) were purchased from Jackson Laboratory and intercrossed by the Wagner laboratory to generate mice lacking PAD4, specifically in the hematopoietic lineage (*Padi4*$^{Vav1Cre/+}$). ASC-deficient mice (C57BL/6J background) used for antibody validation were a kind gift of A. Yazdi (Aachen University, Germany) and were previously described (40). All offsprings were housed in the according institutional animal facility, and mice of both sexes were randomly assigned for experiments. Data analysis was blinded to the identity of the sample.

All experimental animal procedures in this study were approved by the Institutional Animal Care and Use Committee of Boston Children's Hospital under the protocol numbers 20-01-4096R or 20-02-4097R or the Regierungspräsidium Tübingen and were performed under the ARRIVE guidelines.

Flow Restriction Model (DVT)

Flow restriction of the inferior vena cava (IVC) was performed as described elsewhere (41). Briefly, the IVC of 8-week-old male *Nlrp3*$^{-/-}$ and corresponding wild-type mice was exposed, and the renal and iliac veins were ligated. Subsequently, the IVC was partially (90%) ligated with a 7-0 polypropylene suture using a 30-gauge needle as a spacer. After removal of the spacer, the peritoneum and skin were closed by monofilament sutures, and mice were euthanized 6 or 48 hours after surgery. Formed thrombi were harvested for weight and length measurements and cryo-embedded in Tissue-Tek® O.C.T.™.

Immunofluorescence Staining of Thrombi

Cryo-embedded thrombi were cryo-sectioned into 10 µm sections and fixed in 4% paraformaldehyde (PFA) overnight at 4°C. After being washed once with phosphate-buffered saline (PBS), thrombi sections were permeabilized (0.1% Triton X-100, 0.1% sodium citrate) for 10 minutes at 4°C and subsequently incubated with blocking buffer (2.5% BSA, 0.5% Tween-20 in 1x PBS) at 37°C for 1 hour. Following incubation with the primary antibodies H4Cit (1:250) and Ly6G (1:500) at 4°C overnight, the sections were washed 3 times with PBS and incubated with the secondary antibodies (1:1,500) for 2 hours at room temperature (RT). After another 3 washes with PBS, the coverslips were mounted using mounting medium containing 4′,6-diamidin-2-phenylindol (DAPI) and visualized on an Olympus confocal laser scanning microscope (FluoView FV1000) using a 20x air objective with a tile and stitching mode. Images were identically acquired and processed with Fiji/ImageJ to calculate the percentage of H4Cit and Ly6G positive area.

Mouse Neutrophil Isolation

Blood was collected from the retro-orbital plexus of anesthetized mice in 1 mL of ethylenediaminetetraacetic acid (EDTA) anticoagulated buffer supplemented with 1% endotoxin-free BSA in sterile PBS, and peripheral blood neutrophils were subsequently isolated. Bone marrow–derived neutrophils were obtained by flushing the mouse femur 3-4 times with phenol red-free RPMI 1640 medium supplemented with 10 mM HEPES. The bone marrow–cell suspension was strained using a 40 µm cell strainer, and cells were pelleted by 10 minutes of 500 x g centrifugation before finally being resuspended in PBS.

Subsequently, peripheral or bone marrow–derived neutrophils were isolated by Percoll gradient centrifugation, as described elsewhere (7). Neutrophils were then resuspended in phenol red-free RPMI 1640 medium supplemented with 10 mM HEPES, and cell purity was assessed by Wright-Giemsa stain. After the neutrophil count was determined, the required cell density was adjusted by adding HEPES supplemented RPMI 1640 medium.

Human Neutrophil Isolation

The experimental procedure was approved by the Office of Clinical Investigations at Boston Children's Hospital (protocol number IRB-P00003283). Informed consent was provided by donors. Blood was drawn from healthy donors in EDTA-coated vacutainers, and blood samples were de-identified prior to isolation. Neutrophils were isolated using gradient centrifugation, as described elsewhere (7). Cells were resuspended in phenol red free RPMI 1640 medium supplemented with HEPES, assessed for purity by Wright-Giemsa stain, and adjusted to the desired cell density.

Cell Culture of iBMDM Cells

Immortalized mouse bone marrow–derived macrophages (iBMDM) (42) were cultured in Dulbecco's modified Eagle's medium (DMEM) containing 10% fetal bovine serum (FBS), 1% penicillin/streptomycin and supplemented with L-glutamine and sodium pyruvate. Cells were split every 3 days in a 1:10 ratio by detaching them in PBS (pH 7.4) containing 2 mM EDTA.

Gene Editing of iBMDM Cells Overexpressing PAD4

PAD4 overexpressing construct was generated using a murine PAD4-mScarlet vector, which was produced by inserting mScarlet cDNA into the pLV-eGFP plasmid (a gift from Pantelis Tsoulfas, Addgene no: 36083) between XbaI and BamHI sites. The mouse full-length PAD4 insert was amplified and ligated between the AgeI and SalI sites rom he cDNA using the following primers: forward primer of 5'-ACCTCCATAGAAGACACCGACTCTAGAATGGCCCAAGGCGCGGTGATCCA-3', and reverse primer of 5'-CTTGCTCACCATTGAGCCGCTACCGGTGGGCACCATGTGCCACCACTTGA-3'.

Generation of Stable Cell Lines

Stable PAD4-mScarlet overexpressing iBMDM cell lines were generated by a lentiviral transfection approach. To this end, HEK293T cells were co-transfected with 1 µg of pLV plasmid containing the corresponding gene, 750 ng psPAX2 packaging plasmid, and 250 ng pMD2.G envelope plasmid (both plasmids were a gift from Didier Trono, Addgene no: 12260 and 12259, respectively) on day 0 and incubated overnight. On day 1, the medium was removed, replenished with 1 mL fresh medium, and the cells were incubated for another day. On day 2, the supernatant containing the virus was filtered using a 0.45 µm filter and used directly to infect iBMDM cells by spinfection at

2,500 x g for 90 minutes at RT using 8 µg/mL polybrene. Subsequently, cells were incubated in the corresponding culture medium for 24 hours, and positively infected cells were sorted by flow cytometry using mScarlet (PAD4) wavelengths. Positive cell colonies were validated at protein and functional level.

Western Blot

For western blot analysis, cells were lysed in RIPA buffer supplemented with protease and phosphatase inhibitors, according to the manufacturer's protocol, and incubated for 30 minutes on ice. After centrifugation at 20,000 x g for 15 minutes at 4°C, the protein concentration in the supernatant was measured using Bradford reagent. The protein samples were then denatured in LDS buffer and reducing agent for 5 minutes at 95°C. Lysates were separated by 4-12% Bis-Tris gradient gels, and proteins were electrotransferred on a PVDF membrane using the iBlot system. Membranes were blocked with 5% BSA in TBS-T buffer (0.05% Tween-20 in 1x TBS) for 1 hour at RT and incubated overnight at 4°C with anti ASC (1:800), anti NLRP3 (1:1,000), anti caspase-1 (1:1,000), anti PAD4 (1:200) or anti GAPDH (1:5,000) antibodies. For probing with the PAD4 antibody, the membranes were stripped for 20 minutes at RT using 0.5 M NaOH solution, blocked with 5% BSA TBS-T buffer, and incubated for 4 hours at RT using a custom-made mouse-specific PAD4 antibody (Thermo Fisher Scientific) directed against mouse PAD4 peptide DKEDPQASGMDFEDDKILD that does not cross react with mouse PAD2. After incubation with primary antibodies, membranes were washed 3 times with TBS-T buffer before incubation with HRP-conjugated secondary antibodies (1:10,000) and were incubated for 2 hours at RT. Then the membranes were washed 3 more times with TBS-T and subsequently probed with enhanced chemiluminescence (ECL) detection solution.

IL-1ß ELISA

IL-1ß was measured according to the manufacturer's instruction. A 96-well plate was coated with the capturing antibody overnight at 4°C. The following day, the plate was washed 3 times with buffer (PBS + 0.05% Tween-20) and then blocked at RT for 1 hour under gentle shaking. Subsequently, after 3 further washing steps, 100 µL of iBMDM supernatant or standard solution was added per well and incubated for 2 hours at RT under gentle shaking. The plate was again washed 3 times before the addition of the detection antibody. After incubation of the detection antibody for 1 hour at RT, avidin-HRP was added and incubated for 0.5 hours at RT. After final washing steps, TMB solution was supplemented, and 2N H_2SO_4 was used as stop solution. The absorbance was read at 450 and 570 nm. To obtain final values, the 570 nm values were subtracted from the 450 nm values.

qRT-PCR

Total RNA was extracted using the PureLink™ RNA Mini Kit (ThermoFisher) according to the manufacturer's instructions. Complementary DNA (cDNA) was synthesized using All-In-One RT MasterMix following the manufacturer's instructions. Quantitative PCR of specific genes was performed using SYBR Green SuperMix in the StepOnePlus RealTime PCR System. Cycling conditions were as follows: initial denaturation at 95°C for 2 minutes, followed by 40 cycles of 95°C for 15 sec, 55°C for 30 sec, and 70°C for 15 sec. For amplification, the following primer pairs were used (5`- >3`orientation): β-actin: fwd: CGGTTCCG ATGCCCTGAGGCTCTT; rev: CGTCACACTTCATGATGGA ATTGA for isolated peripheral neutrophils and fwd: CATT GCTGACAGGATGCAGAAGG; rev: TGCTGGAAGGT GGACAGTGAGG for iBMDM cells; ASC: fwd: CAGAG TACAGCCAGAACAGGACAC, rev: GTGGTCTCTGCAC GAACTGCCTG; NLRP3: fwd: GTTCTGAGCTCCAACCA TTCT, rev: CACTGTGGGTCCTTCATCTTT; IL1ß: fwd: TGGACCTTCCAGGATGAGGACA; rev: GTTCATCTCGGA GCCTGTAGTG.

To confirm the equal RNA input, β-actin mRNA expression and the relative expression of inflammasome mRNA were calculated with the $\triangle\triangle$Ct method. Specificity of the amplification was checked by melting curve analysis, and data were recorded and analyzed using StepOne Software v2.1.

In Vitro NET Assay

$1.5x10^4$ mouse or human neutrophils per well were resuspended in HEPES supplemented phenol red-free RPMI 1640 medium and plated in a 96-well plate. After allowing the cells to adhere for 30 minutes at 37°C and 5% CO_2 in the absence or presence of 1 µM MCC950, the cells were stimulated with vehicle control, nigericin (15 µM), or ionomycin (4 µM) for 4 hours. Fixation was performed in 2% PFA containing Hoechst 33342 (1:10,000) at 4°C overnight. Cells were washed 3 times with PBS the next day before imaging on a Zeiss Axiovert 200M microscope. The percentage of NETs was analyzed from 8 non-overlapping and randomized visual fields per well by quantifying cells with a web-like chromatin structure and positive citrullinated histone H4 staining. The average percentage of NETing cells was taken from duplicates in each experiment.

Immunofluorescence Staining of ASC Speck in Neutrophils

$6x10^4$ mouse or $1x10^5$ human neutrophils per condition were plated on a sterilized coverslip in a 6-well plate and allowed to adhere for 30 min at 37°C and 5% CO_2 before stimulating the cells with nigericin (15 µM), ionomycin (4 µM), or PMA (50 nM) for 4 hours. The cells were fixed with 4% PFA for 1 hour at RT, washed once with PBS, permeabilized (0.1% Triton X-100, 0.1% sodium citrate) for 10 minutes at 4°C, and incubated with blocking buffer (2.5% BSA, 0.5% Tween-20 in 1x PBS) at 37°C for 1 hour. Samples were incubated at 4°C ON with the primary antibodies against ASC (1:800, mouse neutrophils or 1:200, human neutrophils) and subsequently washed 3 times with PBS before incubation with the secondary antibody (1:1,500) for 2 hours at RT. After another 3 washing steps with PBS, the coverslips were mounted using mounting medium containing DAPI and visualized on a confocal Nikon Eclipse Ti2 microscope using a 60x oil immersion objective (mouse neutrophils) or an

Olympus confocal laser scanning microscope FluoView (FV1000) using a 40x air objective (human neutrophils). Images were identically acquired and processed with Fiji/ImageJ. ASC speck frequency was determined by capturing 37 Z-stacks of 0.1625 µm size from 6 by 6 tiles on a Nikon Eclipse Ti2 A1R confocal microscope (mouse neutrophils) and by 5 non-overlapping and randomized visuals fields on an Olympus FluoView (FV1000) confocal microscope (human neutrophils) in the center of the coverslip. The percentage of neutrophils forming ASC speck was quantified.

Immunofluorescence Staining of ASC Speck in iBMDM

iBMDMs were plated on a 35 mm glass-bottom dish and primed for 4 hours with LPS from E.coli (1 µg/mL) at 37°C and 5% CO_2 before stimulating the cells with nigericin (20 µM) for 30 minutes. iBMDMs were fixed in 3% PFA containing 1:10,000 Hoechst 33342 for 30 minutes at RT, washed twice with PBS for 5 minutes, and permeabilized (0.1% Triton X-100, 0.1% sodium citrate) for 7 minutes at RT, followed by a washing step. Afterwards, cells were blocked for 1 hour at RT with blocking buffer (3% BSA in PBS) and subsequently incubated with the primary antibody ASC (1:1,000) overnight. Followed by extensive washing steps, cells were incubated with the corresponding secondary antibody (1:2,000) the next day for 2 hours at RT. Finally, cells were visualized with an Olympus confocal laser scanning microscope FluoView (FV1000). Images were captured using a 60x water immersion objective with Olympus FluoView version 3.0 viewer software. The images were identically acquired and processed using ImageJ software, and the percentage of iBMDMs developing an ASC speck was quantified.

Time-Lapse Visualization by Spinning Disc Confocal and DIC Microscopy

Time-lapse microscopy was performed using isolated peripheral neutrophils from *Nlrp3*$^{+/+}$ and *Nlrp3*$^{-/-}$ mice. To this end, 1x10^6 mouse neutrophils were stained for 30 min at 37°C and 5% CO_2 using 2 µM SiR-DNA to visualize chromatin and 1 µM ER-tracker red dye to visualize the endoplasmic reticulum and nuclear envelope. Subsequently, cells were washed and resuspended in 300 µL of imaging media (phenol red-free RPMI 1640, 25 mM HEPES, 1% penicillin/streptomycin) before the cell suspension was added and allowed to adhere for 5 min in a non-coated, 24-well glass-bottom plate located on a 37°C pre-warmed microscope stage. 3-10 random fields per well were visualized using a Nikon Eclipse Ti2 microscope equipped with Perfect Focus™, a Yokogawa CSU-X1 spinning disc scanhead, a Nikon motorized stage with XY linear encoders containing a Nano-Z100 piezo insert, and a Hamamatsu Orca-flash 4.0 v3 camera with a Plan Apo Tirf 60x oil 1.49 NA DIC Nikon objective lens. Confocal and DIC images were acquired every 2 minutes for the first 80 minutes and every 5 minutes for the rest of the visualization up to 4 hours. Three images were acquired of unstimulated cells, followed by addition of imaging medium containing ionomycin to achieve a final ionomycin concentration of 4 µM.

Statistical Analysis

All data are presented as mean ± standard error of the mean (SEM). Statistical analysis was performed using GraphPad Prism. Significance was tested with unpaired t-test or, for experiments with more than two groups, with two-way ANOVA multiple comparison test. $p<0.05$ was considered statistically significant.

RESULTS

Neutrophil Activation Induces NLRP3-Dependent ASC Speck Formation Under Sterile Conditions

NLRP3 is expressed in human and mouse neutrophils (22, 23). To investigate whether NLRP3 inflammasome assembles in neutrophils under sterile conditions, human peripheral neutrophils were activated with PMA or nigericin for 4 hours. Both agents induced inflammasome assembly, observed in a subset of cells by immunostaining for ASC speck formation, which was absent in unstimulated neutrophils (**Figure 1A**). Like human neutrophils, isolated peripheral mouse neutrophils displayed ASC speck formation when stimulated with ionomycin or nigericin (**Figure 1B**) and stained with an antibody specific for ASC (**Figure S1**) subsequently. Interestingly, ASC speck formation occurred in NET-forming human or mouse neutrophils upon stimulation with nigericin or ionomycin, respectively (**Figure 1C**). After ionomycin- or nigericin- stimulated NET release, a fraction of neutrophils undergoing NETosis also showed ASC speck or its fragments associated with the expelled extracellular chromatin (**Figure 1C**; red arrowheads).

Next, since activation of pro-caspase-1 upon ASC speck formation is an established hallmark of inflammasome activation, caspase-1 cleavage products were investigated in mouse neutrophils. Stimulation with nigericin or ionomycin caused generation of the characteristic p32 and p20 caspase-1 fragments (**Figure 1D**).

To confirm that the observed ASC speck formation in neutrophils is due to NLRP3 assembly, we treated circulating neutrophils from wild-type (*Nlrp3*$^{+/+}$) and NLRP3-deficient (*Nlrp3*$^{-/-}$) mice with nigericin or ionomycin. As shown in **Figure 1E**, nigericin or ionomycin stimulation induced ASC speck formation in approximately 10% of wild-type neutrophils. By contrast, this activation-dependent increase in ASC speck formation was significantly reduced in neutrophils from *Nlrp3*$^{-/-}$ mice, indicating that the majority of observed ASC speck in the mouse neutrophils was part of the NLRP3 inflammasome (**Figure 1E**).

Taken together, these results demonstrate that neutrophils can assemble a physiologically active inflammasome/ASC speck in the absence of bacteria or LPS.

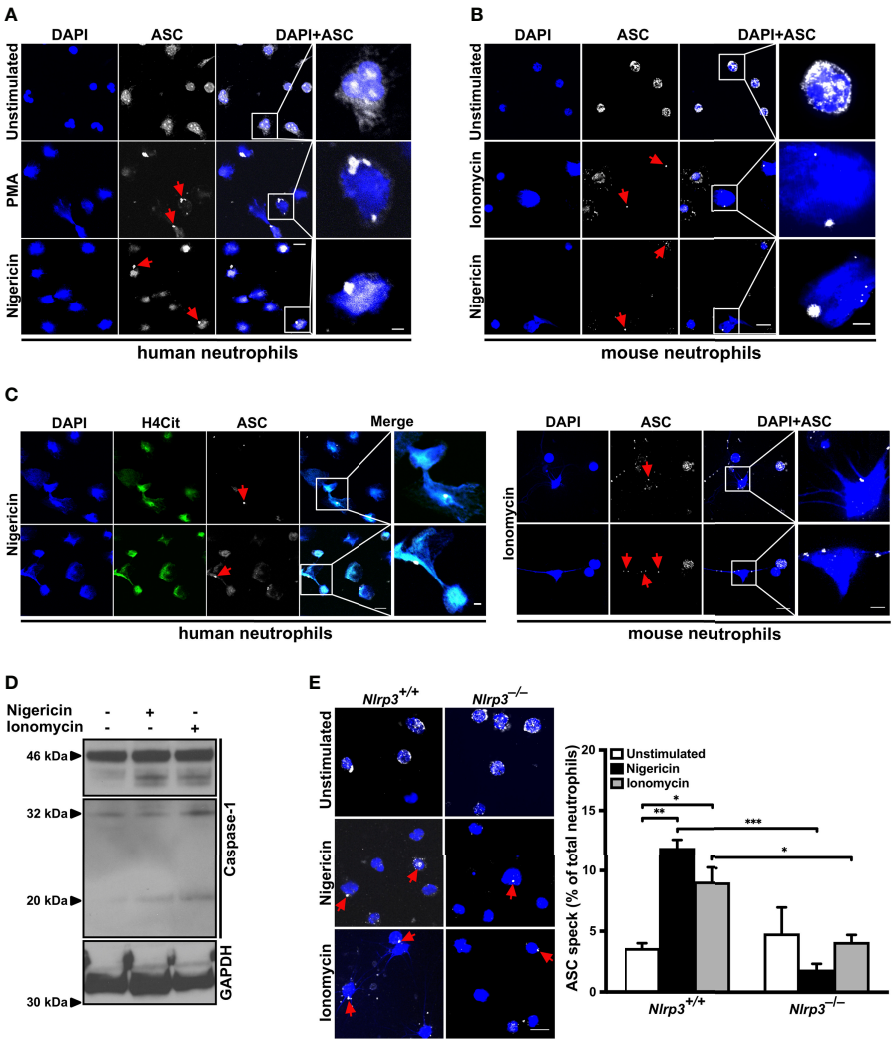

FIGURE 1 | NLRP3 inflammasome-dependent ASC speck formation and release on NETs by stimulated neutrophils **(A)** Confocal microscopy images of immunostained human neutrophils in the absence (unstimulated) or presence of PMA (50 nM) or nigericin (15 μM) for 4 hours. Blue, DNA (DAPI); grey, ASC antibody staining. Red arrows indicate ASC speck. Scale bar equals 10 μm in the overview and 2.5 μm in the zoom panel. Representative of n=4 experiments. **(B)** Confocal microscopy images of immunostained mouse neutrophils in the absence (unstimulated) or presence of ionomycin (4 μM) or nigericin (15 μM) for 4 hours. Blue, DNA (DAPI); grey, ASC antibody staining. Red arrows indicate ASC speck. Scale bar equals 10 μm in the overview and 2.5 μm in the zoom panel. Representative of n=5 experiments. **(C)** Confocal microscopy images of ASC speck formation in NETting cells and associated with NETs in human (left panel) or mouse neutrophils (right panel) in the presence of nigericin (15 μM) or ionomycin (4 μM). Blue, DNA (DAPI); green, H4Cit antibody stain; grey, ASC antibody staining. Red arrows indicate ASC speck. Scale bar equals 10 μm in the overview and 2.5 μm in the zoom panel. Representative of n=4-5 experiments. **(D)** Western blot of caspase-1 cleavage (antibody clone: Casper-1) in neutrophils from wild-type mice in the absence or presence of nigericin (15 μM) or ionomycin (4 μM) for 0.5 hours. Representative of n=3 experiments. **(E)** Representative confocal microscopy images (left panel) and arithmetic means ± SEM (right panel; n=4-5 mice) of ASC speck formation in neutrophils from wild-type (*Nlrp3*$^{+/+}$) or *Nlrp3*$^{-/-}$ mice in the absence (unstimulated, open bars) or presence of nigericin (15 μM, black bars) or ionomycin (4 μM, grey bars) for 4 hours. Blue, DNA (DAPI); grey, ASC antibody staining. Red arrows indicate ASC speck. Scale bar equals 10 μm. *p<0.05, **p<0.01 and ***p<0.001.

PAD4 Supports ASC Speck Formation by Regulation of ASC and NLRP3 Protein Levels

ASC speck forms in stimulated neutrophils, where PAD4 is a prerequisite for NET formation (15). We wondered whether PAD4 may promote ASC speck assembly as well. Since PAD4 can be synthesized by many cell types and can be found in plasma, a hematopoietic cell-specific *Padi4* knockout mouse was generated using Cre-Lox recombination by intercrossing *Padi4*$^{fl/fl}$ with *Vav1-iCre* mice (**Figure S2A**). The resulting PAD4 wild-type (*Padi4*$^{fl/fl}$) and hematopoietic cell-specific knockout (*Padi4*$^{Vav1Cre/+}$) mice showed no differences in blood cell counts (**Figure S2B**) and, in agreement with global *Padi4*$^{-/-}$ mice, *Padi4*$^{Vav1Cre/+}$ mice displayed significantly reduced NETosis (**Figure S2C**).

Immunostaining of unstimulated *Padi4*$^{fl/fl}$ or *Padi4*$^{Vav1Cre/+}$ neutrophils detected ASC speck formation in approximately 2%

of the cells. However, nigericin or ionomycin stimulation resulted in ASC speck formation in about 15% of *Padi4*$^{fl/fl}$ cells, while only 6-8% of neutrophils from *Padi4*$^{Vav1Cre/+}$ mice showed ASC speck formation (**Figure 2A**), which shows that neutrophil PAD4 is needed to fully stimulate ASC speck assembly. Since no LPS pretreatment was needed for induction of ASC speck formation in neutrophils, we decided to compare the protein levels of NLRP3 and ASC in these cells. Interestingly, peripheral neutrophils lacking PAD4 (*Padi4*$^{Vav1Cre/+}$) displayed decreased ASC and NLRP3 protein levels when compared with PAD4-positive neutrophils from *Padi4*$^{fl/fl}$ mice (**Figure 2B**), while LPS pretreatment equalized the ASC and NLRP3 protein levels in these neutrophils (**Figure S2D**). Although protein levels of the NLRP3 inflammasome are transcriptionally regulated by NFκB in macrophages (43), neutrophils from *Padi4*$^{fl/fl}$ and *Padi4*$^{Vav1Cre/+}$ mice showed no difference in NLRP3 and ASC mRNA levels (**Figure 2C**).

These results indicate that PAD4 has the ability to upregulate NLRP3 inflammasome components in a post-transcriptional manner without *de novo* mRNA synthesis in neutrophils.

Overexpresion of PAD4 Bypasses LPS Priming During NLRP3 Inflammasome Assembly in Bone Marrow–Derived Macrophages

To study whether PAD4 also plays a role in ASC speck formation in other cell types, we prepared primary bone marrow–derived macrophages (BMDM) from wild-type and *Padi4*$^{Vav1Cre/+}$ mice. While inhibition of citrullinating activity of several PAD enzymes by Cl-amidine almost completely abrogated ASC speck formation in primary wild-type BMDMs (**Figures S3A, B**), there was no statistically significant difference in ASC speck formation in primary bone marrow–derived macrophages from *Padi4*$^{Vav1Cre/+}$ mice when compared with *Padi4*$^{fl/fl}$ BMDMs after LPS and nigericin exposure (**Figure S3C**). This observation confirms a previous report (44) and indicates that in mouse macrophages, as in neutrophils, citrullination is necessary for ASC speck formation. However, other PAD enzymes may compensate for the lack of PAD4 in macrophages.

To further investigate the role of PAD4 in NLRP3 inflammasome assembly in macrophages, we generated PAD4

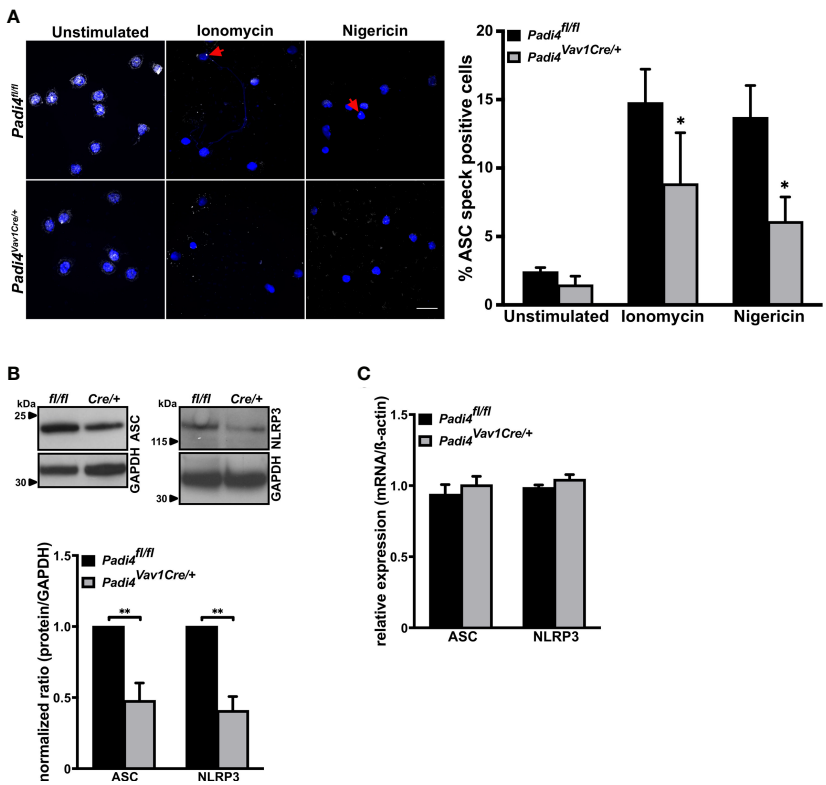

FIGURE 2 | ASC speck formation in neutrophils is, in part, directed by PAD4-dependent regulation of ASC and NLRP3 protein levels **(A)** Representative confocal microscopy images (left panel) and arithmetic means ± SEM (right panel, n=4-6 mice) of ASC speck formation in neutrophils from wild-type (*Padi4*$^{fl/fl}$, black bars) or hematopoietic cell-specific Padi4-deficient mice (*Padi4*$^{Vav1Cre/+}$, grey bars) in the absence (unstimulated) or presence of ionomycin (4 µM) or nigericin (15 µM) for 4 hours. Blue, DNA (DAPI); grey, ASC antibody staining. Red arrows indicate ASC speck. Scale bar equals 10 µm. *p<0.05. **(B)** Representative western blots (upper panel) and arithmetic means ± SEM (lower panel, n=4 mice) of ASC and NLRP3 protein levels in naive neutrophils from wild-type (*Padi4*$^{fl/fl}$, black bars) or hematopoietic specific Padi4-deficient mice (*Padi4*$^{Vav1Cre/+}$, grey bars). **p<0.01. **(C)** Arithmetic means ± SEM (n=3 mice) of relative mRNA levels in naive neutrophils from wild-type (*Padi4*$^{fl/fl}$, black bars) or hematopoietic specific Padi4-deficient mice (*Padi4*$^{Vav1Cre/+}$, grey bars).

overexpressing immortalized bone marrow–derived macrophages (iBMDM). While these cells exhibited a 4-fold increased PAD4 protein level compared with wild-type iBMDM (**Figures S4A, B**), PAD4 overexpression had no effect on IL-1ß mRNA levels in iBMDM (**Figure S4C**). Although *in vitro* stimulation of NLRP3 assembly in iBMDMs requires pretreatment with LPS and subsequent stimulation with nigericin, we observed that nigericin alone was able to induce ample ASC speck formation and IL-1ß production in PAD4 overexpressing iBMDMs (**Figures 3A, B**). Stimulation of control iBMDMs (empty vector-treated cells) with nigericin or LPS alone did not induce ASC speck formation or IL-1ß production (**Figures 3A, B**). In agreement with the observation in neutrophils, PAD4 overexpression in iBMDMs resulted in significantly increased NLRP3 protein levels and a small but significant increase in ASC levels when compared with empty vector expressing cells, without

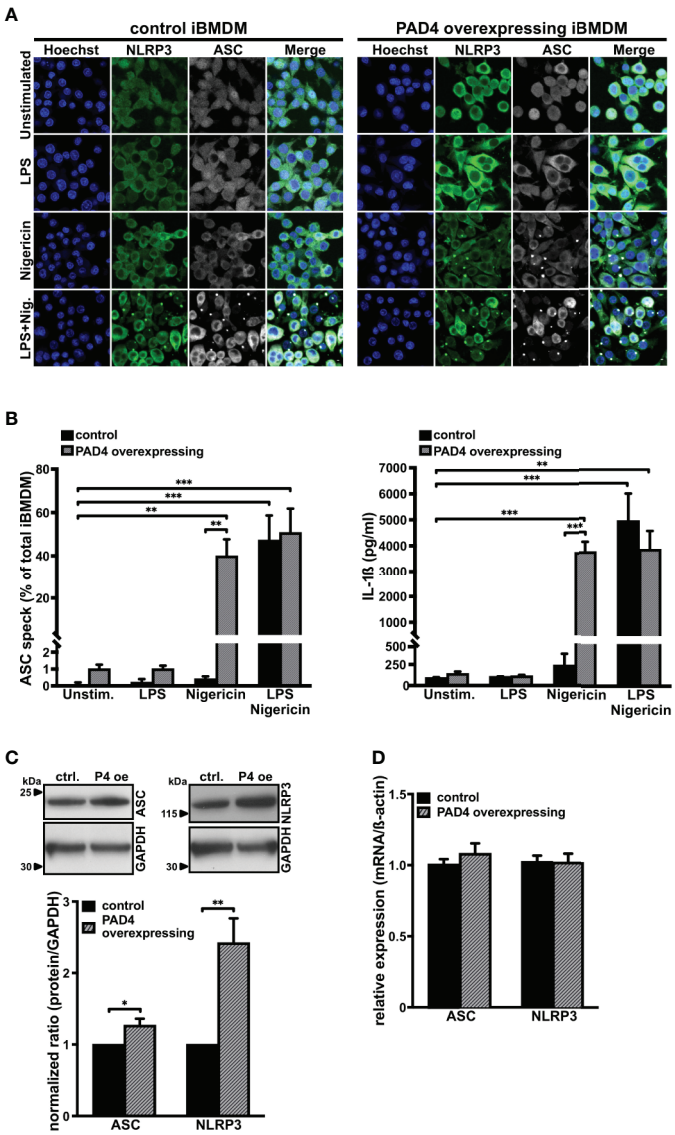

FIGURE 3 | PAD4 overexpression leads to priming-independent ASC speck formation and IL-1ß secretion with an increase in ASC and NLRP3 protein levels in immortalized bone marrow–derived murine macrophages **(A)** Confocal microscopy images of immunostained native mouse immortalized bone marrow–derived macrophages (iBMDM; control, left panel) and PAD4 overexpressing iBMDM (right panel) in the absence (unstimulated) or presence of LPS only (1 µg/mL), nigericin only (15 µM), or LPS and nigericin (15 µM, 0.5 hours). Blue, DNA (Hoechst); green, NLRP3 antibody staining; grey, ASC antibody staining. Scale bar equals 5 µm. Representative of n=4 experiments. **(B)** Arithmetic means ± SEM (n=4) of percentage of ASC speck formation (left panel) and IL-1ß production (right panel) in native iBMDM (control, black bars) or PAD4 overexpressing iBMDM (grey shaded bars) in the absence (unstim.) or presence of LPS only (1 µg/mL), nigericin only (15 µM), or LPS (1 µg/mL) and nigericin (15 µM, 0.5 hours). **p<0.01 and ***p<0.001. **(C)** Representative western blots (upper panel) and arithmetic means ± SEM (lower panel, n=4) of ASC and NLRP3 protein levels in native iBMDM (ctrl.) or PAD4 overexpressing (P4 oe) iBMDM. *p<0.05 and **p<0.01. **(D)** Arithmetic means ± SEM (n=4) of relative mRNA levels in native iBMDM (control) or PAD4 overexpressing iBMDM.

a significant change in the corresponding mRNA levels (**Figures 3C, D**).

These results show the importance of PAD4 activity in inflammasome/ASC speck assembly in iBMDM cells under sterile conditions.

NLRP3 Inflammasome Supports NETosis by Promoting Nuclear Envelope and Plasma Membrane Breakdown

Since ASC speck formation was observed in neutrophils forming NETs, we addressed the importance of the NLRP3 inflammasome assembly on NETosis. To this end, we examined the effects of inflammasome perturbations on NETosis in *in vitro* assays. Neutrophils isolated from *Nlrp3*$^{-/-}$ mice showed significantly decreased NETosis after nigericin or ionomycin stimulation when compared with neutrophils from wild-type mice (**Figure 4A**). The role of NLRP3 was further substantiated both in mouse and human neutrophils by pharmacological inhibition of the NLRP3 inflammasome. Pretreatment for 30 minutes with the specific small molecule NLRP3 inhibitor MCC950 (33) resulted in significantly decreased NETosis after nigericin or ionomycin stimulation than observed in vehicle-treated neutrophils (**Figures 4B, C**). Thereby, the inhibition was more pronounced in mouse than human neutrophils, but was statistically significant in both cases. In line with results from NLRP3 perturbations, we found that pharmacological inhibition of the NLRP3 inflammasome effector molecule caspase-1 also revealed markedly reduced NETosis in human neutrophils (**Figure S5**), indicating that NLRP3-mediated caspase-1 activation is needed for efficient NETosis.

To determine the underlying NLRP3-dependent cellular processes in NETosis, we performed time-lapse microscopy of ionomycin-stimulated neutrophils from *Nlrp3*$^{+/+}$ and *Nlrp3*$^{-/-}$ mice. Spinning disk confocal and DIC microscopy of cells stained with SiR-DNA as a marker of chromatin and ER-tracker as a marker of the endoplasmic reticulum (ER) and nuclear envelope confirmed a significantly impaired NET formation in neutrophils from *Nlrp3*$^{-/-}$ mice when compared with wild-type neutrophils. While neutrophils from *Nlrp3*$^{+/+}$ mice showed a robust breakage of the plasma membrane (NETosis) starting 60 minutes after stimulation, *Nlrp3*-deficient neutrophils displayed four-fold reduced plasma membrane rupture (**Figure 4D**). While nuclear rounding, another described cellular characteristic of NETosis (45), occurred both in neutrophils from *Nlrp3*$^{+/+}$ and *Nlrp3*$^{-/-}$ mice, most *Nlrp3*$^{-/-}$ neutrophils arrested the NETosis process at this stage (**Figure 4E** and **Videos S1, S2**). Accordingly, the rupture of the nuclear envelope was significantly impaired in neutrophils from *Nlrp3*$^{-/-}$ mice when compared with wild-type controls (**Figure 4F**).

The above observations demonstrate an important role of the NLRP3 inflammasome in nuclear envelope and plasma membrane breakdown after sterile inflammation, thus pointing to a central role of the NLRP3 inflammasome in NETosis.

NLRP3 Inflammasome Promotes NETosis *In Vivo* and Supports Venous Thrombus Progression in Mice

We next sought to verify that NLRP3 also regulates NETosis in deep vein thrombosis (DVT) to unravel the physiological importance of our findings. To this end, we applied a mouse model of stenosis-induced DVT, which is an acknowledged murine model for sterile thrombo-inflammation, in wild-type (*Nlrp3*$^{+/+}$) and *Nlrp3*$^{-/-}$ mice. In our previous work with PAD4-deficient mice, we noted that NETs likely stabilize the thrombus, since lack of NETosis displayed a more important phenotype at later timepoints of venous thrombus progression (14). Therefore, we induced vascular stenosis for 6 or 48 hours to monitor thrombus progression. While the incidence of formed thrombi in *Nlrp3*$^{+/+}$ and *Nlrp3*$^{-/-}$ mice was similar at both time points (**Figure 5A**), there was a significant NLRP3-dependent difference in thrombus progression. Interestingly, thrombus length and weight did not differ between *Nlrp3*$^{+/+}$ and *Nlrp3*$^{-/-}$ mice 6 hours after stenosis. By contrast, a significant reduction in thrombus size was observed in *Nlrp3*$^{-/-}$ mice after 48 hours when compared with *Nlrp3*$^{+/+}$ mice. Furthermore, although the thrombi from *Nlrp3*$^{+/+}$ mice increased in weight and length over the 48-hour period, thrombi from NLRP3-deficient mice reached their final small size already after only 6 hours, resulting in smaller thrombi in NLRP3$^{-/-}$ mice when compared with thrombi from wild-type mice (**Figure 5B**). This observation points to a role of NLRP3 in venous thrombosis progression under sterile conditions.

Since thrombus growth in the DVT model is substantially dependent on NETosis, we finally investigated the density of citrullinated histone H4 (H4Cit) in thrombi from *Nlrp3*$^{+/+}$ and *Nlrp3*$^{-/-}$ mice after 48 hours of stenosis as a direct marker for the presence of NETs. As shown in **Figures 5C, D**, NET density, and thus their formation, was significantly reduced in thrombi from *Nlrp3*$^{-/-}$ mice when compared with wild-type controls (**Figures 5C, D**). Neutrophil density in the corresponding thrombi were comparable between *Nlrp3*$^{+/+}$ and *Nlrp3*$^{-/-}$ mice (**Figure 5E**), emphasizing an NLRP3-dependent enhancement of NETosis with subsequent increase in venous thrombus growth *in vivo*.

Our results demonstrate that, at least in the mouse, NLRP3 inflammasome is critical for NETosis *in vivo*.

DISCUSSION

NETs and NLRP3 inflammasome are formed in a similar set of human disorders and infectious diseases. Among these pathologies, noninfectious diseases such as cancer, immunothrombosis, myocardial infarction, and stroke are the main causes of death (46). In particular, it is known that neutrophils and NETosis are major inducers of venous thrombosis (47) and hypoxia-induced venous thrombosis is linked to elevated IL-1ß and NLRP3 levels in thrombi (37, 48). However, it was not known if canonical inflammasome assembly takes place in neutrophils under these noninfectious conditions, and if inflammasome assembly contributes to NETosis.

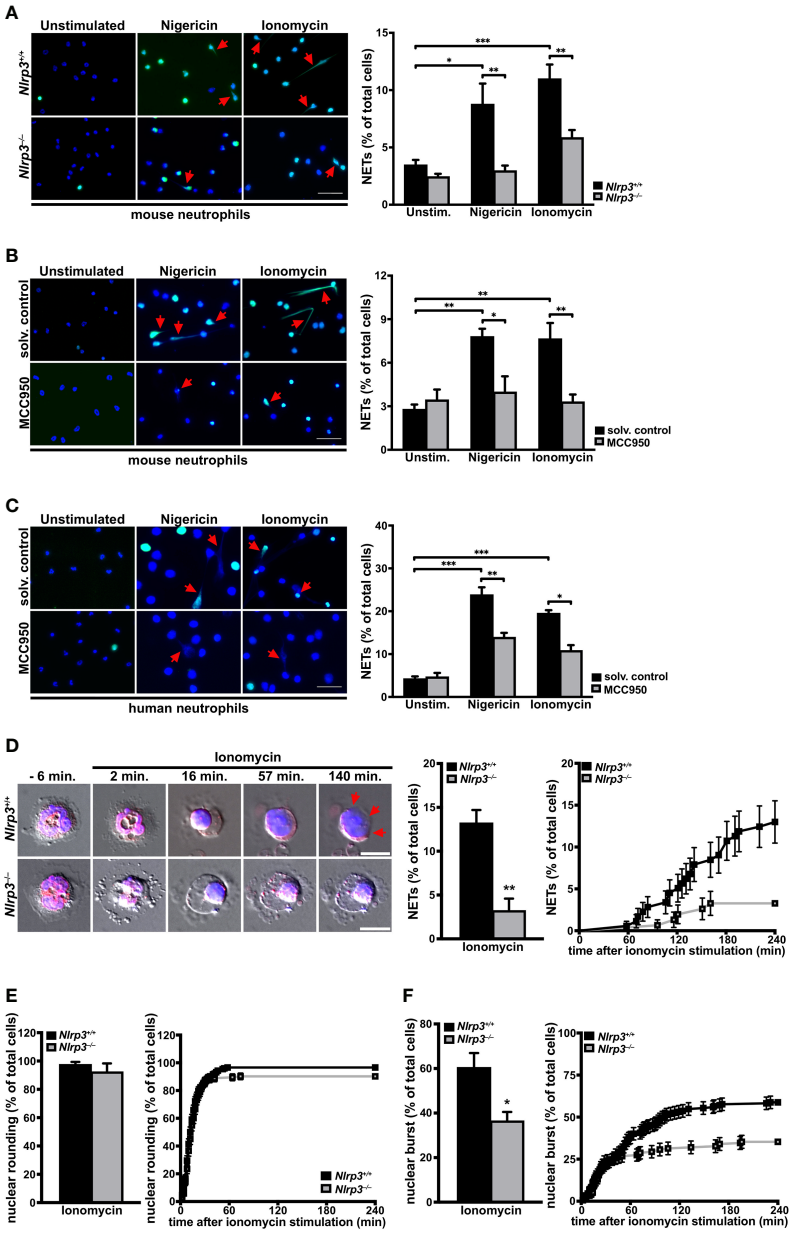

FIGURE 4 | The NLRP3 inflammasome promotes activation-dependent NET formation through nuclear envelope and plasma membrane breakdown in primary neutrophils. **(A)** Overview (left panel) and arithmetic means ± SEM (right, n=5-7 mice) of NET formation by neutrophils from wild-type (*Nlrp3*$^{+/+}$, black bars) or *Nlrp3*$^{-/-}$ mice (grey bars) in the absence (unstimulated) or presence of nigericin (15 µM) or ionomycin (4 µM) for 4 hours. Blue, DNA (DAPI); green, H4Cit antibody stain. Red arrows indicate NETs. Scale bar equals 50 µm. *p<0.05, **p<0.01 and ***p<0.001. **(B)** Overview (left panel) and arithmetic means ± SEM (right, n=5-6 mice) of NET formation in untreated (solvent control, black bars) or MCC950 pretreated (1 µM, grey bars) mouse neutrophils in the absence (unstimulated) or presence of nigericin (15 µM) or ionomycin (4 µM) for 4 hours. Blue, DNA (DAPI); green, H4Cit antibody stain. Red arrows indicate NETs. Scale bar equals 50 µm. *p<0.05 and **p<0.01. **(C)** Overview (left panel) and arithmetic means ± SEM (right, n=4-8 donors) of NET formation in untreated (solvent control, black bars) or MCC950 pretreated (1µM, grey bars) human neutrophils in the absence (unstimulated) or presence of nigericin (15 µM) or ionomycin (4 µM) for 4 hours. Blue, DNA (DAPI); green, H4Cit antibody stain. Red arrows indicate NETs. Scale bar equals 50 µm. *p<0.05, **p<0.01 and ***p<0.001. **(D)** Representative time-lapse differential interference contrast (DIC) spinning-disk confocal microscopy images at indicated time intervals (left panel) and arithmetic means ± SEM (center/right panel; n=5 mice) of percentage of total (middle) and time course (right) of plasma membrane rupture (NETosis) in neutrophils from wild-type (*Nlrp3*$^{+/+}$, black bars) or *Nlrp3*$^{-/-}$ mice (grey bars) in the presence of ionomycin (4 µM). Blue, DNA (siR-DNA); red, nuclear envelope (ER-tracker). Red arrows indicate area of plasma membrane rupture. Scale bar equals 5 µm. **p<0.01. **(E)** Arithmetic means ± SEM (n=5 mice) of percentage of total (left panel) and time course (right panel) of nuclear rounding in neutrophils from wild-type (*Nlrp3*$^{+/+}$, black bars) or *Nlrp3*$^{-/-}$ mice (grey bars) in the presence of ionomycin (4 µM). **(F)** Arithmetic means ± SEM (n=5 mice) of percentage of total (left panel) and time course (right panel) of nuclear envelope rupture in neutrophils from wild-type (*Nlrp3*$^{+/+}$, black bars) or *Nlrp3*$^{-/-}$ mice (grey bars) in the presence of ionomycin (4 µM). *p<0.05.

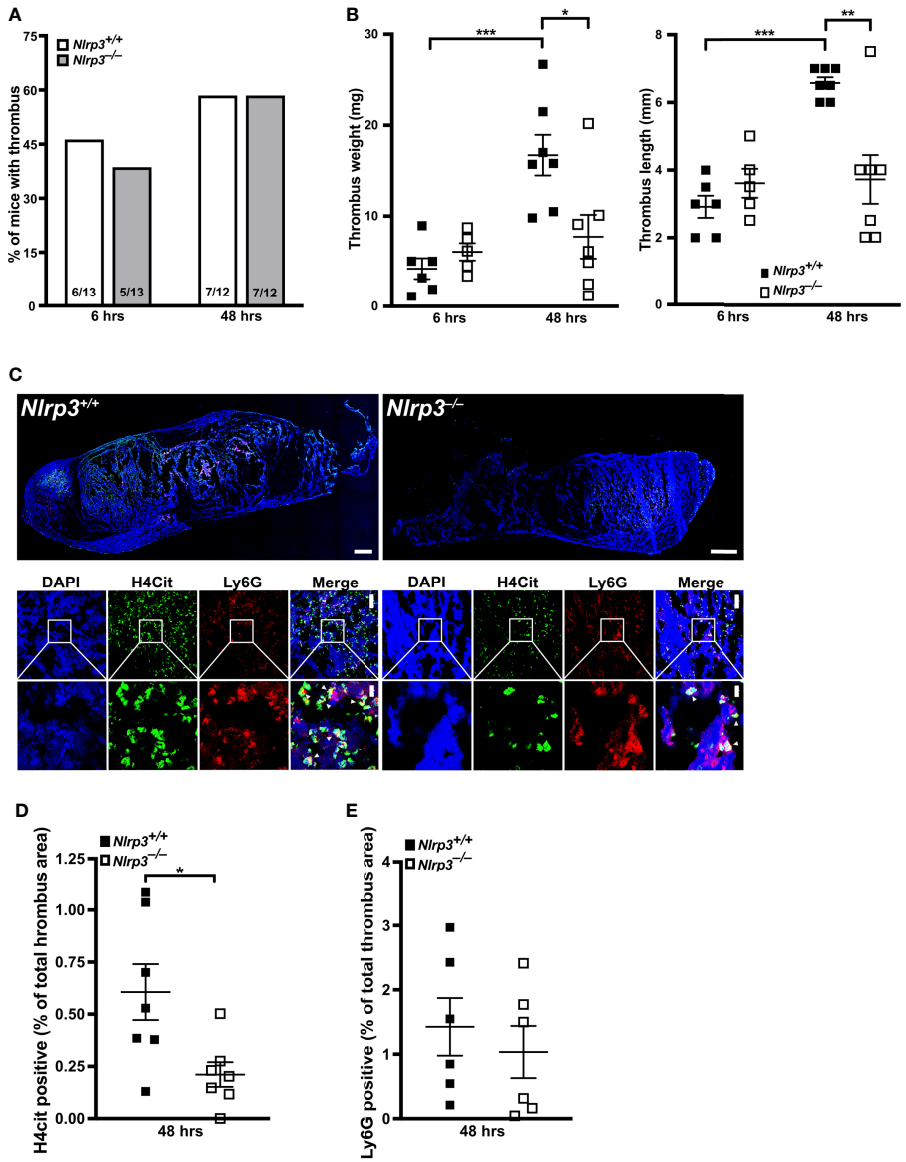

FIGURE 5 | NLRP3 deficiency decreases NETosis and thrombus growth in a stenosis-induced model of deep vein thrombosis. **(A)** Thrombus incidence in wild-type (*Nlrp3*$^{+/+}$, open bars) or *Nlrp3*$^{-/-}$ mice (grey bars) after 6 or 48 hours of stenosis of the inferior vena cava (IVC). **(B)** Thrombus weight (left panel) and thrombus length (right panel) of thrombi from wild-type (*Nlrp3*$^{+/+}$, black) or *Nlrp3*$^{-/-}$ mice (white) after 6 or 48 hours of stenosis of the IVC. Each dot represents a thrombus. *p<0.05, **p<0.01 and ***p<0.001. **(C)** Representative composite images of thrombi by confocal microscopy (upper panels) and zoom images (lower panels) of thrombi from wild-type (*Nlrp3*$^{+/+}$) or *Nlrp3*$^{-/-}$ mice after 48 hours of stenosis of the IVC. Blue, DNA (DAPI); green, H4Cit antibody stain; red, Ly6G antibody staining. Overview images were composed of several photographs. Scale bar equals 300 µm (thrombus overview), 50 µm (upper panel) or 10 µm (lower panel) in the zoom panels. **(D)** Percentage of thrombus area covered by H4Cit in thrombi from wild-type (*Nlrp3*$^{+/+}$, black) or *Nlrp3*$^{-/-}$ mice (white) after 48 hours of stenosis of the IVC. Each dot represents a thrombus. *p<0.05. **(E)** Percentage of thrombus area covered by Ly6G positive cells in thrombi from wild-type (*Nlrp3*$^{+/+}$, black) or *Nlrp3*$^{-/-}$ mice (white) after 48 hours of stenosis of the IVC. Each dot represents a thrombus.

In 2018, two groups of investigators clearly demonstrated that GSDMD pore formation is implicated in NETosis in an NLRP3 inflammasome–independent manner. They proposed that GSDMD is activated either by neutrophil proteases that play a role in NETosis and can cleave GSDMD to its active fragments (49) or by caspase-11-mediated GSDMD cleavage after cytosolic infection by gram-negative bacteria (50). However, as our experiments were exclusively performed under sterile conditions, the observed effects are most likely mediated by caspase-1-dependent mechanisms. In macrophages the cleaved N-terminal GSDMD fragment is established as pore-forming compound (51), while in neutrophils, the elastase (NE)-dependent activation of GSDMD can lead to alternative GSDMD cleavage and localization resulting in pyroptosis-

independent signaling (52). Nevertheless, caspase-11 as well as NE-dependent GSDMD processing affect nuclear extension (49) and nuclear permeabilization (50) in neutrophils. In this context, the importance of caspase-1 or 11 in NETosis is consistent with our collaborative observations showing that caspase-1/11-deficient mice do not expel NETs (53) and that pharmacological perturbation of caspase-1 activity using a specific caspase-1 inhibitor resulted in impaired NET formation (**Figure S5**). Interestingly, all types of sterile stimulation that we tested produced significant ASC speck/inflammasome assembly (**Figure 1**). However, further research is needed to clarify the exact roles of caspase-1 and GSDMD in neutrophil activation. Since occasional speck formation was observed in resting neutrophils and not in naive mononuclear cells, it appears that neutrophils are already primed for inflammasome formation (**Figure 6**).

Apart from NLRP3, other inflammasomes present in neutrophils, such as the NLRC4, NLRP1 and AIM2 inflammasomes, are also known to induce ASC speck-dependent caspase-1 activation (19, 26, 55). NLRP3 and NLRP1 expression levels in neutrophils are higher than in macrophages (56) and especially NLRP1 was recently described as mediator of anthrax lethal toxin induced neutrophil activation (55). Additionally, the AIM2 inflammasome is vastly activated by

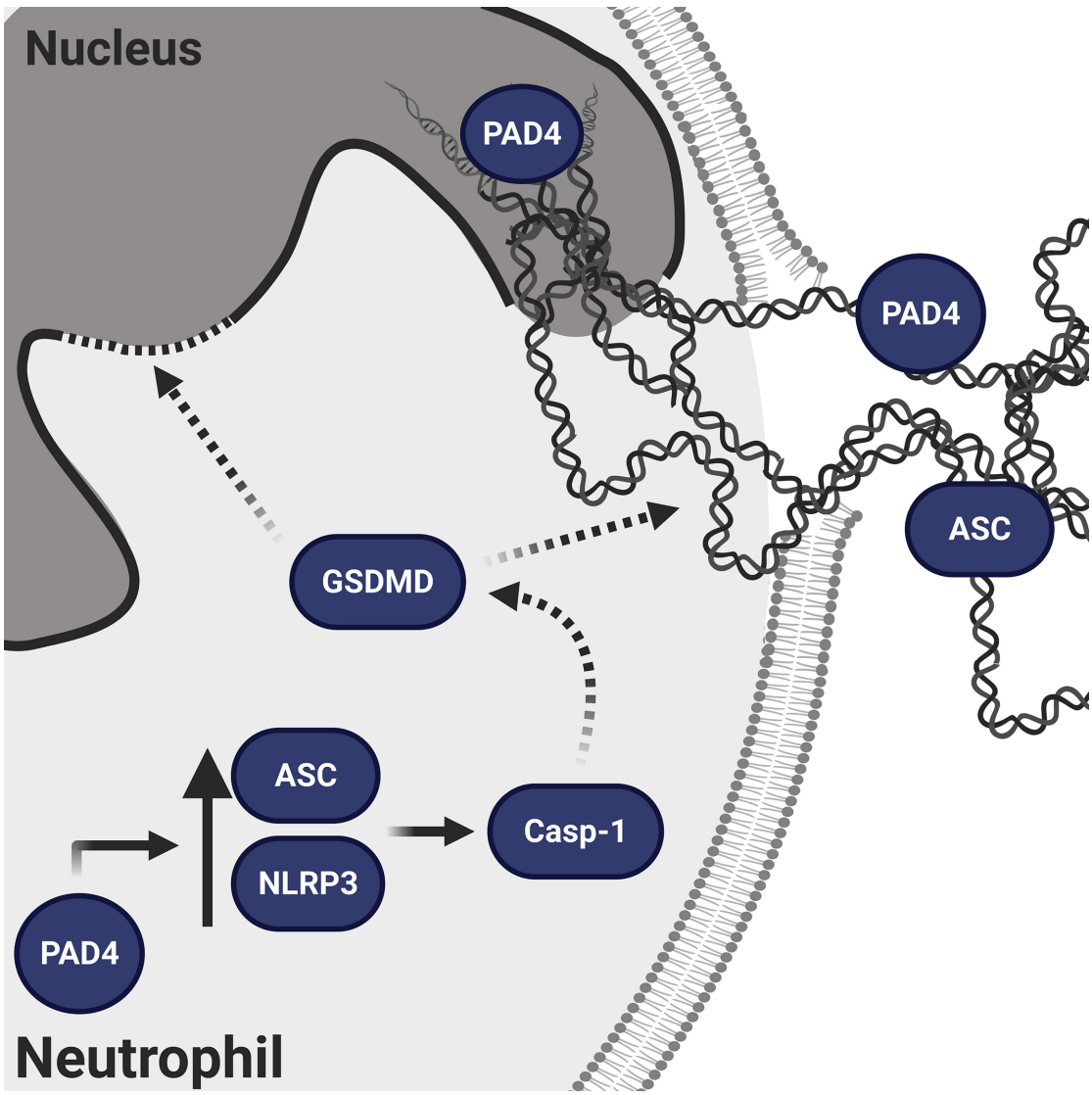

FIGURE 6 | Schematic representation of the proposed mechanism of NLRP3/PAD4-induced NETosis in the absence of infection. PAD4 is present both in the nucleus and cytoplasm (15). In the nucleus, PAD4 orchestrates chromatin decondensation, whereas in the cytoplasm, PAD4 increases NLRP3 and ASC protein levels post-transcriptionally, thus favoring NLRP3 inflammasome/ASC speck assembly. The NLRP3 inflammasome activates caspase-1, which is known to generate the N-terminal fragment of GSDMD pore that facilitates nuclear expansion (49) and nuclear permeabilization (50). In addition to GSDMD, caspase-1 has many other intracellular substrates (54) and therefore its activation could support the cytoskeletal and nuclear disassembly necessary for NETosis (12).

cytosolic dsDNA, which is a characteristic of NETosis. These observations by others may explain why residual ASC speck formation is still observed in *Nlrp3*$^{-/-}$ (**Figure 1E**) or MCC950-treated neutrophils (**Figures 4B, C**). Further investigations are needed to determine the role of inflammasomes other than NLRP3 in NETosis.

PAD4-dependent citrullination events are important in NETosis (12, 15). PAD4 deficiency protects mice from thrombosis, ischemia reperfusion injury, and age-related tissue fibrosis (5, 15). The observation that NLRP3 is linked to similar conditions and functional decline in aging (57, 58) suggested to us that PAD4 could also be regulating the NLRP3 inflammasome. Indeed, we found an impaired ASC speck formation in neutrophils from PAD4-deficient mice when compared with wild-type neutrophils (**Figure 2A**). Recently, a study was published showing that PAD enzymes were also necessary for NLRP3/ASC speck formation in macrophages. While Cl-amidine treatment fully inhibited ASC speck formation, PAD4 deficiency alone, however, had no effect on ASC speck formation (44) (**Figure S3**), showing that PAD4 is more important in neutrophil inflammasome assembly than in macrophages. These observations point to a compensatory effect of other PAD enzymes in macrophages, such as PAD2, which is the main PAD isoform in these leukocytes (59). Since post-translational modifications such as phosphorylation, ubiquitination, or the change in the charge of a single amino acid are known to modify the oligomerization or stability abilities of the NLRP3 inflammasome (60, 61), citrullination of arginine residues by PAD4 could regulate NLRP3 inflammasome oligomerization. Particularly, treatment with the calcium ionophore ionomycin increases intracellular calcium levels and thus likely induce the enzymatic activity of PAD4 with subsequent citrullination of inflammasome components. The same mechanisms is assumed for the potassium ionophore nigericin, by indirectly increasing cytosolic calcium concentrations with subsequent inflammasome activation (62). Another way by which PAD4 could promote inflammasome assembly is the upregulation of NLRP3 production (26, 43). PAD4-dependent citrullination of the NFκB subunit p65 has been described as a mediator of its nuclear translocation (63). Thus, PAD4 elevation in disease (15) could regulate NLRP3 and ASC protein levels in neutrophils and, when overexpressed, also in iBMDMs, as we observed in our study (**Figures 2B**, **3C**). Although nigericin rarely induces caspase-1 activation in unprimed macrophages and monocytes (64, 65), PAD4 overexpression results in LPS-independent inflammasome activation upon stimulation with nigericin (**Figures 3A, B**) without affecting IL-1ß mRNA levels (**Figure S4C**). Remarkably, relative mRNA levels of ASC or NLRP3 were not different in wild-type or PAD4-deficient neutrophils as well as in empty vector or PAD4 overexpressing iBMDMs (**Figures 2C**, **3D**). The post-transcriptional effect of PAD4 on NLRP3 and ASC protein levels was further substantiated, as induction of transcription by LPS priming showed similar ASC and NLRP3 protein levels between wild-type and PAD4-deficient neutrophils (**Figure S2D**). Consequently, these findings show that the inflammasome protein levels are most likely regulated by an increase in translation or a reduced clearance of NLRP3. Indeed, it will be interesting to investigate the mechanism by which citrullination controls NLRP3 inflammasome in the future.

We examined how NLRP3 deficiency impaired NETosis by using time-lapse microscopy. This revealed that initiation of NETosis appeared normal, including plasma membrane vesiculation and nuclear rounding (45); however, following rounding there was diminished rupture of the nuclear envelope and, importantly, almost absent plasma membrane rupture (**Figures 4D, F**). While GSDMD was shown to induce nuclear membrane permeability in neutrophils, it has been suggested that this could promote nuclear membrane breakdown (50). However, plasma membrane rupture during pyroptotic cell death is a well-established event of GSDMD activity after inflammasome activation (51). Since we observed that plasma membrane permeabilization occurs prior to plasma membrane rupture in NETosis (12), inflammasome-dependent GSDMD pore likely prepares the plasma membrane for rupture. In neutrophils, subjected to sterile stimulation, this process is NLRP3 dependent.

Our data point to an important connection between inflammasome/ASC speck and NETosis (**Figure 6**) and thereby possibly promoting inflammatory noninfectious disorders. Diseases that are associated with increased PAD4 expression in neutrophils and elevated susceptibility to NETosis could possibly be linked to elevated NLRP3 inflammasome assembly in both neutrophils and macrophages, as we observed. Neutrophils from diabetic patients for instance showed a four-fold increase in PAD4 levels leading to augmented NETosis (7), and NLRP3 inflammasome is long well-known in type 2 diabetes (66). PAD4-dependent NETosis is also a crucial part of venous thrombosis (14). Thus it is not surprising that we observed that NLRP3 deficiency also diminished venous thrombosis (**Figure 5**). Moreover, considering the clinical importance of excessive IL-1ß generation in a wide variety of thrombo-inflammatory disorders, as shown by the CANTOS trial (67, 68), PAD-dependent regulation of NLRP3 protein levels could be an important mechanism in inflammasome-driven diseases and makes PADs promising new targets in the therapy of cardiovascular diseases (15, 69, 70).

It is likely that inflammasome-driven chronic diseases could be promoted further by neutrophilic inflammasome, as we found ASC speck expelled with extracellular chromatin on NETs (**Figure 1C**). These ASC specks could be taken up by other cells and propagate inflammation. Indeed, ASC has been described as a "prionoid", that, when phagocytosed by macrophages, induce inflammasome assembly (27, 71, 72).

To conclude, here we have evaluated the link between canonical inflammasome and NETosis in sterile environment (**Figure 6**). Our results show inflammasome-dependent signaling is part of NETosis and PAD4 regulates ASC speck formation. These observations open many new avenues that may provide a base for new approaches in the prevention and treatment of inflammatory diseases. Finally, this work revealed additional positive effects of known drugs in development. We show that

an inhibitor of NLRP3 will also reduce the toxic effects of NETs and propose that PAD inhibitors may improve inflammasome-driven human disorders, including cardiovascular disease and thrombosis.

DATA AVAILABILITY STATEMENT

The original contributions presented in the study are included in the article/**Supplementary Material**. Further inquiries can be directed to the corresponding author.

ETHICS STATEMENT

The studies involving human participants were reviewed and approved by Office of Clinical Investigations at Boston Children's Hospital. The patients/participants provided their written informed consent to participate in this study. The animal study was reviewed and approved by Institutional Animal Care and Use Committee of Boston Children's Hospital or the Regierungspräsidium Tübingen.

AUTHOR CONTRIBUTIONS

PM, RN, SF, LM, KA, LC, DC, SG, NS, LS, VM, and ANRW performed experiments and analyzed the data. ANRW provided reagents. PM, RN, RES, CMW, HW, and DDW designed the research. PM and DDW designed the project and wrote the manuscript. All authors contributed to the article and approved the submitted version.

FUNDING

This work was supported by a grant from National Heart, Lung, and Blood Institute of the National Institutes of Health (grant R35 HL135765) and a Steven Berzin family support to DDW, an Individual Erwin Deutsch fellowship by the German, Austrian and Swiss Society of Thrombosis and Hemostasis Research to RES, a Whitman fellowship (MBL) to DDW, and an Individual Marie Skłodowska-Curie Actions fellowship by the European Commission (796365 - COAGULANT) to PM. ANRW was funded by the Deutsche Forschungsgemeinschaft (TRR156/2 – 246807620) and a research grant (We-4195/15-19). CMW was supported by the Division of Intramural Research, NHLBI, NIH.

ACKNOWLEDGMENTS

The authors acknowledge the meticulous help in preparation of the manuscript by Tiffany Frary. We thank the Marine Biological Laboratory (MBL) for support through the Whitman Fellows program and Nikon Instruments for loan of microscopy equipment and support through the Nikon Fellows program at MBL. In particular, we want to acknowledge the outstanding help by John Allen (Nikon Instruments).

SUPPLEMENTARY MATERIAL

The Supplementary Material for this article can be found online at: https://www.frontiersin.org/articles/10.3389/fimmu.2021.683803/full#supplementary-material

REFERENCES

1. Brinkmann V, Reichard U, Goosmann C, Fauler B, Uhlemann Y, Weiss DS, et al. Neutrophil Extracellular Traps Kill Bacteria. *Science* (2004) 303 (5663):1532–5. doi: 10.1126/science.1092385
2. Martinod K, Wagner DD. Thrombosis: Tangled Up in Nets. *Blood* (2014) 123 (18):2768–76. doi: 10.1182/blood-2013-10-463646
3. Sorvillo N, Mizurini DM, Coxon C, Martinod K, Tilvawala R, Cherpokova D, et al. Plasma Peptidylarginine Deiminase IV Promotes VWF-Platelet String Formation and Accelerates Thrombosis After Vessel Injury. *Circ Res* (2019) 125(5):507–19. doi: 10.1161/CIRCRESAHA.118.314571
4. Savchenko AS, Borissoff JI, Martinod K, De Meyer SF, Gallant M, Erpenbeck L, et al. VWF-Mediated Leukocyte Recruitment With Chromatin Decondensation by PAD4 Increases Myocardial Ischemia/Reperfusion Injury in Mice. *Blood* (2014) 123(1):141–8. doi: 10.1182/blood-2013-07-514992
5. Martinod K, Witsch T, Erpenbeck L, Savchenko A, Hayashi H, Cherpokova D, et al. Peptidylarginine Deiminase 4 Promotes Age-Related Organ Fibrosis. *J Exp Med* (2017) 214(2):439–58. doi: 10.1084/jem.20160530
6. Wang J, Li Q, Yin Y, Zhang Y, Cao Y, Lin X, et al. Excessive Neutrophils and Neutrophil Extracellular Traps in COVID-19. *Front Immunol* (2020) 11:2063. doi: 10.3389/fimmu.2020.02063
7. Wong SL, Demers M, Martinod K, Gallant M, Wang Y, Goldfine AB, et al. Diabetes Primes Neutrophils to Undergo NETosis, Which Impairs Wound Healing. *Nat Med* (2015) 21(7):815–9. doi: 10.1038/nm.3887
8. Demers M, Krause DS, Schatzberg D, Martinod K, Voorhees JR, Fuchs TA, et al. Cancers Predispose Neutrophils to Release Extracellular DNA Traps That Contribute to Cancer-Associated Thrombosis. *Proc Natl Acad Sci USA* (2012) 109(32):13076–81. doi: 10.1073/pnas.1200419109
9. Demers M, Wagner DD. Netosis: A New Factor in Tumor Progression and Cancer-Associated Thrombosis. *Semin Thromb Hemost* (2014) 40(3):277–83. doi: 10.1055/s-0034-1370765
10. Albrengues J, Shields MA, Ng D, Park CG, Ambrico A, Poindexter ME, et al. Neutrophil Extracellular Traps Produced During Inflammation Awaken Dormant Cancer Cells in Mice. *Science* (2018) 361(6409). doi: 10.1126/science.aao4227
11. Yipp BG, Kubes P. Netosis: How Vital is it? *Blood* (2013) 122(16):2784–94. doi: 10.1182/blood-2013-04-457671
12. Thiam HR, Wong SL, Qiu R, Kittisopikul M, Vahabikashi A, Goldman AE, et al. Netosis Proceeds by Cytoskeleton and Endomembrane Disassembly and PAD4-mediated Chromatin Decondensation and Nuclear Envelope Rupture. *Proc Natl Acad Sci USA* (2020) 117(13):7326–37. doi: 10.1073/pnas.1909546117
13. Li P, Li M, Lindberg MR, Kennett MJ, Xiong N, Wang Y. PAD4 is Essential for Antibacterial Innate Immunity Mediated by Neutrophil Extracellular Traps. *J Exp Med* (2010) 207(9):1853–62. doi: 10.1084/jem.20100239
14. Martinod K, Demers M, Fuchs TA, Wong SL, Brill A, Gallant M, et al. Neutrophil Histone Modification by Peptidylarginine Deiminase 4 is Critical for Deep Vein Thrombosis in Mice. *Proc Natl Acad Sci USA* (2013) 110 (21):8674–9. doi: 10.1073/pnas.1301059110

15. Wong SL, Wagner DD. Peptidylarginine Deiminase 4: A Nuclear Button Triggering Neutrophil Extracellular Traps in Inflammatory Diseases and Aging. *FASEB J* (2018) 32:6358–70. doi: 10.1096/fj.201800691R
16. Kenny EF, Herzig A, Kruger R, Muth A, Mondal S, Thompson PR, et al. Diverse Stimuli Engage Different Neutrophil Extracellular Trap Pathways. *Elife* (2017) 6. doi: 10.7554/eLife.24437
17. Gupta S, Chan DW, Zaal KJ, Kaplan MJ. A High-Throughput Real-Time Imaging Technique To Quantify NETosis and Distinguish Mechanisms of Cell Death in Human Neutrophils. *J Immunol* (2018) 200(2):869–79. doi: 10.4049/jimmunol.1700905
18. Guarda G, Zenger M, Yazdi AS, Schroder K, Ferrero I, Menu P, et al. Differential Expression of NLRP3 Among Hematopoietic Cells. *J Immunol* (2011) 186(4):2529–34. doi: 10.4049/jimmunol.1002720
19. Chen KW, Gross CJ, Sotomayor FV, Stacey KJ, Tschopp J, Sweet MJ, et al. The Neutrophil NLRC4 Inflammasome Selectively Promotes IL-1beta Maturation Without Pyroptosis During Acute Salmonella Challenge. *Cell Rep* (2014) 8 (2):570–82. doi: 10.1016/j.celrep.2014.06.028
20. Tzeng TC, Schattgen S, Monks B, Wang D, Cerny A, Latz E, et al. A Fluorescent Reporter Mouse for Inflammasome Assembly Demonstrates an Important Role for Cell-Bound and Free Asc Specks During *In Vivo* Infection. *Cell Rep* (2016) 16(2):571–82. doi: 10.1016/j.celrep.2016.06.011
21. Zhang T, Du H, Feng S, Wu R, Chen T, Jiang J, et al. NLRP3/ASC/Caspase-1 Axis and Serine Protease Activity are Involved in Neutrophil IL-1beta Processing During Streptococcus Pneumoniae Infection. *Biochem Biophys Res Commun* (2019) 513(3):675–80. doi: 10.1016/j.bbrc.2019.04.004
22. Karmakar M, Katsnelson MA, Dubyak GR, Pearlman E. Neutrophil P2X7 Receptors Mediate NLRP3 Inflammasome-Dependent IL-1beta Secretion in Response to ATP. *Nat Commun* (2016) 7:10555. doi: 10.1038/ncomms10555
23. Johnson JL, Ramadass M, Haimovich A, McGeough MD, Zhang J, Hoffman HM, et al. Increased Neutrophil Secretion Induced by NLRP3 Mutation Links the Inflammasome to Azurophilic Granule Exocytosis. *Front Cell Infect Microbiol* (2017) 7:507. doi: 10.3389/fcimb.2017.00507
24. Skendros P, Papagoras C, Mitroulis I, Ritis K. Autoinflammation: Lessons From the Study of Familial Mediterranean Fever. *J Autoimmun* (2019) 104:102305. doi: 10.1016/j.jaut.2019.102305
25. Stoler I, Freytag J, Orak B, Unterwalder N, Henning S, Heim K, et al. Gene-Dose Effect of MEFV Gain-of-Function Mutations Determines *Ex Vivo* Neutrophil Activation in Familial Mediterranean Fever. *Front Immunol* (2020) 11:716. doi: 10.3389/fimmu.2020.00716
26. Schroder K, Tschopp J. The Inflammasomes. *Cell* (2010) 140(6):821–32. doi: 10.1016/j.cell.2010.01.040
27. Grebe A, Hoss F, Latz E. Nlrp3 Inflammasome and the IL-1 Pathway in Atherosclerosis. *Circ Res* (2018) 122(12):1722–40. doi: 10.1161/CIRCRESAHA.118.311362
28. Sharif H, Wang L, Wang WL, Magupalli VG, Andreeva L, Qiao Q, et al. Structural Mechanism for NEK7-licensed Activation of NLRP3 Inflammasome. *Nature* (2019) 570(7761):338–43. doi: 10.1038/s41586-019-1295-z
29. He Y, Zeng MY, Yang D, Motro B, Nunez G. NEK7 is an Essential Mediator of NLRP3 Activation Downstream of Potassium Efflux. *Nature* (2016) 530 (7590):354–7. doi: 10.1038/nature16959
30. Franklin BS, Latz E, Schmidt FI. The Intra- and Extracellular Functions of ASC Specks. *Immunol Rev* (2018) 281(1):74–87. doi: 10.1111/imr.12611
31. Boucher D, Monteleone M, Coll RC, Chen KW, Ross CM, Teo JL, et al. Caspase-1 Self-Cleavage is an Intrinsic Mechanism to Terminate Inflammasome Activity. *J Exp Med* (2018) 215(3):827–40. doi: 10.1084/jem.20172222
32. Shi J, Zhao Y, Wang K, Shi X, Wang Y, Huang H, et al. Cleavage of GSDMD by Inflammatory Caspases Determines Pyroptotic Cell Death. *Nature* (2015) 526(7575):660–5. doi: 10.1038/nature15514
33. Coll RC, Robertson AA, Chae JJ, Higgins SC, Munoz-Planillo R, Inserra MC, et al. A Small-Molecule Inhibitor of the NLRP3 Inflammasome for the Treatment of Inflammatory Diseases. *Nat Med* (2015) 21(3):248–55. doi: 10.1038/nm.3806
34. Coll RC, Hill JR, Day CJ, Zamoshnikova A, Boucher D, Massey NL, et al. MCC950 Directly Targets the NLRP3 ATP-Hydrolysis Motif for Inflammasome Inhibition. *Nat Chem Biol* (2019) 15(6):556–9. doi: 10.1038/s41589-019-0277-7
35. Tapia-Abellan A, Angosto-Bazarra D, Martinez-Banaclocha H, de Torre-Minguela C, Ceron-Carrasco JP, Perez-Sanchez H, et al. MCC950 Closes the Active Conformation of NLRP3 to an Inactive State. *Nat Chem Biol* (2019) 15 (6):560–4. doi: 10.1038/s41589-019-0278-6
36. Cho JS, Guo Y, Ramos RI, Hebroni F, Plaisier SB, Xuan C, et al. Neutrophil-Derived IL-1beta is Sufficient for Abscess Formation in Immunity Against Staphylococcus Aureus in Mice. *PloS Pathog* (2012) 8(11):e1003047. doi: 10.1371/journal.ppat.1003047
37. Gupta N, Sahu A, Prabhakar A, Chatterjee T, Tyagi T, Kumari B, et al. Activation of NLRP3 Inflammasome Complex Potentiates Venous Thrombosis in Response to Hypoxia. *Proc Natl Acad Sci USA* (2017) 114 (18):4763–8. doi: 10.1073/pnas.1620458114
38. Nazir S, Gadi I, Al-Dabet MM, Elwakiel A, Kohli S, Ghosh S, et al. Cytoprotective Activated Protein C Averts Nlrp3 Inflammasome-Induced Ischemia-Reperfusion Injury *Via* mTORC1 Inhibition. *Blood* (2017) 130 (24):2664–77. doi: 10.1182/blood-2017-05-782102
39. Hemmers S, Teijaro JR, Arandjelovic S, Mowen KA. PAD4-Mediated Neutrophil Extracellular Trap Formation is Not Required for Immunity Against Influenza Infection. *PloS One* (2011) 6(7):e22043. doi: 10.1371/journal.pone.0022043
40. Drexler SK, Bonsignore L, Masin M, Tardivel A, Jackstadt R, Hermeking H, et al. Tissue-Specific Opposing Functions of the Inflammasome Adaptor ASC in the Regulation of Epithelial Skin Carcinogenesis. *Proc Natl Acad Sci USA* (2012) 109(45):18384–9. doi: 10.1073/pnas.1209171109
41. Brill A, Fuchs TA, Chauhan AK, Yang JJ, De Meyer SF, Kollnberger M, et al. Von Willebrand Factor-Mediated Platelet Adhesion is Critical for Deep Vein Thrombosis in Mouse Models. *Blood* (2011) 117(4):1400–7. doi: 10.1182/blood-2010-05-287623
42. Magupalli VG, Negro R, Tian Y, Hauenstein AV, Di Caprio G, Skillern W, et al. HDAC6 Mediates an Aggresome-Like Mechanism for NLRP3 and Pyrin Inflammasome Activation. *Science* (2020) 369(6510). doi: 10.1126/science.aas8995
43. Bauernfeind FG, Horvath G, Stutz A, Alnemri ES, MacDonald K, Speert D, et al. Cutting Edge: NF-kappaB Activating Pattern Recognition and Cytokine Receptors License NLRP3 Inflammasome Activation by Regulating NLRP3 Expression. *J Immunol* (2009) 183(2):787–91. doi: 10.4049/jimmunol.0901363
44. Mishra N, Schwerdtner L, Sams K, Mondal S, Ahmad F, Schmidt RE, et al. Cutting Edge: Protein Arginine Deiminase 2 and 4 Regulate Nlrp3 Inflammasome-Dependent IL-1beta Maturation and ASC Speck Formation in Macrophages. *J Immunol* (2019) 203(4):795–800. doi: 10.4049/jimmunol.1800720
45. Thiam HR, Wong SL, Wagner DD, Waterman CM. Cellular Mechanisms of NETosis. *Annu Rev Cell Dev Biol* (2020) 36:191–218. doi: 10.1146/annurev-cellbio-020520-111016
46. Mortality GBD. Causes of Death C. Global, Regional, and National Age-Sex Specific All-Cause and Cause-Specific Mortality for 240 Causes of Death, 1990-2013: A Systematic Analysis for the Global Burden of Disease Study 2013. *Lancet* (2015) 385(9963):117–71. doi: 10.1016/S0140-6736(14)61682-2
47. Brill A, Suidan GL, Wagner DD. Hypoxia, Such as Encountered at High Altitude, Promotes Deep Vein Thrombosis in Mice. *J Thromb Haemost* (2013) 11(9):1773–5. doi: 10.1111/jth.12310
48. Yadav V, Chi L, Zhao R, Tourdot BE, Yalavarthi S, Jacobs BN, et al. Ectonucleotidase Tri(Di)Phosphohydrolase-1 (ENTPD-1) Disrupts Inflammasome/Interleukin 1beta-Driven Venous Thrombosis. *J Clin Invest* (2019) 129(7):2872–7. doi: 10.1172/JCI124804
49. Sollberger G, Choidas A, Burn GL, Habenberger P, Di Lucrezia R, Kordes S, et al. Gasdermin D Plays a Vital Role in the Generation of Neutrophil Extracellular Traps. *Sci Immunol* (2018) 3(26). doi: 10.1126/sciimmunol.aar6689
50. Chen KW, Monteleone M, Boucher D, Sollberger G, Ramnath D, Condon ND, et al. Noncanonical Inflammasome Signaling Elicits Gasdermin D-dependent Neutrophil Extracellular Traps. *Sci Immunol* (2018) 3(26). doi: 10.1126/sciimmunol.aar6676
51. Lieberman J, Wu H, Kagan JC. Gasdermin D Activity in Inflammation and Host Defense. *Sci Immunol* (2019) 4(39). doi: 10.1126/sciimmunol.aav1447
52. Karmakar M, Minns M, Greenberg EN, Diaz-Aponte J, Pestonjamasp K, Johnson JL, et al. N-GSDMD Trafficking to Neutrophil Organelles Facilitates

IL-1beta Release Independently of Plasma Membrane Pores and Pyroptosis. *Nat Commun* (2020) 11(1):2212. doi: 10.1038/s41467-020-16043-9
53. Pillai PS, Molony RD, Martinod K, Dong H, Pang IK, Tal MC, et al. Mx1 Reveals Innate Pathways to Antiviral Resistance and Lethal Influenza Disease. *Science* (2016) 352(6284):463–6. doi: 10.1126/science.aaf3926
54. Denes A, Lopez-Castejon G, Brough D. Caspase-1: Is IL-1 Just the Tip of the Iceberg? *Cell Death Dis* (2012) 3:e338. doi: 10.1038/cddis.2012.86
55. Greaney AJ, Portley MK, O'Mard D, Crown D, Maier NK, Mendenhall MA, et al. Frontline Science: Anthrax Lethal Toxin-Induced, NLRP1-mediated Il-1beta Release is a Neutrophil and PAD4-dependent Event. *J Leukoc Biol* (2020) 108(3):773–86. doi: 10.1002/JLB.4HI0320-028R
56. Mankan AK, Dau T, Jenne D, Hornung V. The NLRP3/ASC/Caspase-1 Axis Regulates IL-1beta Processing in Neutrophils. *Eur J Immunol* (2012) 42 (3):710–5. doi: 10.1002/eji.201141921
57. Youm YH, Grant RW, McCabe LR, Albarado DC, Nguyen KY, Ravussin A, et al. Canonical Nlrp3 Inflammasome Links Systemic Low-Grade Inflammation to Functional Decline in Aging. *Cell Metab* (2013) 18(4):519–32. doi: 10.1016/j.cmet.2013.09.010
58. Coll RC, O'Neill L, Schroder K. Questions and Controversies in Innate Immune Research: What is the Physiological Role of NLRP3? *Cell Death Discovery* (2016) 2:16019. doi: 10.1038/cddiscovery.2016.19
59. Vossenaar ER, Radstake TR, van der Heijden A, van Mansum MA, Dieteren C, de Rooij DJ, et al. Expression and Activity of Citrullinating Peptidylarginine Deiminase Enzymes in Monocytes and Macrophages. *Ann Rheum Dis* (2004) 63(4):373–81. doi: 10.1136/ard.2003.012211
60. Stutz A, Kolbe CC, Stahl R, Horvath GL, Franklin BS, van Ray O, et al. NLRP3 Inflammasome Assembly is Regulated by Phosphorylation of the Pyrin Domain. *J Exp Med* (2017) 214(6):1725–36. doi: 10.1084/jem.20160933
61. Tang J, Tu S, Lin G, Guo H, Yan C, Liu Q, et al. Sequential Ubiquitination of NLRP3 by RNF125 and Cbl-b Limits Inflammasome Activation and Endotoxemia. *J Exp Med* (2020) 217(4). doi: 10.1084/jem.20182091
62. Yaron JR, Gangaraju S, Rao MY, Kong X, Zhang L, Su F, et al. K(+) Regulates Ca(2+) to Drive Inflammasome Signaling: Dynamic Visualization of Ion Flux in Live Cells. *Cell Death Dis* (2015) 6:e1954. doi: 10.1038/cddis.2015.277
63. Sun B, Dwivedi N, Bechtel TJ, Paulsen JL, Muth A, Bawadekar M, et al. Citrullination of NF-kappaB p65 Promotes its Nuclear Localization and TLR-induced Expression of IL-1beta and TNFalpha. *Sci Immunol* (2017) 2(12). doi: 10.1126/sciimmunol.aal3062
64. Lawlor KE, Khan N, Mildenhall A, Gerlic M, Croker BA, D'Cruz AA, et al. RIPK3 Promotes Cell Death and NLRP3 Inflammasome Activation in the Absence of MLKL. *Nat Commun* (2015) 6:6282. doi: 10.1038/ncomms7282
65. Gritsenko A, Yu S, Martin-Sanchez F, Diaz-Del-Olmo I, Nichols EM, Davis DM, et al. Priming Is Dispensable for NLRP3 Inflammasome Activation in Human Monocytes In Vitro. *Front Immunol* (2020) 11:565924. doi: 10.3389/fimmu.2020.565924
66. Lee HM, Kim JJ, Kim HJ, Shong M, Ku BJ, Jo EK. Upregulated NLRP3 Inflammasome Activation in Patients With Type 2 Diabetes. *Diabetes* (2013) 62(1):194–204. doi: 10.2337/db12-0420
67. Ridker PM, Everett BM, Thuren T, MacFadyen JG, Chang WH, Ballantyne C, et al. Antiinflammatory Therapy With Canakinumab for Atherosclerotic Disease. *N Engl J Med* (2017) 377(12):1119–31. doi: 10.1056/NEJMoa1707914
68. Ridker PM, MacFadyen JG, Thuren T, Everett BM, Libby P, Glynn RJ, et al. Effect of interleukin-1beta Inhibition With Canakinumab on Incident Lung Cancer in Patients With Atherosclerosis: Exploratory Results From a Randomised, Double-Blind, Placebo-Controlled Trial. *Lancet* (2017) 390 (10105):1833–42. doi: 10.1016/S0140-6736(17)32247-X
69. Abbate A, Toldo S, Marchetti C, Kron J, Van Tassell BW, Dinarello CA. Interleukin-1 and the Inflammasome as Therapeutic Targets in Cardiovascular Disease. *Circ Res* (2020) 126(9):1260–80. doi: 10.1161/CIRCRESAHA.120.315937
70. Gomes T, Varady CBS, Lourenco AL, Mizurini DM, Rondon AMR, Leal AC, et al. IL-1beta Blockade Attenuates Thrombosis in a Neutrophil Extracellular Trap-Dependent Breast Cancer Model. *Front Immunol* (2019) 10:2088. doi: 10.3389/fimmu.2019.02088
71. Baroja-Mazo A, Martin-Sanchez F, Gomez AI, Martinez CM, Amores-Iniesta J, Compan V, et al. The NLRP3 Inflammasome is Released as a Particulate Danger Signal That Amplifies the Inflammatory Response. *Nat Immunol* (2014) 15(8):738–48. doi: 10.1038/ni.2919
72. Franklin BS, Bossaller L, De Nardo D, Ratter JM, Stutz A, Engels G, et al. The Adaptor ASC has Extracellular and 'Prionoid' Activities That Propagate Inflammation. *Nat Immunol* (2014) 15(8):727–37. doi: 10.1038/ni.2913

Conflict of Interest: DDW is on the Scientific Advisory Board of Neutrolis, a preclinical-stage biotech company focused on DNases.

The remaining authors declare that the research was conducted in the absence of any commercial or financial relationships that could be construed as a potential conflict of interest.

frontiers in Immunology

ORIGINAL RESEARCH
published: 28 September 2021
doi: 10.3389/fimmu.2021.720655

Internalization of the Membrane Attack Complex Triggers NLRP3 Inflammasome Activation and IL-1β Secretion in Human Macrophages

*Ines Diaz-del-Olmo[1], Jonathan Worboys[1], Fatima Martin-Sanchez[1], Anna Gritsenko[1], Ashley R. Ambrose[1], Gillian M. Tannahill[2], Eva-Maria Nichols[2], Gloria Lopez-Castejon[1] and Daniel M. Davis[1]**

[1] Division of Infection, Immunity and Respiratory Medicine, Faculty of Biology, Medicine and Health, Lydia Becker Institute of Immunology and Inflammation, The University of Manchester, Manchester, United Kingdom, [2] Adaptive Immunity Research Unit, GSK, Stevenage, United Kingdom

OPEN ACCESS

Edited by:
Zvi Fishelson,
Tel Aviv University, Israel

Reviewed by:
Jordan S. Pober,
Yale University, United States
Bryan Paul Morgan,
Cardiff University, United Kingdom

***Correspondence:**
Daniel M. Davis
daniel.davis@manchester.ac.uk

Specialty section:
This article was submitted to Molecular Innate Immunity, a section of the journal Frontiers in Immunology

Received: 04 June 2021
Accepted: 13 September 2021
Published: 28 September 2021

Citation:
Diaz-del-Olmo I, Worboys J, Martin-Sanchez F, Gritsenko A, Ambrose AR, Tannahill GM, Nichols E-M, Lopez-Castejon G and Davis DM (2021) Internalization of the Membrane Attack Complex Triggers NLRP3 Inflammasome Activation and IL-1β Secretion in Human Macrophages. Front. Immunol. 12:720655. doi: 10.3389/fimmu.2021.720655

Interleukin 1β (IL-1β) plays a major role in inflammation and is secreted by immune cells, such as macrophages, upon recognition of danger signals. Its secretion is regulated by the inflammasome, the assembly of which results in caspase 1 activation leading to gasdermin D (GSDMD) pore formation and IL-1β release. During inflammation, danger signals also activate the complement cascade, resulting in the formation of the membrane attack complex (MAC). Here, we report that stimulation of LPS-primed human macrophages with sub-lytic levels of MAC results in activation of the NOD-like receptor 3 (NLRP3) inflammasome and GSDMD-mediated IL-1β release. The MAC is first internalized into endosomes and then colocalizes with inflammasome components; adapter protein apoptosis associated speck-like protein containing a CARD (ASC) and NLRP3. Pharmacological inhibitors established that MAC-triggered activation of the NLRP3 inflammasome was dependent on MAC endocytosis. Internalization of the MAC also caused dispersion of the trans-Golgi network. Thus, these data uncover a role for the MAC in activating the inflammasome and triggering IL-1β release in human macrophages.

Keywords: membrane attack complex, inflammasome, macrophage, IL-1β, complement, NLRP3

INTRODUCTION

Interleukin 1β (IL-1β) is a pro-inflammatory cytokine with multiple roles in inflammation. When dysregulated, however, IL-1β also underlies the pathology observed in several inflammatory diseases including toxic shock syndrome, rheumatoid arthritis, and type 2 diabetes (1). Thus, production of its active form is tightly regulated by a multi-protein complex termed the inflammasome. The best studied inflammasome is the NOD-like receptor pyrin domain-containing protein 3 (NLRP3) inflammasome and is canonically activated by the detection of two consecutive signals: a priming signal, such as exogenous lipopolysaccharide (LPS), followed by an activation signal, such as the toxin nigericin. Oligomerization of the NLRP3 inflammasome results in the recruitment of multiple proteins to the complex, including the adaptor protein ASC and the effector protease caspase 1,

resulting in the activation of caspase 1 (2–4). Active caspase 1 processes gasdermin D (GSDMD) to form pores in the cell membrane and cleaves pro-IL-1β into its mature active form to be secreted from the cell (5–7).

The complement system is also activated upon recognition of damage-associated and pathogen-associated molecular patterns (DAMPs and PAMPs), such as LPS. This acts in a cascade of protein interactions which results in the formation of the membrane attack complex (MAC), also known as terminal complement complex (TCC) (8). The MAC is formed by the complement proteins C5b, C6, C7, C8 and C9 and has traditionally been studied for its ability to form pores in the membrane of pathogens and dysfunctional cells in order to clear them.

Healthy host cells have mechanisms to prevent lysis by MAC pores. During homeostasis, CD59 blocks MAC insertion into the cell membrane. However, this receptor can become exhausted during prolonged inflammation, allowing MAC pore formation (9). Additionally, nucleated cells are able to remove the MAC from the cell membrane by endocytosis, exocytosis or ectocytosis, also known as outward vesiculation (10–13). In murine cells and human epithelial and endothelial cells, sub-lytic levels of the MAC can activate caspase 1 and trigger IL-1β secretion (14–16). This is important because multiple inflammatory diseases are characterized by increased levels of both IL-1β and complement (17–20). However, it is not clear whether the MAC can directly impact inflammasome activation in human myeloid cells, a primary source of IL-1β. Here, we show that LPS-primed human macrophages internalize the MAC into EEA1+ endosomes, which leads to dispersion of the trans-Golgi network, activation of the NLRP3 inflammasome and secretion of IL-1β to the extracellular milieu.

MATERIALS AND METHODS

Cell Culture and Differentiation

Human primary macrophages were differentiated from monocytes isolated from blood provided by the National Blood Transfusion Service (Manchester, UK) with ethical approval from the Research Governance, Ethics, and Integrity Committee at the University of Manchester (REC 05/0401/108). In brief, peripheral blood mononuclear cells (PBMCs) were isolated from leukocyte cones by ficoll gradient centrifugation. Monocytes were isolated using the human CD14 MACS separation kit (Miltenyi Biotec) and cultured at a concentration of 5 x 10^5 cells/mL for 7 days in complete RPMI media containing RPMI-1640 (Sigma), 10% FBS (Gibco), 1% L-glutamine (Gibco), 1% penicillin/streptomycin (Gibco). Media was supplemented with 50 ng/mL M-CSF (Peprotech) for differentiation into monocyte-derived macrophages (MDMs).

The THP1 cell lines were cultured using complete RPMI media at a density of 5 x 10^5 cells/mL and, differentiated towards a macrophage-like phenotype using 0.5 μM phorbol-12-myristate 13-acetate (PMA, Sigma) for 16 hrs. Cells were rested for 24 hrs in RPMI complete media before cell activation. THP1 wild type cells (TIB-202) were obtained from ATTC and THP1$^{nlrp3-/-}$ cells were a gift from Prof. Veit Hornung (Gene Center Munich) (21). These cells were used to generate THP1$^{nlrp3-/-}$/eGFP-NLRP3 cells as indicated below.

Virus Production and Transduction of THP1$^{nlrp3-/-}$/eGFP-NLRP3

Human NLRP3 was cloned by the Gateway cloning system in a lentiviral destination vector, pLNT-UbC-eGFP-#, generated by Dr Pawel Pazek (University of Manchester) (22). Packaging plasmids psPAX2 and pMD2.G were a gift from Didier Trono (Addgene plasmid #12260 and #12259). HEK293T cells were plated at a concentration of 3.5 × 10^5 cell/mL for 24 hrs and transfected using Lipofectamine 2000 (Invitrogen) following the manufacturer's instructions. In short, 8 μl Lipofectamine, 1.2 μg pMD2.G, 0.4 μg psPAX2 and 1.5 μg of pLNT-UbC-eGFP-NLRP3 were used per reaction. The following day, the media was replaced, and cells were further incubated for 2 days. Supernatants were then filtered with a 0.45-μm filter to obtain a cell-free extract of viral particles. Viral particles containing our vector of interest were used to transduce 5 × 10^4 THP1$^{nlrp3-/-}$ cells, with 8 μg/mL polybrene (Sigma). Cells, together with both the viral particles and polybrene, were centrifuged at 1000 g for 1 hr at 30°C. Pelleted cells were then re-suspended in fresh complete RPMI media.

Cell Stimulation

For inflammasome activation, MDMs or THP1 cells were primed with 1 μg/mL LPS (lipopolysaccharide from Escherichia coli O26:B6, Sigma) in complete media for 3 hrs, washed with serum-free RPMI media, and treated with 10 μM nigericin for 45 mins or the Membrane Attack Complex (MAC) for the indicated time in serum free RPMI media. To form the MAC, cells were treated for 15 mins with 10 μg/mL C5b6, unless otherwise specified, and 10 μg/mL anti-CD59 mAb followed by treatment with 10 μg/mL C7, 10 μg/mL C8 and 10 μg/mL C9 (Complement Technologies). NLRP3 inflammasome activation was impaired using 1 μM MCC950 (Pepreotech). GSDMD processing was blocked using 10 μM NSA (Calbiochem). Endocytosis was blocked with 0.1 μg/mL nystatin (Merck), 10 μM cytochalasin D (Merck), or 10 μM dynasore (Calbiochem), unless otherwise specified. All inhibitors were used for 30 mins before and during stimulation with nigericin or the MAC in serum free RPMI media.

Cell Death Assay

Cell death was established by measuring lactate dehydrogenase (LDH) release in supernatants. Upon treatment, supernatants were collected, centrifuged at 500 g to remove cell debris and LDH release was assessed using a quantitative colorimetric assay (CytoTox96® Non-Radioactive Cytotoxicity Assay, Promega), following manufacturer's instructions. Results were expressed as cell death percentage, relative to a lysis control representing 100%.

Caspase-Glo® 1 Inflammasome Assay

The activity of caspase 1 was assessed using a quantitative luminescence assay (Caspase-Glo® 1 Inflammasome kit,

Promega). In brief, cell supernatants were combined with the aminoluciferin substrate Z-WEHD for 1 hr and luminescence was measured. Results were expressed as fold-increase relative to vehicle-only treated cells.

Enzyme-Linked Immunosorbent Assay (ELISA)

Cytokine release was measured in supernatants using the Human IL-1β or IL-18 DuoSet ELISA kit (R&D) following manufacturer's instructions.

The amount of MAC, also known as terminal complement complex (TCC), was measured in cell lysates using a human TCC ELISA kit (HycultBiotech) following manufacturer's instructions.

Immunoblot

Cell lysates were prepared in RIPA buffer (50 mM Tris-HCl pH 7.4, 1% NP-40, 0.25% Na-deoxycholate, 150 mM NaCl and 1 mM EDTA in miliQ dH_2O) supplemented with protease inhibitor cocktail (Calbiochem) for 30 mins on ice. Lysates were centrifuged at 18,000 g for 20 mins at 4°C to eliminate the insoluble fraction. Protein concentration in cell lysates was determined using a Bicinchoninic Acid Protein Assay (Pierce™ BCA Protein Assay Kit, Life Technologies) and samples were diluted to an equal protein amount of 30 µg. Cell supernatants were centrifuged at 500 g for 5 mins to remove cell debris and concentrated using centrifugal cellulose filters (10 kDa MW Amicon centrifugal filter devices, Merck Millipore), as indicated by the manufacturer. Cell lysates and supernatants were diluted to 1x reducing Laemmli buffer containing 10 mM 1,4-Dithiothreitol (Sigma), heated at 95°C for 10 mins, and separated by 4-12% Bis-Tris NuPAGE gels (Invitrogen) in NuPAGE MES buffer (Invitrogen) at 165 V for 35 mins. A color protein standard (P7719, New England Biolabs or Precision Plus, Bio-Rad), was used for MW references. Proteins were transferred onto 0.2 µm PVDF membranes (GE Healthcare), blocked with 5% Bovine Serum Albumin (BSA, Sigma) in TBST (10 mM Tris-HCl, 15 mM NaCl, 0.05% Tween® 20 at pH 7.5) for 1 hr at room temperature and incubated with the indicated primary antibody in blocking buffer overnight at 4°C. Membranes were washed and incubated for 1 hr at room temperature with the appropriate HRP-conjugated secondary antibody. Membranes were washed and developed using the Clarity Western ECL Substrate (Bio-Rad) and protein bands were visualized using a ChemiDoc™ MP Imager (Bio-Rad).

The primary antibodies used for immunoblotting and their final concentrations were goat Ab anti-human IL-1β (0.1 µg/mL, R&D Systems), rabbit Ab anti-human GSDMD (0.14 µg/mL, Novus Biologicals), rabbit mAb anti-human caspase-1 (1:1000, D7F10, Cell Signalling Technology), mouse mAb anti-human NLRP3 (1 µg/mL, Cryo-2, Adipogen), mouse mAb anti-β-actin-HRP (0.2 µg/mL, AC-15, Sigma). HRP conjugated secondary antibodies used were rabbit Ab anti-goat-HRP (0.13 µg/mL, Sigma), goat Ab anti-rabbit-HRP (1:3000, Bio-Rad), and goat Ab anti-mouse-HRP (1:3000, Bio-Rad).

Confocal Imaging

Cells were cultured in chambered coverglasses (Nunc™ Lab-Tek™ II, Thermo Scientific™) at a concentration of 2 x 10^5 cells/mL. Cells were differentiated, primed with LPS and activated with the MAC or nigericin, as above, fixed with 4% PFA for 15 mins, blocked and permeabilized with 2% BSA and 0.1% Triton (Sigma) in PBS for 30 mins and stained overnight at 4°C with the indicated primary antibody in 2% BSA in PBS. Cells were washed, and matched secondary antibodies were added for 1 hr in 2% BSA in PBS when needed. Samples were then washed 3 times with PBS before being imaged. For all imaging experiments C9 was conjugated in-house with Janelia Fluor 549 NHS ester (Tocris, 6147) or Alexa Fluor 647 NHS ester (Thermo Fisher Scientific, A20006). In brief, 50 µl of C9 (1 mg/mL) was mixed with 5 µl of Janelia Fluor 549 or Alexa Fluor 647 NHS ester (1 mg/mL) in 100 µM $NaHCO_3$ in PBS and incubated for 1 hr at room temperature on a rotator. The excess dye was removed using size-exclusion chromatography (7K MWCO Zeba™ Spin Desalting Column Thermo Scientific) by centrifugation at 1500 g for 2 mins. Protein concentration and degree of labelling were measured by absorption and calculated according to the manufacturer's instructions. Imaging was performed with an inverted confocal microscope (Leica TCS SP8) using a 100x/1.40NA oil-immersion objective or a 63x/1.20NA oil-immersion objective. Excitation was performed with a pulsed white-light laser and emission was detected using time-gated HyD detectors functioning in standard mode. Images were exported and analyzed using ImageJ (23). The proportion of NIK fluorescence within the cytoplasm was calculated by subtracting the nuclear fluorescence from the cell total fluorescence and expressing this relative to the fluorescence of NIK within the entire cell. Nuclei and cell outlines were identified manually using brightfield images.

The primary antibodies used for immunostaining and their final concentrations were as follows: mouse IgG1 mAb anti-human ASC (2 µg/mL, O93E9, BioLegend), mouse IgG2a mAb anti-human TCC (5 µg/mL, aE11, Abcam), sheep Ab anti-human TGN46 (1.25 µg/mL, Bio-Rad), rabbit mAb anti-human EEA1 (1:200, C45B10, Cell Signaling Technology), rabbit Ab anti-NIK (1:200, Cell Signaling Technology). The secondary antibodies used were goat Ab anti-mouse IgG2a Alexa Fluor 488 (2 µg/mL, Invitrogen), goat Ab anti-mouse IgG1 Alexa Fluor 568 or 647 (2 µg/mL, Invitrogen), donkey Ab anti-sheep Alexa Fluor 488 (2 µg/mL, Abcam) and goat Ab anti-rabbit Alexa Fluor 488 (2 µg/mL, Invitrogen).

Statistical Analysis

The normality of the results was analyzed by the Shapiro-Wilk normality test. Normally distributed results were analyzed by parametrical one-way ANOVA and non-normally distributed results using Friedman test. Results were expressed as the mean ± standard deviation (SD). Significant differences between samples were established where $p<0.05$ (*), $p<0.01$(**), $p<0.001$ (***), and $p<0.0001$ (****). Graphpad Prism v9 was used to analyze and graphically represent all results.

RESULTS

The Membrane Attack Complex Activates the Inflammasome in Human Macrophages

It is well-established that complement deposition is highly increased in IL-1β-driven diseases and thus, we set out to test whether IL-1β secretion may be triggered from human macrophages by the terminal complement complex, the MAC. Initially, we used the human monocyte-like cell line, THP1, which was differentiated with PMA to obtain a macrophage-like phenotype. Cells were then primed with LPS for 3 hrs and treated with the complement components C5b6, C7, C8 and C9 added sequentially to form the MAC, and incubated for a further 3 hrs. To permit MAC deposition on the cell membrane, C5b6 treatment was carried out in the presence of an anti-CD59 mAb (15). As a positive control, cells were primed with LPS and then treated with nigericin (Nig) for 45 mins, a widely used potent activator for the NLRP3 inflammasome.

Treatment with the MAC resulted in extracellular release of IL-1β (**Figure 1A**). In agreement with this, a p17 fragment corresponding with mature IL-1β was detected in cell supernatants, by immunoblotting (**Figure 1B**). Stimulation of LPS-primed cells with the MAC also led to GSDMD processing as shown by the detection in cell lysates of a p31 fragment, corresponding with the pore-forming N-terminal subunit (NT-GSDMD; **Figure 1C**).

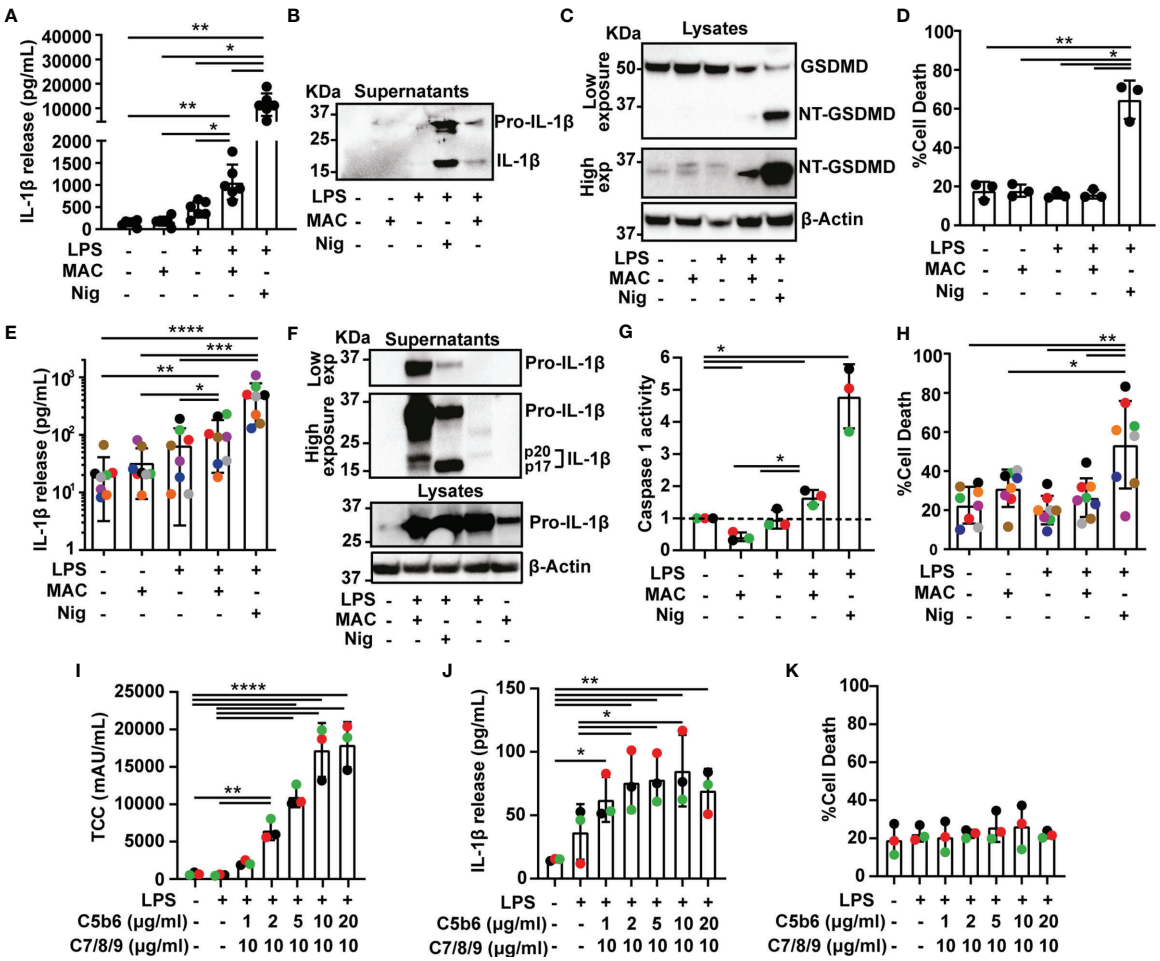

FIGURE 1 | The Membrane Attack Complex induces inflammasome activation in human macrophages. **(A–K)** THP1 cells **(A–D)** and human MDMs **(E–K)** were treated with vehicles or primed with 1 μg/mL LPS for 3 hrs followed by stimulation with 10 μM nigericin (Nig) for 45 mins or with 10 μg/mL anti-CD59 mAb, 10 μg/mL C5b6, unless otherwise specified, C7, C8 and C9 (MAC) for 3 hrs. **(A, E, J)** IL-1β secretion was measured by ELISA. **(B, F)** IL-1β cleavage was analyzed in supernatants by immunoblot. **(C)** GSDMD processing was analyzed in lysates by immunoblot. **(D, H, K)** LDH release was measured as a proxy for cell death. **(F)** Pro-IL-1β production was analyzed in supernatants and cell lysates by immunoblot. **(G)** Caspase 1 activity was measured in cell supernatants and expressed as fold increase *vs* untreated cells. **(I)** TCC (MAC) amount in cell lysates was measured by ELISA. **(A, D, E, G–K)** Data is plotted as mean ± SD and is representative of three **(D, G, I–K)**, six **(A)**, seven **(E)** or eight **(H)** independent experiments. **(E, G–K)** Each color represents a matched donor. **(A, D)** Each dot represents a repeat. **(A, D, E, G–K)** Statistical significance was measured by one-way ANOVA **(A, D, G–K)** or Friedman test **(E)** (*$p < 0.05$, **$p < 0.01$, ***$p < 0.001$, ****$p < 0.0001$). **(B, C, F)** Blots are representative of two independent experiments with similar results.

Cell death, as measured by LDH release from cells, was not significantly increased in MAC-stimulated cells, establishing that cells were not lysed by the complex (**Figure 1D**). Thus, the inflammasome can be activated in PMA-differentiated THP1 cells by the MAC.

We next set to test whether MAC-mediated inflammasome activation occurs in primary human cells. To test this, human monocyte-derived macrophages (MDMs) were activated with LPS and the MAC, which led to processing and secretion of IL-1β (**Figures 1E, F** and **Supplementary Figure 1A**). Furthermore, pro-IL-1β was also detected in lysates of MDMs treated with the MAC alone, indicating that the MAC can regulate IL-1β production (**Figure 1F**). A p20 fragment of IL-1β was also released in LPS-primed MDMs upon MAC activation which could indicate a caspase 1-independent cleavage of this cytokine (**Figure 1F**) (24). To directly test whether stimulation with the MAC triggered caspase 1 activation, treated cells were assayed for caspase 1 activity using a luminescence assay in cell supernatants. Caspase 1 activity was significantly increased upon stimulation with the MAC, as expected (**Figure 1G** and **Supplementary Figure 1B**). Similar to THP1 cells, the MAC did not increase cell death in human MDMs indicating that this complex had a sub-lytic effect (**Figure 1H**). Thus, stimulation of human MDMs with sub-lytic levels of the MAC triggered IL-1β secretion and caspase 1 activation indicating inflammasome activation.

To test the dose-dependency of MAC-mediated inflammasome activation, LPS-primed MDMs were stimulated with concentrations from 1 to 20 μg/mL of C5b6, which is the limiting component for MAC formation, in the presence of 10 μg/mL anti-CD59 and followed by 10 μg/mL of C7, C8 and C9 for 3 hrs. The amount of terminal complement complex (TCC or MAC) was measured in cell lysates by ELISA. As expected, the amount of MAC detected in cell lysates increased with increasing concentration of C5b6 (**Figure 1I**). The greatest levels of IL-1β release were observed when 10 μg/mL C5b6 was used (**Figure 1J**). Cell death was not significantly increased with any of the concentrations used, indicating that MAC formation was always sub-lytic (**Figure 1K**). Subsequent experiments were carried out with 10 μg/mL C5b6.

MAC-Mediated IL-1β Secretion Is Dependent on Both NLRP3 and GSDMD

We next set out to establish whether inflammasome activation triggered by the MAC was dependent on NLRP3. To test this, MDMs were primed with LPS and stimulated with nigericin or the MAC as mentioned previously, in the presence or absence of the NLRP3 inflammasome inhibitor MCC950 (25). The use of MCC950 significantly reduced IL-1β secretion (**Figure 2A**). In contrast, there was no statistically significant change in LDH release produced by the MAC in the presence of MCC950, establishing that cell death was not affected by the inhibitor (**Figure 2B**). For an alternative approach to test the role of NLRP3 in MAC-mediated inflammasome activation, we used THP1$^{nlrp3-/-}$ cells, generated using CRISPR-Cas9 technology as previously described (21). The lack of NLRP3 in these cells was confirmed by immunoblotting (**Figure 2C**). Following LPS and MAC stimulation, IL-1β secretion was impaired in THP1$^{nlrp3-/-}$ cells (**Figure 2D**). As in wild-type THP1 cells, the MAC did not trigger cell death in THP1$^{nlrp3-/-}$ cells, evidenced by no change in LDH release (**Figure 2E**). Thus, NLRP3 is essential for IL-1β secretion triggered by the MAC in human macrophages.

Given the importance of GSDMD for IL-1β secretion upon canonical activation of the NLRP3 inflammasome and the fact that GSDMD cleavage was detected in MAC-stimulated THP1 cells (**Figure 1C**), we next investigated whether GSDMD is involved in MAC-mediated IL-1β release in MDMs. To test this, LPS-primed human MDMs were treated with the MAC in the presence or absence of the GSDMD pore inhibitor necrosulfonamide (NSA) (26). Stimulation with the MAC resulted in the cleavage of GSDMD, and GSDMD processing was impaired by NSA, evidenced by a lack of NT-GSDMD detection by immunoblotting (**Figure 2F**). Crucially, NSA-treated MDMs released significantly less IL-1β upon stimulation with the MAC (**Figure 2G**). Cell death, on the other hand, was not significantly affected (**Figure 2H**). These data are consistent with the idea that GSDMD processing, and therefore pore formation, is important for MAC-mediated IL-1β release in MDMs.

The MAC Localizes With the NLRP3 Inflammasome in Human Macrophages

As MAC-mediated IL-1β secretion in human macrophages is dependent on NLRP3 (**Figures 2A–E**), we next set out to establish the localization of NLRP3 and the MAC within human macrophages. The MAC is formed by a single subunit of C5b6, C7 and C8 and multiple C9 subunits (27). Therefore, to visualize this complex, C9 was directly conjugated to a fluorescent dye (C9-AF647 or C9-JF549). Using confocal imaging, C9 was observed at the cell periphery, indicative of membrane localization, within minutes of stimulation with the MAC (**Supplementary Figures 2A, B**), but after 30 mins C9 was mainly detected intracellularly (**Supplementary Figures 2A, B**), indicating that the MAC was rapidly internalized upon deposition in the cell membrane.

Given that canonical NLRP3 activation is characterized by the oligomerization of the adaptor protein ASC into a speck, cells were stained with an anti-ASC mAb to visualize the inflammasome complex after stimulation with the MAC using C9-JF549. Confocal microscopy revealed ASC speck formation in LPS-primed MDMs after 90 mins of MAC stimulation, indicative of inflammasome assembly (**Figures 3A, B**). The percentage of cells with ASC specks increased over 3 hrs following stimulation (**Figures 3A, B**). Likewise, the percentage of cells with readily detectable intracellular C9 was also increased over 3 hrs (**Figures 3A, C**). Surprisingly, C9 accumulated in specific regions of the cell interior and formed structures with a similar appearance to the ASC specks (**Figures 3A, D**). Further research using specific markers is needed to determine the intracellular trafficking of C9, but strikingly, after 3 hrs of MAC-stimulation, ASC and C9 colocalized in the majority of cells containing ASC specks (**Figures 3D, E**). The MAC is formed by multiple complement components and thus, an accumulation of C9 does

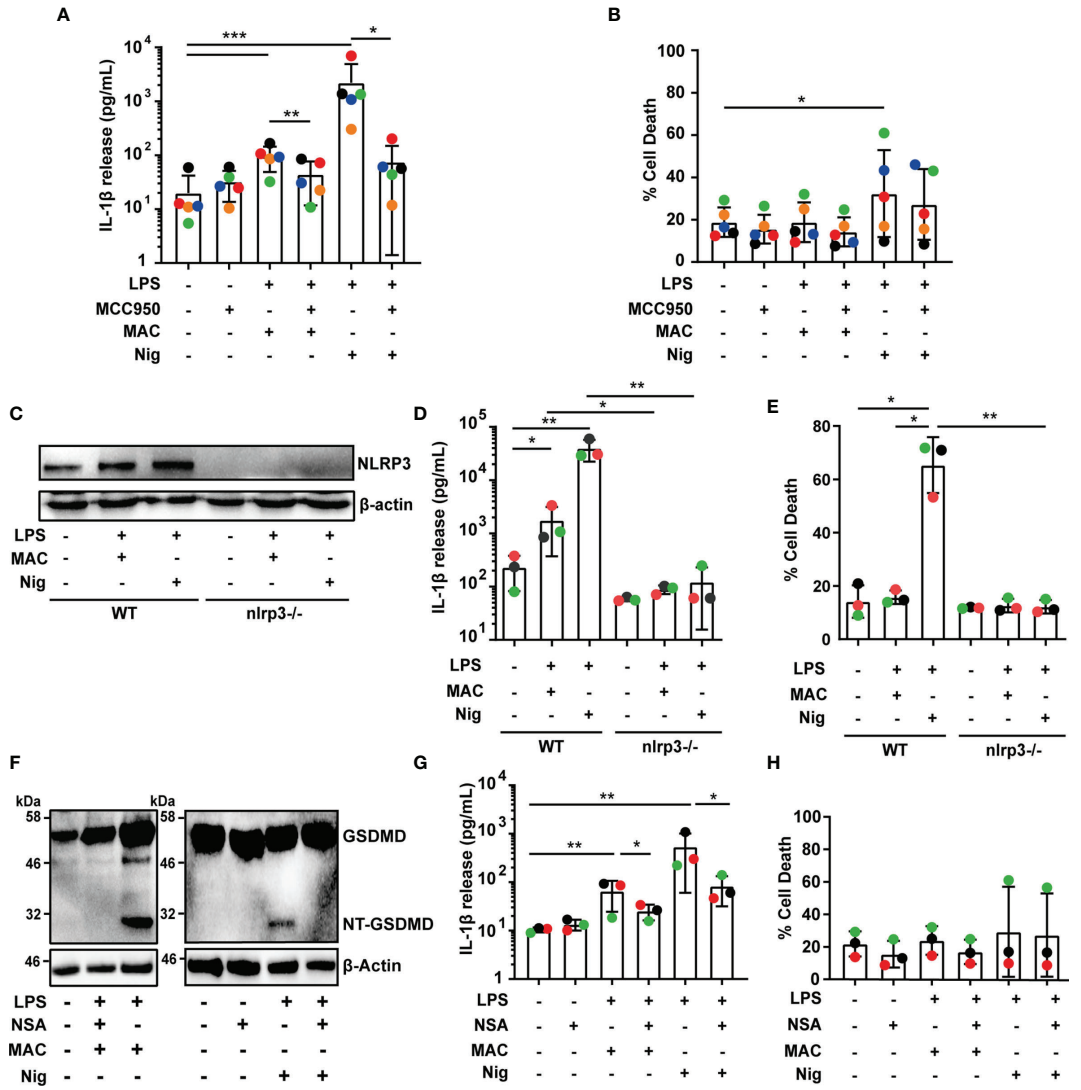

FIGURE 2 | MAC-mediated IL-1β secretion is dependent on NLRP3 and GSDMD. **(A–H)** Human MDMs **(A, B, F–H)** and wild-type THP1 or THP1$^{nlrp3-/-}$ **(C–E)** cells were treated with vehicles or primed with 1 μg/mL LPS for 3 hrs followed by stimulation with 10 μM nigericin (Nig) for 45 mins or with 10 μg/mL anti-CD59 mAb, C5b6, C7, C8 and C9 (MAC) for 3 hrs. **(A, B, F–H)** MAC treatment was carried out in the presence or absence of 1 μM MCC950 **(A, B)** or 10 μM NSA **(F–H)**. **(A, D, G)** IL-1β secretion was measured by ELISA. **(B, E, H)** LDH release was measured as a proxy for cell death. **(C, F)** NLRP3 **(C)** and GSDMD **(F)** production were analyzed in cell lysates by immunoblot. **(A, B, D, E, G, H)** Data is plotted as mean ± SD and is representative of five **(A, B)** or three **(D, E, G, H)** independent experiments. **(A, B, G, H)** Each color represents a matched single donor. **(D, E)** Each color represents a repeat. **(A, B, D, E, G, H)** Statistical significance was measured by Friedman test **(A)** or one-way ANOVA **(B, D, E, G, H)** (*p < 0.05, **p < 0.01, ***p < 0.001). **(C, F)** Blots are representative of two independent experiments with similar results.

not necessarily indicate that fully formed MAC structures remain present intracellularly in the macrophages. To investigate whether the fully formed MAC is internalized, MDMs were also stained with a mAb targeting the TCC. This anti-TCC mAb binds a neoepitope of the MAC, which is only present when C5b6, C7 and C8 are assembled in the complex. Indeed, this mAb also marked regions where both C9 and ASC were detected (**Figure 3D**), establishing that the complete MAC complex is internalized by macrophages. Considering that MAC formation and internalization occurs within minutes of treatment with C5b6, C7, C8 and C9 (**Supplementary Figure 2A**) and that inflammasome assembly occurs 90 mins after stimulation, this implies that the MAC triggers downstream events that over time activate the inflammasome.

To further test whether NLRP3 oligomerization could be directly triggered upon stimulation with the MAC, we generated a THP1 cell line that stably expressed eGFP-NLRP3 in a nlrp3$^{-/-}$ background by transducing THP1$^{nlrp3-/-}$ cells with lentiviral particles containing the vector pLNT-UbC-eGFP-NLRP3. Expression of eGFP-NLRP3 in these cells, which otherwise

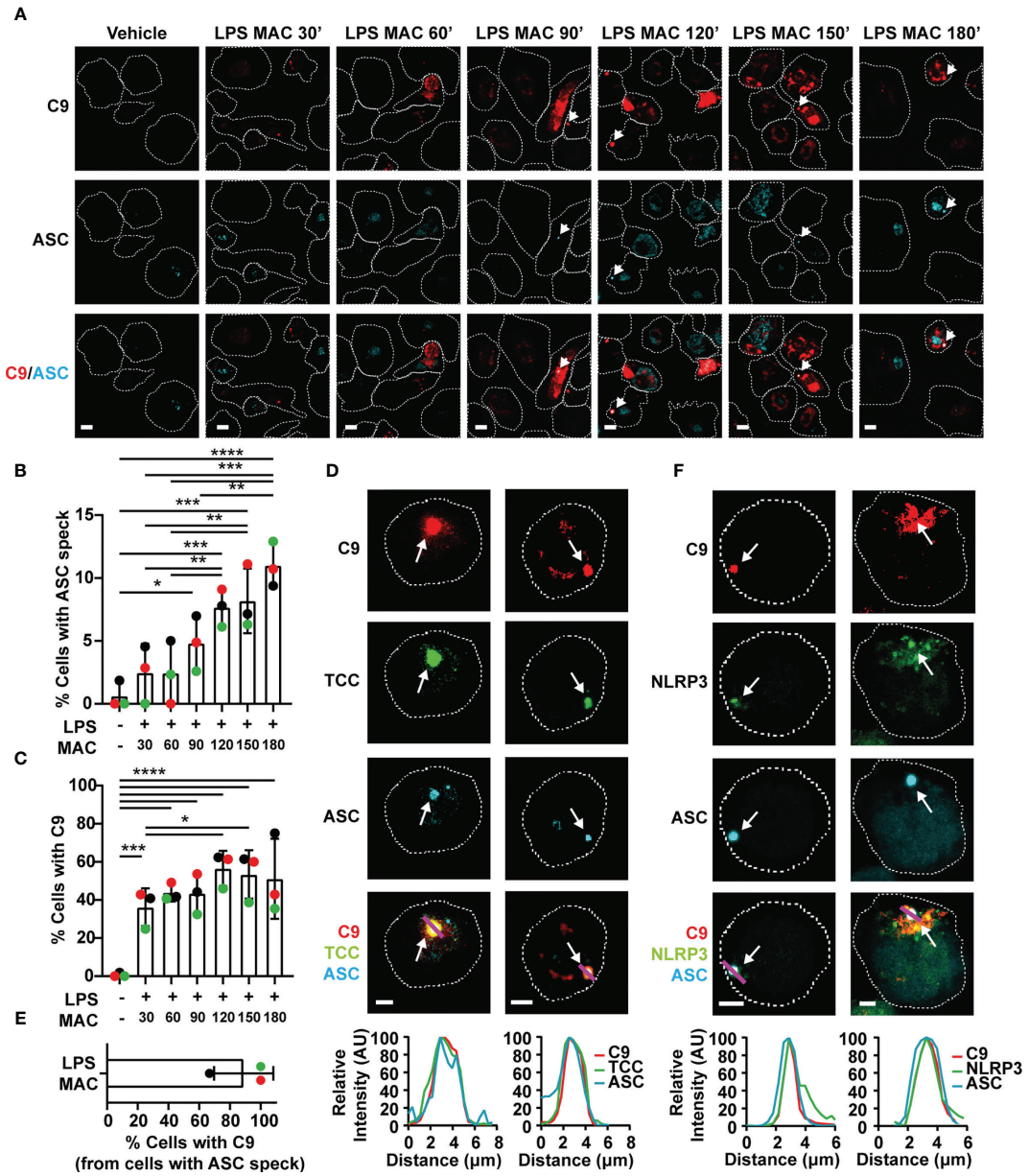

FIGURE 3 | The MAC triggers inflammasome assembly and localizes to the NLRP3-ASC speck. **(A–F)** Human MDMs **(A–E)** and THP1$^{nlrp3-/-}$/eGFP-nlrp3 cells **(F)** were treated with vehicles or primed with 1 μg/mL LPS for 3 hrs followed by stimulation with 10 μg/mL anti-CD59 mAb, C5b6, C7, C8 and C9 labelled with JF-549 (MAC) for the indicated time **(A–C)** or 3hrs **(D–F)**. **(A)** Representative confocal images of C9 (red) and ASC (cyan) overtime. **(B)** Percentage of cells with ASC specks over time. **(C)** Percentage of cells with C9 over time. **(D)** Confocal imaging of C9 (red), ASC (cyan) and TCC (green). **(E)** Percentage of ASC speck positive cells with C9 in the speck. **(F)** Confocal imaging of C9 (red), ASC (cyan) and NLRP3 (green). **(A, D, F)** Dashed lines represent the outline of the cell, arrows point to specks, magenta lines correspond to the plotted line profiles and scale bars are 10 μm **(A)** and 5 μm **(D, F)**. **(B, C, E)** Data is plotted as mean ± SD, each color represents a matched donor. **(B, C)** Statistical significance was measured by one-way ANOVA (*p < 0.05, **p < 0.01, ***p < 0.001, ****p < 0.0001). **(A–F)** Data is representative of 3 independent experiments.

lacked NLRP3, restored their ability to form an active inflammasome upon stimulation with nigericin as shown by IL-18 secretion (**Supplementary Figure 3A**), increased cell death (**Supplementary Figure 3B**), and NLRP3 and ASC speck formation (**Supplementary Figures 3C, D**). Moreover, the use of the NLRP3 inhibitor MCC950 impaired IL-18 secretion, cell death and ASC speck formation (**Supplementary Figures 3A, B, D**). Stimulation with LPS and nigericin led to caspase 1 (Casp-1) and IL-1β processing (**Supplementary Figure 3E**). These results demonstrate that eGFP-NLRP3 is functionally active. More importantly, treatment of these cells with the MAC led to ASC speck formation. At the speck, there was also an accumulation of

C9 and NLRP3 (**Figure 3F**). This provides further evidence that the MAC triggers ASC oligomerization and NLRP3 inflammasome assembly in human macrophages.

The MAC Is Internalized in EEA1 Positive Endosomes

The observation that the MAC is internalized, led us to investigate how this complex is taken up by macrophages. To study this, LPS-primed MDMs were treated with all components of the MAC including C9-AF647. After 30, 90 or 180 mins, cells were fixed and co-stained with an Ab against EEA1 to mark early endosomes. Following 30 mins of MAC treatment, multiple C9 puncta were distributed in the cytosol of the cell (**Figure 4A** and **Supplementary Figure 2A**). These puncta were encircled by the early endosomal marker EEA1 (**Figures 4A, B**). This suggests that C9 is internalized by MDMs *via* EEA1+ endosomes. At later time points, colocalization of C9 and EEA1 was reduced, concurrent with C9 accumulating in larger puncta resembling the structure of inflammasome specks (**Figures 4A, B**). Thus, the MAC is initially internalized into early endosomes before being trafficked to the inflammasome.

MAC-Mediated Inflammasome Activation Is Dependent on Endocytosis

Ion fluxes produced by pore formation in the cell membrane can trigger activation of the NLRP3 inflammasome (28). Therefore, we next investigated whether pore formation by the MAC in the cell membrane is what activates the inflammasome or alternatively, if internalization of the MAC triggers this process. To test this, LPS-primed MDMs were stimulated with the MAC for 3 hrs in the presence or absence of different endocytosis inhibitors: nystatin (Nys), cytochalasin D (Cyt) or dynasore (Dyn) (29–32). Strikingly, all three inhibitors abrogated IL-1β secretion triggered by the MAC (**Figure 4C**), while cell death was unaffected (**Figure 4D**).

Previous work showed that lysis of K562 cells treated with human serum increases in the presence of 40-100 μM dynasore (32). Here, treatment of LPS-primed MDMs with 40-160 μM dynasore, in the absence of the MAC, induced IL-1β secretion but did not trigger cell death (**Supplementary Figures 4A, B**). On the other hand, 10-20 μM dynasore did not result in cytokine secretion by itself, and did not trigger cell death, but significantly reduced MAC-mediated IL-1β release (**Supplementary Figures 4C, D**).

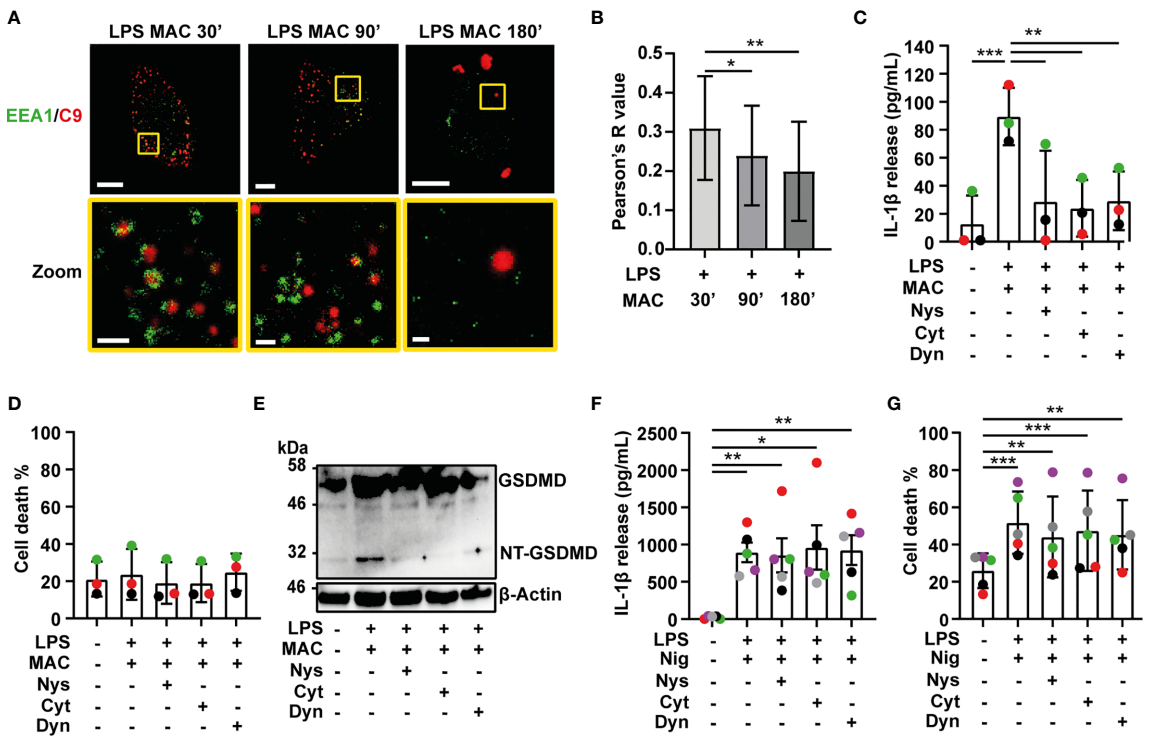

FIGURE 4 | Internalization of the MAC is required for inflammasome activation. **(A, B)** LPS-primed human MDMs were treated with 10 μg/mL anti-CD59 mAb, C5b6, C7, C8 and C9 labelled with AF-647 (MAC) for the indicated time. **(A)** Confocal imaging of EEA1(green) and C9 (red). Yellow squares represent zoom regions and scale bars are 10 μm in full cell pictures and 1 μm in zoom regions. **(B)** Pearson's correlation coefficient of C9 compared to EEA1. **(C–G)** Human MDMs were treated with vehicles or primed with 1 μg/mL LPS for 3 hrs followed by stimulation with 10 μg/mL anti-CD59 mAb, C5b6, C7, C8 and C9 for 3 hrs **(C–E)** or 10 μM nigericin (Nig) for 45 mins **(F, G)** in the presence or absence of 0.1 μg/mL nystatin (Nys), 10 μM cytochalasin D (Cyt) or 10 μM dyanasore (Dyn). **(C, F)** IL-1β secretion was measured by ELISA. **(D, G)** LDH release was measured as a proxy for cell death. **(E)** GSDMD processing was analyzed in cell lysates by immunoblot. **(C, D, F, H)** Data is plotted as mean ± SD, each color represents a matched donor and statistical significance was measured by one-way ANOVA **(B–D, G)** or Friedman's test **(F)** (*$p < 0.05$, **$p < 0.01$, ***$p < 0.001$). **(A–G)** Data is representative of 3 **(A–E)** or 5 **(F, G)** independent experiments.

The NT-GSDMD fragment was not detected in cell lysates of cells treated with any of the endocytosis inhibitors (**Figure 4E**). This shows that inhibition of endocytosis reduced downstream caspase 1 activity and prevented processing of GSDMD. Endocytosis inhibitors did not impair IL-1β secretion in general, since neither IL-1β secretion nor cell death were affected by these inhibitors when cells were stimulated with nigericin (**Figures 4F, G**). Thus, IL-1β secretion following complement-mediated inflammasome activation is specifically dependent on endocytosis of the MAC.

In endothelial cells, endocytosis of the MAC results in the recruitment of various proteins including NF-κB inducing kinase (NIK) that can phosphorylate and activate the NLRP3 sensor to assemble the inflammasome complex (16, 17, 33). To investigate whether NIK is involved in inflammasome activation in MDMs, cells were treated with LPS for 3 hrs, followed by the MAC incorporating C9-AF647 for the indicated time (**Supplementary Figure 5A**). Treatment with the MAC resulted in a change of localization of NIK (**Supplementary Figures 5A, B**). Specifically, the relative abundance of NIK in the cytoplasm increased from early time points after stimulation with the MAC and was decreased after 90 mins, reaching similar levels to cells treated only with LPS (**Supplementary Figures 5A, B**). Whilst NIK localization clearly changed over time, we did not detect colocalization with C9 (**Supplementary Figure 5C**) suggesting that the MAC and NIK may not directly associate.

MAC-Internalization Results in Disruption of the TGN

The dispersion of the trans-Golgi network (TGN) and the recruitment of NLRP3 to the dispersed TGN have been described as upstream events to NLRP3 inflammasome assembly, with multiple inflammasome activators, including nigericin (34). Thus, we next tested if MAC-mediated inflammasome activation is also preceded by dispersion of the TGN. MDMs were treated with LPS followed by the MAC, including the labelled form of C9 (C9-AF647) as previously, for 30, 90 or 180 mins, or nigericin for 45 mins. Cells were then fixed and stained with an Ab against TGN46, a resident membrane protein of the TGN. Different structures of the TGN were revealed by this stain and thus, we classified each cell as exhibiting one of three specific conformations: (i) an intact TGN (iTGN), characterized by a compact single structure; (ii) a fragmented TGN (fTGN), characterized by various stranded structures; or (iii) a dispersed TGN (dTGN), characterized by multiple granular-like dispersed formations (examples shown in **Figure 5A**).

The dispersed TGN structure was observed in LPS-primed MDMs treated with either the MAC or nigericin but not in unstimulated cells (**Figures 5B, C**). This establishes that either type of stimulation triggers this phenomenon for inflammasome activation, and indeed provides further evidence of the MAC to be able to activate the NLRP3 inflammasome. Except in cells stimulated with nigericin, the percentage of cells with fTGN was very similar across conditions (**Figure 5D**). The percentage of cells exhibiting a dTGN was increased in MAC-treated cells from 30 mins of stimulation, although not to the same extent as nigericin-treated cells (**Figure 5B**). The percentage of cells with dTGN remained similar after 90 mins of stimulation (25.5 ± 9% at 30 mins, 25.8 ± 18.9% at 90 mins) and was reduced by 180 mins (18.7 ± 7.3%) (**Figure 5B**). This suggests that dispersion of the TGN occurs soon after internalization of the MAC. Inhibition of MAC endocytosis using nystatin (Nys) reduced dispersion of the TGN (**Figures 5E, F**). However, TGN dispersion did not decrease with the use of the NLRP3 inhibitor MCC950 (**Figures 5E, F**). Thus, TGN dispersion occurs downstream of MAC internalization and upstream of NLRP3 inflammasome assembly. Together, these data establish that the MAC can be internalized by human macrophages into EEA1+ endosomes, which results in disruption of the TGN, the assembly of the NLRP3 inflammasome, caspase 1 activation, GSDMD processing and secretion of IL-1β (**Figure 6**).

DISCUSSION

The terminal pathway of the complement system plays an important role in the development of multiple IL-1β-mediated diseases. For instance, C5b-9 is significantly increased in the serum of patients with bacterial sepsis (19, 20) and in the plasma and synovial fluid of patients with rheumatoid arthritis and osteoarthritis (18, 35, 36). However, whether the terminal complement complex directly impacts macrophage secretion of IL-1β has not been established. Here, we show that formation of the MAC triggers NLRP3-dependent IL-1β secretion providing a link between the terminal pathway of the complement system and IL-1β release in human macrophages. As inflammation and complement activation are intricately linked, this mechanism is likely to be involved in a range of acute and chronic inflammatory diseases.

Specifically, we found that sequential addition of the complement proteins C5b6, C7, C8 and C9 in serum-free media triggered NLRP3-dependent IL-1β release in human macrophages demonstrating that the MAC can activate the inflammasome. MAC-mediated NLRP3 inflammasome activation has been previously described in lung epithelial cells, endothelial cells and myeloid cells (14–16, 37). As well as using different cell types, these prior studies used serum as a source of complement. Bioactive molecules and growth factors present in serum, such as complement component 5a or fibroblast growth factor (38, 39), could enhance MAC-mediated inflammasome responses. Thus, our data clarifies that the MAC can activate the inflammasome independently of other serum components and more importantly, that human macrophages are activated in this way, being a vital source of this cytokine in the human body.

Phagocytosis of particles opsonized by complement-containing serum can trigger IL-1β release in human macrophages (37). However, our data show that deposition of the MAC can directly trigger caspase 1 activation, GSDMD processing and IL-1β secretion in the absence of phagocytosis. This gives a broader role for this complex in promoting

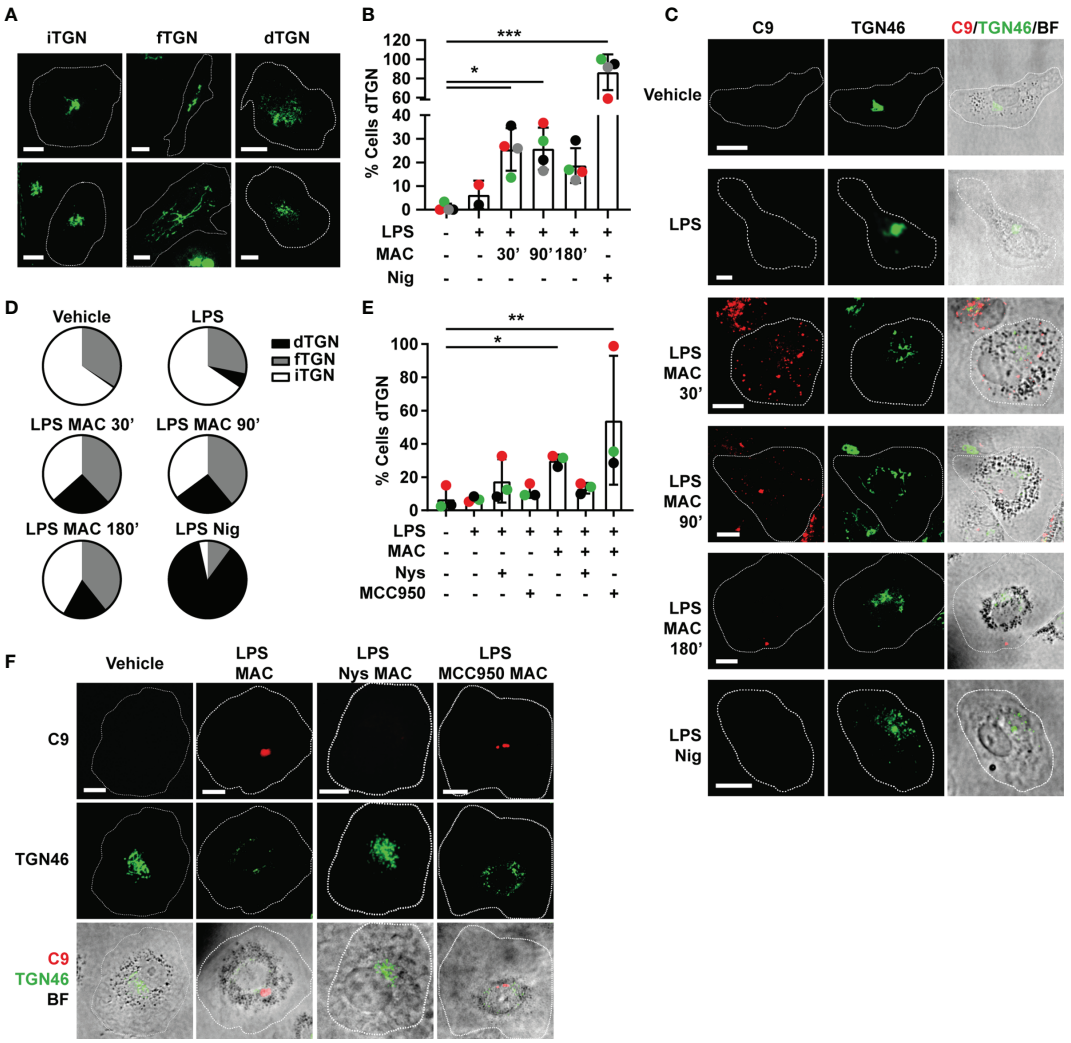

FIGURE 5 | Endocytosis of the MAC triggers disruption of the TGN. **(A–D)** Human MDMs were treated with vehicles or primed with 1 μg/mL LPS for 3 hrs followed by stimulation with 10 μg/mL anti-CD59 mAb, C5b6, C7, C8 and C9 labelled with AF-647 (MAC) for the indicated time or nigericin (Nig) for 45 mins. **(E, F)** Human MDMs were treated with vehicles or primed with LPS and the MAC for 3 hrs in the presence or absence of 0.1 μg/mL nystatin (Nys) or 1 μM MCC950. **(A)** Representative confocal images of the different TGN conformations: intact TGN (iTGN), fragmented TGN (fTGN) and dispersed TGN (dTGN). **(B, E)** Percentage of cells with dTGN. **(C)** Representative confocal images of the results analyzed in panel **(B)**. **(F)** Representative confocal images of the results analyzed in panel **(E)**. **(C, F)** TGN46 (green) and C9 (red) and brightfield images (gray). Dashed lines represent cell outlines and scale bars are 10 μm. **(D)** Pie charts representing the percentage of cells with dTGN, fTGN and iTGN in each condition. **(B, E)** Data is plotted as mean ± SD, each color represents a matched donor and statistical significance was measured by Friedman's test (*$p < 0.05$, **$p < 0.01$, ***$p < 0.001$). **(B–E)** Data is representative of 3 **(E, F)** or 4 **(B–D)** independent experiments.

proinflammatory responses, including in the context of sterile inflammation when inflammasome priming is provided by endogenous DAMPs such as amyloids aggregates and cholesterol crystals (40). Moreover, the MAC triggers IL-1β secretion in the absence of cell death, suggesting that it drives macrophages into a state of hyperactivation, in which they secrete IL-1β while maintaining viability (5). Hyperactive macrophages secrete less IL-1β than macrophages undergoing pyroptosis, which fits with our observation that IL-1β secretion upon stimulation with the MAC occurs to a lesser extent than in nigericin-stimulated cells. Importantly, low levels of IL-1β are able to activate downstream signaling pathways in target cells (41–45) suggesting that the levels of MAC-mediated inflammasome activation and IL-1β release seen in our experiments can be biologically important.

Pro-IL-1β is not considered biologically active. However, proteases derived from neutrophils and pathogens such as *S. aureus* are able to process pro-IL-1β into active molecules (46, 47). Specifically, in models of acute arthritis, proteinase 3 from neutrophils can cleave pro-IL-1β (48) and MAC deposition is known to be elevated in the context of arthritis (17, 18). Thus, the high levels of pro-IL-1β secretion observed after stimulation with the MAC can be relevant both in the context of sterile inflammation and during infection.

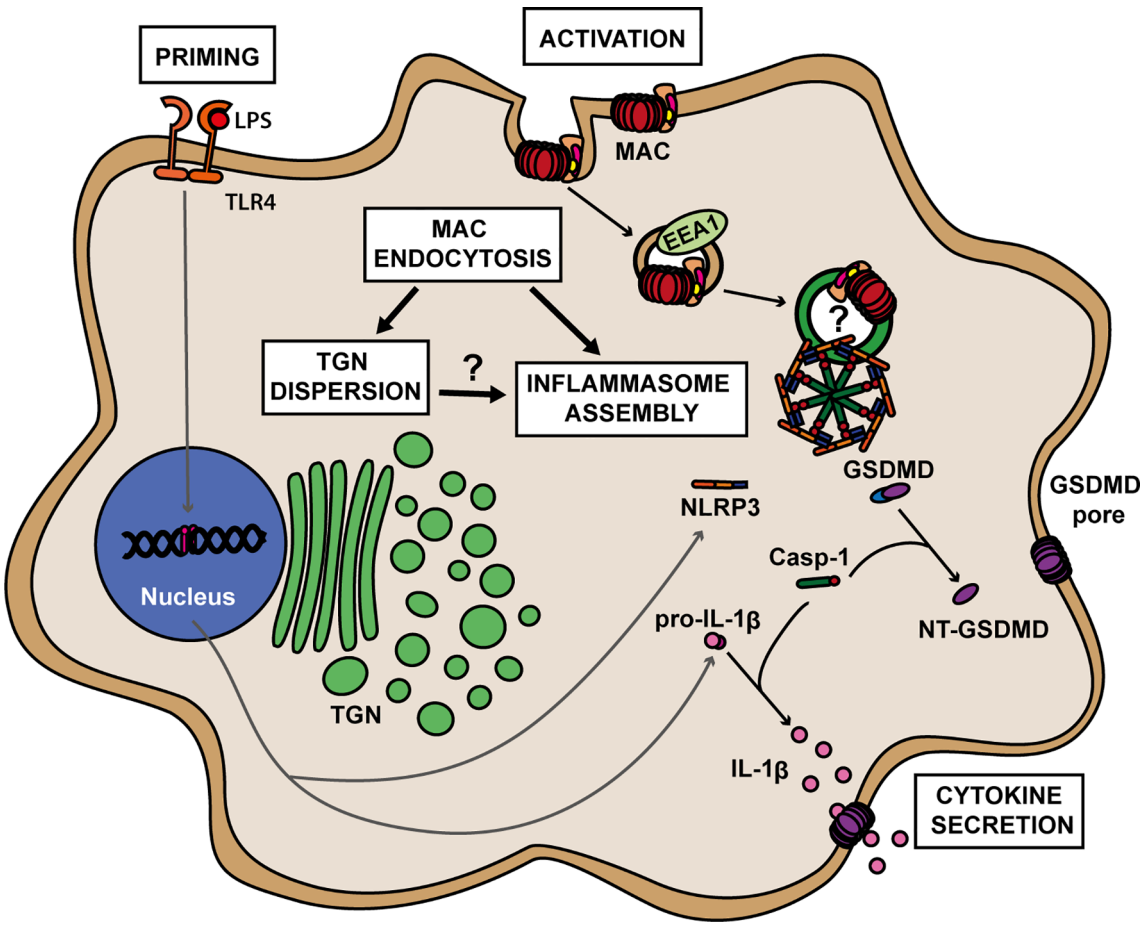

FIGURE 6 | A proposed model for MAC-mediated NLRP3 inflammasome activation in human macrophages. Formation of the MAC in the cell membrane triggers its internalization *via* EEA1+ endosomes. Endocytosis of the MAC leads to dispersion of the trans-Golgi network (TGN) and to the assembly of the NLRP3 inflammasome. The roles of TGN dispersion as well as any direct involvement of MAC components on inflammasome assembly remain to be elucidated. Within the NLRP3 complex, caspase 1 (Casp-1) becomes active and cleaves GSDMD into its pore-forming subunit, NT-GSDMD, and pro-IL-1β into its active form IL-1β. Multiple NT-GSDMD subunits assemble in the cell membrane to form GSDMD pores resulting in the release of IL-1β to the extracellular milieu.

Intracellular LPS can activate caspases 4 and 5 that in turn activate the NLRP3 inflammasome (49, 50). Here, macrophages were primed with LPS prior to MAC treatment. LPS was washed off before MAC stimulation. However, residual levels of LPS could feasibly enter the cell through the MAC and activate caspases 4 and 5. LPS from gram-negative bacteria can activate the complement cascade (51, 52). Therefore, determining whether the entrance of LPS through MAC pores leads to the activation of caspases 4 and 5 and downstream signaling pathways would be interesting to explore further in the context of infection.

In general, mechanisms by which complement activates cells are complex, multi-faceted and vary by cell type. MAC formation in human lung epithelial cells triggers increased cytosolic Ca^{2+} and loss of membrane potential in the mitochondria, with both processes being suggested to be responsible for the activation of the NLRP3 inflammasome (15). Here, we found that, in human macrophages, the MAC is internalized in EEA1+ endosomes from early time points and that endocytosis is required for inflammasome activation. This suggests that ion fluxes caused by MAC deposition in the cell surface membrane might not be sufficient to activate the inflammasome in macrophages but may trigger the internalization of the complex that in turn initiates inflammasome activation. In support of this, dispersion of the trans-Golgi network (TGN), an event that occurs with canonical NLRP3 inflammasome assembly (34), is triggered only upon internalization of the MAC. Previous work has established that other pore-forming toxins including α-haemolysin and streptolysin activate the NLRP3 inflammasome (53). These toxins are also known to be removed from the cell membrane through different mechanisms, including endocytosis (40, 54). Thus, it is possible that internalization of a pore-forming complex is, broadly, able to trigger inflammasome activation.

In response to antibody-mediated complement activation, endothelial cells internalize the MAC in Rab5+ and EEA1+ early endosomes, which results in the recruitment of NLRP3 in a process involving NF-κB–inducing kinase (NIK) (16, 17, 33).

We did not observe colocalization of NIK and C9 at time points where C9 localized to early endosomes or to the inflammasome speck. However, the observation of a change in localization of NIK, going from the nucleus to the cytoplasm after stimulation with the MAC could reflect a role for NIK in MAC-mediated NLRP3 inflammasome assembly in human macrophages as shown in endothelial cells (16, 17, 33).

In retinal epithelial cells, MAC internalization in endosomes and subsequent migration to lysosomes for degradation contributes to the reduction of lytic effects of membrane-bound MAC (29). Podocytes target the MAC for degradation through the autophagic-lysosomal pathway, with the expression of the autophagy markers LC3 and p62 enhanced during this process (55). In THP1 cells, LC3, p62 and ASC are found together upon NLRP3 inflammasome stimulation (56, 57). Overall, this suggests a crosslink between the autophagic-lysosomal pathway in the NLRP3 and the MAC signaling cascades. In addition, internalization of particulate matter such as silica or alum can lead to lysosomal disruption and K^+ efflux, leading to assembly of the inflammasome (58, 59). Given that MAC endocytosis is key to triggering inflammasome assembly in human macrophages and that the level of intracellular C9 is reduced over time, this indicates that the MAC could be targeted for degradation through the lysosomal pathway as in podocytes and retinal epithelial cells. As such, MAC internalization could result in lysosomal damage and subsequent activation of the inflammasome.

It is also possible that disruption of the TGN triggered by MAC internalization plays a role in inflammasome assembly. Endosomes constantly exchange cargo with the TGN and EEA1 can localize to the TGN in various cell types (60). In HeLa cells expressing exogeneous NLRP3 and EEA1, these proteins colocalized with the TGN protein TGN38 upon stimulation with NLRP3 activators (34) indicating the interaction between the endosomal compartment, the TGN and the NLRP3 sensor. NLRP3 can be recruited to the TGN by interaction with phosphatidylinositol-4-phosphate that is exposed in the dispersed TGN (34). In macrophages, NLRP3 activators also trigger the recruitment of mitochondria-associated endoplasmic reticulum membranes (MAMs) to the Golgi. At these MAMs, NLRP3 is phosphorylated leading to its activation (61, 62). Then, upon activation at the MAMs, NLRP3 sensors can be transported to the centrosome where inflammasome assembly occurs upon recruitment of ASC and caspase 1 (56). Considering that our findings show that dispersion of the TGN occurs before inflammasome activation, interaction of MAC-containing EEA1+ endosomes with the TGN may trigger its dispersion leading to NLRP3 recruitment and the consequent assembly of the inflammasome complex. However, further investigation using specific cell compartment markers is needed to determine precisely where the MAC locates within the cell.

These details are important because the complement system plays a role in the pathogenesis of multiple pro-inflammatory diseases characterized by increased levels of IL-1β, including septic shock and rheumatoid arthritis (17–20, 63). Direct or indirect blocking of IL-1β using drugs, such as anakinra or canakinumab, has been used in the treatment of such inflammatory diseases (1). However, the effectiveness of IL-1β blockade is context dependent, varying among patients and diseases (1). Considering that the complement system plays a role in the development of these pathologies and that the MAC triggers IL-1β secretion in human macrophages, one of the main sources of this cytokine, future therapies for IL-1β-mediated diseases could consider targeting the upstream events that trigger cytokine secretion. Specifically, the growing mechanistic evidence of how the MAC modulates inflammation through activation of the inflammasome may lay the foundations for a broader application of anti-MAC therapies in the treatment of inflammatory diseases in which the complement system and IL-1β play an important role, including osteoarthritis, rheumatoid arthritis, and diseases of the central nervous system.

DATA AVAILABILITY STATEMENT

The original contributions presented in the study are included in the article/**Supplementary Material**. Further inquiries can be directed to the corresponding author.

AUTHOR CONTRIBUTIONS

ID-d-O and AA: Acquisition and analysis of data. ID-d-O, JW, GT, E-MN, GL-C, and DMD: Conceptual design. ID-d-O, JW, E-MN, GL-C, DMD: Wrote the manuscript. FM-S and AG: provided novel reagents. All authors contributed to the article and approved the submitted version.

FUNDING

This work was supported by a PhD studentship funded by GSK (to ID-d-O), a Wellcome Trust Investigator Award (110091/Z/15/Z), a Wellcome Trust Sir Henry Dale Fellowship (104192/Z/14/Z) to GL-C, and the Manchester Collaborative Centre for Inflammation Research (funded by a precompetitive open-innovation award from GSK, AstraZeneca, and The University of Manchester, United Kingdom). GSK was not involved in the study design, collection, analysis, interpretation of data, the writing of this article or the decision to submit it for publication.

ACKNOWLEDGMENTS

We thank Prof. Veit Hornung for kindly providing the $THP1^{nlrp3-/-}$ cell line and Dr Pawel Pazek for sharing with us the lentiviral destination vector, pLNT-UbC-eGFP-#. The authors thank everyone in the Davis Laboratory for discussion and Kevin Stacey for cell isolations.

SUPPLEMENTARY MATERIAL

The Supplementary Material for this article can be found online at: https://www.frontiersin.org/articles/10.3389/fimmu.2021.720655/full#supplementary-material

REFERENCES

1. Dinarello CA, Simon A, van der Meer JWM. Treating Inflammation by Blocking Interleukin-1 in a Broad Spectrum of Diseases. *Nat Rev Drug Discovery* (2012) 12:633–52. doi: 10.1038/nrd3800
2. Brough D, Rothwell NJ. Caspase-1-Dependent Processing of Pro-Interleukin-1beta is Cytosolic and Precedes Cell Death. *J Cell Sci* (2007) 120:772–81. doi: 10.1242/jcs.03377
3. Fernandes-Alnemri T, Wu J, Yu JW, Datta P, Miller B, Jankowski W, et al. The Pyroptosome: A Supramolecular Assembly of ASC Dimers Mediating Inflammatory Cell Death *via* Caspase-1 Activation. *Cell Death Differ* (2007) 14:1590–604. doi: 10.1038/sj.cdd.4402194
4. Latz E, Xiao T, Stutz A. Activation and Regulation of the Inflammasomes. *Nat Rev Immunol* (2013) 13:397–411. doi: 10.1038/nri34522013;13:23702978
5. Evavold CL, Ruan J, Tan Y, Xia S, Wu H, Kagan JC. The Pore-Forming Protein Gasdermin D Regulates Interleukin-1 Secretion From Living Macrophages. *Immunity* (2018) 48:35–44. doi: 10.1016/j.immuni.2017.11.013
6. Liu X, Zhang Z, Ruan J, Pan Y, Magupalli VG, Wu H, et al. Inflammasome-Activated Gasdermin D Causes Pyroptosis by Forming Membrane Pores. *Nature* (2016) 535:153–8. doi: 10.1038/nature18629
7. Shi J, Zhao Y, Wang K, Shi X, Wang Y, Huang H, et al. Cleavage of GSDMD by Inflammatory Caspases Determines Pyroptotic Cell Death. *Nature* (2015) 526:660–5. doi: 10.1038/nature15514
8. Ricklin D, Hajishengallis G, Yang K, Lambris JD. Complement: A Key System for Immune Surveillance and Homeostasis. *Nat Immunol* (2010) 11:785–97. doi: 10.1038/ni.1923
9. Morgan BP. The Membrane Attack Complex as an Inflammatory Trigger. *Immunobiology* (2016) 221:747–51. doi: 10.1016/j.imbio.2015.04.006
10. Moskovich O, Fishelson Z. Live Cell Imaging of Outward and Inward Vesiculation Induced by the Complement C5b-9 Complex. *J Biol Chem* (2007) 282:29977–86. doi: 10.1074/jbc.M703742200
11. Scolding NJ, Morgan BP, Houston WAJ, Linington C, Campbell AK, Compston DAS. Vesicular Removal by Oligodendrocytes of Membrane Attack Complexes Formed by Activated Complement. *Nature* (1989) 339:620–2. doi: 10.1038/339620a0
12. Kerjaschki D, Schulze M, Binder S, Kain R, Ojha PP, Susani M, et al. Transcellular Transport and Membrane Insertion of the C5b-9 Membrane Attack Complex of Complement by Glomerular Epithelial Cells in Experimental Membranous Nephropathy. *J Immunol* (1989) 143:546–52.
13. Morgan BP, Dankert JR, Esser AF. Recovery of Human Neutrophils From Complement Attack: Removal of the Membrane Attack Complex by Endocytosis and Exocytosis. *J Immunol* (1987) 138:246–53.
14. Laudisi F, Spreafico R, Evrard M, Hughes TR, Mandriani B, Kandasamy M, et al. Cutting Edge: The NLRP3 Inflammasome Links Complement-Mediated Inflammation and IL-1β Release. *J Immunol* (2013) 191:1006–10. doi: 10.4049/jimmunol.1300489
15. Triantafilou K, Hughes TR, Triantafilou M, Morgan BP. The Complement Membrane Attack Complex Triggers Intracellular Ca2+ Fluxes Leading to NLRP3 Inflammasome Activation. *J Cell Sci* (2013) 126:2903–13. doi: 10.1242/jcs.124388
16. Xie CB, Qin L, Li G, Fang C, Kirkiles-Smith NC, Tellides G, et al. Complement Membrane Attack Complexes Assemble NLRP3 Inflammasomes Triggering IL-1 Activation of IFN-γ–Primed Human Endothelium. *Circ Res* (2019) 124:1747–59. doi: 10.1161/CIRCRESAHA.119.314845
17. Fang C, Manes TD, Liu L, Liu K, Qin L, Li G, et al. ZFYVE21 is a Complement-Induced Rab5 Effector That Activates non-Canonical NF-κb *via* Phosphoinosotide Remodeling of Endosomes. *Nat Commun* (2019) 10:2247. doi: 10.1038/s41467-019-10041-2
18. Bemis EA, Norris JM, Seifert J, Frazer-Abel A, Okamoto Y, Feser ML, et al. Complement and its Environmental Determinants in the Progression of Human Rheumatoid Arthritis. *Mol Immunol* (2019) 112:256–65. doi: 10.1016/j.molimm.2019.05.012
19. Furebring M, Håkansson LD, Venge P, Nilsson B, Sjölin J. Expression of the C5a Receptor (CD88) on Granulocytes and Monocytes in Patients With Severe Sepsis. *Crit Care* (2002) 6:363–70. doi: 10.1186/cc1524
20. Unnewehr H, Rittirsch D, Sarma JV, Zetoune F, Flierl MA, Perl M, et al. Changes and Regulation of the C5a Receptor on Neutrophils During Septic Shock in Humans. *J Immunol* (2013) 190:4215–25. doi: 10.4049/jimmunol.1200534
21. Schmid-Burgk JL, Gaidt MM, Schmidt T, Ebert TS, Bartok E, Hornung V. Caspase-4 Mediates non-Canonical Activation of the NLRP3 Inflammasome in Human Myeloid Cells. *Eur J Immunol* (2015) 45:2911–7. doi: 10.1002/eji.201545523
22. Bagnall J, Boddington C, Boyd J, Brignall R, Rowe W, Jones NA, et al. Quantitative Dynamic Imaging of Immune Cell Signalling Using Lentiviral Gene Transfer. *Integr Biol* (2015) 7:713–25. doi: 10.1039/c5ib00067j
23. Schneider CA, Rasband WS, Eliceiri KW. NIH Image to ImageJ: 25 Years of Image Analysis. *Nat Methods* (2012) 9:671–5. doi: 10.1038/nmeth.2089
24. Edye ME, Lopez-Castejon G, Allan SM, Brough D. Acidosis Drives Damage-Associated Molecular Pattern (DAMP)-Induced Interleukin-1 Secretion *via* a Caspase-1-Independent Pathway. *J Biol Chem* (2013) 288:30485–94. doi: 10.1074/jbc.M113.478941
25. Coll RC, Robertson AAB, Chae JJ, Higgins SC, Muñoz- R, Inserra MC, et al. A Small Molecule Inhibitior of the NLRP3 Inflammasome is a Potential Therapeutic for Inflammatory Diseases. *Nat Med* (2015) 21:248–55. doi: 10.1038/nm.380621(3):248–55
26. Rathkey JK, Zhao J, Liu Z, Chen Y, Yang J, Kondolf HC, et al. Chemical Disruption of the Pyroptotic Pore-Forming Protein Gasdermin D Inhibits Inflammatory Cell Death and Sepsis. *Sci Immunol* (2018) 3:eaat2738. doi: 10.1126/sciimmunol.aat27386
27. Serna M, Giles JL, Morgan BP, Bubeck D. Structural Basis of Complement Membrane Attack Complex Formation. *Nat Commun* (2016) 7:10587. doi: 10.1038/ncomms10587A
28. Gong T, Yang Y, Jin T, Jiang W, Zhou R. Orchestration of NLRP3 Inflammasome Activation by Ion Fluxes. *Trends Immunol* (2018) 39:393–406. doi: 10.1016/j.it.2018.01.009
29. Georgiannakis A, Burgoyne T, Lueck K, Futter C, Greenwood J, Moss SE. Retinal Pigment Epithelial Cells Mitigate the Effects of Complement Attack by Endocytosis of C5b-9. *J Immunol* (2015) 195:3382–9. doi: 10.4049/jimmunol.1500937
30. Macia E, Ehrlich M, Massol R, Boucrot E, Brunner C, Kirchhausen T. Dynasore, a Cell-Permeable Inhibitor of Dynamin. *Dev Cell* (2006) 10:839–50. doi: 10.1016/j.devcel.2006.04.002
31. Payne CK, Jones SA, Chen C, Zhuang X. Internalization and Trafficking of Cell Surface Proteoglycans and Proteoglycan-Binding Ligands. *Traffic* (2007) 8:389–401. doi: 10.1111/j.1600-0854.2007.00540.x
32. Moskovich O, Herzog L-OO, Ehrlich M, Fishelson Z. Caveolin-1 and Dynamin-2 Are Essential for Removal of the Complement C5b-9 Complex *via* Endocytosis. *J Biol Chem* (2012) 287:19904–15. doi: 10.1074/jbc.M111.333039
33. Jane-wit D, Surovtseva YV, Qin L, Li G, Liu R, Clark P, et al. Complement Membrane Attack Complexes Activate Noncanonical NF-κb by Forming an Akt + NIK + Signalosome on Rab5 + Endosomes. *Proc Natl Acad Sci USA* (2015) 112:9686–91. doi: 10.1073/pnas.150353511t
34. Chen J, Chen ZJ. PtdIns4P on Dispersed Trans-Golgi Network Mediates NLRP3 Inflammasome Activation. *Nature* (2018) 564:71–6. doi: 10.1038/s41586-018-0761-3
35. Morgan BP, Daniels RH, Williams BD. Measurement of Terminal Complement Complexes in Rheumatoid Arthritis. *Clin Exp Immunol* (1988) 73:473–78.
36. Struglics A, Okroj M, Swärd P, Frobell R, Saxne T, Lohmander LS, et al. The Complement System is Activated in Synovial Fluid From Subjects With Knee Injury and From Patients With Osteoarthritis. *Arthritis Res Ther* (2016) 18:1–11. doi: 10.1186/s13075-016-1123-x
37. Suresh R, Chandrasekaran P, Sutterwala FS, Mosser DM. Complement-Mediated 'Bystander' Damage Initiates Host NLRP3 Inflammasome Activation. *J Cell Sci* (2016) 129:1928–39. doi: 10.1242/jcs.179291
38. Khameneh HJ, Ho AWS, Laudisi F, Derks H, Kandasamy M, Sivasankar B, et al. C5a Regulates IL-1β Production and Leukocyte Recruitment in a Murine Model of Monosodium Urate Crystal-Induced Peritonitis. *Front Pharmacol* (2017) 8:10. doi: 10.3389/fphar.2017.00010
39. ZhuGe DL, Javaid HMA, Sahar NE, Zhao YZ, Huh JY. Fibroblast Growth Factor 2 Exacerbates Inflammation in Adipocytes Through NLRP3 Inflammasome Activation. *Arch Pharm Res* (2020) 43:1311–24. doi: 10.1007/s12272-020-01295-2
40. Patel MN, Carroll RG, Galván-Peña S, Mills EL, Olden R, Triantafilou M, et al. Inflammasome Priming in Sterile Inflammatory Disease. *Trends Mol Med* (2017) 23:165–80. doi: 10.1016/j.molmed.2016.12.007

41. Friedman W, Thakur S, Seidman L, Rabson A. Regulation of Nerve Growth Factor mRNA by Interleukin-1 in Rat Hippocampal Astrocytes Is Mediated by Nfκb. *J Biol Chem* (1996) 271:31115–20. doi: 10.1074/jbc.271.49.31115
42. Silva I, Peccerella T, Mueller S, Rausch V. IL-1 Beta-Mediated Macrophage-Hepatocyte Crosstalk Upregulates Hepcidin Under Physiological Low Oxygen Levels. *Redox Biol* (2019) 24:101209. doi: 10.1016/j.redox.2019.101209
43. Andersen PAK, Petrenko V, Rose PH, Koomen M, Fischer N, Ghiasi SM, et al. Proinflammatory Cytokines Perturb Mouse and Human Pancreatic Islet Circadian Rhythmicity and Induce Uncoordinated β-Cell Clock Gene Expression *via* Nitric Oxide, Lysine Deacetylases, and Immunoproteasomal Activity. *Int J Mol Sci* (2021) 22:1–25. doi: 10.3390/ijms22010083
44. McNulty AL, Rothfusz NE, Leddy HA, Guilak F. Synovial Fluid Concentrations and Relative Potency of Interleukin-1 Alpha and Beta in Cartilage and Meniscus Degradation. *J Orthop Res* (2013) 31:1039–45. doi: 10.1002/jor.22334
45. Huang Y, Smith DE, Ibáñez-Sandoval O, Sims JE, Friedman WJ. Neuron-Specific Effects of Interleukin-1β Are Mediated by a Novel Isoform of the IL-1 Receptor Accessory Protein. *J Neurosci* (2011) 31:18048–59. doi: 10.1523/JNEUROSCI.4067-11.2011
46. Black RA, Kronheim SR, Cantrell M, Deeley MC, March CJ, Prickett KS, et al. Generation of Biologically Active Interleukin-1 Beta by Proteolytic Cleavage of the Inactive Precursor. *J Biol Chem* (1988) 263:9437–42. doi: 10.1016/S0021-9258(19)76559-4
47. Fantuzzi G, Ku G, Harding MW, Livingston DJ, Sipe JD, Kuida K, et al. Response to Local Inflammation of IL-1 Beta-Converting Enzyme- Deficient Mice. *J Immunol* (1997) 158:1818–24.
48. Joosten LAB, Netea MG, Fantuzzi G, Koenders MI, Helsen MMA, Sparrer H, et al. Inflammatory Arthritis in Caspase-1 Gene Deficient Mice: Contribution of Proteinase 3 for Caspase-1-Independent Production of Bioactive IL-1β. *Arthritis Rheum* (2009) 60:3651–62. doi: 10.1002/art.25006
49. Casson CN, Yu J, Reyes VM, Taschuk FO, Yadav A, Copenhaver AM, et al. Human Caspase-4 Mediates Noncanonical Inflammasome Activation Against Gram-Negative Bacterial Pathogens. *Proc Natl Acad Sci USA* (2015) 112:6688–93. doi: 10.1073/pnas.1421699112
50. Shi J, Zhao Y, Wang Y, Gao W, Ding J, Li P, et al. Inflammatory Caspases are Innate Immune Receptors for Intracellular LPS. *Nature* (2014) 514:187–92. doi: 10.1038/nature13683
51. Brandtzaeg P, Hagåsen K, Kierulf P, Mollnes TE. The Excessive Complement Activation in Fulminant Meningococcal Septicemia Is Predominantly Caused by Alternative Pathway Activation. *J Infect Dis* (1996) 173:647–55. doi: 10.1093/infdis/173.3.647
52. Hsueh W, Sun X, Rioja LN, Gonzalez-Crussi F. The Role of the Complement System in Shock and Tissue Injury Induced by Tumour Necrosis Factor and Endotoxin. *Immunology* (1990) 70:309.
53. Jing W, Lo Pilato J, Kay C, Man SM. Activation Mechanisms of Inflammasomes by Bacterial Toxins. *Cell Microbiol* (2021) 23:e13309. doi: 10.1111/cmi.13309
54. Husmann M, Beckmann E, Boller K, Kloft N, Tenzer S, Bobkiewicz W, et al. Elimination of a Bacterial Pore-Forming Toxin by Sequential Endocytosis and Exocytosis. *FEBS Lett* (2009) 583:337–44. doi: 10.1016/j.febslet.2008.12.028
55. Liu X, Lieberman J. A Mechanistic Understanding of Pyroptosis: The Fiery Death Triggered by Invasive Infection. *Adv Immunol* (2017) 135:81–117. doi: 10.1016/bs.ai.2017.02.002
56. Magupalli VG, Negro R, Tian Y, Hauenstein AV, Caprio G, Skillern W, et al. HDAC6 Mediates an Aggresome-Like Mechanism for NLRP3 and Pyrin Inflammasome Activation. *Science* (2020) 369:eaas8995. doi: 10.1126/science.aas8995
57. Shi CS, Shenderov K, Huang NN, Kabat J, Abu-Asab M, Fitzgerald KA, et al. Activation of Autophagy by Inflammatory Signals Limits IL-1β Production by Targeting Ubiquitinated Inflammasomes for Destruction. *Nat Immunol* (2012) 13:255–63. doi: 10.1038/ni.2215
58. Hornung V, Bauernfeind F, Halle A, Samstad EO, Kono H, Rock KL, et al. Silica Crystals and Aluminum Salts Activate the NALP3 Inflammasome Through Phagosomal Destabilization. *Nat Immunol* (2008) 9:847–56. doi: 10.1038/ni.1631
59. Muñoz-Planillo R, Kuffa P, Martínez-Colón G, Smith BL, Rajendiran TM, Núñez G. K+ Efflux Is the Common Trigger of NLRP3 Inflammasome Activation by Bacterial Toxins and Particulate Matter. *Immunity* (2013) 38:1142–53. doi: 10.1016/j.immuni.2013.05.016
60. Tu Y, Zhao L, Billadeau DD, Jia D. Endosome-To-TGN Trafficking: Organelle-Vesicle and Organelle-Organelle Interactions. *Front Cell Dev Biol* (2020) 8:163. doi: 10.3389/fcell.2020.00163
61. Zhou R, Yazdi AS, Menu P, Tschopp J. A Role for Mitochondria in NLRP3 Inflammasome Activation. *Nature* (2011) 469:221–6. doi: 10.1038/nature09663
62. Misawa T, Takahama M, Kozaki T, Lee H, Zou J, Saitoh T, et al. Microtubule-Driven Spatial Arrangement of Mitochondria Promotes Activation of the NLRP3 Inflammasome. *Nat Immunol* (2013) 14:454–60. doi: 10.1038/ni.2550
63. Fu X, Ju J, Lin Z, Xiao W, Li X, Zhuang B, et al. Target Deletion of Complement Component 9 Attenuates Antibody-Mediated Hemolysis and Lipopolysaccharide (LPS)-Induced Acute Shock in Mice. *Sci Rep* (2016) 6:1–12. doi: 10.1038/srep30239

Conflict of Interest: Authors GT and E-MN are employed by GSK. DMD is a consultant and advisor to GSK.

The remaining authors declare that the research was conducted in the absence of any commercial or financial relationships that could be construed as a potential conflict of interest.

Publisher's Note: All claims expressed in this article are solely those of the authors and do not necessarily represent those of their affiliated organizations, or those of the publisher, the editors and the reviewers. Any product that may be evaluated in this article, or claim that may be made by its manufacturer, is not guaranteed or endorsed by the publisher.

frontiers in Immunology

ORIGINAL RESEARCH
published: 29 September 2021
doi: 10.3389/fimmu.2021.746032

Neutrophils Facilitate Prolonged Inflammasome Response in the DAMP-Rich Inflammatory Milieu

*Seunghwan Son[1], Sung-Hyun Yoon[1], Byeong Jun Chae[1], Inhwa Hwang[1], Do-Wan Shim[1], Young Ho Choe[2], Young-Min Hyun[2] and Je-Wook Yu[1]**

[1] Department of Microbiology and Immunology, Institute for Immunology and Immunological Diseases, Brain Korea 21 Project for Medical Science, Yonsei University College of Medicine, Seoul, South Korea, [2] Department of Anatomy, Brain Korea 21 Project for Medical Science, Yonsei University College of Medicine, Seoul, South Korea

Aberrant inflammasome activation contributes to various chronic inflammatory diseases; however, pyroptosis of inflammasome-active cells promptly terminates local inflammasome response. Molecular mechanisms underlying prolonged inflammasome signaling thus require further elucidation. Here, we report that neutrophil-specific resistance to pyroptosis and NLRP3 desensitization can facilitate sustained inflammasome response and interleukin-1β secretion. Unlike macrophages, inflammasome-activated neutrophils did not undergo pyroptosis, indicated by using *in vitro* cell-based assay and *in vivo* mouse model. Intriguingly, danger-associated molecular patterns (DAMP)-rich milieu in the inflammatory region significantly abrogated NLRP3-activating potential of macrophages, but not of neutrophils. This macrophage-specific NLRP3 desensitization was associated with DAMP-induced mitochondrial depolarization that was not observed in neutrophils due to a lack of SARM1 expression. Indeed, valinomycin-induced compulsory mitochondrial depolarization in neutrophils restored inflammasome-dependent cell death and ATP-induced NLRP3 desensitization in neutrophils. Alongside prolonged inflammasome-activating potential, neutrophils predominantly secreted interleukin-1β rather than other proinflammatory cytokines upon NLRP3 stimulation. Furthermore, inflammasome-activated neutrophils did not trigger efferocytosis-mediated M2 macrophage polarization essential for the initiation of inflammation resolution. Taken together, our results indicate that neutrophils can prolong inflammasome response *via* mitochondria-dependent resistance to NLRP3 desensitization and function as major interleukin-1β-secreting cells in DAMP-rich inflammatory region.

Keywords: neutrophil, inflammasome, pyroptosis, DAMP, NLRP3 desensitization, SARM1, efferocytosis

OPEN ACCESS

Edited by:
Philippe Georgel, Université de Strasbourg, France

Reviewed by:
Ioannis Mitroulis, Democritus University of Thrace, Greece
Marco Di Gioia, Boston Children's Hospital and Harvard Medical School, United States

****Correspondence:***
Je-Wook Yu
jewookyu@yuhs.ac

Specialty section:
This article was submitted to Molecular Innate Immunity, a section of the journal Frontiers in Immunology

Received: *23 July 2021*
Accepted: *14 September 2021*
Published: *29 September 2021*

Citation:
Son S, Yoon S-H, Chae BJ, Hwang I, Shim D-W, Choe YH, Hyun Y-M and Yu J-W (2021) Neutrophils Facilitate Prolonged Inflammasome Response in the DAMP-Rich Inflammatory Milieu. Front. Immunol. 12:746032. doi: 10.3389/fimmu.2021.746032

INTRODUCTION

Neutrophils are the first and most abundant cells that infiltrate inflamed sites following microbial invasion or tissue injury (1). Upon microbial infection, neutrophils play a key role in host defense by phagocytosing microbes and releasing granule-contained antimicrobial factors and neutrophil extracellular traps (1, 2). Although neutrophils have relatively short lifespan, their sustained antimicrobial activity is detrimental to host cells or tissues (3). During the progression of

inflammation, inflammatory cells such as neutrophils infiltrate into the inflamed region, where high levels of damage-associated molecular patterns (DAMPs) or danger signals from injured cells are present. Therefore, the effects of DAMP- or danger signals-rich milieu on the inflammatory potential of infiltrating cells warrant careful investigation.

Of interest, neutrophils also contribute to the resolution of inflammation. The phagocytosis of apoptotic neutrophils by resident macrophages, known as efferocytosis, triggers anti-inflammatory signaling by macrophages to resolve inflammation (4). Defective efferocytosis is a primary cause of prolonged inflammation and subsequent inflammatory diseases (5, 6). Since abnormal neutrophil activity is thought to play an important role in the pathogenesis of chronic inflammatory disorders (3), such as rheumatoid arthritis, neutrophil function must be optimally regulated to avoid unnecessary collateral damage to the host.

The inflammasome is a key molecular complex, mainly present in myeloid cells, to initiate inflammatory responses by inducing inflammatory mediator secretion, like interleukin (IL)-1β or IL-18 (7). In response to microbe- or tissue injury-derived factors, inflammasome sensor molecules, such as NOD-like receptor family, pyrin domain-containing 3 (NLRP3), are converted into their active form and assemble adaptor molecule apoptosis-associated speck-like protein containing a caspase recruitment domain (ASC) and procaspase-1 to form the inflammasome complex (8). The assembled inflammasome promptly leads to caspase-1 activation, which then induces pro-IL-1β and gasdermin D (GSDMD) cleavage into their active forms (9).

Unlike other inflammasome sensor molecules, NLRP3 can be exclusively activated by a broad spectrum of stimuli, ranging from microbial toxins to endogenous metabolites (8). These results suggest that NLRP3 can act as a typical sensor to initiate inflammation in response to diverse abnormalities. Recent studies have closely implicated NLRP3 inflammasome activation in the pathogenesis of many chronic metabolic or degenerative diseases, such as type 2 diabetes, atherosclerosis and Alzheimer's disease (10–12). Despite the important role of NLRP3 inflammasome in a wide range of chronic diseases, inflammasome activation promptly results in the pyroptotic cell death of inflammasome-active cells by causing the formation of GSDMD pores (13). Consequently, inflammasome-activated cells such as macrophages are unlikely to survive and support sustained inflammasome response. As such, it remains largely unknown which type of stimuli or cells contribute to prolonged inflammasome signaling under physiological conditions that lead to chronic inflammatory diseases.

Intriguingly, recent studies demonstrated that neutrophils do not undergo pyroptosis upon canonical inflammasome activation (14, 15). Moreover, considering the importance of neutrophils in resolving inflammation, it is highly possible to speculate that neutrophils may act as an essential regulator of persistent or sustained inflammation. In this context, the cellular function and physiological significance of inflammasome-active neutrophils requires further clarification. Here, we explored whether the key inflammatory cells macrophages or neutrophils can support sustained inflammation with a prolonged inflammasome response under diverse conditions.

MATERIALS AND METHODS

Mice

C57BL/6 (Orient Bio, Gyeonggi-do, Korea), *Nlrp3* $^{-/-}$ (Jackson Laboratory, Bar Harbor, ME, USA), *Gsdmd* $^{-/-}$ (Jackson Laboratory) and *LysM* $^{gfp/+}$ (provided by Dr. Pilhan Kim, Korea Advanced Institute of Science and Technology) (16) mice were bred at Yonsei University College of Medicine. All mice (C57BL/6 background) were maintained under specific pathogen-free conditions, and female mice were used for experiments at 8–10 weeks of age. Protocols for the animal experiments were approved by the Institutional Ethical Committee, Yonsei University College of Medicine. All experiments were performed in accordance with the approved guidelines of the Institutional Ethical Committee.

Mice Treatment

Mice were injected intraperitoneally with 1 mg/kg of LPS for 24 h. Peritoneal lavage fluid was obtained by washing twice with 5 mL of PBS and centrifuging (300 × *g* for 5 min) to pellet cells. The collected cells were stained with anti-CD11b, anti-Ly6G, and anti-F4/80 antibodies conjugated with an appropriate fluorescent dye (eBioscience, San Diego, CA, USA). Cell fluorescence was monitored and analyzed using flow cytometry (FACSVerse, BD, Franklin Lakes, NJ, USA). All flow cytometry data are representative of at least three independent experiments.

Cell Culture

Bone marrow cells were isolated from mouse femurs and differentiated into BMDMs in L929-conditioned medium, as described previously (17). All BMDMs were maintained in L929-conditioned DMEM supplemented with 10% fetal bovine serum (FBS, Gibco, Waltham, MA, USA) and antibiotics. BMNs were obtained from mouse bone marrow cells using an EasySep™ mouse neutrophil enrichment kit (STEMCELL Technologies, Vancouver, Canada) according to the manufacturer's protocols or using Ficoll-Paque density gradient medium. BMNs were cultured in RPMI 1640 supplemented with 10% FBS and antibiotics and used for experiments. Isolated BMNs were analyzed using flow cytometry after co-staining with anti-CD11b, anti-Ly6G, and anti-F4/80 antibodies (eBioscience). Spleen neutrophils were prepared from mouse spleen-derived single-cell suspension using an EasySep™ mouse neutrophil enrichment kit. Mouse peritoneal macrophages were obtained from the peritoneal lavage fluid five days after intraperitoneal injection with 3% thioglycolate medium (1.5 mL). After removing non-adherent cells, peritoneal macrophages were cultured in RPMI 1640 supplemented with 10% FBS and antibiotics. Immortalized NLRP3-GFP-expressing BMDMs were provided by Dr. E.S. Alnemri (Thomas Jefferson University, Philadelphia, PA,

USA). To transfect Sarm1 into BMNs, DOTAP or Lipofectamine 2000 liposomal transfection reagent were used as described previously (18). Briefly, cells were incubated with a mixture of cDNA construct and liposomal reagent in Opti-MEM for 4 h. Then, normal FBS-containing culture medium was added and cells were further incubated for additional 18 h.

Preparation of Cell-Free Supernatants From Injured Cells

To isolate DAMP-rich conditioned medium, mouse BMDMs were treated with staurosporine (2 μg/mL) for 3 h, washed with fresh medium and incubated for an additional 18 h before the supernatant was collected. Alternatively, mouse BMDMs were subjected to four freeze/thaw cycles and the culture supernatant was collected.

Reagents and Antibodies

LPS, ATP, nigericin, poly dA:dT, staurosporine, cytochalasin D, valinomycin, and apyrase were purchased from Sigma-Aldrich (St. Louis, MO, USA). JC-1 and MitoSox were obtained from Invitrogen (San Diego, CA, USA). zVAD-FMK,and ac-YVAD-CMK were purchased from Bachem (Torrance, CA, USA). Mammalian expression constructs for mouse Sarm1 (pGW1-Myc-Sarm1) was purchased from Addgene (Watertown, MA, USA). The following antibodies were used for detecting mouse caspase-1 (Adipogen, San Diego, CA, USA), NLRP3 (Adipogen), IL-1β (R&D Systems, Minneapolis, MN, USA), ASC (Santa Cruz Biotechnology, Dallas, TX, USA), β-actin (Santa Cruz Biotechnology), caspase-3 (Cell Signaling, Beverly, MA, USA), gasdermin D (Abcam, Cambridge, MA, USA), and Sarm1 (Cell Signaling).

Immunoblot Analysis

Cells were lysed in buffer containing 25 mM Tris-Cl (pH 7.5), 150 mM NaCl, 1% NP-40, 1% sodium deoxycholate, 0.1% SDS, and protease inhibitors. Soluble lysates were fractionated using SDS-polyacrylamide gel electrophoresis and transferred to polyvinylidene difluoride membranes. Some supernatants were precipitated using a methanol/chloroform mixture as described previously (19) and immunoblotted. All blot images are representative of at least three independent experiments and have been cropped for presentation.

mRNA Quantification

Total RNA was isolated using an RNeasy Mini Kit (Intron, Gyeonggi-do, Korea) or TRIzol reagent (Invitrogen, Waltham, MA, USA) and reverse-transcribed using a Power cDNA Synthesis Kit (Intron). Quantitative real-time PCR was performed using SYBR Premix Ex Taq (Takara, Tokyo, Japan) while RT-PCR was performed using AccuPower HotStart PCR premix (Bioneer, Daejeon, Korea). The following primers (mouse) were used: *Il-10*, 5′-CCA AGC CTT ATC GGA AAT GA-3′ and 5′-TTT TCA CAG GGG AGA AAT CG-3′; *Il-6*, 5'-AGT TGC CTT CTT GGG ACT GA-3' and 5'-TCC ACG ATT TCC CAG AGA AC-3'; *Tnfα*, 5'-CGT CAG CCG ATT TGC TAT CT-3' and 5'-CGG ACT CCG CAA AGT CTA AG-3'; *Gapdh*, 5'-AAC TTT GGC ATT GTG GAA GG-3' and 5'-ACA CAT TGG GGG TAG GAA CA-3'; *Sarm1*, 5'-CGC TGC CCT GTA CTG GAG G-3' and 5'-CTT CAG GAG GCT GGC CAG CT-3'; *β-actin*, 5'-CCT TCC TGG GCA TGG AGT CCT G-3' and 5'-GGA GCA ATG ATC TTG ATC TTC-3'.

Inflammasome/Caspase-1 Activation Assay

To induce conventional NLRP3 inflammasome activation, cells were primed with LPS (0.25 μg/mL) for 2.5 h and then treated with ATP (2.5 mM) for 30 min. In some experiments, cells were primed with LPS, washed with PBS, and then treated with ATP. To stimulate NLRC4 and AIM2 inflammasome signaling, cells were transfected with flagellin (NLRC4) using N-(2,3-dioleoyloxy-1-propyl) trimethylammonium methyl sulfate (DOTAP) or poly dA:dT (AIM2) using Lipofectamine 2000. Inflammasome activation was determined by the presence of active caspase-1 p20 and active IL-1β in culture supernatant immunoblots and extracellular IL-1β quantification using ELISA. To detect ASC oligomerization, disuccinimidyl suberate (DSS, Thermo Scientific)-mediated cross-linking assays were performed as described previously (20). To determine NLRP3 oligomerization, speck-like aggregates of NLRP3-GFP were assessed by confocal microscopy in NLRP3-GFP-expressing BMDMs.

Cytokine Production Assay

IL-1β, IL-6, and MMP9 levels in the culture supernatants were quantified using mouse IL-1β, IL-6, or MMP9 ELISA kits (R&D Systems), respectively. Inflammatory cytokines in the culture supernatants were quantified using a Cytometric Bead Array Mouse Inflammatory Kit (BD). All assays were performed according to the manufacturer's protocols.

Cell Death Assay

To quantify pyroptotic cell death, extracellular lactate dehydrogenase (LDH) release was measured using a CytoTox96 non-radioactive cytotoxicity assay kit (Promega) and calculated as [extracellular LDH/(intracellular LDH + extracellular LDH) × 100]. Dead cells were labeled with PI or Annexin V-FITC according to the manufacturer's protocol and fluorescence was measured using flow cytometry (FACSVerse, BD). All flow cytometry data are representative of at least three independent experiments. To assess efferocytosis, peritoneal macrophages were treated with untreated, apoptotic, or inflammasome-activated neutrophils (1/4 volume) for 1 h, washed to remove non-engulfed cells, and treated with LPS (0.1 μg/mL) for 18 h.

Immunofluorescence Assay

Cells grown on coverslips in a 12-well plate were fixed with 4% formaldehyde and permeabilized with 0.2% Triton X-100. After blocking with 4% BSA, cells were incubated with anti-α-tubulin primary antibodies (Santa Cruz Biotechnology) followed by Alexa Fluor 488-conjugated anti-mouse IgG (Invitrogen). F-actin was stained using rhodamine-phalloidin (Thermo) and nuclei were visualized by counterstaining with DAPI. Images were acquired using confocal microscopy (LSM 700, Carl Zeiss, Oberkochen, Germany) and processed using ZEN2011 software.

Phagocytosis Assay

To measure phagocytic activity, cells were incubated with zymosan-FITC (Invitrogen; 1:5 ratio) for 30 min, washed, and their fluorescence analyzed using flow cytometry (FACSVerse, BD). All flow cytometry data are representative of at least three independent experiments.

Neutrophil *In Vitro* Migration Assay

To track neutrophil migration, neutrophils were prepared from $LysM^{gfp/+}$ mice. Prior to neutrophil seeding, confocal dishes were coated with fibronectin (Gibco) diluted in PBS. Then, neutrophils were plated with or without LPS (0.25 μg/mL), incubated for 2 h 30 min, followed by the treatment of ATP (2.5 mM) for 30 min or 1 h. *In vitro* migration was imaged using a Nikon Eclipse Ti2 inverted microscope, with DIC and FITC channels captured every 10 s and terminated after 30 min. All imaging data (.nd2) were imported into volocity software v6.3.1 (Perkin Elmer) and processed using IMARIS software v7.2.3 (Bitplane). Tracking analysis was performed using an autoregressive motion in spots tool.

Mitochondrial Membrane Potential and ROS Measurement

To measure mitochondrial membrane potential, cells were stained with JC-1 (Invitrogen) according to the manufacturer's protocol and their fluorescence was monitored and analyzed using flow cytometry (FACSVerse, BD). To measure mitochondrial ROS production, cells were stained with MitoSOX (Invitrogen) after the appropriate treatments and analyzed using flow cytometry, based on the level of MitoSOX. All flow cytometry data are representative of at least three independent experiments.

Statistical Analysis

All values are expressed as the mean ± SEM of individual samples. *n* indicates the number of independent experiments. Data were analyzed using one-way analysis of variance (ANOVA) followed by Dunnett's *post hoc* test to compare all groups with the control group, or Student's *t*-test. Statistical significance was set at $p \leq 0.05$. All analyses were performed using GraphPad Prism.

RESULTS

Inflammasome Activation Induces Pyroptotic Cell Death in Macrophages but Not Neutrophils

To examine the potential outcome of inflammasome activation in major inflammatory cells, we prepared and analyzed bone marrow-derived neutrophils (BMNs) and bone marrow-derived macrophages (BMDMs) from isolated mouse bone marrow cells (**Supplementary Figure S1**). First, we examined the inflammasome response of both cell types following diverse stimulations. NLRP3 inflammasome activation by lipopolysaccharide (LPS) plus ATP or nigericin treatment was observed in BMNs and BMDMs, as determined by extracellular IL-1β secretion (**Figure 1A**). Similarly, neutrophils exhibited normal NLR family, CARD-containing 4 (NLRC4)- and absent in melanoma 2 (AIM2)-mediated inflammasome activation triggered by flagellin or poly dA:dT transfection (**Figure 1A**). Consistently, all forms of inflammasome-activating stimulation caused a robust caspase-1 processing in both cells, as determined by the presence of cleaved caspase-1 (p20) in the cell culture supernatants (**Figure 1B**).

Inflammasome/caspase-1 activation resulted in profound pyroptosis in macrophages, as indicated by lactic acid dehydrogenase (LDH) release into the extracellular medium (**Figure 1C**). Interestingly, this inflammasome-dependent LDH release was not evident in BMNs, irrespective of robust inflammasome activation (**Figures 1C, D**). Consistently, LPS/ATP-induced pyroptosis was not observed in splenic neutrophils (**Figure 1E**). This pyroptosis resistance of neutrophils was also confirmed by using propidium iodide (PI) staining (**Figure 1F** and **Supplementary Figure S2**). However, the well-known apoptosis inducer, staurosporine, promoted robust cell death in neutrophils, as detected by using PI staining and caspase-3 cleavage (**Figures 1F, G**), indicating that neutrophils are susceptible to apoptosis but not pyroptosis. Both neutrophils and macrophages displayed comparable phosphatidylserine exposure levels, a typical eat-me signal, in response to staurosporine, as measured using annexin V staining (**Figure 1H**). However, neutrophils exhibited significantly lower LPS/ATP-induced phosphatidylserine exposure (**Figure 1H**) and cell death (**Figure 1I**) than macrophages. Together, these data demonstrate that neutrophils are inflammasome-competent and secret robust amounts of mature IL-1β, but are resistant to inflammasome-driven pyroptotic cell death.

DAMP-Rich Milieu Desensitizes the NLRP3 Inflammasome-Activating Potential of Macrophages but Not Neutrophils

During the initial stages of inflammation, host tissues or cells at inflamed sites are damaged, leading to the extracellular release of many cellular components (21). Consequently, infiltrated cells such as neutrophils are likely to encounter danger signals or DAMPs released by injured cells in the inflamed region (22). To examine whether exposure to danger signal-rich milieu affects the inflammasome-activating potential of infiltrated cells, we exposed neutrophils or macrophages to injured cell-derived supernatants before inflammasome-activating stimulants (**Figure 2A**). *In vitro* cell injury was induced in BMDMs by staurosporine treatment or repeated freeze-thaw cycles. Of notice, pretreatment with DAMP-rich medium did not affect LPS/ATP-induced IL-1β secretion from neutrophils, but significantly decreased IL-1β secretion from BMDMs (**Figure 2B**). Consistently, the exposure with danger signal-rich medium abolished caspase-1 processing in macrophages following LPS/ATP stimulation, but not in neutrophils (**Figure 2C**). These results indicate that danger signals-rich milieu can abrogate macrophage inflammasome-activating potential at the post-translational level. However, similar to BMNs, splenic neutrophils were resistant to DAMP-rich medium-induced NLRP3 desensitization (**Figure 2D**).

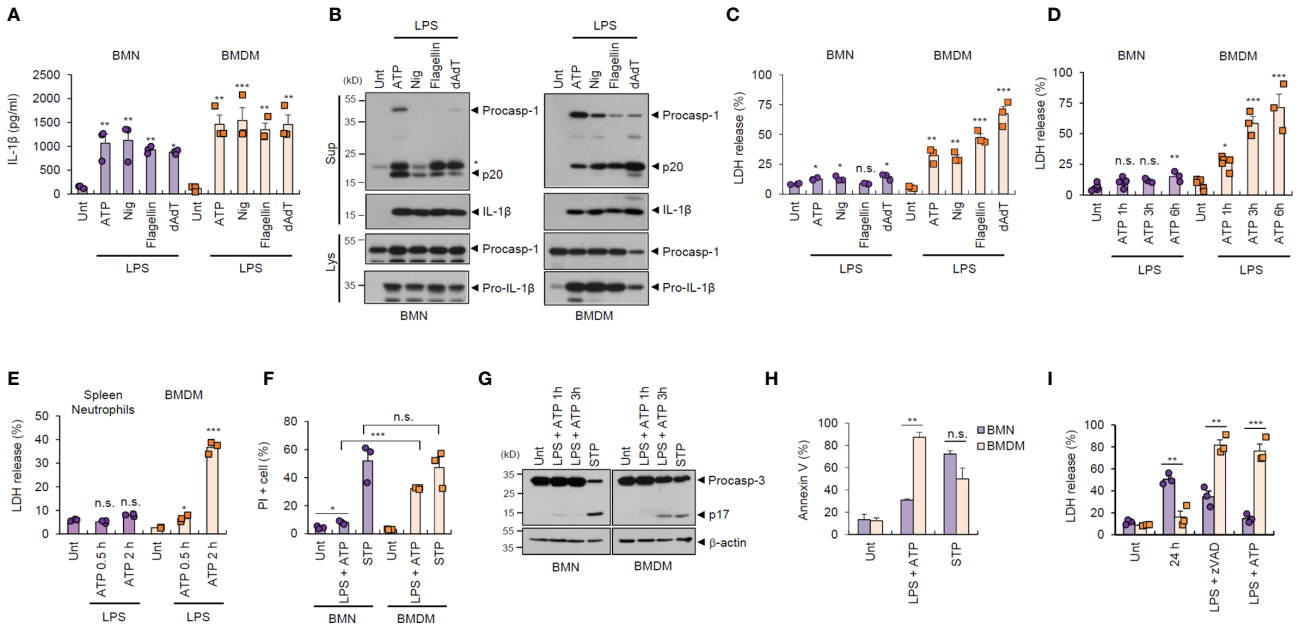

FIGURE 1 | Neutrophils resist inflammasome-dependent cell death. **(A)** Quantification of IL-1β in the culture supernatants of mouse bone marrow-derived neutrophils (BMNs) or macrophages (BMDMs) untreated (Unt) or primed with LPS (0.25 μg/mL, 2.5 h), followed by ATP (2.5 mM, 1 h) or nigericin (Nig, 5 μM, 1 h) treatment, or flagellin (500 μg/mL, 6 h) or poly dA:dT (1 μg/mL, 6 h) transfection (n = 3). **(B)** Immunoblots of mouse BMNs or BMDMs treated as in **(A)**. Culture supernatants (Sup) or cell lysates (Lys) immunoblotted with the indicated antibodies. The asterisk indicates a nonspecific band. **(C, D)** Quantification of LDH in the culture supernatants of mouse BMNs or BMDMs treated as in **(A)** (C, n = 3) or primed with LPS (0.25 μg/mL, 2.5 h) and treated with ATP (2.5 mM, 1, 3, 6 h) (D, n = 3-5). **(E)** Quantification of LDH in the culture supernatant of mouse splenic neutrophils or BMDMs primed with LPS, followed by ATP treatment (0.5 or 2 h). (n = 3) **(F)** Quantification of PI-positive mouse BMNs or BMDMs primed with LPS, followed by ATP (2.5 mM, 1 h) or treated with staurosporine (STP, 2 μg/mL, 6 h), as determined by flow cytometric analysis after propidium iodide (PI) staining. (n = 3). **(G)** Immunoblots of cell lysates from mouse BMNs or BMDMs primed with LPS followed by ATP (1 or 3 h), or staurosporine (STP, 2 μg/mL, 6 h) treatment. **(H)** Quantification of phosphatidylserine-positive mouse BMNs or BMDMs treated with LPS (0.25 μg/mL), followed by ATP (2 h) or staurosporine (STP, 5 h), as determined by flow cytometric analysis after Annexin V-FITC staining (n = 2 or 3). **(I)** Quantification of LDH release into the culture supernatant of mouse BMNs or BMDMs incubated with culture medium (24 h), treated with LPS (0.25 μg/mL, 24 h) in the presence of zVAD (20 μM) or treated with LPS (0.25 μg/mL, 2.5 h) followed by ATP (2.5 mM, 3 h) (n = 3). Data are expressed as the mean ± SEM. $^*P < 0.05$, $^{**}P < 0.01$, $^{***}P < 0.001$, n.s. not significant.

Extracellular ATP is a major danger signal released by damaged cells and plays an important role in the inflammaroty processes (23). To examine whether ATP is critical for the DAMP-induced NLRP3 inflammasome desensitization observed in macrophages, we used apyrase to remove ATP in the DAMP-rich medium. Intriguingly, apyrase significantly restored NLRP3 desensitization by freeze-thaw-induced DAMP-rich medium (**Figure 2E**). Then, we pretreated neutrophils or macrophages with ATP before conventional NLRP3-activating stimulation. Similar to the effects observed following treatment with DAMP-rich medium, ATP pretreatment markedly attenuated IL-1β secretion from macrophages, but not from neutrophils, in response to LPS/ATP or LPS/nigericin stimulation (**Figure 2F**). Pre-exposure with ATP for 15 min was sufficient to desensitize LPS/ATP-stimulated inflammasome activation in macrophages (**Figure 2G**). Like DAMP-rich medium, ATP pretreatment markedly blocked NLRP3-mediated caspase-1 cleavage in macrophages, but not neutrophils (**Figure 2H**). We also found that DAMP-rich medium or ATP treatment alone did not trigger a profound production of proinflammatory cytokine in both cells (**Supplementary Figure S3**).

NLRP3 oligomerization is an essential process in the assembly of the NLRP3 inflammasome complex (24). Consistent with the above data, ATP pretreatment remarkably blocked LPS/nigericin-induced NLRP3 oligomerization in macrophages, as determined by NLRP3 speck formation (**Figure 2I** and **Supplementary Figure S4**). Furthermore, ATP pretreatment abolished ASC oligomerization in BMDMs stimulated with LPS/ATP (**Figure 2J**), but did not inhibit NLRC4- and AIM2-dependent caspase-1 processing in macrophages following flagellin and poly dA:dT transfection, respectively (**Figure 2K**). These data demonstrate that extracellular DAMP- or ATP-rich milieu at the inflamed site can desensitize the NLRP3 inflammasome-activating potential of macrophages but not neutrophils.

Neutrophils Are Resistant to Inflammasome-Dependent Gasdermin D Cleavage and DAMP-Induced Mitochondrial Depolarization

To provide a molecular insight into the distinct resistance of neutrophil to pyroptosis and NLRP3 desensitization, we first

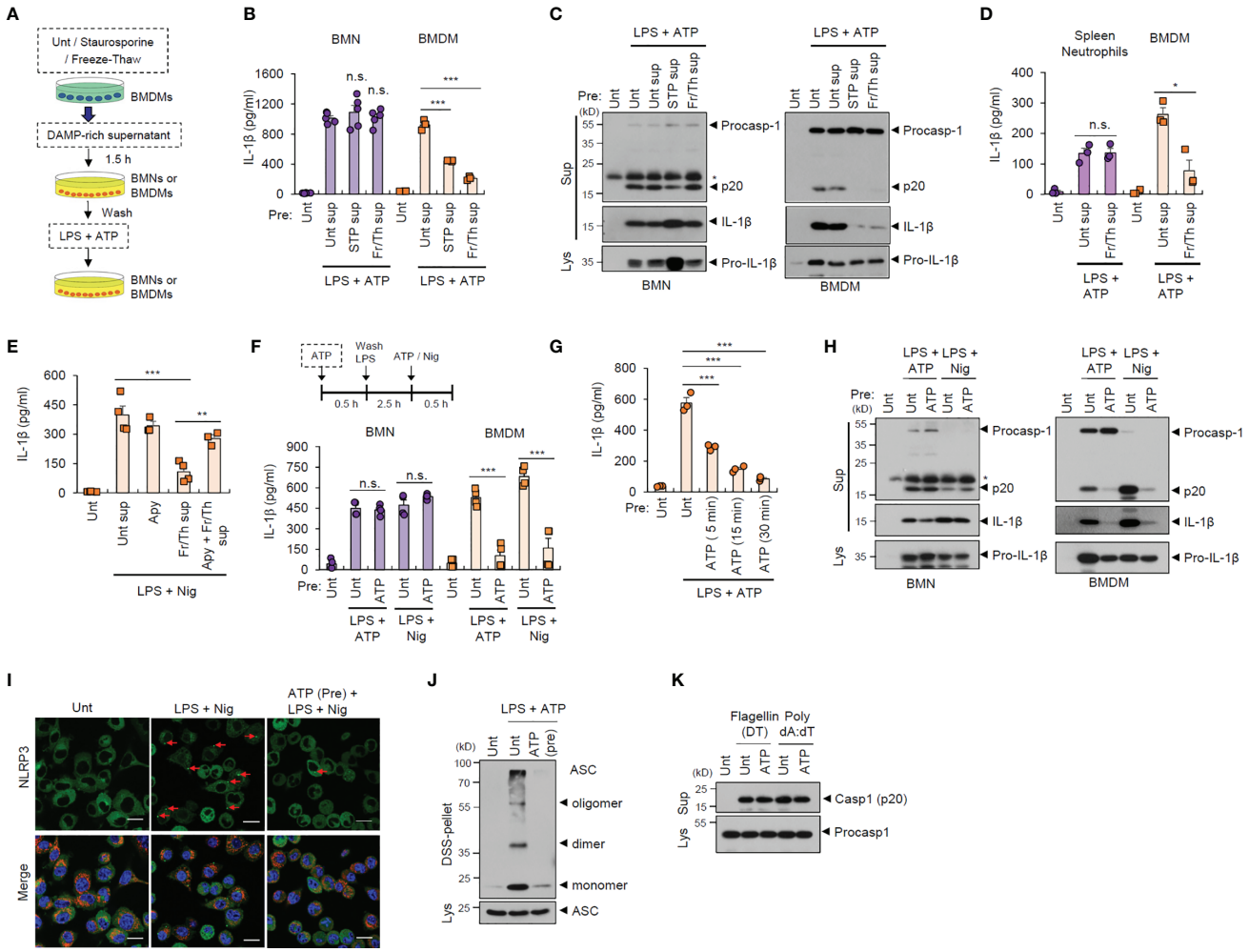

FIGURE 2 | Danger signal-rich medium pretreatment desensitizes NLRP3 inflammasome-activating potential of macrophages but not neutrophils. **(A)** Experimental scheme for determining the potential effect of cell-free supernatants from normal BMDMs or those injured by staurosporine (STP) or repeated freeze/thaw cycles on NLRP3 inflammasome activation of neutrophils or macrophages. **(B)** Quantification of IL-1β in the culture supernatants of mouse BMNs or BMDMs pretreated with cell-free supernatants from untreated or injured BMDMs as in **(A)** and then treated with LPS (0.25 μg/mL, 2.5 h) followed by ATP (2.5 mM, 30 min) treatment (n = 5, BMNs; n = 3, BMDMs). **(C)** Immunoblots from mouse BMNs or BMDMs treated as in **(B)**. The asterisk indicates a nonspecific band. **(D)** Quantification of IL-1β in the culture supernatants of mouse splenic neutrophils or BMDMs pretreated with cell-free supernatants from untreated or injured BMDMsa by freeze/thaw cycles (2.5 mM, 30 min), and then treated with LPS, followed by ATP (2.5 mM, 30 min) treatment (n = 4). **(E)** Quantification of IL-1β in the culture supernatants of mouse BMDMs pretreated with DAMP-rich medium by freeze/thaw cycles in the presence of apyrase (15 U/ml), and then treated with LPS followed by nigericin (5 μM, 40 min) treatment (n = 3 or 4) **(F)** Quantification of IL-1β in the culture supernatants of mouse BMNs or BMDMs pretreated with ATP (2.5 mM, 30 min), washed and treated with LPS (0.25 μg/mL, 2.5 h), followed by ATP (2.5 mM, 30 min) or nigericin (Nig, 5 μM, 40 min) treatment (n = 4). **(G)** Quantification of IL-1β in the culture supernatants of mouse BMDMs pretreated with ATP (5, 15, 30 min), and then treated with LPS, followed by ATP treatment (n = 3). **(H)** Immunoblots from mouse BMNs or BMDMs treated as in **(F)**. **(I)** Representative immunofluorescence images of NLRP3-GFP-expressing immortalized BMDMs pretreated with ATP (2 mM, 30 min) and then treated with LPS (0.25 μg/mL, 3 h), followed by nigericin (Nig, 5 μM, 30 min) treatment after anti-Tom20 antibody staining (red). Nuclei were stained with DAPI (blue). Scale bars, 20 μm. Red arrows indicate NLRP3-oligomerized specks. **(J)** Immunoblots of DSS-crosslinked pellets (DSS-pel) or cellular lysates (Lys) from BMDMs pretreated with ATP (2.5 mM, 30 min) and then treated with LPS (0.25 μg/mL) and ATP (2.5 mM). **(K)** Immunoblots of mouse BMDMs pretreated with ATP (2.5 mM, 30 min) and then transfected with flagellin (500 ng/mL, 4 h) or poly dA:dT (2 μg/mL, 4 h). Culture supernatants (Sup) or cell lysates (Lys) were immunoblotted with the indicated antibodies. *P < 0.05, **P < 0.01, ***P < 0.001, n.s. not significant.

measured inflammasome component expression. We found that neutrophils displayed lower active caspase-1 (p20) levels than macrophages (**Figure 3A**), but similar levels of active IL-1β secretion (**Supplementary Figure S5A**). Likewise, GSDMD cleavage was much weaker in neutrophils than in macrophages (**Figures 3A, B** and **Supplementary Figure S5B**). These findings suggest that impaired GSDMD cleavage led to reduced GSDMD pore formation in the neutrophil plasma membrane. Indeed, GSDMD deficiency completely abrogated LPS/ATP-induced cell death in macrophages (**Figure 3C**). Moreover, LPS/ATP stimulation substantially disrupted plasma membrane integrity in macrophages but not neutrophils (**Figure 3D**). Consistently,

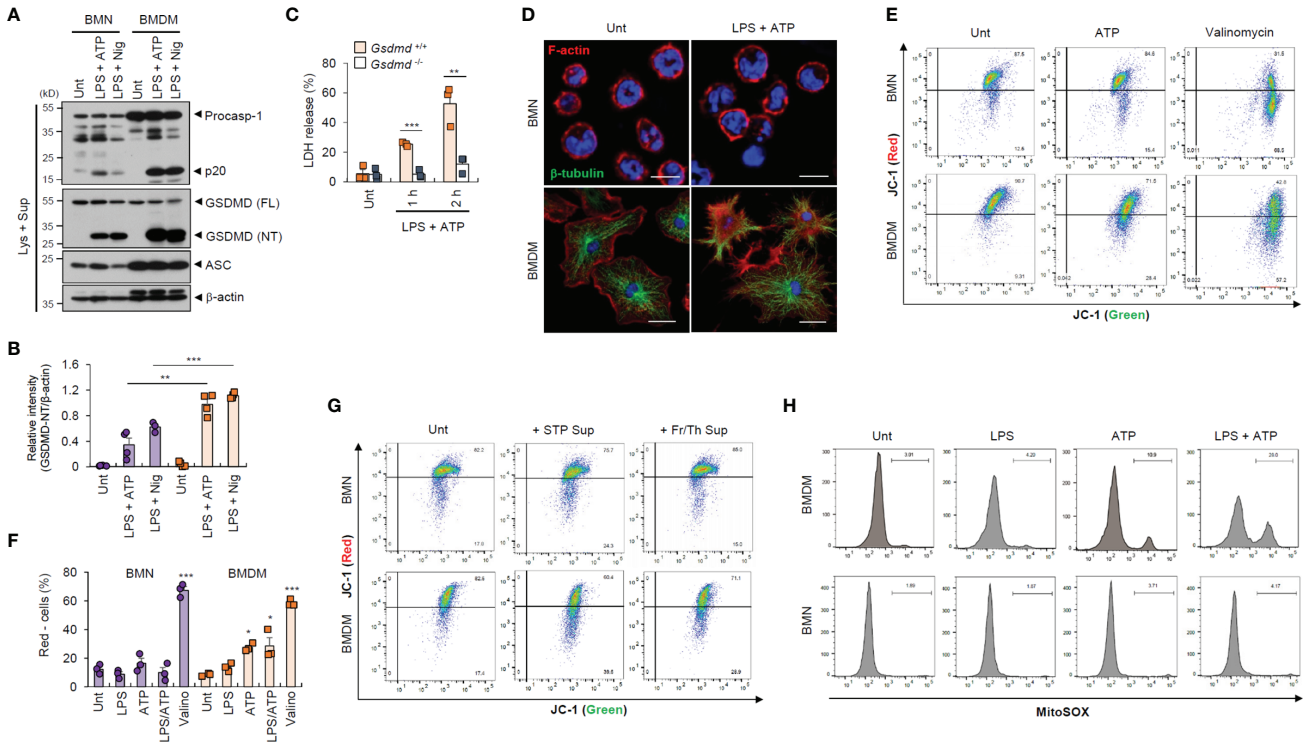

FIGURE 3 | Neutrophils exhibit weaker gasdermin D cleavage and mitochondrial depolarization than macrophages in response to NLRP3 stimulation. **(A)** Immunoblots from mouse BMNs or BMDMs untreated (Unt) or primed with LPS (0.25 μg/mL, 2.5 h), followed by ATP (2.5 mM, 1h) or nigericin (Nig, 5 μM, 1 h) treatment. **(B)** Quantification of relative GSDMD (NT) band intensity versus β-actin band in **(A)**. (n = 4). **(C)** Quantification of LDH release into the culture supernatants of wild-type or *Gsdmd*-deficient mouse BMDMs primed with LPS followed by ATP (2.5 mM, 1 or 2 h) treatment (n = 3). **(D)** Representative immunofluorescence images of mouse BMNs or BMDMs treated with LPS followed by ATP (2 mM, 1 h) treatment after staining with anti-F-actin (red) and anti-α-tubulin (green) antibodies. Nuclei were stained with DAPI (blue). Scale bars, 10 μm (BMNs) or 20 μm (BMDMs). **(E)** Flow cytometric analysis of mouse BMNs or BMDMs treated with ATP (2.5 mM, 30 min) or valinomycin (5 μM, 30 min) treatment after JC-1 staining. **(F)** Quantification of JC-1 (red)-negative mouse BMDM or BMN populations treated with LPS alone, ATP alone, LPS followed by ATP or valinomycin (n = 3). **(G)** Flow cytometric analysis of mouse BMDMs or BMNs treated with cell-free supernatants of untreated cells or those injured by staurosporine treatment or repeated freeze/thaw cycles for 1.5 h after JC-1 staining. **(H)** Flow cytometric analysis of mouse BMDMs or BMNs treated with LPS alone (0.25 μg/mL, 2.5 h), ATP alone (2.5 mM, 0.5 h) or LPS followed by ATP treatment after MitoSOX staining. GSDMD; gasdermin D, FL; full length, NT; N-terminal. $^*P < 0.05$, $^{**}P < 0.01$, $^{***}P < 0.001$.

LPS/ATP stimulation significantly increased membrane permeability and phosphatidylserine exposure in macrophages but much less in neutrophils (**Figures 1F, H**). These results indicate that lower GSDMD pore formation may partly explain the pyroptosis resistance of neutrophils.

Mitochondria are important signaling organelles in regulating NLRP3 inflammasome activation and many types of cell death (24, 25). To explore whether mitochondrial alterations are involved in the distinct pyroptosis resistance of neutrophils, we examined mitochondrial phenotype under inflammasome-activating conditions. Unexpectedly, ATP treatment and LPS/ATP stimulation led to profound mitochondrial depolarization in macrophages but not neutrophils, as indicated by an increase in the JC-1 (red)-negative population (**Figures 3E, F**). The selective caspase-1 inhibitor, ac-YVAD-cmk, did not protect macrophages against LPS/ATP-promoted mitochondria depolarization (**Supplementary Figure S6**), indicating that ATP treatment, but not active caspase-1, primarily caused the loss of mitochondrial membrane potential in macrophages. In neutrophils, mitochondrial depolarization was detected by valinomycin, widely used to cause the loss of mitochondrial membrane potential, but not by LPS/ATP stimulation (**Figures 3E, F**). Like ATP treatment, the DAMP-rich medium markedly impaired the mitochondrial membrane potential of macrophages but not neutrophils (**Figure 3G**). Moreover, ATP treatment induced a profound mitochondrial reactive oxygen species (ROS) production only in macrophages (**Figure 3H**), suggesting that DAMP or ATP may damage macrophage mitochondrial integrity but not that of neutrophils.

Distinct Resistance of Neutrophils to Pyroptosis and NLRP3 Desensitization Is Associated With the Absence of SARM1-Induced Mitochondrial Depolarization

To examine whether intact mitochondrial membrane potential can explain the unique resistance of neutrophils to pyroptosis and NLRP3 desensitization, we treated cells with valinomycin to induce compulsory mitochondrial depolarization. Interestingly,

valinomycin treatment (10 min after ATP treatment) did not affect LPS/ATP-promoted IL-1β secretion by neutrophils (**Figure 4A**) but caused a significant pyroptosis in neutrophils (**Figure 4B**), indicating that mitochondrial membrane potential plays a key role in determining pyroptosis resistance. Moreover, pretreatment with valinomycin significantly abolished NLRP3 inflammasome activation in neutrophils, while ATP pretreatment failed to attenuate LPS/ATP-triggered IL-1β secretion (**Figure 4C**). Consistently, rotenone, another chemical to cause mitochondrial depolarization, pretreatment led to impaired IL-1β production by neutrophils (**Supplementary Figure S7**). These observations suggest that intact mitochondrial membrane potential at the moment of second signal, such as ATP or nigericin, is prerequisite for normal NLRP3 inflammasome-activating potential. Accordingly, valinomycin pretreatment clearly diminished LPS/ATP-triggered caspase-1 activation (**Figure 4D**) and ASC oligomerization in neutrophils (**Figure 4E**).

We were then keen to unveil the mechanism underlying the different status of the mitochondrial membrane potential of both cells exposed to the DAMP- or ATP-rich milieu. A recent study demonstrates that Sterile α- and heat armadillo motif-containing protein 1 (SARM1) clustering contributes to the induction of mitochondrial depolarization upon treatment with NLRP3

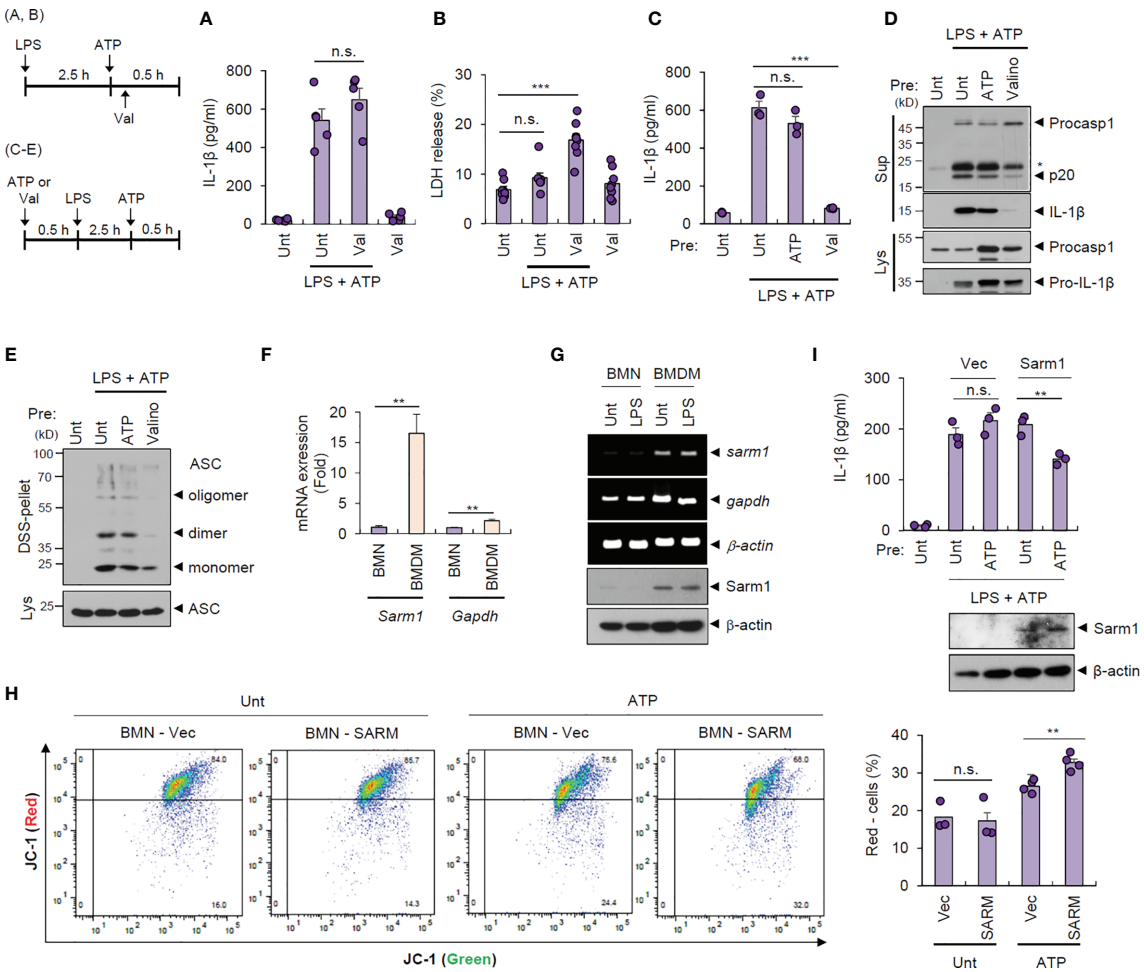

FIGURE 4 | Cell type-specific changes in mitochondrial integrity determine pyroptosis resistance and NLRP3 desensitization. **(A, B)** Quantification of IL-1β **(A)** or LDH **(B)** release into the culture supernatant from mouse BMNs primed with LPS (0.25 μg/ml, 2.5 h) followed by ATP (2.5 mM, 1 h) treatment in the presence of valinomycin (10 μM, last 50 min) (n = 5 or 8). **(C, D)** Quantification of IL-1β in the culture supernatant **(C)** or immunoblots from mouse BMNs pretreated with ATP (2.5 mM) or valinomycin (10 μM) for 30 min, washed and primed with LPS (0.25 μg/mL, 2.5 h) followed by ATP (2.5 mM, 30 min) treatment (n = 3). The asterisk indicates a nonspecific band **(D)**. **(E)** Immunoblots of DSS-crosslinked pellets (DSS-pel) or cell lysates (Lys) from BMNs treated as in **(C, D)**. **(F)** Quantification of *sarm1* or *gapdh* mRNA levels in mouse BMNs or BMDMs (n = 5). **(G)** RT-PCR analysis and immunoblots of *sarm1* or *gapdh* in mouse BMNs or BMDMs untreated or treated with LPS (0.5 μg/mL, 3 h). **(H)** Mouse BMNs were transfected with vector or Sarm1-expressing construct using DOTAP liposomal reagent and then treated with ATP (2.5 mM, 1 h). Flow cytometric analysis of these cells after JC-1 staining (left panel). Quantification of JC-1 (red)-negative mouse BMN populations (right panel, n = 3 or 4). **(I)** Quantification of IL-1β (upper panel) or immunoblots (lower panel) of mouse BMNs transfected with empty vector or Sarm1-expressing construct, and treated with ATP (2 mM, 20 min), and then treated with LPS followed by ATP treatment. (n = 3). Culture supernatants (Sup) or cell lysates (Lys) were immunoblotted with the indicated antibodies. $^{**}P < 0.01$, $^{***}P < 0.001$, n.s., not significant.

stimulants (26). Intriguingly, neutrophils displayed negligible Sarm1 expression compared to macrophages (**Figures 4F, G**). We thus speculate that the absence of Sarm1 expression is implicated in the neutrophil resistance to mitochondrial depolarization by ATP stimulation. Indeed, liposome-mediated Sarm1 transfection caused a considerable increase in the ATP-driven mitochondrial depolarization in neutrophils (**Figure 4H**). Sarm1 transfection did not impair cell viability of neutrophils (**Supplementary Figure S8**), but significantly diminished IL-1β secretion from neutrophils in response to the following LPS/ATP stimulation (**Figure 4I**). These results indicate that sarm1-deficiency is potentially implicated in the neutrophil resistance to NLRP3 desensitization.

Neutrophils Drive Sustained IL-1β-Specialized Inflammatory Responses

As shown above, neutrophils exhibited much lower caspase-1 cleavage than macrophages, but equivalent IL-1β secretion. To determine whether a protease other than caspase-1 was implicated in IL-1β processing and secretion in neutrophils, we measured IL-1β production in the presence of the caspase-1-selective inhibitor, YVAD. In neutrophils, YVAD markedly blocked active IL-1β production in response to NLRP3 stimulation (**Supplementary Figures S9A, B**). Moreover, NLRP3 was essential for ATP- or nigericin-triggered IL-1β secretion by neutrophils (**Supplementary Figure S9C**), indicating that IL-1β secretion by neutrophil is NLRP3/caspase-1-dependent similar to macrophages.

GSDMD pore is the major conduit for IL-1β secretion in macrophages (27). As neutrophils displayed much weaker GSDMD pore formation than macrophages (**Figure 3**), we determined IL-1β secretion levels in wild-type and *Gsdmd*-deficient cells. GSDMD presence was essential for early IL-1β secretion by neutrophils, but partial GSDMD-independent IL-1β secretion was observed in neutrophils after 2 h of ATP stimulation (**Figures 5A, B**). Besides, neutrophils displayed more rapid IL-1β secretion than macrophages (**Supplementary Figure S9D**), suggesting that neutrophil may have a somewhat different IL-1β secretion mechanism to macrophages.

Intriguingly, we noticed that IL-6 production in response to NLRP3-activating or LPS stimulations was very low in neutrophils but robust in macrophages (**Figure 5C**). Indeed, neutrophils elicited more IL-1β-oriented production than macrophages under NLRP3 inflammasome-activating conditions (**Figure 5D**). Then, we measured the secretion of several cytokines from both cell types in response to LPS stimulation using cytokine-bead array experiments. LPS alone caused robust IL-6, MCP-1 and TNF-α production in macrophages, but none or much less from neutrophils, whereas IL-1β secretion was similar in both cell types following LPS/ATP stimulation (**Figures 5E–H**). Furthermore,

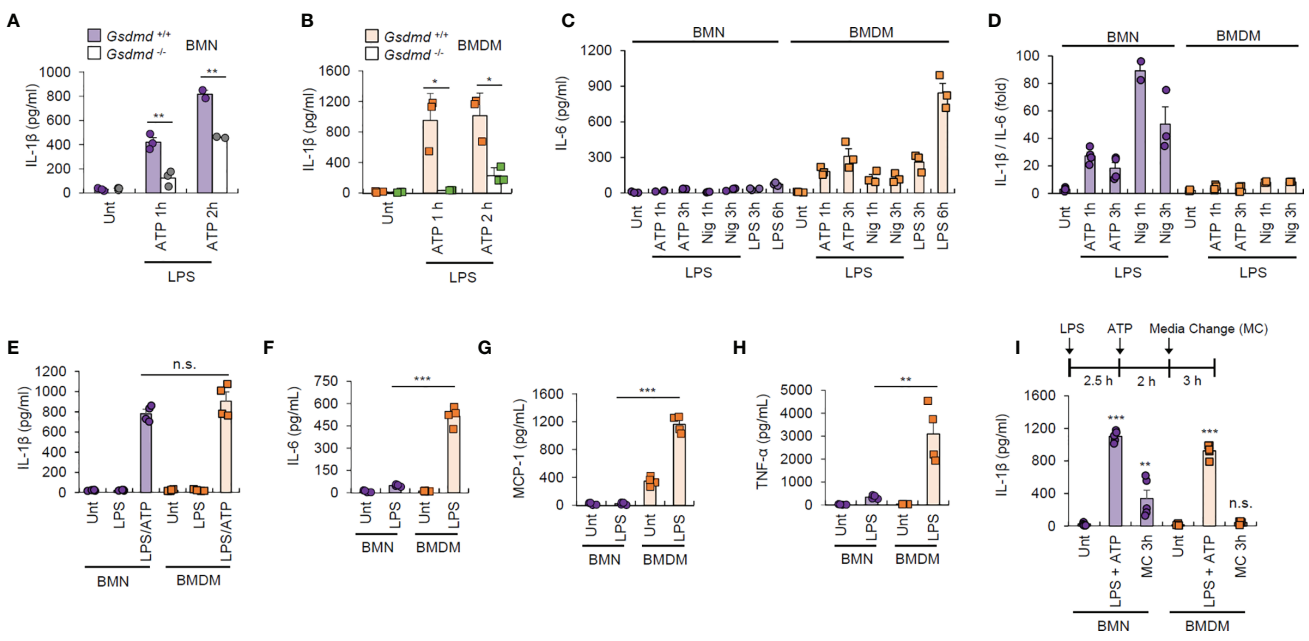

FIGURE 5 | Neutrophils exhibit unique IL-1β-oriented cytokine production. **(A, B)** Quantification of IL-1β in the culture supernatant of *Gsdmd* $^{+/+}$ or *Gsdmd* $^{-/-}$ mouse BMNs **(A)** or BMDMs **(B)** treated with LPS (0.25 μg/mL, 2.5 h) followed by ATP (2.5 mM, 1 or 2 h) treatment (n = 3). **(C, D)** Quantification of IL-6 **(C)** or the relative IL-1β/IL-6 ratio **(D)** in the culture supernatant of mouse BMNs or BMDMs primed with LPS (0.25 μg/mL, 2.5 h), washed and treated with ATP (2.5 mM) or nigericin (5 μM) for 1 or 3 h, or treated with LPS alone (n = 3). **(E)** Quantification of IL-1β in the culture supernatant of mouse BMNs or BMDMs primed with LPS (0.25 μg/mL, 2.5 h) followed by ATP (2.5 mM, 1 h) treatment (n = 4). **(F–H)** Quantification of IL-6 **(F)**, MCP-1 **(G)**, and TNF-α **(H)** in the culture supernatant of mouse BMNs or BMDMs treated with LPS (0.25 μg/mL, 3 h) (n = 4). **(I)** Quantification of IL-1β in the culture supernatant of mouse BMNs or BMDMs treated with LPS (0.25 μg/mL, 2.5 h) followed by ATP (2.5 mM, 2 h) treatment, washed and incubated for 3 h in the presence of additional LPS and ATP (n = 5). Culture supernatants (Sup) or cell lysates (Lys) were immunoblotted with the indicated antibodies. *P < 0.05, **P < 0.01, ***P < 0.001, n.s. not significant.

neutrophils facilitated persistent IL-1β secretion after media change following 2 h of ATP stimulation, unlike macrophages (**Figure 5I**). Together, these data demonstrate that neutrophils can drive IL-1β–oriented inflammatory responses more persistently than macrophages.

Inflammasome-Active Neutrophils Maintain Antimicrobial Functions but Do Not Trigger Efferocytosis-Mediated M2-Like Macrophage Polarization

Next, we determined the traditional function of neutrophils after inflammasome activation. We examined the phagocytic activity of inflammasome-active neutrophils and macrophages using a zymosan phagocytosis assay. Cytochalasin D, an actin polymerization inhibitor, was used as a control for the inhibition of phagocytosis. NLRP3 inflammasome-activating LPS/ATP stimulation did not affect zymosan uptake in neutrophils but markedly impaired this process in macrophages (**Figure 6A** and **Supplementary Figure S10**), indicating that inflammasome activation may impair the phagocytic activity of macrophages but not neutrophils. We also examined whether inflammasome activation can regulate neutrophil degranulation activity. Consistent with its effect on phagocytosis, NLRP3 inflammasome activation did not significantly affect neutrophil degranulation by measuring the extracellular release of matrix metallopeptidase 9 (MMP-9) triggered by phorbol-12-myristate-13-acetate (PMA) (**Figure 6B**).

Additionally, we measured the migration ability of neutrophils after inflammasome activation using an *in vitro* migration assay. Interestingly, LPS/ATP stimulation did not alter neutrophil migration speed (**Supplementary Figure S11**) but significantly increased their total migration track length (**Figure 6C**). Of note, LPS/ATP treatment reduced the straightness of neutrophil migration (**Figure 6D**) and enhanced random migration patterns (**Figure 6E** and **Supplementary Movie 1**). Together, these findings indicate that inflammasome activation does not impair but slightly increase neutrophil migration ability.

As shown in **Figure 1H**, NLRP3 inflammasome activation caused much less phosphatidylserine exposure, a typical eat-me signal, in neutrophils than in macrophages. Dying neutrophils are engulfed by macrophages in a process known as efferocytosis, leading to M2-like macrophage polarization and inflammation resolution (4, 28). We thus examined whether inflammasome-active neutrophils could promote efferocytosis-mediated signaling of target macrophages (**Figure 6F**). Consistent with previous reports (28), staurosporine-treated neutrophils significantly increased IL-10 production by peritoneal macrophages stimulated with LPS (**Figure 6G**); however, LPS/ATP-stimulated neutrophils did not alter IL-10 production in macrophages (**Figure 6G**), indicating that inflammasome-active neutrophils do not induce efferocytosis-mediated M2 macrophage polarization. Supporting this finding, LPS/ATP-treated neutrophils failed to affect the production of proinflammatory cytokines, including TNF-α (**Figure 6H**) and IL-6 (**Figure 6I**), by peritoneal macrophages upon LPS stimulation, whereas staurosporine-stimulated neutrophils significantly abolished proinflammatory cytokine production in these macrophages. Together, these findings suggest that inflammasome-activated neutrophils do not immunologically silence target macrophages but instead mediates prolonged inflammation in the inflamed region.

Neutrophils Resist Pyroptosis in LPS-Challenged *In Vivo* Mouse Model

To confirm pyroptosis resistance in neutrophils under physiological conditions, we intraperitoneally injected mice with PBS or LPS and analyzed cells in the peritoneal lavage after 24 h of LPS challenge. We found that considerably more $Ly6G^+$ neutrophils were isolated from the peritoneal lavage fluid of LPS-treated mice than PBS-treated mice (**Figure 7A**). Although PI-stained dead neutrophils population was less than 10%, even in the LPS-treated mice (**Figure 7B**), LPS administration dramatically increased the population of PI-positive dead small and large peritoneal macrophages (**Figures 7A, B**). Thus, these *in vivo* data indicate that LPS challenge causes significant cell death in macrophages from peritoneal lavage fluid, but much less cell death in neutrophils.

To examine whether the above macrophage cell death was inflammasome-dependent, we performed the experiments using wild-type and *Nlrp3*-deficient mice. Notably, the LPS-driven increase in the $Ly6G^+$ neutrophils in the peritoneal lavage of wild-type mice was significantly diminished in the peritoneal lavage of NLRP3-knockout mice (**Figure 7C**), while LPS administration profoundly increased cell death in small macrophages from the peritoneal lavage of wild-type mice compared to *Nlrp3*-deficient mice (**Figures 7D, E**). These *in vivo* results indicate that NLRP3 inflammasome-activating conditions lead to the apparent NLRP3-dependent cell death of macrophages under physiological conditions.

DISCUSSION

Chronic and sustained inflammation or inflammasome activation can be detrimental to host tissues and exacerbates the pathogenesis of diverse inflammatory or metabolic diseases (29). However, inflammasome assembly promptly induces the caspase-1 or caspase-11-dependent GSDMD cleavage and subsequent GSDMD pore formation in the plasma membrane leading to pyroptosis (30). The pyroptosis of inflammasome-activated cells can, therefore, terminate the inflammasome response and IL-1β production in the inflammatory region to prevent sustained inflammasome activation. Consistently, previous studies have demonstrated that pyroptotic macrophages lose their functional integrity upon inflammasome activation (31). Pyroptosis occurs in various inflammasome-active cell types, including macrophages, monocytes, dendritic cells and endothelial cells (32–34); therefore, it remains unclear which cell types can overcome pyroptosis and facilitate sustained inflammasome responses in chronic inflammasome-related diseases.

Consistent with recent reports (9, 14, 15, 35), we clarified pyroptosis resistance of neutrophils using diverse *in vitro* experiments and *in vivo* conditions. Molecular mechanisms

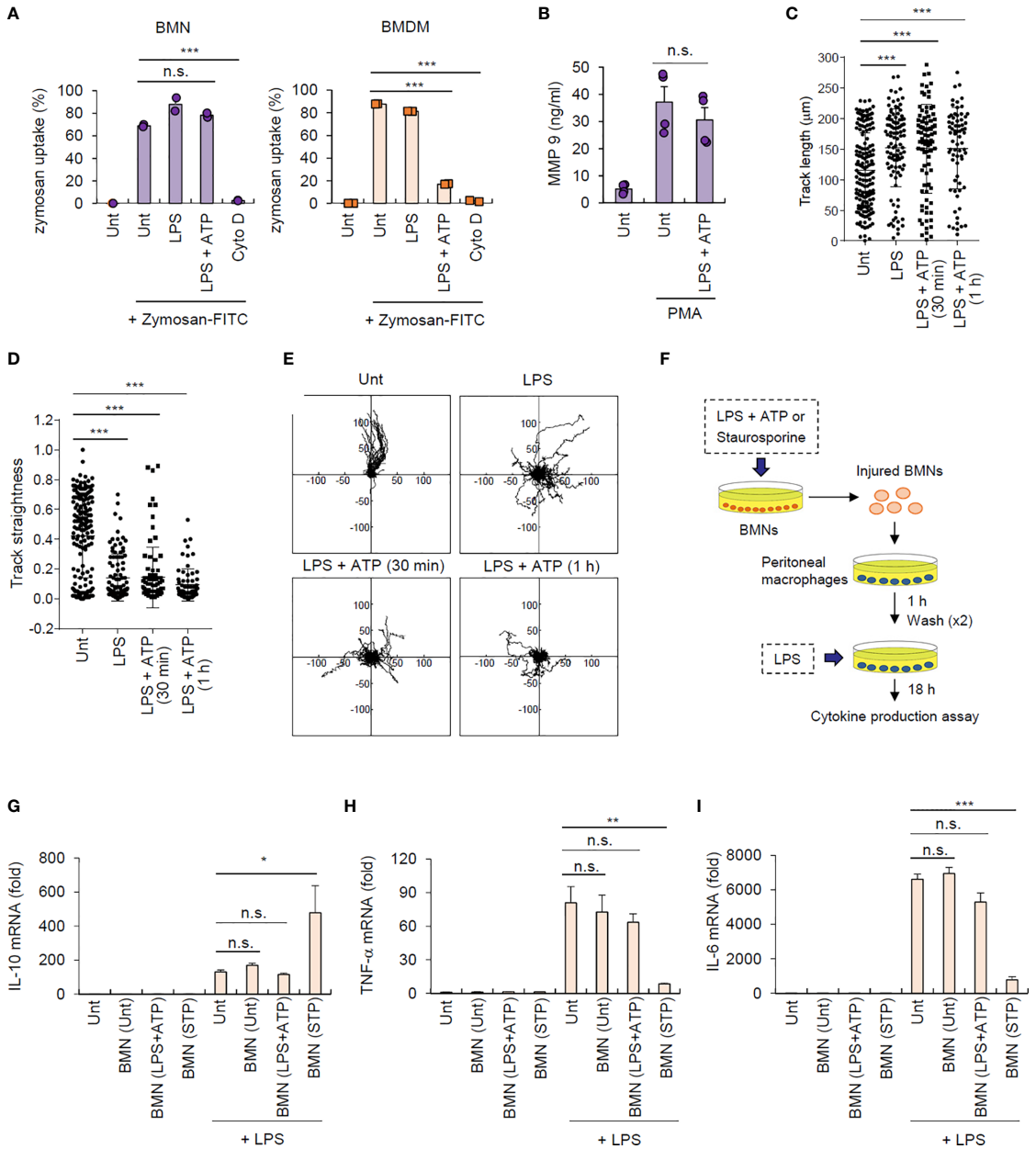

FIGURE 6 | Inflammasome-active neutrophils maintain phagocytosis, degranulation, and migration activities, but do not trigger efferocytic anti-inflammatory macrophage polarization. **(A)** Mouse BMNs or BMDMs were untreated (Unt) or treated with LPS (0.25 μg/mL, 2.5 h) alone, LPS followed by ATP (2.5 mM, 1 h), or cytochalasin D (Cyto D, 10 μM, 30 min) as determined using flow cytometric analysis after incubating with zymosan-FITC (5 particles/cell, 30 min) (n = 3). **(B)** Quantification of MMP-9 in the culture supernatants of mouse BMNs treated with LPS (0.25 μg/mL, 2.5 h) followed by ATP (2.5 mM, 1 h), washed and treated with PMA (1 μM, 2 h) (n = 3). **(C, D)** Quantification of track length **(C)** and track straightness **(D)** of BMNs treated with LPS (0.25 μg/mL, 2.5 h) alone or followed by ATP (2.5 mM), as determined using *in vitro* migration assays. **(E)** Representative migration tracks of BMNs treated as in **(C, D)**. **(F)** Experimental scheme for determining the potential effect of inflammasome-active neutrophils on efferocytosis. **(G–I)** Mouse BMNs were untreated or treated with LPS (0.25 μg/mL, 2.5 h) followed by ATP (2.5 mM, 2 h) or staurosporine (2 μg/mL, 5 h). Mouse peritoneal macrophages were treated with the injured BMNs (1:2.5 ratio, macrophages: neutrophils) for 1 h, washed and treated with LPS (0.1 μg/mL) for 18 **(H)** Quantification of *IL-10* **(G)**, *TNF-α* **(H)**, or *Il-6* **(I)** mRNA levels in mouse peritoneal macrophages treated as above (n = 3). $^*P < 0.05$, $^{**}P < 0.01$, $^{***}P < 0.001$, n.s. not significant.

underlying the pyroptosis resistance of neutrophils remain elusive. It was previously suggested that smaller ASC speck in neutrophils might implicate pyroptosis resistance (36). In the present study, our data revealed that neutrophils exhibited weaker caspase-1 processing and GSDMD cleavage than macrophages, which led to the reduced number of GSDMD pores in the plasma membrane of neutrophils, thereby affecting their resistance to pyroptosis. Of interest, a recent study demonstrated that cleaved GSDMD does

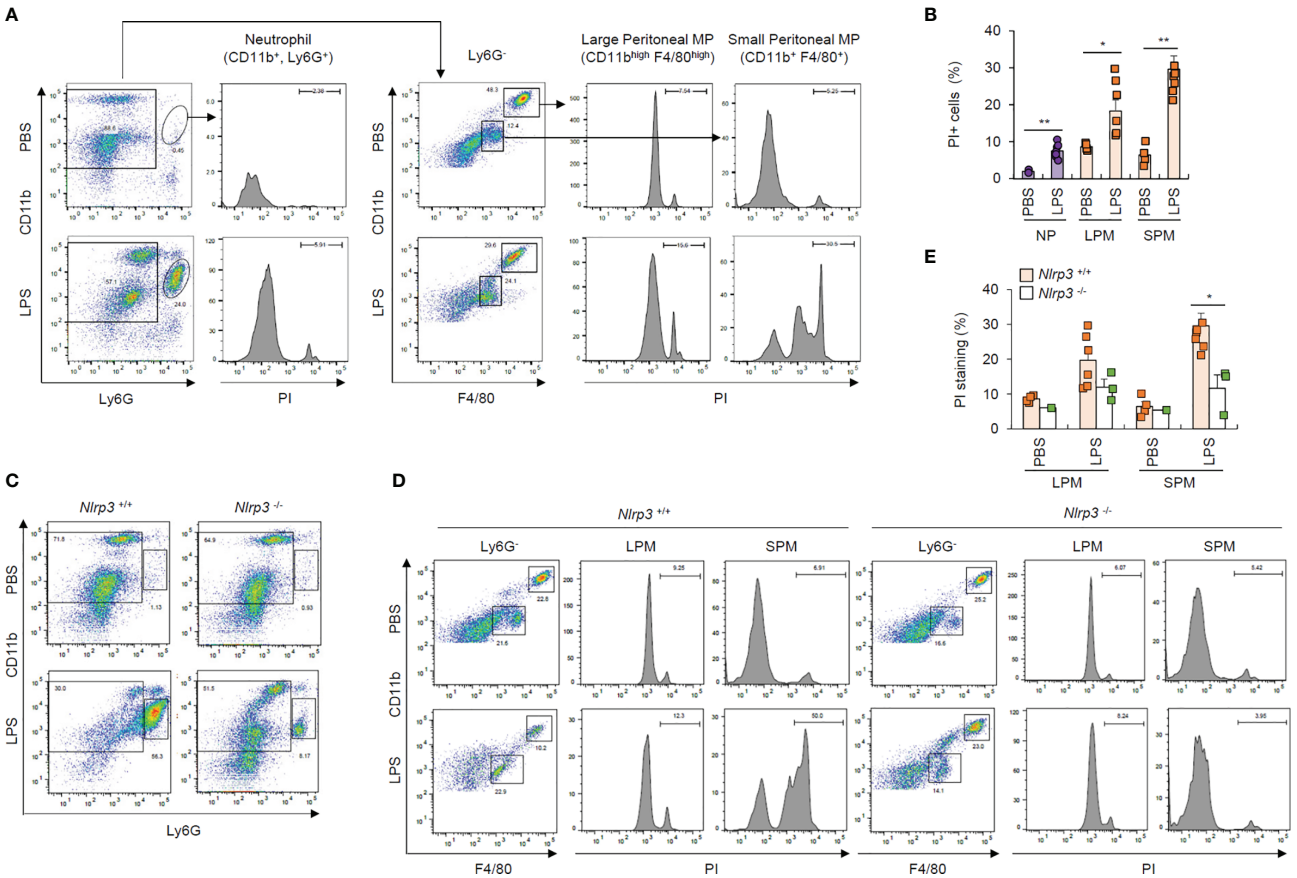

FIGURE 7 | Neutrophils resist pyroptosis in an *in vivo* mouse model. **(A)** Flow cytometric analysis of peritoneal lavage from mice administered PBS or LPS (1 mg/kg, 24 h) after staining with anti-CD11b, Ly6G, and F4/80 antibodies and propidium iodide (PI). **(B)** Quantification of PI-positive cells of neutrophils (NP), large or small peritoneal macrophages (LPM or SPM) as indicated in **(A)** (n = 2~7). **(C, D)** Flow cytometric analysis of mouse peritoneal lavage from wild-type or *Nlrp3*-deficient mice administered PBS or LPS (1 mg/kg, 24 h) after staining with anti-CD11b, Ly6G, and F4/80 antibodies and PI. **(E)** Quantification of PI-positive cells of LPM or SPM as treated in **(D)** (n = 2~7). *P < 0.05, **P < 0.01.

not localize to the plasma membrane, but migrates to azurophilic granules in neutrophils (37), supporting our hypothesis that neutrophils exhibit impaired GSDMD pore formation in the plasma membrane. On the other hand, our data also indicate that mitochondrial membrane potential is critical for determining pyroptosis. Carty et al. recently reported that SARM1-dependent mitochondrial depolarization regulates pyroptosis in macrophages (26). Interestingly, we found that SARM1 expression was not observed in neutrophils and the preservation of mitochondrial membrane potential under NLRP3-activating stimulation contributes to the pyroptosis resistance of neutrophils.

GSDMD pore in the plasma membrane has been shown to act as a major conduit for IL-1β secretion in macrophages (27). Despite reduced GSDMD pore formation, neutrophils displayed similar levels of IL-1β secretion to macrophages. At present, the mechanism underlying this phenomenon is not yet completely understood. Our data demonstrated that neutrophil IL-1β secretion is still caspase-1 activity- and GSDMD presence-dependent. A recent study proposed that N-GSDMD localizes to azurophilic granules and autophagosomes in neutrophils rather than the plasma membrane (37), with this unique pattern of GSDMD trafficking driving IL-1β secretion in a GSDMD/ATG7-dependent manner. In accordance with this finding, our current study supports the possibility that neutrophil IL-1β secretion depends on GSDMD but not GSDMD pores in the plasma membrane. Of interest, a slower GSDMD-independent IL-1β secretion was recently proposed in the non-pyroptotic cells such as neutrophils (38). Consistently, we also found that some GSDMD-independent IL-1β release was observed after 2 h of ATP stimulation.

We also demonstrated that neutrophils induced more rapid IL-1β secretion than macrophages in response to NLRP3 activation. Since rapid IL-1β secretion was found to involve microvesicle shedding in THP-1 monocytes (39), it is possible that neutrophils may also use microvesicle shedding rather than GSDMD pore for very early IL-1β secretion following NLRP3 stimulation. Therefore, the detailed molecular mechanism *via* which neutrophils secret IL-1β after NLRP3 inflammasome activation remains to be further elucidated. Interestingly, our study revealed that neutrophils predominantly secrete IL-1β rather than other proinflammatory cytokines upon NLRP3

stimulation. Similarly, previous studies demonstrated that neutrophils produce much lower levels of proinflammatory cytokines in response to diverse types of stimulation (40, 41). Moreover, Bakele et al. showed that NLRP3 activation caused a robust IL-1β, but not IL-18 secretion by neutrophils, while macrophages produced both cytokines (42). Based on these observations, we propose that neutrophils can act as specialized IL-1β-producing cells under NLRP3 agonist-rich circumstances.

During the initial phase of inflammation, some resident cells are injured or die, leading to the release of cellular contents that produce a danger signal-rich milieu (21). To maintain prolonged inflammasome activation in such inflamed tissues, recruited fresh myeloid cells must promote a robust inflammasome response. Interestingly, we noticed that danger signal-rich medium or ATP clearly abrogated the NLRP3 inflammasome-activating capacity of macrophages. This observation is consistent with a recent study demonstrating that ATP-P2X7 signaling compromises NLRP3 inflammasome activation in macrophages (43). Unexpectedly, our study revealed that danger signal or ATP pretreatment failed to mitigate NLRP3-activating potential of neutrophils, strongly suggesting that recruited or infiltrated neutrophils can activate NLRP3 inflammasome signaling in danger signal-rich inflamed tissues and that neutrophils are major inflammasome-activating cells, particularly under ATP-rich conditions (**Supplementary Figure S12**).

Although the detailed molecular mechanism for the desensitization of NLRP3 inflammasome by danger signals remains unclear, we found that mitochondrial membrane potential status is closely associated with this phenomenon. Indeed, pretreatment with danger signal-rich medium or ATP caused mitochondrial depolarization in macrophages but not in neutrophils, while valinomycin-induced mitochondrial depolarization significantly abolished the NLRP3 inflammasome-activating potential of neutrophils. SARM is a potent candidate marker for macrophage-specific mitochondrial depolarization to determine cellular fate after inflammasome activation (26). Our data revealed that no robust SARM expression was detected in neutrophils. We also found that intact mitochondrial membrane potential is vital for the assembly and activation of NLRP3 inflammasome during treatment with NLRP3-activating second signals such as ATP or nigericin. These results suggest that intact mitochondria may act as a molecular platform for NLRP3 inflammasome assembly.

In addition to this sustained inflammasome-activating potential of neutrophils, our data further indicate that inflammasome-activated neutrophils do not induce efferocytosis-mediated M2-like macrophage polarization. Previous reports have shown that inflammasome-activated macrophages can trigger efferocytosis and downstream signaling of engulfed macrophages *via* exposing eat-me and find-me signals (44, 45). In our study, phosphatidylserine exposure, a typical eat-me signal, was unequivocally observed in inflammasome-activated macrophages, but not neutrophils. These findings indicate that inflammasome-active macrophages can contribute to efferocytosis-mediated inflammation resolution, while inflammasome-active neutrophils do not support efferocytosis but rather facilitate prolonged inflammasome responses (**Supplementary Figure S12**).

Taken together, our data provide new insights into the physiological role of neutrophil inflammasome signaling. In particular, distinct resistance of neutrophils to pyroptosis and DAMP-induced NLRP3 desensitization can prolong robust NLRP3 inflammasome response in danger signal-rich milieu during the propagation stage of inflammation. Thus, our results highlight the importance of neutrophils in the persistent inflammasome activation in response to chronic insult of endogenous metabolites, but not to acute microbial infection. Furthermore, our data suggest that this prolonged inflammasome-activating potential of neutrophils may contribute to the pathogenesis of chronic neutrophil-mediated inflammatory diseases.

DATA AVAILABILITY STATEMENT

The original contributions presented in the study are included in the article/**Supplementary Material**. Further inquiries can be directed to the corresponding author.

ETHICS STATEMENT

The animal study was reviewed and approved by Institutional Ethical Committee, Yonsei University College of Medicine.

AUTHOR CONTRIBUTIONS

SS, S-HY, BC, IH, and D-WS performed experiments and analyzed the data. YC and Y-MH performed and analyzed the experiments regarding neutrophil migration. J-WY supervised the entire project. SS and J-WY wrote the manuscript. All authors contributed to the article and approved the submitted version.

FUNDING

This work was supported by the National Research Foundation of Korea Grant funded by the Korean Government (2017R1A 2B2007467, 2020R1A2B5B02001823, 2020R1A4A1019009) and the "Dongwha" Faculty Research Assistance Program of Yonsei University College of Medicine (6-2019-0122).

SUPPLEMENTARY MATERIAL

The Supplementary Material for this article can be found online at: https://www.frontiersin.org/articles/10.3389/fimmu.2021.746032/full#supplementary-material

REFERENCES

1. Bardoel BW, Kenny EF, Sollberger G, Zychlinsky A. The Balancing Act of Neutrophils. *Cell Host Microbe* (2014) 15:526–36. doi: 10.1016/j.chom.2014.04.011
2. Faurschou M, Borregaard N. Neutrophil Granules and Secretory Vesicles in Inflammation. *Microbes Infect* (2003) 5:1317–27. doi: 10.1016/j.micinf.2003.09.008
3. Kruger P, Saffarzadeh M, Weber AN, Rieber N, Radsak M, von Bernuth H, et al. Neutrophils: Between Host Defence, Immune Modulation, and Tissue Injury. *PloS Pathog* (2015) 11:e1004651. doi: 10.1371/journal.ppat.1004651
4. Nagata S. Apoptosis and Clearance of Apoptotic Cells. *Annu Rev Immunol* (2018) 36:489–517. doi: 10.1146/annurev-immunol-042617-053010
5. Kawano M, Nagata S. Lupus-Like Autoimmune Disease Caused by a Lack of Xkr8, a Caspase-Dependent Phospholipid Scramblase. *Proc Natl Acad Sci USA* (2018) 115:2132–7. doi: 10.1073/pnas.1720732115
6. Abdolmaleki F, Farahani N, Gheibi Hayat SM, Pirro M, Bianconi V, Barreto GE, et al. The Role of Efferocytosis in Autoimmune Diseases. *Front Immunol* (2018) 9:1645. doi: 10.3389/fimmu.2018.01645
7. Rathinam VA, Fitzgerald KA. Inflammasome Complexes: Emerging Mechanisms and Effector Functions. *Cell* (2016) 165:792–800. doi: 10.1016/j.cell.2016.03.046
8. Yu JW, Lee MS. Mitochondria and the NLRP3 Inflammasome: Physiological and Pathological Relevance. *Arch Pharm Res* (2016) 39:1503–18. doi: 10.1007/s12272-016-0827-4
9. Chen KW, Demarco B, Broz P. Beyond Inflammasomes: Emerging Function of Gasdermins During Apoptosis and NETosis. *EMBO J* (2020) 39:e103397. doi: 10.15252/embj.2019103397
10. Mangan MSJ, Olhava EJ, Roush WR, Seidel HM, Glick GD, Latz E. Targeting the NLRP3 Inflammasome in Inflammatory Diseases. *Nat Rev Drug Discov* (2018) 17:588–606. doi: 10.1038/nrd.2018.97
11. Ising C, Venegas C, Zhang S, Scheiblich H, Schmidt SV, Vieira-Saecker A, et al. NLRP3 Inflammasome Activation Drives Tau Pathology. *Nature* (2019) 575:669–73. doi: 10.1038/s41586-019-1769-z
12. Lee E, Hwang I, Park S, Hong S, Hwang B, Cho Y, et al. MPTP-Driven NLRP3 Inflammasome Activation in Microglia Plays a Central Role in Dopaminergic Neurodegeneration. *Cell Death Differ* (2019) 26:213–28. doi: 10.1038/s41418-018-0124-5
13. Shi J, Zhao Y, Wang K, Shi X, Wang Y, Huang H, et al. Cleavage of GSDMD by Inflammatory Caspases Determines Pyroptotic Cell Death. *Nature* (2015) 526:660–5. doi: 10.1038/nature15514
14. Karmakar M, Katsnelson MA, Dubyak GR, Pearlman E. Neutrophil P2X7 Receptors Mediate NLRP3 Inflammasome-Dependent IL-1beta Secretion in Response to ATP. *Nat Commun* (2016) 7:10555. doi: 10.1038/ncomms10555
15. Chen KW, Monteleone M, Boucher D, Sollberger G, Ramnath D, Condon ND, et al. Noncanonical Inflammasome Signaling Elicits Gasdermin D-Dependent Neutrophil Extracellular Traps. *Sci Immunol* (2018) 3(26). doi: 10.1126/sciimmunol.aar6676
16. Faust N, Varas F, Kelly LM, Heck S, Graf T. Insertion of Enhanced Green Fluorescent Protein Into the Lysozyme Gene Creates Mice With Green Fluorescent Granulocytes and Macrophages. *Blood* (2000) 96:719–26. doi: 10.1182/blood.V96.2.719
17. Fernandes-Alnemri T, Yu JW, Juliana C, Solorzano L, Kang S, Wu J, et al. The AIM2 Inflammasome Is Critical for Innate Immunity to Francisella Tularensis. *Nat Immunol* (2010) 11:385–93. doi: 10.1038/ni.1859
18. Yang J, Lee KM, Park S, Cho Y, Lee E, Park JH, et al. Bacterial Secretant From Pseudomonas Aeruginosa Dampens Inflammasome Activation in a Quorum Sensing-Dependent Manner. *Front Immunol* (2017) 8:333. doi: 10.3389/fimmu.2017.00333
19. Fernandes-Alnemri T, Yu JW, Datta P, Wu J, Alnemri ES. AIM2 Activates the Inflammasome and Cell Death in Response to Cytoplasmic DNA. *Nature* (2009) 458:509–13. doi: 10.1038/nature07710
20. Yu JW, Fernandes-Alnemri T, Datta P, Wu J, Juliana C, Solorzano L, et al. Pyrin Activates the ASC Pyroptosome in Response to Engagement by Autoinflammatory PSTPIP1 Mutants. *Mol Cell* (2007) 28:214–27. doi: 10.1016/j.molcel.2007.08.029
21. Davies LC, Jenkins SJ, Allen JE, Taylor PR. Tissue-Resident Macrophages. *Nat Immunol* (2013) 14:986–95. doi: 10.1038/ni.2705
22. de Oliveira S, Rosowski EE, Huttenlocher A. Neutrophil Migration in Infection and Wound Repair: Going Forward in Reverse. *Nat Rev Immunol* (2016) 16:378–91. doi: 10.1038/nri.2016.49
23. Trautmann A. Extracellular ATP in the Immune System: More Than Just a "Danger Signal". *Sci Signal* (2009) 2:pe6. doi: 10.1126/scisignal.256pe6
24. Park S, Juliana C, Hong S, Datta P, Hwang I, Fernandes-Alnemri T, et al. The Mitochondrial Antiviral Protein MAVS Associates With NLRP3 and Regulates Its Inflammasome Activity. *J Immunol* (2013) 191:4358–66. doi: 10.4049/jimmunol.1301170
25. Gurung P, Lukens JR, Kanneganti TD. Mitochondria: Diversity in the Regulation of the NLRP3 Inflammasome. *Trends Mol Med* (2015) 21:193–201. doi: 10.1016/j.molmed.2014.11.008
26. Carty M, Kearney J, Shanahan KA, Hams E, Sugisawa R, Connolly D, et al. Cell Survival and Cytokine Release After Inflammasome Activation Is Regulated by the Toll-IL-1r Protein SARM. *Immunity* (2019) 50:1412–1424 e1416. doi: 10.1016/j.immuni.2019.04.005
27. Heilig R, Dick MS, Sborgi L, Meunier E, Hiller S, Broz P. The Gasdermin-D Pore Acts as a Conduit for IL-1beta Secretion in Mice. *Eur J Immunol* (2018) 48:584–92. doi: 10.1002/eji.201747404
28. Sugimoto MA, Vago JP, Perretti M, Teixeira MM. Mediators of the Resolution of the Inflammatory Response. *Trends Immunol* (2019) 40:212–27. doi: 10.1016/j.it.2019.01.007
29. Chawla A, Nguyen KD, Goh YP. Macrophage-Mediated Inflammation in Metabolic Disease. *Nat Rev Immunol* (2011) 11:738–49. doi: 10.1038/nri3071
30. Orning P, Lien E, Fitzgerald KA. Gasdermins and Their Role in Immunity and Inflammation. *J Exp Med* (2019) 216:2453–65. doi: 10.1084/jem.20190545
31. Evavold CL, Ruan J, Tan Y, Xia S, Wu H, Kagan JC. The Pore-Forming Protein Gasdermin D Regulates Interleukin-1 Secretion From Living Macrophages. *Immunity* (2018) 48:35–44 e36. doi: 10.1016/j.immuni.2017.11.013
32. Zanoni I, Tan Y, Di Gioia M, Springstead JR, Kagan JC. By Capturing Inflammatory Lipids Released From Dying Cells, the Receptor CD14 Induces Inflammasome-Dependent Phagocyte Hyperactivation. *Immunity* (2017) 47:697–709 e693. doi: 10.1016/j.immuni.2017.09.010
33. Deng M, Tang Y, Li W, Wang X, Zhang R, Zhang X, et al. The Endotoxin Delivery Protein HMGB1 Mediates Caspase-11-Dependent Lethality in Sepsis. *Immunity* (2018) 49:740–753 e747. doi: 10.1016/j.immuni.2018.08.016
34. Cheng KT, Xiong S, Ye Z, Hong Z, Di A, Tsang KM, et al. Caspase-11-Mediated Endothelial Pyroptosis Underlies Endotoxemia-Induced Lung Injury. *J Clin Invest* (2017) 127:4124–35. doi: 10.1172/JCI94495
35. Chen KW, Gross CJ, Sotomayor FV, Stacey KJ, Tschopp J, Sweet MJ, et al. The Neutrophil NLRC4 Inflammasome Selectively Promotes IL-1beta Maturation Without Pyroptosis During Acute Salmonella Challenge. *Cell Rep* (2014) 8:570–82. doi: 10.1016/j.celrep.2014.06.028
36. Boucher D, Monteleone M, Coll RC, Chen KW, Ross CM, Teo JL, et al. Caspase-1 Self-Cleavage Is an Intrinsic Mechanism to Terminate Inflammasome Activity. *J Exp Med* (2018) 215:827–40. doi: 10.1084/jem.20172222
37. Karmakar M, Minns M, Greenberg EN, Diaz-Aponte J, Pestonjamasp K, Johnson JL, et al. N-GSDMD Trafficking to Neutrophil Organelles Facilitates IL-1beta Release Independently of Plasma Membrane Pores and Pyroptosis. *Nat Commun* (2020) 11:2212. doi: 10.1038/s41467-020-16043-9
38. Monteleone M, Stanley AC, Chen KW, Brown DL, Bezbradica JS, von Pein JB, et al. Interleukin-1beta Maturation Triggers Its Relocation to the Plasma Membrane for Gasdermin-D-Dependent and -Independent Secretion. *Cell Rep* (2018) 24:1425–33. doi: 10.1016/j.celrep.2018.07.027
39. MacKenzie A, Wilson HL, Kiss-Toth E, Dower SK, North RA, Surprenant A, et al. Rapid Secretion of Interleukin-1beta by Microvesicle Shedding. *Immunity* (2001) 15:825–35. doi: 10.1016/S1074-7613(01)00229-1
40. Tamassia N, Bianchetto-Aguilera F, Arruda-Silva F, Gardiman E, Gasperini S, Calzetti F, et al. Cytokine Production by Human Neutrophils: Revisiting the "Dark Side of the Moon". *Eur J Clin Invest* (2018) 48(Suppl 2):e12952. doi: 10.1111/eci.12952
41. Zhang X, Majlessi L, Deriaud E, Leclerc C, Lo-Man R. Coactivation of Syk Kinase and MyD88 Adaptor Protein Pathways by Bacteria Promotes Regulatory Properties of Neutrophils. *Immunity* (2009) 31:761–71. doi: 10.1016/j.immuni.2009.09.016
42. Bakele M, Joos M, Burdi S, Allgaier N, Poschel S, Fehrenbacher B, et al. Localization and Functionality of the Inflammasome in Neutrophils. *J Biol Chem* (2014) 289:5320–9. doi: 10.1074/jbc.M113.505636
43. Martinez-Garcia JJ, Martinez-Banaclocha H, Angosto-Bazarra D, de Torre-Minguela C, Baroja-Mazo A, Alarcon-Vila C, et al. P2X7 Receptor Induces

Mitochondrial Failure in Monocytes and Compromises NLRP3 Inflammasome Activation During Sepsis. *Nat Commun* (2019) 10:2711. doi: 10.1038/s41467-019-10626-x
44. Wang Q, Imamura R, Motani K, Kushiyama H, Nagata S, Suda T. Pyroptotic Cells Externalize Eat-Me and Release Find-Me Signals and Are Efficiently Engulfed by Macrophages. *Int Immunol* (2013) 25:363–72. doi: 10.1093/intimm/dxs161
45. Lu J, Shi W, Liang B, Chen C, Wu R, Lin H, et al. Efficient Engulfment of Necroptotic and Pyroptotic Cells by Nonprofessional and Professional Phagocytes. *Cell Discov* (2019) 5:39. doi: 10.1038/s41421-019-0108-8

Conflict of Interest: The authors declare that the research was conducted in the absence of any commercial or financial relationships that could be construed as a potential conflict of interest.

Publisher's Note: All claims expressed in this article are solely those of the authors and do not necessarily represent those of their affiliated organizations, or those of the publisher, the editors and the reviewers. Any product that may be evaluated in this article, or claim that may be made by its manufacturer, is not guaranteed or endorsed by the publisher.

frontiers in Immunology

ORIGINAL RESEARCH
published: 10 February 2022
doi: 10.3389/fimmu.2022.812164

A 4-Benzene-Indol Derivative Alleviates LPS-Induced Acute Lung Injury Through Inhibiting the NLRP3 Inflammasome

Junmei Li[1†], Yang Bai[1†], Yiting Tang[2], Xiangyu Wang[1], María José Cavagnaro[3], Ling Li[1], Zhaozheng Li[1], Yi Zhang[4] and Jian Shi[1,5*]*

[1] Department of Hematology and Critical Care Medicine, The Third Xiangya Hospital, Central South University, Changsha, China, [2] Department of Physiology, School of Basic Medical Science, Central South University, Changsha, China, [3] College of Medicine-Phoenix, University of Arizona, Phoenix, AZ, United States, [4] Department of Gastrointestinal Surgery, The Third Xiangya Hospital, Central South University, Changsha, China, [5] Department of Spine Surgery, The Third Xiangya Hospital, Central South University, Changsha, China

OPEN ACCESS

Edited by:
Chaofeng Han, Second Military Medical University, China

Reviewed by:
Jin Zhu, Nanjing Medical University, China
Dong-Yun Ouyang, Jinan University, China

***Correspondence:**
Yi Zhang
yzhangxy3@csu.edu.cn
Jian Shi
xyshijian@csu.edu.cn

[†]These authors have contributed equally to this work

Specialty section:
This article was submitted to Molecular Innate Immunity, a section of the journal Frontiers in Immunology

Received: *09 November 2021*
Accepted: *10 January 2022*
Published: *10 February 2022*

Citation:
Li J, Bai Y, Tang Y, Wang X, Cavagnaro MJ, Li L, Li Z, Zhang Y and Shi J (2022) A 4-Benzene-Indol Derivative Alleviates LPS-Induced Acute Lung Injury Through Inhibiting the NLRP3 Inflammasome. Front. Immunol. 13:812164. doi: 10.3389/fimmu.2022.812164

Acute lung injury (ALI) is a common complication of critical illness that could frequently lead to acute respiratory distress syndrome and other serious clinical consequences. Sepsis is one of the major and most common inducements among all causes of ALI. Due to its high incidence and mortality rate and also the complexity in treatment, sepsis-related ALI has become an urgent clinical problem waiting to be solved effectively. At present, only the protective ventilation strategy, restrictive fluid management, and antibiotics application are measures that can improve the prognosis with evidence-based medical proof. No pharmacological treatment is currently available to protect or significantly reverse the prognosis. Seeking for effective interventions measures for sepsis-related ALI is one of the most necessitous research directions. In this research, a conspicuous discovery of treatment-related translational use for a 4-benzene-indol derivative was elaborated by screening a large number of chemical compounds. The results showed that 4-benzene-indol derivative could not only suppress the activation of NLRP3 inflammasome both *in vitro* and alleviate LPS-induced ALI *in vivo* but also suppress the NLRP3 inflammasome in human myeloid leukemia mononuclear cells (THP-1) cell lines. Mechanistically, 1,2-diol blocks the NLRP3 inflammasome activation by disrupting NLRP3–NEK7 interaction and the subsequent NLRP3 inflammasome assembly and activation. To summarize, this research indicated that the newly-discovered 4-benzene-indol derivative targets NLRP3 inflammasome signaling, which consequently alleviates sepsis-related ALI. Collectively, the 4-benzene-indol derivative may serve as a potential therapeutic drug and NLRP3 inflammasome signaling would be a novel pharmaceutical target for clinical treatment of sepsis-related ALI.

Keywords: sepsis, acute lung injury, NLRP3 inflammasome, 4-benzene-indol derivative, pharmaceutical target, inflammatory cytokines, critical care medicine, basic and clinic immunology

INTRODUCTION

As a life-threatening multiple organ dysfunction attributable to maladjusted host immune responses to infection, sepsis is usually the common pathway to serious prognosis such as systemic inflammatory response syndrome (SIRS), multiple organ dysfunctions (MODS) and a high risk of death (1–3). In sepsis-induced MODS, the lung is the most vulnerable organ (4), several studies have demonstrated that more than 50% of patients with sepsis will eventually become acute lung injury (ALI) or acute respiratory distress syndrome (ARDS) (5, 6), which characterized by acute onset noncardiogenic pulmonary edema and hypoxemia (7). Despite the considerable efforts to find potential treatment strategies, the protective ventilation strategy, restrictive fluid management, and antibiotics application are the only available treatment options for patients with sepsis and ALI. Nevertheless, these measures have limited effect on decreasing the high mortality rate from sepsis (8, 9).

Recently, multiple studies have highlighted the crucial component of the NLR family pyrin domain containing 3 (NLRP3) inflammasome in sepsis (10, 11). As a multiple-protein complex, NLRP3 inflammasome is composed by NLRP3, apoptosis-associated speck-like protein containing a CARD (ASC) and Caspase-1 which are known as innate immune sensors (12). The assembly of NLRP3 inflammasome will lead to the activation of Caspase-1, and Caspase-1 will then promote the cleavage of GSDMD and also pro-IL-1β and pro-IL-18. Hence, NLRP3 inflammasome plays an essential role in inflammation and innate immunity (13). Production of proinflammatory cytokines interleukin such as IL-1β and IL-18 and NLRP3 inflammasome in macrophages, jointly result in the pyroptosis process of macrophages during ALI (14–16). Moreover, several inhibitors of NLRP3 inflammasome have been demonstrated to exert beneficial effects for ALI in animal model tests which suggest that NLPR3 inflammasome might be a novel potential pharmaceutical target for the clinical treatment of ALI (17, 18).

In this study, by screening a large number of chemical compounds, we identified 4-[2-(1H-indol-3-yl)-1,3-thiazol-4-yl] benzene-1,2-diol (1,2-diol), a 4-benzene-indol derivative, suppressed NLRP3 inflammasome activation both *in vitro* and alleviates LPS-induced ALI *in vivo*. Mechanistically, 1,2-diol blocks the NLRP3 inflammasome activation by disrupting NLRP3-NEK7 interaction and the subsequent NLRP3 inflammasome assembly and activation. Furthermore, 1,2-diol can also suppress the NLRP3 inflammasome in human myeloid leukemia mononuclear cells (THP-1) cell lines. Collectively, this study provides a new avenue for LPS induced ALI, which may facilitate the therapeutic strategy of sepsis and ALI.

MATERIALS AND METHODS

Animals

C57BL/6 mice (8–10 weeks old) weighing 25–28 g were purchased from the Hunan SJA Laboratory Animal Co. Ltd. (Changsha, China). *NLRP3*$^{-/-}$ mice were provided by Professor Rongbin Zhou. Mice were kept under specific pathogen-free (SPF) conditions. All animal experiments were approved by the Institutional Animal Care and Use Committee of Central South University.

Cell Culture

THP-1 cells were obtained from American Type Culture Collection (Manassas, VA). Primary peritoneal macrophages from C57BL/6 mice were isolated by peritoneal lavage with 10 ml RPMI 1640 medium (Gibco™ |Thermo Fisher Scientific).THP-1 cells and primary peritoneal macrophages were cultured in RPMI 1640 medium which was supplemented with 10% FBS (Gibco™ |Thermo Fisher Scientific) and 1% penicillin/streptomycin at 37°C in a humidified incubator of 5% CO_2.

Inflammasome Activation

Primary peritoneal macrophages from C57BL/6 mice or THP1 cells were seeded in 24-well (5×10^5) or 6-well (2×10^6) culture plates. The next day, we removed medium and primed macrophages with LPS (InvivoGen tlrl-3pelps,100 ng/ml) for 3 h followed by 1,2-diol for 1 h. At the last, we treated macrophages with stimulation as follows: ATP (InvivoGen tlrl-atp, 5 mmol/L) or nigericin (InvivoGen tlrl-nig, 10 μmol/L) for 1 h and MSU (InvivoGen tlrl-msu, 200μg/ml) or SiO_2 (InvivoGen tlrl-sio, 20 μg/ml) for 6 h. THP-1 cells should be treated with 100 ng/ml PMA for 12 h before seeding in culture plates.

ELISA Assay for Cytokines

ELISA kits were used to detect the mouse IL-1β (eBioscience), TNF-α (eBioscience), IL-6 (eBioscience), and human IL-1β (Biolegend, #437004), human TNF-α (eBioscience) according to the manufacturer's instructions.

ASC Speck Formation

Primary peritoneal macrophages were seeded in chamber slides and the following day, the cells were given with indicated stimuli. Then we used 4% Paraformaldehyde (PFA) to fix the cells for 15 min at room temperature. Then the cells were washed with PBS, permeabilized with 0.1% Triton X-100, and blocked with PBS buffer which were containing 3% BSA. Then we used the anti-ASC (Adipogen AL177, 1:200 at 4°C overnight) to incubate with the cells and used DyLight 488-labeled as the secondary antibody (1:50 at room temperature for 45 min). Finally, DAPI was used to stain nuclei and cells were visualized by fluorescence microscope (Nikon Ti2-U).

Immunoprecipitation and Western Blot

Peritoneal macrophages which were treated with stimulation were lysed in immunoprecipitation (IP) buffer, namely, a protease inhibitor cocktail, and then the cell lysates were incubated overnight at 4°C with the specific antibodies. The next day, immunoprecipitates were washed by IP buffer 4 times and incubated with Protein A/G plus-agarose(Santa Cruz sc-2003) at 4°C for 4 h. At last, immunoprecipitates were boiled with 1% (w/v) SDS sample buffer. The proteins bound by antibody were precipitated by protein A/G beads and subjected

to immunoblotting analysis. The proteins were separated by SDS-PAGE, and then we have translated the proteins onto PVDF membranes for immunoblot analysis. After that, the membranes were blocked with 5% dried milk in TBS-T (50 mM Tris/HCL, 150 mM NaCl, pH 7.6 and 0.1% Tween-20) for 1 h at room temperature. After blocking, PVDF membranes were incubated with various primary antibodies such as human IL-1β (Abcam ab9722), human GSDMD (Abcam ab210070), Caspase-1 (Abcam ab179515), IL-1β (RD systems AF-401-NA), NLRP3 (Adipogen), ASC (Adipogen AL177), GSDMD (Abcam ab133514) and NEK7 (Abcam ab133514) at 4°C overnight. The next day, membranes were washed with TBS-T and incubated in corresponding horseradish peroxidase-conjugated secondary antibodies (1:5,000, KPL) for 1 h at room temperature.

ASC Oligomerization

Peritoneal macrophages were treated with indicated stimuli, then the cells were lysed with Triton buffer [50 mM Tris–HCl (pH 7.5), 50 mM NaCl, 0.5% Triton X-100], 0.1 mM phenylmethylsulfonyl fluoride (PMSF) and EDTA-free protease inhibitor cocktail at 4°C for 10 min. The lysates were centrifuged at 6,000*g* at 4°C for 15 min, the supernatant was collected and pellets were washed twice and re-suspended in 200 μl Triton buffer, then added 2 mM disuccinimidyl suberate (DSS) and cross-linked at 37°C for 30 min. Samples were centrifuged and the pellets were dissolved in sodium dodecyl sulfate (SDS) loading buffer for western blotting.

Intracellular K+ Level

Peritoneal macrophages were treated with indicated stimuli, then the medium was removed and cells were washed with PBS 2 times, and then cells were soaked with 0.9% NS for 15 min. We scraped cells and collected them to count under the microscope. At last, cells were added 0.9% NS so that its concentration becames 1×10^6, and then tested the K^+ level by Hitachi 7600 automatic biochemical analyzer (Hitachi Coro, Tokyo, Japan).

ALI and Endotoxemia Model

For ALI model, C57BL/6 mice were anesthetized using 1% Pentobarbital administered intraperitoneally and mice were injected intraperitoneally (i.p) with 40 mg/kg 1,2-diol or DMSO 30 min before intratracheally (i.t) instilled with 15 mg/kg LPS (*E. coli* O111:B4; Sigma). After 48 h, we killed the mice, harvested the lung tissue and collected the bronchoalveolar lavage fluid. For endotoxemia model, C57BL/6 mice were injected intraperitoneally with 40 mg/kg 1,2-diol or DMSO 30 min before i.p. with 25 mg/kg LPS. After 16 h, we killed the mice, harvested the lung tissue and collected the serum.

Histology

The lung tissue sections from mouse were fixed in 4% PFA and embedded by paraffin. Tissue sections were deparaffinized and rehydrated. The sections were prepared and stained with H&E using standard procedures. Slides were examined under a Nikon ECL IPSE Ci biological microscope, and images were captured with a Nikon DS-U3 color digital camera.

Statistical Analysis

All data were analyzed using GraphPad Prism software (version 8.2). Data were analyzed using by student's t-test and were used for comparison between two groups or one-way ANOVA followed by *post-hoc* Bonferroni test for multiple comparisons. A p-value <0.05 was considered statistically significant for all experiments. All values are presented as the mean ± SD.

RESULTS

1,2-Diol Blocks NLRP3 Activation in Mouse Peritoneal Macrophages

To discover a potential approach for the treatment of NLRP3-driven diseases, we screened NLRP3 inflammasome inhibitors in a bioactive compound library purchased from Selleck. We treated mouse peritoneal macrophages with nigericin and LPS to activate NLRP3 inflammasome and detected IL-1β release (**Figure 1A**). After screening 110 compounds, we identified 4-[2-(1H-indol-3-yl)-1,3-thiazol-4-yl]benzene-1,2-diol (1,2-diol), a novel indole-based small molecule compound, as the most potent inhibitor for NLRP3 inflammasome (**Figures 1B, C**). The results showed that 1,2-diol exhibited dose-dependent inhibitory effects on NLRP3-dependent IL-1β secretion, but had no effects on inflammasome-independent cytokine TNF-α production (**Figure 1D**). As revealed by western-blot, 1,2-diol significantly attenuated Caspase-1 and GSDMD cleavage, the release of IL-1β, but did not inhibit the precursors of IL-1β and Caspase-1 expression (**Figure 1E**). To further verify the inhibitory effect of 1,2-diol on NLRP3 inflammasome, we used other NLRP3 agonists, such as monosodium urate crystals (MSU), ATP or silicon crystals (SiO_2).The results showed 1,2-diol can also abolish the secretion of IL-1β, but had no effects on inflammasome-independent cytokine TNF-α production (**Figure 1D**). The cleaved of Caspase-1,GSDMD and the release of IL-1β were impaired, and also the precursors of IL-1β and Caspase-1 expression did not affect either (**Figure 1F**). Thus, these results suggest that 1,2-diol can be an inhibitor of NLRP3 inflammasome.

1,2-Diol Suppresses NLRP3 Inflammasome Activation in THP-1 Cells

Next, we examine whether 1,2-diol can suppress NLPR3 inflammasome in human cells. Consistent with mouse peritoneal macrophages, after treating 1,2-diol with PMA-primed THP-1 cells and challenged with the above-mentioned agonists, IL-1β secretion was dose-dependent inhibited (**Figure 2A**). Western blot analysis revealed that 1,2-diol suppressed the activation of Caspase-1 and IL-1β in the supernatant, and attenuated the cleavage of GSDMD but did not impair the precursors of IL-1β and Caspase-1 (**Figure 2B**). Together, these results indicated that 1,2-diol also inhibits NLRP3 inflammasome in human cells.

1,2-Diol Inhibits ASC Oligomerization and Inflammasome Assembly

We next investigated how 1,2-diol inhibited NLRP3 inflammasome activation. It has been proposed that potassium

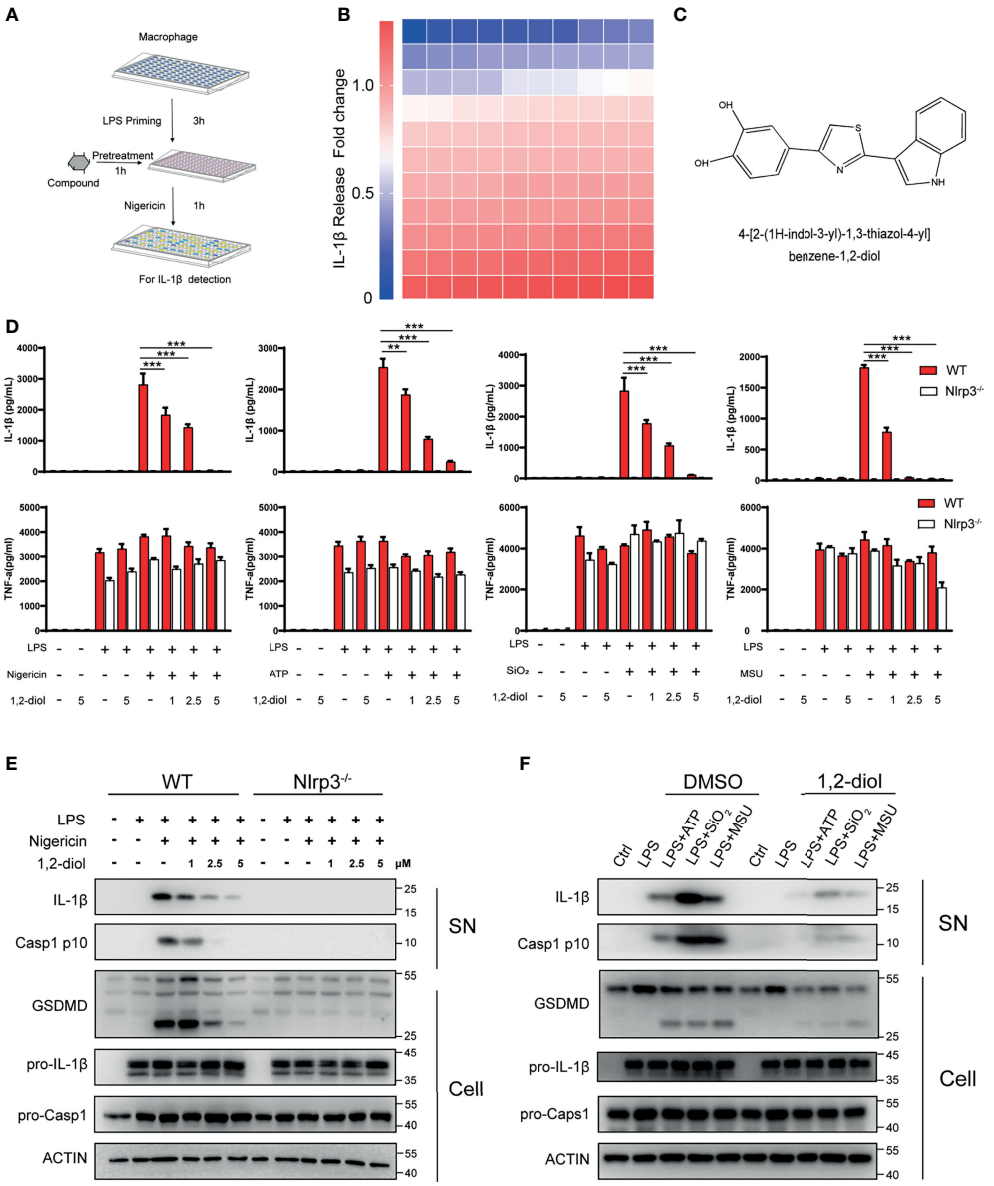

FIGURE 1 | 1,2-Diol blocks NLRP3 activation in mouse peritoneal macrophages.**(A)** Schematic diagram of the screening steps from the compound library in mouse macrophage stimulated with nigericin and LPS. **(B)** Heatmap of IL-1β release changes in LPS-primed primary macrophages treated with 5 μM inhibitors and then stimulated with nigericin with 110 bioactive compounds library. **(C)** Chemical structure of 4-[2-(1H-indol-3-yl)-1,3-thiazol-4-yl]benzene-1,2-diol. **(D)** cytokines (IL-1β and TNFα) release from WT or Nlrp3$^{-/-}$ peritoneal macrophages primed by LPS and stimulated with nigericin, ATP, SiO_2 or MSU in the absence or not of 1,2-diol with different doses. **(E)** Western blots for Caspase-1 and IL-1β in the supernatant or the cleavage of GSDMD, the expression of pro-Caspase-1 and pro-IL-1β in the cell lysates of WT or Nlrp3$^{-/-}$ peritoneal macrophages primed by LPS and stimulated with nigericin in the absence or not of 1,2-diol with different doses. **(F)** Western blots for Caspase-1 and IL-1β in the supernatant or the cleavage of GSDMD, the expression of pro-Caspase-1 and pro-IL-1β in the cell lysates of peritoneal macrophages primed by LPS and stimulated with ATP, SiO2 or MSU in the absence or not of 1,2-diol with 5 μM dose. Graphs show the mean ± SD of technical replicates and are representative of at least three independent experiments. (**p < 0.01; ***p < 0.001).

(K^+) efflux is a trigger common to several NLRP3 activators, namely, nigericin, ATP, MSU and SiO_2. So we tested whether 1,2-diol could block potassium. The results confirmed that 1,2-diol could not block nigericin-induced potassium efflux (**Figure 3A**), indicating that 1,2-diol does not affect the potassium efflux during NLRP3 inflammasome activation.

Since ASC oligomerization and the formation of ASC speck are essential steps for NLRP3 activation, we next examined the formation of nigericin-induced ASC oligomers and ASC speck. The results demonstrated that 1,2-diol could significantly suppress the formation of ASC oligomers (**Figure 3B**) and could reduce the percentage of cells containing ASC speck

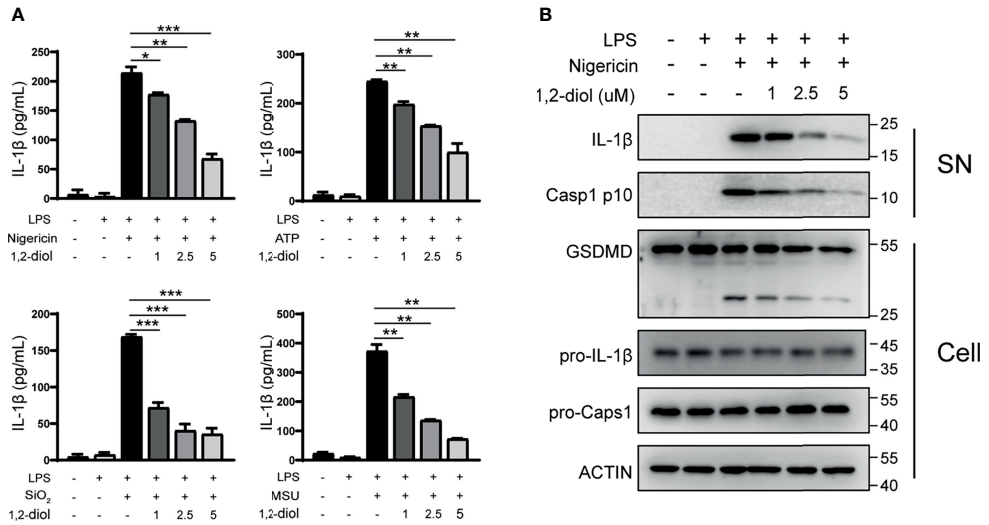

FIGURE 2 | 1,2-Diol suppresses NLRP3 inflammasome activation in THP-1 cells. **(A)** ELISA of IL-1β in supernatant from PMA-primed THP-1 cells treated with LPS stimulation, after that the cells were treated with or without different doses of 1,2-diol and stimulated with ATP, nigericin SiO_2 or MSU. **(B)** Western blots for Caspase-1 and IL-1β in the supernatant or the cleavage of GSDMD, the expression of pro-Caspase-1 and pro-IL-1β in the cell lysates of PMA-primed THP-1 cells treated with LPS stimulation, after that the cells were treated with or without different doses of 1,2-diol and stimulated with nigericin. (*$p < 0.05$; **$p < 0.01$; ***$p < 0.001$).

(**Figure 3C**), suggesting that 1,2-diol may affect the ASC oligomerization or the upstream of ASC oligomerization to suppress the NLRP3 inflammasome activation.

Next, we assessed whether 1,2-diol could impact the NLRP3-ASC interaction which is a critical step for ASC oligomerization and NLRP3 inflammasome. The results showed that 1,2-diol inhibited the endogenous interaction between NLRP3 and ASC in nigericin-treated macrophages (**Figure 3D**). Thus, these results investigate that 1,2-diol could block NLRP3-ASC complex formation to inhibit ASC speck formation and NLRP3 inflammasome activation.

Recently, NEK7 has been proposed as an essential component of NLRP3 inflammasome and NEK7–NLRP3 interaction is important for subsequent NLRP3 inflammasome assembly and recruitment of ASC to NLRP3 (11). So we used immunoprecipitation and immunoblotting assays to verify whether 1,2-diol could suppress the endogenous interaction between NEK7 and NLRP3 promoted by nigericin. The results showed 1,2-diol could markedly prevent the interaction of NEK7 and NLRP3 (**Figure 3E**). Thus, these results suggest 1,2-diol may block ASC speck formation and NLRP3 inflammasome assembly by preventing NLRP3–NEK7 interaction.

1,2-Diol Was Readily Docked With NLRP3

To further evaluate how 1,2-diol inhibited NLRP3 inflammasome, we performed molecular interactions of 1,2-diol and template structure of NLRP3 (Protein Data Bank accession no. 6NPY) by AutoDock4. After calculating, the results showed that 1,2-diol was readily docked into the NLRP3 pocket with −7.93 kcal/mol binding energy (**Figure 4A**). The interaction residues of NLRP3 with 1,2-diol including PHE523, LEU411, PRO410, TRP414, TYR166, LEU169, and THR167 (**Figures 4B, C**). Thus, these results suggest that 1,2-diol may have an affinity binding site to the NLRP3 inflammasome.

1,2-Diol Inhibits NLRP3 Activation *In Vivo* and has Beneficial Effects in LPS Induced Mouse Models of ALI

We next examined whether 1,2-diol could inhibit NLRP3 activation *in vivo* and has beneficial effects in mouse models of LPS induce ALI. We first induced ALI by intra-tracheal delivery LPS.The results showed that the level of IL-1β in the lung BALF was significantly decreased after 1,2-diol treatment and IL-6 was only slightly decreased (**Figure 5A**). Furthermore, we observed a marked decreased ALI pathology by treating 1,2-diol (**Figure 5B**). Meanwhile, the body weight and temperature of mice were detected every 24 h with comprehensive, detailed records and statistics (**Figure 5C**). To further investigate whether 1,2-diol could inhibit NLRP3 inflammasome *in vivo*, then we induced endotoxemia model by i.p. injection of LPS. We observed a marked decrease in sepsis-related lung injury by 1,2-diol treatment as evaluated by the histopathology (**Figure 5D**). In addition, we detect the cleavage of GSDMD, the pro-Caspase-1 and cleavage Caspase-1 in lung tissues. Treatment of 1,2-diol significantly inhibited the cleavage of GSDMD and Caspase-1 in lung tissue in endotoxemia mice (**Figure 5E**). At last, we found that the level of IL-1β in the serum was significantly decreased by treatment with 1,2-diol in endotoxemia mice (**Figure 5F**). Overall, 1,2-diol inhibits NLRP3 activation *in vivo* and has beneficial effects in mouse models of LPS induce ALI.

DISCUSSION

As a severe respiratory inflammatory syndrome, ALI is considered to be one of the most important causes of

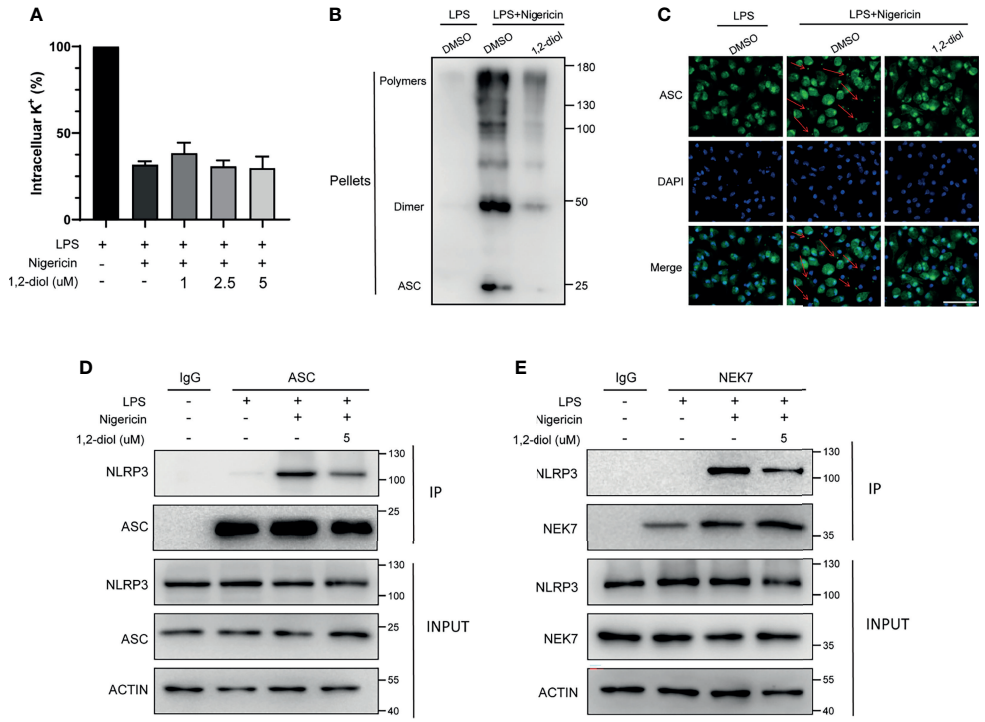

FIGURE 3 | 1,2-diol inhibits ASC oligomerization and inflammasome assembly **(A)** Qualification of potassium efflux in LPS-primed peritoneal macrophages treated with different doses of 1,2-diol and then stimulated with nigericin. **(B)** Immunoblot analysis of ASC oligomerization in the cell lysates of LPS-primed peritoneal macrophages treated with 1,2-diol and then stimulated with nigericin. **(C)** Immunofluorescent staining of ASC and representative images of ASC speck. **(D)** IP and immunoblot analysis of the interaction of NLRP3 and ASC in the cell lysates of LPS-primed peritoneal macrophages treated with 1,2-diol and then stimulated with nigericin. **(E)** IP and immunoblot analysis of the interaction of NLRP3 and NEK7 in the cell lysates of LPS-primed peritoneal macrophages treated with 1,2-diol and then stimulated with nigericin.

morbidity and mortality in critically ill patients (19, 20). Destruction of the alveolar epithelium, exudation of protein-rich liquid into the alveoli and related external factors such as the collapse of lung tissues jointly caused and exacerbated the development of ALI (21). Meanwhile, infectious etiologies, such as sepsis and pneumonia, are also the significant catalysts and leading causes of ALI/ARDS (22). ALI not only has serious consequences for general health, but also is one major contributor to intensive care unit (ICU) costs. Despite the treatment strategies have some marked improvements in the delivery of critical care, the mortality of ALI still remains high, with no new and effective pharmacologic therapies or alternative medicine approved (23).

In the present study, we used i.t. administration of LPS, the component of the Gram-negative bacterial cell membrane which has been widely used to induce pulmonary inflammation in animal models of severe lung injury to induce ALI, with characteristic symptoms, namely, pulmonary edema, intrapulmonary hemorrhage and excessive leukocyte accumulation (15). Here we have surprisingly found a novel small molecule compound 4-benzene-indol derivative (1,2-diol), ameliorated LPS-induced sepsis-related ALI by inhibiting the NLRP3 inflammasome.

NLRP3 inflammasome is a multiple-protein complex that in humans is encoded by the NLRP3 gene, which is located on the long arm of human chromosome (24). NLRP3 inflammasome is expressed preponderantly in macrophages and could trigger an array of immune responses after being activated (25). Because the immune system is the very first body system to be affected by sepsis and the indispensable role played by NLRP3 inflammasome, a series of approaches have been researched to modulate it in the initiation, progression, and clinical therapy. Some pieces of evidence had already demonstrated that NLRP3 inflammasome activation could induce significant changes in different body systems affected by sepsis, among which, the effects of NLRP3 inflammasome on the respiratory system includes immunological influences like edema formation, neutrophil infiltration, and elevated levels of inflammatory cytokines such as IL-1β and IL-18 in the lung tissue (26). Meanwhile, the therapeutic efficacy on respiratory system of targeting the NLRP3 inflammasome pathway has been extensively studied and has some practical applications (27). For example, the administration of cinnamaldehyde, a phenolic compound from Cinnamon species, can reduce the expression level of IL-1β and NLRP3 in the lungs of LPS-injected mice (28). Another study demonstrated that hemin (an inducer of HO-1) was able to decrease the expression of ASC, Caspase-1 and NLRP3, the activation of NLRP3 inflammasome could also be weakened (29). The protective effects for CLP-induced acute lung injury of mice by using dihydromyricetin have also been proved which could inhibit the activation of NLRP3

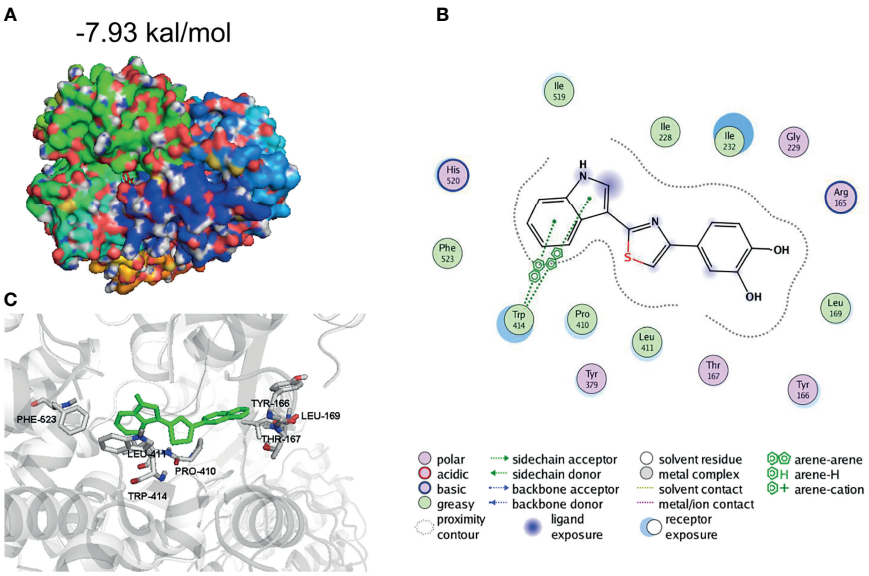

FIGURE 4 | 1,2-Diol was readily docked with NLRP3. **(A, B)** 3D binding mode diagrams between NLRP3 and the chemical 1,2-diol. The protein is shown in cartoon and colored in gray, key amino acid residues were shown as sticks. Docking score is −7.93kcal/mol. **(C)** 2D mode diagrams the key amino residues in the ligand –protein complexes.

inflammasome then reduce pyroptosis (30). Up to the present, molecular mechanisms and related signaling pathways indicate that preventing the assembly and activation of NLRP3 inflammasome could reduce the inflammatory response in sepsis.

In this research, a conspicuous discovery of treatment-related translational use for a 4-benzene-indol derivative (1,2-diol) was elaborated by screening a large number of chemical compounds. The results showed that 1,2-diol could not only suppress the activation of NLRP3 inflammasome both *in vitro* and alleviate LPS-induced ALI *in vivo*, but also suppress the NLRP3 inflammasome in human myeloid leukemia mononuclear cells (THP-1) cell lines. Mechanistically, we found out that the inhibition effect of 1,2-diol did not depend on the potassium (K+) efflux, which has been well accepted as an essential process both necessary and sufficient for NLRP3 inflammasome activation, because of the stable results of intracellular potassium concentration. However, the combination of NLRP3 and ASC was significantly affected. It has been widely confirmed that NLRP3 inflammasome is composed of the sensor protein NLRP3 connected to Caspase-1 through the adaptor protein ASC, upon inflammasome activation functional oligomeric inflammasome particles of NLRP3 and ASC were released from cells, acting as danger signals to amplify inflammation by promoting the activation of Caspase-1 extracellularly (25, 31, 32). Our immunoprecipitation (IP) experiment also showed that 1,2-diol could affect the combining of NLRP3 and ASC. Further exploration of upstream mechanism has shown that the combination of NLRP3 and NEK7 was markedly inhibited, since NEK7 is considered as an essential mediator of NLRP3 activation downstream of potassium efflux. Therefore, the abovementioned experimental results comprehensively demonstrate that 1,2-diol firstly affected the combination of NEK7 and NLRP3, then affected the expression of the downstream target ASC and thus affecting the activation of NLRP3, thereby influencing the splicing of Caspase-11 as well as the release of IL-1β. The possible molecular targets were further predicted by software which showed that NLRP3 might tightly linked to 1,2-diol (**Figure 6**, created with BioRender). Collectively, 1,2-diol blocks the NLRP3 inflammasome activation by disrupting NLRP3-NEK7 interaction and the subsequent NLRP3 inflammasome assembly and activation. 1,2-diol may serve as a potential therapeutic drug and NLRP3 inflammasome signaling would be a novel pharmaceutical target for clinical treatment of sepsis-related ALI. The pieces of evidence presented here demonstrated that inhibiting the assembly and activation of this NLRP3 inflammasome could prevent the inflammatory response normally visualized in sepsis-related ALI. Still, further studies on 1,2-diol are necessary to demonstrate the detailed influence exerted by the NLPR3 inflammasome on sepsis pathophysiology and to design new treatment approaches such as decreasing toxicity and increasing efficacy, pharmaceutical and related translational research.

CONCLUSIONS

Overall, our research provides a new promising therapeutic drug 4-benzene-indol derivative (1,2-diol) in avoiding the establishment of sepsis-related ALI. The 1,2-diol marks a new pharmacological approach for treating NLRP3 inflammasome-related diseases, whereas the effectiveness in mankind cases clinically requires more investigations nonetheless.

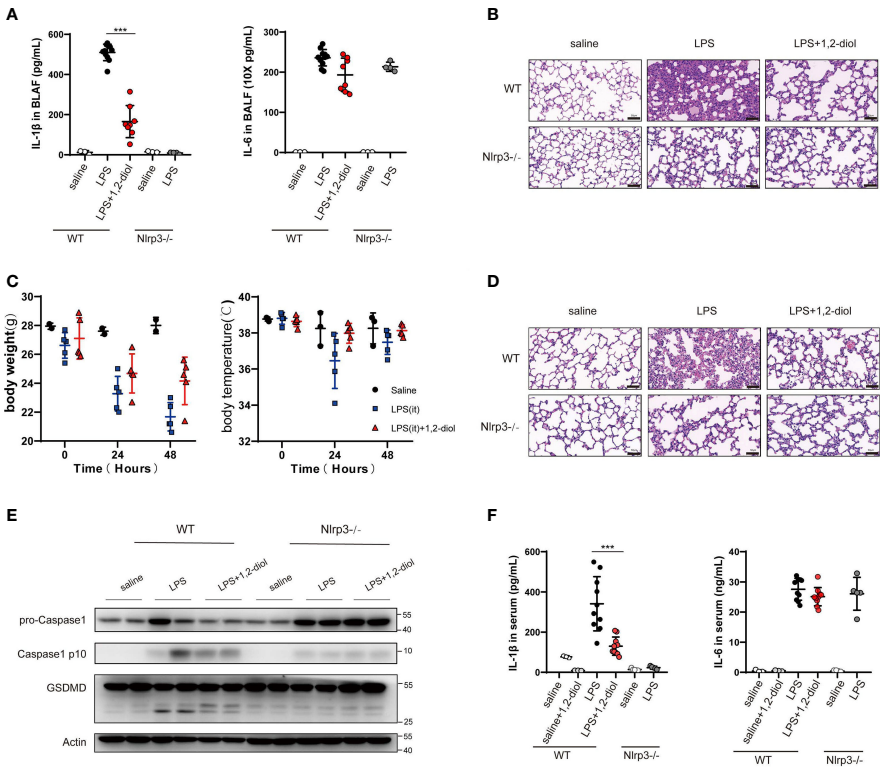

FIGURE 5 | 1,2-Diol inhibits NLRP3 activation *in vivo* and has beneficial effects in mouse models of LPS induce ALI. **(A)** IL-1β and IL-6 release in the BLAF were measured by ELISA. WT or Nlrp3$^{-/-}$ mice were pretreated with 40 mg/kg, 12-diol by intraperitoneal injection 30 min before i.t. instilled with 15 mg/kg LPS. **(B)** H&E staining show representative images of lung in WT or Nlrp3$^{-/-}$ mice which i.t. instilled with 15 mg/kg LPS (scale bar, 50 μm). **(C)** The body weight and the body temperature were recorded during ALI. 1,2-diol treatment has a tendency to reduce the loss of body temperature and body weight. **(D)** H&E staining showed representative images of lung in WT or Nlrp3$^{-/-}$ mice which was intraperitoneal challenged with LPS 25 mg/kg (scale bar, 50 μm). **(E)** Western blots for the cleavage of GSDMD and the expression of Caspase-1 in lung. WT or Nlrp3$^{-/-}$ mice were pretreated with 40 mg/kg 1,2-diol by intraperitoneal injection 30min before intraperitoneally challenged with LPS 25 mg/kg. **(F)** IL-1β and IL-6 released in the serum were measured by ELISA. WT or Nlrp3$^{-/-}$ mice were pretreated with 40 mg/kg 1,2-diol by intraperitoneal injection 30 min before intraperitoneally challenged with LPS 25 mg/kg. (***p <0.001).

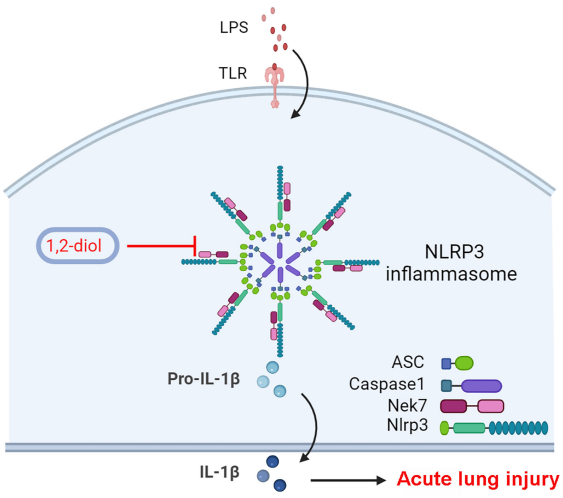

FIGURE 6 | Schematic diagram of suppressive role of 1,2-diol on NLRP3 inflammasome.

DATA AVAILABILITY STATEMENT

The original contributions presented in the study are included in the article, further inquiries can be directed to the corresponding authors.

ETHICS STATEMENT

The animal study was reviewed and approved by the Central South University.

AUTHOR CONTRIBUTIONS

YB, JL and JS contributed to study design. JL, YB and JS conducted animal experiments. YZ, XW, LL and ZL performed data analysis. YB, JS and MC wrote the original manuscript. YZ and YT edited the manuscript. JS, JL and YB made the revision. All authors listed have made a substantial, direct, and intellectual contribution to the work and approved it for publication.

FUNDING

This research was supported by the National Natural Science Foundation of China (Nos. 81971893, 81700127), the Excellent Postdoctoral Program for Innovative Talent of Hunan (2021M693564), the China Postdoctoral Science Foundation (2020TQ0364) and Fundamental Research Funds for the Central Universities of Central South University (2021zzts0405).

ACKNOWLEDGMENTS

The authors thank Professor Rongbin Zhou (Institute of Immunology School of Life Sciences. University of Science & Technology of China) for sharing mouse strains ($Nlrp3^{-/-}$ mice) and Professor Ben Lu (The Third Xiangya Hospital, Central South University) for his continous help and support with meaningful advices on the manuscript.

REFERENCES

1. Kaukonen KM, Bailey M, Pilcher D, Cooper DJ, Bellomo R. Systemic Inflammatory Response Syndrome Criteria in Defining Severe Sepsis. *N Engl J Med* (2015) 372:1629–38. doi: 10.1056/NEJMoa1415236
2. Fry DE. Sepsis, Systemic Inflammatory Response, and Multiple Organ Dysfunction: The Mystery Continues. *Am Surgeon* (2012) 78:1–8. doi: 10.1177/000313481207800102
3. Chen AX, Simpson SQ, Pallin DJ. Sepsis Guidelines. *N Engl J Med* (2019) 380:1369–71. doi: 10.1056/NEJMclde1815472
4. Vincent JL, Zambon M. Why do Patients Who Have Acute Lung Injury/ Acute Respiratory Distress Syndrome Die From Multiple Organ Dysfunction Syndrome? Implications for management. *Clinics Chest Med* (2006) 27:725–31; abstract x-xi. doi: 10.1016/j.ccm.2006.06.010
5. Matuschak GM, Lechner AJ. Acute Lung Injury and the Acute Respiratory Distress Syndrome: Pathophysiology and Treatment. *Missouri Med* (2010) 107:252–8.
6. Ranieri VM, Rubenfeld GD, Thompson BT, Ferguson ND, Caldwell E, Fan E, et al. Acute Respiratory Distress Syndrome: The Berlin Definition. *Jama* (2012) 307:2526–33. doi: 10.1001/jama.2012.5669
7. Matthay MA, Zemans RL, Zimmerman GA, Arabi YM, Beitler JR, Mercat A, et al. Acute Respiratory Distress Syndrome. *Nat Rev Dis Primers* (2019) 5:18. doi: 10.1038/s41572-019-0069-0
8. Parekh D, Dancer RC, Thickett DR. Acute Lung Injury. *Clin Med (London England)* (2011) 11:615–8. doi: 10.7861/clinmedicine.11-6-615
9. Tsushima K, King LS, Aggarwal NR, De Gorordo A, D'Alessio FR, Kubo K. Acute Lung Injury Review. *Internal Med (Tokyo Japan)* (2009) 48:621–30. doi: 10.2169/internalmedicine.48.1741
10. Ting JP, Lovering RC, Alnemri ES, Bertin J, Boss JM, Davis BK, et al. The NLR Gene Family: A Standard Nomenclature. *Immunity* (2008) 28:285–7. doi: 10.1016/j.immuni.2008.02.005
11. He Y, Hara H, Núñez G. Mechanism and Regulation of NLRP3 Inflammasome Activation. *Trends Biochem Sci* (2016) 41:1012–21. doi: 10.1016/j.tibs.2016.09.002
12. Jin C, Flavell RA. Molecular Mechanism of NLRP3 Inflammasome Activation. *J Clin Immunol* (2010) 30:628–31. doi: 10.1007/s10875-010-9440-3
13. Xiao TS. Innate Immunity and Inflammation. *Cell Mol Immunol* (2017) 14:1–3. doi: 10.1038/cmi.2016.45
14. Grailer JJ, Canning BA, Kalbitz M, Haggadone MD, Dhond RM, Andjelkovic AV, et al. Critical Role for the NLRP3 Inflammasome During Acute Lung Injury. *J Immunol (Baltimore Md 1950)* (2014) 192:5974–83. doi: 10.4049/jimmunol.1400368
15. Zhang Y, Li X, Grailer JJ, Wang N, Wang M, Yao J, et al. Melatonin Alleviates Acute Lung Injury Through Inhibiting the NLRP3 Inflammasome. *J Pineal Res* (2016) 60:405–14. doi: 10.1111/jpi.12322
16. Zheng D, Liwinski T, Elinav E. Inflammasome Activation and Regulation: Toward a Better Understanding of Complex Mechanisms. *Cell Discov* (2020) 6:36. doi: 10.1038/s41421-020-0167-x
17. Liu Y, Shang L, Zhou J, Pan G, Zhou F, Yang S. Emodin Attenuates LPS-Induced Acute Lung Injury by Inhibiting NLRP3 Inflammasome-Dependent Pyroptosis Signaling Pathway *In Vitro* and *In Vivo*. *Inflammation* (2021) 17:1–5. doi: 10.1007/s10753-021-01581-1
18. Cao F, Tian X, Li Z, Lv Y, Han J, Zhuang R, et al. Suppression of NLRP3 Inflammasome by Erythropoietin *via* the EPOR/JAK2/STAT3 Pathway Contributes to Attenuation of Acute Lung Injury in Mice. *Front Pharmacol* (2020) 11:306. doi: 10.3389/fphar.2020.00306
19. Shah CV, Localio AR, Lanken PN, Kahn JM, Bellamy S, Gallop R, et al. The Impact of Development of Acute Lung Injury on Hospital Mortality in Critically Ill Trauma Patients. *Crit Care Med* (2008) 36:2309–15. doi: 10.1097/CCM.0b013e318180dc74
20. Rubenfeld GD, Herridge MS. Epidemiology and Outcomes of Acute Lung Injury. *Chest* (2007) 131:554–62. doi: 10.1378/chest.06-1976
21. Butt Y, Kurdowska A, Allen TC. Acute Lung Injury: A Clinical and Molecular Review. *Arch Pathol Lab Med* (2016) 140:345–50. doi: 10.5858/arpa.2015-0519-RA
22. Blank R, Napolitano LM. Epidemiology of ARDS and ALI. *Crit Care Clinics* (2011) 27:439–58. doi: 10.1016/j.ccc.2011.05.005
23. Patel VJ, Biswas Roy S, Mehta HJ, Joo M, Sadikot RT. Alternative and Natural Therapies for Acute Lung Injury and Acute Respiratory Distress Syndrome. *BioMed Res Int* (2018) 2018:2476824. doi: 10.1155/2018/2476824
24. Shim DW, Lee KH. Posttranslational Regulation of the NLR Family Pyrin Domain-Containing 3 Inflammasome. *Front Immunol* (2018) 9:1054. doi: 10.3389/fimmu.2018.01054
25. Paik S, Kim JK, Silwal P, Sasakawa C, Jo EK. An Update on the Regulatory Mechanisms of NLRP3 Inflammasome Activation. *Cell Mol Immunol* (2021) 18:1141–60. doi: 10.1038/s41423-021-00670-3
26. Danielski LG, Giustina AD, Bonfante S, Barichello T, Petronilho F. The NLRP3 Inflammasome and Its Role in Sepsis Development. *Inflammation* (2020) 43:24–31. doi: 10.1007/s10753-019-01124-9
27. McElvaney OJ, Zaslona Z, Becker-Flegler K, Palsson-McDermott EM, Boland F, Gunaratnam C, et al. Specific Inhibition of the NLRP3 Inflammasome as an Antiinflammatory Strategy in Cystic Fibrosis. *Am J Respir Crit Care Med* (2019) 200:1381–91. doi: 10.1164/rccm.201905-1013OC
28. Xu F, Wang F, Wen T, Sang W, Wang D, Zeng N. Inhibition of NLRP3 Inflammasome: A New Protective Mechanism of Cinnamaldehyde in Endotoxin Poisoning of Mice. *Immunopharmacol Immunotoxicol* (2017) 39:296–304. doi: 10.1080/08923973.2017.1355377
29. Luo YP, Jiang L, Kang K, Fei DS, Meng XL, Nan CC, et al. Hemin Inhibits NLRP3 Inflammasome Activation in Sepsis-Induced Acute Lung Injury, Involving Heme Oxygenase-1. *Int Immunopharmacol* (2014) 20:24–32. doi: 10.1016/j.intimp.2014.02.017
30. Wang YC, Liu QX, Zheng Q, Liu T, Xu XE, Liu XH, et al. Dihydromyricetin Alleviates Sepsis-Induced Acute Lung Injury Through Inhibiting NLRP3 Inflammasome-Dependent Pyroptosis in Mice Model. *Inflammation* (2019) 42:1301–10. doi: 10.1007/s10753-019-00990-7
31. Yang Y, Wang H, Kouadir M, Song H, Shi F. Recent Advances in the Mechanisms of NLRP3 Inflammasome Activation and Its Inhibitors. *Cell Death Dis* (2019) 10:128. doi: 10.1038/s41419-019-1413-8
32. Mankan AK, Dau T, Jenne D, Hornung V. The NLRP3/ASC/Caspase-1 Axis Regulates IL-1β Processing in Neutrophils. *Eur J Immunol* (2012) 42:710–5. doi: 10.1002/eji.201141921

Conflict of Interest: The authors declare that the research was conducted in the absence of any commercial or financial relationships that could be construed as a potential conflict of interest.

Publisher's Note: All claims expressed in this article are solely those of the authors and do not necessarily represent those of their affiliated organizations, or those of the publisher, the editors and the reviewers. Any product that may be evaluated in

this article, or claim that may be made by its manufacturer, is not guaranteed or endorsed by the publisher.

frontiers | Frontiers in Immunology

ORIGINAL RESEARCH
published: 19 April 2022
doi: 10.3389/fimmu.2022.856296

Oleamide-Mediated Polarization of M1 Macrophages and IL-1β Production by Regulating NLRP3-Inflammasome Activation in Primary Human Monocyte-Derived Macrophages

OPEN ACCESS

Edited by:
Chaofeng Han,
Second Military Medical University, China

Reviewed by:
Paola Italiani,
National Research Council (CNR), Italy
Razif Abas,
Universiti Putra Malaysia, Malaysia

***Correspondence:**
Kanchana Usuwanthim
kanchanau@nu.ac.th

Specialty section:
This article was submitted to Molecular Innate Immunity, a section of the journal Frontiers in Immunology

Received: *17 January 2022*
Accepted: *23 March 2022*
Published: *19 April 2022*

Citation:
Wisitpongpun P, Potup P and Usuwanthim K (2022) Oleamide-Mediated Polarization of M1 Macrophages and IL-1β Production by Regulating NLRP3-Inflammasome Activation in Primary Human Monocyte-Derived Macrophages. Front. Immunol. 13:856296. doi: 10.3389/fimmu.2022.856296

Prapakorn Wisitpongpun, Pachuen Potup and Kanchana Usuwanthim*

Cellular and Molecular Immunology Research Unit (CMIRU), Faculty of Allied Health Sciences, Naresuan University, Phitsanulok, Thailand

Macrophages are a type of innate immune cell that activates the NLRP3 inflammasome, causing the release of the cytokine IL-1β, which is a crucial mediator of the inflammatory response. NLRP3 activation that is dysregulated worsens a variety of inflammatory and autoimmune diseases, as well as neurodegenerative diseases. Oleamide is an endogenous fatty acid amide that was first determined as a sleep-inducing molecule and later shown to have wide-ranging beneficial effects on the central nervous system. How oleamide influences human macrophage polarization and NLRP3-inflammasome activation remains unclear. The effect of oleamide on macrophage polarization was explored using an *in vitro* culture of primary human monocyte-derived macrophages (MDMs) supplemented with human serum-containing media. Cellular and molecular mechanisms of oleamide-regulated MDMs polarization were also investigated. Results showed that oleamide promoted naïve macrophages (M0) toward the M1 phenotype by upregulating M1-associated genes (*IL-1β*, *iNOS*, *CXCL10*), along with downregulation of M2-associated genes (*Arg-1*, *CD206*, *CCL22*). Cell surface expression indicated that oleamide enhanced CD80 expression in M0 naïve macrophages and hider CD206 and CD163 expression in M2 macrophages. Higher production of IL-1β cytokine was observed but with no alteration in IL-6 and TNF-α levels by MDMs and differentiated THP-1 models. Whether oleamide functioned as a second signal that activated the NLRP3 inflammasome and mediated IL-1β production was further investigated using LPS-primed MDMs followed by oleamide treatment that induced activation of inflammasome-related proteins including NLRP3, ASC, cleaved casp-1, and cleaved IL-1β. These findings

suggested that oleamide promoted M1 macrophage polarization and increased IL-1β production by activating the NLRP3 inflammasome in primary MDMs. This research reveals a new function for oleamide as well as prospective targets for treating NLRP3-related inflammatory disorders.

Keywords: MDMs, monocyte-derived macrophages, macrophage - cell, polarization, oleamide (OA), inflammasome

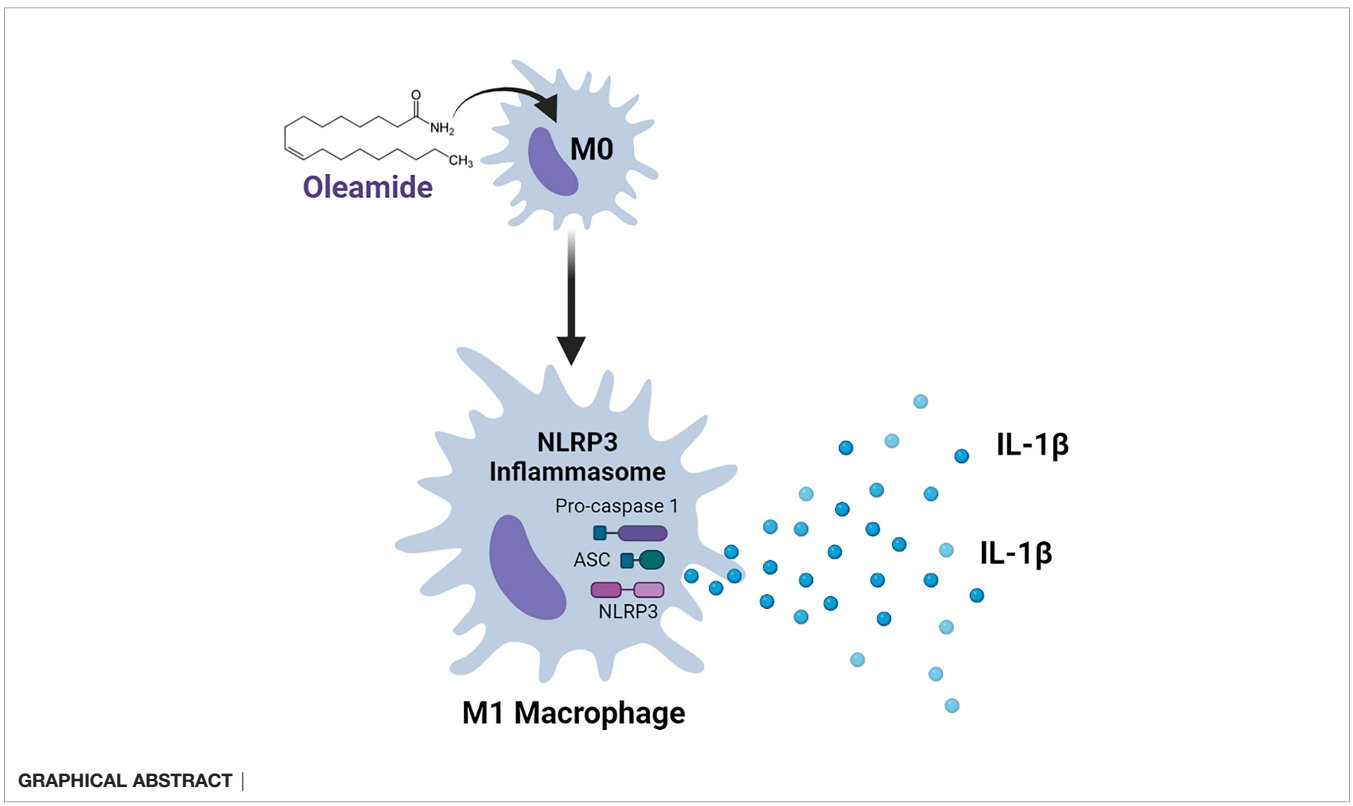

GRAPHICAL ABSTRACT |

INTRODUCTION

Macrophages comprise a heterogeneous population of the innate immune system involved in several processes of health and disease (1–3). The heterogeneity of macrophages is commonly referred to as polarization, a process by which macrophages display different functional phenotypes in response to specific microenvironmental stimuli and signals (4). Macrophage polarization is conventionally divided into three groups as naïve macrophages (MØ; also called M0), which readily differentiate into two major phenotypes as classically activated macrophages (M1) and alternatively activated macrophages (M2) (1–3). M1 macrophages, also known as pro-inflammatory macrophages, are characterized by high levels of reactive oxygen species (ROS) and nitric oxide (NO) and the production of pro-inflammatory cytokines (1, 5). Inflammation and microbicidal activity are linked to M1 macrophages (1, 5). M2 macrophages, commonly known as anti-inflammatory macrophages, have multiple receptors expressed, including the mannose receptor (MRC1), scavenging receptor CD163, dectin-1, and DC-SIGN (1, 5). Immunosuppression, wound repair, and tumor promotion are all mechanisms related with M2 macrophages (3).

Interleukin-1β (IL-1β) is a pro-inflammatory cytokine produced mainly by innate immune cells as a response to infection and injury (6). In macrophages, NLRP3 inflammasome-mediate IL-1β production can be primed by TLRs activation (Signal 1), which activates NF-κB or a non-NF-κB pathway to produce pro-IL-1β and pro-IL-18. The second signal is the oligomerization of NLRP3, pro-caspase 1, and ASC (apoptosis-associated speck-like protein containing a caspase recruitment domain), an adapter protein (7). The assembly of these proteins activates caspase-1, which then converts pro-IL-1β and pro-IL-18 into mature IL-1β and IL-18 that are released, resulting in inflammatory reactions (8, 9). As a result, dysregulation of the NLRP3 inflammasome has been linked to the advancement of a number of inflammatory and autoimmune disorders, including neurodegenerative diseases like Alzheimer's, Parkinson's, and amyotrophic lateral sclerosis (10–12). This shows that targeting the NLRP3 inflammasome as a therapeutic strategy for treating NLRP3-related inflammatory disorders may be feasible.

Oleamide (Cis-9,10-octadecenamide) is an endogenous fatty acid discovered in the cerebrospinal fluid of sleep-deprived cats and later identified as an endogenous sleep-inducing agent (13). Oleamide has a variety of effects on the central nervous system, including antiepileptic (14), memory regulation (15, 16), and hypothermia elicitation (17). In addition, oleamide has been shown to decrease LPS-induced iNOS and COX-2 production in BV2 murine microglial cells through inhibiting NF-κB activation (18). Oleamide has recently been identified as a dual-active component that both decreases amyloid-β (Aβ) accumulation through increased microglial phagocytosis and suppresses LPS-induced microglial inflammation by reducing TNF-α and MIP-1α production (19). These findings in microglial cells suggested that oleamide might affect macrophage activity, although it is still uncertain how oleamide influences macrophage polarization and the NLRP3 inflammasome.

This study investigated the regulatory effects of oleamide on the progression of M1/M2 macrophage polarization using an *in vitro* culture of primary human monocyte-derived macrophages (MDMs) as a model. Results showed that oleamide promoted naïve macrophages (M0) toward the M1 phenotype and hider development of the M2 phenotype. Moreover, oleamide critically regulates IL-1β production in MDMs by stimulating the NLRP3 inflammasome.

MATERIAL AND METHODS

Isolation of Human MDMs

MDMs were isolated from a blood buffy coat of healthy blood donors. Briefly, buffy coats were transferred into 50 ml tubes and centrifuged at 3,000 rpm for 30 min. The WBC layer was collected and then diluted 1:1 in PBS-EDTA (1 mM). Diluted WBCs were gently overlaid on top of Ficoll-Paque solution (density 1.077 g/ml, GE Healthcare, Chicago, USA) at a 1:1 ratio and then centrifuged at 3,000 rpm for 30 min. The peripheral blood mononuclear cell (PBMC) layer at the interface was transferred to a new 50 ml tube and washed once with 40 ml PBS-EDTA by centrifugation at 1500 rpm for 5 min. The PBMCs were then diluted in 15 ml PBS-EDTA and overlaid on 46% Percoll solution (density 1.131 g/ml, GE Healthcare, Chicago, USA) at a 1:1 ratio followed by centrifugation at 3,000 rpm for 30 min. Then monocyte layer at the interface was collected into a new 50 ml tube, washed 3-5 times in 40 ml PBS-EDTA, and cultured in desired conditions. The purity of MDMs on days 0-6 was shown in **Supplementary Figure 1**.

MDMs Culture and Polarization

MDMs were cultured in RPMI 1640 supplemented with 10% human serum from buffy coats of healthy donors and 1% antibiotic-antimycotic (Gibco™, USA #15240062) at 37°C with 5% CO_2. The M0 macrophages condition, monocytes were grown in a complete medium without stimulation for 6 days. In the M1 macrophages, monocytes were cultured in the presence of 50 ng/ml of GM-CSF (ImmunoTools GmbH, Germany) for 6 days. In the M2 macrophages, monocytes were cultured in 50 ng/ml M-CSF (ImmunoTools GmbH, Germany) for 6 days. Cell culture mediums were replaced every 3 days in all conditions. On day 6, M0 macrophages were incubated in complete medium alone for 24 h to serve as naïve macrophage or negative control cells. M1 macrophages were polarized with 20 ng/ml IFN-γ (ImmunoTools GmbH, Germany) and 10 ng/ml LPS of *Escherichia coli* O55:B5 (Sigma Aldrich, MO, USA) for 24 h. M2 macrophages were polarized using 20 ng/ml IL-4 (ImmunoTools GmbH, Germany) for 24 h. For experimental groups, M0, M1, and M2 macrophages (day 6) were cultured in desired conditions plus oleamide for 24 h.

THP-1 Cell Culture and Differentiation

THP-1 cells obtained from ATCC were maintained in RPMI-1640 supplemented with 10% FBS and 1% Antibiotic-Antimycotic (Gibco™, USA #15240062) at 37°C with 5% CO_2. THP-1 were differentiated into macrophages by incubating with 100 nM phorbol-12-myristate-13-acetate (PMA) (Sigma-Aldrich, St. Louis, MO, USA) for 24 h and then replaced with PMA-free complete medium for 72 h. Following differentiation, cells were polarized into M1 macrophages by incubation with 20 ng/ml IFN-γ (ImmunoTools GmbH, Germany) and 10 ng/ml LPS (Sigma Aldrich, MO, USA) for 24 h. M2 macrophages were obtained by incubation with 20 ng/ml IL-4 (ImmunoTools GmbH, Germany) for 24 h. M0 macrophages were incubated with a complete medium only for 24. For experimental groups, M0, M1, and M2 macrophages were cultured in desired conditions plus oleamide for 24 h.

Inflammasome Activation

Isolated monocytes (Day 0) were seeded at a density of 4 x 10^5 cells/well in 12-well plates and differentiated for 6 days in complete medium. Cell culture medium was replaced every 3 days. On day 6, MDMs were stimulated with 100 ng/ml LPS for 3 h. Cells were then stimulated with oleamide (10-40 μg/ml) (Sigma Aldrich, St. Louis, MO, USA) or adenosine triphosphate (ATP) (Sigma-Aldrich, St. Louis, MO, USA) as the positive control for 1 and 3 h. After stimulation, supernatants were collected, and cytokine levels were measured using an ELISA. Cells were collected, and qRT-PCR was used to examine mRNA expression.

Cell Viability Assay

Cell viability was determined using the Methyl Thiazol Tetrazolium (MTT) assay. MDMs (Day 6) were seeded at a density of 2.0 x 10^4 cells/well in a 96-well plate and incubated with the serial concentration of oleamide for 48 h. The MTT salt solution (Thermo Fisher Scientific, Waltham, MA, USA) was then added and incubated for 3 h at 37°C. To dissolve the formazan crystal, 100 μl of dimethyl sulfoxide (DMSO) (VWR International, West Chester, PA, USA) was added to each well. Plates were gently shaken for 5-10 min. The absorbance was measured at 570 nm using a microplate reader (PerkinElmer, Inc., USA).

Flow Cytometry

After stimulation, MDMs were harvested using Trypsin-EDTA for 15 min followed by a cell scraper. Cells were washed once with ice-cold PBS and resuspended in ice-cold FACS buffer (0.5% BSA and

0.05% sodium azide in PBS). Cells (2 x 10^5 cells) were stained with the fluorochrome-conjugated anti-human antibodies, including CD80-FITC, CD163-PE, and CD206-FITC (BioLegend, San Diego, CA, USA), CD14-PE, CD16-FITC, and isotype control (ImmunoTools GmbH, Germany) for 30 min at 4°C in FACS buffer. The cells were then washed three times in ice-cold PBS and fixed with 2% formaldehyde (Sigma Aldrich, MO, USA) at 4°C for 10 min. After fixation, cells were washed once in PBS, resuspended in FACS buffer, and stored at 4°C in the dark until used. Cell surface expressions were detected using CytoFlex S (Beckman Coulter Life Sciences, Indiana, USA) and analyzed with CytoExpert software.

Reverse Transcription-Quantitative Real-Time PCR (RT-qPCR)

Total RNA was extracted using Trizol reagent (Invitrogen, Carlsbad, CA, USA) according to the manufacturer's instructions. cDNA was synthesized using Tetro cDNA Synthesis Kit (Bioline, Tennessee, USA). The resulting cDNAs were amplified with different primers (**Supplementary Table 1**) using the SensiFAST™ SYBR ® No-ROX Kit (Bioline USA Inc., Taunton, MA, USA). Results were analyzed using the relative gene expression method. Briefly, the relative expression of the target genes was calculated by relating the Ct-value of the target gene to unstimulated M0 macrophage. The quantitative cycle (Ct) values were used to calculate relative variations in gene expression between groups. These values were normalized to a housekeeping gene (β-actin) in the same sample (ΔCt) and expressed as the fold-change over control ($2^{-\Delta\Delta Ct}$). Real-time fluorescence detection was performed using a CFX96 Touch Real-Time PCR Detection System (Bio-Rad).

Scanning Electron Microscope (SEM)

MDM cells were plated into 12-cell well plate containing sterile coverslips. After differentiation, samples were fixed with 4% paraformaldehyde and 2.5% glutaraldehyde in 0.1 M phosphate buffer (1.14 g NaH_2PO_4, 1.69 g Na_2HPO_4 in a 100-ml final volume of ddH_2O, pH 7.4) for 30 min at 4°C. Samples were washed three times for 5 min each in 0.1 M phosphate buffer and then dehydrated with graded ethanol (EtOH) series beginning with 25%, 50%, 75%, 95%, and 100% EtOH (5 min for each). Then, the cells were further dehydrated with 1:1 [Hexamethyldisilazane (HMDS): ETOH] for 5 min and 100% HMDS two times for 5 min at room temperature. Samples were then coated with gold particles and imaged with an Apreo 2 SEM (Thermo Fisher Scientific) using a 5 kV incident beam.

Enzyme-Linked Immunosorbent (ELISA) Assay

Levels of TNF-α, IL-6, IL-1ß and IL-18 cytokines were measured by a sandwich ELISA Kit according to the manufacturer's instructions (Sino Biological Inc., China). Absorbance of the reaction was measured at 450 nm using an EnSpire® Multimode microplate reader (PerkinElmer, Inc., MA, USA).

LDH Assay

The release of lactate dehydrogenase (LDH) was measured using the CyQUANT LDH Cytotoxicity Assay (Thermo Fisher, Waltham, USA). MDMs were plated into a 96-well plate at a density of 2.0 x 10^4 cells/well overnight, and then incubated with LPS for 3 h followed by oleamide (10 - 40 μg/ml) or ATP (30 mM) for 3 h. After incubation, 50 μl of culture medium was transferred to a new 96-well plate and 50 μl of LDH reaction mixture was added, mixed, and incubated for 30 min at room temperature. Then, 50 μl of stop solution was added to terminate the reactions. Absorbances of the reaction mixtures were measured at 490 nm and 680 nm.

Western Blot Analysis

Cells were washed with ice-cold PBS and lysed with RIPA buffer containing 1X Protease/Phosphatase Inhibitor Cocktail (Sigma Aldrich, St. Louis, MO, USA) for 30 min on ice. The lysate was then transferred into microcentrifuge tubes and centrifuged at 12,000 rpm for 10 min under 4°C. The supernatant containing whole protein was collected and measured for protein concentration by the Bradford assay. Equal amounts of each sample were loaded and separated in 8-12% of SDS-PAGE at 100 V for 1.30 h. Protein was then transferred onto PVDF membrane at 100 V for 1.30 h in an icebox. The membranes were blocked with TBST containing 5% BSA for 1 h and subsequently incubated with the appropriate primary antibodies; Rabbit mAb against IL-1β, cleaved- IL-1β, caspase-1, cleaved caspase-1, NLRP3, ASC/TMS1, P2X7 receptor (Cell Signaling Technology, MA, USA) at 4°C overnight. Membranes were washed 3-5 times in TBST for 5 min each and then incubated with Anti-rabbit IgG, HRP-linked Antibody (Cell Signaling Technology, MA, USA) for 1 h at RT. After incubation, membranes were washed in TBST 3-5 times for 5 min each and the blots were developed by chemiluminescence solution for 1 min. Then, the protein was detected using ChemiDoc™ Touch Imaging System (Bio-Rad, Hercules, CA, USA).

Statistical Analysis

All data were expressed as mean ± standard deviation (n = 3). For comparisons of more than two groups, one-way ANOVA was performed with multiple comparison correction (Dunnett test) using GraphPad Prism 6.0 software (GraphPad Software Inc., San Diego, CA, USA). p-values < 0.05 were considered statistically significant.

RESULTS

Generation of *In Vitro* Culture and Polarization of MDMs

To imitate naturally occurring macrophages, monocytes were freshly isolated from the blood buffy coat of healthy donors. MDMs were cultured in complete medium containing human serum alone (M0 cells), or complete medium containing GM-CSF (M1-like cells) or M-CSF (M2-like cells) for 6 days. MDMs were further cultivated for 24 h in the same medium (M0 macrophage) or in the presence of LPS plus IFN-γ (M1 macrophage) or IL-4 (M2 macrophage) (**Figure 1A**). The presence of GM-CSF led to a majority of round adhered with short-elongated shape, whereas the presence of M-CSF enhanced more elongation. MDMs cultured

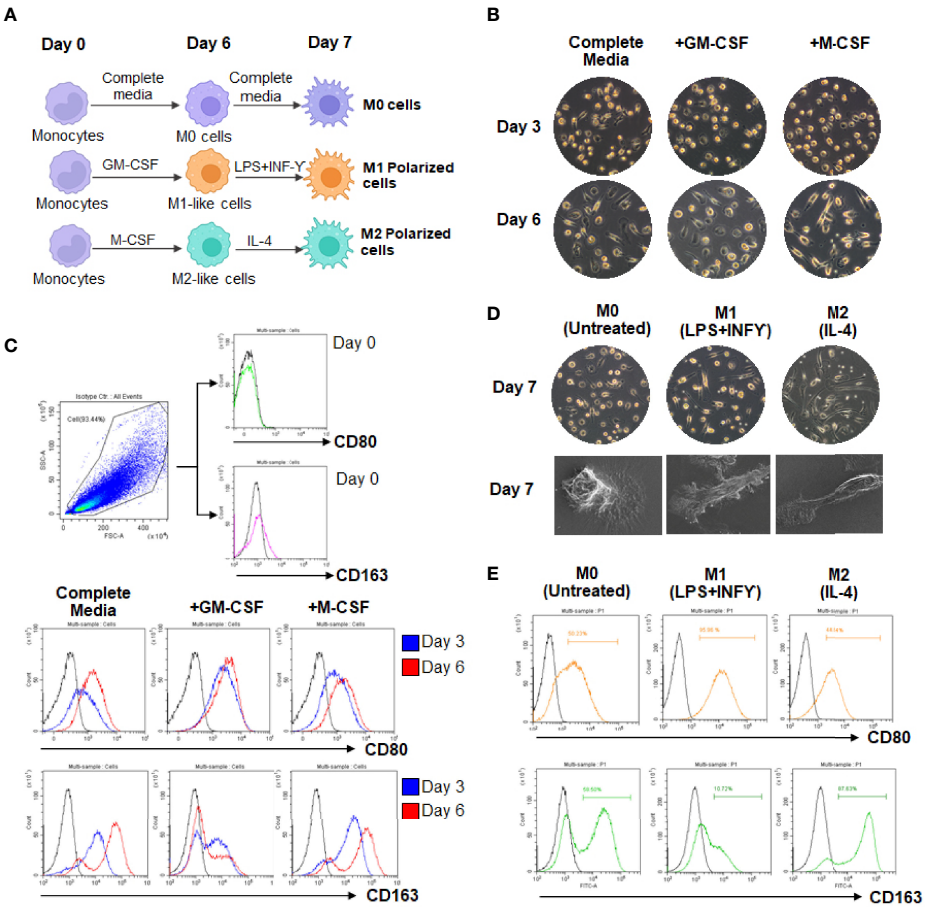

FIGURE 1 | Morphologic and phenotypic characterization of cultured MDMs. **(A)** Scheme of monocyte-derived macrophages (MDMs) culture and polarization. **(B, C)** Differentiation of MDMs at day 3 and 6. **(D)** Polarization of MDMs in complete medium containing M1 (LPS plus IFN-γ)- or M2 (IL-4). (E) Flow cytometry analysis of CD80 and CD163 expressions in culture MDMs at day 7.

in complete medium containing human serum alone exhibited dual morphology (round adherend and elongated shape), indicating the mixed phenotypes in the M0 macrophages (**Figure 1B** and **Supplementary Figure 3**). Differentiation of MDMs at days 0-6 were analyzed by flow cytometry using CD80 (M1 marker) and CD163 (M2 marker). Results showed that M1-like cells or the presence of GM-CSF upregulated CD80 expression, correlating with downregulation of CD163 at days 0-6, respectively. By contrast, M2-like cells displayed upregulation of CD163 expression with downregulation of CD80. MDMs cultured in a medium containing human serum alone displayed increased expression of CD163 rather than CD80 on the cell surface (**Figure 1C**). For fully polarized macrophages, LPS plus IFN-γ treated cells displayed strong induction of CD80 and downregulation of CD163 compared to unpolarized M0 cells. Conversely, IL-4-treated cells displayed high expression of CD163 and low levels of CD80 expression (**Figure 1E**). By using an inverted microscope and a SEM, the exhibit morphology of fully M0, M1, and M2 (**Figure 1D**). Collectively, these data confirmed the M1 and M2 polarization state of LPS plus IFN-γ and IL-4-treated MDMs.

Oleamide Mediated M1 Macrophages Polarization and IL-1β Production

To investigate the effect of oleamide on macrophage polarization, MDMs were cultured in conditioned media for M1 (LPS + IFN-γ), M2 (IL-4), and M0 (untreated) in the presence or absence of oleamide. These cells were characterized in different conditions based on surface markers, gene expression, and cytokine production. The presence of oleamide enhanced greater elongation as spindle-like shapes of the M0 and M1 macrophages (**Supplementary Figure 4**). Surface expressions were analyzed by flow cytometry using polarization markers including CD80 for the M1 phenotype and CD163 and CD206 for the M2 phenotype. Flow cytometry assay revealed that CD80 expression was upregulated in M0 phenotypes treated with oleamide (from 53.09% to 62.17%), whereas CD163 and CD206 were downregulated in M0 phenotypes treated with oleamide compared to the untreated control (from 58.50% to 42.10% and 63.85% to 56.24%, respectively). For the M1 phenotype, CD163 and CD206 expression levels were downregulated (from 10.72% to 5.36% and 74.14% to 54.20%, respectively), whereas CD80 was not differenced in M1 treated

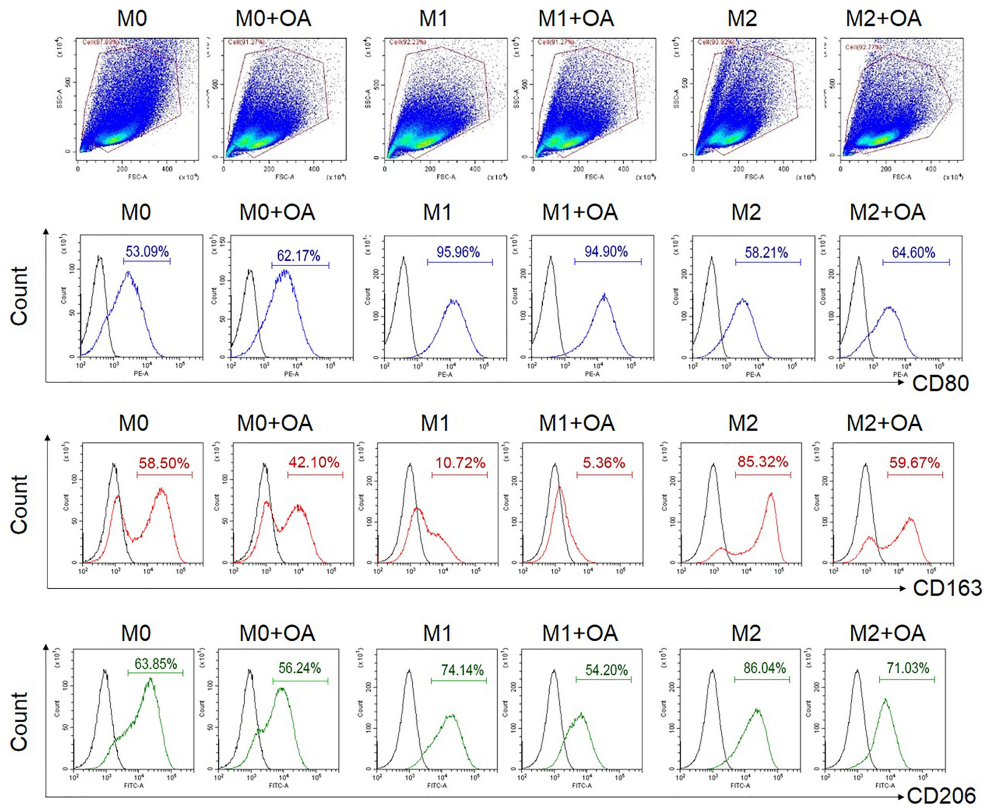

FIGURE 2 | Flow cytometry analysis of surface expressions. MDMs at day 6 were cultured in complete medium only (M0), LPS + INF-γ (M1), or IL-4 (M2) in the presence or absence of oleamide (15 μg/ml) for 24h. LPS, lipopolysaccharides; OA, oleamide.

with oleamide compared to M1 untreated control. For the M2 phenotype, CD163 and CD206 expression levels were downregulated (from 85.32% to 59.67% and 86.04% to 71.03%, respectively), whereas CD80 was upregulated in M2 treated with oleamide compared to the control (58.21% to 64.60%) (**Figure 2**).

M1/M2 phenotypes were further confirmed by studying the expression of M1-associated genes (*TNFα, IL-1β, IL-6, iNOS, CXCL10*), along with the expression of M2-associated genes (*Arg-1, CD206, and CCL22*) using RT-qPCR. Results showed that M0 macrophages treated with oleamide displayed increased expression of *TNF-α*, *IL-1β*, *IL-6*, and *iNOS* genes, while M2 macrophages treated with oleamide displayed defective expression of M2-associated genes (*Arg-1*, *CD206*, and *CCL22*) along with increased expression of the *IL-1β* gene. For M1 macrophages, treatment with oleamide displayed a minor change in both M1and M2-associated genes (**Figure 3A**). To support these results, pro-inflammatory cytokines IL-1β, IL-6, and TNF-α were determined by ELISA.

Interestingly, augment releasing of IL-1β was observed in all macrophage phenotypes after treatment with oleamide, whereas TNF-α and IL-6 increased in M0 macrophages but not significantly (**Figure 3B**). To confirm these results, cytokine production was further investigated using the THP-1 derived macrophage model. Surprisingly, increasing IL-1β production was also observed in M0 macrophages treated with oleamide, similar to the MDM model (**Figure 3C**). Therefore, this suggested that oleamide induced IL-1 β production in both MDMs and THP-1 cells. Taken together, these results indicated that oleamide mediated naïve macrophages (M0) toward the M1 phenotype and promoted IL-1β production while hindering the polarization of M2 phenotypes.

Oleamide Induced IL-1β Production in LPS-Primed MDMs Involves Activation of the NLRP3- Inflammasome Pathway

An increase of IL-1β production was observed in both MDMs and THP-1 treated with oleamide, suggesting that oleamide functioned as a secondary signal to trigger NLRP3 inflammasome activation and lead to the production of IL-1β. To explore this hypothesis, naïve macrophages (M0) were primed with LPS (signal 1) followed by oleamide treatment for 1-3 h (**Figure 4A**). Then, cell morphology was observed using a bright-field microscope (**Figure 4B**). Cell-free supernatant was detected for IL-1β and IL-18 secretion and inflammasome-related genes (*IL-1β, IL-18, ASC, NLRP3*) were analyzed by RT-qPCR. As predicted, IL-1β and IL-18 were readily produced in LPS-primed MDMs exposed to oleamide in a dose- and time-dependent manner (**Figure 4C**). Furthermore, a high concentration of oleamide (30-40 μg/ml) induced IL-1β and IL-18 production equivalent to ATP, which is known as the NLRP3 inflammasome activation molecule. Consistent with results obtained using cell-free supernatant, oleamide induced upregulation of NLRP3, IL-1β, and IL-18 mRNA expression

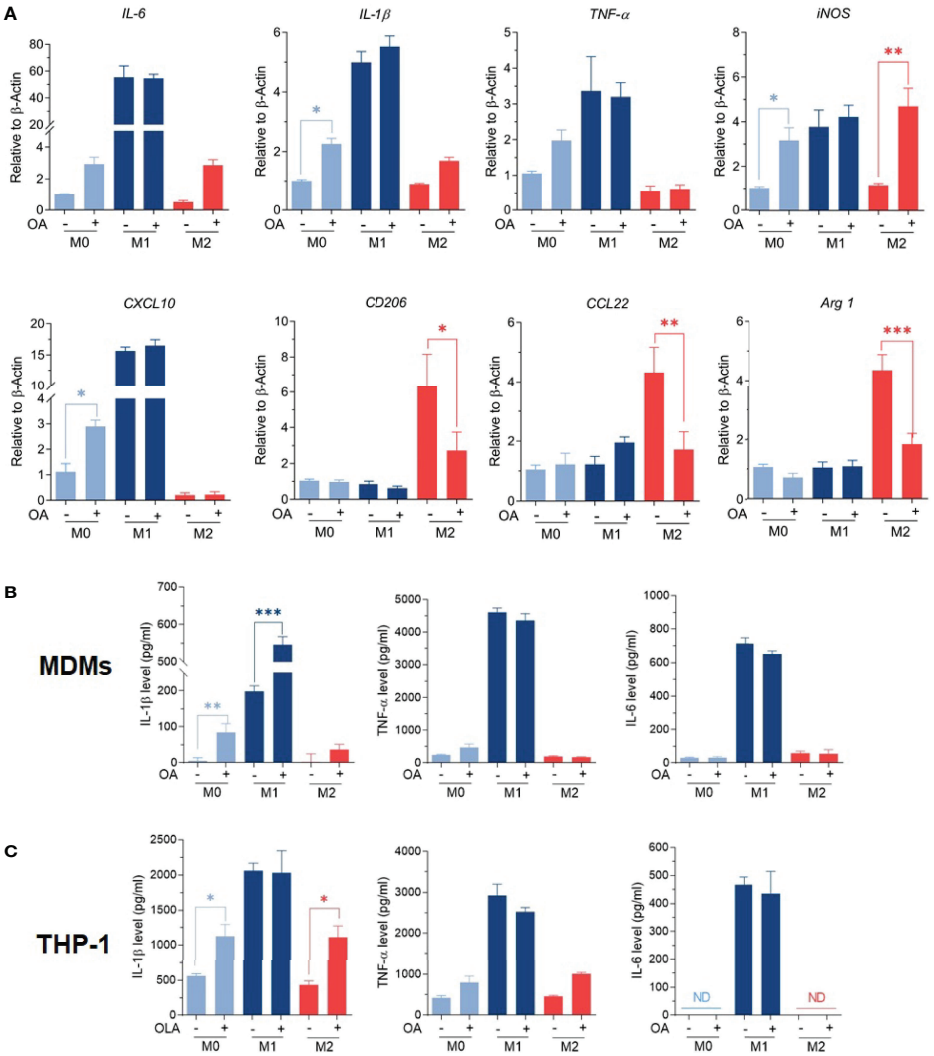

FIGURE 3 | Oleamide mediated M1 macrophage polarization. **(A)** M1/M2 gene expression by RT-qPCR. **(B, C)** Cytokine levels by ELISA. MDMs (Day 6) or differentiated THP-1 were cultured in complete medium only (M0), LPS + INF-γ (M1), or IL-4 (M2) in the presence or absence of oleamide (15 μg/ml) for 24h in all experiments. One-way ANOVA was performed with multiple comparison corrections (Dunnett test). Data represent the mean ± SEM of three independent experiments. (*$p < 0.05$, **$p < 0.01$, ***$p < 0.001$).

compared to the control cells (**Figure 4D**). Therefore, results suggested that oleamide mediated IL-1β and IL-18 production by triggering the NLRP3 inflammasome pathway.

Oleamide Mediated IL-1β Production by Regulating NLRP3-Inflammasome in LPS-Primed MDMs

To further investigate how oleamide impacted NLRP3 inflammasome activation and IL-1β production, LPS-primed MDMs were treated with oleamide for 3 h. Results showed that oleamide induced activation of NLRP3 and ASC speck formation similar to induction by ATP, which activated the NLRP3 inflammasome *via* the purinergic P2X7 receptor (**Figure 5A**). Both IL-1β and IL-18 are initially produced as biologically inactive pro-forms that require cleavage into mature cytokines. Typically, this processing is mediated by caspase-1, which is activated following the formation of an inflammasome (20). Our results showed that oleamide induced upregulation of cleaved caspase 1 and cleaved IL-1β in the supernatant, correlating to downregulation of these proteins in cell lysate (**Figure 5A**). The release of lactate dehydrogenase (LDH) induced by oleamide in LPS-primed MDMs significantly increased in a dose-dependent manner (**Figure 5B**), suggesting that oleamide increased caspase-1-mediated pyroptosis. Similar to LDH, an increase in cell death was observed in a dose-dependent manner (**Figure 5C**). These findings

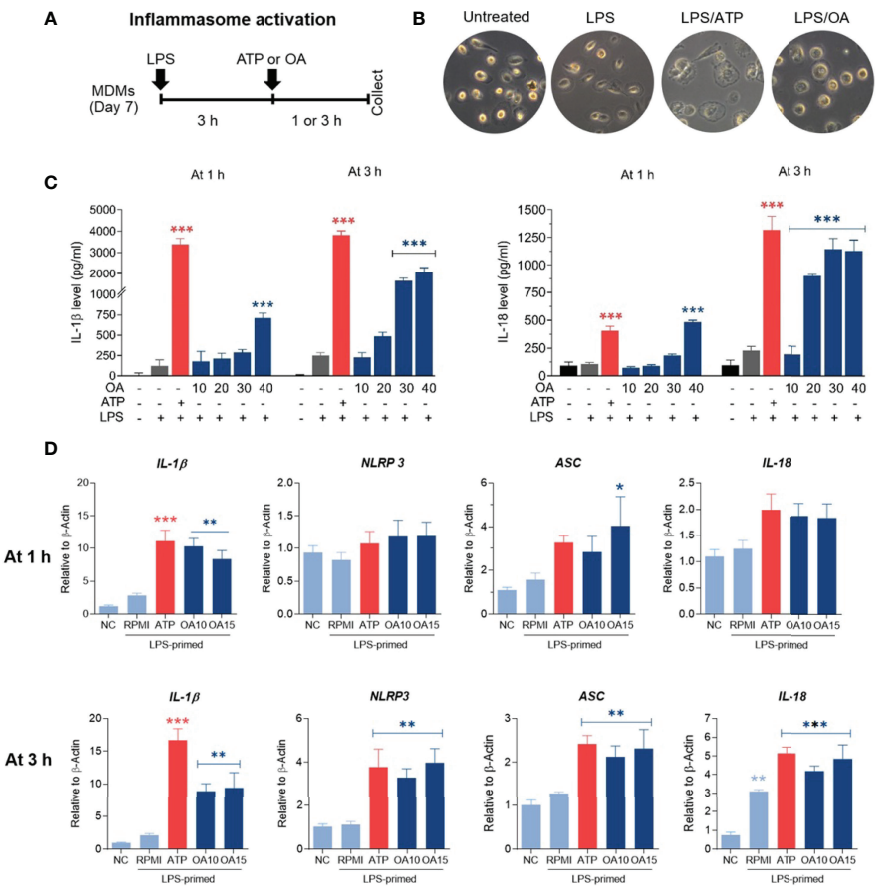

FIGURE 4 | Oleamide mediated inflammasome activation and IL-1β and IL-18 production in LPS-primed MDMs. **(A)** Scheme of inflammasome activation. **(B)** Cell morphology by invested microscope. **(C)** IL-1β and IL-18 levels by ELISA. **(D)** Inflammasome-related gene expression by qRT-PCR. MDMs were primed with LPS (100 ng/ml) for 3 h followed by oleamide (OA) (15 μg/ml) or ATP (30 mM) for 1-3 h in all experiments. Data represents the mean ± SEM of three independent experiments (*p < 0.05, **p < 0.01, ***p < 0.001). NC, negative control; LPS, lipopolysaccharides; ATP, adenosine triphosphate; OA, oleamide; ASC, apoptosis-associated speck-like protein containing a C-terminal caspase recruitment domain; NLRP3, NOD-, LRR- and pyrin domain-containing protein 3.

suggested that oleamide induced activation of the NLRP3 inflammasome pathway and mediated IL-1β production in LPS-primed MDMs.

DISCUSSION

Macrophage polarization is a process whereby macrophages adopt different functional phenotypes in response to specific microenvironmental stimuli and signals (2). This process is crucial for inflammation, tissue repair, and homeostasis maintenance (21). This study explored the immunoregulatory effects of oleamide focusing on macrophage polarization. Results indicated that oleamide mediated naïve macrophages (M0) toward the M1 phenotype and promoted NLRP-3 inflammasome-mediated IL-1β production in primary human monocyte-derived macrophages (MDMs) *in vitro*.

Macrophage polarization is conventionally subdivided into three groups as naïve macrophages (MØ; also called M0), which readily differentiate into the other two major phenotypes as classically activated macrophages (M1) and alternatively activated macrophages (M2) (1–3). Most research on macrophage polarization used simply *in vitro* techniques. Generally, macrophages derived from *in vitro* culture in the presence of specific cytokines stimulate M1 or M2 polarization. Here, M1 polarization was stimulated by LPS and IFN-γ, which are toll-like receptor (TLR) agonists. M2 polarization was stimulated by IL-4, designed to mimic what happens when macrophages are exposed to polarized $CD4^+$ T cells, producing their distinctive cytokine combinations (3). M0 macrophages were cultured in complete media only without polarizing agents and considered naïve macrophages that had not been exposed to any pro- or anti-inflammatory stimuli or environment. This also avoids discrepancy from M-CSF or GM-CSF–dependent culture (22, 23). These three groups were cultured in the presence or

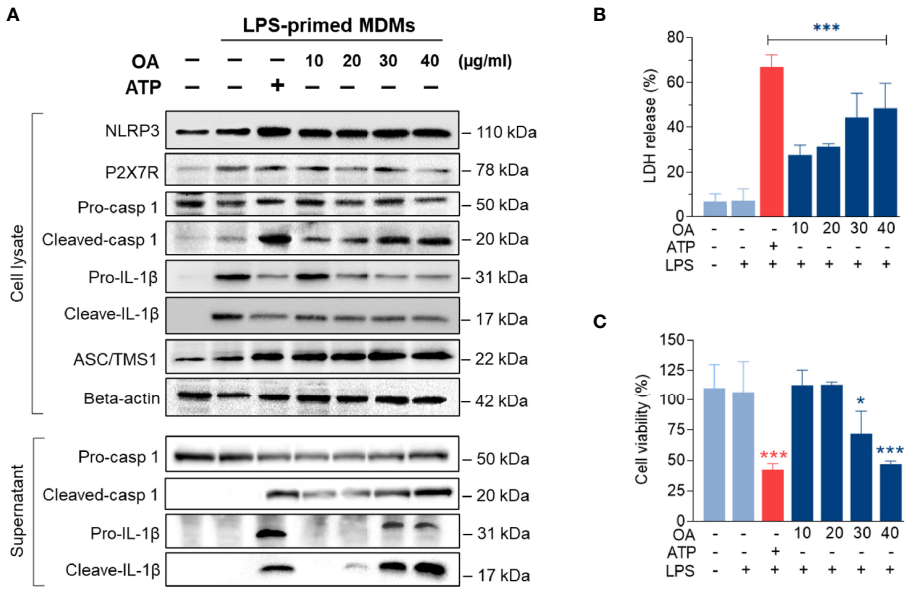

FIGURE 5 | Oleamide promoted NLRP3 inflammasome activation in LPS-primed MDMs. **(A)** Western blot of whole cell lysate and supernatant from LPS-primed MDMs treated with oleamide (OA) (10 - 40 μg/ml) or ATP (30 mM) for 3 h **(B)** Release of LDH and **(C)** Cell viability (%) in LPS-primed MDMs treated with OA (10-40 μg/ml) or ATP (30 mM) for 3h Data represent the mean ± SEM of three independent experiments (*$p < 0.05$, ***$p < 0.001$). LPS, lipopolysaccharides; ATP, adenosine triphosphate; OA, oleamide; LDH, lactate dehydrogenase; ASC, apoptosis-associated speck-like protein containing a C-terminal caspase recruitment domain; NLRP3, NOD-, LRR- and pyrin domain-containing protein 3; P2X7R, purinergic P2X7 receptor.

absence of oleamide. The M0 and M2 macrophages displayed upregulation of CD80 coupled with downregulation of CD163 and CD206 on the cell surface after treatment with oleamide. In M1 macrophages, CD80 expression remained stable but displayed downregulation of CD163 and CD206 on the cell surface after treatment with oleamide (**Figure 2**). CD206 (also known as macrophage mannose receptor; MMR) is primarily expressed on the surface of macrophages and immature dendritic cells, where it acts as a pattern recognition receptor (PRR) (24, 25). Expression of CD206 is generally used as a marker of M2 macrophages (26–28). However, more than half of the M0, M1, and M2 phenotypes exhibited CD206 on the cell surface, indicating that using CD206 as an M2 marker in MDMs should be considered in terms of specificity.

Macrophage polarization is also characterized by the production of cytokines and the expression of M1/M2-associated genes. M1 macrophages are characterized by the production of proinflammatory cytokines like TNF-α, IL-1β, and IL-6. M2 macrophages are characterized by the production of IL-10 and TGF-β. Surprisingly, oleamide treatment did not alter the basal levels of IL-6 and TNF-α but specifically stimulated the production of IL-1β in both MDMs and differentiated THP-1 (**Figure 3C**). This indicated that oleamide might have some impact on IL-1β signaling and/or NLRP3 inflammasome.

IL-1β is a master regulator of inflammation by controlling a variety of innate immune cells (6, 8, 9, 29). In macrophages, inflammasome activation is required to process pro-IL-1β and pro-IL-18 into their mature forms and secrete active forms (IL-1β and IL-18), resulting in initiating inflammation. Currently, a two-step model is used for initiating inflammasome activation (6, 8, 9, 29). The first step or priming step (signal 1) typically involves an NF-κB-dependent upregulation of cellular NLRP3, pro-IL-1β, and pro-IL-18 protein synthesis. The second step (signal 2) is the activation of NLRP3 oligomerization. This step can be induced by numerous PAMP or DAMP such as extracellular ATP and K^+efflux through the ATP-gated P2X7 channel, nigericin toxin as well as lysosomal destabilization agents (6, 8, 9). Upon activation, NLRP3 triggers self-oligomerization and recruitment of apoptosis-associated speck-like protein containing a caspase-recruitment domain (ASC) and pro-caspase-1, leading to the assembly of inflammasome complex (6, 8, 9). NLRP3 inflammasome activation results in active caspase-1, which cleaves the pro-IL-1β and pro-IL-18 into their mature forms, which then facilitates the robust immune responses and pyroptosis (6, 8, 9).

Dysregulation of NLRP3 inflammasome activation is linked with the development of many diseases, especially age-associated ailments such as neurologic disorders and metabolic diseases. Enhanced NLRP3 inflammasome-mediated IL-1β secretion in microglia is associated with the progression of Alzheimer's disease by reducing the phagocytosis of Aβ from microglia (22, 30). The previous study by Yasuhisa Ano et al. reported that oleamide reduces amyloid-β (Aβ) accumulation *via* enhanced microglial phagocytosis, we hypothesized that oleamide could affect human macrophage NLRP3 inflammatory activation. Surprisingly, our research discovered that oleamide has a divisive effect on human macrophages. Results showed that oleamide mediated IL-1β and IL-18 secretion in LPS-primed

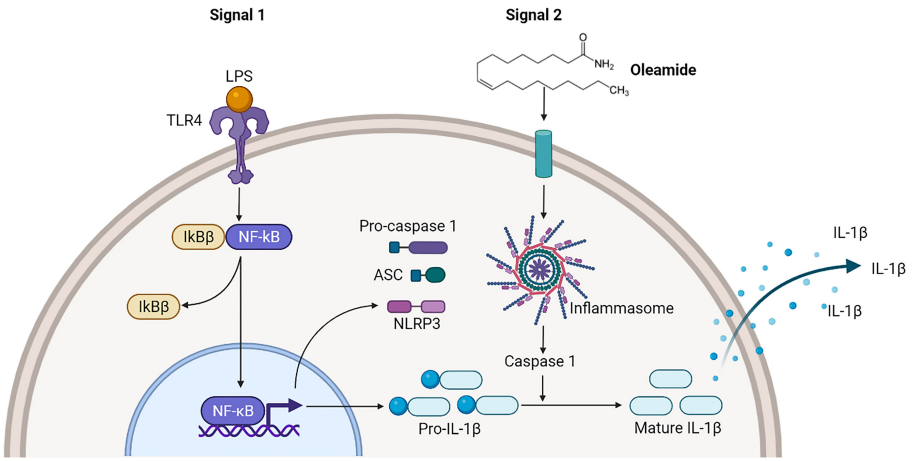

FIGURE 6 | Oleamide activation of NLRP3 inflammasome of M1 phenotypes. The priming step (signal 1) by LPS involved an NF-κB-dependent upregulation of cellular NLRP3 and pro-IL-1β, while the second step (signal 2) was induced by oleamide activating inflammasome and cleaving IL-1β. The released IL-1β may help to induce the polarization of naive macrophages (M0) into M1 phenotypes by supporting oleamide.

MDMs nearly to ATP (**Figure 4C**). Moreover, oleamide induced activation of intracellular inflammasome-associated proteins including NLRP-3, ASC, cleaved casp-1and cleaved IL-1β, correlating with upregulation of cleaved IL-1β and cleaved casp-1 in the supernatant or secreted proteins (**Figure 5A**). However, no alteration of purinergic P2X7 receptor expression was observed after treatment with oleamide. This result indicated that oleamide-mediated NLRP-3 inflammasome activation was not involved in the activation of the P2X7 receptor. A previous study has been reported that P2Y type receptors, a family of G protein-coupled receptors, are potential targets of oleamide in primary murine microglia and human dendritic cells (30). P2Y type receptors involve the coupling of several intracellular pathways and second messengers but act more slowly than P2X receptors (22). However, the regulatory effect of oleamide *via* the P2Y receptor in the inflammasome activation has not been studied. Therefore, how oleamide regulates the NLRP3 inflammasome still requires further investigation. Furthermore, our findings were the first to show that oleamide can cause M1 macrophage polarization and inflammasome activation as well as IL-1β release in MDMs. However, the exact mechanism by which these released IL-1β regulate MDM polarizations is unknown.

Oleamide is an endogenous fatty acid amide that was first reported as a sleep-inducing substance and was later identified as having a wide range of receptors and neurotransmitter systems (15, 16, 23, 31). Nervous and immune systems are often cross-regulated and the potential immunoregulatory activity of oleamide was also studied. Oleamide suppressed the expression of iNOS and COX-2 and secretion of pro-inflammatory cytokines including TNF-α, IL-1β, and IL-6 in LPS-induced RAW264.7 murine macrophages (32). Surprisingly, this study found an opposite effect of oleamide that promoted the production of IL-1β and NLRP3 inflammasome activation in LPS-primed human MDMs. These opposite results were due to different experimental designs (pre-treatment vs. post-treatment), cell culture models (RAW264.7 cell vs. MDMs).

This study explored the immunoregulatory effects of oleamide on human macrophage polarization and NLRP3 inflammasome activation using primary human MDMs cultured in a medium containing human serum as a model. Our results indicated that oleamide promoted naïve macrophages (M0) toward the M1 phenotype and IL-1β production by regulating NLRP3 inflammasome activation in MDMs. This research shows that oleamide has a new effect on human MDMs and could be used as a therapeutic target for NLRP3-related inflammatory diseases, particularly neurodegenerative disorders.

CONCLUSION

Findings demonstrated that oleamide induced NLRP3 inflammasome activation and subsequently activated caspase 1, leading to the production of mature IL-1β, which secreted and promoted polarization of naive macrophages (M0) into M1 phenotypes (**Figure 6**). As a conclusion, oleamide could be a possible target for regulating the activation of the NLRP3 inflammasome and its implications for the treatment of inflammatory diseases.

DATA AVAILABILITY STATEMENT

The original contributions presented in the study are included in the article/**Supplementary Material**. Further inquiries can be directed to the corresponding author.

AUTHOR CONTRIBUTIONS

Conceptualization, PW and KU. Methodology, PW. Software, PW. Formal analysis, PW. Investigation, PW. Writing—original draft preparation, PW. Writing—review and editing, KU. Funding acquisition, KU and PP. Supervision, KU. Project administration, KU. All authors have read and agreed to the published version of the manuscript.

FUNDING

This research was funded by the Royal Golden Jubilee Ph.D. Program (PhD/0002/2559), and the Thailand Science Research and Innovation, and Naresuan University (FF 2566).

ACKNOWLEDGMENTS

We would like to thank the staff of the Blood Bank Unit of Naresuan University Hospital, Thailand for providing blood samples.

SUPPLEMENTARY MATERIAL

The Supplementary Material for this article can be found online at: https://www.frontiersin.org/articles/10.3389/fimmu.2022.856296/full#supplementary-material

REFERENCES

1. Genin M, Clement F, Fattaccioli A, Raes M, Michiels C. M1 and M2 Macrophages Derived From THP-1 Cells Differentially Modulate the Response of Cancer Cells to Etoposide. *BMC Cancer* (2015) 15(1):577. doi: 10.1186/s12885-015-1546-9
2. Orecchioni M, Ghosheh Y, Pramod AB, Ley K. Macrophage Polarization: Different Gene Signatures in M1(LPS+) vs. Classically and M2(LPS–) vs. Alternatively Activated Macrophages. *Front Immunol* (2019) 10:1084–98. doi: 10.3389/fimmu.2019.01084
3. Murray PJ. Macrophage Polarization. *Annu Rev Physiol* (2017) 79(1):541–66. doi: 10.1146/annurev-physiol-022516-034339
4. Yao Y, Xu X-H, Jin L. Macrophage Polarization in Physiological and Pathological Pregnancy. *Front Immunol* (2019) 10:792. doi: 10.3389/fimmu.2019.00792
5. Li C, Levin M, Kaplan DL. Bioelectric Modulation of Macrophage Polarization. *Sci Rep* (2016) 6(1):21044. doi: 10.1038/srep21044
6. Lopez-Castejon G, Brough D. Understanding the Mechanism of IL-1β Secretion. *Cytokine Growth Factor Rev* (2011) 22(4):189–95. doi: 10.1016/j.cytogfr.2011.10.001
7. Lee H, Fessler MB, Qu P, Heymann J, Kopp JB. Macrophage Polarization in Innate Immune Responses Contributing to Pathogenesis of Chronic Kidney Disease. *BMC Nephrol* (2020) 21(1):270. doi: 10.1186/s12882-020-01921-7
8. Paik S, Kim JK, Silwal P, Sasakawa C, Jo E-K. An Update on the Regulatory Mechanisms of NLRP3 Inflammasome Activation. *Cell Mol Immunol* (2021) 18(5):1141–60. doi: 10.1038/s41423-021-00670-3
9. Martín-Sánchez F, Diamond C, Zeitler M, Gomez AI, Baroja-Mazo A, Bagnall J, et al. Inflammasome-Dependent IL-1β Release Depends Upon Membrane Permeabilisation. *Cell Death Differ* (2016) 23(7):1219–31. doi: 10.1038/cdd.2015.176
10. Holbrook JA, Jarosz-Griffiths HH, Caseley E, Lara-Reyna S, Poulter JA, Williams-Gray CH, et al. Neurodegenerative Disease and the NLRP3 Inflammasome. *Front Pharmacol* (2021) 12. doi: 10.3389/fphar.2021.643254
11. Kwon HS, Koh S-H. Neuroinflammation in Neurodegenerative Disorders: The Roles of Microglia and Astrocytes. *Trans Neurodegener* (2020) 9(1):42. doi: 10.1186/s40035-020-00221-2
12. Guo H, Callaway JB, Ting JPY. Inflammasomes: Mechanism of Action, Role in Disease, and Therapeutics. *Nat Med* (2015) 21(7):677–87. doi: 10.1038/nm.3893
13. Boger DL, Henriksen SJ, Cravatt BF. Oleamide: An Endogenous Sleep-Inducing Lipid and Prototypical Member of a New Class of Biological Signaling Molecules. *Curr Pharm Des* (1998) 4(4):303–14.
14. Nam HY, Na EJ, Lee E, Kwon Y, Kim H-J. Antiepileptic and Neuroprotective Effects of Oleamide in Rat Striatum on Kainate-Induced Behavioral Seizure and Excitotoxic Damage *via* Calpain Inhibition. *Front Pharmacol* (2017) 8. doi: 10.3389/fphar.2017.00817
15. Akanmu MA, Adeosun SO, Ilesanmi OR. Neuropharmacological Effects of Oleamide in Male and Female Mice. *Behav Brain Res* (2007) 182(1):88–94. doi: 10.1016/j.bbr.2007.05.006
16. Murillo-Rodríguez E, Giordano M, Cabeza R, Henriksen SJ, Méndez Díaz M, Navarro L, et al. Oleamide Modulates Memory in Rats. *Neurosci Lett* (2001) 313(1-2):61–4. doi: 10.1016/S0304-3940(01)02256-X
17. Mendelson WB, Basile AS. The Hypnotic Actions of the Fatty Acid Amide, Oleamide. *Neuropsychopharmacology* (2001) 25(1):S36–S9. doi: 10.1016/S0893-133X(01)00341-4
18. Oh YT, Lee JY, Lee J, Lee JH, Kim JE, Ha J, et al. Oleamide Suppresses Lipopolysaccharide-Induced Expression of iNOS and COX-2 Through Inhibition of NF-kappaB Activation in BV2 Murine Microglial Cells. *Neurosci Lett* (2010) 474(3):148–53. doi: 10.1016/j.neulet.2010.03.026
19. Ano Y, Ozawa M, Kutsukake T, Sugiyama S, Uchida K, Yoshida A, et al. Preventive Effects of a Fermented Dairy Product Against Alzheimer's Disease and Identification of a Novel Oleamide With Enhanced Microglial Phagocytosis and Anti-Inflammatory Activity. *PloS One* (2015) 10(3):e0118512. doi: 10.1371/journal.pone.0118512
20. Lang T, Lee JPW, Elgass K, Pinar AA, Tate MD, Aitken EH, et al. Macrophage Migration Inhibitory Factor is Required for NLRP3 Inflammasome Activation. *Nat Commun* (2018) 9(1):2223. doi: 10.1038/s41467-018-04581-2
21. Patel U, Rajasingh S, Samanta S, Cao T, Dawn B, Rajasingh J. Macrophage Polarization in Response to Epigenetic Modifiers During Infection and Inflammation. *Drug Discov. Today* (2017) 22(1):186–93. doi: 10.1016/j.drudis.2016.08.006
22. Zhang Y, Dong Z, Song W. NLRP3 Inflammasome as a Novel Therapeutic Target for Alzheimer's Disease. *Signal Transduct Target Ther* (2020) 5(1):37. doi: 10.1038/s41392-020-0145-7
23. Boger DL, Patterson JE, Guan X, Cravatt BF, Lerner RA, Gilula NB. Chemical Requirements for Inhibition of Gap Junction Communication by the Biologically Active Lipid Oleamide. *Proc Natl Acad Sci USA* (1998) 95(9):4810–5. doi: 10.1073/pnas.95.9.4810
24. Azad AK, Rajaram MV, Schlesinger LS. Exploitation of the Macrophage Mannose Receptor (CD206) in Infectious Disease Diagnostics and Therapeutics. *J Cytol Mol Biol* (2014) 1(1):1000003. doi: 10.13188/2325-4653.1000003
25. Jaynes JM, Sable R, Ronzetti M, Bautista W, Knotts Z, Abisoye-Ogunniyan A, et al. Mannose Receptor (CD206) Activation in Tumor-Associated Macrophages Enhances Adaptive and Innate Antitumor Immune Responses. *Sci Trans Med* (2020) 12(530):eaax6337. doi: 10.1126/scitranslmed.aax6337
26. Bertani FR, Mozetic P, Fioramonti M, Iuliani M, Ribelli G, Pantano F, et al. Classification of M1/M2-Polarized Human Macrophages by Label-Free Hyperspectral Reflectance Confocal Microscopy and Multivariate Analysis. *Sci Rep* (2017) 7(1):8965. doi: 10.1038/s41598-017-08121-8
27. Zhu Y, Zhang L, Lu Q, Gao Y, Cai Y, Sui A, et al. Identification of Different Macrophage Subpopulations With Distinct Activities in a Mouse Model of Oxygen-Induced Retinopathy. *Int J Mol Med* (2017) 40(2):281–92. doi: 10.3892/ijmm.2017.3022
28. Smith TD, Tse MJ, Read EL, Liu WF. Regulation of Macrophage Polarization and Plasticity by Complex Activation Signals. *Integr Biol: Quant Biosci Nano Macro* (2016) 8(9):946–55. doi: 10.1039/c6ib00105j

29. Gritsenko A, Yu S, Martin-Sanchez F, Diaz-del-Olmo I, Nichols E-M, Davis DM, et al. Priming Is Dispensable for NLRP3 Inflammasome Activation in Human Monocytes *In Vitro*. *Front Immunol* (2020) 11:2573. doi: 10.3389/fimmu.2020.565924
30. Hanslik KL, Ulland TK. The Role of Microglia and the Nlrp3 Inflammasome in Alzheimer's Disease. *Front Neurol* (2020) 11:570711. doi: 10.3389/fneur.2020.570711
31. Guan X, Cravatt BF, Ehring GR, Hall JE, Boger DL, Lerner RA, et al. The Sleep-Inducing Lipid Oleamide Deconvolutes Gap Junction Communication and Calcium Wave Transmission in Glial Cells. *J Cell Biol* (1997) 139 (7):1785–92. doi: 10.1083/jcb.139.7.1785
32. Moon SM, Lee SA, Hong JH, Kim JS, Kim DK, Kim CS. Oleamide Suppresses Inflammatory Responses in LPS-Induced RAW264.7 Murine Macrophages and Alleviates Paw Edema in a Carrageenan-Induced Inflammatory Rat Model. *Int Immunopharmacol* (2018) 56:179–85. doi: 10.1016/j.intimp.2018.01.032

Conflict of Interest: The authors declare that the research was conducted in the absence of any commercial or financial relationships that could be construed as a potential conflict of interest.

frontiers | Frontiers in Immunology

REVIEW
published: 30 May 2022
doi: 10.3389/fimmu.2022.896473

Inflammasomes and Pyroptosis of Liver Cells in Liver Fibrosis

Can Gan[1,2†], *Qiuyu Cai*[1,2†], *Chengwei Tang*[1,2*] *and Jinhang Gao*[1,2*]

[1] *Lab of Gastroenterology and Hepatology, West China Hospital, Sichuan University, Chengdu, China,* [2] *Department of Gastroenterology, West China Hospital, Sichuan University, Chengdu, China*

Inflammasomes are multiprotein complexes that can sense danger signals and activate caspase-1 to mediate pro-inflammatory cytokines release and pyroptotic cell death. There are two main canonical and non-canonical signaling pathways that trigger inflammasome activation. Inflammasomes are expressed and assembled in parenchymal and nonparenchymal cells in response to liver injury in the liver. Additionally, the hepatocytes, biliary epithelial cells (cholangiocytes), hepatic stellate cells (HSCs), hepatic macrophages, and liver sinusoidal endothelial cells (LSECs) contribute to liver fibrosis *via* different mechanisms. However, the underlying mechanism of the inflammasome and pyroptosis in these liver cells in liver fibrosis remains elusive. This review summarizes the activation and function of inflammasome complexes and then discusses the association between inflammasomes, pyroptosis, and liver fibrosis. Unlike other similar reviewers, we will focus on the effect of inflammasome activation and pyroptosis in the various liver cells during the development of liver fibrosis. We will also highlight the latest progress of pharmacological intervention in inflammasome-mediated liver fibrosis.

Keywords: inflammasome activation, pyroptosis, caspase-1, IL-1β, IL-18, liver cirrhosis

OPEN ACCESS

Edited by:
Alessandra Mortellaro, San Raffaele Telethon Institute for Gene Therapy (SR-Tiget), Italy

Reviewed by:
Alessio Cantore, San Raffaele Scientific Institute (IRCCS), Italy
Edward N. Harris, University of Nebraska System, United States
Steven O'Reilly, STipe Therapeutics, Denmark

***Correspondence:**
Jinhang Gao
Gao.jinhang@scu.edu.cn;
Gao.jinhang@qq.com
Chengwei Tang
shcqcdmed@163.com

†These authors contributed equally to this work

Specialty section:
This article was submitted to Molecular Innate Immunity, a section of the journal Frontiers in Immunology

Received: *15 March 2022*
Accepted: *04 May 2022*
Published: *30 May 2022*

Citation:
Gan C, Cai Q, Tang C and Gao J (2022) Inflammasomes and Pyroptosis of Liver Cells in Liver Fibrosis. Front. Immunol. 13:896473. doi: 10.3389/fimmu.2022.896473

1 INTRODUCTION

Inflammasomes are signaling platforms in response to infectious diseases or chronic sterile inflammation. These multimeric complexes respond to molecular patterns from pathogens and cellular damage by releasing pro-inflammatory cytokines and inducing pyroptotic cell death (1). In general, inflammasome complexes are composed of a pattern-recognition receptor, an effector caspase-1, and an adaptor connecting these two components. There are two groups of inflammasomes in terms of receptors: the NLR family containing NLRP1, 2, 3, 6, NLRC4 and NLRP12; pyrin and HIN domain-containing (PYHIN) family including absent in melanoma 2 (AIM2) and pyrin (2). The inflammasomes could either aggravate inflammation *via* interleukin (IL)-1β and IL-18 or induce pyroptosis *via* gasdermin D (GSDMD). Although the inflammasome and its related pyroptosis have been well studied in infectious diseases, the role and mechanism of inflammasome and pyroptosis in liver fibrosis remain unclear.

Liver fibrosis is characterized by excessive extracellular matrix (ECM) deposition in response to chronic liver injury, including virus infection, non-alcoholic steatohepatitis (NASH), alcoholic liver disease (ALD), and autoimmune diseases (3, 4). Generally, activated HSCs are primary myofibroblasts that produce and secrete ECM. In addition, hepatocytes, Kupffer cells (KCs), LSECs, cholangiocytes, and recruited cell types (*e.g.*, bone marrow-derived macrophages) also contribute to liver fibrosis (5, 6). The mechanisms of liver fibrosis are complicated and involve different cells, signaling pathways, and cross-

talk between individual cells. Recent studies have shown that inflammasomes and inflammasome-related pyroptosis are involved in liver fibrogenesis from various pathologies (7). The detailed mechanism of the inflammasome and pyroptosis in liver fibrosis is not well-defined. Collaboration of multiple liver cells maintains hepatic homeostasis in health and contributes to disturbed hepatic homeostasis in liver fibrosis (8). This review summarizes the progress of inflammasome and inflammasome-related pyroptosis in liver fibrosis. The roles and mechanisms of inflammasomes and pyroptosis in various liver cells and their cross-talks will also be described. Eventually, the potential therapeutic targets and future directions will also be implied based on the current progress.

2 INFLAMMASOME BIOLOGY AND ACTIVATION

There are five main kinds of inflammasome sensor complexes in terms of receptors, NLRP1, NLRP3, NLRC4, AIM2, and pyrin (**Figure 1**). The inflammasome receptor oligomerizes and recruits the adaptor ASC and effector caspase-1 to assemble inflammasome complexes after sensing pathogens or host-derived injuries. After activation, the cleaved caspase-1 mediates the maturation and secretion of IL-1β and IL-18 and pyroptotic cell death (9). In this section, we will compare the structures of different inflammasomes and discuss the mechanism of inflammasome activation.

2.1 Inflammasome Assembly and Structure

2.1.1 NLRP1 Inflammasome

NLRP1 was the first inflammasome to be identified; however, little research has focused on NLRP1 inflammasome due to the complexity and differences in structures between humans and mice. Human NLRP1 inflammasome has two domains in NOD-like receptor (NLR): an N−terminal pyrin domain (PYD) and a C−terminal caspase activation and recruitment domain (10). In contrast, the mouse genome encodes Nlrp1a, Nlrp1b, and Nlrp1c, which activate caspase-1 without the help of an ASC

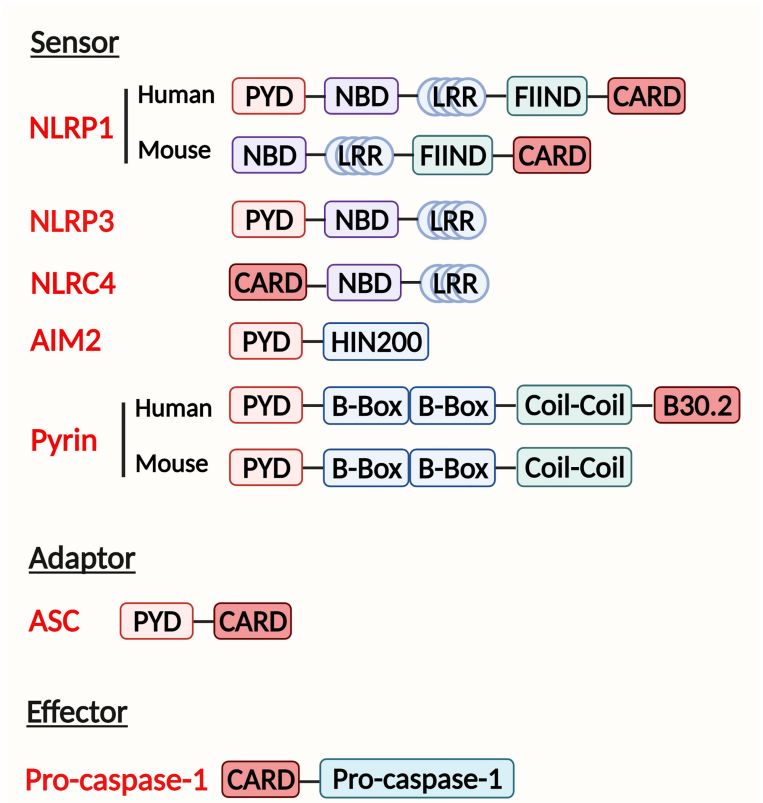

FIGURE 1 | Domain structure and inflammasome assembly. The inflammasome complex contains a sensor, adapter, and effector protein. There are two kinds of sensors: the NOD-like receptor (NLR) family and the PYHIN (pyrin and HIN200 (hematopoietic interferon-inducible nuclear antigens with 200 amino-acid repeats) domain-containing protein) family. The NLR family includes NLRP1, NLRP3, NLRC4 sensors. They contain a nucleotide-binding domain (NBD), carboxy-terminal leucine-rich repeat (LRR), either a pyrin domain (PYD) or a caspase activation and recruitment domain (CARD). Additionally, NLRP1 has a function-to-find domain (FIIND) at the C terminal. The PYHIN family AIM2 receptor has a PYD and HIN200 domain, whereas pyrin contains a PYD, two B boxes, and a coil-coil domain. Human pyrin has an additional B30.2 domain. Adaptor has a PYD to combine with the sensor and a CARD with the effector. The effector is composed of a CARD and pro-caspase-1, which will be cleaved when inflammasome assembly.

adaptor due to the lack of a PYD domain in the receptor (11). But a function-to-find domain (FIIND) at the C–terminal is required in both humans and mice to participate in the activation of the NLRP1 inflammasome (**Figure 1**) (12).

Regarding inflammasome activation, Bacillus anthracis lethal toxin (LT) was involved in the NLRP1 inflammasome activation and subsequent caspase-1–dependent cytokine release and pyroptosis (13). Moreover, extracellular ATP was also demonstrated to trigger the NLRP1 inflammasome by activating the P2X7 receptor and potassium efflux (14, 15). As the NLRP1 inflammasome is less well-studied, the role of the NLRP1 inflammasome in chronic liver disease and liver fibrosis remains unclear.

2.1.2 NLRP3 Inflammasome

The NLRP3 inflammasome contains the NOD-like receptor NLRP3, the adaptor ASC, and the effector pro-caspase-1 (**Figure 1**). The NLRP3 inflammasome is the most widely studied and the best-characterized inflammasome in infectious and chronic inflammatory diseases (16).

The stimuli involved in NLRP3 activation include pathogen-associated molecular patterns (PAMPs) ligands (17), such as bacterial, fungal, and viral components, pore-forming toxins, nucleic acids; and damage-associated molecular patterns (DAMPs) such as extracellular ATP (18), uric acid crystals (19), and amyloid (20). Activation by these PAMPs and DAMPs indicates that the NLRP3 inflammasome is a common sensor of cellular stress or injury. Activation of the NLRP3 inflammasome requires two steps. First, extracellular stimuli prime cells, *e.g.*, LPS binds to TLR4 to activate NF-κB and subsequent transcription and translation of IL–1β. Then secondary stimuli such as ATP induce inflammasome complex assembly and IL-1β cleavage and secretion. An increasing number of studies have confirmed the critical roles of NLRP3 inflammasome activation in pro-inflammatory cytokines release and pyroptosis initiation. The NLRP3 inflammasome-mediated cellular communication among different liver cell types in acute and chronic liver diseases from diverse liver injuries was also well-defined (21, 22), indicating the pivotal role of NLRP3 inflammasome in the development of liver diseases.

2.1.3 NLRC4 Inflammasome

The NLRC4 inflammasome is activated in response to Flagellin infection (23), Salmonella infection (24), and bacterial type 3 secretion systems (T3SSs) (25). These stimulators bind to NLRC4 indirectly. During infection, neuronal apoptosis inhibitory proteins (NAIPs) interact with the ligand and NLRC4 receptor, activating the assembly of the NLRC4 inflammasome (**Figure 1**) (26). A few studies showed that bacterial flagellin induced NLRC4 inflammasome activation in hepatocytes and KCs (27, 28). Moreover, the NLRC4-driven IL-1 release was also involved in liver fibrosis (27, 28). Though these studies show an important role of NLRC4 inflammasome in bacterial infection in liver cells, more studies are needed to explore the potential mechanisms of NLRC4 inflammasome activation and its role in liver fibrosis.

2.1.4 AIM2 Inflammasome

The AIM2 inflammasome is a cytosolic receptor that senses double-stranded DNA (dsDNA). It contains an N-terminal PYD domain and a C-terminal hematopoietic interferon-inducible nuclear protein with a 200-amino acid repeat (HIN200) domain (**Figure 1**) (29). When dsDNA binds to the AIM2 receptor, ASC and pro-caspase-1 are recruited for inflammasome complex formation and activation (30, 31). Previous studies have found that the AIM2 inflammasome induction in hepatocytes and macrophages participates in chronic liver diseases *via* the pyroptosis pathway (32–35). However, the mechanism of AIM2 inflammasome regulation is not well-studied.

2.1.5 Pyrin Inflammasome

Pyrin, encoded by the MEFV gene, contains a PYD, two B–boxes, a coiled-coil domain, and a SPRY/PRY domain (**Figure 1**). Pyrin was recently recognized as an inflammasome-forming and pyroptosis-initiating protein. Pyrin inflammasome was reported to stimulate pyroptosis, but there is no evidence showing its direct effect on the progression of liver fibrosis (36, 37).

2.2 Functions of Effector Components in Inflammasomes

Inflammasome assembly activates caspase-1, which cleaves the pro-IL-1β and pro-IL-18 into active IL-1β and IL-18. Meanwhile, GSDMD is cleaved by caspase-1 to N-terminal fragments (GSDMD-NT), which are inserted into the cell lipid membrane to assemble arc- and slit-like oligomers and grow into large and stable ring-like oligomers to form transmembrane pores. This process leads to cell membrane rupture and resultant pyroptosis (38). We next explored the functions of these effector components in inflammasomes.

2.2.1 IL Maturation and Secretion

Activation of inflammasome complexes cleaves pro-caspase-1 and triggers IL-1β and IL-18 maturation and secretion. IL–1β and IL–18 are crucial cytokines involved in immune responses and trigger the inflammatory cascade (39). However, there have been many debates about how IL-1 is secreted out of cells. Recent studies have shown that *Gsdmd* knockout macrophages mature IL–1β normally but fail to secrete it due to lack of pyroptosis, suggesting that IL-1β is secreted through cell membrane rupture and lysis (40). However, whether IL-1 is released *via* pyroptosis in other cell types remains unknown; further studies are needed.

2.2.2 Pyroptosis

Pyroptosis is a distinct type of programmed cell death characterized by the formation of cell membrane pores, the release of intracellular contents, nuclear condensation, and cell lysis (41). Compared with pyroptosis, apoptosis and necroptosis are caspase-3/7 and receptor-interacting serine-threonine kinase-1/3 (RIPK-1/3) mediated programmed cell death, respectively (42). Pyroptosis depends on inflammatory caspase-1 to cleave gasdermins to form membrane pores. Of all gasdermins, GSDMD has been demonstrated to play a central role in pyroptotic cell death. Active caspases cleave GSDMD to

GSDMD-NT, which causes membrane pores and induces pyroptosis *via* both canonical and non-canonical signaling pathways (41, 43). However, the mechanism by which GSDMD executes cell death is poorly explored.

2.3 Canonical and Non-Canonical Signaling Pathways of Inflammasome Activation

As previously reviewed, inflammasomes are initiated and assembled *via* a canonical or non-canonical signaling pathway (2). There are two steps to process inflammasome activation in the canonical signaling pathway (**Figure 2**) (44). In the first step, PAMPs, such as LPS, bind to TLRs and elicit the downstream MyD88–NF-κB signaling pathway to produce pro-IL-1β and pro-IL-18. In the second step, endogenous danger signals activate inflammasome assembly and caspase-1. A combination of PRR, ASC, and pro-caspase-1 helps activate caspase-1, which cleaves GSDMD into GSDMD-NT as well as cleaves pro-IL-1β and pro-IL-18 into mature IL-1β and IL-18. There are three main mechanisms involved in the second step. Firstly, extracellular ATP binds to the P2X7 receptor and opens a pore on the cell membrane through pannexin 1 protein, causing potassium efflux and NLRP3 activation (18). Secondly, uric acid crystals and amyloid endocytosed by phagosome lysosomes contribute to lysosome rupture and release of cathepsin B, which helps inflammasome assembly (19). Thirdly, thioredoxin-interacting protein (TXNIP) detached from thioredoxin and mitochondrial DNA (mtDNA) accumulation in a ROS-dependent manner activates inflammasomes (45).

Apart from the canonical signaling pathway, inflammasomes are also activated by the non-canonical signaling pathway (**Figure 2**). In this process, intracellular LPS or toxin initiates caspase-11, promoting inflammasome assembly and caspase-1 activation. Then both active caspase-11 and caspase-1 cleave GSDMD into GSDMD-NT, leading to cascaded reactions similar to the canonical signaling pathway (46). Inflammasome activation is a complex process that involves multiple proteins. It remains unclear whether the cross-talk of the canonical signaling pathway and the non-canonical signaling pathway also revokes inflammasome activation.

3 INFLAMMASOME AND PYROPTOSIS IN LIVER FIBROSIS

Liver fibrosis is a dynamic process characterized by an imbalance in ECM deposition and degradation due to chronic liver injury of

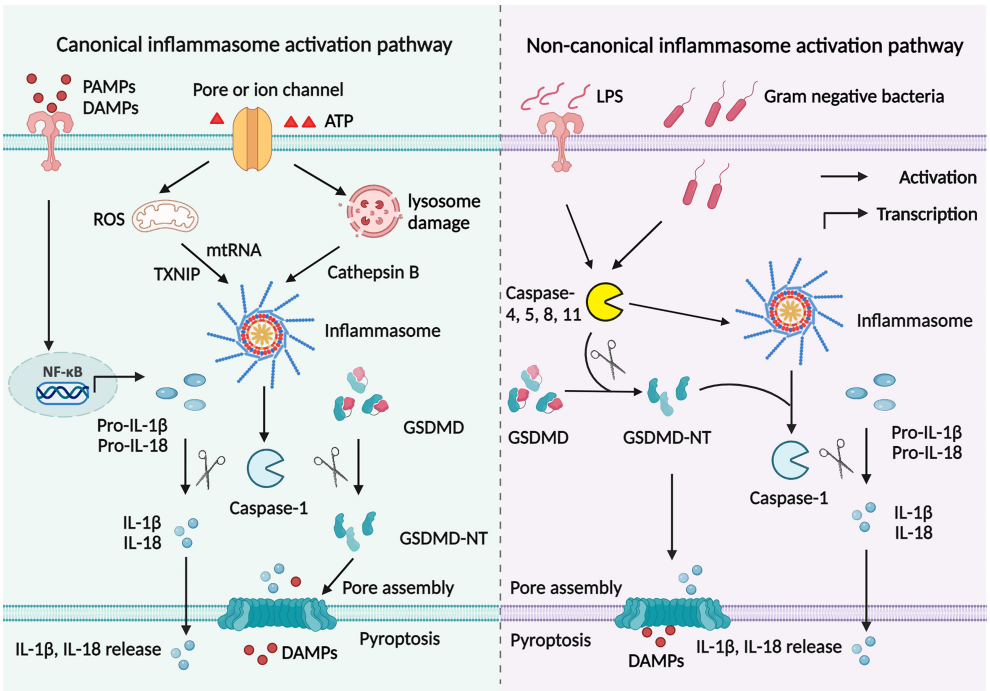

FIGURE 2 | Canonical and non-canonical signaling pathways to activate inflammasomes. Canonical signaling pathway to activate inflammasomes is mediated by two signaling steps. The priming step involves PAMPs or DAMPs binding to TLRs to initiate NF- κB signaling pathway, which promotes pro-IL-1β and pro-IL-18 production. Then endogenous danger signals activate inflammasome assembly and caspase-1 in the second step. Active caspase-1 cleaves GSDMD into GSDMD-NT; cut pro-IL-1β and pro-IL-18 into mature IL-1β and IL-18. The GSDMD breaks a pore on the cell membrane to help IL-1β and IL-18 secretion. There are three main mechanisms involved in inflammasome activation. Extracellular ATP binds to the P2X7 receptor and causes potassium efflux and NLRP3 activation. Uric acid and amyloid are endocytosed in a lysosome-dependent manner, promoting lysosome rupture and cathepsin B release and resultant inflammasome assembly. TXNIP and mtDNA accumulation in a ROS-dependent manner activates inflammasomes. However, in the non-canonical signaling pathway, intracellular LPS or toxin initiates caspase-11, promoting inflammasomes assembly and caspase-1 activation. Then both active caspase-11 and caspase-1 cleave GSDMD into GSDMD-NT, leading to cascaded reactions similar to the canonical signaling pathway.

various etiologies (5). During this process, quiescent HSCs transdifferentiate into fibrogenic activated phenotype, representing the dominant collagen-producing myofibroblasts in different chronic injury models (5, 7, 47). Stimulators of chronic liver injuries, such as fatty acid, alcohol, toxin, and virus infection, affect hepatocytes, hepatic macrophages, LSECs, and cholangiocytes. Damaged liver cells interact with HSCs by releasing pro-inflammatory and pro-fibrotic factors, promoting HSC activation and resultant liver fibrosis (48–50). It is worth noting that inflammasome activation and pyroptosis play a central role in the inflammatory cascade (51). Previous studies have demonstrated that inflammasome components are widely expressed in these liver cell types in response to liver injury (52–54). Moreover, inflammasomes could induce liver fibrosis both directly and indirectly. Inflammasome activation in HSCs directly leads to HSCs activation, which is responsible for ECM formation and liver fibrosis. Indirectly, pro-inflammatory cytokine release or pyroptotic cell death in hepatocytes and other nonparenchymal cells induces HSC activation and eventually leads to liver fibrosis (**Figure 3**) (55).

3.1 Inflammasomes and Pyroptosis in Hepatocytes

Although inflammasomes are predominately expressed in immune cells, hepatocytes, which are the most abundant cell type in the liver and predisposed to liver injury, also express inflammasomes (52). Recently, increasing studies have demonstrated important roles of hepatocellular inflammasomes activation, the subsequent pyroptotic death, and inflammasome-implicated cross-talk with HSCs in chronic liver injury from various liver pathologies.

3.1.1 Hepatocellular NLRP3 Inflammasome in NAFLD and NASH-Related Liver Fibrosis

Hepatocellular NLRP3 inflammasome activation and caspase-1-mediated pyroptosis play a crucial role in the progression of non-alcoholic fatty liver disease (NAFLD). Lipid exposure resulted in hepatocellular NLRP3 inflammasome activation and cleavage of mature IL-1β and IL-18 by caspase-1 in high fructose-induced NAFLD mouse model. The inflammatory response aggravated hepatocellular lipid accumulation as well as impaired insulin sensitivity in JAK/STAT3-dependent (56) and PI3K/AKT-dependent manner (57), respectively. The evidence indicates that NLRP3 inflammasome mediates lipid and glucose metabolism in hepatocytes. Mechanically, NLRP3 inflammasome and cytokine production are induced by mitochondrial reactive oxygen species (ROS) in fatty hepatocytes (58, 59). Furthermore, the binding of IL-1β and IL-18 to HSC-derived IL-1 receptor, as well as DAMPs released from pyroptotic hepatocytes transdifferentiated HSCs into activated phenotype for fibrotic scar formation (57). Liver inflammation and ECM deposition are relieved in hepatocyte-specific *caspase-11*-deficient mice with high sucrose and high fat diet, where the production of IL-1β and GSDMD was blocked, further proving the role of inflammasomes in liver fibrosis (60). In summary, these studies have demonstrated that hepatocellular

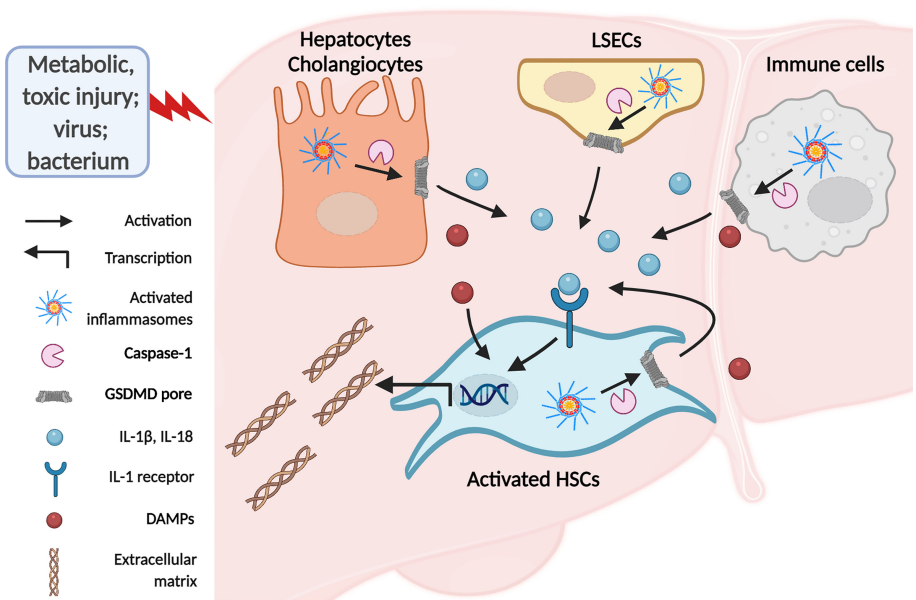

FIGURE 3 | The inflammasomes in liver fibrosis. Activated HSCs are the primary source of extracellular matrix deposition in response to chronic liver injury. There are direct and indirect ways involved in inflammasome to stimulate HSCs. Activation of inflammasomes in hepatocytes and macrophages due to chronic liver injury leads to IL-1β and IL-18 release and pyroptotic cell death. Secreted IL-1β and IL-18 bind to IL-1 receptors on HSCs and induce HSCs activation and resultant ECM formation. In addition, DAMPs from pyroptotic cells promote HSCs activation and liver fibrosis. Meanwhile, PAMPs or DAMPs may directly target HSCs to induce inflammasome-dependent IL-1 release and pyroptosis, eliciting HSCs activation in an autocrine or paracrine manner.

NLRP3 inflammasome and pyroptosis contribute to the development of NAFLD and liver fibrosis *via* the cross-talk between hepatocytes and HSCs.

3.1.2 Hepatocellular NLRP3 Inflammasome in Liver Fibrosis

Hepatocyte pyroptosis and the release of inflammasome particles caused by DAMPs and PAMPs were internalized by HSCs and further induced HSC activation and liver fibrosis (55, 61). It seems that the NLRP3 inflammasome in hepatocytes may play a pivotal role in developing liver fibrosis. Ethanol was shown to trigger hepatocyte NLRP3 inflammasome-dependent IL-1β production and pyroptosis by TXNIP overexpression (62) and the caspase-4/11–GSDMD non-canonical signaling pathway in ALD (63). Elevated inflammation accompanied apoptotic and necroptotic cell death in the *Nlrp3*-knockout acute BDL model. In contrast, decreased liver injury and bridge fibrosis in the *Nlrp3*-knockout chronic BDL model showed diverse roles of NLRP3 in acute and chronic cholestatic liver injury (64). Mechanically, endoplasmic reticulum (ER) stress is the central process involved in NLRP3 inflammasome activation in hepatocytes. The IRE1α–sXBP1–ER stress signaling pathway mediated hepatocellular NLRP3 inflammasome activation (65). In comparison, this NLRP3 inflammasome activation was relieved in XBP1 knockout mice (65). In the LPS- and CCl_4-induced chronic liver injury model, NLRP3 inflammasome-mediated hepatocyte pyroptotic cell death was relieved after ER stress abrogation *via* either CHOP knockdown (66) or FXR regulation (67). The above studies demonstrate that ER stress-dependent inflammasome activation mediates chronic liver injury and fibrosis. However, further studies that use hepatocyte-specific NLRP3 deletion mice are urgently needed. Although many studies have revealed that NLPR3 is upregulated in hepatocytes, few studies have focused on the transcriptional regulation of NLRP3.

3.1.3 Other Hepatocellular Inflammasomes in Liver Fibrosis

In addition to NLRP3, other inflammasomes in hepatocytes are also involved in liver injury and liver fibrosis. AIM2 inflammasome activation by mtDNA resulted in increased expression of IL-1β and GSDMD in hepatocytes. The release of IL-1β promoted liver steatosis, inflammation, and activated IL-1 receptor on HSCs, contributing to the fibrogenic phenotype of HSCs (32); whereas HMGB1 redox status inhibited activation of caspase-1 through AIM2 inflammasome in chronic liver inflammation (33). In addition, NLRC4 inflammasome activation and pro-inflammatory cytokines induced by bacterial flagellin were rescued by hepatocyte Toll-Like Receptor 5 (27). The progression of NASH was attenuated by the deletion of NLRC4 inflammasome and the subsequent decrease in hepatocyte pyroptosis (68). The above studies show hepatocytes express and activate other inflammasomes, which participate in cellular communication with HSCs to induce liver fibrosis. Compared to the NLRP3 inflammasome, the effect of other inflammasomes remains unclear, and further studies are needed.

In summary, various chronic injuries lead to inflammasome assembly in hepatocytes *via* canonical and non-canonical signaling pathways. Then inflammasomes and pyroptosis in hepatocytes initiate liver fibrosis mainly *via* HSC activation.

3.2 Inflammasomes and Pyroptosis in Hepatic Macrophages

There are two phenotypes of macrophages in the liver: liver resident KCs and bone marrow-derived macrophages (BMDMs). KCs are the predominant macrophages in healthy conditions, whereas BMDMs infiltrate into the liver in response to danger signals (49, 69). Macrophages are recognized as the primary source of inflammasomes and pro-inflammatory cytokines (70). Generally, inflammasome activation and the subsequent pyroptosis in macrophages promote chronic liver inflammation by IL-1 and DAMPs release, which bind to receptors on HSCs and initiate HSCs-mediated fibrosis from various etiologies.

3.2.1 Hepatic Macrophage NLRP3 Inflammasome in NAFLD and NASH-Related Liver Fibrosis

In NASH models, the NLRP3 inflammasome activation in KCs or BMDMs caused inflammatory cytokine production, contributing to lipid synthesis in hepatocytes and fibrotic collagen production in HSCs (71–73). Furthermore, macrophage-specific *Nrf2* knockout aggravated NASH progression by initiating ROS and IL-1β in a yes-associated protein (YAP)–NLRP3-dependent manner (74). This finding demonstrates the role of ROS in activating the NLRP3 inflammasome in NASH. Similarly, the activation of the kinase receptor-interacting protein 1 (RIP1) in BMDMs, which induced inflammasome assembly and pyroptotic cell death, also contributed to the pathogenesis of NASH (75). Mechanically, NLRP3-mediated M1 macrophage polarization was blocked by the TGR5 signaling pathway, which further restored liver steatosis, inflammatory infiltration, and liver fibrosis (76). TLR2 and palmitic acid cooperatively stimulated the NLRP3 inflammasome in KCs and BMDMs. Then the activated NLRP3 inflammasome enhanced macrophage autophagy *via* the release of IL-1β to induce HSC activation (77, 78). Accordingly, inhibiting the NLRP3 inflammasome by TIM-4 *via* LKB1–AMPKα-mediated autophagy in macrophages suppressed the progression of NAFLD (79).

Moreover, the caspase-1–IL-1β signaling pathway in macrophages leads to lipid accumulation, inflammatory infiltration, and liver fibrosis in NASH mouse models by mediating macrophage–hepatocyte and macrophage–HSC interactions (80). However, this progression was blocked by ezetimibe administration in an autophagy-dependent manner (80). Consistently, by exposing hepatocytes and KCs to cholesterol crystals, NLRP3 inflammasome activation was demonstrated to be involved in the development of NASH (81). The above investigations confirmed the vital role of autophagy in regulating macrophage-derived inflammasome assembly in NASH. Nevertheless, the role of macrophage-derived autophagy in inducing disrupted cross-talk in sinusoids and liver fibrosis in NASH remains unclear. Further

studies that focus on cellular cross-talk in the sinusoids are urgently needed.

3.2.2 Hepatic Macrophage NLRP3 Inflammasome in Liver Fibrosis

NLRP3 inflammasome activation in KCs and BMDMs drove the caspase-1 signaling pathway, leading to IL-1 secretion and pyroptotic death in response to LPS-induced injury *in vivo* and *in vitro (*82, 83). However, NLRP3 inflammasome-derived IL-1β secretion and pyroptosis in macrophages and collagens deposition were blocked by pharmaceutical inhibition or genetic knockdown of COX-2 (84). Consistently, COX-2 promotes the development of liver cirrhosis (85) by inducing ROS (86, 87) and ER stress (88), indicating that COX-2 might contribute to liver cirrhosis *via* macrophage-derived inflammasomes. However, further studies are needed to determine how COX-2 regulates the activation of macrophage-derived inflammasomes and pyroptosis of macrophages in the context of liver fibrosis.

Studies confirmed that NLRP3 activation was not only required for hepatic inflammation and fibrosis but also as an essential mediator to amplify and perpetuate programmed inflammatory pyroptotic cell death (55). LPS from the damaged gut barrier and endogenous danger signals from hepatocytes damaged by ethanol (extracellular ATP and uric acid) are responsible for macrophage recruitment and subsequent inflammatory cytokine processing and pyroptotic cell death (89–92). The process is termed classically activated (M1) macrophage polarization (93). Increased NLRP3 and subsequent IL-1β maturation and secretion in macrophages exacerbated liver inflammation and fibrosis in ALD *via* induction of IL-1 receptor expression on HSCs and facilitated ECM secretion and formation (91). However, macrophage-specific *Atg5* knockout promoted caspase-1 activation, and pro-inflammatory M1 macrophage polarization, resulting in liver fibrosis during chronic ethanol exposure. Autophagy, a conserved cellular process to remove the damaged or unnecessary component, plays an important role in negatively regulating NLRP3 inflammasome in macrophages by degrading mitochondrial-derived DAMPs and inflammasome complexes. Research has demonstrated that autophagy in macrophages is protective against alcohol-induced liver injury in an NLRP3 inflammasome-dependent manner (94). Taken together, NLRP3 inflammasome induction in macrophages polarizes M1 phenotype, which is under the negative regulation of the autophagy signaling pathway.

Patients with chronic HCV infection and cirrhosis have elevated serum Il-1β and IL-18 levels (95, 96). Increased serum IL-1β and IL-18 are the components of NLRP3 inflammasome activation in response to HCV uptake by liver macrophages (95, 96). The current results confirm that NLRP3 inflammasome assembly and activation are central to mitigating HCV-related inflammation and fibrosis (95–97). Besides, NLRP3 inflammasomes expressed in KCs cause inflammatory cytokine production and fibrotic collagen formation in schistosomiasis-induced liver fibrosis (SSLF) (98) and idiosyncratic liver injury-induced fibrosis (99, 100). The above observation confirms that the NLRP3 inflammasomes in hepatic macrophages are crucial in initiating and propagating liver fibrosis from different etiologies.

3.2.3 Other Hepatic Macrophage Inflammasomes in Liver Fibrosis

Not only NLRP3 inflammasome but also other inflammasome complexes are involved in liver injury and liver fibrosis. Assembly of the AIM2 inflammasome in KCs led to the processing of IL-1β and IL-18 in response to hepatitis B virus infection, aggregating the development of liver cirrhosis (34, 101). Moreover, perfluorooctane sulfonate (PFOS), a chemical that causes chronic systematic inflammation, activated the AIM2 inflammasome *via* the Ca(2+)–PKC–NF-κB/JNK–BAX/BAK axis (35). In contrast, deletion of the AIM2 suppressed PFOS-induced inflammation and fibrosis in the liver and other organs (35). This study shows the critical role of the AIM2 inflammasome in toxin-induced chronic inflammation (35).

The NLRP6 inflammasome promotes the onset of hepatic granuloma and collagen deposition, indicating that NLRP6 is a crucial trigger for SSLF (102). Activation of the NLRC4 inflammasome and the subsequent pyroptosis and IL-18 and IL-1β secretion in macrophages promotes cross-talk with HSCs, exacerbating inflammation and fibrosis development in NAFLD (28). Furthermore, the NLRP12 inflammasome negatively modulated inflammatory responses by blocking the NF-κB and MAPK signaling pathways as well as IL-1β release from BMDMs in mouse liver and spleen against the infection of Brucella abortus, which is a kind of Gram-negative bacterium infection causing innate immunity and subsequent chronic inflammation in the host (103).

In summary, inflammasome activation mediates the polarization of liver macrophages and subsequent interaction with HSCs, contributing to the progression of liver fibrosis.

3.3 Inflammasomes and Pyroptosis in Cholangiocytes

Cholangiopathies, *e.g.*, primary sclerosing cholangitis (PSC) and primary biliary cholangitis (PBC), represent an autoimmune inflammatory liver disease characterized by chronic inflammation and subsequent sclerosis and destruction of intrahepatic small bile ducts (104). Increased NLRP3 expression in reactive cholangiocytes resulted in pro-inflammatory IL-18 production and influenced the epithelial integrity of cholangiocytes in both murine PSC model and patients with PSC (105). Meanwhile, inflammasome activation in cholangiocytes interacts with nuclear translocation of pSer675β-catenin and transcriptional activation, which recruits M1 macrophages in a CXC-chemokine ligand-1/10/12 (CXCL-1/10/12) dependent manner and activates HSCs in a transforming growth factor-β (TGF-β) dependent manner. These liver cell phenotype changes initiate biliary inflammation and fibrosis (106, 107). Furthermore, galectin-3, a pleiotropic lectin that mediates cell-cell adhesion, is secreted by these inflammatory macrophages and exacerbates cholangiocyte injury. While

inflammasome activation and PBC-induced fibrosis can be improved by deleting macrophage-derived galectin-3 expression in the mouse model (108).

3.4 Inflammasomes and Pyroptosis in HSCs

In addition to cross-talk through inflammasomes between other liver cell types and HSCs, HSC-derived inflammasomes can be remarkably induced in pathological conditions. Inflammasome activation in HSCs initiates a range of functional changes such as transdifferentiating into a fibrogenic activated phenotype, as well as inhibition of chemotaxis (109).

3.4.1 HSC NLRP3 Inflammasome in Liver Fibrosis

Palmitic acid upregulated the NLRP3–IL-1β axis in HSCs *via* the TLR4–MyD88–NF-κB signaling pathway (110) and hedgehog signaling pathway (111). Then the activated NLRP3 facilitates IL-1 receptor expression on HSCs and the consequent fibrotic induction with the development of NASH (111). Alternatively, the HSC-derived NLRP3 inflammasome could also be activated *via* the PDGFβR–NLRP3–caspase-1 signaling pathway (112), and result in increased expression of fibrotic markers alpha-smooth muscle actin (α-SMA), connective tissue growth factor (CTGF), and tissue inhibitors of matrix metalloproteinase 1 (TIMP1) in the CCl_4 mouse model. Mechanically, many molecules are involved in the activation of the NLRP3 inflammasome. ROS plays a vital role in activating the NLRP3–IL-1β signaling pathway in HSCs (113). Angiotensin II-mediated NLRP3 inflammasome assembly contributed to cholestatic liver fibrosis (114), whereas *Nlrp3* knockout or inhibition of Ang- (1–7) reduced ECM synthesis and deposition (115). The vitamin D receptor (VDR) agonist calcipotriol alleviated cholestatic fibrosis *via* YAP1 mediated inactivation of the NLRP3 inflammasome and caspase-1 (116). The P2X7 receptor, which binds with endogenous danger extracellular ATP, is involved in the immune response and inflammation by activating the NLRP3 inflammasome and increasing IL-1β production and pyroptosis in HSCs during the development of chronic alcoholic liver fibrosis (117). Meanwhile, the release of inflammasome components from pyroptotic HSCs, in turn, activates quiescent HSCs (117). Cysteine–cysteine chemokine ligand 5 (CCL5) secreted from macrophages, activated HSC-derived NLRP3, IL-1β, and IL-6 and upregulated liver fibrosis markers α-SMA and TGF-β1 (118). In contrast, blocking antibodies against CCL5 inhibited HSCs activation and HCV-related liver fibrosis (118).

3.4.2 HSC Inflammasomes in Infection-Related and Hormone-Related Liver Fibrosis

Brucella abortus infection not only affected macrophages but also triggered NLRP3 and AIM2 inflammasome assembly in HSCs, which eventually led to collagens deposition in mouse liver (119). Schistosoma Japonicum is a parasite that causes granulomatous inflammation and tissue damage. Infection with Schistosoma Japonicum stimulated the NLRP3 inflammasome *via* Dectin-1, and JNK signaling pathways, contributing to SSLF (120). Aldosterone, the main mineralocorticoid steroid hormone secreted by the adrenal gland, was shown to play a role in regulating myofibroblast contraction and proliferation by assembly of NLRP3 inflammasome in HSCs. NLRP3 depletion in primary mouse HSCs attenuated liver fibrosis in the presence of aldosterone, indicating the crucial role of NLRP3 inflammasome in aldosterone-mediated liver fibrosis (121).

The above research indicates that the NLRP3 inflammasome is the most well-studied inflammasome in HSCs. Whether other inflammasomes in HSCs are also involved in the development of liver fibrosis remains unclear.

3.5 Inflammasomes and Pyroptosis in Other Liver Cells

Apart from the abovementioned cells, inflammasome activation has also existed in other liver cells. DAMPs from fatty hepatocytes initiate NLRP3 inflammasome complex assembly *via* the P2X7 receptor on sinusoidal lining cells such as LSECs (122), resulting in NASH-associated fibrosis (123). Inflammasome activation in natural killer (NK) cells promotes HSC apoptosis and alleviates the progression of liver fibrosis in a TRAIL-dependent degranulation manner (124). In contrast, natural killer T (NKT) cells had dual roles in regulating liver fibrosis *via* activating the NLRP3 inflammasome (125). Besides, the NLRC4 inflammasome in neutrophils initiated auto-inflammatory disease, and these effects were attenuated in Asc knockout mice or after IL-1 receptor inhibitor administration (126).

The impact of the different inflammasomes in individual cells varies in liver diseases and animal models. Research that uses high-throughput technologies might help us establish the landscape of inflammasomes in liver cells cross-talk. Additionally, more attention should be paid to the mechanism of inflammasome-induced pyroptosis of individual liver cells during different pathological stimulations.

4 INFLAMMASOME-TARGETING THERAPIES IN LIVER FIBROSIS

An increasing number of studies have confirmed the involvement of inflammasomes in the development of chronic inflammation-induced liver fibrosis, indicating the possibility of therapies targeting inflammasome complex activation as well as signaling pathways involved in IL-1β and IL-18. Here, we summarized the pharmacological therapies targeting inflammasome- and pyroptosis-related signaling pathways on chronic liver injury-induced fibrosis from clinical trials and pre-clinical experimental studies (**Table 1**).

4.1 IL-1 Inhibitors

Macrophages, hepatocytes, and HSCs are the major cells that produce inflammasome-driven IL-1β due to ethanol and LPS stimulation. Recombinant IL-1R antagonist administration in mice inhibited the IL-1 signaling pathway and reversed alcohol-induced liver steatosis, inflammation, and fibrosis (91, 129). Anakinra, a recombinant form of human IL-1R antagonist, is

TABLE 1 | Potential Therapeutic Agents for liver fibrosis.

Targeting molecule	Therapeutic agent	Targeted disease	Species	Reference
IL-1 receptor Inhibitor	Anakinra	ALD, Diabetes; Toxin-induced liver fibrosis	Human; Mouse	(55, 91, 127–129)
IL-1 inhibitor	Canakinumab	ALD, CVD	Human	(122)
Caspase-1 inhibitor	Ac-YVAD	NASH associated fibrosis	Mouse	(130)
	Vx-166 (pan-caspases)	NASH associated fibrosis	Mouse	(131)
	Emricasan (pan-caspases)	NASH associated fibrosis	Mouse	(132)
NLRP3 inhibitor	MCC950	NASH associated fibrosis	Mouse	(133)
	P2X7R	Toxin-induced liver fibrosis; NASH associated fibrosis	Mouse; Human cell	(18, 134)

FDA approved medicine to treat rheumatoid arthritis and neonatal-onset multisystem inflammatory disease (135). It was shown that Anakinra could relieve macrophage infiltration, lipid accumulation, and liver fibrosis in a mouse model of ALD (129). Moreover, Anakinra treatment alleviated liver injury and inflammation without affecting fibrosis in a mouse model of CCl_4-induced liver fibrosis, as shown by a decrease in caspase-1 and IL-1β with unchanged CTGF and TIMP expression (55). Since good efficiency in treating experimental liver diseases, Anakinra combined with zinc and pentoxifylline is used to treat patients with severe alcoholic hepatitis and type 2 diabetes. Unfortunately, Anakinra did not affect 30-day mortality in research focused on 3-month and 6-month survival rates (ClinicalTrials.gov, AH/NCT01809132) (127). In another clinical trial, Anakinra was administered to patients with type 2 diabetes. They found a decrease in insulin resistance and systematic inflammation, which also participate in the progression of NASH (128). Further clinical trials on Anakinra in patients with NASH are needed. Canakinumab, a monoclonal antibody against IL-1β, was beneficial in patients with cardiovascular diseases (122), and a clinical trial about its effect on patients with severe alcoholic hepatitis is ongoing (ClinicalTrials.gov, AH/NCT03775109). Although many basic studies have shown beneficial effects by inhibiting the IL-1 singling pathway, few have been translated into clinical treatment of chronic liver diseases and liver fibrosis. More clinical trials are needed to explore the role of IL-1 in liver fibrosis.

4.2 Caspase-1 Inhibitors

The pan-caspase inhibitors, Vx-166 and Emricasan, showed a beneficial role in liver inflammation and fibrosis in NASH mice by decreasing the expression of IL-1β and IL-18 and inactivating HSCs (131, 132). A caspase-1 specific inhibitor, Ac-YVAD, was demonstrated to block liver steatosis and fibrosis in mice fed with HFD (130). In view of the excellent effect on animal models, clinical trials of caspase-1 inhibitors on chronic liver diseases are urgently needed in the future.

4.3 Inflammasomes and Their Upstream Inhibitors

The NLRP3 inflammasome inhibitor MCC950 was reported to relieve liver inflammation *via* polarizing macrophages into M2 phenotype in CCl_4-induced liver injury (136) and fibrosis *via* decreasing plasma and hepatic IL-1β and IL-6 in a mouse model of NASH (133), suggesting the pivotal role of MCC950 in attenuating liver inflammation from various etiologies. As the upstream molecule of the inflammasome, the P2X7 receptor induces inflammasome activation (18, 117). P2X7 receptor pharmacological inhibitor SGM-1019 was shown to block IL-1β secretion in KCs, HSC activation, and collagen deposition in human cells from NASH and in the primate model from CCl_4-induced liver fibrosis (134). Although inflammasome inhibitors showed promising effects in experimental models, whether these inhibitors could improve liver inflammation and fibrosis in patients with liver cirrhosis remains obscure.

5 FUTURE PERSPECTIVES

Inflammasome, a double-edged sword in liver injury, could protect the liver from pathogen infection, metabolism syndrome, and oxidative stress by eliminating the initial cause of cell injury and promoting wound healing. However, excessive and chronic inflammasome activation contributes to the pathogenesis of various liver diseases, which is the primary topic of our review. In summary, the pathological role of inflammasomes in liver fibrosis has gained substantial recognition from diverse chronic liver injury models. Exogenous and endogenous danger signals activate inflammasomes *via* canonical or non-canonical signaling pathways, leading to increased IL-1β, IL-18, and pyroptotic cell death. *In vivo* and *in vitro* studies over the recent years have evidenced central roles of IL-1β, IL-18, and pyroptotic cell death in NLRP3 inflammasome-induced biological responses, but the functions of the non-canonical inflammasome activation signaling pathway and other NLR genes in liver fibrosis remains poorly understood. Further studies are needed to explore the cellular source of other inflammasomes and their roles in liver fibrosis. In addition, the mechanism of GSDMD assembly leading to cell lysis is largely unknown. Apart from IL-1, inflammasomes also regulate the release of other immune factors, such as leukotrienes and prostaglandins (137), which could regulate liver fibrosis progression (85). Therefore, further studies are required to explore the potential mechanisms.

Quiescent HSCs change phenotypes and have different cell fates after stimuli, including activation, senescence, and inactivation. These phenotypes can be transdifferentiated from each other (5). Most studies illustrate that HSCs are activated by paracrine profibrogenic cytokines and danger signals, while

other molecules from pyroptotic cells that regulate HSC fate have scarcely been investigated. Specifically, it remains unclear whether inhibition of inflammasome-mediated cell interactions with HSCs could regress liver fibrosis. Although IL-1 from inflammatory hepatic macrophages could activate HSCs, the release of matrix metalloproteinases (MMPs) from these inflammatory macrophages degrades ECM and resolves fibrosis (138). Inflammasome-activated NK cells and NKT cells secreted inflammatory cytokine IL-1 to promote liver fibrogenesis, whereas IFN-γ secreted from the two kinds of cells have an antifibrotic role and trigger HSC apoptosis, promoting the regression of liver fibrosis (139, 140). Therefore, the cell-specific mechanisms of intercellular cross-talk in HSC activation need in-depth investigation.

In recent years, the pharmacological treatment of inflammasomes in chronic liver injury mainly focuses on IL-1β and IL-1 receptors. Research on blocking other molecules in the inflammasome pathway, such as caspase-1 and GSDMD, is missing. Though a recent study has shown that IL-18 inhibitor attenuates renal fibrosis in the ischemia-reperfusion murine model (141), there is no research on IL-18 inhibitors treating liver fibrosis in either animal models or human. Further studies are urgent to explore the potential of blocking IL-18, as well as caspase-1 and GSDMD in treating liver fibrosis. Although inflammasomes have been confirmed to have critical effects in many experimental animal models and *in vitro cell lines*, no direct evidence demonstrates that inflammasomes mediate liver fibrosis in humans. Organoids are self-organized 3D tissue cultures from stem cells that could recapitulate the function of the represented organ (142). Hence, organoids may be a novel research method to explore the mechanism of the inflammasome in regulating liver fibrosis. It is shown that bone marrow-derived mesenchymal stem cells (BM-MSCs) injection could decrease inflammasomes in the ischemic stroke rat model (143). Therefore, cell therapy by *in vivo* delivery of BM-MSCs may be helpful to mitigate inflammasomes during the development of liver fibrosis. Further studies are needed to target the novel direction. In summary, targeting inflammasome signaling pathways to treat liver fibrosis is promising, and more basic research and clinical trials are demanded in the future.

AUTHOR CONTRIBUTIONS

CT and JG designed and coordinated the study. CG, QC, CT, and JG analyzed articles and finalized the figures. CG, QC, and JG wrote the manuscript. All authors contributed to the article and approved the submitted version.

FUNDING

This work was supported by the National Natural Science Fund of China (82170623, 82170625, U1702281, 81873584, 82000613, and 82000574), National Key R&D Program of China (2017YFA0205404), Sichuan Science and Technology Program (2020YJ0084 and 2021YFS0147), and the 135 projects for disciplines of excellence of West China Hospital, Sichuan University (ZYGD18004).

REFERENCES

1. Broz P, Dixit VM. Inflammasomes: Mechanism of Assembly, Regulation and Signalling. *Nat Rev Immunol* (2016) 16(7):407–20. doi: 10.1038/nri.2016.58
2. Christgen S, Place DE, Kanneganti TD. Toward Targeting Inflammasomes: Insights Into Their Regulation and Activation. *Cell Res* (2020) 30(4):315–27. doi: 10.1038/s41422-020-0295-8
3. Zeng XH, Yuan XL, Cai QY, Tang CW, Gao JH. Circular Rna as an Epigenetic Regulator in Chronic Liver Diseases. *Cells* (2021) 10(8):1945–59. doi: 10.3390/cells10081945
4. Cai Q, Gan C, Tang C, Wu H, Gao J. Mechanism and Therapeutic Opportunities of Histone Modifications in Chronic Liver Disease. *Front Pharmacol* (2021) 12:784591. doi: 10.3389/fphar.2021.784591
5. Kisseleva T, Brenner D. Molecular and Cellular Mechanisms of Liver Fibrosis and Its Regression. *Nat Rev Gastroenterol Hepatol* (2021) 18 (3):151–66. doi: 10.1038/s41575-020-00372-7
6. Koyama Y, Brenner DA. Liver Inflammation and Fibrosis. *J Clin Invest* (2017) 127(1):55–64. doi: 10.1172/jci88881
7. Tsuchida T, Friedman SL. Mechanisms of Hepatic Stellate Cell Activation. *Nat Rev Gastroenterol Hepatol* (2017) 14(7):397–411. doi: 10.1038/nrgastro.2017.38
8. Cao S, Liu M, Sehrawat TS, Shah VH. Regulation and Functional Roles of Chemokines in Liver Diseases. *Nat Rev Gastroenterol Hepatol* (2021) 18 (9):630–47. doi: 10.1038/s41575-021-00444-2
9. Vanaja SK, Rathinam VA, Fitzgerald KA. Mechanisms of Inflammasome Activation: Recent Advances and Novel Insights. *Trends Cell Biol* (2015) 25 (5):308–15. doi: 10.1016/j.tcb.2014.12.009
10. Martínez-Cardona C, Lozano-Ruiz B, Bachiller V, Peiró G, Algaba-Chueca F, Gómez-Hurtado I, et al. Aim2 Deficiency Reduces the Development of Hepatocellular Carcinoma in Mice. *Int J Cancer* (2018) 143(11):2997–3007. doi: 10.1002/ijc.31827
11. Faustin B, Lartigue L, Bruey JM, Luciano F, Sergienko E, Bailly-Maitre B, et al. Reconstituted Nalp1 Inflammasome Reveals Two-Step Mechanism of Caspase-1 Activation. *Mol Cell* (2007) 25(5):713–24. doi: 10.1016/j.molcel.2007.01.032
12. Finger JN, Lich JD, Dare LC, Cook MN, Brown KK, Duraiswami C, et al. Autolytic Proteolysis Within the Function to Find Domain (Fiind) Is Required for Nlrp1 Inflammasome Activity. *J Biol Chem* (2012) 287 (30):25030–7. doi: 10.1074/jbc.M112.378323
13. Moayeri M, Sastalla I, Leppla SH. Anthrax and the Inflammasome. *Microbes Infect* (2012) 14(5):392–400. doi: 10.1016/j.micinf.2011.12.005
14. Pelegrin P, Surprenant A. Pannexin-1 Mediates Large Pore Formation and Interleukin-1beta Release by the Atp-Gated P2x7 Receptor. *EMBO J* (2006) 25(21):5071–82. doi: 10.1038/sj.emboj.7601378
15. Wickliffe KE, Leppla SH, Moayeri M. Anthrax Lethal Toxin-Induced Inflammasome Formation and Caspase-1 Activation Are Late Events Dependent on Ion Fluxes and the Proteasome. *Cell Microbiol* (2008) 10 (2):332–43. doi: 10.1111/j.1462-5822.2007.01044.x
16. Latz E, Xiao TS, Stutz A. Activation and Regulation of the Inflammasomes. *Nat Rev Immunol* (2013) 13(6):397–411. doi: 10.1038/nri3452
17. Duncan JA, Gao X, Huang MT, O'Connor BP, Thomas CE, Willingham SB, et al. Neisseria Gonorrhoeae Activates the Proteinase Cathepsin B to Mediate the Signaling Activities of the Nlrp3 and Asc-Containing Inflammasome. *J Immunol* (2009) 182(10):6460–9. doi: 10.4049/jimmunol.0802696

18. Mariathasan S, Weiss DS, Newton K, McBride J, O'Rourke K, Roose-Girma M, et al. Cryopyrin Activates the Inflammasome in Response to Toxins and Atp. *Nature* (2006) 440(7081):228–32. doi: 10.1038/nature04515
19. Martinon F, Pétrilli V, Mayor A, Tardivel A, Tschopp J. Gout-Associated Uric Acid Crystals Activate the Nalp3 Inflammasome. *Nature* (2006) 440 (7081):237–41. doi: 10.1038/nature04516
20. Halle A, Hornung V, Petzold GC, Stewart CR, Monks BG, Reinheckel T, et al. The Nalp3 Inflammasome Is Involved in the Innate Immune Response to Amyloid-Beta. *Nat Immunol* (2008) 9(8):857–65. doi: 10.1038/ni.1636
21. Woolbright BL, Jaeschke H. Role of the Inflammasome in Acetaminophen-Induced Liver Injury and Acute Liver Failure. *J Hepatol* (2017) 66(4):836–48. doi: 10.1016/j.jhep.2016.11.017
22. Szabo G, Csak T. Inflammasomes in Liver Diseases. *J Hepatol* (2012) 57 (3):642–54. doi: 10.1016/j.jhep.2012.03.035
23. Miao EA, Alpuche-Aranda CM, Dors M, Clark AE, Bader MW, Miller SI, et al. Cytoplasmic Flagellin Activates Caspase-1 and Secretion of Interleukin 1beta *Via* Ipaf. *Nat Immunol* (2006) 7(6):569–75. doi: 10.1038/ni1344
24. Mariathasan S, Newton K, Monack DM, Vucic D, French DM, Lee WP, et al. Differential Activation of the Inflammasome by Caspase-1 Adaptors Asc and Ipaf. *Nature* (2004) 430(6996):213–8. doi: 10.1038/nature02664
25. Miao EA, Mao DP, Yudkovsky N, Bonneau R, Lorang CG, Warren SE, et al. Innate Immune Detection of the Type Iii Secretion Apparatus Through the Nlrc4 Inflammasome. *Proc Natl Acad Sci U S A* (2010) 107(7):3076–80. doi: 10.1073/pnas.0913087107
26. Tenthorey JL, Kofoed EM, Daugherty MD, Malik HS, Vance RE. Molecular Basis for Specific Recognition of Bacterial Ligands by Naip/Nlrc4 Inflammasomes. *Mol Cell* (2014) 54(1):17–29. doi: 10.1016/j.molcel.2014.02.018
27. Etienne-Mesmin L, Vijay-Kumar M, Gewirtz AT, Chassaing B. Hepatocyte Toll-Like Receptor 5 Promotes Bacterial Clearance and Protects Mice Against High-Fat Diet-Induced Liver Disease. *Cell Mol Gastroenterol Hepatol* (2016) 2(5):584–604. doi: 10.1016/j.jcmgh.2016.04.007
28. Chen Y, Ma K. Nlrc4 Inflammasome Activation Regulated by Tnf-α Promotes Inflammatory Responses in Nonalcoholic Fatty Liver Disease. *Biochem Biophys Res Commun* (2019) 511(3):524–30. doi: 10.1016/j.bbrc.2019.02.099
29. Rathinam VA, Jiang Z, Waggoner SN, Sharma S, Cole LE, Waggoner L, et al. The Aim2 Inflammasome Is Essential for Host Defense Against Cytosolic Bacteria and DNA Viruses. *Nat Immunol* (2010) 11(5):395–402. doi: 10.1038/ni.1864
30. Hornung V, Ablasser A, Charrel-Dennis M, Bauernfeind F, Horvath G, Caffrey DR, et al. Aim2 Recognizes Cytosolic Dsdna and Forms a Caspase-1-Activating Inflammasome With Asc. *Nature* (2009) 458(7237):514–8. doi: 10.1038/nature07725
31. Mambwe B, Neo K, Javanmard Khameneh H, Leong KWK, Colantuoni M, Vacca M, et al. Tyrosine Dephosphorylation of Asc Modulates the Activation of the Nlrp3 and Aim2 Inflammasomes. *Front Immunol* (2019) 10:1556. doi: 10.3389/fimmu.2019.01556
32. Xu L, Zhou J, Che J, Wang H, Yang W, Zhou W, et al. Mitochondrial DNA Enables Aim2 Inflammasome Activation and Hepatocyte Pyroptosis in Nonalcoholic Fatty Liver Disease. *Am J Physiol Gastrointest Liver Physiol* (2021) 320(6):G1034–g44. doi: 10.1152/ajpgi.00431.2020
33. Sun Q, Loughran P, Shapiro R, Shrivastava IH, Antoine DJ, Li T, et al. Redox-Dependent Regulation of Hepatocyte Absent in Melanoma 2 Inflammasome Activation in Sterile Liver Injury in Mice. *Hepatology* (2017) 65(1):253–68. doi: 10.1002/hep.28893
34. Lozano-Ruiz B, Bachiller V, García-Martínez I, Zapater P, Gómez-Hurtado I, Moratalla A, et al. Absent in Melanoma 2 Triggers a Heightened Inflammasome Response in Ascitic Fluid Macrophages of Patients With Cirrhosis. *J Hepatol* (2015) 62(1):64–71. doi: 10.1016/j.jhep.2014.08.027
35. Wang LQ, Liu T, Yang S, Sun L, Zhao ZY, Li LY, et al. Perfluoroalkyl Substance Pollutants Activate the Innate Immune System Through the Aim2 Inflammasome. *Nat Commun* (2021) 12(1):2915. doi: 10.1038/s41467-021-23201-0
36. Schnappauf O, Chae JJ, Kastner DL, Aksentijevich I. The Pyrin Inflammasome in Health and Disease. *Front Immunol* (2019) 10:1745. doi: 10.3389/fimmu.2019.01745
37. Heilig R, Broz P. Function and Mechanism of the Pyrin Inflammasome. *Eur J Immunol* (2018) 48(2):230–8. doi: 10.1002/eji.201746947
38. Mulvihill E, Sborgi L, Mari SA, Pfreundschuh M, Hiller S, Müller DJ. Mechanism of Membrane Pore Formation by Human Gasdermin-D. *EMBO J* (2018) 37(14):e98321–31. doi: 10.15252/embj.201798321
39. Rathinam VA, Fitzgerald KA. Inflammasome Complexes: Emerging Mechanisms and Effector Functions. *Cell* (2016) 165(4):792–800. doi: 10.1016/j.cell.2016.03.046
40. He WT, Wan H, Hu L, Chen P, Wang X, Huang Z, et al. Gasdermin D Is an Executor of Pyroptosis and Required for Interleukin-1β Secretion. *Cell Res* (2015) 25(12):1285–98. doi: 10.1038/cr.2015.139
41. Shi J, Zhao Y, Wang K, Shi X, Wang Y, Huang H, et al. Cleavage of Gsdmd by Inflammatory Caspases Determines Pyroptotic Cell Death. *Nature* (2015) 526(7575):660–5. doi: 10.1038/nature15514
42. Kist M, Vucic D. Cell Death Pathways: Intricate Connections and Disease Implications. *EMBO J* (2021) 40(5):e106700. doi: 10.15252/embj.2020106700
43. Kayagaki N, Stowe IB, Lee BL, O'Rourke K, Anderson K, Warming S, et al. Caspase-11 Cleaves Gasdermin D for Non-Canonical Inflammasome Signalling. *Nature* (2015) 526(7575):666–71. doi: 10.1038/nature15541
44. Bauernfeind FG, Horvath G, Stutz A, Alnemri ES, MacDonald K, Speert D, et al. Cutting Edge: Nf-Kappab Activating Pattern Recognition and Cytokine Receptors License Nlrp3 Inflammasome Activation by Regulating Nlrp3 Expression. *J Immunol* (2009) 183(2):787–91. doi: 10.4049/jimmunol.0901363
45. Zhou R, Yazdi AS, Menu P, Tschopp J. A Role for Mitochondria in Nlrp3 Inflammasome Activation. *Nature* (2011) 469(7329):221–5. doi: 10.1038/nature09663
46. Rühl S, Broz P. Caspase-11 Activates a Canonical Nlrp3 Inflammasome by Promoting K(+) Efflux. *Eur J Immunol* (2015) 45(10):2927–36. doi: 10.1002/eji.201545772
47. Parola M, Pinzani M. Liver Fibrosis: Pathophysiology, Pathogenetic Targets and Clinical Issues. *Mol Aspects Med* (2019) 65:37–55. doi: 10.1016/j.mam.2018.09.002
48. Marrone G, Shah VH, Gracia-Sancho J. Sinusoidal Communication in Liver Fibrosis and Regeneration. *J Hepatol* (2016) 65(3):608–17. doi: 10.1016/j.jhep.2016.04.018
49. Gao J, Wei B, Liu M, Hirsova P, Sehrawat TS, Cao S, et al. Endothelial P300 Promotes Portal Hypertension and Hepatic Fibrosis Through C-C Motif Chemokine Ligand 2-Mediated Angiocrine Signaling. *Hepatology* (2021) 73 (6):2468–83. doi: 10.1002/hep.31617
50. Gao J, Wei B, de Assuncao TM, Liu Z, Hu X, Ibrahim S, et al. Hepatic Stellate Cell Autophagy Inhibits Extracellular Vesicle Release to Attenuate Liver Fibrosis. *J Hepatol* (2020) 73(5):1144–54. doi: 10.1016/j.jhep.2020.04.044
51. Strowig T, Henao-Mejia J, Elinav E, Flavell R. Inflammasomes in Health and Disease. *Nature* (2012) 481(7381):278–86. doi: 10.1038/nature10759
52. Szabo G, Petrasek J. Inflammasome Activation and Function in Liver Disease. *Nat Rev Gastroenterol Hepatol* (2015) 12(7):387–400. doi: 10.1038/nrgastro.2015.94
53. Schuster-Gaul S, Geisler LJ, McGeough MD, Johnson CD, Zagorska A, Li L, et al. Ask1 Inhibition Reduces Cell Death and Hepatic Fibrosis in an Nlrp3 Mutant Liver Injury Model. *JCI Insight* (2020) 5(2):e123294–308. doi: 10.1172/jci.insight.123294
54. Luan J, Ju D. Inflammasome: A Double-Edged Sword in Liver Diseases. *Front Immunol* (2018) 9:2201. doi: 10.3389/fimmu.2018.02201
55. Wree A, Eguchi A, McGeough MD, Pena CA, Johnson CD, Canbay A, et al. Nlrp3 Inflammasome Activation Results in Hepatocyte Pyroptosis, Liver Inflammation, and Fibrosis in Mice. *Hepatology* (2014) 59(3):898–910. doi: 10.1002/hep.26592
56. Zhang X, Zhang JH, Chen XY, Hu QH, Wang MX, Jin R, et al. Reactive Oxygen Species-Induced Txnip Drives Fructose-Mediated Hepatic Inflammation and Lipid Accumulation Through Nlrp3 Inflammasome Activation. *Antioxid Redox Signal* (2015) 22(10):848–70. doi: 10.1089/ars.2014.5868
57. Wan X, Xu C, Lin Y, Lu C, Li D, Sang J, et al. Uric Acid Regulates Hepatic Steatosis and Insulin Resistance Through the Nlrp3 Inflammasome-Dependent Mechanism. *J Hepatol* (2016) 64(4):925–32. doi: 10.1016/j.jhep.2015.11.022

58. Zhang NP, Liu XJ, Xie L, Shen XZ, Wu J. Impaired Mitophagy Triggers Nlrp3 Inflammasome Activation During the Progression From Nonalcoholic Fatty Liver to Nonalcoholic Steatohepatitis. *Lab Invest* (2019) 99(6):749–63. doi: 10.1038/s41374-018-0177-6
59. Yu X, Hao M, Liu Y, Ma X, Lin W, Xu Q, et al. Liraglutide Ameliorates Non-Alcoholic Steatohepatitis by Inhibiting Nlrp3 Inflammasome and Pyroptosis Activation *Via* Mitophagy. *Eur J Pharmacol* (2019) 864:172715. doi: 10.1016/j.ejphar.2019.172715
60. Zhu Y, Zhao H, Lu J, Lin K, Ni J, Wu G, et al. Caspase-11-Mediated Hepatocytic Pyroptosis Promotes the Progression of Nonalcoholic Steatohepatitis. *Cell Mol Gastroenterol Hepatol* (2021) 12(2):653–64. doi: 10.1016/j.jcmgh.2021.04.009
61. Gaul S, Leszczynska A, Alegre F, Kaufmann B, Johnson CD, Adams LA, et al. Hepatocyte Pyroptosis and Release of Inflammasome Particles Induce Stellate Cell Activation and Liver Fibrosis. *J Hepatol* (2021) 74(1):156–67. doi: 10.1016/j.jhep.2020.07.041
62. Heo MJ, Kim TH, You JS, Blaya D, Sancho-Bru P, Kim SG. Alcohol Dysregulates Mir-148a in Hepatocytes Through Foxo1, Facilitating Pyroptosis *Via* Txnip Overexpression. *Gut* (2019) 68(4):708–20. doi: 10.1136/gutjnl-2017-315123
63. Khanova E, Wu R, Wang W, Yan R, Chen Y, French SW, et al. Pyroptosis by Caspase11/4-Gasdermin-D Pathway in Alcoholic Hepatitis in Mice and Patients. *Hepatology* (2018) 67(5):1737–53. doi: 10.1002/hep.29645
64. Frissen M, Liao L, Schneider KM, Djudjaj S, Haybaeck J, Wree A, et al. Bidirectional Role of Nlrp3 During Acute and Chronic Cholestatic Liver Injury. *Hepatology* (2021) 73(5):1836–54. doi: 10.1002/hep.31494
65. Lebeaupin C, Vallée D, Rousseau D, Patouraux S, Bonnafous S, Adam G, et al. Bax Inhibitor-1 Protects From Nonalcoholic Steatohepatitis by Limiting Inositol-Requiring Enzyme 1 Alpha Signaling in Mice. *Hepatology* (2018) 68(2):515–32. doi: 10.1002/hep.29847
66. Lebeaupin C, Proics E, de Bieville CH, Rousseau D, Bonnafous S, Patouraux S, et al. Er Stress Induces Nlrp3 Inflammasome Activation and Hepatocyte Death. *Cell Death Dis* (2015) 6(9):e1879. doi: 10.1038/cddis.2015.248
67. Han CY, Rho HS, Kim A, Kim TH, Jang K, Jun DW, et al. Fxr Inhibits Endoplasmic Reticulum Stress-Induced Nlrp3 Inflammasome in Hepatocytes and Ameliorates Liver Injury. *Cell Rep* (2018) 24(11):2985–99. doi: 10.1016/j.celrep.2018.07.068
68. Koh EH, Yoon JE, Ko MS, Leem J, Yun JY, Hong CH, et al. Sphingomyelin Synthase 1 Mediates Hepatocyte Pyroptosis to Trigger Non-Alcoholic Steatohepatitis. *Gut* (2021) 70(10):1954–64. doi: 10.1136/gutjnl-2020-322509
69. Kazankov K, Jørgensen SMD, Thomsen KL, Møller HJ, Vilstrup H, George J, et al. The Role of Macrophages in Nonalcoholic Fatty Liver Disease and Nonalcoholic Steatohepatitis. *Nat Rev Gastroenterol Hepatol* (2019) 16 (3):145–59. doi: 10.1038/s41575-018-0082-x
70. Tacke F. Targeting Hepatic Macrophages to Treat Liver Diseases. *J Hepatol* (2017) 66(6):1300–12. doi: 10.1016/j.jhep.2017.02.026
71. Wang X, Gao Y, Song J, Tang C, Wang M, Que L, et al. The Tir/Bb-Loop Mimetic as-1 Prevents Non-Alcoholic Steatohepatitis and Hepatic Insulin Resistance by Inhibiting Nlrp3-Asc Inflammasome Activation. *Br J Pharmacol* (2017) 174(12):1841–56. doi: 10.1111/bph.13786
72. Wang F, Park JS, Ma Y, Ma H, Lee YJ, Lee GR, et al. Ginseng Saponin Enriched in Rh1 and Rg2 Ameliorates Nonalcoholic Fatty Liver Disease by Inhibiting Inflammasome Activation. *Nutrients* (2021) 13(3):856–72. doi: 10.3390/nu13030856
73. Mohammed S, Nicklas EH, Thadathil N, Selvarani R, Royce GH, Kinter M, et al. Role of Necroptosis in Chronic Hepatic Inflammation and Fibrosis in a Mouse Model of Increased Oxidative Stress. *Free Radic Biol Med* (2021) 164:315–28. doi: 10.1016/j.freeradbiomed.2020.12.449
74. Wang P, Ni M, Tian Y, Wang H, Qiu J, You W, et al. Myeloid Nrf2 Deficiency Aggravates Non-Alcoholic Steatohepatitis Progression by Regulating Yap-Mediated Nlrp3 Inflammasome Signaling. *iScience* (2021) 24(5):102427. doi: 10.1016/j.isci.2021.102427
75. Tao L, Yi Y, Chen Y, Zhang H, Orning P, Lien E, et al. Rip1 Kinase Activity Promotes Steatohepatitis Through Mediating Cell Death and Inflammation in Macrophages. *Cell Death Differ* (2021) 28(4):1418–33. doi: 10.1038/s41418-020-00668-w
76. Shi Y, Su W, Zhang L, Shi C, Zhou J, Wang P, et al. Tgr5 Regulates Macrophage Inflammation in Nonalcoholic Steatohepatitis by Modulating Nlrp3 Inflammasome Activation. *Front Immunol* (2020) 11:609060. doi: 10.3389/fimmu.2020.609060
77. Miura K, Yang L, van Rooijen N, Brenner DA, Ohnishi H, Seki E. Toll-Like Receptor 2 and Palmitic Acid Cooperatively Contribute to the Development of Nonalcoholic Steatohepatitis Through Inflammasome Activation in Mice. *Hepatology* (2013) 57(2):577–89. doi: 10.1002/hep.26081
78. Shen L, Yang Y, Ou T, Key CC, Tong SH, Sequeira RC, et al. Dietary Pufas Attenuate Nlrp3 Inflammasome Activation *Via* Enhancing Macrophage Autophagy. *J Lipid Res* (2017) 58(9):1808–21. doi: 10.1194/jlr.M075879
79. Liu W, Bai F, Wang H, Liang Y, Du X, Liu C, et al. Tim-4 Inhibits Nlrp3 Inflammasome *Via* the Lkb1/Ampkα Pathway in Macrophages. *J Immunol* (2019) 203(4):990–1000. doi: 10.4049/jimmunol.1900117
80. Kim SH, Kim G, Han DH, Lee M, Kim I, Kim B, et al. Ezetimibe Ameliorates Steatohepatitis *Via* Amp Activated Protein Kinase-Tfeb-Mediated Activation of Autophagy and Nlrp3 Inflammasome Inhibition. *Autophagy* (2017) 13(10):1767–81. doi: 10.1080/15548627.2017.1356977
81. Ioannou GN, Van Rooyen DM, Savard C, Haigh WG, Yeh MM, Teoh NC, et al. Cholesterol-Lowering Drugs Cause Dissolution of Cholesterol Crystals and Disperse Kupffer Cell Crown-Like Structures During Resolution of Nash. *J Lipid Res* (2015) 56(2):277–85. doi: 10.1194/jlr.M053785
82. Antonopoulos C, Russo HM, El Sanadi C, Martin BN, Li X, Kaiser WJ, et al. Caspase-8 as an Effector and Regulator of Nlrp3 Inflammasome Signaling. *J Biol Chem* (2015) 290(33):20167–84. doi: 10.1074/jbc.M115.652321
83. Zhang X, Wang G, Gurley EC, Zhou H. Flavonoid Apigenin Inhibits Lipopolysaccharide-Induced Inflammatory Response Through Multiple Mechanisms in Macrophages. *PloS One* (2014) 9(9):e107072. doi: 10.1371/journal.pone.0107072
84. Hua KF, Chou JC, Ka SM, Tasi YL, Chen A, Wu SH, et al. Cyclooxygenase-2 Regulates Nlrp3 Inflammasome-Derived Il-1β Production. *J Cell Physiol* (2015) 230(4):863–74. doi: 10.1002/jcp.24815
85. Gao JH, Wen SL, Feng S, Yang WJ, Lu YY, Tong H, et al. Celecoxib and Octreotide Synergistically Ameliorate Portal Hypertension *Via* Inhibition of Angiogenesis in Cirrhotic Rats. *Angiogenesis* (2016) 19(4):501–11. doi: 10.1007/s10456-016-9522-9
86. Tai Y, Zhao C, Zhang L, Tang S, Jia X, Tong H, et al. Celecoxib Reduces Hepatic Vascular Resistance in Portal Hypertension by Amelioration of Endothelial Oxidative Stress. *J Cell Mol Med* (2021) 25(22):10389–402. doi: 10.1111/jcmm.16968
87. Tang S, Huang Z, Jiang J, Gao J, Zhao C, Tai Y, et al. Celecoxib Ameliorates Liver Cirrhosis *Via* Reducing Inflammation and Oxidative Stress Along Spleen-Liver Axis in Rats. *Life Sci* (2021) 272:119203. doi: 10.1016/j.lfs.2021.119203
88. Su W, Tai Y, Tang SH, Ye YT, Zhao C, Gao JH, et al. Celecoxib Attenuates Hepatocyte Apoptosis by Inhibiting Endoplasmic Reticulum Stress in Thioacetamide-Induced Cirrhotic Rats. *World J Gastroenterol* (2020) 26 (28):4094–107. doi: 10.3748/wjg.v26.i28.4094
89. Shang Y, Li XF, Jin MJ, Li Y, Wu YL, Jin Q, et al. Leucodin Attenuates Inflammatory Response in Macrophages and Lipid Accumulation in Steatotic Hepatocytes *Via* P2x7 Receptor Pathway: A Potential Role in Alcoholic Liver Disease. *BioMed Pharmacother* (2018) 107:374–81. doi: 10.1016/j.biopha.2018.08.009
90. Petrasek J, Iracheta-Vellve A, Saha B, Satishchandran A, Kodys K, Fitzgerald KA, et al. Metabolic Danger Signals, Uric Acid and Atp, Mediate Inflammatory Cross-Talk Between Hepatocytes and Immune Cells in Alcoholic Liver Disease. *J Leukoc Biol* (2015) 98(2):249–56. doi: 10.1189/jlb.3AB1214-590R
91. Mathews S, Gao B. Therapeutic Potential of Interleukin 1 Inhibitors in the Treatment of Alcoholic Liver Disease. *Hepatology* (2013) 57(5):2078–80. doi: 10.1002/hep.26336
92. Kim JW, Roh YS, Jeong H, Yi HK, Lee MH, Lim CW, et al. Spliceosome-Associated Protein 130 Exacerbates Alcohol-Induced Liver Injury by Inducing Nlrp3 Inflammasome-Mediated Il-1β in Mice. *Am J Pathol* (2018) 188(4):967–80. doi: 10.1016/j.ajpath.2017.12.010
93. Orecchioni M, Ghosheh Y, Pramod AB, Ley K. Macrophage Polarization: Different Gene Signatures in M1(Lps+) Vs. Classically and M2(Lps-) Vs.

Alternatively Activated Macrophages. *Front Immunol* (2019) 10:1084. doi: 10.3389/fimmu.2019.01084
94. Ilyas G, Cingolani F, Zhao E, Tanaka K, Czaja MJ. Decreased Macrophage Autophagy Promotes Liver Injury and Inflammation From Alcohol. *Alcohol Clin Exp Res* (2019) 43(7):1403–13. doi: 10.1111/acer.14041
95. Negash AA, Ramos HJ, Crochet N, Lau DT, Doehle B, Papic N, et al. Il-1β Production Through the Nlrp3 Inflammasome by Hepatic Macrophages Links Hepatitis C Virus Infection With Liver Inflammation and Disease. *PloS Pathog* (2013) 9(4):e1003330. doi: 10.1371/journal.ppat.1003330
96. Serti E, Werner JM, Chattergoon M, Cox AL, Lohmann V, Rehermann B. Monocytes Activate Natural Killer Cells *Via* Inflammasome-Induced Interleukin 18 in Response to Hepatitis C Virus Replication. *Gastroenterology* (2014) 147(1):209–20.e3. doi: 10.1053/j.gastro.2014.03.046
97. Negash AA, Olson RM, Griffin S, Gale MJr. Modulation of Calcium Signaling Pathway by Hepatitis C Virus Core Protein Stimulates Nlrp3 Inflammasome Activation. *PloS Pathog* (2019) 15(2):e1007593. doi: 10.1371/journal.ppat.1007593
98. Zhang WJ, Fang ZM, Liu WQ. Nlrp3 Inflammasome Activation From Kupffer Cells Is Involved in Liver Fibrosis of Schistosoma Japonicum-Infected Mice *Via* Nf-κb. *Parasit Vectors* (2019) 12(1):29. doi: 10.1186/s13071-018-3223-8
99. Wang Y, Xu G, Wang Z, Li R, Zhan X, Liu H, et al. Psoralidin, a Major Component of Psoraleae Fructus, Induces Inflammasome Activation and Idiosyncratic Liver Injury. *Int Immunopharmacol* (2021) 92:107352. doi: 10.1016/j.intimp.2020.107352
100. Jia Y, Ma L, Wang Y, Wang W, Shen C, Wang X, et al. Nlrp3 Inflammasome and Related Cytokines Reflect the Immune Status of Patients With Hbv-Aclf. *Mol Immunol* (2020) 120:179–86. doi: 10.1016/j.molimm.2020.01.011
101. Zannetti C, Roblot G, Charrier E, Ainouze M, Tout I, Briat F, et al. Characterization of the Inflammasome in Human Kupffer Cells in Response to Synthetic Agonists and Pathogens. *J Immunol* (2016) 197(1):356–67. doi: 10.4049/jimmunol.1502301
102. Sanches RCO, Souza C, Marinho FV, Mambelli FS, Morais SB, Guimarães ES, et al. Nlrp6 Plays an Important Role in Early Hepatic Immunopathology Caused by Schistosoma Mansoni Infection. *Front Immunol* (2020) 11:795. doi: 10.3389/fimmu.2020.00795
103. Silveira TN, Gomes MT, Oliveira LS, Campos PC, Machado GG, Oliveira SC. Nlrp12 Negatively Regulates Proinflammatory Cytokine Production and Host Defense Against Brucella Abortus. *Eur J Immunol* (2017) 47(1):51–9. doi: 10.1002/eji.201646502
104. Lazaridis KN, LaRusso NF. The Cholangiopathies. *Mayo Clin Proc* (2015) 90(6):791–800. doi: 10.1016/j.mayocp.2015.03.017
105. Maroni L, Agostinelli L, Saccomanno S, Pinto C, Giordano DM, Rychlicki C, et al. Nlrp3 Activation Induces Il-18 Synthesis and Affects the Epithelial Barrier Function in Reactive Cholangiocytes. *Am J Pathol* (2017) 187(2):366–76. doi: 10.1016/j.ajpath.2016.10.010
106. Fabris L, Fiorotto R, Spirli C, Cadamuro M, Mariotti V, Perugorria MJ, et al. Pathobiology of Inherited Biliary Diseases: A Roadmap to Understand Acquired Liver Diseases. *Nat Rev Gastroenterol Hepatol* (2019) 16(8):497–511. doi: 10.1038/s41575-019-0156-4
107. Lan T, Qian S, Tang C, Gao J. Role of Immune Cells in Biliary Repair. *Front Immunol* (2022) 13:866040. doi: 10.3389/fimmu.2022.866040
108. Tian J, Yang G, Chen HY, Hsu DK, Tomilov A, Olson KA, et al. Galectin-3 Regulates Inflammasome Activation in Cholestatic Liver Injury. *FASEB J* (2016) 30(12):4202–13. doi: 10.1096/fj.201600392RR
109. Watanabe A, Sohail MA, Gomes DA, Hashmi A, Nagata J, Sutterwala FS, et al. Inflammasome-Mediated Regulation of Hepatic Stellate Cells. *Am J Physiol Gastrointest Liver Physiol* (2009) 296(6):G1248–57. doi: 10.1152/ajpgi.90223.2008
110. Dong Z, Zhuang Q, Ning M, Wu S, Lu L, Wan X. Palmitic Acid Stimulates Nlrp3 Inflammasome Activation Through Tlr4-Nf-κb Signal Pathway in Hepatic Stellate Cells. *Ann Transl Med* (2020) 8(5):168. doi: 10.21037/atm.2020.02.21
111. Duan NN, Liu XJ, Wu J. Palmitic Acid Elicits Hepatic Stellate Cell Activation Through Inflammasomes and Hedgehog Signaling. *Life Sci* (2017) 176:42–53. doi: 10.1016/j.lfs.2017.03.012
112. Wu X, Zhang F, Xiong X, Lu C, Lian N, Lu Y, et al. Tetramethylpyrazine Reduces Inflammation in Liver Fibrosis and Inhibits Inflammatory Cytokine Expression in Hepatic Stellate Cells by Modulating Nlrp3 Inflammasome Pathway. *IUBMB Life* (2015) 67(4):312–21. doi: 10.1002/iub.1348
113. Zhao Y, Wang Z, Feng D, Zhao H, Lin M, Hu Y, et al. P66shc Contributes to Liver Fibrosis Through the Regulation of Mitochondrial Reactive Oxygen Species. *Theranostics* (2019) 9(5):1510–22. doi: 10.7150/thno.29620
114. Ning ZW, Luo XY, Wang GZ, Li Y, Pan MX, Yang RQ, et al. Microrna-21 Mediates Angiotensin Ii-Induced Liver Fibrosis by Activating Nlrp3 Inflammasome/Il-1β Axis *Via* Targeting Smad7 and Spry1. *Antioxid Redox Signal* (2017) 27(1):1–20. doi: 10.1089/ars.2016.6669
115. Cai SM, Yang RQ, Li Y, Ning ZW, Zhang LL, Zhou GS, et al. Angiotensin-(1-7) Improves Liver Fibrosis by Regulating the Nlrp3 Inflammasome *Via* Redox Balance Modulation. *Antioxid Redox Signal* (2016) 24(14):795–812. doi: 10.1089/ars.2015.6498
116. Wang X, Wang G, Qu J, Yuan Z, Pan R, Li K. Calcipotriol Inhibits Nlrp3 Signal Through Yap1 Activation to Alleviate Cholestatic Liver Injury and Fibrosis. *Front Pharmacol* (2020) 11:200. doi: 10.3389/fphar.2020.00200
117. Shan L, Jiang T, Ci L, Liu Z, Lv X, Li J. Purine Signaling Regulating Hscs Inflammatory Cytokines Secretion, Activation, and Proliferation Plays a Critical Role in Alcoholic Liver Disease. *Mol Cell Biochem* (2020) 466(1-2):91–102. doi: 10.1007/s11010-020-03691-0
118. Sasaki R, Devhare PB, Steele R, Ray R, Ray RB. Hepatitis C Virus-Induced Ccl5 Secretion From Macrophages Activates Hepatic Stellate Cells. *Hepatology* (2017) 66(3):746–57. doi: 10.1002/hep.29170
119. Arriola Benitez PC, Pesce Viglietti AI, Gomes MTR, Oliveira SC, Quarleri JF, Giambartolomei GH, et al. Brucella Abortus Infection Elicited Hepatic Stellate Cell-Mediated Fibrosis Through Inflammasome-Dependent Il-1β Production. *Front Immunol* (2019) 10:3036. doi: 10.3389/fimmu.2019.03036
120. Lu YQ, Zhong S, Meng N, Fan YP, Tang WX. Nlrp3 Inflammasome Activation Results in Liver Inflammation and Fibrosis in Mice Infected With Schistosoma Japonicum in a Syk-Dependent Manner. *Sci Rep* (2017) 7(1):8120. doi: 10.1038/s41598-017-08689-1
121. Li Y, Zhang Y, Chen T, Huang Y, Zhang Y, Geng S, et al. Role of Aldosterone in the Activation of Primary Mice Hepatic Stellate Cell and Liver Fibrosis *Via* Nlrp3 Inflammasome. *J Gastroenterol Hepatol* (2020) 35(6):1069–77. doi: 10.1111/jgh.14961
122. Ridker PM, Everett BM, Thuren T, MacFadyen JG, Chang WH, Ballantyne C, et al. Antiinflammatory Therapy With Canakinumab for Atherosclerotic Disease. *N Engl J Med* (2017) 377(12):1119–31. doi: 10.1056/NEJMoa1707914
123. Blasetti Fantauzzi C, Menini S, Iacobini C, Rossi C, Santini E, Solini A, et al. Deficiency of the Purinergic Receptor 2x(7) Attenuates Nonalcoholic Steatohepatitis Induced by High-Fat Diet: Possible Role of the Nlrp3 Inflammasome. *Oxid Med Cell Longev* (2017) 2017:8962458. doi: 10.1155/2017/8962458
124. Li T, Yang Y, Song H, Li H, Cui A, Liu Y, et al. Activated Nk Cells Kill Hepatic Stellate Cells *Via* P38/Pi3k Signaling in a Trail-Involved Degranulation Manner. *J Leukoc Biol* (2019) 105(4):695–704. doi: 10.1002/jlb.2a0118-031rr
125. Nilsson J, Hörnberg M, Schmidt-Christensen A, Linde K, Nilsson M, Carlus M, et al. Nkt Cells Promote Both Type 1 and Type 2 Inflammatory Responses in a Mouse Model of Liver Fibrosis. *Sci Rep* (2020) 10(1):21778. doi: 10.1038/s41598-020-78688-2
126. Nichols RD, von Moltke J, Vance RE. Naip/Nlrc4 Inflammasome Activation in Mrp8(+) Cells Is Sufficient to Cause Systemic Inflammatory Disease. *Nat Commun* (2017) 8(1):2209. doi: 10.1038/s41467-017-02266-w
127. Szabo G. Clinical Trial Design for Alcoholic Hepatitis. *Semin Liver Dis* (2017) 37(4):332–42. doi: 10.1055/s-0037-1608788
128. Larsen CM, Faulenbach M, Vaag A, Vølund A, Ehses JA, Seifert B, et al. Interleukin-1-Receptor Antagonist in Type 2 Diabetes Mellitus. *N Engl J Med* (2007) 356(15):1517–26. doi: 10.1056/NEJMoa065213
129. Petrasek J, Bala S, Csak T, Lippai D, Kodys K, Menashy V, et al. Il-1 Receptor Antagonist Ameliorates Inflammasome-Dependent Alcoholic Steatohepatitis in Mice. *J Clin Invest* (2012) 122(10):3476–89. doi: 10.1172/jci60777
130. Morrison MC, Mulder P, Salic K, Verheij J, Liang W, van Duyvenvoorde W, et al. Intervention With a Caspase-1 Inhibitor Reduces Obesity-Associated Hyperinsulinemia, Non-Alcoholic Steatohepatitis and Hepatic Fibrosis in

Ldlr-/-. *Leiden Mice Int J Obes (Lond)* (2016) 40(9):1416–23. doi: 10.1038/ijo.2016.74
131. Witek RP, Stone WC, Karaca FG, Syn WK, Pereira TA, Agboola KM, et al. Pan-Caspase Inhibitor Vx-166 Reduces Fibrosis in an Animal Model of Nonalcoholic Steatohepatitis. *Hepatology* (2009) 50(5):1421–30. doi: 10.1002/hep.23167
132. Barreyro FJ, Holod S, Finocchietto PV, Camino AM, Aquino JB, Avagnina A, et al. The Pan-Caspase Inhibitor Emricasan (Idn-6556) Decreases Liver Injury and Fibrosis in a Murine Model of Non-Alcoholic Steatohepatitis. *Liver Int* (2015) 35(3):953–66. doi: 10.1111/liv.12570
133. Mridha AR, Wree A, Robertson AAB, Yeh MM, Johnson CD, Van Rooyen DM, et al. Nlrp3 Inflammasome Blockade Reduces Liver Inflammation and Fibrosis in Experimental Nash in Mice. *J Hepatol* (2017) 66(5):1037–46. doi: 10.1016/j.jhep.2017.01.022
134. Baeza-Raja B, Goodyear A, Liu X, Lam K, Yamamoto L, Li Y, et al. Pharmacological Inhibition of P2rx7 Ameliorates Liver Injury by Reducing Inflammation and Fibrosis. *PloS One* (2020) 15(6):e0234038. doi: 10.1371/journal.pone.0234038
135. Gabay C, Lamacchia C, Palmer G. Il-1 Pathways in Inflammation and Human Diseases. *Nat Rev Rheumatol* (2010) 6(4):232–41. doi: 10.1038/nrrheum.2010.4
136. Yan W, Shen Y, Huang J, Lu L, Zhang Q. Mcc950 Ameliorates Acute Liver Injury Through Modulating Macrophage Polarization and Myeloid-Derived Suppressor Cells Function. *Front Med (Lausanne)* (2021) 8:752223. doi: 10.3389/fmed.2021.752223
137. von Moltke J, Trinidad NJ, Moayeri M, Kintzer AF, Wang SB, van Rooijen N, et al. Rapid Induction of Inflammatory Lipid Mediators by the Inflammasome *in Vivo*. *Nature* (2012) 490(7418):107–11. doi: 10.1038/nature11351
138. Ramachandran P, Pellicoro A, Vernon MA, Boulter L, Aucott RL, Ali A, et al. Differential Ly-6c Expression Identifies the Recruited Macrophage Phenotype, Which Orchestrates the Regression of Murine Liver Fibrosis. *Proc Natl Acad Sci U S A* (2012) 109(46):E3186–95. doi: 10.1073/pnas.1119964109
139. Weng H, Mertens PR, Gressner AM, Dooley S. Ifn-Gamma Abrogates Profibrogenic Tgf-Beta Signaling in Liver by Targeting Expression of Inhibitory and Receptor Smads. *J Hepatol* (2007) 46(2):295–303. doi: 10.1016/j.jhep.2006.09.014
140. Li X, Zhang M, Liu J, Huang Z, Zhao Q, Huang Y, et al. Intrahepatic Nk Cells Function Suppressed in Advanced Liver Fibrosis. *Eur J Clin Invest* (2016) 46(10):864–72. doi: 10.1111/eci.12669
141. Liang H, Xu F, Zhang T, Huang J, Guan Q, Wang H, et al. Inhibition of Il-18 Reduces Renal Fibrosis After Ischemia-Reperfusion. *BioMed Pharmacother* (2018) 106:879–89. doi: 10.1016/j.biopha.2018.07.031
142. Prior N, Inacio P, Huch M. Liver Organoids: From Basic Research to Therapeutic Applications. *Gut* (2019) 68(12):2228–37. doi: 10.1136/gutjnl-2019-319256
143. Sarmah D, Datta A, Kaur H, Kalia K, Borah A, Rodriguez AM, et al. Sirtuin-1 - Mediated Nf-κb Pathway Modulation to Mitigate Inflammasome Signaling and Cellular Apoptosis Is One of the Neuroprotective Effects of Intra-Arterial Mesenchymal Stem Cell Therapy Following Ischemic Stroke. *Stem Cell Rev Rep* (2022) 18(2):821–38. doi: 10.1007/s12015-021-10315-7

Conflict of Interest: The authors declare that the research was conducted in the absence of any commercial or financial relationships that could be construed as a potential conflict of interest.

Publisher's Note: All claims expressed in this article are solely those of the authors and do not necessarily represent those of their affiliated organizations, or those of the publisher, the editors and the reviewers. Any product that may be evaluated in this article, or claim that may be made by its manufacturer, is not guaranteed or endorsed by the publisher.

frontiers | Frontiers in Immunology

TYPE Original Research
PUBLISHED 05 August 2022
DOI 10.3389/fimmu.2022.963582

OPEN ACCESS

EDITED BY
Chaofeng Han,
Second Military Medical University, China

REVIEWED BY
Degang Yang,
School of Medicine, Tongji University, China
Zhi Qi,
Nankai University, China

*CORRESPONDENCE
Xuhua Lu
xuhualu@hotmail.com
Haisong Yang
yangspine@163.com

†These authors share first authorship

SPECIALTY SECTION
This article was submitted to Molecular Innate Immunity, a section of the journal Frontiers in Immunology

RECEIVED 07 June 2022
ACCEPTED 11 July 2022
PUBLISHED 05 August 2022

CITATION
Wang C, Ma H, Zhang B, Hua T, Wang H, Wang L, Han L, Li Q, Wu W, Sun Y, Yang H and Lu X (2022) Inhibition of IL1R1 or CASP4 attenuates spinal cord injury through ameliorating NLRP3 inflammasome-induced pyroptosis.
Front. Immunol. 13:963582.
doi: 10.3389/fimmu.2022.963582

Inhibition of IL1R1 or CASP4 attenuates spinal cord injury through ameliorating NLRP3 inflammasome-induced pyroptosis

Chenfeng Wang[1†], Hongdao Ma[1†], Bangke Zhang[1†], Tong Hua[2], Haibin Wang[1], Liang Wang[1], Lin Han[1], Qisheng Li[1], Weiqing Wu[1], Yulin Sun[1], Haisong Yang[1*] and Xuhua Lu[1*]

[1]Department of Orthopaedics, Shanghai Changzheng Hospital, Shanghai, China, [2]Department of Anesthesiology, Shanghai Changzheng Hospital, Shanghai, China

Spinal cord injury (SCI) is a devastating trauma characterized by serious neuroinflammation and permanent neurological dysfunction. However, the molecular mechanism of SCI remains unclear, and few effective medical therapies are available at present. In this study, multiple bioinformatics methods were used to screen out novel targets for SCI, and the mechanism of these candidates during the progression of neuroinflammation as well as the therapeutic effects were both verified in a rat model of traumatic SCI. As a result, CASP4, IGSF6 and IL1R1 were identified as the potential diagnostic and therapeutic targets for SCI by computational analysis, which were enriched in NF-κB and IL6-JAK-STATA3 signaling pathways. In the injured spinal cord, these three signatures were up-regulated and closely correlated with NLRP3 inflammasome formation and gasdermin D (GSDMD) -induced pyroptosis. Intrathecal injection of inhibitors of IL1R1 or CASP4 improved the functional recovery of SCI rats and decreased the expression of these targets and inflammasome component proteins, such as NLRP3 and GSDMD. This treatment also inhibited the pp65 activation into the nucleus and apoptosis progression. In conclusion, our findings of the three targets shed new light on the pathogenesis of SCI, and the use of immunosuppressive agents targeting these proteins exerted anti-inflammatory effects against spinal cord inflammation by inhibiting NF-kB and NLRP3 inflammasome activation, thus blocking GSDMD -induced pyroptosis and immune activation.

KEYWORDS

spinal cord injury, NLRP3 inflammasome, pyroptosis, IL1R1, CASP4, GSDMD, gasdermin D

Introduction

Spinal cord injury (SCI) is a common nervous system disease which may cause permanent neurological dysfunction (1), with approximately 180,000 new cases diagnosed per year in the world (2). Despite advances in surgical techniques and efforts dedicated to the treatment of SCI, there is currently no effective regimen to treat this devastating neurological disease (3, 4). Given the seriousness of this disease, a comprehensive understanding about the pathomechanism of SCI is primarily important in mining the potential targets and searching for effective treatment strategies.

Continuous progress and development of bioinformatics have made it possible to explore underlying mechanisms of multiple diseases at genetic and molecular levels, and provide guidelines for better treatment. Bioinformatical analysis has demonstrated that hub genes are expressed differentially across the acute, subacute and chronic phases of SCI, which offers some meaningful insights into different pathomechanisms and targeted therapies between acute and chronic SCI (5). Besides, weighted gene co-expression network analysis (WGCNA), as an important bioinformatics method, can assist to explore the underlying mechanism of SCI-induced immune suppression (6). Furthermore, leveraging the benefits of bioinformatics is an innovative way to mine cell markers and immune responses following SCI (7).

Interestingly, an increasing number of studies have proven that immune cell infiltration plays a key role in the advancement of SCI. γδ T cells, a subgroup of T cells, could be recruited into the SCI site for exacerbating inflammation and impeding neurological self-impair *via* CCL2/CCR2 signaling (8). Neutrophils are reported to play an essential role in the progression of SCI, and recruitment of macrophages at the lesion site is regarded as a potential approach for treating SCI (9, 10).

The motivation of this study was to explore key biomarkers of SCI as well as obtaining the therapeutic targets for SCI therapy with the help of bioinformatical analysis and experiments. First, multiple bioinformatics methods were used to screen out novel targets for SCI. Second, the mechanism of these candidates during the progression of neuroinflammation was verified in a rat model of traumatic SCI. Finally, the therapeutic effects of immunosuppressive agents targeting biomarkers for SCI treatment were clarified.

Materials and methods

Data collection

Three transcription datasets GSE5296 (11), GSE47681 (12) and GSE45006 (13) were downloaded from the GEO database (https://www.ncbi.nlm.nih.gov/geo/). The dataset GSE5296 and GSE47681 based on GPL1261 [Mouse430_2] Affymetrix Mouse Genome 430 2.0 Array. The former dataset included 21 murine normal spinal cord and 75 SCI samples, and the latter one included nine normal and 25 SCI samples. To evaluate the efficiency of analysis, the GSE45006 dataset was utilized as the validation set using GPL1355 [Rat230_2] Affymetrix Rat Genome 230 2.0 Array as the platform, which contained four normal samples and 20 SCI samples.

Obtainment of DEGs

To remove the inter-batch difference, GSE5296 and GSE47681 were integrated through the "affy" package (14) and the "sva" package (15), showing in a two-dimensional PCA cluster plot (16). The obtainment of DEGs depended on the "limma" package (17), exhibiting on a volcano figure with the usage of the "ggplot2" package (18). DEGs with $p < 0.05$ and $|\log_2 FC|>1$ were viewed as statistically significant.

Functional enrichment analysis and PPI network

To obtain biological functions and signaling pathways for disease, the Metascape database (www.metascape.org) was used for functional annotation. Gene Ontology (GO) and Kyoto Encyclopedia of Genes and Genomes (KEGG) pathway enrichment analyses were performed for specific genes. Min overlap ≥3 and $p \leq 0.01$ were considered statistically significant.

All the genes were input into the STRING (http://string–db.org) online database for investigating the interaction between proteins and constructing their network. Among the high confidence (score 0.900), a 'tsv' file was imported into the Cytoscape software to visualize the network.

Acquisition and validation of diagnostic markers

LASSO logistic regression (19) and Boruta algorithm (20) were applied to conduct feature selection to screen key markers for SCI. LASSO logistic regression, a machine learning strategy, finds λ to decide the variables when the classification error is littlest. LASSO regression allows the coefficients of the features to be compressed by a penalty function to obtain the optimal constrained model; this approach avoids the overfitting and covariance found in classical analysis methods and also enhances the generalization ability of the model. The Boruta algorithm is a random forest classifier package that finds all the relevant feature variables. They are often utilized to search characteristic variables and assemble an excellent classification model. After quality control, the expression matrices

of the GSE5296, GSE47681, and GSE45006 datasets were merged into an independent dataset for the next analysis. The LASSO logistic regression was utilized through the "glmnet" package (21). Additionally, the Boruta algorithm is a feature-selection algorithm that randomly disrupts the order of each real feature, evaluates the importance of each feature, and iteratively removes features of low relevance to find the best variable. In this study, "Boruta" package (20) was used for feature selection, and a total of 500 trees were constructed to a deeper level of verification for the diagnostic efficiency of these biomarkers. The overlapping genes obtained by these two algorithms are considered as signature genes and they are validated in GSE45006. Three receiver operating characteristic (ROC) curves were generated to estimate the accuracy of the screened biomarkers. The area under the curve (AUC) represents the performance of the model.

Correlation analysis of genes and immune cell infiltration

The CIBERSORT algorithm is widely used to assess immune cell types in various diseases. In this study, data related to spinal cord injury were analyzed using CIBERSORT to infer the relative proportions of 22 immune infiltrating cells and to plot the associated heat map using the "corrplot" and "vioplot" packages. And Spearman correlation analysis was conducted for candidate markers and immune cells that participated in the progress of infiltration, which were visualized by using "ggplot2" package.

To evaluate the influence of genes on immune cell infiltration (22), ssGSEA (23) was used to quantify the infiltration level of immune cells in each sample.

Gene set variation analysis (GSVA)

GSVA (24) is a non-parametric and unsupervised method for assessing gene set enrichment (GSE) and identifying important signaling pathways involved in SCI. The corresponding genomes were downloaded from the Molecular Signature Database (http://gsea-msigdb.org) and the GSVA R package was used to find differential expression pathways and biological processes between high and low expression groups of candidate genes.

Antibodies and reagents

The antibodies and reagents used in this study included anti-IL1R1 (Abclonal, A5727), anti-GAPDH (Proteintech, HRP-60004), anti-CASP4 (Affinity, AF5130), anti-cleaved CASP4 (Affinity, AF5373), anti-IGSF6 (Abclonal, A15128), anti-phospho-NF-κB pp65 (Servicebio, GB13025), anti-Bcl2 (Abclonal, A0208), anti-CASP3 (Abclonal, A2156), anti-IL1B (Abclonal, A16288), anti-NLRP3 (Affinity, DF7438), anti-ASC (Abcam, ab180799), anti-GSDMD (Cell signaling technology, 39754), anti-cleaved GSDMD (Cell signaling technology, 10137), anti-NF-κB p65 (Cell signaling technology, 3033), Goat anti-rabbit IgG-HRP (Proteintech, HRP60004), Goat anti-rabbit pp65 (Servicebio, GB21303), TUNEL (Servicebio, GB1501), DAPI (Servicebio, G1012), Anakinra (MCE, AMG-719), and Belnacasan (Selllock, also known VX-765, S2228).

Establishment of the rat SCI model

SD male rats aged 60 days and weighing 180-200g were used to build the SCI model. Briefly, after successful anesthesia with 1% pentobarbital, laminectomy was performed to expose the spinal cord at T10 level, and then a spinal cord impactor (F69852, RWD, CA, USA) was utilized to make an injury by dropping a 5g rod onto the spinal cord from a height of 6.5 cm. After the operation, the animals were carefully nursed, fed and pressed to promote urination three times a day until the bladder reflex was recovered. Rats in the Sham operation group underwent laminectomy only at the same level.

Basso Beattie Bresnahan (BBB) scale and footprint analysis

BBB scale was used to assess the hindlimb motor function of the rats on day 1, 3, 7, 14, 21, and 28 post-injury in an open field. After the rats had adapted to the environment, two well-trained experimenters observed and scored the locomotor function in 5 minutes, and the mean BBB score of three measurements was used for analysis.

Footprint analysis was performed by dipping the rat hind paws in dye. All rats were allowed to walk across a narrow box measuring 1 m long and 7 cm wide, and the footprints were scanned.

Swimming test

The swimming test is also a scoring system to evaluate functional recovery. All rats were trained to swim from one end to the other end of a water-filled glass tank, and their swimming strokes were scored by the Louisville Swim Scale (LSS) in terms of forelimb dependency, hind limb movement and alternation, trunk instability, and body angle. Each rat was tested twice to calculate the mean score.

Drug administration and animal grouping

Anakinra is an inhibitor of IL1R1, while VX-1765 is an inhibitor of CASP4. As no inhibitor for IGSF6 was available,

it was excluded in the subsequent experiments. Forty-eight rats were randomly divided into four groups: a Sham group, a SCI+normal saline (NS) group, a SCI + Anakinra (SA) group, and a SCI + VX765 (SV) group. Anakinra in SA group was injected intrathecally at a dose of 25μg/5μl on the day of modeling as it was done in SV group. In Sham and NS group, 5μl NS was injected intrathecally on the day of modeling.

Tissue collection

According to the protein expression time curves of the three biomarkers (IL1R1, CASP4 and IGSF6), follow-up experiments were carried out to further verify the accuracy of the signatures. After experimental verification, the injured spinal cord tissues processed in different groups were collected on day 7 after injury. The rats were anesthetized by 1% pentobarbital and perfused with 0.9% saline (containing 50 U/mL heparin) through the endocardium and then perfused with phosphate buffer (containing 4% PFA). A 10-mm spinal cord segment was cut at the injured site, fixed in 4% PFA for 48 h at room temperature, and paraffin-embedded.

Haematoxylin-eosin (HE) staining

The fixed, dehydrated and paraffin-embedded tissues were sliced into 4-μm sections. After deparaffinization and hydration with gradient ethanol, they were stained with hematoxylin for 5 min, differentiated with 1% hydrochloric acid and ethanol, and blued with 5% ammonia. The sections were stained with 0.5% eosin for 1 min, dehydrated and sealed with neutral glue. Pathological changes of the injured spinal cord were observed under an optical microscope.

Immunohistochemistry

The paraffin-embedded tissues were sliced and incubated in 0.3% H2O2 for 30 min, and then in 0.1% Triton X-100 for 20 min. Next, the sections were incubated with primary antibodies, including anti-IL1R1 antibody (1:100), anti-IGSF6 antibody (1:100), and anti-CASP4 antibody (1:100) overnight at 4°C and secondary antibody for 60 min at 37°C. Finally, the sections were stained with DAB for color development and counterstained with hematoxylin.

Immunofluorescence staining

Cryosections of the spinal cord tissue were rinsed with 0.01 M PBS, and then blocked with 5% normal goat serum, 0.1% bovine serum albumin, and 0.2% Triton-X 100 in 0.01 M PBS before applying the primary antibody of rat anti-pp65 (1:100). Target signals were visualized by using rabbit HRP with fluorescence-conjugated secondary antibodies. The TUNEL kit was used to stain at 37°C for 2 h, and confocal images were obtained using a scanning instrument (Pannoramic DESK P-MIDI P250, 3D HISTECH, Hungary).

Western blot analysis

The proteins of the spinal cord (epicenter ± 5mm) were extracted by protein extraction buffer (Beyotime, P00103J) supplemented with 1% protease inhibitor (Beyotime, P1005) in a tissue grinding machine (Servicebio, KZ-III-FP). Cell lysates were centrifuged at 12000g for 15min at 4°C to collect supernatants. The protein concentration was determined by the BCA kit (Beyotime, P0012) and followed by denaturing at 95°C for 10 min in 1×SDS loading buffer. Subsequently, samples with an equal amount of protein were loaded and applied to 10% SDS-PAGE and then transferred onto nitrocellulose membranes (Millipore). The membranes were sealed and then incubated with specific primary and secondary antibodies. Proteins were visualized using enhanced chemiluminescence substrate (Tanon) and then quantified using a Tanon Chemiluminescent Imaging System.

Real-time quantitative PCR (RT-qPCR) analysis

Through machine grinding, total RNA of cracking organizations was extracted using the Trizol reagent (Vazyme) and then converted to cDNA using a reverse transcription kit HiScript II Q RT SuperMix for qPCR (R122-01, Vazyme, China). Next, RT-qPCR was performed using AceQ qPCR SYBR Green Master Mix (Q111-02, Vazyme, China) in a 7500 real-time PCR system (Applied Biosystems, Inc., USA) according to the manufacturer's instruction. The primer sequences used for RT-qPCR are listed in Table 1. The mRNA levels of the target genes were normalized to the Glyceraldehyde-3-phosphate dehydrogenase (GAPDH) expression. Quantification of the RT-qPCR results was performed by the 2ΔΔCt method.

Statistical analysis

The statistical analysis was conducted in R v3.6. All statistical tests were bilateral, and $p < 0.05$ was considered statistically significant. Data between two groups were compared by an unpaired t-test, and comparisons between multiple groups were performed with one-way analysis of variance (ANOVA) whereas pairwise comparison within groups was conducted by *post hoc* test.

TABLE 1 Primer sequences for RT-qPCR.

Gene	Forward	Reverse
GAPDH	GACATGCCGCCTGGAGAAAC	AGCCCAGGATGCCCTTTAGT
CASP4	CTTACGGCTGAGGGCATGGAATC	CAAGTGGTGTGGTGTTGTAGAGTAGAG
IGSF6	ACAGCAATCCAAACAACAGCAAAGAG	GACAGTTACTTCCGCTCTGCCTTC
IL1R1	TTGTCTCATTGTGCCTCTGCTGTC	GCTGATGAATCCTGGAGTCCTTGTC

Results

Normalization and DEGs obtainment

After merging the GSE5296 and GSE47681 datasets, the newly generated gene expression matrix needed processing, which was presented in a two-dimensional PCA cluster layout before and after processing, suggesting that the aid of samples used was reliable. A total of 182 DEGs were identified, including 178 up-regulated genes and four down-regulated genes (Figure 1A).

Functional enrichment analysis and PPI network analysis

By understanding the signaling pathways, biological processes and interactions involved in DEGs, it is an important step to uncover the pathological mechanisms of SCI. Functional enrichment analysis showed that DEGs were associated with inflammatory response, osteoclast differentiation, myeloid leukocyte activation, regulation of cytokine production, and positive regulation of immune response (Figure 1B). Of the 128 nodes and 934 edges, DEGs that did not participate in the construction of PPI network were either hidden or deleted (Figure 1C).

Acquisition and validation of diagnostic markers

To obtain more representative biomarkers, we select two feature selection algorithms and validate the results. 15 DEGs were identified as biomarkers for SCI by LASSO logistic regression (Figures 2A, B) and 43 by the Boruta algorithm (Figure 2C). By overlapping the feature genes, we finally obtained eight feature genes (SLA、IL1R1、NPAS4、CASP4、IGSF6、EGR3、NR4A1 and NAIP5). As described before, GSE45006 was used to further verify the intersecting genes, finding that CASP4 (caspase 4), IGSF6 (immunoglobulin superfamily member 6), and IL1R1 (interleukin 1 receptor type 1) varied significantly in SCI. Three genes were differentially expressed between the normal and SCI samples, which are respectively presented in a box violin map (Figure 2D). In addition, the ROC curve of diagnostic efficacy demonstrated that CASP4 (AUC=0.883), IGSF6 (AUC=0.907), and IL1R1 (AUC=0.942) had a high diagnostic value (Figure 2E). IL1R1 and CASP4 are involved in non-classical pathways of pyroptosis process (25), and as for IGSF6, it plays a significant role in the nerve system (26).

Correlation analysis between biomarkers and infiltrating immune cells

It is known that immune cells contribute to the inflammatory responses in SCI progression. Therefore, we further explored the immune infiltration that is closely associated with SCI. With the help of the CIBERSORT, the difference in immune infiltration was summarized between 100 SCI and 30 normal spinal cord tissues in subpopulations of immune cells (Figure 3A). Compared with the control, the injured spinal cord contained a higher proportion of antigen-presenting cells (APC), macrophages, check-point, Treg, and tumor-infiltrating lymphocytes (TIL) (Figures 3B, 4A).

Correlation analysis demonstrated that CASP4 was positively associated with chemokine receptor (CCR) and para-inflammation, and negatively associated with activated dendritic cells (aDCs); IGSF6 was positively associated with TIL and macrophage, and negatively associated with aDCs and neutrophils; IL1R1 was positively associated with Treg and Parainflammation, and negatively associated with aDCs (Figure 4B).

GSVA analysis

The biological effects of the three biomarkers were evaluated using the GSVA algorithm, and the results demonstrated that there were significant differences in 33 common pathways, including activated pathways such as the IL6-JAK-Akt signaling pathway and TNFα signaling *via* NFκB (Figure 4C).

IL1R1, CASP4, and IGSF6 are upregulated in the injured spinal cord

To explore the role of the biomarkers in the pathophysiology of SCI, RT-qPCR and Western blot were used to determine their

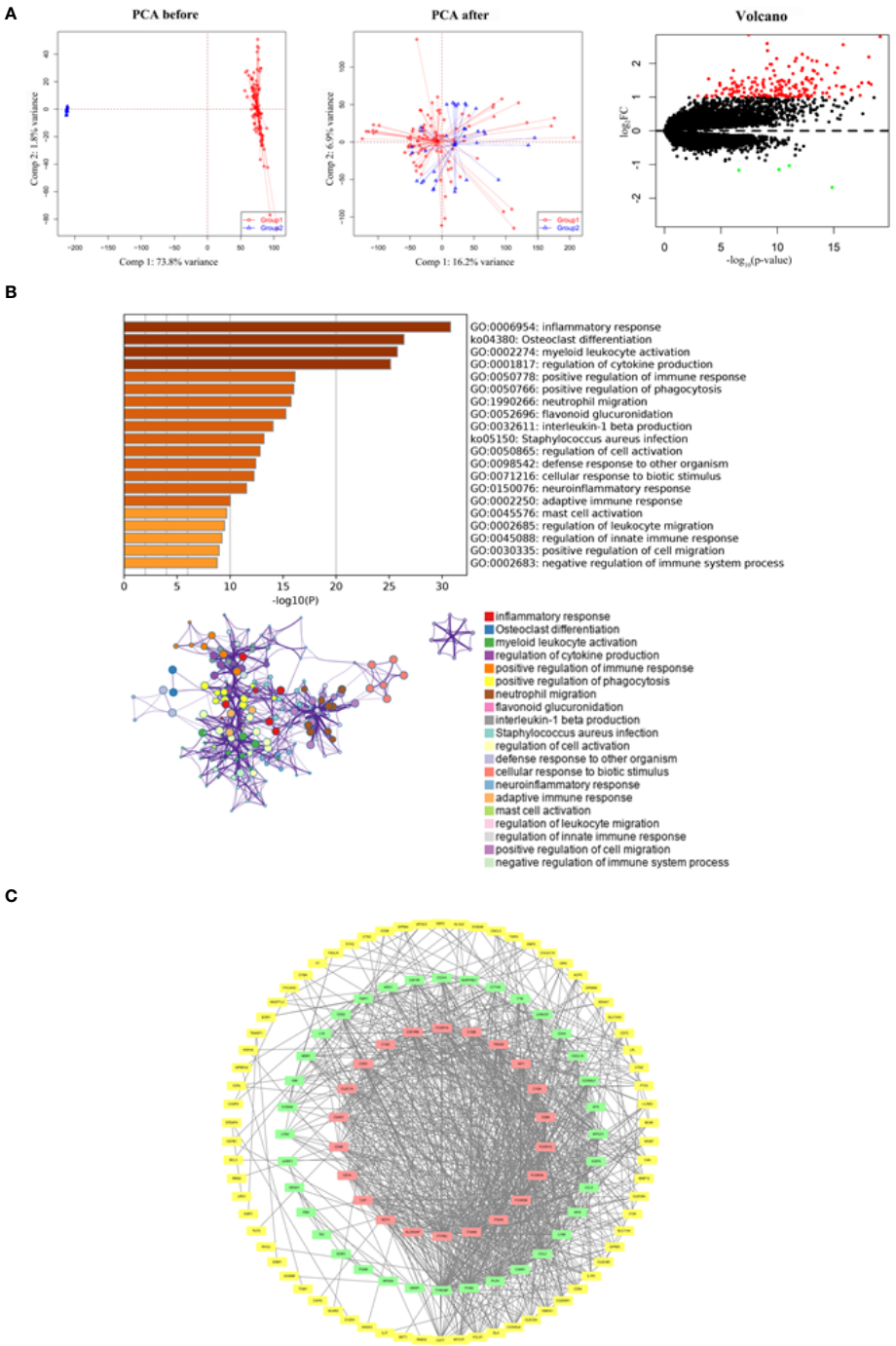

FIGURE 1
Functional enrichment and PPI network analysis of identified DEGs. **(A)** Two-dimensional PCA cluster plot of GSE5296 and GSE47681 datasets before and after normalization: group1 represented the SCI group and. group2 represented the normal control group. Red dots represent up-regulated genes, black dots represent no significant difference, and green dots represent down-regulated genes. **(B)** GO enrichment analysis demonstrated the main biological process and signaling pathways. **(C)** The PPI network construction. The red squares construct the most significant cluster, the green squares represent other clusters, and the yellow squares represent the genes not involved in cluster construction.

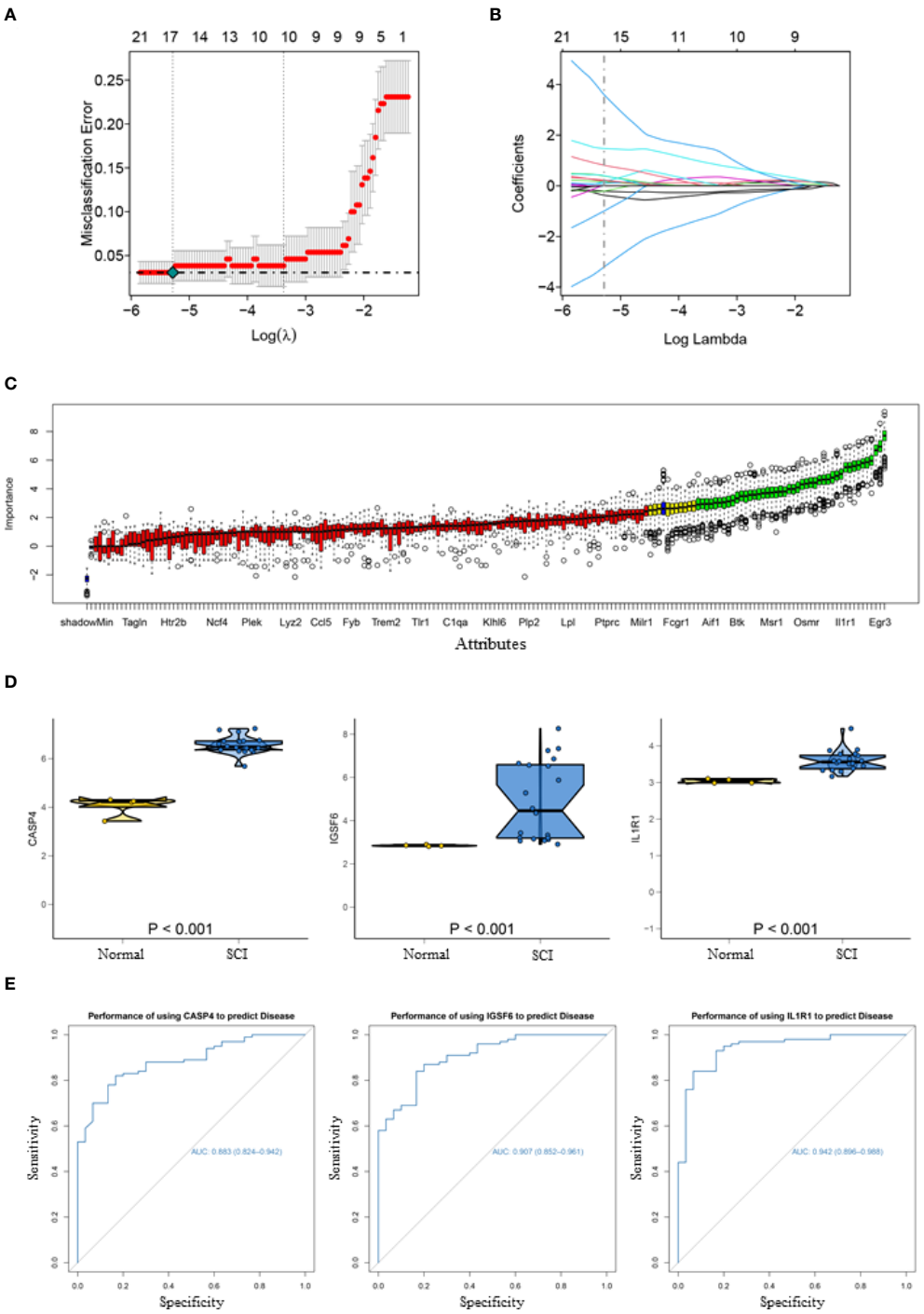

FIGURE 2
Acquisition and validation of candidate diagnostic markers. **(A)** LASSO regression showed the binomial deviation of different quantitative variables. The lower horizontal coordinate indicates the value of the lasso regression model parameter λ, the upper horizontal coordinate indicates the number of coefficients in the corresponding model, and the vertical coordinate indicates the error of the model. There are two dashed lines, the line with the lowest error on the left and the line with fewer features on the right. **(B)** Coefficient of LASSO regression model. As the λ value changes, the later the coefficient is compressed to zero the more important the variable is. **(C)** Boruta algorithm to screen diagnostic biomarkers. **(D)** Box violin maps of CASP4, IGSF6 and IL1R1 indicate that the differential expression in SCI group was significantly different from that in the normal group. **(E)** The ROC curves of the diagnostic efficacy of CASP4 (AUC=0.883), IGSF6 (AUC=0.907) and IL1R1 (AUC=0.942), the area under which was used to evaluate the effectiveness.

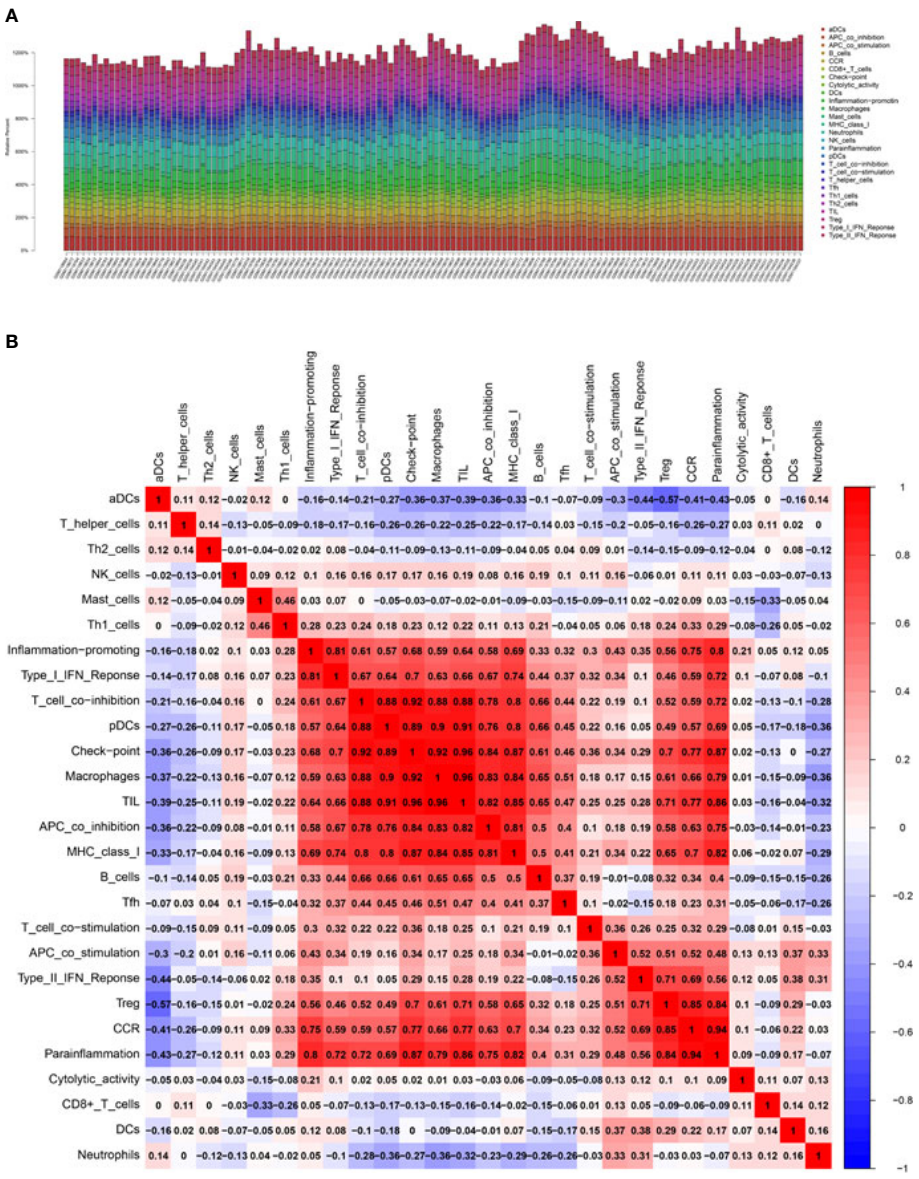

FIGURE 3
Correlation analysis of the biomarkers and infiltrating immune cells. **(A, B)** Relative immune cells and responses in 130 samples from GSE5296 and GSE47681 datasets.

expression patterns in the lesion site at day 1, 3, 5 and 7 after injury. The results showed that the three biomarkers were upregulated in SCI (Figures 5B, C). The protein expression of IL1R1 was the highest at day 1 after injury, and both CASP4 and IGSF6 peaked at day 5 after injury. Besides, the mRNA expression of IL1R1 was significantly upregulated at day 1 after injury; IGSF6 and CASP4 reached the peak level at day 5 after injury, which was coincident with the protein expression (Figure 5A). The HE staining (Figure 5D) showed no significant pathological change in Sham group, while significant abnormalities in the gray and white matter boundary in SCI rats, including focal bleeding, necrosis and cavity formation. Immunohistochemistry showed that the expression of the three signatures increased markedly after SCI (Figure 5E).

Locomotor functional recovery

To validate the potential therapeutic value of the biomarkers, immunosuppressive therapy was performed against the selected

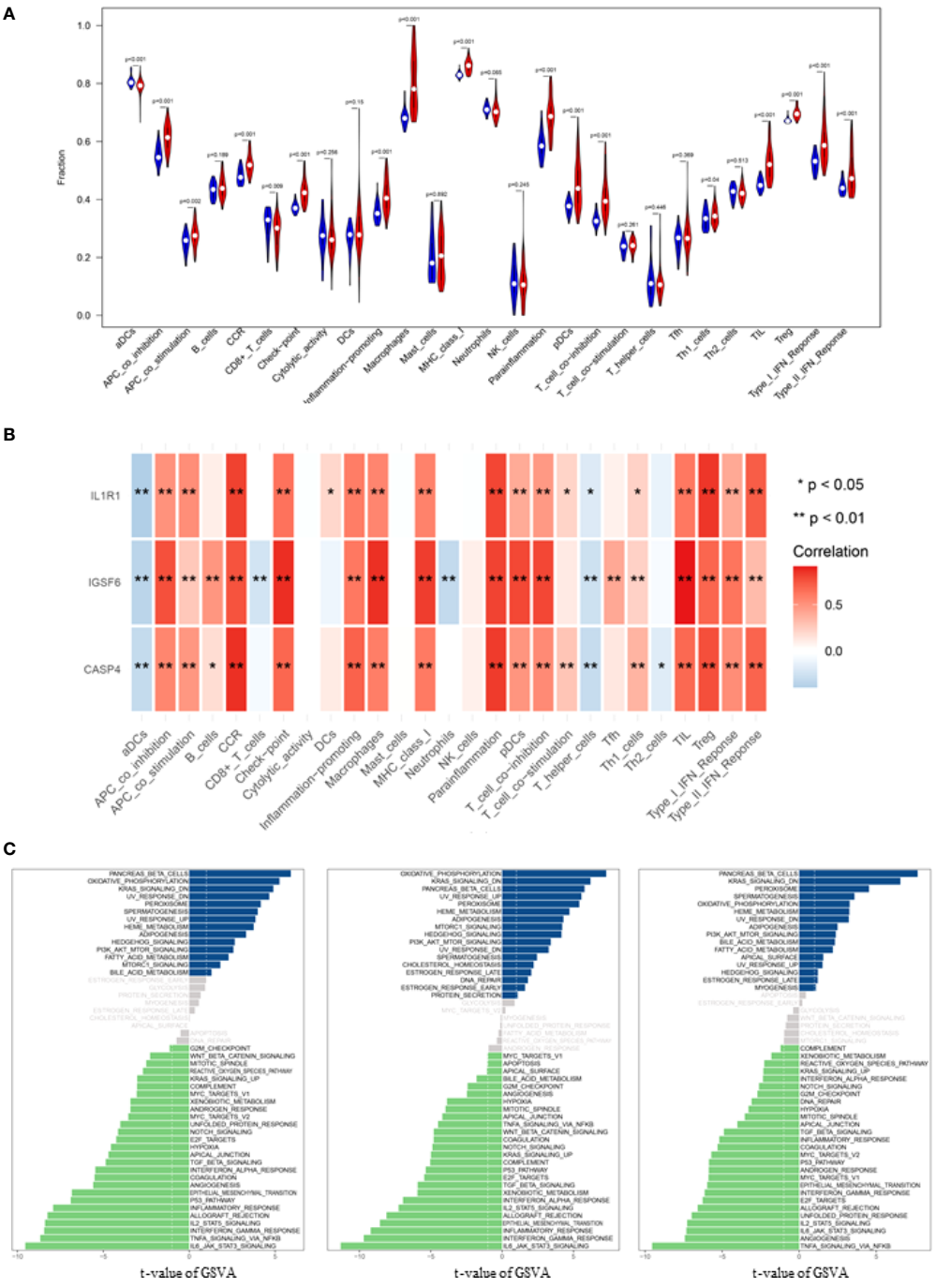

FIGURE 4
Correlation analysis of infiltrating immune cells and Gene set variation analysis (GSVA). **(A)** Differences in immune infiltration between SCI and normal control groups. Blue represents the normal control group, and red represents SCI group. p-value <0.05 was considered statistically significant. **(B)** * p = < 0.05, ** = p < 0.01, and non-* = statistically insignificant. The color of the squares represents the closeness degree of the relationship between the genes and immune cells, the darker the color, the higher the p-value, and the lighter the color, the lower the p-value. **(C)** The GSVA results demonstrated the pathway differences of these key gene expressions in SCI.

targets by selecting appropriate doses of the inhibitors to treat SCI rats for a week to observe the long-term effect. The BBB scale, footprint experiments, and LSS were used to evaluate neurological functional recovery. As indicated in Figures 6A, D, there was no significant difference in BBB and swimming test scores between the four groups before SCI. Yet, the result of locomotor function assessment in SA and SV groups was significantly superior to that in NS group from day 7 after

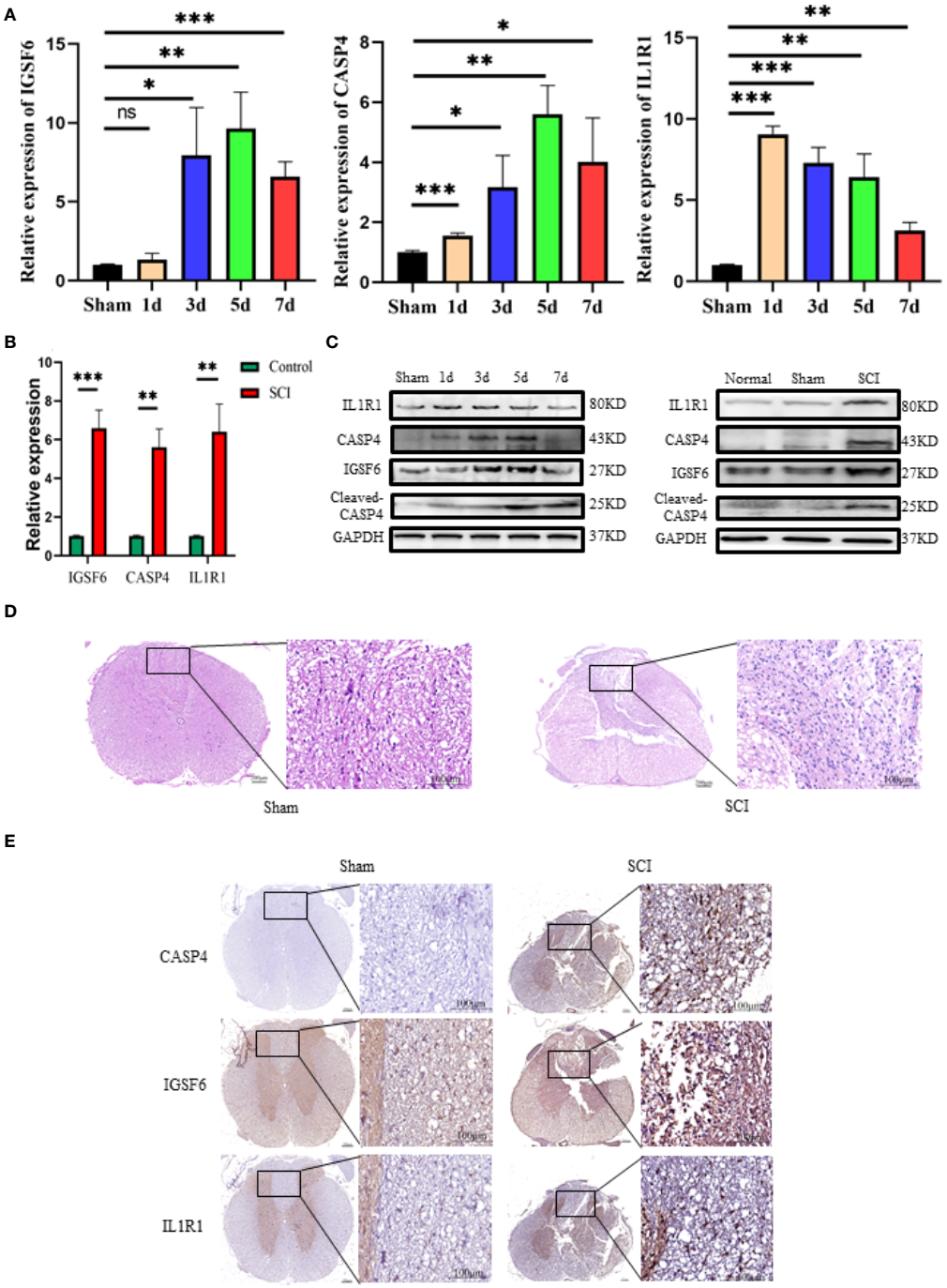

FIGURE 5
Western blot, RT-qPCR and immunohistochemistry of the three biomarkers (IL1R1, CASP4 and IGSF6). **(A)** The time curves of the three biomarkers at mRNA level on day 1, 3, 5 and 7 after SCI or sham surgery (n = 3 rats per group at each time point, values are the mean ± SD, *p < 0.05, **p < 0.01, ***p < 0.001, t-test). **(B)** RT-qPCR validation of the biomarkers expressing in peak: the three signatures were increased significantly in SCI group (n = 3 rats per group, values are the mean ± SD, *p < 0.05, **p < 0.01, ***p < 0.001, t-test). **(C)** Western blot validation of the biomarkers as represented by their time curves at protein level (n = 3 rats per group, values are the mean ± SD, *p < 0.05, t-test). **(D)** Histomorphologically, the injured spinal cord tissue exhibited organizational abnormalities as compared with the normal control (overall scale bars = 200μm, regional-scale bars = 100μm). **(E)** Immunohistochemical validation of the biomarkers: the markers were found to be expressed in both gray matter and white matter (Overall scale bars = 200μm, regional-scale bars = 100μm, the arrows point to the positioning of the marker).

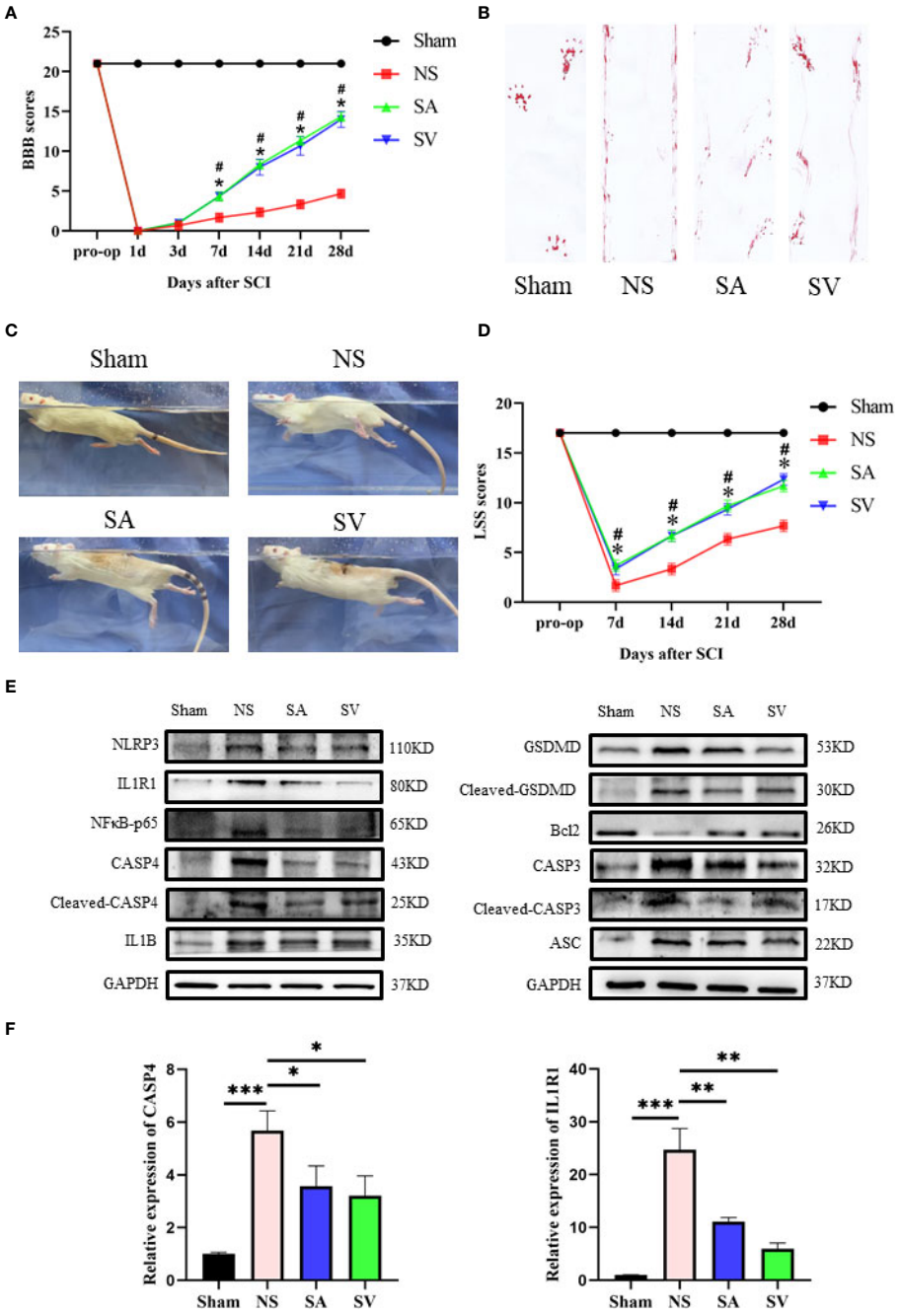

FIGURE 6
Change of the biomarkers and functional recovery in the SCI model after immunosuppressive therapy. **(A)** Statistical analysis of the BBB Scale in Sham, positive control, and treatment groups over 28 days (n = 3 rats per group at each time point, values are the mean ± SD, *p < 0.05, t-test). **(B)** Footprint analysis of different groups. **(C, D)** Statistical analysis of the Louisville Swim Scale in the four groups over 28 days (n = 3 rats per group at each time point, values are the mean ± SD, *p < 0.05, t-test). **(E)** Western blot showed that the expression level of the biomarkers in the treatment groups was between the levels of sham and control groups, and the levels of Bcl2 and CASP3, NFκB, GSDMD, IL1B, ASC, and CASP3 in SA and SV groups were also between those of Sham and control groups (n = 3 rats per group, *p < 0.05, **p < 0.01, ***p < 0.001, t-test). **(F)** RT-qPCR showed that the level of biomarkers was significantly decreased after treatment (n = 3 rats per group, *p < 0.05, **p < 0.01, ***p < 0.001, t-test).

SCI. In addition, the LSS showed that the SCI rats receiving inhibition therapy exhibited less forelimb dependence, faster hind limb alternation, and a smaller angle between the body and water surface from day 7 after injury (Figures 6C, D). Footprint analysis at day 28 showed that rats in SA and SV groups exhibited consistent coordination of the hindlimbs and reduced toe dragging (Figure 6B). On the contrary, no such coordination ability was observed in NS group rats; rather toe dragging was obvious. These findings indicate that the targetable inhibitors could promote the therapeutic effect on the functional improvement of SCI rats.

IL1R1 and CASP4 inhibitors attenuate inflammation and promote repair of the injured spinal cord

The use of IL1R1 and CASP4 inhibitors to reduce the degree of inflammation of secondary SCI and eliminate the cascade reaction may have a positive effect on SCI recovery. NLRP3, GSDMD, ASC, NFκB, IL1B and CASP4 are known to be related to pyroptosis, and Bcl2 and CASP3 are associated with apoptosis. Western blot analysis revealed that the levels of NLRP3, NFκB, GSDMD, IL1B, ASC and CASP3 in treatment groups were lower in SA and SV groups than NS group, while the Bcl2 level in SA and SV groups was significantly higher than that in NS group, which further proved that pyroptosis and apoptosis were involved in the cascade responses after SCI. With respect to the signatures, the expression of CASP4 and IL1R1 was in coincidence with other inflammatory and apoptosis indicators (Figure 6E). Meanwhile, the RT-qPCR of the three biomarkers illustrated that their mRNA expressions were significantly decreased in SCI rats after the inhibitor therapy (Figure 6F). Furthermore, the inhibitory effect on the expression of the biomarkers was detected by immunohistochemistry. It was found that the expression of two biomarkers was markedly decreased as represented by obvious attenuation of the staining area in SA and SV groups (Figure 7A).

As shown in Figure 7B, the phosphorylation-NFκB (pp65) showed red dots, and the nucleus showed blue dots. Compared with Sham group, p65 was activated and then entered the nucleus, turning pink. However, P65 fluorescence expression in SA and SV groups was between Sham and NS groups, showing a small proportion of p65 activation (Figure 7B). Furthermore, immunofluorescence staining also showed that targetable treatment significantly decreased the number of TUNEL+ cells (Figure 8A). Collectively, our results suggested that Anakinra and VX765 utilization inhibited inflammation, decreased cell apoptosis and rehabilitated the physical function of the animals *in vivo*.

To observe the therapeutic effect of the drugs more directly, the spinal cord tissues were observed morphologically. It was found that the biopsy tissues in Sham group exhibited clear boundaries and an integrated morphology. In NS group, the structures of the spinal cord tissues were damaged histopathologically. Compared with NS group, such damage was dramatically reduced in SA and SV groups. The extent of focal hemorrhage and cavity in the gray matter of the treatment groups was mild and between that of Sham and NS groups (Figure 7A).

Discussion

Spinal cord injury may cause nervous system dysfunction and remains a clinical challenge. Many studies have proposed that immune cells play a necessary role in the process of SCI. Therefore, exploration of related biomarkers, molecular mechanism and immune infiltration is indispensable for seeking advantageous treatment solutions and ultimately improving the quality of life of SCI patients. In this study, we employed bioinformatics analysis as an extensive approach to discover the biomarkers and CIBERSORT tools for the sake of finding out the immune cell infiltration patterns of the disease, and then verified the therapeutic effect of immunosuppressants targeting the markers on SCI. Finally, we identified a total of 182 DEGs that were enriched in inflammatory response, myeloid leukocyte activation, regulation of cytokine production, positive regulation of immune response, IL6-JAK-STAT3 signaling pathway, and TNFα signaling *via* NFκB. It was found that down-regulation of IL6-JAK-STAT3 and NFκB signaling pathways could inhibit inflammatory response and promote the recovery of neurological function after SCI (27, 28). Besides, we identified CASP4, IGSF6 and IL1R1 as the biomarkers of SCI by combining the LASSO logistic regression and Boruta algorithm and verified them by experiments. Delightedly, treating SCI with drug-targetable biomarkers could significantly improve the spinal cord morphology, inhibit GSDMD -induced pyroptosis and recover the behavioral ability. All these findings support our data analysis, confirming that the results obtained in this study are reliable and correct.

Some current studies have begun using machine learning and deep learning to select significant features and models. For example, as a learning machine, XGBoost can reliably predict neurological alterations, thereby enhancing personalized management and clinical prognosis of SCI patients (29). Besides, what counts is that effective machine learning can even precisely predict the prolonged ICU stay and the prolonged hospital stay to guide clinical treatment (30). LASSO logistic regression, a machine learning strategy, finds λ to decide the variables when the classification error is littlest. The Boruta algorithm is a random forest classifier package that finds all the relevant feature variables. They are often utilized to search characteristic variables and assemble an excellent classification model (31, 32). In this study, we identified CASP4, IGSF6 and

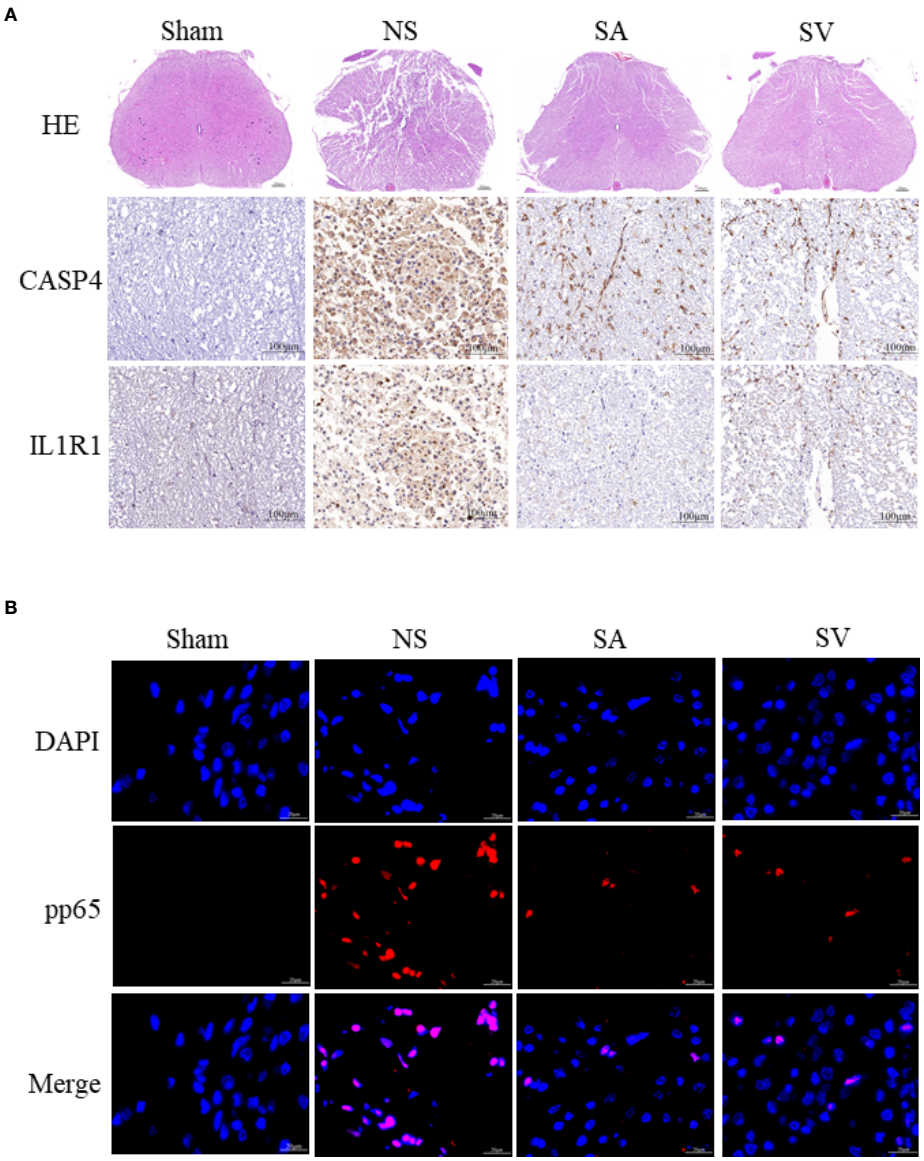

FIGURE 7
Histopathological changes. **(A)** HE staining demonstrated that the structure of the injured spinal cord tissue became clearer after treatment, with fewer cavities and necroses as compared with SCI group (Scale bars = 100μm, the arrows point to cavities and necroses), and the expression level of the biomarkers in the spinal cord was reduced (Scale bars = 20μm) (n = 3 rats per group, *p < 0.05, **p < 0.01, ***p < 0.001, t-test). **(B)** Representative images showing pp65 and DAPI co-staining of the spinal cord sections from the rats of the four groups (Scale bars = 20μm) (n = 3 rats per group, *p < 0.05, **p < 0.01, ***p < 0.001, t-test).

IL1R1 as the biomarkers of SCI by combining the two algorithms.

The biomarkers were likely to relate to pyroptosis. CASP4, the ortholog of CASP11, as the receptor for cytoplasmic lipopolysaccharide, plays a role in the non-canonical inflammasome pathway and development of pyroptosis in SCI. CASP4 performs a similar function to CASP1, and its activation could induce GSDMD-dependent pyroptosis and processing of interleukin-18, further aggravating inflammatory damage (33). IGSF6 is a member of the immunoglobulin superfamily and is highly expressed in the immune tissue. It is considered as a candidate protein for inflammatory bowel disease susceptibility (34). Besides, IGSF6 is closely related to immune cell activity, which may participate in the progress of DC antigen presentation (35) and $CD4^+$ T cell response (36). However, there is no study reporting the role of IGSF6 in SCI has not been reported and further experimental information is required. IL1R1, the ligand-binding receptor of IL1α and IL1β, can regulate IL1-related activities (37)

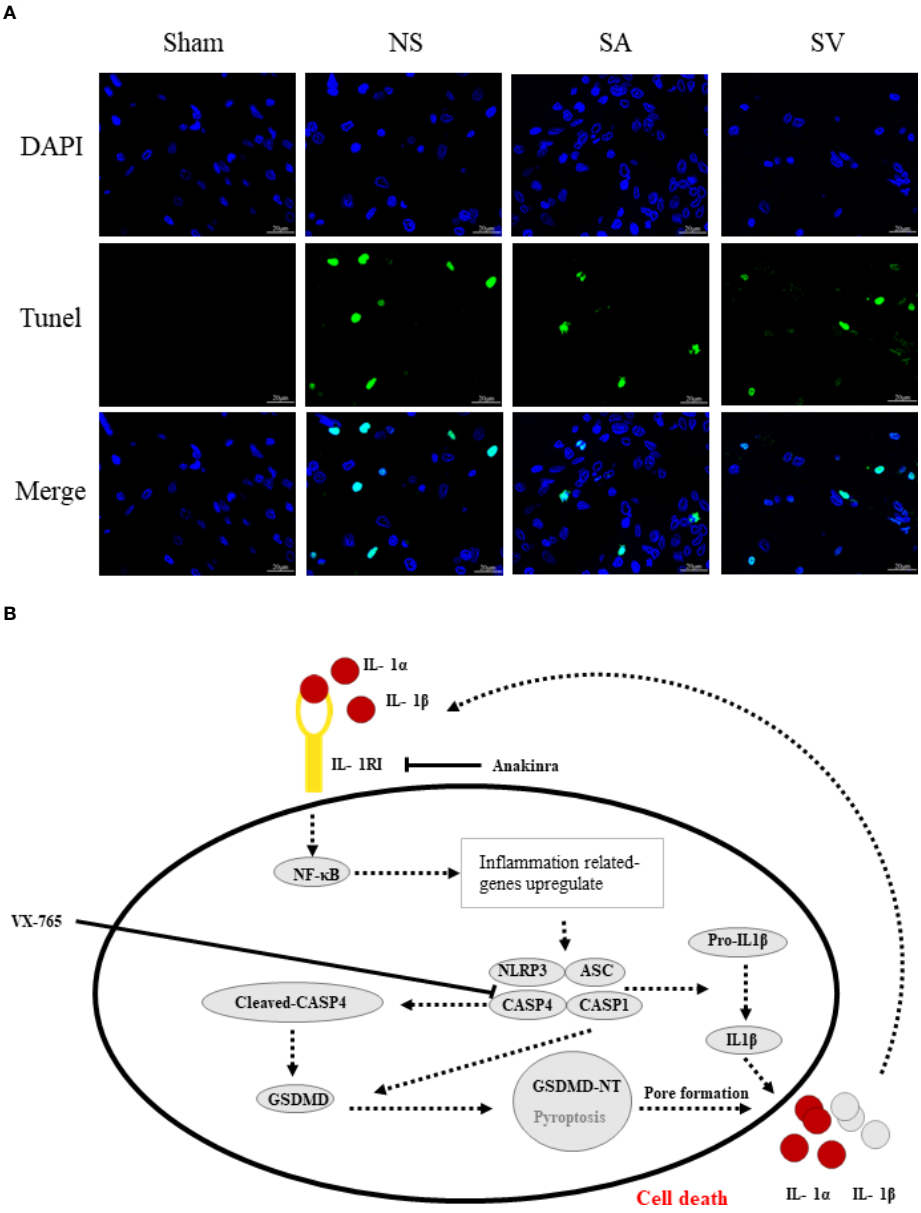

FIGURE 8
The therapeutic effect of the targetable drugs and exploration of the mechanism of spinal cord injury based on the biomarkers. **(A)** Verification of the therapeutic effect of Anakinra and VX765 for SCI by TUNEL staining (Scale bars = 20μm) (n = 3 rats per group, *p < 0.05, **p < 0.01, t-test). **(B)** Speculation for the pathomechanism of SCI.

and is highly expressed in SCI, which may contribute to posttraumatic inflammation response (38). However, IL1/IL1R1 is a double-edged sword, playing an essential role in aggravating or repairing the damage. Some SCI experiments suggested that astrocytes may initiate inflammation by promoting the entry of inflammatory monocytes and neutrophils in an IL1R1-dependent way (39). On the other hand, IL1/IL1R1 can exert beneficial effects, particularly in modest concentrations. For example, Parkinson's disease progressed more rapidly in IL-1RI null mice as compared with their wild-type counterpart (40). Previous studies reported that CASP4, IGSF6 and IL1R1 may play significant roles in SCI and be considered as the biomarkers for SCI.

To gain deeper insights into the effect of immune infiltration in SCI, some studies used CIBERSORT to legitimately assess the relationship between immune cells and biomarkers. They found that CCR could early recruit monocytes to the lesion epicenter following SCI (41) and parainflammation response was closely related to the slow progress of SCI (42, 43). In addition, *in vitro*

maturation of DCs was dramatically reduced in SCI patients (44). It was found that Tregs, an important factor in the immune system, could enhance repair of the injured nerve system by exerting an immunosuppressive effect through modulating multiple mechanisms (45). Cytokines are secreted by macrophages to regulate signaling ways to promote functional recovery after SCI (46). A study has shown that it is advantageous to decrease neutrophil activity to attenuate the pernicious impact of expanded neutrophil burst action (47). Hence, we conjecture that CASP4, IGSF6 and IL1R1 may participate in the occurrence and progression of SCI by increasing the positive-related cells or minimizing the negative-related cells. These suspicions need to be confirmed by more studies on the relationship between biomarkers and immune cells.

Mechanistically, pyroptosis involves two pathways: the canonical CASP1 inflammasome pathway, and the non-canonical CASP4/5/11 inflammasome pathway (48). The similarity between the two pathways is that both induce the maturation of GSDMD to complete pyroptosis, whereas the differences lie in the main components involved in the process of pyroptosis. In canonical pyroptosis centering around CASP1, After receiving stimulation, pro-CASP1 and ASC are recruited (often by NLRP3) to form inflammasomes, and then pro-CASP1 is cleaved to form caspase-1 for cleaving GSDMD (49). NLRP3 inflammasome, a sensor of damage-associated molecular patterns, plays a key role in SCI (50, 51). Our data showed that neuroinflammation caused by SCI increased the level of NLRP3 inflammasome, IL1β and GSDMD. Furthermore, NFκB subunit p65 will be activated by phosphorylation, promoting NLRP3 inflammasome activation. Based on the data currently available (25, 52), we made a speculation about the underlying mechanism (Figure 8B). Initiation of an inflammatory response increases the expression of various inflammatory cytokines such as IL1β and NLRP3. Post-SCI elevation of IL1R1 can activate NFκB signaling pathway by combining with IL1α or IL1β, which further upregulates inflammatory genes that encode IL1R1, pro-IL1α/IL1β and NLRP3. On the other hand, CASP4 that performs similar functions to CASP1 is activated to directly cleava GSDMD to initiate pyroptosis. Rupture of the cell membrane causes the release of inflammatory factors, which begins a new round of pyroptosis by binding to their receptors on the surrounding cell membrane. Interestingly, inhibition of IL1R1 could reduce the levels of pyroptosis-related proteins and apoptosis-related genes such as CASP3 and Bcl2. Inhibition of CASP4 could also decrease the expression of these genes, suggesting that drugs targeting these genes may be a potential strategy for the treatment of SCI by inhibiting the NLRP3 inflammasome formation and GSDMD -induced pyroptosis.

At present, the research on the application of immunosuppressants to SCI has made remarkable progress. Lee et al. (53) found that IL-20 antibodies improved motor function and reduced the formation of scar tissue around the injured spinal cord in rats with SCI, suggesting that IL-20 may be a potential therapeutic target for SCI. Giovanna Casili et al. (54) demonstrated that as an inhibitor of PARP-1/2, ABT888 exerts a protective effect after SCI by reducing autophagy-activating proteins and decreasing the apoptosis-autophagy mechanism. In contrast to these cases, the immunosuppressants we used were obtained by bioinformatic analysis of gene sequencing results, which is clearly directed; secondly, the progression of SCI can be detected by the altered expression of markers during the use of immunosuppressants, which in turn can better guide the application of the corresponding inhibitors; Besides, Anakinra has stable performance and significant therapeutic effect that has been applied to clinical studies of various diseases (55–57), and is expected to be a potential drug for the treatment of spinal cord injury. Yet, Anakinra and VX-765 have not yet been carried out to treat clinical patients with SCI, and further study is needed.

The reliability of the analysis results will be improved after introducing new calculation methods. Innovative scientific methods such as the Boruta algorithm and LASSO logistic regression were employed to prove biomarkers of SCI. As it is difficult to obtain large numbers of human spinal cord samples, we used mouse and rat samples instead, which may cause inaccuracy in genomic analysis. Since the focus of this paper is to explore the reliability of biomarkers and the effectiveness of marker-targeted immunosuppressants, we will perform cellular experiments to explore underlying mechanisms and functional phenotypes in the next step to further demonstrate our results.

In conclusion, CASP4, IGSF6 and IL1R1 were identified as key biomarkers of SCI. Inhibition of these biomarkers was regarded as an effective approach to achieving SCI repair by inhibiting NF-kB and NLRP3 inflammasome activation, thus blocking GSDMD -induced pyroptosis. Besides, TIL, dendritic cells, Treg, macrophages, parainflammation, and neutrophils may play essential roles in the progression of SCI. These findings may help mine the potential mechanism and explore treatment options for SCI.

Data availability statement

The datasets presented in this study can be found in online repositories. The names of the repository/repositories and accession number(s) can be found in the article/supplementary material.

Ethics statement

The animal study was reviewed and approved by animal ethics committee in Shanghai Changzheng Hospital.

Author contributions

CW, HY, and XL designed the experiment. CW, HM, BZ, TH, HW, LW, LH, QL, WW, and YS performed the animal

trials, and sample and data analysis. CW, HM, and BZ wrote the manuscript. HY and XL revised the manuscript. All authors contributed to the article and approved the submitted version.

Funding

This study was supported by the Research Projects of Shanghai Changzheng Hospital (No.0910 and No.2020YCXYJ-ZD06) and the National Natural Science Foundation of China (No. 81572201 and No. 81802185).

Acknowledgments

This work has benefited from GEO. We thank the GEO network for its generous sharing of large amounts of data.

Conflict of interest

The authors declare that the research was conducted in the absence of any commercial or financial relationships that could be construed as a potential conflict of interest.

The handling editor declared a shared parent affiliation with the authors at the time of review.

Publisher's note

References

1. Shrestha R, Qiao J, Shen F, Bista K, Zhao Z, Yang J. Intra-spinal bone marrow mononuclear cells transplantation inhibits the expression of nuclear factor-κB in acute transection spinal cord injury in rats. *J Korean Neurosurg Soc* (2014) 56 (5):375–82. doi: 10.3340/jkns.2014.56.5.375

2. van Dijsseldonk RB, van Nes IJW, Geurts ACH, Keijsers NLW. Exoskeleton home and community use in people with complete spinal cord injury. *Sci Rep* (2020) 10(1):15600. doi: 10.1038/s41598-020-72397-6

3. Calvert JS, Grahn PJ, Zhao KD, Lee KH. Emergence of epidural electrical stimulation to facilitate sensorimotor network functionality after spinal cord injury. *Neuromodulation* (2019) 22(3):244–52. doi: 10.1111/ner.12938

4. Lavis T, Goetz LL. Comprehensive care for persons with spinal cord injury. *Phys Med Rehabil Clinics North America* (2019) 30(1):55–72. doi: j.biopha.2017.09.133/j.pmr.2018.08.010

5. Niu S-P, Zhang Y-J, Han N, Yin X-F, Zhang D-Y, Kou Y-H. Identification of four differentially expressed genes associated with acute and chronic spinal cord injury based on bioinformatics data. *Neural Regen Res* (2021) 16(5):865–70. doi: 10.4103/1673-5374.297087

6. Wang T, Wu B, Zhang X, Zhang M, Zhang S, Huang W, et al. Identification of gene coexpression modules, hub genes, and pathways related to spinal cord injury using integrated bioinformatics methods. *J Cell Biochem* (2019) 120 (5):6988–97. doi: 10.1002/jcb.27908

7. Yao X, Liu Z, Chen J, Huang Z, Liu J, Sun B, et al. Proteomics and bioinformatics reveal insights into neuroinflammation in the acute to subacute phases in rat models of spinal cord contusion injury. *FASEB J* (2021) 35(7):. doi: 10.1096/fj.202100081RR

8. Xu P, Zhang F, Chang M-M, Zhong C, Sun C-H, Zhu H-R, et al. Recruitment of γδ T cells to the lesion *via* the CCL2/CCR2 signaling after spinal cord injury. *J Neuroinflamm* (2021) 18(1):64. doi: 10.1186/s12974-021-02115-0

9. Torabi S, Anjamrooz SH, Zeraatpisheh Z, Aligholi H, Azari H. Ibrutinib reduces neutrophil infiltration, preserves neural tissue and enhances locomotor recovery in mouse contusion model of spinal cord injury. *Anat Cell Biol* (2021) 54 (3):350–60. doi: 10.5115/acb.20.299

10. Yates AG, Jogia T, Gillespie ER, Couch Y, Ruitenberg MJ, Anthony DC. Acute IL-1RA treatment suppresses the peripheral and central inflammatory response to spinal cord injury. *J Neuroinflamm* (2021) 18(1):15. doi: 10.1186/s12974-020-02050-6

11. Zhang G, Yang P. Bioinformatics genes and pathway analysis for chronic neuropathic pain after spinal cord injury. *BioMed Res Int* (2017) 2017:6423021. doi: 10.1155/2017/6423021

12. Wu J, Renn CL, Faden AI, Dorsey SG. TrkB.T1 contributes to neuropathic pain after spinal cord injury through regulation of cell cycle pathways. *J Neurosci* (2013) 33(30):12447–63. doi: 10.1523/JNEUROSCI.0846-13.2013

13. Ma S, Wang J, Liu L, Xia L, Tao R. Identification of temporal genes involved in the mechanisms of spinal cord injury. *Spinal Cord* (2017) 55(4):355–61. doi: 10.1038/sc.2016.183

14. Gautier L, Cope L, Bolstad BM, Irizarry RA. Affy–analysis of affymetrix GeneChip data at the probe level. *Bioinformatics* (2004) 20(3):307–15. doi: 10.1093/bioinformatics/btg405

15. Parker HS, Leek JT, Favorov AV, Considine M, Xia X, Chavan S, et al. Preserving biological heterogeneity with a permuted surrogate variable analysis for genomics batch correction. *Bioinformatics* (2014) 30(19):2757–63. doi: 10.1093/bioinformatics/btu375

16. Deng YJ, Ren EH, Yuan WH, Zhang GZ, Wu ZL, Xie QQ. GRB10 and E2F3 as diagnostic markers of osteoarthritis and their correlation with immune infiltration. *Diagn (Basel)* (2020) 10(3):171. doi: 10.3390/diagnostics10030171

17. Ritchie ME, Phipson B, Wu D, Hu Y, Law CW, Shi W, et al. Limma powers differential expression analyses for RNA-sequencing and microarray studies. *Nucleic Acids Res* (2015) 43(7):e47. doi: 10.1093/nar/gkv007

18. Ginestet C. ggplot2: Elegant graphics for data analysis. *R Stat Soc* (2011) 174 (1):245–6. doi: 10.1111/j.1467-985X.2010.00676_9.x

19. Tibshirani R. Regression shrinkage and selection *Via* the lasso. *R Stat Soc* (1996) 58(1):267–88. doi: 10.1111/j.2517-6161.1996.tb02080.x

20. Breiman L. Random forests. *Mach Learn* (2001) 45(1):5–32. doi: 10.1023/A:1010933404324

21. Friedman J, Hastie T, Tibshirani R. Regularization paths for generalized linear models *via* coordinate descent. *J Stat Softw* (2010) 33(1):1–22. doi: 10.18637/jss.v033.i01

22. Cai W, Li H, Zhang Y, Han G. Identification of key biomarkers and immune infiltration in the synovial tissue of osteoarthritis by bioinformatics analysis. *PeerJ* (2020) 8:e8390. doi: 10.7717/peerj.8390

23. Subramanian A, Tamayo P, Mootha V, Mukherjee S, Ebert B, Gillette M, et al. Gene set enrichment analysis: a knowledge-based approach for interpreting genome-wide expression profiles. *Proc Natl Acad Sci United States America* (2005) 102(43):15545–50. doi: 10.1073/pnas.0506580102

24. Hänzelmann S, Castelo R, Guinney J. GSVA: gene set variation analysis for microarray and RNA-seq data. *BMC Bioinf* (2013) 14:7. doi: 10.1186/1471-2105-14-7

25. Al Mamun A, Wu Y, Monalisa I, Jia C, Zhou K, Munir F, et al. Role of pyroptosis in spinal cord injury and its therapeutic implications. *J Adv Res* (2021) 28:97-109. doi: j.biopha.2017.09.133/j.jare.2020.08.004

26. Rougon G, Hobert O. New insights into the diversity and function of neuronal immunoglobulin superfamily molecules. *Annu Rev Neurosci* (2003) 26:207–38. doi: 10.1146/annurev.neuro.26.041002.131014

27. Xu L, Botchway BOA, Zhang S, Zhou J, Liu X. Inhibition of NF-kappaB signaling pathway by resveratrol improves spinal cord injury. *Front Neurosci* (2018) 12:690. doi: 10.3389/fnins.2018.00690

28. Ning S, Zhu H, Shao J, Liu Y, Lan J, Miao J, et al. MiR-21 inhibitor improves locomotor function recovery by inhibiting IL-6R/JAK-STAT pathway-mediated inflammation after spinal cord injury in model of rat. *Eur Rev Med Pharmacol Sci* (2019) 23(2):433–40. doi: 10.26355/eurrev_201901_16852

29. Inoue T, Ichikawa D, Ueno T, Cheong M, Inoue T, Whetstone WD, et al. XGBoost, a machine learning method, predicts neurological recovery in patients with cervical spinal cord injury. *Neurotrauma Rep* (2020) 1(1):8-16. doi: 10.1089/neur.2020.0009

30. Fan G, Yang S, Liu H, Xu N, Chen Y, He J, et al. Machine learning-based prediction of prolonged ICU- stay for critical patients with spinal cord injury. *Spine* (2021) 47(9):E390-E398. doi: 10.1097/BRS.0000000000004267

31. Vidyasagar M. Identifying predictive features in drug response using machine learning: Opportunities and challenges. *Annu Rev Pharmacol Toxicol* (2015) 55(1):15–34. doi: 10.1146/annurev-pharmtox-010814-124502

32. Veen KM, de Angst IB, Mokhles MM, Westgeest HM, Kuppen M, Groot CAU, et al. A clinician's guide for developing a prediction model: a case study using real-world data of patients with castration-resistant prostate cancer. *J Cancer Res Clin Oncol* (2020) 146(8):2067–75. doi: 10.1007/s00432-020-03286-8

33. Wandel MP, Kim BH, Park ES, Boyle KB, Nayak K, Lagrange B, et al. Guanylate-binding proteins convert cytosolic bacteria into caspase-4 signaling platforms. *Nat Immunol* (2020) 21(8):880–91. doi: 10.1038/s41590-020-0697-2

34. King K, Moody A, Fisher S, Mirza M, Cuthbert A, Hampe J, et al. Genetic variation in the IGSF6 gene and lack of association with inflammatory bowel disease. *Eur J Immunogenetics* (2003) 30(3):187–90. doi: 10.1046/j.1365-2370.2003.00387.x

35. Yang AX, Chong N, Jiang Y, Catalano J, Puri RK, Khleif SN. Molecular characterization of antigen-peptide pulsed dendritic cells: immature dendritic cells develop a distinct molecular profile when pulsed with antigen peptide. *PloS One* (2014) 9(1):e86306. doi: 10.1371/journal.pone.0086306

36. Gridley DS, Pecaut MJ, Rizvi A, Coutrakon GB, Luo-Owen X, Makinde AY, et al. Low-dose, low-dose-rate proton radiation modulates CD4(+) T cell gene expression. *Int J Radiat Biol* (2009) 85(3):250–61. doi: 10.1080/09553000902748609

37. Boraschi D, Italiani P, Weil S, Martin MU. The family of the interleukin-1 receptors. *Immunol Rev* (2018) 281(1):197–232. doi: 10.1111/imr.12606

38. Wang XF, Huang LD, Yu PP, Hu JG, Yin L, Wang L, et al. Upregulation of type I interleukin-1 receptor after traumatic spinal cord injury in adult rats. *Acta Neuropathol* (2006) 111(3):220–8. doi: 10.1007/s00401-005-0016-x

39. Pineau I, Sun L, Bastien D, Lacroix S. Astrocytes initiate inflammation in the injured mouse spinal cord by promoting the entry of neutrophils and inflammatory monocytes in an IL-1 receptor/MyD88-dependent fashion. *Brain Behav Immun* (2010) 24(4):540–53. doi: j.biopha.2017.09.133/j.bbi.2009.11.007

40. Parish CL, Finkelstein DI, Tripanichkul W, Satoskar AR, Drago J, Horne MK. The role of interleukin-1, interleukin-6, and glia in inducing growth of neuronal terminal arbors in mice. *J Neurosci* (2002) 22(18):8034–41. doi: 10.1523/JNEUROSCI.22-18-08034.2002

41. Ma M, Wei T, Boring L, Charo IF, Ransohoff RM, Jakeman LB. Monocyte recruitment and myelin removal are delayed following spinal cord injury in mice with CCR2 chemokine receptor deletion. *J Neurosci Res* (2002) 68(6):691–702. doi: 10.1002/jnr.10269

42. Chen M, Xu H. Parainflammation, chronic inflammation, and age-related macular degeneration. *J Leukoc Biol* (2015) 98(5):713–25. doi: 10.1189/jlb.3RI0615-239R

43. Galbavy W, Lu Y, Kaczocha M, Puopolo M, Liu L, Rebecchi MJ. Transcriptomic evidence of a para-inflammatory state in the middle aged lumbar spinal cord. *Immun Ageing* (2017) 14:9. doi: 10.1186/s12979-017-0091-6

44. Picotto G, Morse LR, Nguyen N, Saltzman J, Battaglino R. TMEM176A and TMEM176B are candidate regulators of inhibition of dendritic cell maturation and function after chronic spinal cord injury. *J Neurotrauma* (2020) 37(3):528–33. doi: 10.1089/neu.2019.6498

45. Huan Y, He Y, Liu B, Li Y, Jia L, Qu C, et al. Zhenbao pill reduces the percentage of treg cells by inducing HSP27 expression. *BioMed Pharmacother* (2017) 96:818–24. doi: j.biopha.2017.09.133/j.biopha.2017.09.133

46. Chen J, Wang Z, Zheng Z, Chen Y, Khor S, Shi K, et al. Neuron and microglia/macrophage-derived FGF10 activate neuronal FGFR2/PI3K/Akt signaling and inhibit microglia/macrophages TLR4/NF-kappaB-dependent neuroinflammation to improve functional recovery after spinal cord injury. *Cell Death Dis* (2017) 8(10):e3090. doi: 10.1038/cddis.2017.490

47. Kanyilmaz S, Hepguler S, Atamaz FC, Gokmen NM, Ardeniz O, Sin A. Phagocytic and oxidative burst activity of neutrophils in patients with spinal cord injury. *Arch Phys Med Rehabil* (2013) 94(2):369–74. doi: j.biopha.2017.09.133/j.apmr.2012.09.015

48. Wang YY, Liu XL, Zhao R. Induction of pyroptosis and its implications in cancer management. *Front Oncol* (2019) 9:971. doi: 10.3389/fonc.2019.00971

49. Tsuchiya K. Inflammasome-associated cell death: Pyroptosis, apoptosis, and physiological implications. *Microbiol Immunol* (2020) 64(4):252–69. doi: 10.1111/1348-0421.12771

50. He Y, Hara H, Núñez G. Mechanism and regulation of NLRP3 inflammasome activation. *Trends Biochem Sci* (2016) 41(12):1012–21. doi: j.biopha.2017.09.133/j.tibs.2016.09.002

51. Jiang W, Li M, He F, Zhou S, Zhu L. Targeting the NLRP3 inflammasome to attenuate spinal cord injury in mice. *J Neuroinflamm* (2017) 14(1):207. doi: 10.1186/s12974-017-0980-9

52. Gehrke N, Hövelmeyer N, Waisman A, Straub BK, Weinmann-Menke J, Wörns MA, et al. Hepatocyte-specific deletion of IL1-RI attenuates liver injury by blocking IL-1 driven autoinflammation. *J Hepatol* (2018) 68(5):986–95. doi: j.biopha.2017.09.133/j.jhep.2018.01.008

53. Lee JS, Hsu YH, Chiu YS, Jou IM, Chang MS. Anti-IL-20 antibody improved motor function and reduced glial scar formation after traumatic spinal cord injury in rats. *J Neuroinflamm* (2020) 17(1):156. doi: 10.1186/s12974-020-01814-4

54. Casili G, Campolo M, Lanza M, Filippone A, Scuderi S, Messina S, et al. Role of ABT888, a novel Poly(ADP-ribose) polymerase (PARP) inhibitor in countering autophagy and apoptotic processes associated to spinal cord injury. *Mol Neurobiol* (2020) 57(11):4394–407. doi: 10.1007/s12035-020-02033-x

55. Brucato A, Imazio M, Gattorno M, Lazaros G, Maestroni S, Carraro M, et al. Effect of anakinra on recurrent pericarditis among patients with colchicine resistance and corticosteroid dependence: The AIRTRIP randomized clinical trial. *Jama* (2016) 316(18):1906–12. doi: 10.1001/jama.2016.15826

56. Tzanetakou V, Kanni T, Giatrakou S, Katoulis A, Papadavid E, Netea MG, et al. Safety and efficacy of anakinra in severe hidradenitis suppurativa: A randomized clinical trial. *JAMA Dermatol* (2016) 152(1):52–9. doi: 10.1001/jamadermatol.2015.3903

57. Saag KG, Khanna PP, Keenan RT, Ohlman S, Osterling Koskinen L, Sparve E, et al. A randomized, phase II study evaluating the efficacy and safety of anakinra in the treatment of gout flares. *Arthritis Rheumatol* (2021) 73(8):1533–42. doi: 10.1002/art.41699

frontiers | Frontiers in Immunology

TYPE Original Research
PUBLISHED 15 August 2022
DOI 10.3389/fimmu.2022.918507

OPEN ACCESS

EDITED BY
Alessandra Mortellaro,
San Raffaele Telethon Institute for Gene Therapy (SR-Tiget), Italy

REVIEWED BY
Sreya Ghosh,
Boston Children's Hospital and Harvard Medical School, United States
Shah S. Hussain,
University of Alabama at Birmingham, United States

*CORRESPONDENCE
Isabelle Couillin
isabelle.couillin@cnrs-orleans.fr
Nicolas Riteau
nicolas.riteau@cnrs-orleans.fr

SPECIALTY SECTION
This article was submitted to Molecular Innate Immunity, a section of the journal Frontiers in Immunology

RECEIVED 12 April 2022
ACCEPTED 26 July 2022
PUBLISHED 15 August 2022

CITATION
Huot-Marchand S, Nascimento M, Culerier E, Bourenane M, Savigny F, Panek C, Serdjebi C, Le Bert M, Quesniaux VFJ, Ryffel B, Broz P, Riteau N, Gombault A and Couillin I (2022) Cigarette smoke-induced gasdermin D activation in bronchoalveolar macrophages and bronchial epithelial cells dependently on NLRP3.
Front. Immunol. 13:918507.
doi: 10.3389/fimmu.2022.918507

Cigarette smoke-induced gasdermin D activation in bronchoalveolar macrophages and bronchial epithelial cells dependently on NLRP3

Sarah Huot-Marchand[1], Mégane Nascimento[1], Elodie Culerier[1], Mélissa Bourenane[1], Florence Savigny[1], Corinne Panek[1], Cindy Serdjebi[2], Marc Le Bert[1], Valérie F. J. Quesniaux[1], Bernhard Ryffel[1], Petr Broz[3], Nicolas Riteau[1*], Aurélie Gombault[1] and Isabelle Couillin[1*]

[1]University of Orleans and CNRS, INEM-UMR7355, Orleans, France, [2]Biocellvia, Marseille, France, [3]Department of Biochemistry, University of Lausanne, Lausanne, Switzerland

Chronic pulmonary inflammation and chronic obstructive pulmonary disease (COPD) are major health issues largely due to air pollution and cigarette smoke (CS) exposure. The role of the innate receptor NLRP3 (nucleotide-binding domain and leucine-rich repeat containing protein 3) orchestrating inflammation through formation of an inflammasome complex in CS-induced inflammation or COPD remains controversial. Using acute and subchronic CS exposure models, we found that *Nlrp3*-deficient mice or wild-type mice treated with the NLRP3 inhibitor MCC950 presented an important reduction of inflammatory cells recruited into the bronchoalveolar space and of pulmonary inflammation with decreased chemokines and cytokines production, in particular IL-1β demonstrating the key role of NLRP3. Furthermore, mice deficient for *Caspase-1/Caspase-11* presented also decreased inflammation parameters, suggesting a role for the NLRP3 inflammasome. Importantly we showed that acute CS-exposure promotes NLRP3-dependent cleavage of gasdermin D in macrophages present in the bronchoalveolar space and in bronchial airway epithelial cells. Finally, *Gsdmd*-deficiency reduced acute CS-induced lung and bronchoalveolar space inflammation and IL-1β secretion. Thus, we demonstrated in our model that NLRP3 and gasdermin D are key players in CS-induced pulmonary inflammation and IL-1β release potentially through gasdermin D forming-pore and/or pyroptoctic cell death.

KEYWORDS

cigarette smoke, NLRP3 inflammasome, gasdermin D, lung, mice

Introduction

Among lung inflammatory diseases, chronic obstructive pulmonary disease (COPD) represents one of the most important public health issue. This illness is now the third leading cause of death in the world as predicted by the World Health Organization (WHO). COPD is characterized by chronic inflammation and mucus hypersecretion responsible for bronchial obstruction and that may lead to alveolar wall destruction and impaired lung functions (1, 2). Cigarette smoking (CS) is the major cause of COPD including emphysema with more than 95% of cases in industrialized countries (3). Inflammation can persist when smoking has been stopped and still be present even decades later. Frequent exacerbations of lung inflammation occur during respiratory infections which are characterized by impaired immune response to invading pathogens (4). Current treatments have limited efficiency (5) and thus research efforts to better understand the cellular and molecular mechanisms involved in airway inflammation leading to the pathophysiology of COPD have become a priority. COPD patients display a significant increase of airway recruited alveolar macrophages and neutrophils, which correlates with the disease severity (1, 2, 6).

Inflammasomes are cytoplasmic multiprotein complexes that orchestrate diverse functions during homeostasis and inflammation (7). Among the various inflammasomes, NLRP3 inflammasome demonstrated the most significant clinical relevance to date (8). The canonical NLRP3 inflammasome consists of the sensory protein NLRP3, the adaptor protein ASC (apoptosis-associated speck-like protein containing a CARD), and the effector protein caspase-1 (9, 10). NLRP3 activation requires a first signal resulting in transcriptional and post-transcriptional priming of NLRP3 and to pro-IL-1β, and pro-IL-18 expression and a second signal to promote NLRP3 inflammasome complex formation and subsequent caspase-1 activation, and pro-IL-1β and/or pro-IL-18 maturation (7).

The role of the NLRP3 inflammasome in CS-induced pulmonary inflammation and CS-resulting COPD is unclear. NLRP3 overexpression was reported in lungs of COPD patients and correlated with airway obstruction (11). *In vivo* studies reported increased NLRP3 and pro-IL-1β protein expression upon CS exposure in adult mice (12) or in offspring after maternal CS exposure (13). Mice exposure to cigarette smoke condensate (CSC) also activates NLRP3 inflammasome (14). In contrast, CS was shown to repress NLRP3 inflammasome-dependent innate immune response to asbestos in mice (15). In addition, cigarette smoke extract (CSE) or CSC induce activation of NLRP3 inflammasome in bronchial and alveolar epithelial cells and/or monocytic cells in *in vitro* experiments (16–18). Finally, CSE was shown to inhibit the NLRP3 inflammasome and to lead to caspase-1 activation *via* TLR4-TRIF-Caspase-8 axis in human macrophages (19).

Inflammasome-dependent activation of caspase-1 also leads to gasdermin D (GSDMD) protein cleavage thereby releasing its N-terminal domain, which forms pores in plasma and organellar membranes. GSDMD-N pore-forming protein was first described as the executor of pyroptosis, a programmed cell death dependent on inflammasome activation and as a part of the host innate immune defense allowing to kill bacteria-infected cells and restrict pathogen infection (20). Pyroptosis cell death leads to the release of pro-inflammatory cytokines and endogenous danger signals that amplify inflammation (21–23). On the other hand, GSDMD-mediated pyroptosis can be induced directly by caspase-8 or by the noncanonical inflammasome, *via* caspase-11-dependent cleavage (24). Besides macrophages, pyroptosis was also detected in neutrophils upon activation of non-canonical inflammasome leading to neutrophil extracellular trap (NET) formation dependent on GSDMD and caspase-11 (25), and in tissue cells in particular airway epithelial cells, exacerbating airway inflammation (26).

Importantly, GSDMD-forming pores at the plasma membrane were recently identified as the most important mechanism to explain IL-1β secretion, taking into account that this cytokine lacks a signal sequence preventing classical secretion through the endoplasmic reticulum/Golgi compartment (27). GSDMD pores were shown to be selective channels for cytokine release and ion fluxes, permitting passage of small molecules up to 25-50 kDa in particular of mature IL-1β and IL-18, independently of cell lysis, whereas larger proteins, such as the heterotetrameric caspase-1 p10/p20 (60 kDa), are released after lysis of pyroptotic macrophages (28). Interestingly, calcium influx through GSDMD pores promotes membrane repair and epithelial cell survival, highlighting that GSDMD activation may result in different fate (28, 29).

The NLRP3/caspase-1 GSDMD pathway was shown to be involved in the induction of human airway epithelial cell pyroptosis by CSE or nicotine, and associated with COPD progression (30, 31). However, whether GSDMD activation also contributes to CS-mediated pulmonary inflammation and/or COPD was poorly studied with mostly *in vitro* data and remains to be elucidated.

We here addressed the involvement of the NLRP3 inflammasome and gasdermin D in pulmonary cell influx and cytokine secretion upon acute or subchronic CS exposure.

Using an acute murine model of CS exposure which could mimic exacerbation phases of COPD or pulmonary diseases, already used to describe recent papers (32, 33), we showed that *Nlrp3*- or *Caspase-1/11*-deficiency or pharmacological treatment with the NLRP3 inhibitor MCC950 strongly reduced pulmonary inflammation and remodeling. Importantly, NLRP3 depletion reduced IL-1β levels in the bronchoalveolar space. Due to the pivotal role of IL-1β release in multiple inflammatory diseases, we hypothesized that GSDMD-forming pores contribute to CS-induced pulmonary inflammation. We showed for the first time

that mouse acute CS exposure induces GSDMD activation in lung tissue and macrophages recruited into the bronchoalveolar space, through a NLRP3 dependent manner. In addition, using *Gsdmd*-deficient mice, we demonstrated that GSDMD is a key player in acute CS-induced lung inflammation.

Results

Nlrp3 deficiency dampens pulmonary inflammation and remodeling in response to cigarette smoke exposure

Since the role of the NLRP3 inflammasome in cigarette smoke (CS)-induced pulmonary inflammation is not well-established *in vivo*, we analyzed the impact of *Nlrp3* deficiency using first a subchronic models of mouse CS-exposure during 6 weeks which leads to pulmonary inflammation, in comparison to chronic model of 12 weeks often used to induce experimental COPD in mice. Wild-type (WT) and *Nlrp3*-deficient (*Nlrp3*$^{-/-}$) mice were exposed to CS three times a day, five days a week for six weeks (Figure 1A). As compared to unexposed (Air) mice, subchronically CS-exposed WT mice presented increased numbers of bronchoalveolar lavage (BAL) cells (Figure 1B), in particular macrophages (Figure 1C), neutrophils (Figure 1D) and lymphocytes (Figure 1E). Importantly, neutrophils and lymphocytes recruitment into the BAL was significantly attenuated in CS-exposed *Nlrp3*$^{-/-}$ mice. Neutrophils play a major role in the pathogenesis developed in response to CS exposure (34, 35). As a marker of recruited neutrophils, BAL levels of myeloperoxidase (MPO) (Figure 1F), an enzyme present in neutrophil granules, and of the neutrophilic chemokine CXCL1 (Figure 1G) were elevated in CS-exposed WT mice and significantly decreased in CS-exposed *Nlrp3*$^{-/-}$ mice. In lung homogenates MPO (Figure 1H) and CXCL1 (Figure 1I) were also significantly reduced in CS-exposed Nlrp3$^{-/-}$ mice compared to CS-exposed WT mice. In addition, we observed significantly reduction of IL-1β protein (Figure 1J) and *proIl-18* mRNA (Figure 1K) levels in the lungs of CS-exposed *Nlrp3*$^{-/-}$ mice compared to CS-exposed WT mice.

We next analyzed the balance between expression of remodeling proteases involved in the progression to COPD and their inhibitors. We focused on matrix metalloproteinase (MMP)-9, a gelatinase produced by alveolar macrophages and neutrophils that degrades extracellular matrix proteins and promotes neutrophil chemotaxis, and MMP-12 an elastase mainly produced by alveolar macrophages that contributes to alveolar damages (36) and their inhibitor tissue inhibitor of matrix metalloproteinase 1 (TIMP-1). MMP-9 and TIMP-1 protein levels (Figures 2A, B) in BAL and in lungs (Figures 2C, D) were significantly decreased in subchronically CS-exposed *Nlrp3*$^{-/-}$ mice as compared to WT mice. *Mmp-12* mRNA levels in lungs (Figure 2E) were reduced in CS-exposed *Nlrp3*$^{-/-}$ mice as compared to WT mice. Further, lung microsections and histology analysis showed increased cell recruitment and inflammation in lung tissue of CS-exposed WT mice compared to Air-exposed mice, which were attenuated in CS-exposed *Nlrp3*$^{-/-}$ mice (Figures 2F, G). These findings were confirmed by an increase in Ly6G labelling in lungs of CS-exposed WT mice (Figures 2H, I). In lungs of *Nlrp3*$^{-/-}$ mice, however, CS exposure did not affect the neutrophil count compared to Air-exposed deficient mice.

We next performed acute CS exposures during 4 days (Figure S1A) that confirmed reduced inflammation in *Nlrp3*$^{-/-}$ in comparison to WT mice. Total cells (Figure S1B), macrophages (Figure S1C) and neutrophils (Figure S1D) numbers in BAL were significantly attenuated in *Nlrp3*$^{-/-}$ mice acutely exposed to CS as compared to CS-exposed WT mice. BAL levels of MPO (Figure S1E), CXCL1 (Figure S1F), IL-1β (Figure S1G), as well as MMP-9 (Figure S1H) and TIMP-1 (Figure S1I) were significantly reduced in CS-exposed *Nlrp3*$^{-/-}$ mice compared to CS-exposed WT mice. We also observed significant reduction of CXCL1 (Figure S1J), IL-1β (Figure S1K) in lungs of CS-exposed *Nlrp3*$^{-/-}$ mice. Finally, MMP-9 (Figure S1L) and TIMP-1 (Figure S1M) levels in lungs of CS-exposed *Nlrp3*$^{-/-}$ mice were non significantly reduced as compared to WT mice. Infiltrating cells were not detected on histology slides after only 4 days of CS (data not shown). Our results demonstrate that the NLRP3 sensor is important for pulmonary inflammation and remodeling in response to CS exposure. Since our data show the role of NLRP3 in pulmonary inflammation induced by both acute and subchronic CS-exposure in mice, we next used the acute exposure model as previously (32, 33) in order to investigate the mechanism of NLRP3-mediated lung inflammation.

Pharmacological MCC950 treatment inhibits lung inflammation induced by cigarette smoke

To confirm NLRP3 implication as a sensor in CS-induced pulmonary inflammation, we treated mice intraperitonealy with MCC950, a potent specific inhibitor of NLRP3 inflammasome activation (37, 38). MCC950 is active in different NLRP3-dependent inflammatory mouse models, impairing *in vivo* IL-1β production and attenuating the severity in inflammatory disease models (39). WT mice exposed to CS during 4 days were treated daily with MCC950 or vehicle (20mg/kg) (Figure 3A). BAL total cells (Figure 3B), macrophages (Figure 3C) and neutrophils (Figure 3D) were significantly reduced in MCC950-treated CS-exposed mice as compared to control group. Moreover, BAL levels of MPO levels (Figure 3E), of the neutrophil gelatinase-associated lipocalin (LCN)-2 (Figure 3F), a protein expressed by neutrophils and involved in innate immunity, of the neutrophilic chemokine CXCL1 (Figure 3G)

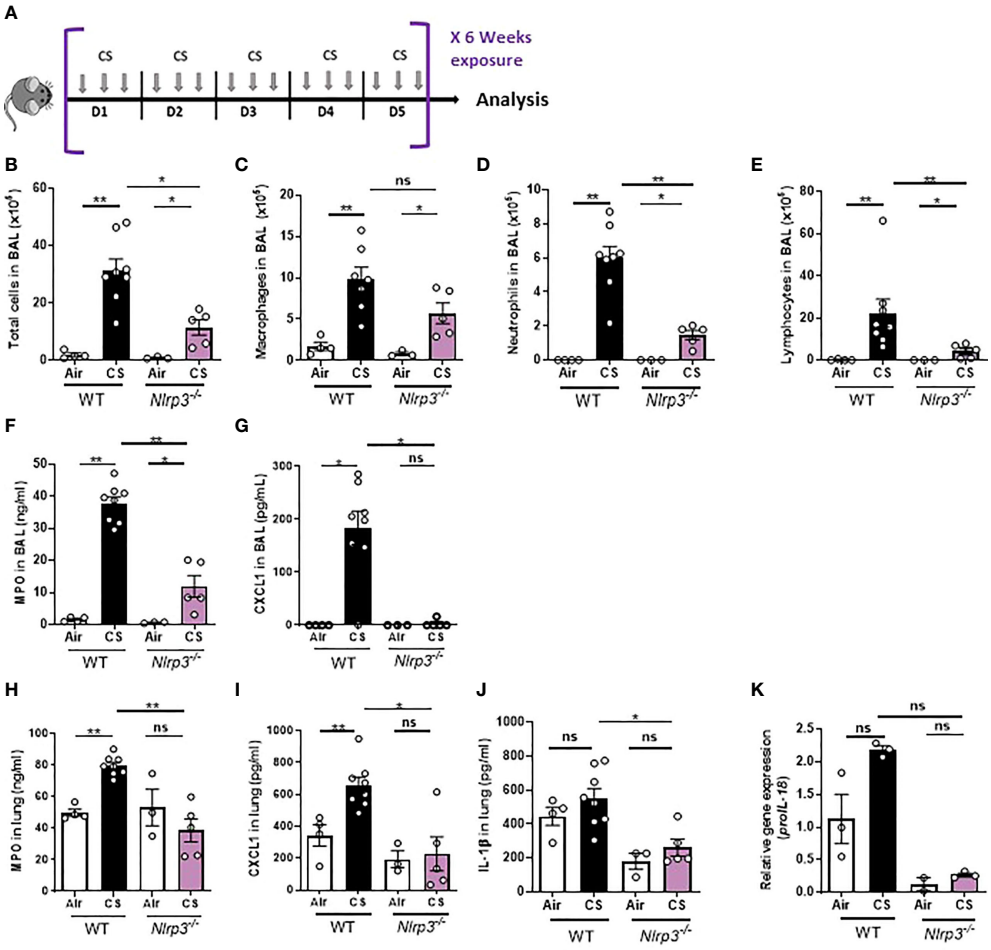

FIGURE 1
Nlrp3 deficiency impairs inflammation to subchronic cigarette smoke (CS) exposure in mice. WT and *Nlrp3*$^{-/-}$ mice were exposed to CS or Air during 6 weeks **(A)**. CS exposure led to significant decrease counts of total cells **(B)**, macrophages **(C)**, neutrophils **(D)** and lymphocytes **(E)** into BAL of *Nlrp3*$^{-/-}$ mice compared to exposed WT mice. Levels of myeloperoxidase (MPO) **(F)**, CXCL1 **(G)** in BAL, and MPO **(H)**, CXCL1 **(I)** and IL-1β **(J)** in lung were reduced in *Nlrp3*$^{-/-}$ mice exposed to CS compared to CS WT mice. The *proIL-18* mRNA expression **(K)** was reduced in CS *Nlrp3*$^{-/-}$ mice as compared to exposed WT mice. Data are representative of one experiment and are expressed as mean values ± SEM (n= 6-9 mice per group, *p < 0.05, **p < 0.01, ns, non significant, using a Mann Whitney test).

and also of CXCL5 (Figure 3H) and CXCL15 (Figure 3I), two neutrophilic chemokines mainly produced by epithelial cells, were significantly reduced in BAL of MCC950-treated CS-exposed mice compared to CS-exposed WT mice. Importantly, BAL levels of the proinflammatory cytokines IL-1β (Figure 3J) was significantly decreased in MCC950-treated CS-exposed mice. Levels of MMP-9 (Figure 3K) and TIMP-1 (Figure 3L) were significantly and non significative reduced respectively in BAL of MCC950-treated CS-exposed mice. Furthermore, in lung tissues, levels of MPO, LCN-2, CXCL1, CXCL5, CXCL15, IL-1β, MMP-9 and TIMP-1 (Figures 3M-T) were significantly decreased in MCC950-treated CS-exposed compared to CS-exposed WT mice. Thus, results with NLRP3 pharmacological inhibition confirmed those obtained with NLRP3 gene deletion, showing that this receptor is involved in acute inflammation and remodeling induced by CS in mice.

Caspase-1 and/or caspase 11 play a key role in acute CS-induced pulmonary inflammation

In order to investigate the role of the canonical and/or non canonical inflammasome in pulmonary inflammation to CS, we used mice double deficient for caspase-1 and caspase-11 (*Caspase-1/11*$^{-/-}$). Acute CS-exposure led to reduced inflammation in *Caspase-1/11*$^{-/-}$ mice in comparison to WT mice with a strong decrease in BAL total cells, macrophages

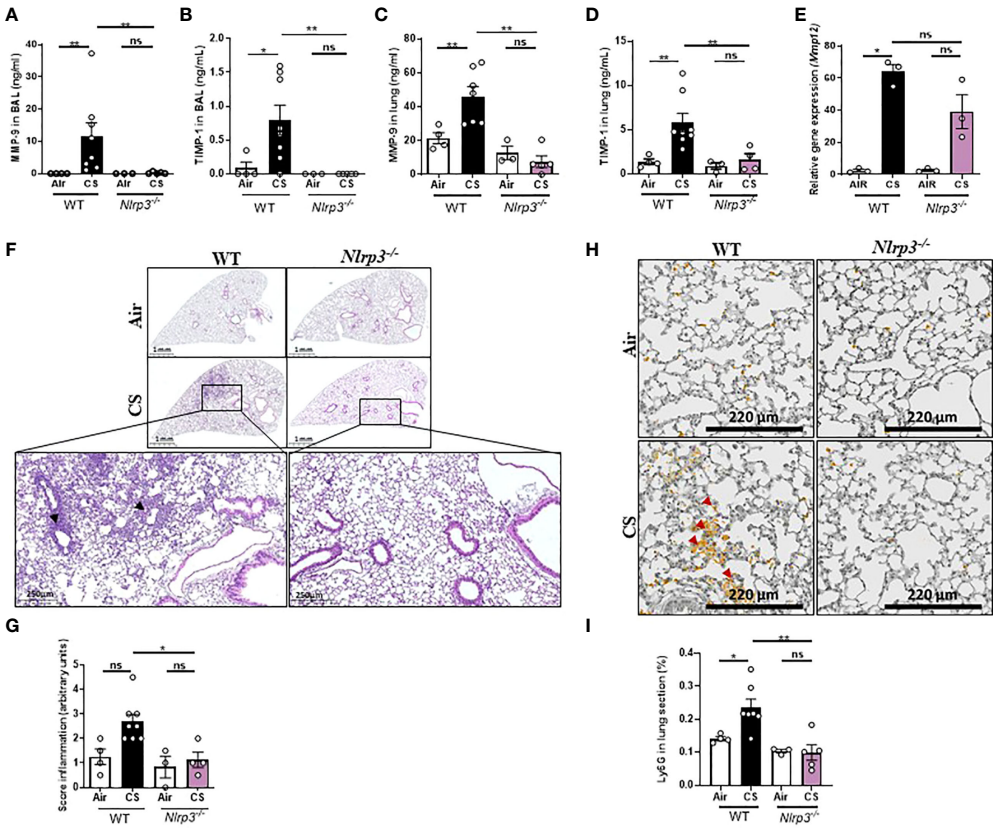

FIGURE 2
Nlrp3 deficiency decreases remodeling factor expression and lung tissue inflammation upon subchronic cigarette smoke (CS) exposure. WT and *Nlrp3*$^{-/-}$ mice were exposed to CS or Air during 6 weeks and protein levels of remodeling factor such as MMP-9 **(A)**, TIMP-1 **(B)** in BAL, and MMP-9 **(C)**, TIMP-1 **(D)** in lung tissue were measured by ELISA whereas lung MMP-12 mRNA expression was measured by quantitative RT-PCR **(E)**. All these parameters were decreased in response to CS exposure in *Nlrp3*$^{-/-}$ mice as compared to exposed WT mice. Histological analysis of pulmonary inflammation and cell recruitment were evaluated from histology sections **(F)** and inflammation score were determined **(G)**. Ly6G immunostaining was performed on WT and *Nlrp3*$^{-/-}$ lung sections **(H)**. Percentage of Ly6G positive area per tissue section **(I)**. Data are representative of five experiments for A-G and one experiment for H and I, and are expressed as mean values ± SEM (n= 4-6 mice per group, *p < 0.05, **p < 0.01, ns, non significant, using a Mann Whitney test).

and neutrophils (Figures 4A-C). BAL levels of MPO (Figure 4D) and LCN-2 (Figure 4E), CXCL1 (Figure 4F) and CXCL5 (Figure 4G) were significantly decreased in acutely CS-exposed *Caspase-1/11*$^{-/-}$ mice in comparison to WT. In lungs levels of LCN-2, CXCL1 and CXCL5 (Figures 4H-J) were also significantly reduced in *Caspase-1/11*$^{-/-}$ CS-exposed mice compared to WT CS-exposed mice. Importantly, IL-1β levels (Figure 4K) were significantly reduced in the lungs of *Caspase-1/11*$^{-/-}$ mice. These results indicate that either a canonical NLRP3/Caspase-1 inflammasome and/or the non-canonical inflammasome pathway (i.e. caspase-11 and NLRP3/Caspase-1 inflammasome) are involved in acute CS-induced lung inflammation.

In order to determine if acute CS exposure induces activation of the canonical inflammasome in alveolar macrophages and/or neutrophils recruited into the BAL, we probed for caspase-1 cleavage. Immunostaining with an antibody specific for the cleaved form (Asp 296) of murine caspase-1 showed that BAL recruited macrophages of acute CS-exposed mice, identified by their large uni-lobulated DAPI-stained nucleus, featured high levels of active processed caspase-1 in comparison to BAL cells from air-exposed mice (Figures 5A, B). In addition, BAL recruited neutrophils, identified by their tri-lobulated nucleus and small size compared to macrophages presented a weak expression of cleaved caspase-1. In contrast, cleaved caspase-1 was almost not detectable in BAL alveolar macrophages from MCC950-treated acute CS-exposed WT mice or from CS-exposed *Nlrp3*$^{-/-}$ mice (Figures 5A, B). These results indicate that acute CS-exposure promotes NLRP3-dependent caspase-1 activation in macrophages and recruited neutrophils of the bronchoalveolar space.

10.3389/fimmu.2022.918507

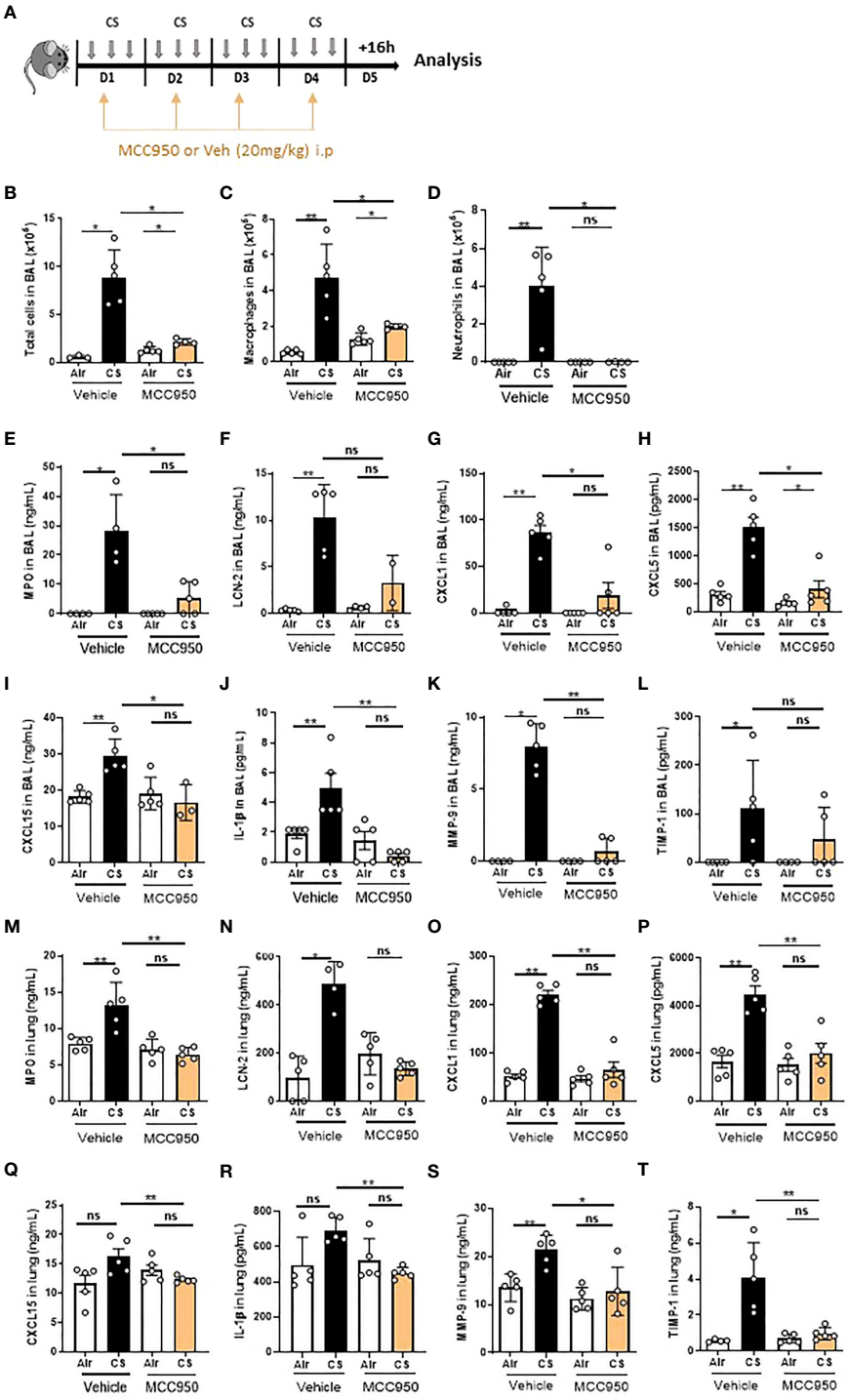

FIGURE 3
The NLRP3 inhibitor MCC950 impairs pulmonary inflammation upon acute cigarette smoke (CS) exposure. WT mice, treated or not with MCC950 (20mg/kg i.p. daily) were exposed to CS or Air during 4 days **(A)**. CS exposure led to significant decrease of total cells **(B)**, macrophages **(C)**, neutrophils **(D)** into BAL of MCC950 treated mice compared to untreated exposed WT mice. Myeloperoxidase (MPO) **(E)**, lipocaline 2 (LCN-2) **(F)**, CXCL1 **(G)**, CXCL5 **(H)** and CXCL15 **(I)** and IL-1β **(J)**, MMP-9 **(K)** and TIMP-1 **(L)** levels were measured in BAL by ELISA. All these parameters were decreased in response to CS exposure in MCC950-treated mice as compared to untreated exposed WT mice. Lung levels of MPO **(M)**, lipocaline 2 (LCN-2) **(N)**, CXCL1 **(O)**, CXCL5 **(P)**, CXCL15 **(Q)**, IL-1β **(R)**, MMP-9 **(S)** and TIMP-1 **(T)** were significantly decreased in MCC950 treated CS-exposed mice as compared to exposed WT mice. Data are representative of two experiments and are expressed as mean values ± SEM (n= 4-6 mice per group, *p < 0.05, **p < 0.01, ns, non significant, using a Mann Whitney test).

10.3389/fimmu.2022.918507

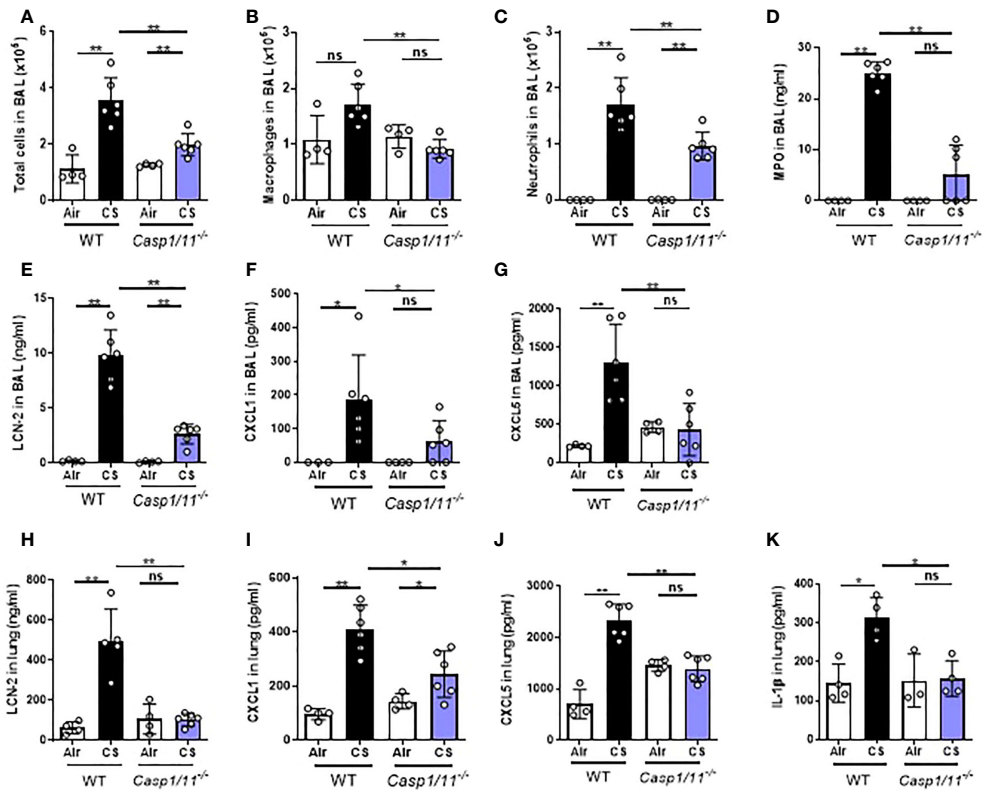

FIGURE 4
Caspase1/11-deficient mice (*caspase1/11*$^{-/-}$) have reduced pulmonary inflammation after acute cigarette smoke (CS) exposure. WT and *caspase1/11*$^{-/-}$ mice were exposed to CS or Air during 4 days. Total cells **(A)**, macrophages **(B)** and neutrophils **(C)** counts and MPO levels **(D)** in BAL are shown. Lipocaline 2 (LCN-2) **(E)**, CXCL1 **(F)**, CXCL5 **(G)** levels were reduced in BAL of *caspase1/11*$^{-/-}$ CS-exposed mice. LCN-2 **(H)**, CXCL1 **(I)**, CXCL5 **(J)** and IL-1β **(K)** were also significantly reduced in lungs of *caspase1/11*$^{-/-}$ CS-exposed mice compared to CS-exposed WT mice. Data are representative of four experiments and are expressed as mean values ± SEM (n= 4-6 mice per group, *p < 0.05, **p < 0.01, ns, non significant, using a Mann Whitney test).

CS exposure promotes NLRP3-dependent activation of gasdermin D in lung tissue

To better understand the mechanisms of inflammation in response to acute CS-exposure, we investigated whether NLRP3 activation leads to gasdermin D (GSDMD) cleavage and possibly to IL-1β secretion or pyroptosis, an immunogenic cell death (ICD) associated with NLRP3 activation. GSDMD is a 53.2 kDa protein that is cleaved by caspase-1 and/or caspase-11 upon NLRP3 activation, resulting in the generation of the GSDMD-N p31 fragment. The active GSDMD-N forms pores in the plasma membrane, allowing small cytokine release such as mature IL-1β and/or ion fluxes that may lead to cell swelling and to pyroptosis. We first analysed the level of the p53 full-length GSDMD and/or the GSDMD-N p31 active form in the lungs of acute CS-exposed mice by western blot. We observed that acute CS exposure increased lung tissue expression of the pro-GSDMD p53 in WT mice that was strongly reduced in acutely CS-exposed *Nlrp3*$^{-/-}$ mice (Figures 6A, B; Figure S2). Importantly, using an antibody specifically recognizing the cleaved form of GSDMD at its N-terminal domain, we show that acute CS-exposure induced lung expression of the cleaved GSDMD p31 protein in WT mice but less importantly in lungs of *Nlrp3*$^{-/-}$ acute CS-exposed mice (Figures 6A-C; Figure S2). Furthermore, lung section immunostaining analysis indicates that acute CS induced expression of the cleaved GSDMD p31 in bronchial airway epithelial cells that was reduced in lung of *Nlrp3*$^{-/-}$ mice and absent in *Gsdmd*$^{-/-}$ mice as compared to WT mice (Figure 6D). However we did not observe cleaved GSDMD expression in lung alveolar regions or in infiltrating cells that were not detectable on histology slides after only 4 days of CS exposure. These results demonstrate that acute CS exposure induces NLRP3 activation which is involved in GSDMD protein cleavage in bronchial airway epithelial cells.

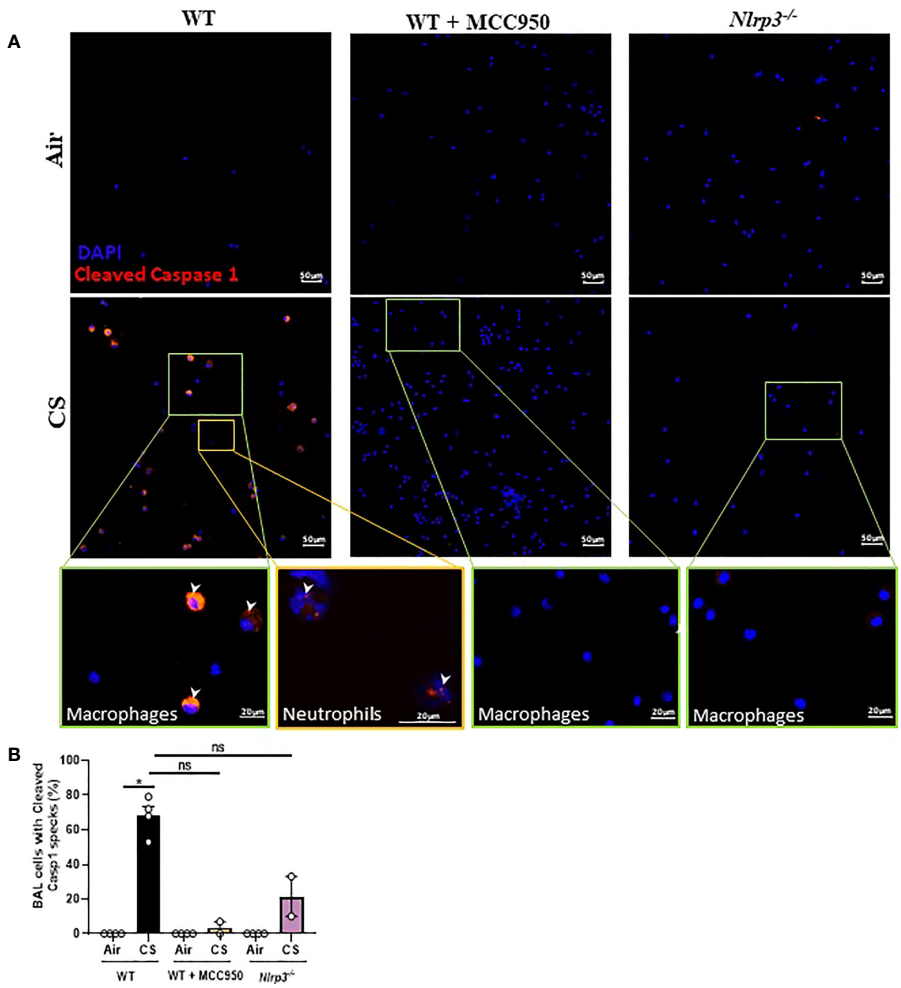

FIGURE 5
Cigarette Smoke (CS) exposure promotes caspase-1 cleavage in BAL macrophages and neutrophils in an NLRP3-dependent manner. Cleaved caspase-1 immunostaining on BAL cells collected after Air or CS exposure of WT, MCC950 WT treated mice and *Nlrp3*$^{-/-}$ mice. Cleaved caspase-1 is shown in red and nucleus in blue (DAPI) **(A)**. BAL cells fluorescence intensity quantification **(B)**. Data are representative of three experiments. Bar graph is expressed as mean ± SEM (n =2–4 mice per group, *p < 0.05 ns, non significant, using a Mann Whitney test).

Mouse CS exposure induces NLRP3-dependent activation of GSDMD in bronchoalveolar space macrophages

We next determined whether GSDMD activation occurs in BAL cells upon CS exposure by immunostaining using the specific antibody that recognizes the cleaved N-terminal domain of GSDMD. We observed that airway macrophages, identified by their large unit-lobulated DAPI-stained nucleus, show cleaved GSDMD in response to acute CS-exposure of WT mice but not in recruited neutrophils (Figures 7A, B). Importantly, cleaved GSDMD levels in macrophages were reduced in CS-exposed WT mice treated with MCC950 and importantly reduced in CS-exposed *Nlrp3*$^{-/-}$ mice (Figures 7A, B). These results demonstrate that CS-exposure induces NLRP3 dependent GSDMD cleavage in bronchoalveolar space macrophages potentially through NLRP3 inflammasome activation.

GSDMD deficient mice have reduced pulmonary inflammation to CS exposure

Finally, in order to confirm that GSDMD participates in pulmonary inflammation to acute CS exposure, we exposed WT and *Gsdmd*-deficient (*Gsdmd*$^{-/-}$) mice to Air or CS for 4 days. We observed that total cells, macrophages and neutrophils (Figures 8A-C) together with MPO, CXCL1, CXCL5 and CXCL15 (Figures 8D-G) levels were significantly decreased in

10.3389/fimmu.2022.918507

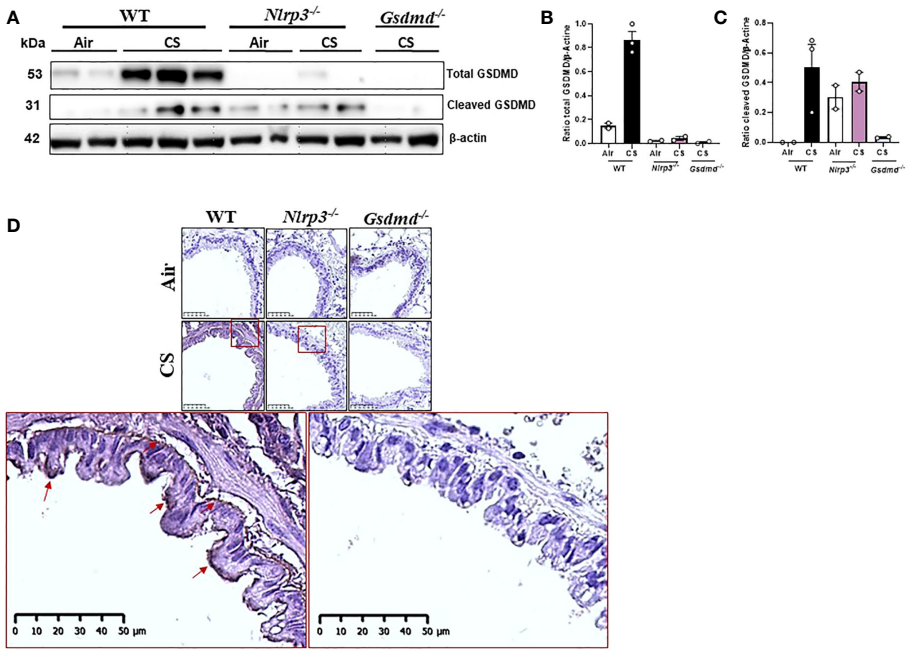

FIGURE 6
Cigarette Smoke (CS) exposure induces GSDMD cleavage in bronchial epithelial cells in an NLRP3-dependent manner. Immunoblot for total and cleaved GSDMD proteins in lung homogenates of Air or CS-exposed mice of WT, *Nlrp3*$^{-/-}$ or *Gsdmd*$^{-/-}$ mice **(A)** and quantification of total GSDMD **(B)** and cleaved GSDMD **(C)** immunoblot were shown. Cleaved GSDMD immunostaining was performed on lung sections of Air or CS-exposed WT, *Nlrp3*$^{-/-}$ and *Gsdmd*$^{-/-}$ mice **(D)**. Data are representative of three experiments. Bar graph are expressed ± SEM (n =2–4 mice per group).

BAL of acutely CS-exposed *Gsdmd*$^{-/-}$ mice as compared to WT mice. Importantly, IL-1β levels in BAL (Figure 8H) was significantly reduced in *Gsdmd*$^{-/-}$ mice indicating a role of GSDMD in IL-1β release. In addition, BAL levels of MMP-9 (Figure 8I) and TIMP-1 (Figure 8J) were significantly and non-significantly reduced respectively in acutely CS-exposed *Gsdmd*$^{-/-}$ mice as compared to WT CS-exposed mice. Finally, IL-1β (Figure 8K) levels in lungs of acutely CS-exposed *Gsdmd*$^{-/-}$ mice was also significantly reduced, as well as MMP-9 and TIMP-1 (Figures 8L, M) compared to WT mice. Altogether, these results confirm that GSDMD protein is a key player of pulmonary inflammatory responses to acute CS exposure.

Discussion

We investigated whether NLRP3 is involved in pulmonary inflammation induced by acute or subchronical experimental CS-exposure. We previously demonstrated that murine CS-induced airway inflammation depends on the IL-1R1/MyD88 signaling pathway and showed that *ex vivo* stimulation of bone marrow-derived macrophages with LPS and ATP, promotes caspase-1-dependent IL-1β maturation and secretion, suggesting involvement of an inflammasome complex (40). However, subsequent *in vivo* studies were controversial regarding the role of NLRP3 in inflammation to CS (12–15).

We demonstrate here that NLRP3 is a key player in pulmonary inflammation and remodeling upon acute or subchronical mouse CS exposure. Macrophages and neutrophils are innate immune cells infiltrating lung and recruited in bronchoalveolar space upon CS exposure and also associated with COPD pathogenesis (1, 2). Pro-inflammatory cytokines, chemokines and proteases, secreted by pulmonary recruited cells and lung resident cells amplify organ inflammation and damages. Here we highlighted a decrease of bronchoalveolar space and lung tissue cell influx, cytokines/chemokines expression and/or release upon acute and subchronic CS exposure after knockdown of the NLRP3 sensor. Influx of macrophages, and neutrophils and importantly IL-1β secretion in the bronchoalveolar space of acutely of subchronically CS-exposed mice were dependent on NLRP3. Furthermore, we report attenuated inflammation and remodeling responses to acute CS exposure after pharmacological inhibition of the NLRP3 inflammasome by MCC950 treatment. MCC950 was shown to directly targets the NLRP3 ATP hydrolysis motif to specifically inhibit canonical and non-canonical NLRP3 formation at nanomolar concentrations (38). MCC950 is active *in vivo* in multiple

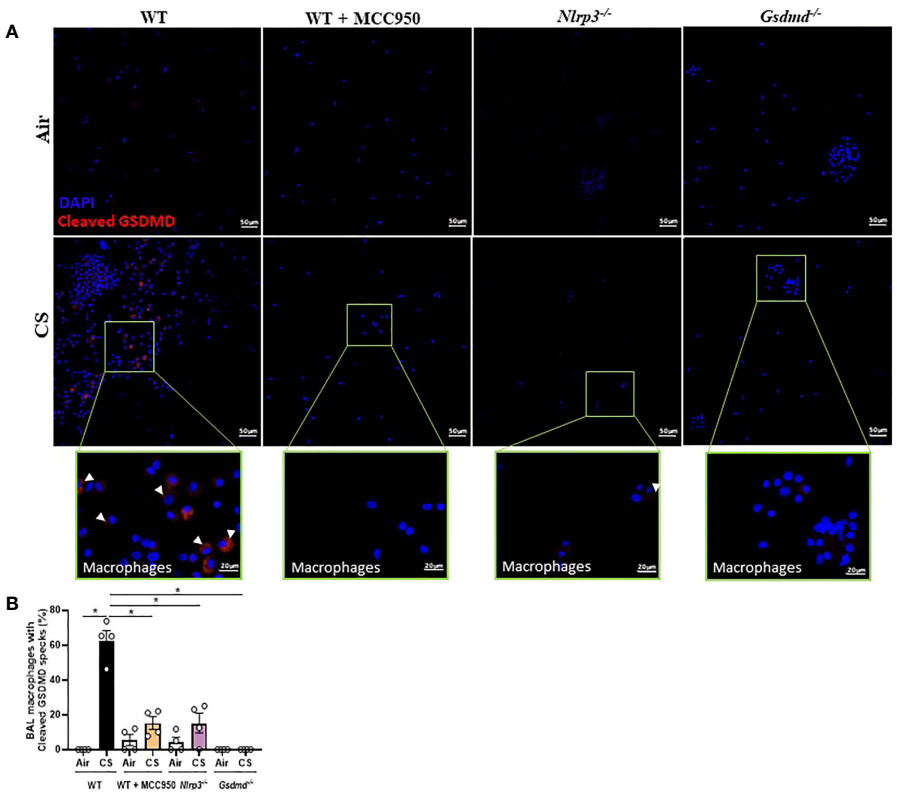

FIGURE 7
Cigarette Smoke (CS) exposure promotes GSDMD expression and cleavage in BAL alveolar macrophages dependently of NLRP3. Cleaved GSDMD immunostaining on BAL cells collected after Air or CS exposure in WT, MCC950-treated WT mice, *Nlrp3*$^{-/-}$ and *Gsdmd*$^{-/-}$ mice. Cleaved GSDMD is shown in red and nucleus in blue (DAPI) **(A)**. Airway macrophages fluorescence intensity quantification **(B)**. Data are representative of three experiments. Bar graph is expressed as mean ± SEM (n =2–4 mice per group, *p < 0.05 using a Mann Whitney test).

NLRP3-dependent mouse models, impairing IL-1β production and attenuating the severity of inflammatory disease models (37). Although we cannot exclude that MCC950 may non-specifically inhibit other targets, our data with genetic depletion and pharmacological inhibition strongly suggest that NLRP3 is a key sensor of pulmonary injury and in particular induced by acute CS exposure but possibly after other noxious airway exposure, open new fields to investigate. Importantly, MCC950 treatment might be beneficial in preventing pulmonary inflammation and this hypothesis could be tested in chronically CS-exposed mice models. However, although MCC950 inhibited the NLRP3 inflammasome in a lot of nonclinical models of inflammatory diseases with very high specificity and at nanomolar concentrations, this inhibitor presents pharmacokinetic and toxicokinetic properties that may limit its therapeutic development in the clinic. Several improved next-generation inhibitors are now in clinical trials (39). We further showed that *Caspase1/11* deficiency leads to reduced pulmonary inflammation suggesting that NLRP3-canonical and/or non-canonical inflammasome pathways are involved in acute CS exposure-induced lung inflammation. Moreover, mouse CS exposure induced cleaved caspase-1 in macrophages and neutrophils present in the bronchoalveolar space, which was dampened after knockdown or pharmacological inhibition of the NLRP3 sensor. These results demonstrated that the canonical NLRP3 inflammasome is a key player of acute CS exposure-induced inflammation mediated by macrophages and neutrophils in the bronchoalveolar space.

In addition, we investigated the role of the gasdermin D (GSDMD) in pulmonary inflammation upon mouse acute CS exposure. GSDMD-forming pores is known to drive a rapid pro-inflammatory form of cell death known as pyroptosis and release pro-inflammatory cytokines and endogenous danger signals (21–23). Importantly, GSDMD-forming pores were also identified as the most important way for the secretion of mature IL-1β (27). GSDMD activation may result in different fate such as membrane repair and cell survival depending on cell types (28, 29). Interestingly, we demonstrated that NLRP3 mediates GSDMD activation in bronchial epithelial cells and in macrophages of the bronchoalveolar space upon acute CS exposure of mice, possibly through NLRP3 inflammasome activation. Finally we demonstrated for the first time in *Gsdmd*

10.3389/fimmu.2022.918507

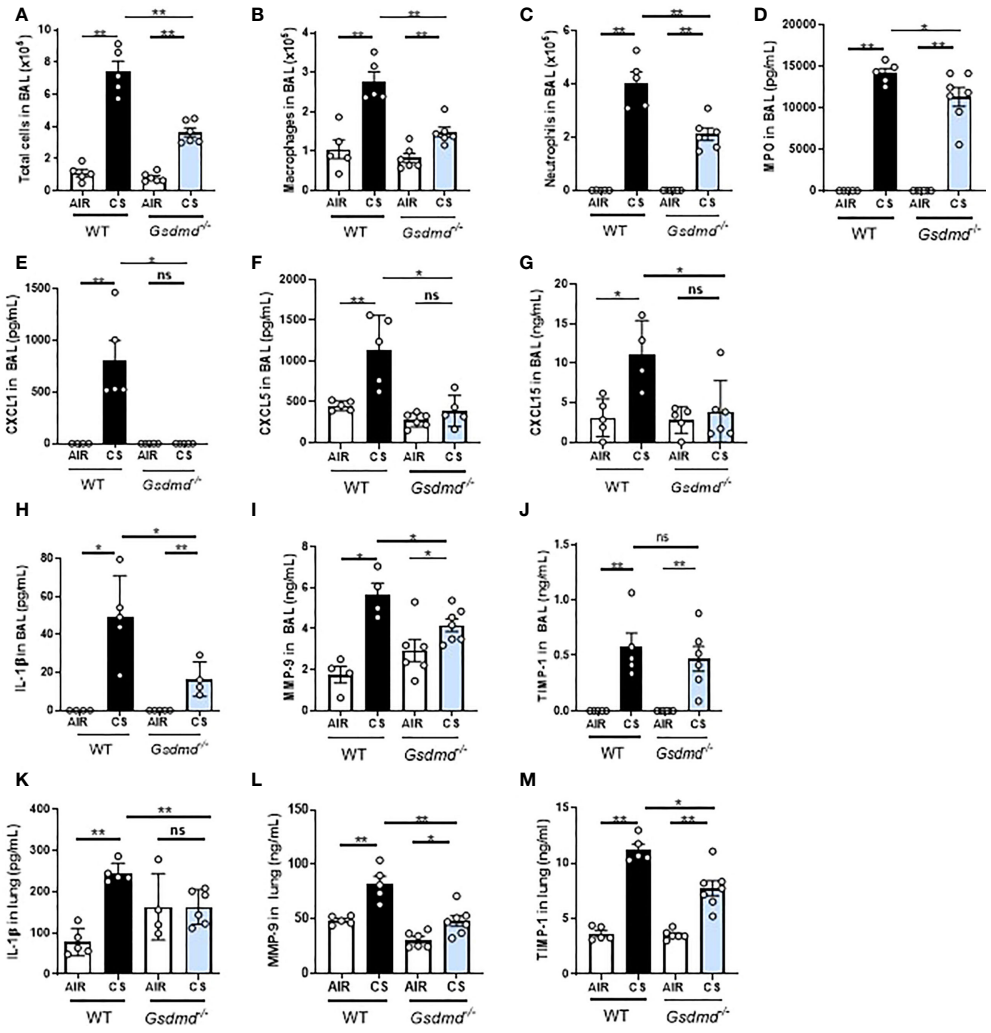

FIGURE 8
Gasdermin d-deficient mice (*Gsdmd*$^{-/-}$) have reduced pulmonary inflammation and remodeling after acute smoke cigarette (CS) exposure. WT and *Gsdmd*$^{-/-}$ mice were exposed to CS or Air during 4 days. Total cells **(A)**, macrophages **(B)** and neutrophils **(C)** counts and MPO level in BAL **(D)** are shown. CXCL1 **(E)**, CXCL5 **(F)**, CXCL15 **(G)** and IL-1β **(H)** levels were measured in BAL. MMP-9 **(I)** and TIMP-1 **(J)** remodeling factor levels were measured in BAL. In lungs, levels of IL-1β **(K)**, MMP-9 **(L)** and TIMP-1 **(M)** were also measured. All parameters decreased in *Gsdmd*$^{-/-}$ mice exposed to CS as compared to CS WT mice. Data are representative of four experiments and are expressed as mean values ± SEM (n= 4-6 mice per group, *p < 0.05, **p < 0.01, ns, non significant, using a Mann Whitney test).

deficient mice that this pore-forming protein is central to airway inflammation upon mouse acute CS exposure, probably through GSDMD expression and activation in bronchoalveolar space recruited macrophages and in bronchial airway epithelial cells.

Importantly, implication of GSDMD activation in acute CS-induced lung inflammation opens new potential studies in chronical CS-induced lung inflammation, using GSDMD inhibitors such as disulfiram that blocks pore formation (41). Pore forming ability of GSDMD represents a drug target to block IL-1β release during inflammasome-driven sterile inflammatory diseases.

Collectively, our data report a key role of the NLRP3 sensor and of the pore-forming GSDMD protein, in pulmonary inflammation to acute CS exposure in mice.

Materials and methods

Mice

Wild type C57BL/6J (WT) male mice were purchased from the Janvier Laboratory.

Caspase1/11$^{-/-}$ (42) were provided by Seshadri Tara at BASF Bioresearch corporation, *Nlrp3*$^{-/-}$ (10) by Dr. Jürg Tschopp and *Gsdmd*$^{-/-}$ (27) by Dr Petr Broz. Mice were backcrossed 10 times or made on C57BL/6J background. All mice were housed at the animal facility at transgenose institute (TAAM) in CNRS of Orleans, France. For experiments, adults (8-11 weeks old) were kept in sterile, isolated and ventilated cages. All animal experiments followed the French government's ethical and animal experiment regulations (APAFIS 2020 #26177).

Cigarette smoke model

Cigarette smoke (CS) exposure was performed using a calibrated EMKA InExpose smoking robot. Mice were exposed to mainstream cigarette smoke in a whole-body chamber for 20 min, 3 times a day for 4 days for acute model and on 5 consecutive days for 6 weeks for subchronic model. We used 3R4F research cigarettes (University of Kentucky) without filter removed and the cigarettes were puffed once per minute, 4s duration, 200 ml puff volume. The experimental bias flow, required to deliver CS and fresh air to the mice, is calibrated at 3.10^7 L.min^{-1} and maintained constant. The concentration of smoke particulates is estimated to be 350 mg/cubic meter as mentioned by the manufacturer as previously described (32, 33). Our cigarette smoke exposure models are based on classical experimental models used to analyse the mechanism of CS-induced inflammation and/or COPD in mice (43, 44). These smoke exposure models mimic important features observed in human including epithelial injury and pulmonary inflammation with neutrophils influx (1, 2, 6).

MCC950 mice treatment

Mice were treated intraperitoneally with 20mg/kg of MCC950 provided by Luke O'Neill (Coll, 2015 #3697), dissolved in (2-Hydroxypropyl)-β-cyclodextrin (H31133, Alfa Aesar) vehicle or with vehicle alone everyday between the first and the second CS exposition.

Broncho-alveolar lavage (BAL)

BAL was performed as previously described (32, 33). Differential cell counts were performed by counting an average of 250 cells on cytospin preparations (Shandon CytoSpin 3, ThermoFisher Scientific™, Illkirch, France) after May-Grünwald-Giemsa staining (Diff Quick, Medion Diagnostics, Düdingen, Switzerland) according to manufacturer's instructions.

Lung homogenates

After BAL the lung were perfused with Isoton® (Beckman Coulter France, Villepinte) to flush the vascular content. For protein analysis, the trilobed lung part was homogenized by a rotor-stator (Ultra-turrax®) in 1ml of T-Per protein extraction buffer (ThermoFisher Scientific™) mixed with protease and phosphatase inhibitor (ThermoFisher Scientific™). The extract was centrifuged 10 min at 10000 rpm and the supernatant was stored at -80°C before mediator measurement and immunoblotting analysis.

Lung histology and Ly6G immunohistochemistry (IHC)

The left lobe of lung was fixed in 4% buffered formaldehyde (PFA), processed and paraffin embedded under standard conditions. Three microns sections were cut and stained with hematoxylin and eosin (HE). Cell infiltration was assessed by a semi-quantitative score on infiltrated area compared to the entire lung tissue area with increasing severity 0 (without any inflammation) to 5 (severe inflammation) by two independent observers on the HE-stained sections. Two additional slides per animal were cut and labelled with an anti-Ly6G antibody (ab238132, Abcam). Lung sections were scanned at X20 (0.452 µm/pixel) using a NanoZoomer-SQ and their whole slide image (WSI) captured using the NDP.view 2 software (both from Hamamatsu Corporation, Japan).

Digital quantification of Ly6G IHC

Quantification of Ly6G was performed on the digitized sections using MorphoQuant™ software (Biocellvia, France), initially developed to measure lung lesions induced by pulmonary fibrosis or emphysema (45, 46). Briefly, neutrophils were quantified through positive labelling with Ly6G, using the classic diaminobenzidine. Positive elements appear in brown in the section and were quantified on the digitized sections using MorphoQuant™, a digital pathology software relying on morphometric analysis. In the Ly6G-labelled sections, all brown pixels were considered as Ly6G positive elements. The total number of positive Ly6G pixels was thus divided by the total number of pixels describing the whole sections, and the ratio was expressed in percent.

Cleaved gasdermin D immunostaining

The left lobe of lung was fixed in 4% PFA for 72h, embedded in paraffin and sectioned at 3 µm. Lung sections were dewaxed

and rehydrated, then heated 20 min at 80°C in citrate buffer 10 mM pH=6 for antigen retrieval (unmasking step). Lung sections were permeabilized in PBS 0.5% triton X-100, blocked with 5% FCS for 1h at RT and then incubated overnight with primary mouse anti-cleaved Gasdermin D (1:100, #10137, Cell Signaling). After washing, sections were incubated with the appropriate second antibody conjugated to horseradish peroxidase (1:200 anti-rabbit IgG, Sigma Aldrich®) in 1% FCS 1h at RT. Following washing, lung sections were incubated with HRP Substrate, DAB (Vector Laboratories®), following the manufacturer's protocol. After distilled water washing, Gill hematoxyline counterstaining on lung sections was done. Then, lung sections were dehydrated, fixed and mounted onto microscope slides (Eukitt). Slides were examined by using a scanner NDP view.

Mediator measurements

For cytokine determination, BAL supernatant and lung homogenates were analysed by ELISA assay kits for murine: CXCL1, CXCL5, CXCL15, MPO, LCN-2, MMP-9, TIMP-1 (Mouse DuoSet, R&D system, Minneapolis, USA) according to manufacturer's instructions. IL-1β mesurment in BAL was measured using multiplex immunoassay according to manufacturers' instructions (ProcartaPlex, Invitrogen™). Data were acquired on Luminex equipment (MagPix, BioRad) and analyzed using Bioplex Manager software (BioRad).

Quantitative RT-PCR

RNA was purified from lung homogenates by using Trizol extraction protocol. Reverse transcription of RNA into cDNA was carried out with Go script reverse kit (Promega). RT-PCR was performed with Fast SYBR Green master mix on an ARIA MX (Stratagene MX3005P, Agilent technologies). Primers were synthetized (Qiagen, Hilden, Germany). The expression of *pro-IL-18* and *Mmp12* mRNA, relative to housekeeping 18S mRNA, were analyzed using Quantitect gene expression assays (Qiagen). For all experiments, biological quadruplicate and technical triplicate were performed.

Immunoblotting

Protein concentrations were determined in lung tissue by using DC™ protein Assay (BIO-RAD, France). 40 µg of proteins were denatured by boiling (95°C, 5 min) in reducing SDS sample buffer. Samples were resolved on 13% polyacrylamide gel and run at 160V for 45min using the Mini gel Tank (ThermoFisher Scientific™). Total protein were immunoblotted to 0.2 µm nitrocellulose membrane (Amersham™) using a Trans-Blot SD Transfer System (Bio-Rad) at 100V for 45 min. Successful protein transfer was confirmed by using Ponceau S staining. Membranes were blocked 2 hours with 5% non-fat milk (Cell signaling) in 1X TBS- 0,1% Tween® 20 (20 mM Tris Trizma® Base, 150 mM sodium chloride, and 0.05% Tween® 20 pH 7.6) at room temperature. Then, membranes were incubated with primary antibodies, mouse anti-Gasdermin (1:500, ab209845, Abcam), anti-cleaved Gasdermin (1:500, #10137, Cell Signaling) in 5% non fat dried milk in 1X TBS- 0,1% Tween® 20, over nigh at 4°C. Mouse anti-actin (1:10 000, #A3854; Sigma-Aldrich) was incubated 1h at room temperature. Membranes were then washed 3 times in 1X TBS- 0,1% Tween® 20 and incubated with the appropriate second antibody conjugated to horseradish peroxidase (anti-rabbit IgG, Sigma-Aldrich) 1h at room temperature. Protein bands were visualized following exposure of the membrane to Amersham ECL™ prime substrate solution using PXi gel doc system® Syngene, and quantified using ImageJ software.

Immunostaining on Cytospin

Cytospin slides were fixed in 4% PFA (Sigma-Aldrich). Cells were washed 3 times in TBS, incubated 15 min in TBS-0.3% Triton X-100, then washed 3 times in TBS, blocked in TBS-10% Bovine Serum Albumin (BSA) for 45min and incubated overnight with primary rabbit anti-Cleaved Caspase1 (1:100, #89332, Cell Signaling) or anti-Cleaved Gasdermin (1:100, #10137, Cell Signaling). After washing, cytospins were incubated with goat anti-rabbit IgG secondary antibodies conjugated with Alexa® Fluor 594 (1:200, # A-11037, Invitrogen) in 1% FCS. Following washing, cells were stained with DAPI (1:2000) for 5 min, washed with PBS, and mounted onto microscope slides (Fluoromount). Immunofluorescence staining were blindly examined by using a Leica microscope at 20X magnification (Leica, Solms, Germany). Images were treated using Zen blue Zeiss software. Quantifications were realized at least for 2 mice per group, on different cytospin spots for each one.

Statistical analysis

Statistical tests of selected populations were performed using Mann-Whitney non-parametric test. Data represent mean ± SEM. P values <0.05 were considered statistically significant.

Data availability statement

The raw data supporting the conclusions of this article will be made available by the authors, without undue reservation.

Ethics statement

The animal study was reviewed and approved by APAFIS N° 26177-2019021818223038v15.

Author contributions

SH-M, MN, EC, MB, AG, FS, CP, and NR performed the experiments. SH-M, MN, AG, and IC, conceived the experiments and analyzed the data. ML supervised the breeding of knock-out mice. PB provided *Gsdmd* deficient mice. SH-M, AG, VQ, BR, PB, NR, CS, and IC discussed the results. SH-M, AG, NR, PB, and IC wrote the manuscript and IC and VQ provided funding and IC overall supervision of this study.

Funding

Grant support by the «Agence nationale de Recherche» (ANR AAPG2019 CES15 Smoke6) and the "Fondation pour la Recherche Médicale" (EQU202003010405) and the Centre National de Recherche Scientifique (CNRS) and the University of Orleans. This work was supported by CNRS, University of Orleans, the «Agence nationale de Recherche» (ANR AAPG2019 CES15 Smoke6) and the "Fondation pour la Recherche Médicale" (EQU202003010405).

Acknowledgments

We also thank Luke O'Neill for providing us with the MCC950 inhibitor. We also thank Nathalie Froux, Pauline Abgrall, and all technicians from our specific pathogen-free animal facility at CNRS (TAAM UPS44, Orléans, France) for breeding and animal care.

Conflict of interest

The authors declare that the research was conducted in the absence of any commercial or financial relationships that could be construed as a potential conflict of interest.

Publisher's note

All claims expressed in this article are solely those of the authors and do not necessarily represent those of their affiliated organizations, or those of the publisher, the editors and the reviewers. Any product that may be evaluated in this article, or claim that may be made by its manufacturer, is not guaranteed or endorsed by the publisher.

Supplementary material

The Supplementary Material for this article can be found online at: https://www.frontiersin.org/articles/10.3389/fimmu.2022.918507/full#supplementary-material

SUPPLEMENTARY FIGURE 1
Nlrp3-deficient mice (*Nlrp3*$^{-/-}$) have reduced pulmonary inflammation after acute cigarette smoke (CS) exposure. WT and *Nlrp3*$^{-/-}$ mice were exposed to CS or Air during 4 days **(A)**. Total cells **(B)**, macrophages **(C)**, neutrophils **(D)** counts and MPO **(E)**, CXCL1 **(F)**, IL-1β **(G)** and remodeling factors MMP-9 **(H)** and TIMP-1 **(I)** levels in BAL were decreased in *Nlrp3*$^{-/-}$ mice exposed to CS compared to CS WT mice. CXCL1 **(J)**, IL-1β **(K)** and MMP-9 **(L)** and TIMP-1 **(M)** levels in lungs are shown. Data are representative of four experiments and are expressed as mean values ± SEM (n= 4-6 mice per group, *p < 0.05, **p < 0.01, using a Mann Whitney test).

SUPPLEMENTARY FIGURE 2
Total red ponceau membrane. Total protein migration was verified on total membrane using red ponceau staining for the following immunoblot analysis. Data are representative of three experiments.

References

1. Barnes PJ. Cellular and molecular mechanisms of chronic obstructive pulmonary disease. *Clin Chest Med* (2014) 35:71–86. doi: 10.1016/j.ccm.2013.10.004

2. Barnes PJ. Mediators of chronic obstructive pulmonary disease. *Pharmacol Rev* (2004) 56:515–48. doi: 10.1124/pr.56.4.2

3. Barnes PJ, Burney PG, Silverman EK, Celli BR, Vestbo J, Wedzicha JA, et al. Chronic obstructive pulmonary disease. *Nat Rev Dis Primers* (2015) 1:15076. doi: 10.1038/nrdp.2015.76

4. Wedzicha JA, Singh R, Mackay AJ. Acute COPD exacerbations. *Clin Chest Med* (2014) 35:157–63. doi: 10.1016/j.ccm.2013.11.001

5. Barnes PJ. New anti-inflammatory targets for chronic obstructive pulmonary disease. *Nat Rev Drug Discovery* (2013) 12:543–59. doi: 10.1038/nrd4025

6. Sethi S, Evans N, Grant BJ, Murphy TF. New strains of bacteria and exacerbations of chronic obstructive pulmonary disease. *N Engl J Med* (2002) 347:465–71. doi: 10.1056/NEJMoa012561

7. Broderick L, De Nardo D, Franklin BS, Hoffman HM, Latz E. The inflammasomes and autoinflammatory syndromes. *Annu Rev Pathol* (2015) 10:395–424. doi: 10.1146/annurev-pathol-012414-040431

8. de Zoete MR, Palm NW, Zhu S, Flavell RA. Inflammasomes. *Cold Spring Harbor Perspect Biol* (2014) 6:a016287. doi: 10.1101/cshperspect.a016287

9. Christgen S, Place DE, Kanneganti TD. Toward targeting inflammasomes: insights into their regulation and activation. *Cell Res* (2020) 30:315–27. doi: 10.1038/s41422-020-0295-8

10. Martinon F, Petrilli V, Mayor A, Tardivel A, Tschopp J. Gout-associated uric acid crystals activate the NALP3 inflammasome. *Nature* (2006) 440:237–41. doi: 10.1038/nature04516

11. Faner R, Sobradillo P, Noguera A, Gomez C, Cruz T, Lopez-Giraldo A, et al. The inflammasome pathway in stable COPD and acute exacerbations. *ERJ Open Res* (2016) 2(3):0002. doi: 10.1183/23120541.00002-2016

12. Mahalanobish S, Dutta S, Saha S, Sil PC. Melatonin induced suppression of ER stress and mitochondrial dysfunction inhibited NLRP3 inflammasome activation in COPD mice. *Food Chem Toxicol* (2020) 144:111588. doi: 10.1016/j.fct.2020.111588

13. Wang B, Chan YL, Zhou S, Saad S, Chen H, Oliver BG. Offspring sex affects the susceptibility to maternal smoking-induced lung inflammation and the effect of maternal antioxidant supplementation in mice. *J Inflamm (Lond)* (2020) 17:24. doi: 10.1186/s12950-020-00253-5

14. Mehta S, Srivastava N, Bhatia A, Dhawan V. Exposure of cigarette smoke condensate activates NLRP3 inflammasome *in vitro* and *in vivo*: A connotation of innate immunity and atherosclerosis. *Int Immunopharmacol* (2020) 84:106561. doi: 10.1016/j.intimp.2020.106561

15. Morris GF, Danchuk S, Wang Y, Xu B, Rando RJ, Brody AR, et al. Cigarette smoke represses the innate immune response to asbestos. *Physiol Rep* (2015) 3 (12):92. doi: 10.14814/phy2.12652

16. Rumora L, Hlapcic I, Hulina-Tomaskovic A, Somborac-Bacura A, Bosnar M, Rajkovic MG. Pathogen-associated molecular patterns and extracellular Hsp70 interplay in NLRP3 inflammasome activation in monocytic and bronchial epithelial cellular models of COPD exacerbations. *APMIS* (2021) 129:80–90. doi: 10.1111/apm.13089

17. Nachmias N, Langier S, Brzezinski RY, Siterman M, Stark M, Etkin S, et al. NLRP3 inflammasome activity is upregulated in an in-vitro model of COPD exacerbation. *PloS One* (2019) 14:e0214622. doi: 10.1371/journal.pone.0214622

18. Mehta S, Dhawan V. Exposure of cigarette smoke condensate activates NLRP3 inflammasome in THP-1 cells in a stage-specific manner: An underlying role of innate immunity in atherosclerosis. *Cell Signal* (2020) 72:109645. doi: 10.1016/j.cellsig.2020.109645

19. Buscetta M, Di Vincenzo S, Miele M, Badami E, Pace E, Cipollina C. Cigarette smoke inhibits the NLRP3 inflammasome and leads to caspase-1 activation *via* the TLR4-TRIF-caspase-8 axis in human macrophages. *FASEB J* (2020) 34:1819–32. doi: 10.1096/fj.201901239R

20. Demarco B, Chen KW, Broz P. Cross talk between intracellular pathogens and cell death. *Immunol Rev* (2020) 297:174–93. doi: 10.1111/imr.12892

21. Broz P. Immunology: Caspase target drives pyroptosis. *Nature* (2015) 526:642–3. doi: 10.1038/nature15632

22. Aglietti RA, Dueber EC. Recent insights into the molecular mechanisms underlying pyroptosis and gasdermin family functions. *Trends Immunol* (2017) 38:261–71. doi: 10.1016/j.it.2017.01.003

23. Broz P, Pelegrin P, Shao F. The gasdermins, a protein family executing cell death and inflammation. *Nat Rev Immunol* (2020) 20:143–57. doi: 10.1038/s41577-019-0228-2

24. Shi J, Zhao Y, Wang K, Shi X, Wang Y, Huang H, et al. Cleavage of GSDMD by inflammatory caspases determines pyroptotic cell death. *Nature* (2015) 526:660–5. doi: 10.1038/nature15514

25. Chen KW, Monteleone M, Boucher D, Sollberger G, Ramnath D, Condon ND, et al. Noncanonical inflammasome signaling elicits gasdermin d-dependent neutrophil extracellular traps. *Sci Immunol* (2018) 3(26):eaar6676. doi: 10.1126/sciimmunol.aar6676

26. Zhuang J, Cui H, Zhuang L, Zhai Z, Yang F, Luo G, et al. Bronchial epithelial pyroptosis promotes airway inflammation in a murine model of toluene diisocyanate-induced asthma. *BioMed Pharmacother* (2020) 125:109925. doi: 10.1016/j.biopha.2020.109925

27. Heilig R, Dick MS, Sborgi L, Meunier E, Hiller S, Broz P. The gasdermin-d pore acts as a conduit for IL-1beta secretion in mice. *Eur J Immunol* (2018) 48:584–92. doi: 10.1002/eji.201747404

28. Ruhl S, Broz P. Regulation of lytic and non-lytic functions of gasdermin pores. *J Mol Biol* (2022) 434:167246. doi: 10.1016/j.jmb.2021.167246

29. Ruhl S, Shkarina K, Demarco B, Heilig R, Santos JC, Broz P. ESCRT-dependent membrane repair negatively regulates pyroptosis downstream of GSDMD activation. *Science* (2018) 362:956–60. doi: 10.1126/science.aar7607

30. Zhang MY, Jiang YX, Yang YC, Liu JY, Huo C, Ji XL, et al. Cigarette smoke extract induces pyroptosis in human bronchial epithelial cells through the ROS/NLRP3/caspase-1 pathway. *Life Sci* (2021) 269:119090. doi: 10.1016/j.lfs.2021.119090

31. Mo R, Zhang J, Chen Y, Ding Y. Nicotine promotes chronic obstructive pulmonary disease *via* inducing pyroptosis activation in bronchial epithelial cells. *Mol Med Rep* (2022) 25(3):92. doi: 10.3892/mmr.2022.12608

32. Nascimento M, Gombault A, Lacerda-Queiroz N, Panek C, Savigny F, Sbeity M, et al. Self-DNA release and STING-dependent sensing drives inflammation to cigarette smoke in mice. *Sci Rep* (2019) 9:14848. doi: 10.1038/s41598-019-51427-y

33. Nascimento M, Huot-Marchand S, Gombault A, Panek C, Bourinet M, Fanny M, et al. B-cell activating factor secreted by neutrophils is a critical player in lung inflammation to cigarette smoke exposure. *Front Immunol* (2020) 11:1622. doi: 10.3389/fimmu.2020.01622

34. Balamayooran G, Batra S, Cai S, Mei J, Worthen GS, Penn AL, et al. Role of CXCL5 in leukocyte recruitment to the lungs during secondhand smoke exposure. *Am J Respir Cell Mol Biol* (2012) 47:104–11. doi: 10.1165/rcmb.2011-0260OC

35. Morissette MC, Jobse BN, Thayaparan D, Nikota JK, Shen P, Labiris NR, et al. Persistence of pulmonary tertiary lymphoid tissues and anti-nuclear antibodies following cessation of cigarette smoke exposure. *Respir Res* (2014) 15:49. doi: 10.1186/1465-9921-15-49

36. Chukowry PS, Spittle DA, Turner AM, Disease SA. Biomarkers and COPD: Where are we? *Int J Chron Obstruct Pulmon Dis* (2021) 16:351–65. doi: 10.2147/COPD.S280157

37. Coll RC, Robertson AA, Chae JJ, Higgins SC, Munoz-Planillo R, Inserra MC, et al. A small-molecule inhibitor of the NLRP3 inflammasome for the treatment of inflammatory diseases. *Nat Med* (2015) 21:248–55. doi: 10.1038/nm.3806

38. Coll RC, Hill JR, Day CJ, Zamoshnikova A, Boucher D, Massey NL, et al. MCC950 directly targets the NLRP3 ATP-hydrolysis motif for inflammasome inhibition. *Nat Chem Biol* (2019) 15:556–9. doi: 10.1038/s41589-019-0277-7

39. Corcoran SE, Halai R, Cooper MA. Pharmacological inhibition of the nod-like receptor family pyrin domain containing 3 inflammasome with MCC950. *Pharmacol Rev* (2021) 73:968–1000. doi: 10.1124/pharmrev.120.000171

40. Doz E, Noulin N, Boichot E, Guenon I, Fick L, Le Bert M, et al. Cigarette smoke-induced pulmonary inflammation is TLR4/MyD88 and IL-1R1/MyD88 signaling dependent. *J Immunol* (2008) 180:1169–78. doi: 10.4049/jimmunol.180.2.1169

41. Hu JJ, Liu X, Xia S, Zhang Z, Zhang Y, Zhao J, et al. FDA-Approved disulfiram inhibits pyroptosis by blocking gasdermin d pore formation. *Nat Immunol* (2020) 21:736–45. doi: 10.1038/s41590-020-0669-6

42. Kuida K, Lippke JA, Ku G, Harding MW, Livingston DJ, Su MS, et al. Altered cytokine export and apoptosis in mice deficient in interleukin-1 beta converting enzyme. *Science* (1995) 267:2000–3. doi: 10.1126/science.7535475

43. Lu Z, Van Eeckhoutte HP, Liu G, Nair PM, Jones B, Gillis CM, et al. Necroptosis signaling promotes inflammation, airway remodeling, and emphysema in chronic obstructive pulmonary disease. *Am J Respir Crit Care Med* (2021) 204:667–81. doi: 10.1164/rccm.202009-3442OC

44. Le Roux M, Ollivier A, Kervoaze G, Beke T, Gillet L, Pichavant M, et al. IL-20 cytokines are involved in epithelial lesions associated with virus-induced COPD exacerbation in mice. *Biomedicines* (2021) 9(12):1838. doi: 10.3390/biomedicines9121838

45. Gilhodes JC, Jule Y, Kreuz S, Stierstorfer B, Stiller D, Wollin L. Quantification of pulmonary fibrosis in a bleomycin mouse model using automated histological image analysis. *PloS One* (2017) 12:e0170561. doi: 10.1371/journal.pone.0170561

46. Michaudel C, Fauconnier L, Jule Y, Ryffel B. Functional and morphological differences of the lung upon acute and chronic ozone exposure in mice. *Sci Rep* (2018) 8:10611. doi: 10.1038/s41598-018-28261-9

frontiers | Frontiers in Immunology

TYPE Original Research
PUBLISHED 25 August 2022
DOI 10.3389/fimmu.2022.832306

OPEN ACCESS

EDITED BY
Alessandra Mortellaro,
San Raffaele Telethon Institute for Gene Therapy (SR-Tiget), Italy

REVIEWED BY
Benoit Briard,
Institut National de la Santéet de la Recherche Médicale (INSERM), France
Ayan Mondal,
Stanford School of Medicine, Pediatrics, United States

*CORRESPONDENCE
Analia S. Trevani
analiatrevani@yahoo.com.ar
atrevani@fmed.uba.ar

SPECIALTY SECTION
This article was submitted to Molecular Innate Immunity, a section of the journal Frontiers in Immunology

RECEIVED 09 December 2021
ACCEPTED 03 August 2022
PUBLISHED 25 August 2022

CITATION
Keitelman IA, Shiromizu CM, Zgajnar NR, Danielián S, Jancic CC, Martí MA, Fuentes F, Yancoski J, Vera Aguilar D, Rosso DA, Goris V, Buda G, Katsicas MM, Galigniana MD, Galletti JG, Sabbione F and Trevani AS (2022) The interplay between serine proteases and caspase-1 regulates the autophagy-mediated secretion of Interleukin-1 beta in human neutrophils.
Front. Immunol. 13:832306.
doi: 10.3389/fimmu.2022.832306

The interplay between serine proteases and caspase-1 regulates the autophagy-mediated secretion of Interleukin-1 beta in human neutrophils

Irene A. Keitelman[1], Carolina M. Shiromizu[1], Nadia R. Zgajnar[2], Silvia Danielián[3], Carolina C. Jancic[1,4], Marcelo A. Martí[5,6], Federico Fuentes[7], Judith Yancoski[3], Douglas Vera Aguilar[1], David A. Rosso[1], Verónica Goris[8], Guadalupe Buda[5,6], María Martha Katsicas[9], Mario D. Galigniana[2,5], Jeremías G. Galletti[1], Florencia Sabbione[1] and Analia S. Trevani[1,4]*

[1]Laboratorio de Inmunidad Innata, Instituto de Medicina Experimental (IMEX) - CONICET, Academia Nacional de Medicina, Buenos Aires, Argentina, [2]Laboratorio de receptores nucleares, Instituto de Biología y Medicina Experimental (IBYME)-CONICET, Buenos Aires, Argentina, [3]Laboratorio de Biología Molecular Inmunología, Hospital de Pediatría "Juan P. Garrahan", Buenos Aires, Argentina, [4]Departamento de Microbiología, Parasitología e Inmunología, Facultad de Medicina, Universidad de Buenos Aires, Buenos Aires, Argentina, [5]Departamento de Química Biológica, Facultad de Ciencias Exactas y Naturales (FCEyN), Universidad de Buenos Aires (UBA), Buenos Aires, Argentina, [6]Instituto de Química Biológica de la Facultad de Ciencias Exactas y Naturales (IQUIBICEN) – CONICET, Facultad de Ciencias Exactas y Naturales (FCEyN), Universidad de Buenos Aires (UBA), Buenos Aires, Argentina, [7]Laboratorio de Microscopía, Instituto de Medicina Experimental (IMEX) - CONICET, Academia Nacional de Medicina, Buenos Aires, Argentina, [8]Unidad de Genómica. Laboratorio de Biología Molecular de Inmunología, Hospital de Pediatría "Juan P. Garrahan", Buenos Aires, Argentina, [9]Servicio de Inmunología y Reumatología, Hospital de Pediatría "Juan P. Garrahan", Buenos Aires, Argentina

Neutrophils play major roles against bacteria and fungi infections not only due to their microbicide properties but also because they release mediators like Interleukin-1 beta (IL-1β) that contribute to orchestrate the inflammatory response. This cytokine is a leaderless protein synthesized in the cytoplasm as a precursor (pro-IL-1β) that is proteolytically processed to its active isoform and released from human neutrophils by secretory autophagy. In most myeloid cells, pro-IL-1β is processed by caspase-1 upon inflammasome activation. Here we employed neutrophils from both healthy donors and patients with a gain-of-function (GOF) *NLRP3*-mutation to dissect IL-1β processing in these cells. We found that although caspase-1 is required for IL-1β secretion, it undergoes rapid inactivation, and instead, neutrophil serine proteases play a key role in pro-IL-1β processing. Our findings bring to light distinctive features

of the regulation of caspase-1 activity in human neutrophils and reveal new molecular mechanisms that control human neutrophil IL-1β secretion.

KEYWORDS

autophagosome, granulocytes, inflammasome, neutral proteases, unconventional protein secretion

Introduction

Neutrophils are key actors of the innate immune system that play a major role as the first line of defense against infections (1). These granulocytes, the most abundant leukocytes in human circulation, are massively recruited to infection foci where they deploy a battery of antimicrobial weapons to fight against the potentially harmful invaders. The crucial role of neutrophils in the immune response is evidenced by the severe, and often fatal, course of infections in patients with congenital neutrophil deficiencies.

Neutrophils are terminally differentiated cells with a short lifespan that kill microbes by phagocytosis and extracellular traps formation. However, their role in the immune system goes far beyond these functions. These cells also contribute to coordinate the immune response by means of the release of preformed, and *de novo* synthesized proinflammatory mediators (2). Among them, is the highly inflammatory cytokine Interleukin-1 beta (IL-1β) which plays major roles in host defense and immune pathology (3).

Neutrophils are characterized by the presence of heterogeneous granules containing a variety of enzymes and anti-microbial peptides that exert key functions as part of the non-oxidative arm of their microbicidal actions. Among these granules, the azurophilic ones contain the potent neutral serine proteases elastase (NE), proteinase 3 (PR3), cathepsin G (CG), and neutrophil serine protease 4 (NSP4) (4).

Neutrophil serine proteases (NSPs) are synthesized during the promyelocytic stage of granulopoiesis in the bone marrow, and under homeostatic conditions, they are stored within the azurophilic granules of circulating neutrophils (5). Upon microbe internalization, azurophilic granules fuse with phagosome membranes in a process that licenses these enzymes to degrade the internalized cargo. Also, granule binding to plasma membrane allows serine proteases to have extracellular microbicidal action as well as tissue-degrading effects. Cumulative evidence indicates that NSPs also exert other actions outside granules and phagosomes either intracellularly or extracellularly (6). In fact, in aging neutrophils, PR3 is released to the cytosol *via* lysosomal membrane permeabilization, an event that leads to pro-caspase-3 cleavage and apoptosis. The cytosolic PR3 activity is counteracted by the suicide protease inhibitor SERPINB1. The final balance between PR3 and SERPINB1 controls neutrophil spontaneous death (7). Furthermore, PR3 is also expressed bound to CD177 on the plasma membrane of freshly isolated neutrophils. There is also evidence that not only PR3 but also NE and CG can associate with the plasma membrane under inflammatory conditions (6). On the other hand, upon stimulation with agonists that induce neutrophil extracellular traps formation, NE escapes from azurophilic granules through a reactive oxygen species (ROS)-dependent process (8). In the cytosol, NE binds and degrades F-actin to arrest actin dynamics, and subsequently it translocates to the nucleus, where it partially degrades specific histones promoting chromatin decondensation (9). Recent studies also determined that N-Gasdermin D (N-GSDMD), the pore-forming fragment of Gasdermin D generated by active caspase-1, in neutrophils traffics to the membrane of azurophilic granules, thus mediating the leakage of neutrophil elastase into the cytosol. This event, in turn, facilitates a secondary cascade of serine protease-dependent GSDMD processing (10).

Interleukin-1β is a pro-inflammatory cytokine that lacks a signal peptide. It is synthesized as an inactive precursor (pro-IL-1β) in the cytosol, where it is processed by enzymatic cleavage. In myeloid cells, the precursor processing usually relies on the action of the enzyme caspase-1, which in turn is activated upon the formation of the intracellular macromolecular complexes called inflammasomes (11, 12). The canonical inflammasomes comprise an inflammasome sensor protein, such as the nucleotide-binding domain and leucine-rich-repeat containing protein 3 (NLRP3), which binds to caspase-1 usually *via* the adapter ASC (apoptosis-associated speck-like protein containing the caspase activation and recruitment domain [CARD]). NLRP3 is activated by pathogen- and danger-associated molecular patterns representative of infection, cellular damage, or cell stress, which promotes its oligomerization (13). This, in turn, leads to ASC recruitment and polymerization, originating an ASC-speck structure, to which full-length caspase-1 binds. Full-length caspase-1 dimerization in the inflammasome structure triggers its protease activity, which allows its self-cleavage to generate a fully active p33/p10 species, which remains bound to the inflammasome and is responsible for pro-IL-1β processing, i.e., the generation of the mature 17-kDa IL-1β isoform (14). Then, caspase-1 self-cleaves again generating

a p20/p10 species. This cleavage releases caspase-1 from the inflammasome and terminates its protease activity and cytokine processing (3, 14).

Interestingly, other studies showed that NSPs can also process pro-IL-1β into a bioactive fragment and attributed a role to these enzymes in the extracellular processing of pro-IL-1β released at inflammatory environments (15–17).

Previously we determined that highly purified human neutrophils produce and secrete IL-1β (18, 19). These studies showed that human neutrophil IL-1β secretion is restrained by both caspase-1 and NSPs inhibition, and that cytokine secretion, but not pro-IL-1β processing, is dependent on NADPH oxidase-derived ROS (18). As pro-IL-1β is a leaderless protein synthesized in the cytosol, once processed, IL-1β is usually released by unconventional secretory mechanisms. Our previous studies also determined that human neutrophils release IL-1β by an autophagy-mediated secretory mechanism (19). In fact, pharmacological inhibition of autophagy as well as ATG5 knockdown, reduced IL-1β secretion, while autophagy stimulation by starvation increased it. Additional studies performed by using ATG7-deficient mouse cells confirmed these findings (10).

Considering that both caspase-1 and NSPs are required for the release of active IL-1β, we conducted this study to address the role of these enzymes in the mechanisms involved in pro-IL-1β processing in human neutrophils and those leading to IL-1β secretion. By studying the responses of human neutrophils from healthy donors and from patients with a GOF *NLRP3*-mutation, we found that even though caspase-1 is activated after inflammasome activation and is required for IL-1β secretion, it mostly undergoes rapid inactivation and NSPs accomplish a major role in pro-IL-1β processing.

Materials and methods

The experimental protocols performed have been approved by the Biosafety and Research Review boards of the "Instituto de Medicina Experimental (IMEX)-CONICET-Academia Nacional de Medicina" and the Ethical Committee of the "Institutos de la Academia Nacional de Medicina".

Reagents and materials

RPMI 1640 culture medium, Earle's Balanced Salt Solution (EBSS), LysoTracker™ Red DND-99, ammonium persulfate, Pierce LDH Cytotoxicity Assay Kit, dextran 500, and TMB substrate were purchased from Thermo Fisher Scientific Life Technologies (MA, USA). Fetal bovine serum (FBS) and bovine serum albumin were purchased from Internegocios (Buenos Aires, Argentina). Ficoll-Paque was purchased from GE Healthcare (Munich, Germany). BD OptEIA™ Human IL-1β ELISA Set II and Human IL-8/CXCL8 ELISA Set were purchased from BD Biosciences (Franklin Lakes, NJ, USA). Quantikine Human Pro-IL-1β/IL-1F2 Immunoassay and Human IL-1β/IL-1F2 Propeptide Antibody (MAB6964) were purchased from R&D (Minneapolis, MN, USA). Secondary antibodies were purchased from Jackson Immunoresearch Laboratories (West Grove, PA, USA): Alexa Fluor® 647 AffiniPure F (ab')$_2$ Fragment Goat Anti-Rabbit IgG (H + L), cat. #111-606-144; Alexa Fluor® 488 AffiniPure F(ab')$_2$ Fragment Goat Anti-Rabbit IgG (H + L) cat. #111-546-144; DyLight 549 conjugated AffiniPure F(ab')$_2$ Fragment Goat Anti-mouse IgG (H + L), cat. #115-506-062; Cy™3 AffiniPure F(ab')2 Fragment Goat Anti-Mouse IgG (H+L), cat. #115-166-146. TO-PRO-3 was obtained from Life Technologies (Carlsbad, CA, USA). Phycoerythrin-conjugated anti-CD14 antibody was purchased from eBioscience (San Diego, CA, USA). Aqua Poly/Mount Coverslipping Medium was purchased from Polysciences (Warrington, PA, USA). Rabbit polyclonal antibody anti-microtubule-associated protein 1 light chain 3 beta (LC3B) cat. #sc28266; rabbit polyclonal antibody anti-IL-1 cat. #sc7884, anti-caspase-1 p10(C-20) cat. #515 antibody and cat. #sc-56036 were from Santa Cruz Biotechnology (Dallas, TX, USA); rabbit polyclonal anti-human IL-1 beta cat. NB600-633 was from Novus Biologicals (Co, USA); rabbit polyclonal anti-human-myeloperoxidase cat.#A0398 was from Dako (Glostrup, Denmark); rabbit polyclonal anti-sequestosome 1(SQSTM1)/p62 cat.# F48010 was from NSJ Bioreagents (San Diego, CA, USA); and purified mouse IgG1, κ isotype control cat. #555746 and rabbit polyclonal IgG was purchased from Jackson Immunoresearch. Complete™, EDTA-free Protease Inhibitor Cocktail, cat. #11873580001 was from Roche (Basel, Switzerland). Hyperfilm ECL Amersham and Hybond PVDF membrane were from Amersham Cytiva (Marlborough, MA, US). AEBSF (4-(2-aminoethyl)-benzenesulfonyl fluoride, monohydrochloride), Ac-YVAD-CMK (N-acetyl-L-tyrosyl-L-valyl-N-[(1S)-1-(carboxymethyl)-3-chloro-2-oxo-propyl]-L-alaninamide), Z-VAD-FMK, Bafilomycin A1, and 3-methyladenine (3-MA) and VX-765 were purchased from Cayman Chemical (Michigan, USA), Annexin V-FITC cat. # 31490013 was purchased from Immunotools (Gladiolenweg, Germany). FAM-FLICA® Caspase-1 Assay Kit and FAM-FLISP FLCK Serine protease kit were purchased from Immunochemistry Technologies (Bloomington, MN, USA). All other chemicals employed were purchased from Sigma Aldrich (St. Louis, MO, USA).

Human neutrophil isolation

Cells were isolated from ACD-anticoagulated human blood from healthy adult donors or from patients with the gain-of-function (GOF) *NLRP3* mutation c.1322C>T (p.Ala441Val) validated as Pathogenic on the Infevers Database, classification proposed by the International Study Group for Systemic Autoinflammatory Diseases (20) and aged-matched control donors. Neutrophils were isolated by centrifugation on Ficoll-Paque, dextran sedimentation, and hypotonic lysis. Cells were suspended at 6×10^6/mL in RPMI 1640 supplemented with penicillin (100 U/mL), streptomycin (100 µg/mL), and 10% FBS.

After isolation, neutrophil preparations were stained with an anti-CD14-PE antibody and analyzed with a Partec Cyflow cytometer to guarantee that monocyte contamination was less than 0.5% as previously described (19). Cells were used immediately after isolation.

Neutrophil stimulation

Neutrophils ($5x10^6$/ml) were treated for 2 h with or without 150 ng/mL LPS from *Escherichia coli* O111:B4. Then, they were stimulated or not with 2.5 mM ATP and cultured for the specified times. Where indicated, before LPS stimulation, cells were pretreated for 30 min with AEBSF (1 mM or 0.35 mM) and/or Ac-YVAD-CMK (50 μM), VX-765 (50 μM) or Z-VAD-FMK (50 μM). After culture, cell supernatants, and where indicated, also the cell pellets, were collected and pro-IL-1β, IL-1β and IL-8 concentrations were quantitated by ELISA. In cell pellets, viability was determined by annexin V-FITC/propidium iodide (PI) staining and flow cytometry analysis. Alternatively, at the specified time, cell pellets were fixed with 4% paraformaldehyde (PFA) and processed for either confocal laser scanning microscopy (CLSM) or flow cytometry. In some experiments, inhibitors were added at different time points after ATP treatment and at 5 h post-LPS stimulation, supernatants and pellets were collected and IL-1β was determined by ELISA.

Intracellular immunostainings and CLSM acquisition

After fixation with PFA 4% for 30 min, cells were blocked with PBS-glycine (0.1 M) for 15 min, permeabilized with chilled acetone (−20°C) for 7 min, rehydrated with PBS and blocked with PBS supplemented with 5% goat serum overnight at 4°C. Then, neutrophils were incubated with the primary antibodies in blocking buffer for 1 h at room temperature, washed, and then incubated with the corresponding secondary antibodies for 1 h at room temperature. In some experiments TO-PRO-3 was added for nuclei staining. Then cells were washed, cyto-spinned, mounted with Aqua-Poly/mount mounting medium, and stored at 4°C until microscopy examination. Image acquisition was performed by using a FluoView FV1000 confocal microscope (Olympus, Tokyo, Japan) equipped with a Plapon 60X/1.42 objective. Images were analyzed with ImageJ software (NIH) and fluorescence was quantitated. Some CLSM experiments were performed by seeding neutrophils on poly-L-lysine coated Lab-Tek chambers (Nalge Nunc International, New York, NY, USA).

Phalloidin staining

Cells were fixed with PFA 4% for 20 min, then stained with Phalloidin-TRITC (50 μg/mL) for 40 min and washed thoroughly with PBS. Next, cells were subjected to flow cytometry or CLSM image acquisition.

Flow cytometry analysis

For certain experiments, after immunostaining, cell fluorescence was determined by flow cytometry using a Partec Cyflow cytometer. Data were analyzed by using the FlowJo software (FlowJo v10.3 for Windows; Treestar Inc, Ashland, OR, USA).

Determination of caspase-1 activation

Neutrophils were stimulated as described above and at the specified times for each experiment, FAM-FLICA (FLICA) reagent was added according to manufacturer's instructions. After additional culture, neutrophils were washed thoroughly, and analyzed for caspase-1 activation by flow cytometry. Alternatively, neutrophils were seeded in Cellview glass bottom dishes chambers (GBO) pre-treated with poly-L-lysine (0.01%), stimulated with LPS and two hours later, inflammasome activation was triggered by the addition of ATP (2.5 mM). The chamber was incubated at 37°C and 5% CO2 in the microscope incubator, and the FLICA probe was added ten minutes after ATP. Images were captured each 5 sec.

Lactate dehydrogenase (LDH) Assay

Culture supernatants were harvested and LDH levels were measured by using a Pierce LDH Cytotoxicity Assay Kit according to manufacturer's instructions. The same number of cells were lysed with 0.5% Triton X-100 and used as a positive control.

Cytokine quantification

After neutrophil stimulation, cell supernatants were collected, and in the indicated cases, the cell pellets were treated with 0.1% Triton-X100 and protease inhibitors. Cytokines were quantified by ELISA following the manufacturer's instructions.

Automated image analysis

Images were analyzed using Fiji software and macros for automatized image quantification were designed as previously described (19). Regions of interest (ROIs) of cells were generated using the TRITC-phalloidin signal or the LC3B signal on the

corresponding images. Briefly, a low threshold was applied for the creation of a mask image and individual ROIs were determined by size. For F-actin determination, the TRITC raw intensity density of the phalloidin signal was measured in each individual ROI. To quantify the degree of colocalization between LC3B and ASC, we performed an image analysis by using the Manders' coefficients. The values of these coefficients range from 0 to 1, for no colocalization to perfect colocalization, respectively. For the colocalization of vesicular LC3B and ASC, a threshold was established and Manders' M1 (LC3B) and M2 (ASC) coefficients of individual cells were determined using the coloc2 plugin.

Whole cell extract and western blot analysis

Extracts from $5x10^6$ neutrophils were denatured in lysis buffer (Tris-HCl 60 mM, 1% SDS) with the addition of a 2.5X final concentration of protease inhibitors (cOmplete™, EDTA-free Protease Inhibitor Cocktail) for 10 min at 95°C. Then centrifuged at 13.000 rpm for 10 min at room temperature and supernatants were collected. Protein concentration was measured, and samples (65 µg per lane) were prepared with sample buffer 6X. Next, samples were separated in SDS-PAGE gel with 12% of polyacrylamide, and electrophoretically transferred onto polyvinylidene difluoride membranes (PVDF) membranes. Non-specific binding sites were blocked by soaking the membranes in Tris buffer saline (TBS), with 0.1% BSA, 0.4% Tween 20 and 1 mM EDTA for 1 hour at room temperature. The different proteins (as indicated in the figures and figure legends) were detected with specific primary antibodies and their corresponding horseradish peroxidase (HRP)-conjugated secondary antibodies followed by incubation and development with ECL. Note: Raw films of western blots are shown in Supplementary Figure S10.

Statistical Analysis

Statistical analysis was performed using GraphPad Prism 7 for Windows version 7.04, GraphPad Software, La Jolla, CA, USA or InfoStat software (Córdoba, Argentina) for Kruskall-Wallis analysis. Statistical significance was defined as $p < 0.05$.

Results

Human neutrophil treatment with the serine protease inhibitor AEBSF restrains autophagy impairing IL-1β secretion

In a previous work, we determined that an autophagy-dependent mechanism is involved in IL-1β secretion in human neutrophils (19). In that study, we determined that neutrophil treatment with the NSPs inhibitor AEBSF (1 mM) added 1 h post-LPS-stimulation (p.s.) inhibited IL-1β secretion. This inhibitor did not induce the accumulation of intracellular mature IL-1β, although it tended to increase intracellular pro-IL-1β levels at 5 h p.s (19). We hypothesized that this was a consequence of a balance between two opposite effects of NSPs, on the one hand, their potential contribution to pro-IL-1β processing, and on the other one, their capacity to mediate IL-1β degradation inside the autolysosomes. However, NSPs might also modulate neutrophil IL-1β secretion by other pathways. To get insight into these other possibilities, we first performed assays to determine whether the addition of AEBSF before LPS stimulation reproduced the effects we observed when it was added later. Treatment of neutrophils with AEBSF (1 mM or 0.35 mM) 30 min before LPS stimulation nearly abrogated IL-1β secretion at 5 h p.s., a time point that according to our previous studies maximal IL-1β secretion is detected (Figures 1A, B). Moreover, AEBSF also abolished intracellular IL-1β levels (Figures 1A, B). These findings could not be attributed to cell death because even though AEBSF 1 mM induced a marked reduction in cell viability evaluated by either Annexin V and propidium iodide (PI) staining (Figures 1C, D and Supplementary Figure S1) and LDH release (Figure 1E), most of the cells were viable when treated with AEBSF 0.35 mM. Furthermore, AEBSF did not inhibit pro-IL-1β synthesis as indicated by flow cytometry assays using a specific antibody that recognizes this precursor (Figure 1F).

Considering that IL-1β is exported from human neutrophils by an autophagy-dependent mechanism (19), we first evaluated the impact of AEBSF on the autophagic pathway. To this aim, we took advantage of the fact that in cells undergoing autophagy, the cytoplasmic protein LC3B-I conjugates with phosphatidylethanolamine in the membrane of autophagosomes (LC3B-II) and both isoforms can be identified by western blot. Thus, we treated or not human neutrophils with AEBSF and stimulated them or not with LPS and ATP as we previously showed that these stimuli induce the neutrophil autophagy flux. As a control, we employed the autolysosomal degradation blocker Bafilomycin A1 (Baf A1) to determine the effect of the inhibition of autophagy flux in these cells. As depicted in Figure 2A, inhibition of NSPs with AEBSF induced a strong increase in the LC3B-I band in both unstimulated and LPS+ATP stimulated cells. As expected, treatment with Baf A1 increased the LC3B-II isoform especially in LPS+ATP-stimulated neutrophils. But more importantly, the combined treatment of AEBSF and Baf A1 did not increase LC3B-II expression compared to Baf A1 treatment alone, suggesting that AEBSF inhibits autophagy induction but does not block the autophagy flux.

We also evaluated the expression of SQSTM1/p62, a protein that links LC3 with ubiquitinated substrates to incorporate them into autophagosomes for degradation. Thus, inhibition of

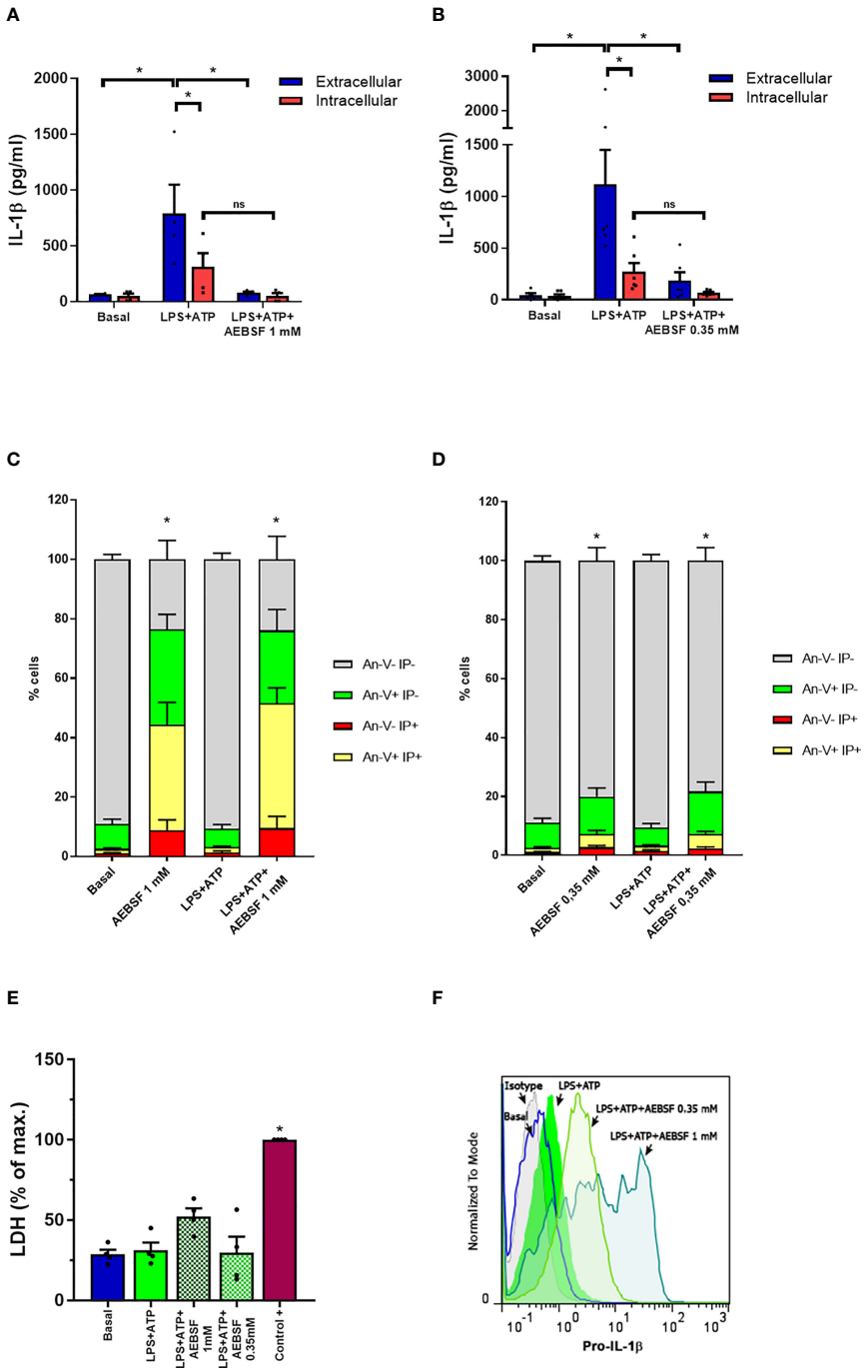

FIGURE 1
Treatment of neutrophils with the NSPs inhibitor AEBSF reduces IL-1β secretion without compromising pro-IL-1β synthesis. **(A, B)** Extracellular (blue bars) and intracellular (red bars) concentrations of IL-1β in culture supernatants of unstimulated (basal) or LPS + ATP-stimulated neutrophils for 5 h in the absence or presence of AEBSF added 30 min before LPS stimulation. Data represent the mean ± SEM of experiments performed in triplicate with 4 donors. **(C, D)** Apoptosis evaluated by annexin V-PI staining and flow cytometry in the cell pellets of the same donors evaluated in **(A)** and **(B)**. **(E)** LDH levels determined in culture supernatants of neutrophils treated as indicated and expressed as % of maximal LDH content, represented by the amount of LDH of a whole extract of the same number of neutrophils employed in the assay (control+). Data represent the mean ± SEM of experiments performed with 4 donors. **(F)** Pro-IL-1β expression in neutrophils stimulated or not with LPS+ATP (2.5 h p.s.) and pretreated or not with AEBSF (0.35 or 1 mM) evaluated by immunostaining and flow cytometry. Histograms are representative of experiments with 4 donors. *p<0.05. Two-way ANOVA followed by Bonferroni's multiple comparisons test. ns, non-significant..

autophagy induction usually correlates with increased SQSTM1/p62 levels. Results from flow cytometry studies indicated that inhibition of NSPs markedly increased SQSTM1/p62 levels (Figure 2B). In assays performed by immunostaining and confocal microscopy, we also detected an accumulation of cytosolic LC3B when LPS-stimulated cells were treated with AEBSF (Figures 2C, D). Altogether, our findings suggest that NSPs inhibition modulates the neutrophil autophagy process. Thus, the ability of AEBSF to reduce neutrophil IL-1β secretion could be due to its capacity to impair IL-1β entry into autophagy vesicles.

Autophagy and NSPs modulate caspase-1 activity

As determined in our previous studies, and as confirmed here by time-lapse microscopy (Supplementary video 1), neutrophil stimulation with LPS+ATP induces caspase-1 activation, and its inhibition significantly reduces neutrophil IL-1β secretion (18). Caspase-1 is activated within the inflammasomes and prior reports in macrophages indicated that autophagy engulfs inflammasomes and mediates their degradation (21). Thus, we reasoned that AEBSF by inhibiting autophagy might modulate the stability of active caspase-1. Therefore, we first determined if inflammasomes in human neutrophils are also targeted to autophagosomes. Supporting this possibility, the ASC adaptor molecule could be found colocalizing with LC3B puncta by immunostaining and CLSM, especially when cells were stimulated with LPS+ATP (Figures 3A–C).

Hence, subsequently, we determined the effect of AEBSF on caspase-1 by employing FLICA, a fluorescent probe that irreversibly binds to active caspase-1. As expected, stimulation of neutrophils with LPS+ATP increased the percentage of cells with active caspase-1. Treatment with AEBSF considerably increased this number further (Figure 4A). Intriguingly, we detected a similar percentage of cells with active caspase-1 in

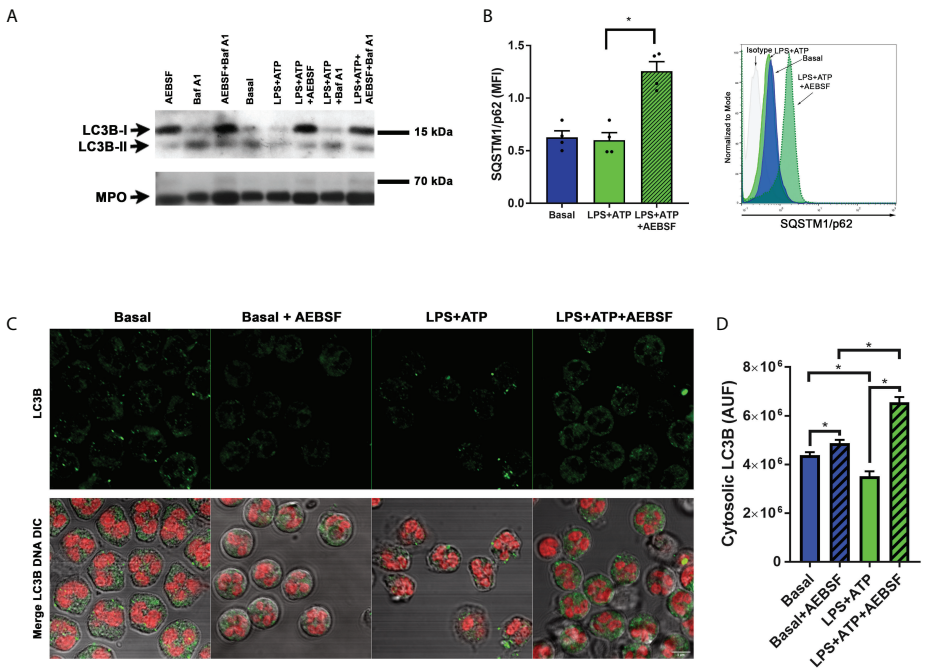

FIGURE 2
Treatment of neutrophils with AEBSF inhibits autophagy induction. **(A)** Immunoblot analysis of LC3B in lysates of human neutrophils pre-treated or not with AEBSF (0.35 mM; t= -30 min), then stimulated or not with LPS (t= 0); treated or not with the autophagy flux blocker Baf A1 (t= 1 h), and with ATP (t= 2 h), assessed at 2 h and 15 min post-LPS stimulation. Immunoblot is representative of 2 independent experiments. Myeloperoxidase (MPO) was employed as loading control. **(B)** Median fluorescence intensity (MFI) levels of the autophagy receptor p62/SQSTM1 evaluated by immunostaining and flow cytometry at 2 h and 15 min post-LPS stimulation. Data represent the mean ± SEM of experiments performed with 4 donors (left) and representative histograms of one of these experiments (right). *p < 0.05. One-way ANOVA followed by Holm-Sidak's multiple comparisons test. **(C)** Representative CLSM images of neutrophils pre-treated or not with AEBSF and stimulated or not with LPS+ATP for 4 h. Cells were stained with a specific antibody anti-LC3B and the corresponding secondary antibody and DNA was stained with ToPro-3. Images are representative of experiments with 3 different donors. **(D)** Quantification of the images of experiments performed with 3 donors as shown in **(C)** Data represent the fluorescence corresponding to cytosolic LC3B expressed in arbitrary units of fluorescence (AUF). *p<0.05. Kruskal-Wallis test.

either unstimulated (Figure 4A left panels) or LPS+ATP-stimulated neutrophils (Figure 4A right panels) when treated with AEBSF. These findings suggested that inhibition of either autophagy or NSPs conducted to an increase in the active caspase-1 levels independently of the cellular stimulation status. Since treatment of either unstimulated- or LPS+ATP-stimulated neutrophils with the autophagy flux blocking agent Baf A1 also markedly increased the percentage of cells with active caspase-1 (Figure 4A; lower panels), our results suggest that inhibition of neutrophil autophagy leads to caspase-1 activation. These findings are in agreement with previous observations in macrophages stimulated with LPS+ATP in which the deficiency in the autophagic proteins LC3B and beclin 1 enhanced the activation of caspase-1 (22). However, it is important to note that our findings do not rule out that part of the active caspase-1 we detected was also due to an increase in its stability because it can no longer be degraded inside autophagosomes (see below in Figure 4G).

In western blot assays performed using an antibody raised against the C-terminus of the human caspase-1 (p10 subunit), we detected a 10 kDa band which represents a post-activation cleavage product of this enzyme, either in unstimulated or LPS+ATP-stimulated neutrophils (Figure 4B), although in the last case, a much more intense band was detected. These results suggest that some caspase-1 might be found constitutively active in neutrophils. In agreement with results obtained by FLICA staining, treatment of neutrophils with AEBSF elicited an increased p10 band confirming that inhibition of autophagy led to caspase-1 activation.

Noteworthy, treatment with AEBSF also induced the appearance of the p46 kDa isoform. Previous studies showed that the dominant species of active caspase-1 elicited by inflammasomes consists of dimers of the full-length p46 and a transient species, p33/p10 (14). That work indicated that further p33/p10 auto-processing releases p20/p10 from the inflammasome, whereupon the tetramer becomes unstable in cells and protease activity is terminated. According to these findings, treatment with Ac-YVAD-CMK, which irreversibly bind to active caspase-1, should lead to the stabilization of the dimers of p46 isoform (and the p33/10 isoform) on the inflammasome since it would avoid caspase-1 self-inactivating cleavage. However, when we treated human neutrophils with Ac-YVAD-CMK, we were unable to detect an accumulation of the p46 isoform and the levels of the p10 band were similar to those observed upon LPS+ATP stimulation alone (Figure 4B). These results suggest that in contrast to what happens in macrophages, when the neutrophil's caspase-1 is irreversibly inhibited by Ac-YVAD-CMK, it can still be cleaved by other proteases. In fact, with this antibody (sc-515) we only detected the p46 kDa isoform upon treatment with AEBSF, the condition that, according to FLICA assays, increases the percentage of cells with active caspase-1, and upon simultaneous treatment with AEBSF and Ac-YVAD-CMK (Figure 4B). We surmise that AEBSF avoided active caspase-1 cleavage, increasing its intracellular concentration in such a way that it exceeded the threshold limit of detection by the antibody. However, as the full-length p46 isoform is expected to be present even in its monomeric (inactive) state under basal conditions, we repeated the assays by employing another anti-caspase-1 antibody (sc-56036). This antibody was more effective in recognizing the caspase-1 precursor, allowing us to detect the p46 kDa band under all the conditions evaluated even in unstimulated (basal) cells (Figure 4C). Of mention, in these new set of assays, we also examined the effect of VX-765, a caspase-1/4 inhibitor either alone or together with AEBSF. As observed with Ac-YVAD-CMK, inhibition of caspase-1/4 with VX-765 did not increased full-length caspase-1, something that was observed when it was added together with AEBSF (Figure 4C).

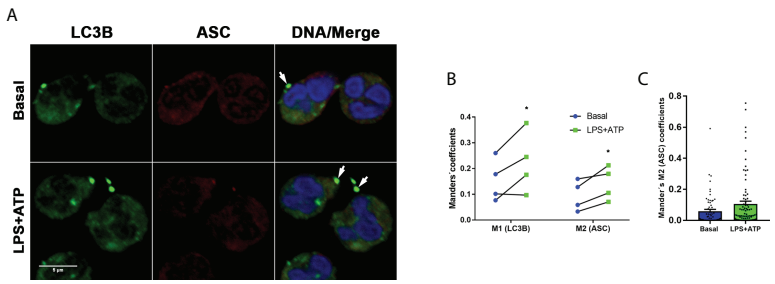

FIGURE 3
Inflammasomes are targeted to autophagosomes. **(A)** Representative CLSM images of neutrophils stimulated or not with LPS and 2 hours later treated or not with ATP. At 4 h post-LPS stimulation, cells were fixed, permeabilized and stained with specific antibodies anti-LC3B (green) and ASC (red). Images are representative of experiments with 4 different donors. **(B)** Manders´ coefficients (M1; the amount of vesicular LC3B that colocalizes with ASC) and M2 (the amount of ASC that colocalizes with LC3B) calculated by image quantification of experiments performed with 4 donors as in **(A)** in which at least 60 cells were analyzed for each condition by using a specific macro with Fiji software. Each data in the graph corresponds to the mean of Manders´ coefficients of at least 60 cells of each individual donor per experimental condition. *p<0.05. Kruskal-Wallis test. **(C)** Data from a representative experiment of those included in the graph depicted in B, from which the mean value of the Mander's M2 coefficient for LC3B was calculated.

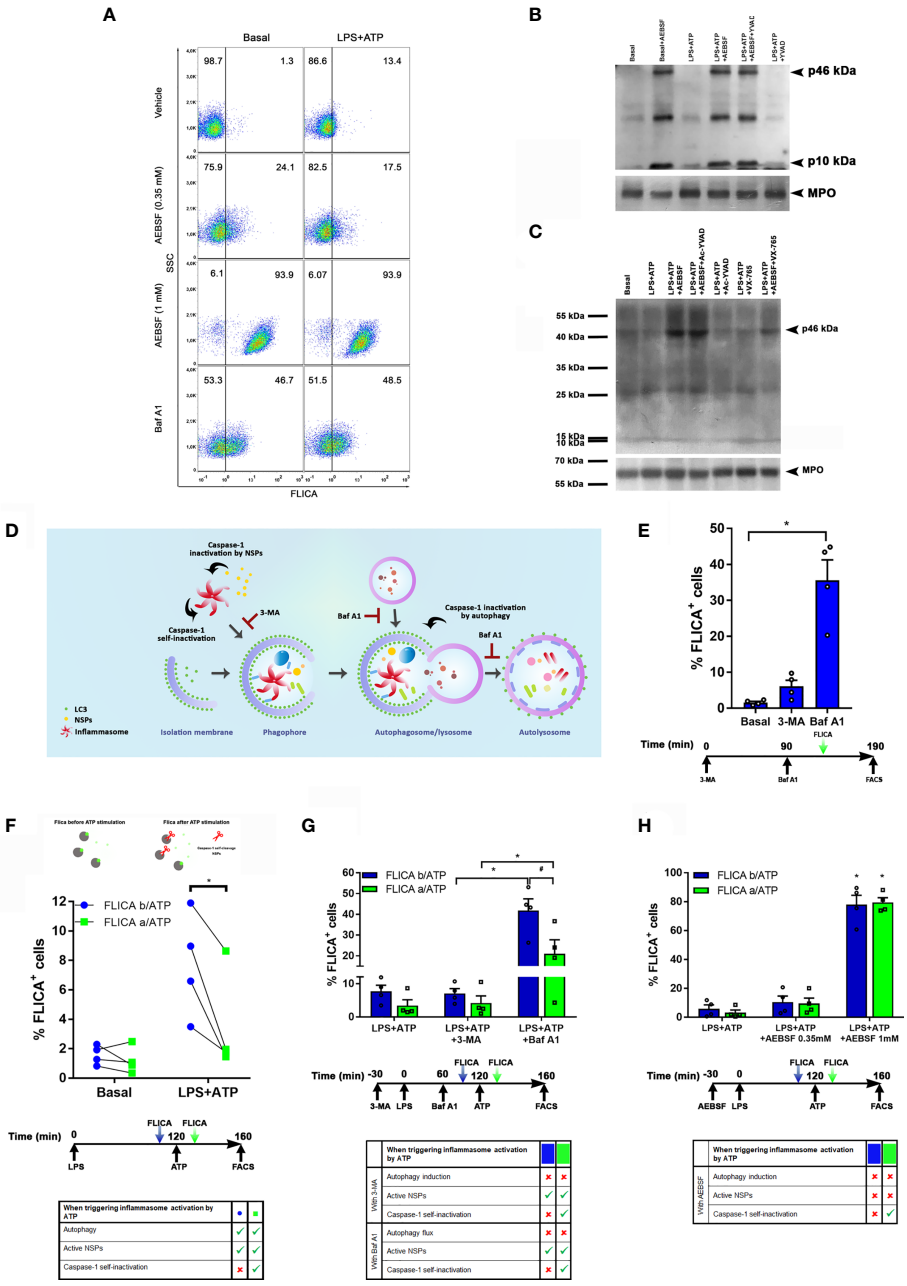

FIGURE 4
Caspase-1 activity is regulated by autophagy, self-inactivation and by NSPs. **(A)** Neutrophils were pre-treated or not with AEBSF (t= -30 min), then stimulated or not with LPS (t= 0); and treated or not with Baf A1 (t= 1 h). At 1 h 50 min the FLICA probe was added and inflammasome activation was stimulated by ATP at 2 h and cells were assessed at 2 h 40 min by flow cytometry. Dot plots are representative of experiments with 4 donors. (B and C) Immunoblot analysis of caspase-1 in lysates of human neutrophils pre-treated or not with AEBSF (0.35 mM), Ac-YVAD-CMK (50 μM), VX-765 (50 μM) or AEBSF and the corresponding caspase-1 inhibitor together, at t= -30 min, then stimulated or not with LPS (t=0) and ATP (t= 2 h) and assessed at 3 h 30 min post-LPS stimulation. MPO levels are shown as loading control. Immunoblots are representative of 3 **(B)** and 2 **(C)** independent experiments. **(D)** Rationale model to explain how the different inhibitors would impact on caspase-1 activity and its detection. **(E)** Neutrophils were treated or not with 3-MA or Baf A1 as indicated in the schedule below the graph, stained with the FLICA probe and cell fluorescence was determined by flow cytometry. **(F–H)** Neutrophils were treated as indicated in the schedule below each graph. Where indicated the FLICA probe was added 10 min before (b/ATP; blue symbols/bars) or 10 min after (a/ATP; green symbols/bars) inflammasome activation by ATP, and fluorescence was determined by flow cytometry. (F; top part) depicts the rationale of the assay; grey: caspase-1, green: FLICA probe, red scissors: proteolytic cleavage. *p<0.05 **(D)** One way ANOVA followed by Sidak's multiple comparisons test; **(E)** Paired t test; **(F–G)** Two-way ANOVA followed by Tukey's multiple comparisons test. #p<0.05 **(F)** Two-way ANOVA followed by Sidak's multiple comparisons test.

These results, together with those of FLICA assays, suggest that the inhibition of autophagy elicits inflammasome activation, and that inhibition of NSPs either directly or by its effect on autophagy, might control the stability of the active caspase-1 isoform. Thus, we then compared caspase-1 activation levels by FLICA staining in neutrophils in which autophagy was inhibited by 3-MA and Baf A1. We reasoned that as 3-MA inhibits autophagy induction, even though it leads to inflammasome activation, it would impair its targeting to the autophagosomes. Thus, after activation, caspase-1 might self-inactivate or eventually be a target of cytosolic NSPs. By contrast, as Baf A1 inhibits the autophagy flux avoiding autolysosome degradation, even if Baf A1 could induce inflammasome activation, this complex might still be targeted to the autophagosome. Thus, under these conditions, caspase-1 might undergo self-inactivation, but it would be protected from the action of cytosolic NSPs (Figure 4D). As shown in Figure 4E, both autophagy inhibitors increased the percentage of cells with active caspase-1 with respect to basal conditions. However, in accordance with our presumption, these levels were higher upon treatment with Baf A1. These findings suggest that active caspase-1 is susceptible to inactivation in the cytosol.

Afterwards, we performed assays in which we added to LPS +ATP-stimulated neutrophils the FLICA probe either 10 min before or after inflammasome activation by ATP. Since this probe rapidly diffuses inside the cell and irreversibly binds to and disables active caspase-1, we reasoned that if it is added before inflammasome activation, it would hamper the potential caspase-1 self-inactivation. By contrast, when it is added after ATP, a portion of caspase-1 might self-inactivate before FLICA has the chance to bind to its active-site (Figure 4F top). In fact, we detected higher levels of active caspase-1 when FLICA was added before ATP treatment (Figure 4F; bottom), suggesting that, as previously reported, caspase-1 can undergo self-inactivation.

We also reasoned that as 3-MA inhibits autophagy induction, upon treatment of neutrophils with this inhibitor, caspase-1 not only might undergo self-inactivation but also be more susceptible to inactivation by cytosolic NSPs. Also, upon treatment with Baf A1, caspase-1 might remain active longer because it could still be incorporated in autophagosomes but not degraded. Thus, the comparison of FLICA signal upon treatment with both inhibitors might provide information of the contribution of autophagy to caspase-1 inactivation. Moreover, by adding FLICA before and after ATP stimulation we could also obtain an estimation of the level of caspase-1 self-inactivation under these conditions. Results in Figure 4G showed a higher percentage of FLICA positive cells when neutrophils were treated with Baf A1 compared to those treated with 3-MA, suggesting that autophagy markedly contributes to active caspase-1 removal. Moreover, we detected lower levels of cells with active caspase-1 when FLICA was added after ATP stimulation under all the conditions evaluated (Figure 4G), suggesting that caspase-1 self-inactivation also takes place rapidly after activation as determined by Schroder's group. Of note, we observed similar levels of cells with active caspase-1 even if they were treated or not with 3-MA, suggesting that if caspase-1 is not incorporated into autophagosomes it can be rapidly inactivated in the cytosol.

Finally, we performed additional assays with LPS+ATP-stimulated neutrophils in which we evaluated caspase-1 activation by adding FLICA either before or after ATP treatment in the presence or absence of AEBSF (Figure 4H). AEBSF augmented the percentage of cells with active caspase-1 but this increase was independent of the moment at which the FLICA probe was added. These results suggest that when autophagy induction is inhibited, mainly NSPs contribute to caspase-1 inactivation.

Caspase-1 inactivation was also evident in studies performed with cells from pediatric patients with a GOF *NLRP3*-mutation (Figure 5A). In those neutrophils, we could detect some constitutive active caspase-1 although we also found activation in age-matched control neutrophils. However, when we stimulated cells with LPS+ATP and added FLICA 10 min after inflammasome activation by ATP, we not only detected a reduction in the percentage of cells with active caspase-1, but also, a decrease in FLICA fluorescence intensity in the whole cell population. A similar behavior was observed in neutrophils from the patients' mother (patient 4) who is also carrier of the *NLRP3* mutation even though the constitutive caspase-1 activation level was lower than in her offspring's. In neutrophils of the aged-matched control donors a decrease in FLICA fluorescence intensity was also observed after LPS+ATP stimulation as compared to that in unstimulated neutrophils, although the reduction was not as pronounced as in patients' neutrophils (Figure 5A).

Comparison of the median FLICA fluorescence intensity of unstimulated neutrophils with LPS+ATP-stimulated neutrophils of adult healthy donors when FLICA was added 10 min after ATP stimulation, also showed a reduction in active caspase-1 in 8 out of 14 donors (Supplementary Figure S2).

Altogether these results suggest that after inflammasome activation, caspase-1 substantially undergoes rapid deactivation by NSPs, autophagy and self-inactivation.

Caspase-1 activation is necessary but not sufficient for neutrophil IL-1β secretion.

Intriguingly, despite the increased constitutive activity of caspase-1 observed in the neutrophils from some patients carrying a GOF-*NLRP3* mutation and in control donor 3, these cells did not exhibit an augmented IL-1β secretion either basally or when they were stimulated with LPS+ATP (Figure 5B) or LPS alone (Supplementary Figure S3). However, the secretion of IL-8, a cytokine that does not involve caspase-1 processing, was similar among control donors and patients' neutrophils

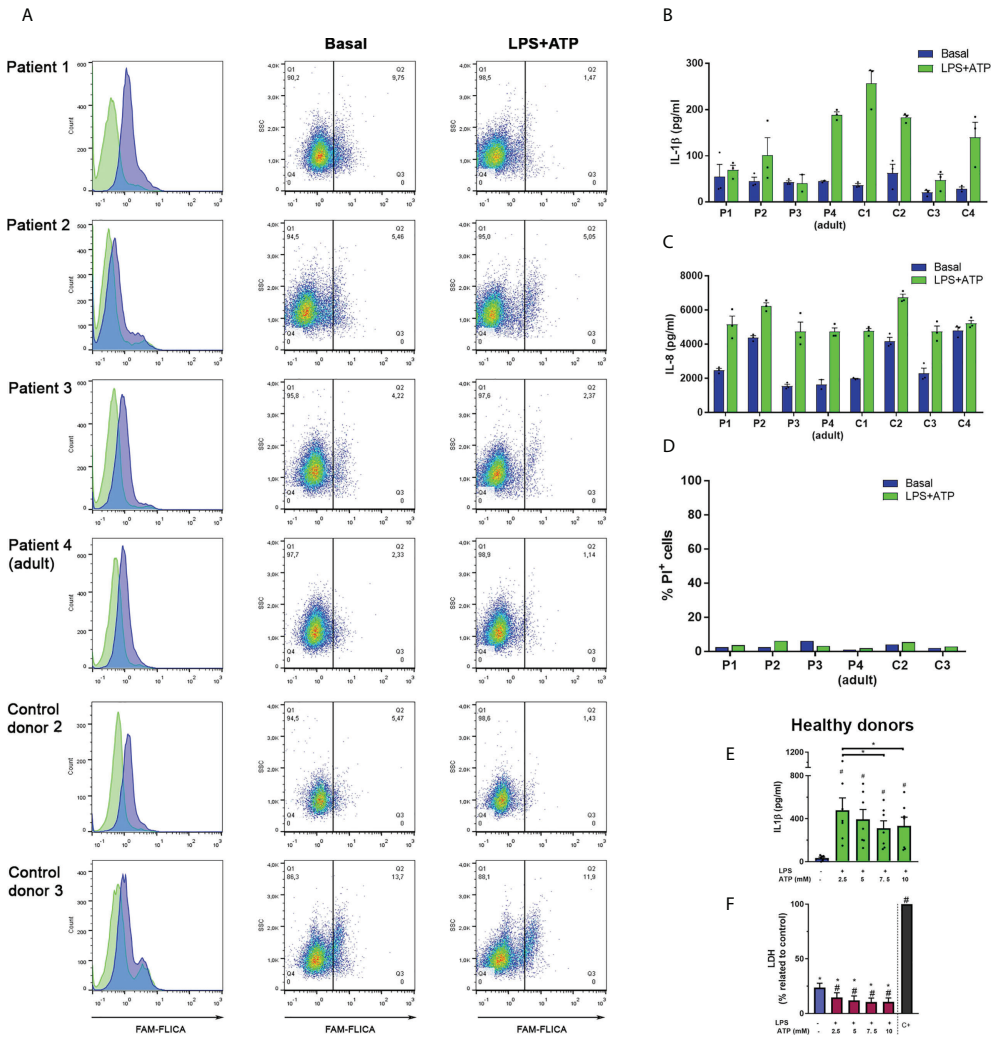

FIGURE 5
Responses of neutrophils isolated from patients who are carriers of the GOF *NLRP3* c.1322C>T (p.A441V) mutation. **(A)** Neutrophils from patients and aged-matched control donors were stimulated or not with LPS (t= 0) and 2 h later were stimulated or not with ATP. Ten min later, the FLICA probe was added, and cell fluorescence was determined at 2 h 40 min by flow cytometry. Data are depicted as histograms (blue, basal -unstimulated- condition; green, LPS+ATP-stimulated cells) to appreciate FLICA signal reduction upon stimulation; and dot plots, to show the % of cells with FLICA signal higher than the same arbitrary threshold set for all donors. **(B–D)** Neutrophils from patients and aged-matched control donors were stimulated or not with LPS (t= 0) and 2 h later were stimulated or not with ATP. At 5 h post-LPS stimulation IL-1β **(B)** or IL-8 **(C)** concentrations in culture supernatants were determined by ELISA and PI incorporation in the cell pellets was evaluated by flow cytometry **(D)**. In **(B)** and **(C)**, each bar represents the mean+SEM of the cytokine concentrations of an individual donor evaluated in triplicate. **(E, F)** Neutrophils from healthy donors were treated or not with LPS, and 2 h later with the indicated ATP concentrations. At 5 h post-LPS stimulation IL-1β **(E)** or LDH activity **(F)** were determined. Two-way ANOVA followed by Tukey's multiple comparisons test. # and *p < 0.05. # vs basal **(E, F)**; * vs positive control **(F)**.

(Figure 5C). In fact, patients' neutrophils secreted lower IL-1β amounts when stimulated by LPS+ATP than those released by neutrophils from most age-matched control donors, although their monocytes exhibited an increased IL-1β release (Supplementary Figure S4). The differences in the capacity to secrete IL-1β were not due to cell death, as neutrophils from patients' and control donors incorporated low and similar levels of PI (Figure 5D). Noteworthy, the neutrophils from the patients' mother (patient 4) which carry the same *NLRP3* mutation, did not show differences in IL-1β secretion regarding most control donors and were still able to respond to LPS+ATP stimulation. However, her neutrophils showed low levels of constitutive caspase-1 activation. By contrast, control donor 3 (C3) neutrophils, which showed a remarkable high level of constitutive caspase-1 activation, exhibited a reduced capacity to release IL-1β.

Our previous findings (18), confirmed in this work (Supplementary Figure S5) indicated that inhibition of caspase-1 with either Ac-YVAD-CMK or with VX-765 constrains IL-1β secretion. Thus, these findings together with results of this study suggest that caspase-1 activation is necessary for neutrophil IL-1β secretion, but its increased activation might be detrimental to this end. In agreement with this possibility, IL-1β secretion from healthy donors' neutrophils stimulated with LPS, was reduced upon treatment with increasing concentrations of ATP (Figure 5E). Of note, this reduction was not due to cell death (Figure 5F).

One of the causes underlying these observations might be that a greater caspase-1 activity could lead to an increase in cytosolic NSPs that might contribute not only to process, but also to degrade pro-IL-1β. In fact, previous studies showed that in neutrophils, active caspase-1 cleaves Gasdermin D (GSDMD) generating N-GSDMD that polymerizes on the membrane of azurophil granules and causes leakage of NE into the cytosol (10). As the human pro-IL-1β sequence has many NE and other NSPs cleavage target sites [Supplementary Figure S6 and (23)], we speculated that after caspase-1 activation and N-GSDMD polymerization on the azurophil granules membranes, NSPs might be released to the cytosol not only being able to inactivate caspase-1 (as we showed above) but also process and/or degrade pro-IL-1β.

To get insight in this issue, we first analyzed if LPS+ATP stimulation induces NSPs activation by employing the fluorescent probe FAM-FLISP that binds to active serine proteases. We confirmed its activation by flow cytometry upon LPS+ATP treatment (Figures 6A, B). Then, we determined if under our experimental conditions, NSPs are released in an active state into the cytosol by employing FAM-FLISP and analyzing its cell distribution by time-lapse CLSM. In these assays we also employed Lysotracker red to discriminate the acidic compartments, among them azurophil granules. Figures 6C, D, and Supplementary video 2, 3 show that upon LPS+ATP stimulation active NSPs are not found in the acidic granular compartments. However, a diffuse signal of active NSPs was detected in these cells, consistent with the notion that they were in the cytosol.

This possibility was further supported by results of additional assays that evaluated F-actin levels, since previous studies showed that when NE is released to the cytosol it binds and degrades F-actin (9). By employing phalloidin staining and flow cytometry, we detected a reduction of phalloidin fluorescence levels in LPS +ATP-stimulated neutrophils indicating, as expected, a promotion of the actin dynamics (Figure 6E). By contrast, inhibition of NSPs with AEBSF markedly increased phalloidin fluorescence over that observed upon LPS+ATP stimulation (Figure 6E). Similar findings were made when phalloidin staining was evaluated by CLSM (Figures 6F, G).

Altogether, these results support that neutrophil stimulation with LPS+ATP induces active NSPs leakage to the cytosol where they might contribute to inactivate the caspase-1 and to either process or eventually cleave/degrade pro-IL-1β.

To obtain further evidence of these possibilities, we stimulated neutrophils with LPS, and before or after the addition of ATP, we treated them either with AEBSF, VX-765 or both inhibitors together. At the end of the culture, we determined pro-IL-1β processing by evaluating the total levels (intracellular + extracellular) of mature IL-1β (Figure 7A). We found that both, AEBSF and VX-765 partially inhibited IL-1β processing at all the time points they were added. However, we detected greater IL-1β processing (higher levels of mature IL-1β) when NSPs were inhibited either 10 min before or 2 min after inflammasome activation with ATP, than when caspase-1 was inhibited with VX-765 at the same time points, suggesting that immediately after inflammasome activation the caspase-1 exerts a major role in pro-IL-1β processing. However, when the caspase-1 inhibitor was added 10 min after the inflammasome activation, it had a lower impact in IL-1β processing, but if NSPs were simultaneously inhibited by AEBSF, IL-1β processing was markedly reduced. These results suggest that caspase-1 was less relevant for IL-1β processing at this time point, in agreement with the possibility that part of the enzyme had undergone inactivation. The fact that both inhibitors added together reduced even more the processing of the cytokine than caspase-1 inhibition alone, confirms that NSPs also play a role in IL-1β processing at this moment. The results we obtained when inhibitors were added at 30 min post-ATP indicating that caspase-1 inhibition reduced even less IL-1β processing in contrast to NSPs inhibition, suggested that by this time NSPs play a major role in the processing of the cytokine.

Furthermore, to get insight if NSPs are involved in the caspase-1 activity reduction that we observed at 10 min after inflammasome activation, we performed additional assays with the FLICA probe (Figure 7B). In these assays, we added or not AEBSF simultaneously with FLICA at different time points post-inflammasome activation with ATP and incubated them during a 5 minutes-lapse to allow FLICA to bind all active caspase-1 that could be present in this time frame. We observed a reduction in FLICA signal at 10 min post-ATP in the absence of the inhibitor (top panel), while the addition of AEBSF increased active caspase-1 levels. Moreover, the addition of AEBSF led to a maximal increase in active caspase-1 levels when it was added at 15 min post-ATP, but these values were reduced again when AEBSF was added at 30 min post-ATP. These results are in agreement with the possibility that by this time-point part of the caspase-1 had undergone inactivation being unable to be trapped by FLICA. Considering that in these assays we only analyzed the FLICA signal that accumulated in a 5-min lapse time, and AEBSF was acting only during this period, these results probably reflect the effects of the NSPs inhibition on caspase-1 instead of the contribution of AEBSF to autophagy inhibition.

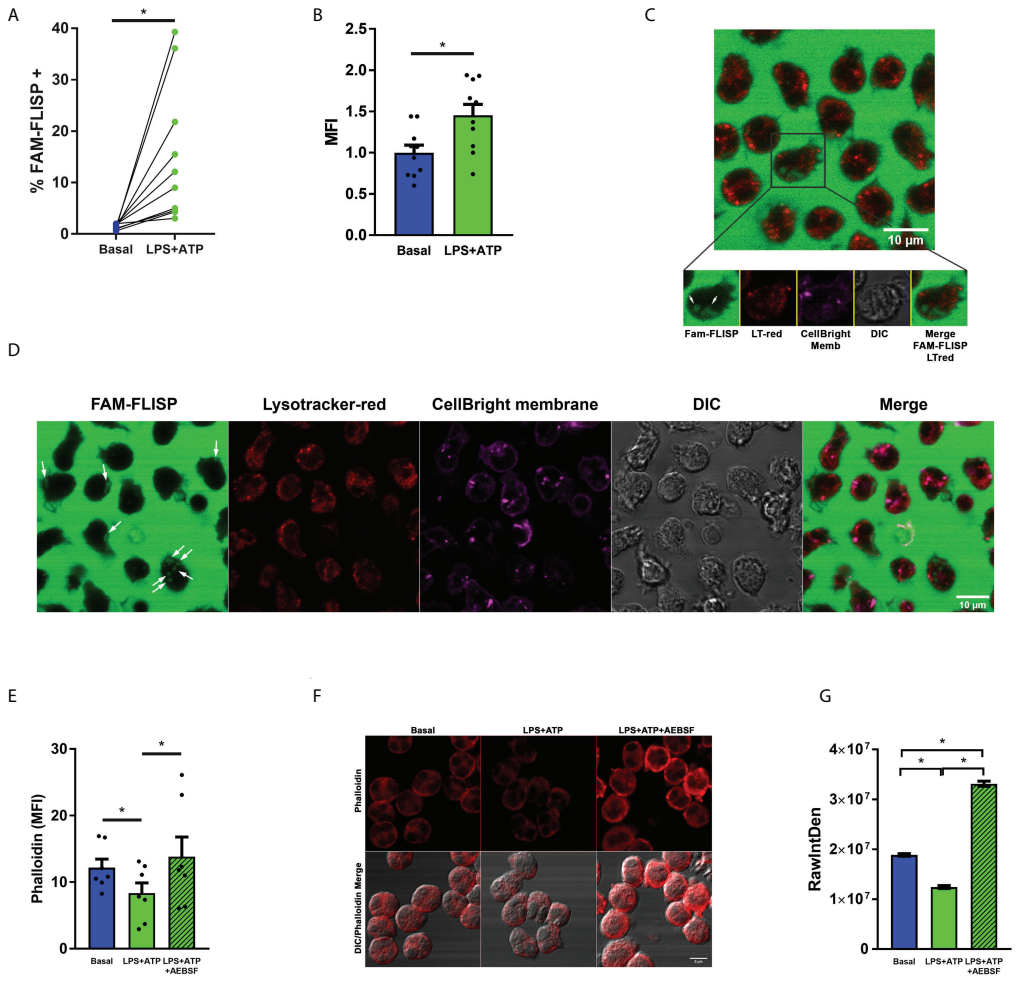

FIGURE 6
Neutrophil serine proteases undergo activation upon LPS+ATP stimulation. **(A, B)** Neutrophils from healthy donors were stimulated or not with LPS (t= 0), stained with the fluorescent probe FAM-FLISP (t= 115 min), stimulated or not with ATP (t= 120 min) and fluorescence was recorded by flow cytometry (t= 155 min). **(A)** Each point depicts the % of cells with FAM-FLISP positive signal. Results corresponding to each donor are linked with a line. **(B)** Mean ± SEM of the median fluorescence intensity (MFI) values of FAM-FLICA signal. *p<0.05 One-tailed Paired t test. **(C, D)** Representative images acquired by time-lapse confocal microscopy of neutrophils stained with CellBrite fix640 to delimit cell contour (magenta) and the fluorescent probes FAM-FLISP to detect active NSPs (green) and Lysotracker red (red). Cells were stimulated with LPS (1 µg/ml in C or 150 pg/ml in D) and treated with ATP (2.5 mM; t= 2h). Images were acquired every 2 min **(C)** and 63 sec **(D)**. White arrows show the diffuse pattern of active NSPs. Images are representative of 3 **(C)** and 1 **(D)** experiments. Of note, the intense green fluorescence outside the cells is emitted by the probe that had to be present during the whole experiment to increase the sensitivity of the assay. **(E–G)** Actin dynamic evaluated as a surrogate marker of NSP enzymatic activity in the cytosol. Neutrophils were pre-treated or not with AEBSF (0.35 mM), stimulated or not with LPS and 2 h later treated or not with ATP. Then, cells were fixed, permeabilized and stained with TRITC-Phalloidin. Cell fluorescence was evaluated by flow cytometry **(E)** and images were acquired by CLSM **(F)** and quantitated **(G)**. TRITC raw intensity density of the phalloidin signal was measured for each individual cell. **(G)** Graph depicts the mean ± SEM of raw intensity density values of 3 independent experiments in which at least 63 cells were analyzed. *p<0.05 One-way ANOVA **(D)** and Kruskal-Wallis test **(F)**.

NSPs play a major role in pro-IL-1β processing

On the other hand, to further examine if NSPs contribute to process pro-IL-1β, we reasoned that AEBSF, that when added 30 min before LPS inhibited the induction of neutrophil autophagy, should impair IL-1β to enter autophagy vesicles and its secretion. Thus, by employing this compound we would be able to study in more depth the impact of NSPs and caspase-1 on the cytoplasmic processing of pro-IL-1β. To this end, we pre-treated LPS+ATP-stimulated neutrophils with AEBSF, Ac-YVAD-CMK, VX-765 or the combination of AEBSF with either caspase-1 inhibitors to compare their effects on pro-IL-1β expression and its processing in whole cell lysates by western blot at 3.5 h post-LPS stimulation (Figure 8A upper part and 8B) and in the supernatants of the

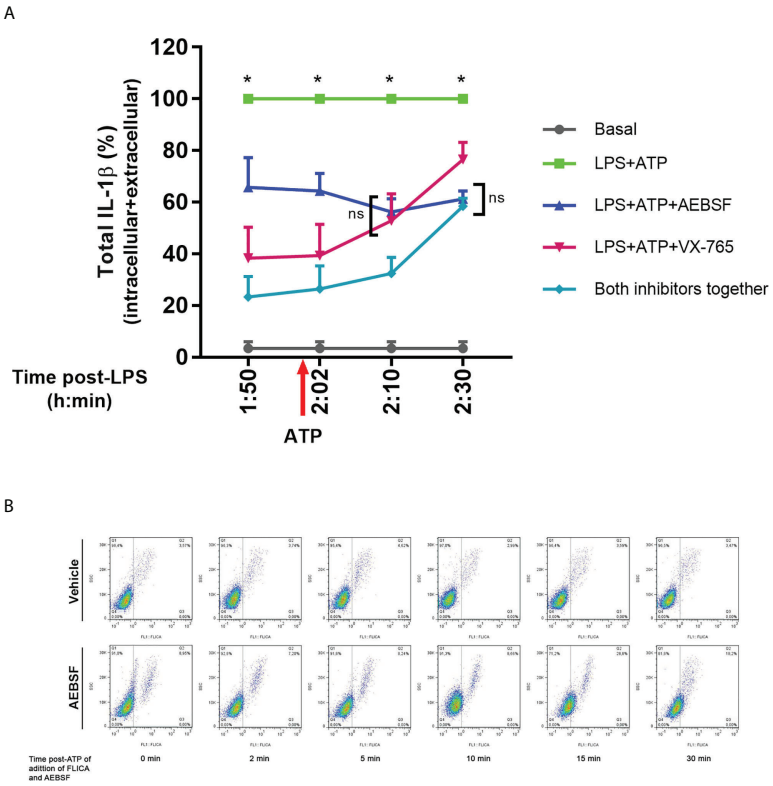

FIGURE 7
Dynamic of pro-IL-1β processing by caspase-1 and NSPs. **(A)** Total (intracellular+extracellular) mature IL-1β levels determined by ELISA in neutrophils stimulated with LPS+ATP either in the presence of AEBSF, VX-765 (caspase-1/4 inhibitor) and both inhibitors together, added at different time points before and after inflammasome activation with ATP. Neutrophils were stimulated or not with LPS and 2 h later with ATP. Ten min before ATP treatment or 2, 10 or 30 min after, cells were treated with AEBSF (0.35 mM), VX-765 (50 μM) or both inhibitors together. At 5 h post-LPS stimulation, total (intracellular+extracellular) concentrations of mature IL-1β were determined by ELISA. Data are depicted as % of the levels of mature IL-1β produced upon LPS+ATP stimulation alone and represent the mean ± SEM of experiments performed in duplicate with 4 donors. *p<0.05 LPS+ATP vs each treatment at the corresponding time point; ns: non-significant; Two-way ANOVA with Tukey's multiple comparisons test. **(B)** Effect of inhibition of NSPs at different time points after inflammasome activation with ATP on caspase-1 activity. Neutrophils were stimulated with LPS for 2 h, and then were treated with ATP to induce inflammasome activation. At the time points post ATP-addition indicated below each dot plot, FLICA was added or not simultaneously with AEBSF to trap during a 5 minutes-lapse all active caspase-1. Images depict representative dot plots of experiments performed with 4 donors showing FLICA fluorescence of neutrophils after having excluded the doublets.

same cells by quantitation of IL-1β concentrations by ELISA (Figure 8A bottom part). Of mention, the same extracts were probed with two different anti-IL-1β antibodies to confirm the results (Figure 8A upper part and 8B). As expected, and according to our previous studies (18), in cells stimulated with LPS+ATP we barely detected the pro-IL-1β band and most of the mature IL-1β was found in the culture supernatant (Figure 8A bottom part). Treatment with AEBSF alone, or in combination with Ac-YVAD-CMK or VX-765, markedly increased the band corresponding to pro-IL-1β. By contrast, treatment only with the caspase-1 inhibitors did not markedly modulate the pro-IL-1β and mature IL-1β bands compared to those observed with LPS+ATP alone as would be expected if caspase-1 plays a major role in processing this cytokine. However, both AEBSF and the caspase-1 inhibitors inhibited IL-1β release (Figure 8A bottom part) as we have already described for Ac-YVAD-CMK (18, 19) and confirmed in this work (Supplementary Figure S5). These assays indicated that pro-IL-1β accumulated not only when NSPs were inhibited and caspase-1 was expected to be active for a longer time (AEBSF condition; see Figure 4A), but also when both NSPs and caspase-1 were expected to be inactive (AEBSF+Ac-YVAD-CMK or AEBSF+VX-765 conditions). Besides, we did not detect extracellular IL-1β when LPS+ATP-stimulated cells were incubated with these inhibitors, even though cells in their absence secreted huge amounts of IL-1β (Figure 8A bottom part).

Of mention, due to differences in IL-1β secretion dynamics, in some donors we could detect a band corresponding to mature IL-1β upon LPS+ATP stimulation (Supplementary Figure S7)

because it was not totally released at the time point analyzed. In these cases, we also detected mature IL-1β upon Ac-YVAD-CMK treatment, confirming that even when caspase-1 was inhibited IL-1β could still be processed. Altogether, these findings suggest that NSPs mainly contribute to pro-IL-1β processing in human neutrophils.

Finally, we performed additional assays to quantitate by specific ELISAs the intracellular and extracellular pro-IL-1β and IL-1β levels upon treatment with the inhibitors (Figures 8C, D). In agreement with western blot results, treatment with AEBSF alone or together with Ac-YVAD-CMK markedly increased the intracellular levels of pro-IL-1β (Figure 8C). Treatment with Ac-YVAD-CMK did not lead to pro-IL-1β accumulation. A similar behavior was detected by intracellular immunostaining and flow cytometry (Supplementary Figure S8). Furthermore, inhibition of caspase-1 neither modulated mature intracellular IL-1β levels

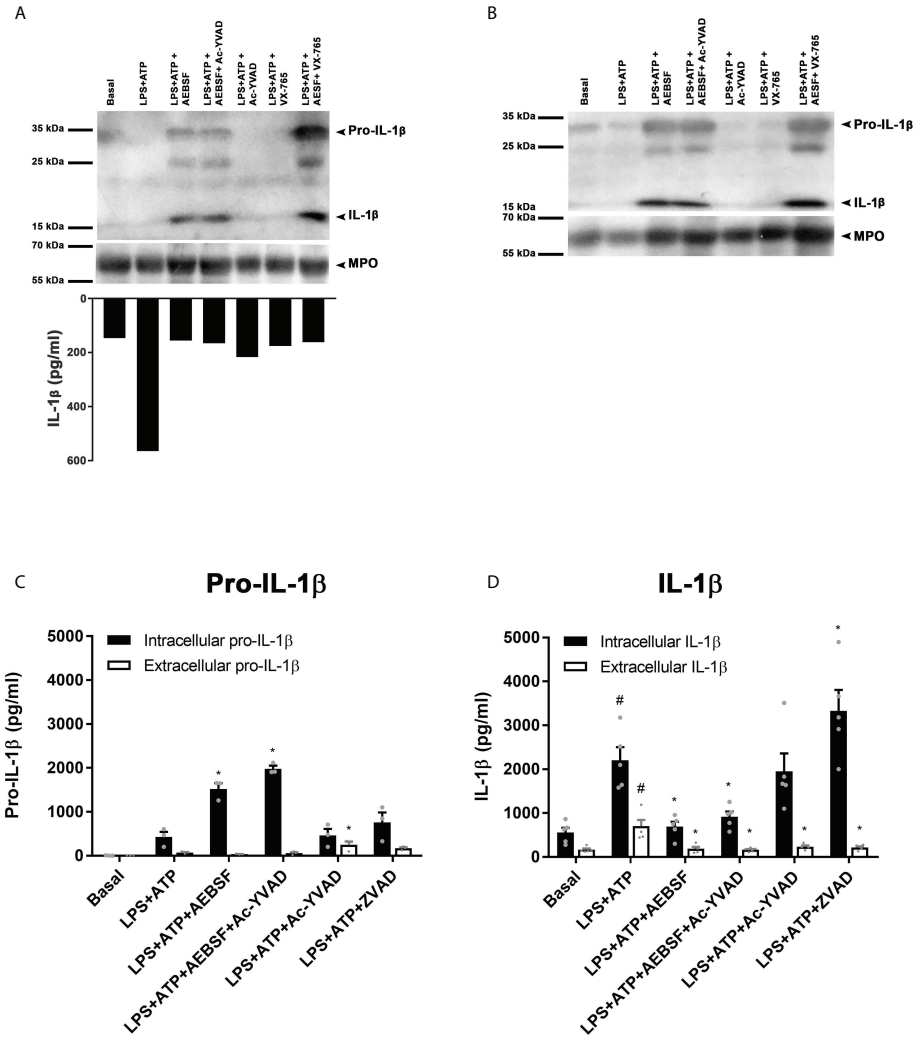

FIGURE 8
NSPs but not caspase-1 play a major role in pro-IL-1β processing. (**A** upper part and **B**) Neutrophils were pre-treated for 30 min in the presence or absence of AEBSF (1 mM), Ac-YVAD-CMK (50 μM), VX-765 (50 μM) or their combination of AEBSF and one of the caspase-1 inhibitors, then cultured with or without LPS for 2 h and after were stimulated or not with ATP (2.5 mM) for another 1.5 h. Then, whole cell extracts were subjected to Western blot **(A, B)** and supernatants collected for ELISA quantification (A; bottom part). Western blots in A and B belong to the same cells extracts that were electrophoresed and electro-transferred twice, one probed with an anti-human IL-1β antibody from Santa Cruz (antibody H-153; A) and the other one with a Novus Biological antibody (NB600-633; B). (**A**, upper part and **B**) Representative Western blot assay (n=6; **A** and n=2; **B**) of pro-IL-1β and mature IL-1β expression; and (A, bottom part) IL-1β concentration in culture supernatants of the same cells from which lysates were immunoblotted in **(A)** and **(B)**. **(C, D)** Concentrations determined by specific ELISAs of pro-IL-1β **(C)** and IL-1β **(D)** in culture supernatants and cell pellets of neutrophils stimulated in the absence or presence of AEBSF (0.35 mM), Ac-YVAD-CMK (50 μM), the combination of AEBSF and Ac-YVAD-CMK, or Z-VAD-FMK (50 μM) added 30 min before LPS stimulation, then stimulated or not for 2 h with LPS and then treated or not with ATP for another 1.5 h. Data represent the mean ± SEM of experiments with 3 **(C)** or 5 **(D)** donors performed in duplicate. *p<0.05 vs LPS+ATP; #p<0.05 vs Basal. One-way ANOVA with Sidak´s multiple comparisons test.

as compared to those observed with LPS+ATP (Figure 8D). To determine if another caspase might overcome the absence of active caspase-1 in cells treated with Ac-YVAD-CMK, we evaluated the impact of the pan-caspase inhibitor Z-VAD-FMK (ZVAD) on pro-IL-1β processing and IL-1β secretion. However, this inhibitor increased further pro-IL-1β processing, rising the intracellular levels of mature IL-1β, even though it did not promote its secretion, ruling out that possibility. As expected, according to our previous results (18, 19), treatment with either AEBSF or Ac-YVAD-CMK did not induce IL-1β secretion, suggesting that even though caspase-1 does not play a major role in pro-IL-1β processing it is still required for IL-1β secretion. Of mention, an elastase inhibitor, AZD9668, was also able to reduce IL-1β secretion (Supplementary Figure S9)

Altogether, our results indicated that NSPs but not caspase-1 mainly contribute to pro-IL-1β processing in human neutrophils and caspase-1 is necessary for IL-1β secretion, even though the role of this enzyme remains to be determined and deserves future studies.

Discussion

Previous studies indicated that human neutrophils produce IL-1β and secrete this cytokine by an autophagy-dependent mechanism (10, 18, 19). Our previous data also showed that not only caspase-1 but also NSPs inhibition (NE and/or PR3) reduces IL-1β secretion, however, the role of these enzymes in the mechanisms that lead to IL-1β secretion had not been elucidated (18, 19). Recent studies also indicated that in NLRP3-activated human neutrophils, N-GSDMD oligomerizes on azurophil granule membranes causing leakage of NE into the cytosol that results in secondary cleavage of GSDMD to an alternatively cleaved N-GSDMD product (10). Other studies also showed that NSPs, especially NE, process GSDMD generating fragments able to originate pores that produce HEK cell lysis (24, 25). Additional work also showed that *in vitro* both elastase, CG and PR3 efficiently process pro-IL-1β (15, 26). Thus, considering the abundant content of serine proteases in neutrophils (6), here we investigated the role of caspase-1 and NSPs in the mechanisms involved in pro-IL-1β processing in human neutrophils and those that lead to IL-1β secretion. Our main findings indicated that even though caspase-1 is activated in NLRP3-stimulated human neutrophils and is required for IL-1β secretion, it undergoes rapid inactivation, and instead, NSPs accomplish a major role in pro-IL-1β processing.

We found that AEBSF, a pan-serine protease inhibitor, markedly inhibited IL-1β secretion. Even though we determined this inhibitor blocked autophagy induction, its ability to prevent IL-1β secretion was not entirely associated with this effect but also to its capacity to impair pro-IL-1β processing. In accordance with a previous work (10), which by subcellular fractionation showed the presence of NSPs in the cytosolic fractions of NLRP3-activated murine neutrophils, we detected the presence of active serine proteases in the cytosol of human neutrophils by confocal microscopy. We also determined that these proteases modulated actin dynamic, indicating they are competent to mediate proteolytic actions in the cytosol, such as the pro-IL-1β processing. The major role of NSPs in pro-IL-1β processing in human neutrophils is probably related to the short stability of active caspase-1 in these cells. In fact, our findings indicated that the duration of caspase-1 activity in neutrophils is determined by an intricate weave of regulatory mechanisms that involve its self-inactivation, its inactivation by NSPs and the inflammasome degradation by autophagy.

Previous studies by Schroder's et al. showed that the inflammasome–caspase-1 complex functions as a holoenzyme that directs the location of caspase-1 activity (14). The authors reported that active caspase-1 species (p46 dimers and p33/10 dimers) can undergo inactivation by a self-cleavage that releases p20/p10 dimers from the inflammasome and ceases the protease activity. Based on the fact they found that murine neutrophils assemble smaller ASC speck than macrophages between 1 and 5 h post-Nigericin stimulation, and they were able to find some active caspase-1 until 8 h post-Nigericin stimulation, the authors concluded that neutrophil caspase-1 activity duration is extended relative to macrophages. However, in human neutrophils we found that a great proportion of caspase-1 undergoes rapid inactivation even earlier than one hour after inflammasome activation. Furthermore, our results suggest that caspase-1 self-inactivation is only one of the mechanisms that control caspase-1 deactivation. In fact, as previously reported in macrophages (21, 27), our findings indicated that inflammasomes can be found colocalizing with autophagosomes, and autophagy also controls the duration of caspase-1 activity. Cytosolic serine proteases also contribute to caspase-1 inactivation. Indeed, when employing AEBSF, which inhibits both autophagy induction and NSPs activity, the addition of FLICA before or after inflammasome activation by ATP did not affect the percentage of cells with active caspase-1 (Figure 4H). By contrast, when only autophagy was inhibited by 3-MA or Baf A1, but NSP were still active, a reduction in the percentage of cells with active caspase-1 was observed if FLICA was added 10 min after inflammasome activation, indicating that in this frame of time some caspase-1 underwent cytosolic inactivation (Figure 4G). Thus, once in the cytosol, NSPs not only contribute to pro-IL-1β processing but also to caspase-1 inactivation.

Considering previous studies indicating that caspase-1 process GSDMD allowing N-GSDMD to polymerize on azurophil granule membranes leading to NSPs leakage to the cytosol (10), the consequences of this outflow will probably depend on the strength or nature of the stimulus that triggers inflammasome activation. Our findings with neutrophils from patients with a GOF *NLRP3*-mutation suggest that a greater caspase-1 activation might be detrimental for neutrophil IL-1β

secretion. This possibility was further supported by results indicating that a stronger inflammasome stimulation with increasing ATP concentrations reduced IL-1β secretion. Considering the presence of many NSPs target sites in IL-1β sequence, it is possible to speculate that those stimuli which induce weak caspase-1 activation will probably allow NSPs to process pro-IL-1β; while those which induce strong activation of caspase-1 might induce a larger NSPs leakage contributing to rapid caspase-1 inactivation and IL-1β degradation. Thus, human neutrophils might modulate its IL-1β-dependent pro-inflammatory potential by means of an intrinsic mechanism that, by limiting the stability of active caspase-1, controls the cytosolic NSPs availability determining whether pro-IL-1β is processed to its active state or degraded.

Our studies showed that inhibition of autophagy also contributes to an increase in caspase-1 activation. This effect appears to be caused by both an augmented activation of the enzyme and a limited remotion of inflammasomes. Previous studies in autophagy-deficient macrophages showed that these cells accumulate dysfunctional mitochondria which release ROS and mitochondrial DNA in the cytosol, leading to NLRP3 activation, an effect that was potentiated by LPS and/or ATP (22, 28). However, mitochondria are scant in human neutrophils and differ from those in other myeloid cells, and the number of copies of mitochondrial DNA is 10-15-fold lower than in peripheral blood mononuclear cells (29). Thus, further studies are required to elucidate if the same events take place in human neutrophils and lead to caspase-1 activation upon autophagy inhibition.

Regarding the role of autophagy as a suppressor of inflammasome activity, our findings are in line with previous work in THP-1 cells, macrophages and monocytes that showed that the activation of inflammasomes lead to autophagy induction and to polyubiquitination of ASC in the inflammasomes, which recruits the autophagic adaptor SQSTM1/p62 resulting in inflammasome degradation by selective autophagy (21). However, we speculate that in macrophages and neutrophils, inflammasome removal by autophagy might have different consequences. In macrophages it might restrain IL-1β secretion, but in neutrophils, it might limit the massive leakage of NSPs from azurophil granules avoiding IL-1β degradation.

Our results showing that autophagy inhibition increased caspase-1 activation even in unstimulated neutrophils, are also in accordance with previous work that suggested that lower autophagy levels might keep inadvertent inflammasome activity in check (21).

Early studies in mice with serine protease activity deficiency, showed a diminished recruitment of neutrophils to air pouches in response to zymosan, which were accompanied by reduced IL-1β levels (30). Additional literature reported a role of NSPs in IL-1β-mediated pathologies in mice models (17). In fact, studies in a mouse model of *P. aeruginosa* corneal infection showed that neutrophils are the primary source of mature IL-1β, and the processing of cytokine's precursor is dependent on serine proteases, although in this case, neither NLRC4 nor caspase-1 were involved (31). Furthermore, *in vivo* studies also showed that PR3 and elastase can compensate caspase-1 absence for pro-IL-1β processing both in a serum transfer–induced arthritis model and in the monosodium urate monohydrate crystal–induced peritonitis model (32). Results of our study add to previous literature elucidating one mechanism by which NSPs might contribute to different IL-1β-mediated diseases dominated by neutrophil recruitment.

Altogether, the results of our study indicate that NSPs regulate the unconventional IL-1β secretion in human neutrophils. Furthermore, caspase-1 activation is necessary but not sufficient for IL-1β secretion as it appears to play a minor role in pro-IL-1β processing probably because it is rapidly inactivated after inflammasome activation. Autophagy not only controls IL-1β secretion but also the frame time caspase-1 is active by targeting inflammasomes for degradation.

Our findings reveal the usefulness to study potential therapeutic interventions directed to inactivate NSPs, which might be more cost-effective than targeting IL-1β to control inflammation in those pathologies where neutrophil-derived IL-1β plays a key pathogenic role, without extensively compromising broad host defense against pathogens.

Data availability statement

The original contributions presented in the study are included in the article/Supplementary Material. Further inquiries can be directed to the corresponding author.

Ethics statement

The studies involving human participants were reviewed and approved by Ethical Committee of the "Institutos de la Academia Nacional de Medicina". Written informed consent to participate in this study was provided by the participants or the participants' legal guardian/next of kin.

Author contributions

IK, FS and CS conducted most of the assays; IK, FS and AT designed the study, analyzed the data, and wrote the paper; NZ, CJ, DR, DVA and JG performed some experiments; SD, JY, MM and GB, conducted some assays with patients and/or analyzed data; FF programmed the image quantification macros, and performed microscopy acquisitions together with IK and AT; VG contributed to patients' sequences analysis; MK was involved in clinical workup of patients; and MG provided

scientific expertise and analyzed data. All authors contributed to the article and approved the submitted version.

Funding

This work was supported by grants from Agencia Nacional de Promoción Científica y Tecnológica, Ministerio de Ciencia, Tecnología e Innovación, Argentina [PICT2016-1418 and PICT-2018-02338 (A T); and PICT 2018-0546 (MG)], and Consejo Nacional de Investigaciones Científicas y Técnicas (CONICET), Buenos Aires, Argentina. This study also received funding from Novartis (MM). The funder was not involved in the study design, collection, analysis, interpretation of data, the writing of this article or the decision to submit it for publication.

Conflict of interest

MM receives a scientific research grant from Novartis; MK gives lectures for Pfizer and Novartis.

The remaining authors declare that the research was conducted in the absence of any commercial or financial relationships that could be construed as a potential conflict of interest.

Publisher's note

Supplementary material

The Supplementary Material for this article can be found online at: https://www.frontiersin.org/articles/10.3389/fimmu.2022.832306/full#supplementary-material

References

1. Ley K, Hoffman HM, Kubes P, Cassatella MA, Zychlinsky A, Hedrick CC, et al. Neutrophils: New insights and open questions. *Sci Immunol* (2018) 3(30): eaat4579. doi: 10.1126/sciimmunol.aat4579

2. Tamassia N, Bianchetto-Aguilera F, Arruda-Silva F, Gardiman E, Gasperini S, Calzetti F, et al. Cytokine production by human neutrophils: Revisiting the "dark side of the moon." *Eur J Clin Invest* (2018) 48(Supp.2):e12952. doi: 10.1111/eci.12952

3. Chan AH, Schroder K. Inflammasome signaling and regulation of interleukin-1 family cytokines. *J Exp Med* (2020) 217(1):1–10. doi: 10.1084/jem.20190314

4. Rørvig S, Østergaard O, Heegaard NHH, Borregaard N. Proteome profiling of human neutrophil granule subsets, secretory vesicles, and cell membrane: correlation with transcriptome profiling of neutrophil precursors. *J Leukoc Biol* (2013) 94(4):711–21. doi: 10.1189/jlb.1212619

5. Majewski P, Majchrzak-Gorecka M, Grygier B, Skrzeczynska-Moncznik J, Osiecka O, Cichy J. Inhibitors of serine proteases in regulating the production and function of neutrophil extracellular traps. *Front Immunol* (2016) 7:1–10. doi: 10.3389/fimmu.2016.00261

6. Kettritz R. Neutral serine proteases of neutrophils. *Immunol Rev* (2016) 273 (1):232–48. doi: 10.1111/imr.12441

7. Liu P, Ye K, Kasorn A, Cao S, Zhou J, Gong H, et al. Proteinase 3–dependent caspase-3 cleavage modulates neutrophil death and inflammation. *J Clin Invest* (2014) 124(10):4445–58. doi: 10.1172/JCI76246

8. Papayannopoulos V, Metzler KD, Hakkim A, Zychlinsky A. Neutrophil elastase and myeloperoxidase regulate the formation of neutrophil extracellular traps. *J Cell Biol* (2010) 191(3):677–91. doi: 10.1083/jcb.201006052

9. Metzler KD, Goosmann C, Lubojemska A, Zychlinsky A. A myeloperoxidase-containing complex regulates neutrophil elastase release and actin dynamics during NETosis. *Cell Rep* (2014) 8(3):883–96. doi: 10.1016/j.celrep.2014.06.044

10. Karmakar M, Minns M, Greenberg EN, Diaz-Aponte J, Pestonjamasp K, Johnson JL, et al. N-GSDMD trafficking to neutrophil organelles facilitates IL-1β release independently of plasma membrane pores and pyroptosis. *Nat Commun* (2020) 11(1):1–14. doi: 10.1038/s41467-020-16043-9

11. Martinon F, Burns K, Rg Tschopp J. The inflammasome: A molecular platform triggering activation of inflammatory caspases and processing of proIL- that they possess several distinct protein/protein inter-action domains which are used to assemble large multi-component complexes. apaf-1, for e. *Mol Cell* (2002) 10 (2):417–26. doi: 10.1016/s1097-2765(02)00599-3

12. Ketelut-Carneiro N, Fitzgerald KA. Inflammasomes. *Curr Biol* (2020) 30 (12):R689–94. doi: 10.1016/j.cub.2020.04.065

13. He Y, Hara H, Núñez G. Mechanism and regulation of NLRP3 inflammasome activation. *Trends Biochem Sci* (2016) 41(12):1012–21. doi: 10.1016/j.tibs.2016.09.002

14. Boucher D, Monteleone M, Coll RC, Chen KW, Ross CM, Teo JL, et al. Caspase-1 self-cleavage is an intrinsic mechanism to terminate inflammasome activity. *J Exp Med* (2018) 215(3):827–40. doi: 10.1084/jem.20172222

15. Greten FR, Arkan MC, Bollrath J, Hsu LC, Goode J, Miething C, et al. NF-κB is a negative regulator of IL-1β secretion as revealed by genetic and pharmacological inhibition of IKKβ. *Cell.* (2007) 130(5):918–31. doi: 10.1016/j.cell.2007.07.009

16. Coeshott C, Ohnemus C, Pilyavskaya A, Ross S, Wieczorek M, Kroona H, et al. Converting enzyme-independent release of tumor necrosis factor α and IL-1β from a stimulated human monocytic cell line in the presence of activated neutrophils or purified proteinase 3. *Proc Natl Acad Sci U S A.* (1999) 96 (11):6261–6. doi: 10.1073/pnas.96.11.6261

17. Netea MG, van de Veerdonk FL, van der Meer JWM, Dinarello CA, Joosten LAB. Inflammasome-independent regulation of IL-1-Family cytokines. *Annu Rev Immunol* (2015) 33(1):49–77. doi: 10.1146/annurev-immunol-032414-112306

18. Gabelloni ML, Sabbione F, Jancic C, Fuxman Bass J, Keitelman I, Iula L, et al. NADPH oxidase derived reactive oxygen species are involved in human neutrophil IL-1β secretion but not in inflammasome activation. *Eur J Immunol* (2013) 43(12):3324–35. doi: 10.1002/eji.201243089

19. Iula L, Keitelman IA, Sabbione F, Fuentes F, Guzman M, Galletti JG, et al. Autophagy mediates interleukin-1β secretion in human neutrophils. *Front Immunol* (2018) 9:1–14. doi: 10.3389/fimmu.2018.00269

20. Van Gijn ME, Ceccherini I, Shinar Y, Carbo EC, Slofstra M, Arostegui JI, et al. New workflow for classification of genetic variants' pathogenicity applied to hereditary recurrent fevers by the international study group for systemic autoinflammatory diseases (INSAID). *J Med Genet* (2018) 55(8):530–7. doi: 10.1136/jmedgenet-2017-105216

21. Shi CS, Shenderov K, Huang NN, Kabat J, Abu-Asab M, Fitzgerald K a, et al. Activation of autophagy by inflammatory signals limits IL-1β production by targeting ubiquitinated inflammasomes for destruction. *Nat Immunol* (2012) 13 (3):255–63. doi: 10.1038/ni.2215

22. Nakahira K, Haspel JA, Rathinam V, Lee S-J, Dolinay T, Lam HC, et al. Autophagy proteins regulate innate immune responses by inhibiting the release of mitochondrial DNA mediated by the NALP3 inflammasome. *Nat Immunol* (2011) 12(3):222–30. doi: 10.1038/ni.1980

23. Afonina IS, Müller C, Martin SJ, Beyaert R. Proteolytic processing of interleukin-1 family cytokines: Variations on a common theme. *Immunity*. (2015) 42(6):991–1004. doi: 10.1016/j.immuni.2015.06.003

24. Kambara H, Liu F, Zhang X, Liu P, Bajrami B, Teng Y, et al. Gasdermin d exerts anti-inflammatory effects by promoting neutrophil death. *Cell Rep* (2018) 22 (11):2924–36. doi: 10.1016/j.celrep.2018.02.067

25. Sollberger G, Choidas A, Burn GL, Habenberger P, Di Lucrezia R, Kordes S, et al. Gasdermin d plays a vital role in the generation of neutrophil extracellular traps. *Sci Immunol* (2018) 3(26):eaar6689. doi: 10.1126/sciimmunol.aar6689

26. Hazuda DJ, Strickler J, Kueppers F, Simon PL, Young PR. Processing of precursor interleukin 1 beta and inflammatory disease. *J Biol Chem* (1990) 265 (11):6318–22. doi: 10.1016/S0021-9258(19)39328-7

27. Harris J, Lang T, Thomas JPW, Sukkar MB, Nabar NR, Kehrl JH. Autophagy and inflammasomes. *Mol Immunol* (2017) 86:10–5. doi: 10.1016/j.molimm.2017.02.013

28. Zhou R, Yazdi AS, Menu P, Tschopp J. A role for mitochondria in NLRP3 inflammasome activation. *Nature* (2011) 469(7329):221–6. doi: 10.1038/nature09663

29. Maianski N a, Geissler J, Srinivasula SM, Alnemri ES, Roos D, Kuijpers TW. Functional characterization of mitochondria in neutrophils: a role restricted to apoptosis. *Cell Death Differ* (2004) 11(2):143–53. doi: 10.1038/sj.cdd.4401320

30. Adkison AM, Raptis SZ, Kelley DG, Pham CTN. Dipeptidyl peptidase I activates neutrophil-derived serine proteases and regulates the development of acute experimental arthritis. *J Clin Invest* (2002) 109(3):363–71. doi: 10.1172/JCI0213462

31. Karmakar M, Sun Y, Hise AG, Rietsch A, Pearlman E. IL-1β processing during pseudomonas aeruginosa infection is mediated by neutrophil serine proteases and is independent of NLRC4 and caspase-1. *J Immunol* (2013) 189 (9):4231–5. doi: 10.4049/jimmunol.1201447

32. Guma M, Ronacher L, Liu-Bryan R, Takai S, Karin M, Corr M. Caspase 1-independent activation of interleukin-1beta in neutrophil-predominant inflammation. *Arthritis Rheum* (2009) 60(12):3642–50. doi: 10.1002/art.24959

Frontiers in Immunology

Explores novel approaches and diagnoses to treat immune disorders.

The official journal of the International Union of Immunological Societies (IUIS) and the most cited in its field, leading the way for research across basic, translational and clinical immunology.

Discover the latest Research Topics

See more →

Frontiers

Avenue du Tribunal-Fédéral 34
1005 Lausanne, Switzerland
frontiersin.org

Contact us

+41 (0)21 510 17 00
frontiersin.org/about/contact